Maria Teresa Borrello

PhD.

University of East Anglia

The School of Pharmacy

August 2016

Supervisor: Prof. A. Ganesan

Second Supervisor: Prof. Mark Searcey

“Der Mensch ist was er isst”

The man is what he eats

Ludwig Feuerbach

Abstract

Environmental factors and lifestyle can alter the way our genes are expressed influencing a network of chemical switches within our cells collectively known as the Epigenome. Among the epigenetic mechanisms orchestrating the gene expression, methylation is of foremost importance and probably fair to say, still incompletely decoded. Dysregulations of histone methylation patterns lead to the repression or activation of signalling pathways that often promote the genesis and progression of disease states.

Lysine specific demethylase 1 (LSD1) oxidatively removes methyl groups from histone H3 and its aberrant activity has been correlated with the development of a broad range of pathologies. Therefore, specific inhibitors of LSD1 have potential in pharmacological applications. Research into LSD1 and its functions in normal and abnormal cells has been hindered by the lack of a specific and potent suppressor. The development of a selective inhibitor could not only foster the understanding of the biological roles of LSD1 but also represent a breakthrough for the design of novel drugs for a range of burdensome diseases. Here we investigate on reversible and irreversible inhibitors of LSD1, with the hope of broadening the current knowledge on this epigenetic target. By analysing the LSD1 interaction with the transcription factor Snail-1, we generated a series of small peptides as potential reversible inhibitors. The synthetic peptides were then evaluated in cellular assays. In search of novel non-covalent LSD1 blockers, we next explored Phage Display technology. Thereafter, we targeted LSD1 covalently by synthesising multiple structural analogues of the clinically used antidepressant TCP (Parnate®), which is a known irreversible suppressor of LSD1 activity. We evaluated their ability of inhibiting LSD1 in a cell-free assay and the compounds showing enzymatic inhibition were tested as potential anti-proliferative and differentiating agents in leukaemia cell lines. Finally, we generated activity-based probes to fluorescently label LSD1 for biological applications.

Acknowledgments

I firstly want to express my sincere gratitude to my Supervisor Prof. Ganesan for his supervision and stewardship during almost four years of PhD work. Thanks Prof. Ganesan for the encouragement, the extreme patience, the help, the support and the scientific discussions and for your help to correct my thesis, my grammar and spelling mistakes.

I also thank my second supervisor Prof. Mark Searcey.

I am indebted to Dr Christopher Morris for his advices and feedbacks on my work through my PhD and to give me the knowledge to perform Phage Display screening. Thanks Dr Chris, for all the patience and assistance, it was a pleasure to work with you.

I share the credits of this work with Prof. Andrea Mattevi for the X-ray crystal structures, Prof. Antonello Mai for the helpful discussions, Dr Rona Ramsay, Dr Patrick Duriez for the help with the enzymatic studies and protein purification and Dr Simon Crabb. I also would like to thank Dr Sarah Bailey and Dr Sergio Regufe da Mota for the biology testing on prostate cancer.

Sincere thanks also to Prof. Kristian Bowles group and especially Dr Stuart Rush worth who have gave me all the knowledge to perform the biological experiments in leukaemia. I am also grateful to Prof. Sven Mangelinckx and Prof. Günter Haufe for providing compounds to test as LSD1 inhibitors.

I owe my deepest gratitude to Dr Peter McCormick and Dr Wafa-Al-Jamal to have allowed me to use their laboratory facilities for biological testing.

In addition, I would like to thank the previous and current members of Prof. Ganesan research group and particularly Dr Hanae Benelkebir, Ke Liu, Carys Thomas, Remy Norozny, Nail and Angus for the nice working environment.

My gratitude goes to Dr Elise Wright and Dr Zöe Waller to have proof read my thesis and encouraged me throughout this journey.

I would like to thank especially my colleague and friend Serena Monaco, whose presence was fundamental in these last months. Thanks Sere, thanks for the help, for the laughter and for the dancing.

I am extremely grateful to my friends Alessia Cominato, Marco Rendina, Grazia Santarpia, Manar Shafat, Esperanza Garcia, David Todd, Amy Gallant and Aidan Pickham who have always gave me precious support along these years.

Finally I would like to thank Marco Bocchio, my fiancé, whose support and love are priceless.

I would like to dedicate this work to my parents Maria Fernanda and Cataldo Borrello, my fiancé Marco and Prof. Ganesan who have been my guides and teachers. This thesis would have remained a dream had it not been for them.
Thank you again for having always stood by me.

To my guides:
my parents Maria Fernanda dos Santos e Cataldo Borrello,
Marco Bocchio and Prof. Ganesan

Contents

List of figures

List of schemes

List of tables

Declaration of authorship

I, Maria Teresa Borrello, certify that the work contained in the thesis "Reversible and irreversible inhibitors of LSD1" submitted by me for the degree of Doctor of Philosophy at the School of Pharmacy is my original work, derived by results of my own research, except where due reference is made to other authors or other researchers. I also certify that it has not been previously submitted by me for a degree at this or any other university.

Parts of this work have been published in the following papers:

Protein Recognition by Small Peptides Reversible Inhibitors of the Chromatin Modifying LSD1/CoREST Lysine Demethylase; Tortorici, M.; Borrello, M. T.; Tardugno, M.; Chiarelli, L. R.; Pilotto, S.; Ciossani, G.; Vellore, N. A.; Bailey, S. G.; Cowan, J.; O'Connell, M.; Crabb, S. J.; Packham, G. K.; Mai, A.; Baron, R.; Ganesan, A.; Mattevi, A. *ACS Chem. Biol*. **2013**, 8, 1677–1682**.**

Expanding the Druggable Space of the LSD1/CoREST Epigenetic Target: New Potential Binding Regions for Drug-Like Molecules, Peptides, Protein Partners, and Chromatin. Robertson, J. C.; Hurley, N. C.; Tortorici, M.; Ciossani, G.; Borrello, M. T.; Vellore, N. A.; Ganesan, A.; Mattevi, A.; Baron, R. *PLoS Comput. Biol.* **2013**, *9*, e1003158.

Cis-Cyclopropylamines as Mechanism-Based Inhibitors of Monoamine Oxidases.
Malcomson, T.; Yelekci, K.; Borrello, M. T.; Ganesan, A.; STDina, E.; De Kimpe, N.; Mangelinckx, S.; Ramsay, R. R. *FEBS J*. **2015**, 282, 3190–3198.

Signed

……

Date

……..

List of abbreviations

A or Ala	Alanine
ABP	Active based probe
ABPP	Activity based probe protein profiling
Ab	antibody
Ac	Acetyl
AcOH	Acetic acid
AcH3K9	Histone 3 lysine 9 acetyl
ADP	Adenosine diphosphate
AML	Acute myeloid leukaemia
AOL	Amino oxidase-like domain
APAO	Polyamine oxidases N^1-acetylpolyamino oxidase
APL	Acute promyelocytic leukaemia
APS	ammonium persulfate
Aq	aqueous
AR	Androgen nuclear receptor
ATP	Adenine triphosphate
ATRA	*trans* retinoic acid
BCA	Bovine carbonic anhydrase
BET	bromodamain ex-terminal
BLAST	Basic Local Alignment Search Tool
Boc	*tert*-butyloxycarbonyl
BODIPY	Boron-dipyrromethene
bp	DNA base pair
br	broad
BSA	Bovine serum albumin
C or Cys	cysteine
CC	Click chemistry
calcd.	calculated
CML	Myelomonocytic leukaemia

CoREST	1.1.1. C-terminal domain of repressor element-1 silencing transcription factor.
CpG	Cytosine-phosphate-guanine
δ	Chemical shift in parts per millions
d	Doublet (NMR)
dd	Double deionised (water), NMR double doublet
D or Asp	Aspartic acid
DCM	Dichloromethane
DHT	5α–Androstan-17β-ol-3-one
DIC	*N*,*N*'-Diisopropylcarbodiimide
DIPEA	*N*,*N*-Diisopropylethylamine
DMAP	*N*,*N*-4-Dimethylaminopyridine
DMF	Dimethylformamide
DMSO	Dimethyl sulfoxide
DNA	Deoxyribonucleic acid
DNMT	DNA methyltransferase
DPPA	Diphenylphosphoryl azide
DTT	Dithiothreitol
E or Glu	glutamic acid
ECL	Enhanced chemiluminescence
EDCI	1-ethyl-3-(3-dimethylaminopropyl) carbodiimide
EDTA	Ethylenediaminetetraacetic acid
ELISA	Enzyme-linked immunoassorbent assay
EMT	Epithelial-to-mesenchymal transition
ERα	Estrogen nuclear receptor
ESI	Electron spray ionisation
Et	Ethyl
EtOAc	Ethyl acetate
equiv.	Equivalents
F or Phe	Phenylalanine
FAB	French-American-British
FAD	Flavin adenine dinucleotide

FBS	Foetal Bovine Serum
FCS	Foetal Calf Serum
FDA	Food and Drug administration
FITC	Fluorescein isothiocyanate
FLT-3	Fms-like tyrosine kinase 3
Fmoc	9-fluorenylmethyloxycarbonyl
FSC	Forward scatter
G or Gly	Glycine
GAPDH	Glyceraldehyde-3-Phosphate Dehydrogenase
GATA	Erythroid transcription factor
h	Hours
H or His	Histidine
H3K4	Histone 3 lysine 4
H3K9	Histone 3 lysine 9
H3K4me1	Histone 3 lysine 4 mono-methylated
H3K4me2	Histone 3 lysine 4 di-methylated
H3S9	Histone 3 serine 9
HAT	Histone acetyltransferase
HDAC	Histone deacetylase
HDACi	HDAC inhibitors
HEK	Human Embryonic Kidney 293 (cell line)
HMT	Histone methyltransferase
HOBt	Hydroxybenzotriazole
HOTAIR	HOX antisense intergenic lncRNA
HPLC	High-performance liquid chromatography
HRMS	High-resolution mass spectrometry
HRP	Horseradish peroxidase
HSC	Hematopoietic stem cells
HSV	Herpes simplex
HTRF	Homogenous time-resolved fluorescence
Hz	Hertz
I or Ile	Isoleucine

IC_{50}	Half maximal inhibitory concentration
IPTG	Isopropyl-β-D-thiogalactoside
ITD	Juxtamembrane region
K or Lys	Lysine
KDM	Lysine demethylase family
K_i	Inhibition constant
K_m	Michaelis constant
L or Leu	Leucine
LB	Lysogeny broth
LNCaP	Lymph node carcinoma of prostate
LncRNA	Long non-coding RNA
LSD1	Lysine specific demthylase 1
LSD2	Lysine specific demethylase 2
m	Multiplet
mA	Milliampere
µM	Micromolar
m^5C	5-methylcytosine
M or met	Methionine
MAO	Mono amino oxidase
MAOIs	MAO inhibitors
mM	Millimolar
MM	Multiple myeloma
min	Minute
miRNA	Micro-RNA
mp	Melting point
mRNA	Messenger RNA
MSD	Myelodisplastic syndrome
MTA	Metastasis associated protein
MTS	[3-(4,5-dimethylthiazol-2-yl)-5-(3-carboxymethoxyphenyl)-2-(4-sulfophenyl)-2H-tetrazolium, inner salt
N or Asn	Asparagine
nM	Nanomolar

NMR	Nuclear magnetic resonance
NuRD or Mi-2	Nuclear remodeling deacetylase complex
ns	Non significant
nt	Non tested
1.2. **NuRD or Mi-2**	Nuclear remodeling deacetylase complex
P or Pro	Proline
PBS	Phosphate buffer saline
PDB	Protein Data Bank
PE	Phycoerythrin
PEG	Polyethylen glycol
PFU	Plaque forming unit
pI	Isoeletric point
ppm	Parts per millions
PSA	Prostate specific antigen
PSSC	Proteins structure similarities search clustering
PTMs	Post translational modifications
PTEN	Phosphatase and tensin homolog
PVDF	Polyvinylidene difluoride
PyBOP	Benzotriazol-1-yl-oxytripyrrolidinophosphonium hexafluorophosphate
Q or Gln	Glutamine
R or Arg	Arginine
R_f	Retention factor
RFU	Relative fluorescence unit
RLU	Relative luminescence unit
RNA	Ribonucleic acid
ROS	Reactive oxygen specie
RP	Reversed phase
rpm	Revolutions per minute
RPMI	Roswell Park Memorial Institute medium
rt	Room temperature
s	Singlet

S or Ser	Serine
SAHA	Suberoylanilide hydroxamic acid
SAR	structure active relationship
SCLC	Small cell lung cancers
SDS	Sodium dodecyl sulfate
SEM	Standard error of the mean
SET	Single electron transfer
SMO	Spermine oxidase
SPPS	Solid phase peptide synthesis
SSC	Side scatter
t	triplet
T or Thr	threonine
TAL1	T-cell acute lymphocytic leukaemia protein 1
TAMRA	tetramethylrhodamine
TBS	Tris buffered saline
TBST	Tris buffered saline and Tween 20®
TBTA	tris-(benzyltriazolylmethyl) amine
TCEP	tris (2-carboxyethyl) phosphine
TCP	Tranylcypromine
TEMED	*N*,*N*,*N′*,*N′*-Tetramethylethylenediamine
TFA	Trifluoroacetic acid
THF	Tetrahydrofuran
THPTA	tris (3-hydroxypropyltriazolylmethyl) amine
TIPS	triisopropylsilane
TKD	point mutation tyrosine kinase
TLC	Thin layer chromatography
TLX	Nuclear receptor
ToF	Time of flight
V or Val	valine
W or Trp	tryptophan
X-gal	5-bromo-4-chloro-3- indolyl-β-D-galactoside
Y or Tyr	tyrosine

Chapter 1 - Introduction

1.1. Epigenetics

Natural selection has been for a long time considered the main evolutionary mechanism of adaptation. Accordingly, the variations in the DNA sequences that confer a fitness advantage for a specific environment would be copied and inherited while the less adequate are left out.[1] Whether there are instead mechanisms that translate adult experience into inherited phenotypes without altering the genotype, has been for long time an important question among the scientific community.[1–4] The potential of environmental exposure to orchestrate the transgenerational phenotypic adaptation without genetic selection was implied in the theories of the biologist J.B. Lamarck in the 18th century.[5] However, given the lack of evidence correlating the environment and alterations of gene expression, which could be inherited through the germ line, such theories have been rejected. On the other hand, the natural selection theories are unable to explain the adaptive features that an organism acquires during lifetime.[6] The cells constituting the human body, for example, are all derived from the same fertilised egg. In the path from embryo to fully developed organism, the initial cell undergoes several modifications that devote the embryo-derived cells to specific functions.[6,7] Another well-described example of environmentally driven adaptation, is the caste polyphenism in social insects. In honeybees' societies, from the same genotype, distinct caste phenotypes are generated, namely fertile queens, sterile female workers and male drones.[8] No genetic differences underlie the caste differentiation between queens and worker bees. In contrast, social environment and nutrition of the larvae are determinant as queens-to be larvae are only nourished with royal jelly.[8] If the honeybee colony loses its queen, sterile females develop ovaries[8] and such phenomenon evidentiate further that the caste differentiation is not decided only by genetic pre-determination.

In these examples, the diversity in phenotypes is achieved without changes in the DNA bases (i.e. the genetic code). The establishment of a functional identity, inherited through generations without altering the DNA sequence is defined **epigenetics** (ἐπί, *epi*: Greek for upon). Through epigenetic modifications, the environment drives cells to tag

the DNA and such acquired modifications can be transmitted to the offspring.[2] These inherited changes consist of chemical alterations to cytosine, histone tails and non-coding RNAs. Methylations, acetylations, ubiquitylation and sumoylation, are among an ever-growing list of histone tail modifications that modulate gene expression during developmental stages, tissue differentiation and diseases states.[9,10] Their presence or absence can alter the state of compaction of chromatin, regulating the way the genes are expressed. These tags have been termed **epigenetic marks**, as they do not modify the primary DNA sequence like base mutations do, while acting upon them.[5]

The salient roles of epigenetics have been described in all aspects of biology and epigenetic dysregulations have been associated with all major human diseases[11] such as cancers, Alzheimer, diabetes and viral infections.[12–14] Mutations in genes encoding for crucial epigenetic regulators have been found in several solid cancers and blood malignancies as for example the gene encoding for the histone acetyltransferase CREBBP and EP300,[15] or the DNA methyltransferase DNMT3A.[16] Furthermore, biological studies have revealed the presence in neoplastic tissues of unusual areas of chromatin, termed epigenetic lesions.[6,17–19] One example is the translocation of *MLL* oncoprotein in the human mixed-lineage leukaemia (MLL), where genes bound to *MLL* display an aberrant distribution of methylation marks on histone 3 (H3).[20,21]

Unlike genetic mutations, epigenetic modifications are reversible and “resetting” the abnormal *epi*genome to the normal state represents a revolutionary new strategy for therapy.[11] High-risk myelodysplasia patients are already receiving benefits from *epi*-drugs with the demethylating agent azacitidine (Vidaza®).[22]

Given the growing scientific evidence for the roles of epigenetic dysfunctions in the onset of diseases together with the tangible advantages of employing epigenetic therapeutics, current research is focusing on whether epigenetic modulators can be targeted for novel pharmacological approaches.

1.2. Chromatin

Chromatin remodeling is of foremost importance in the epigenetic regulation of gene expression. It defines the state in which eukaryotic DNA is packaged with histone proteins to form DNA-histone complexes within cells.[23] The basic unit of chromatin is the nucleosome (Figure 1.1), composed of 147 base pairs (bp) of DNA packed around two copies of four core histone proteins: H2A, H2B, H3 and H4, and a linker histone H1. The latter allows the compaction of chromatin single units into higher-order structures.[24] The core histones are globularly packaged, while their N-terminal tails are unshaped and protrude from the globular region. This feature makes them accessible to histone modifying enzymes.[23]

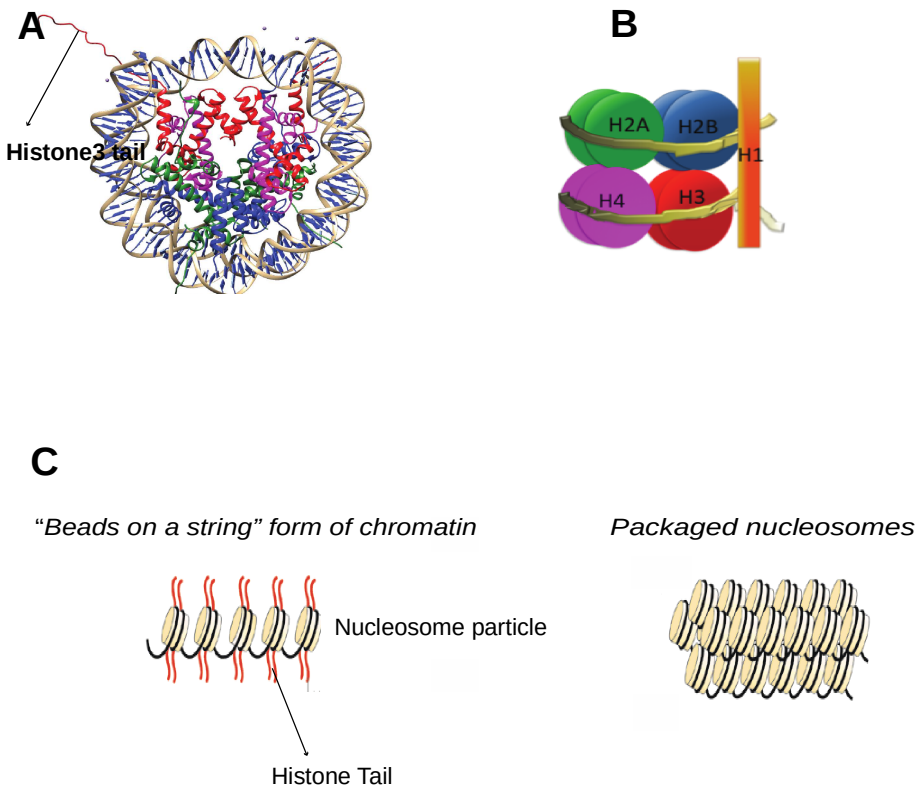

Figure 1.1: Chromatin and histone structure.

(A) High resolution structure of the nucleosome core particle; DNA strand is beige and bases are shown in blue. H3 dimer is shown in red, H4 in magenta, H2A in green and H2B in blue. **(B)** Nucleosome core particle and histones, plus histone linker (H1). **(C)** Beads on string representation (left) and packaged nucleosome representation (right). The nucleosome particles are shown as yellow cylinders. The black strands represent the DNA and the red lines the N-terminal histone tails.

Chromatin in non-dividing cells is classified in two different functional states: heterochromatin, transcriptionally silent and euchromatin, transcriptionally active.[25] Euchromatin, representing 4% of the genome, is characterised by the presence of active and inactive genes, which are accessible to the transcriptional machinery.[26] Meanwhile in heterochromatin, representing the 95% of the genome, the DNA is tightly asSTDbled in a conformation that is inaccessible to the transcription factors. Heterochromatin mainly consists of repetitive non-coding sequences and repressed genes that contribute to the maintenance of chromosomal stability by preventing mutations or translocations of the DNA bases.[27]

The histone tails, protruding from the nucleosome, undergo several chemical modifications leading to chromatin remodeling, altered gene expression and ultimately to phenotypic changes. Such modifications are **DNA methylation** and **histone post-translational modifications**.[14]

1.3. Epigenetic modifications: DNA methylation and histone post-translational modifications

DNA methyltransferases (DNMTs) are a class of enzymes that promote the cytosine methylation at the 5' position of the cytosine ring within cytosine-phosphate-guanine (CpG) dinucleotide and this modification leads to 5-methylcytosine (m^5C).[18] DNMTs are a well characterised class of epigenetic modifiers and are involved in the regulation of embryonic development, chromatin structure and chromosome stability. Hence, aberrant DNA methylation patterns correlate with a huge variety of diseases.[28,29] The mammalian DNA methylations are orchestrated by three classes of DNMTs: DNMT1, DNMT2 and DNMT3. DNMT1 is the most abundant class and acts as a "maintenance methyltransferase", specific for hemi-methylated CpGs: it copies DNA methylation patterns to a newly synthesised DNA strand, promoting the inheritance of the DNA methylation patterns.[30–33] DNMT2 class is devoted mostly to the methylation of transfer RNA; however, its functions have not yet been understood fully.[34] DNMT3A and DNMT3B act as *de novo* methyltransferases, targeting unmethylated CpGs and initiate the methylation process.[35]

In euchromatin, most housekeeping genes and the ones that need regulation are frequently unmethylated, remaining accessible to transcription factors that bind to their gene promoter and initiate the transcriptional process.[31,36] Conversely, the non-coding regions are enriched in methylated DNA and associated with transcriptional silencing and heterochromatin formation.[37–39] As both hypomethylation and hypermethylation states of CpG islands have been described in cancers, DNMT inhibitors (DNMTi) are currently evaluated as therapeutic agents.[40] DNMTi can be classified into two groups: nucleoside and non-nucleoside inhibitors. Nucleoside inhibitors consist of modified cytosine-like molecules that are incorporated into the newly synthesised DNA strand, impeding the methylation by DNMTs.[29]

The Food and Drug Administration (FDA) has approved two nucleosides DNMTi for the therapy of myelodisplastic syndrome (MSD) and chronic myelomonocytic leukaemia (CML). These are 5-azacytidine and 5-aza-2'-deoxycytidine (**1.1** and **1.2,** Figure 1.2).[29]

Although having pharmacokinetic liabilities, the molecules are effective at low doses and are generally well tolerated by MSD and CML patients.[29]

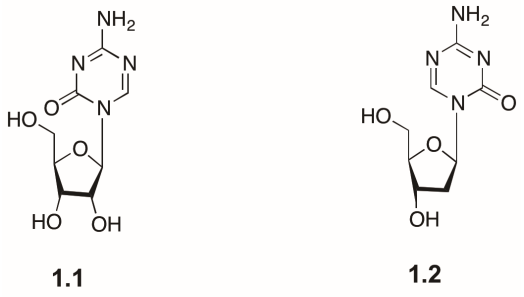

Figure 1.2: Nucleoside based DNMTi.
1.1 5-azacytidine; **1.25**-aza-2' deoxycytidine.

Non-nucleoside agents are investigated to overcome the possible side effects associated with the incorporation of external nucleotides into the DNA, such as the potential to induce mutations.[29,41] These agents inhibit the enzymatic activity by binding to the DNMT's catalytic site (**1.3** and **1.4**, Figure 1.3).[29]

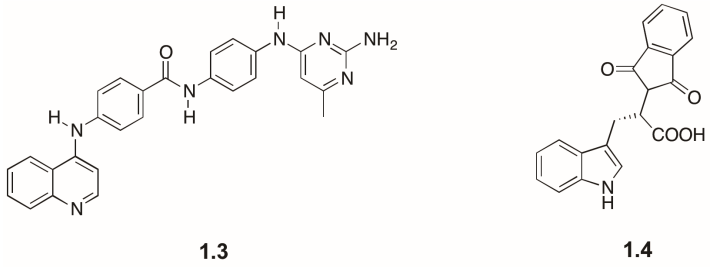

Figure 1.3: Non-nucleoside based DNMTi.
1.3 SGI-1027, a quinolone based compound; **1.4 RG108**, a tryptamine based compound.

The DNA methylation strikingly correlates with histone modifications and their cooperation tightly regulates the genome by promoting chromatin remodeling.[14,31] Three categories of proteins promote the histone N-terminal tail modifications and based on their functions, these are termed as "writers", "erasers" and "readers" (Figure 1.4).[42,43]

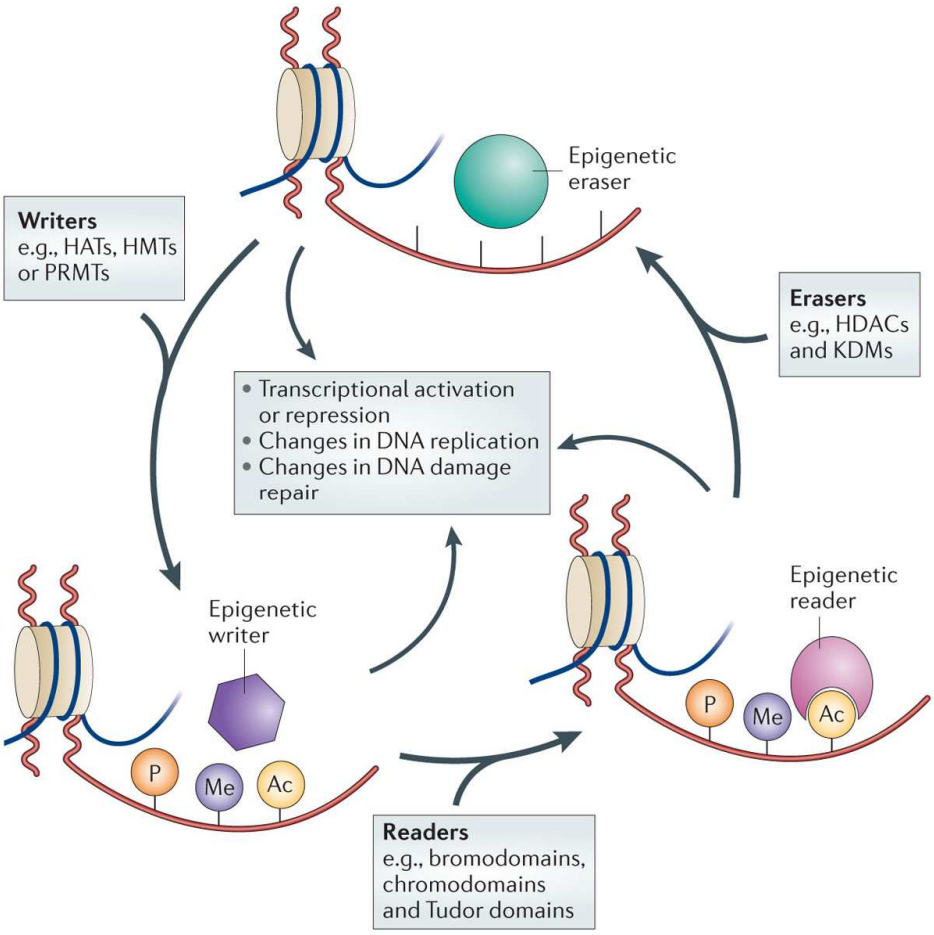

Figure 1.4: Cross talk between epigenetic regulators: writers, erasers and readers.

The writers, like histone acetyltransferases (HATs), histone methyltransferases (HMTs) and arginine methyltransferases, promote the addition of epigenetic marks onto histone tails. The erasers such as histone deacetylases (HDAC) and lysine demethylases (KDMs) families (LSDs and JmjC) remove the epigenetic marks from the histone tails. Readers of the epigenetic marks, like bromodomains and chromodomains, have specialised protein domains that recognise the epigenetic modifications. All together these epigenetic regulators contribute to DNA-dependent processes such as chromatin remodeling, gene transcription and ultimately phenotypic changes. Moreover these actively participate in DNA replication and DNA repair.

Adapted from Falkenberg *et al.*[43]

The **"writers"** lay down epigenetic marks on lysine (Lys or K) and arginine (Arg or R) residues of histone substrates.[43] The histone acetyltransferases (HATs) for example, transfer acetyl groups to lysines residues of H2A and H2B, H3 and H4.[44] Being positively charged, lysine side chains of histones keep chromatin compaction by binding the histone core proteins to the negatively charged chains of DNA. By masking such positive charge, acetylation via HATs elicit euchromatin formation and the access of the transcriptional machinery to DNA gene promoters.[39,44] HATs also promote the

acetylation of non-histone proteins such as p53.[44] The histone methyltransferases (HMTs) are responsible instead for the addition of methyl groups to histones' lysine and arginine residues using *S*-adenosylmethionine as a methyl group donor.[45] As opposite to acetylation, an epigenetic mark exclusively associated with euchromatin and therefore, transcriptional activity, histone methylation conveys either an activating or a repressive mark to genes. The HMTs can add up to three methyl groups on H3 and H4 lysine residues (H3K4, H3K9, H3K27, H3K36 and H4K20). Both the methylation position and the degree of methylation (mono, di or tri- methylation) determine the consequences of such epigenetic modification leading to euchromatin or heterochromatin formation.[42,46] Transcriptionally active regions possess enriched H3K4, H3K36 and H3K79 mono-methyllysine residues, whereas inactive regions display H3K9 H3K29 and H4K27 mono, di-methylation marks.[47,48] Tri-methyl marks at K9 and K27 of H3 are associated with heterochromatin formation and gene silencing whereas H3K9 and H3K27 mono-methylation marks are linked with gene activation. Thus, even at the same lysine residue, different degrees of methylation promote divergent effects.[47,48] Unlike to HATs and HMTs, the epigenetic **"erasers"** remove chemical modifications from histone substrates. The histone deacetylases classes (HDACs) remove the acetyl marks from lysine residues of H3 and by re-establishing the presence of the positive charge on the Lys residues, favour the histone protein binding to the DNA chains and heterochromatin formation (Figure 1.5).[18,43]

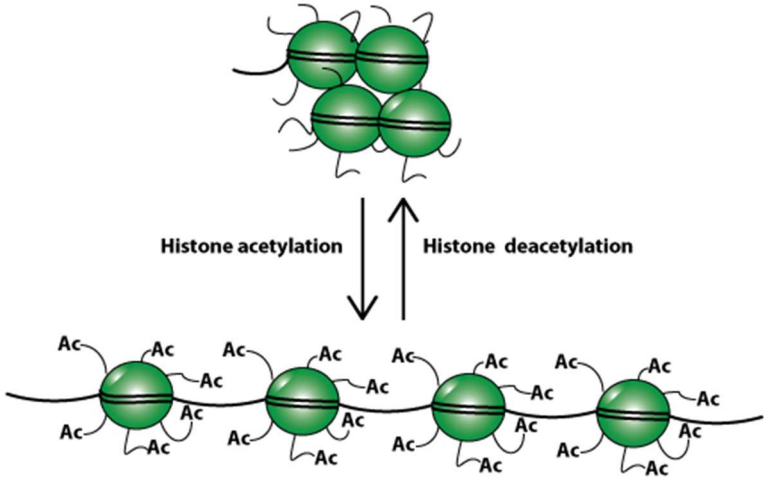

Figure 1.5: Transcriptional consequences of acetylation and deacetylation on histone tails.
Acetylation decreases the affinity of histones for DNA by masking the positive charge on the lysine residues. Deacetylation promotes the removal of acetyl group re-establishing the histone-DNA affinity and thus transcriptional repression.

There are 18 known HDACs, classified into five subclasses based on the activity and phylogenesis (Table 1.1).

Table 1.1: Classes of HDACs.

Class	Enzymes	Zn^{2+}	Localization	Expression
I	HDAC 1,2,3,8	Yes	Nucleus	Ubiquitous
IIa	HDAC 4,5,7,9	Yes	Nucleus and Cytoplasm	Tissue specific
IIb	HDAC 6 and 10	Yes	Cytoplasm	Tissue specific
III	Sirtuins 1-7	No	Variable	Variable
IV	HDAC 11	Yes	Nucleus and Cytoplasm	Ubiquitous

Classes I and II reveal a high enzymatic preference towards histone substrates and are characterised by the presence of a HDAC-Zinc binding domain.[43] The activity of these classes has been successfully inhibited with the use of chelating agents such as hydroxamic acid derivatives.[49] The Sirtuin family of HDACs constitutes class III and several works indicate their importance in human cell development and disease.[49] Seven Sirtuins have been described so far and among them, the SIRT1 group regulates acetylation levels in both histone (H4K16 and H3K9) and non-histone proteins like

p53.[43,46,49] HDAC 11 constitutes class IV and members of this group have been localised in different tissues such as brain, kidney and testis but their activity is still poorly characterised.[49]

Although associated mostly with transcriptional repression, recent studies showed that the HDACs activities can also promote transcriptional activation of specific genes.[50] HDACs are often found as stable subunits of transcriptional repressor complexes, as for example the NuRD complex.[51] Abnormal HDACs activity and expression have been observed in cancer tissues and scientific evidence has proven that the use of HDAC inhibitors (HDACi) is likely to have therapeutic effect in wide range of diseases, such as anti-neoplastic potential by inducing cell-cycle arrest, apoptosis and immunomodulatory effects.[43,49,51] However, it is still not clear how HDACi exert their anti-cancer activity. It has been proposed that they could bind to the HDACs catalytic pocket, chelating Zn^{2+} ion.[43,51]

HDACi have generally a defined pharmacophore, composed of three regions (Figure 1.6):

1. a **cap** region or surface recognition domain that is able to occlude the entrance of the HDAC catalytic pocket;
2. a **zinc binding domain**, which chelates the zinc ion;
3. a **linker** region that connects the cap region to the zinc binding domain;

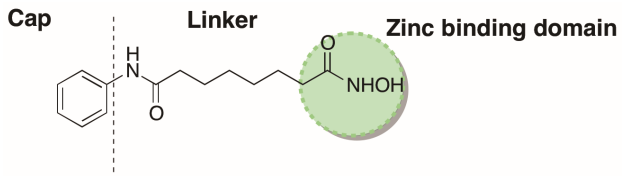

Figure 1.6: Domains of HDACi pharmacophore showed in Vorinostat®.

The most important classes of HDACi are:[43]

1. Hydroxamic acids, generally inhibiting several classes of HDAC;
2. Cyclic tetrapeptides and despipeptides;
3. Benzamides, generally targeting class I HDAC;
4. Epoxides;
5. Aliphatic acids;

The most important drugs belongings to the above-mentioned classes of HDACi are reported in Figure 1.7.

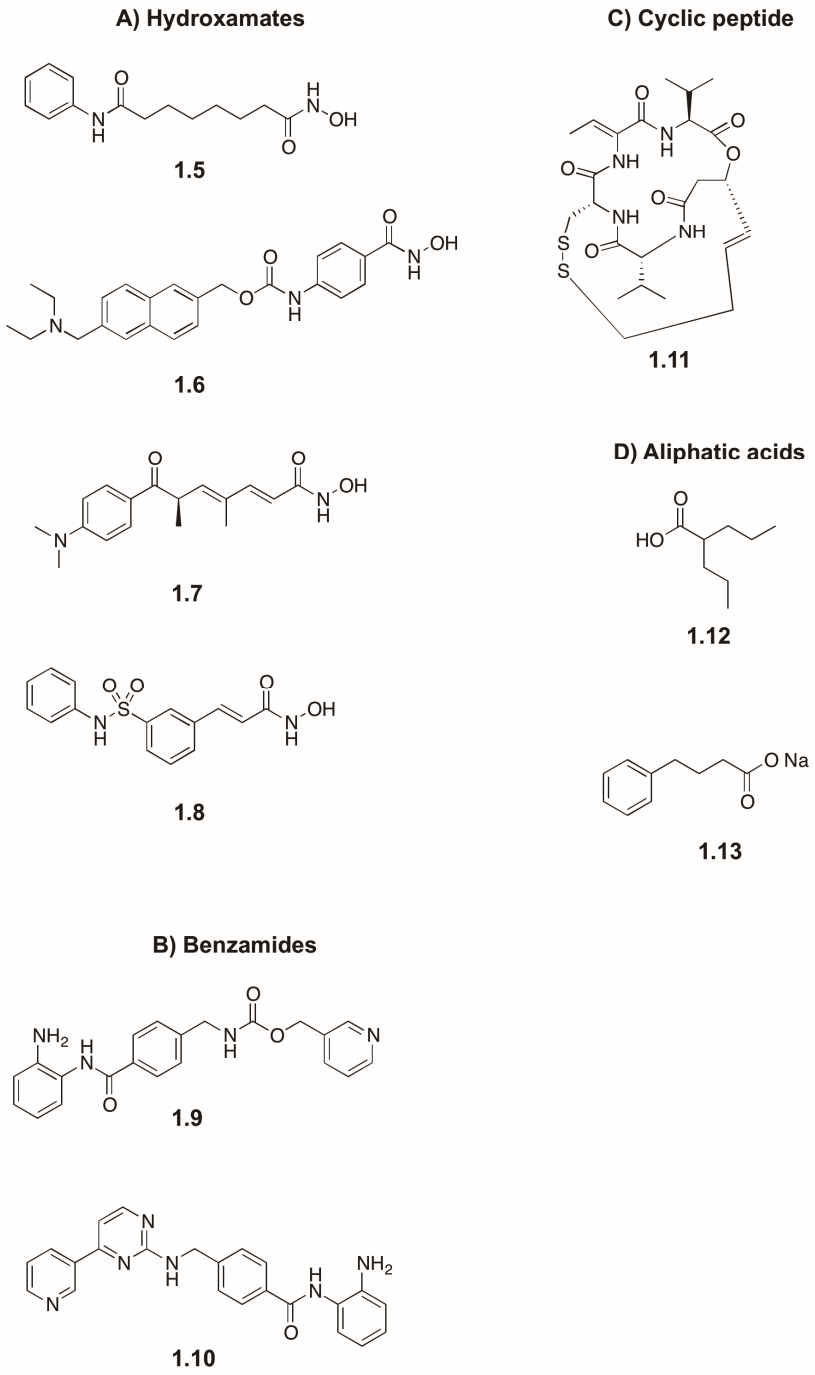

Figure 1.7: Important classes of HDACi and relative compounds and relative active concentrations.
(A) Hydroxamates: 1.5 SAHA (Vorinostat®, Zolinza®), pan-HDACi, µM; **1.6 Givinostat**, pan-HDACi, µM; **1.7 Trichostatin**, pan-HDACi, nM; **1.8 Belinostat**, pan-HDACi, µM. **(B) Benzamides: 1.8 Etinostat,** HDACi I, II, II, µM; **1.9 Mocetinostat,** HDACi class I, µM. **(C)** Cyclic peptide: **1.10 Depsipeptide** (FK228, Romidepsin): HDACi 1 and 2, nM. **(D) Aliphatic acids: 1.11 Valproic acid**, HDACi class I and II, mM; **1.11 Sodium Phenylbutyrate,** HDACi Class I and II, mM.

Lysine demethylases (KDMs) are another class of epigenetic erasers devoted to the removal of methyl groups from lysine residues of H3 and H4. Two classes of KDMs have been identified: **L**ysine **s**pecific **d**emethylase 1 and 2 (LSD1/2) and JumonjiC (JmjC) containing domain family of KDMs.

LSD1/LSD2 are the first discovered human demethylases and catalyse the post-translational demethylation of H3K4me1/me2 and H3K9me1/me2 side chains of histone protein and peptides (see below).[52]

The JmjC proteins are the most recently discovered family of KDMs, comprising approximately twenty human demethylases and classified in five subgroups (KDM2/7, KDM3, KDM4, KDM5 and KDM6).[53] The JmjC KDMs are able to promote the demethylation of mono-di and tri-methylated lysines using 2-oxoglutarate and dioxygen species as co-substrates.[53,54] The demethylation involves five steps and starts with the 2-oxoglutarate binding to the Fe(II) in the enzymatic pocket; the substrate binding promotes the destabilisation of the coordinate water molecule-Fe(II), eliciting the binding of a dioxygen species; subsequently, the dioxygen reacts with 2-oxoglutarate leading to succinate, release of carbon dioxide and formation of an oxoferryl species (Fe(IV)=O). The Fe(IV)=O hydroxylates the methyl-lysine that undergoes hemiaminal hydrolysis loosing the methyl-group (Scheme 1.1).[54]

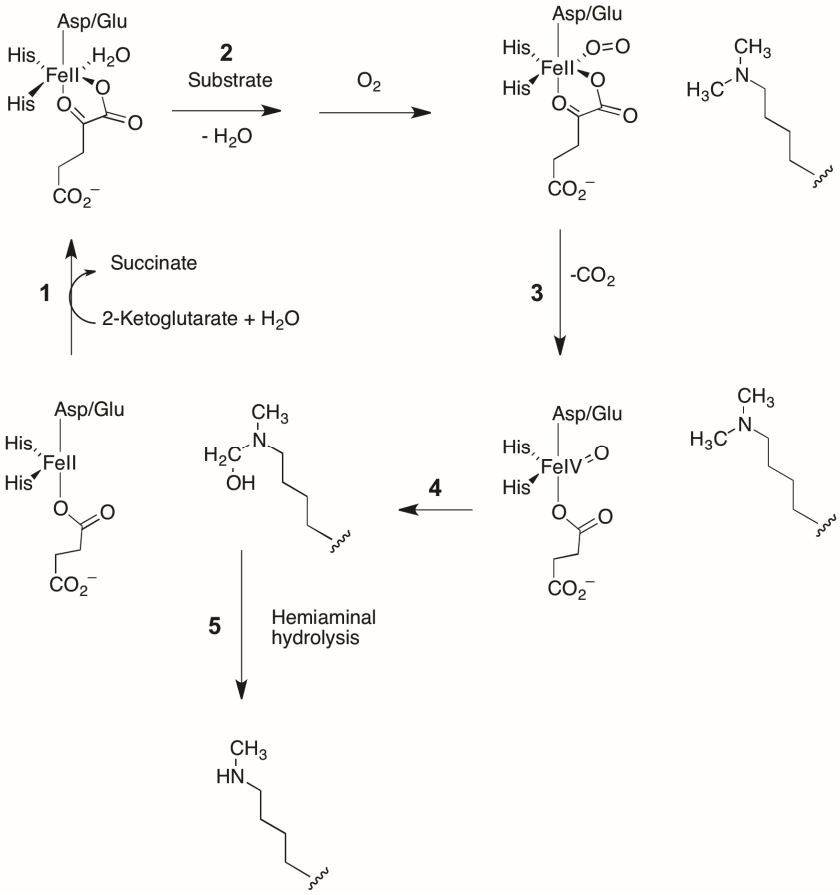

Scheme 1.1: JmjC mechanism of lysine demethylation.

Through this mechanism, the enzymes are able to demethylate lysine residues in all the three methylations states (mono, di and tri-methyllysine). Every sub-class of JmjC KDMs contains in the catalytic site specific amino acids that correlate with the preference for a specific methylation state of lysine.[54,55] The JmjC containing proteins are involved in neural development and their activities are associated with autism, midline defects and mental retardation.[53] Since their discovery, many JmjC inhibitors have been developed and the majority of them antagonise the catalytic activity by binding to the 2-oxoglutarate cofactor in a competitive fashion.[53,56] For example, several 8-hydroxyquinolines have been identified as low micromolar pan-JmjC KDMs inhibitors.[54,57] One derivative of such class, (**1.14**, Figure 1.8), was prepared and evaluated successfully in blocking the reactivation of Herpes simplex virus (HSV) in a mouse model.[58]

The most promising compound for the JmjC inhibition is GSK-J1 from GlaxoSmithKline (**1.15**, Figure 1.8). The compound displays remarkable selectivity for KDM6 class and inhibit the enzymatic activity at sub-micromolar concentrations (60 nM).[59] GSKJ-1 binds to 2-oxoglutarate cofactor and chelates the Fe(II) in the active JmjC catalytic pocket. GSKJ-1 is also effective in modulating the pro-inflammatory macrophagic response.[59]

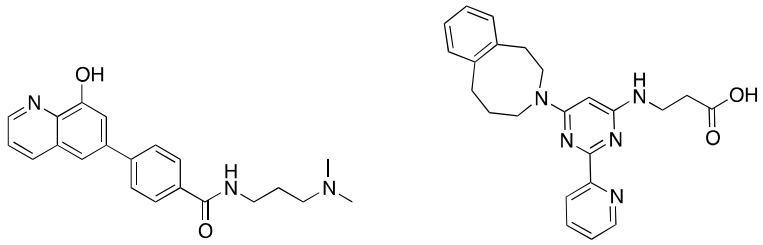

1.14 **1.15**

Figure 1.8: Molecular structure of potent JmjC inhibitors.
1.14 N-(3- (dimethylamino) propyl)-4-(8-hydroxyquinolin-6-yl) benzamide, was tested against HSV in mouse models; **1.15** GSK-J1 effective in inhibition JMJD3 enzymatic activity and reduces pro-inflammatory response.

The **"readers"** represent the last category of epigenetic effectors and actively recognise the chromatin associated histone modifications. Such epigenetic effectors bind directly to post-translational marks on histones via their specialised proteins domains.[60] For example, lysine side chain modifications are recognised by chromobarrel, chromodomain, tandem Tudor domain, whereas acetylation marks are recognised by bromodomains.[60] Proteins containing bromodomains have been identified to be involved in oncogenic rearrangement and control of salient elements for the regulation of the nuclear factor *k*B, a mediator of the inflammatory response pathway.[61] Recently, several small molecules targeting bromodomains and specifically, the bromodamain ex-terminal (BET), have been patented as anti-neoplastic agents.[62]

1.4. LSD1 biology and therapeutic potential

Since its discovery almost 11 years ago, Lysine specific demethylase 1 (LSD1) has intrigued the scientific community because of its multiple biological functions.

To date, research has only partially disentangled LSD1 activity in cell homeostasis in health and disease. As a result, the consequences of LSD1 inhibition are far from being fully understood. The overall information gathered suggests that it tightly regulates chromatin remodeling processes, cell development, cell differentiation, cancer proliferation and metastasis.[55,63–70] On that account, molecules targeting LSD1 have been widely researched for pharmacological interventions and currently, four clinical trials are investigating LSD1 inhibitors for leukaemia and small cell lung cancer.[56,71]

LSD1 has salient roles in cell development and cell differentiation programs: its knockdown or pharmacological inhibition results in impaired development of embryos[72] and precludes the correct differentiation of hematopoietic,[73,74] pituitary,[75] osteogenic[76] and neuronal stem cells.[77–79] Yet LSD1 overexpression correlates with poor outcome of cancers and LSD1 suppression effectively arrests cancer cell proliferation.[80–83] LSD1 is among the most frequent proteins found in human primary acute myeloid leukaemia tissues and an ever-growing body of evidence from pre-clinical and clinical studies, is designing LSD1 as a suitable target in blood-related malignancies.[84–86] High levels of LSD1 are also associated with the invasive behaviour of solid tumours such as colorectal,[87–89] bladder,[90] prostate[81,91] and breast cancers.[92] LSD1 overexpression in prostate carcinomas predicts aggressive biology and correlates with an increased risk of relapses after prostatectomy.[93] Accordingly, treatments with anti-LSD1 agents decrease cell growth of androgen dependent and independent prostate carcinomas in *in vitro* and *in vivo* models.[93–95] In breast cancer biopsies, the presence of LSD1 is a prognostic marker of tumorigenesis and tumour aggressiveness.[92,96–98] In addition, its abnormal expression has been found in receptor negative (ER^-) breast cancers, characterised by a rapid growth, loss of cell differentiation capacity, metastatic potential and insensitivity to estrogen suppressors.[92] It is also reported that the pharmacological inhibition of LSD1 sensitises the breast cancer to HDACi treatments and to hormonal therapy in drug-resistant carcinomas cellular models.[85,99] Furthermore, LSD1 activity is associated with HSV infection and reactivation from latency, broadening the potential applications of LSD1 inhibitors as anti-viral agents.[65,100]

1.4.1. LSD1 structure and enzymatic catalysis on H3K4

LSD1 is a large protein (93 kDa), highly conserved among eukaryotes and belongs to the family of flavin adenine dinucleotide (FAD) -dependent amino oxidase enzyme.[52] It is characterised by three major protein domains:[52] an N-terminal **SWIRM domain** (Swi3p/Rsc8p/Moira, residues 172-270), an **amine oxidase-like domain** (**AOL,** residues 271-417) and a **Tower domain** (residues 428-533).[77,101] The SWIRM domain is important for binding chromatin and forms, together with the AOL domain, a large hydrophobic pocket containing FAD (Figure 1.9).[102] The AOL domain constitutes the catalytic site of the enzyme and reveals a high homology in amino acid sequence to other FAD-dependent enzymes, including mono- and polyamine oxidases.[102,103] The inner surface of the catalytic site is characterised by two different areas, defined by the presence of amino acid residues with different chemical natures. The entrance of the catalytic channel, accommodating the *N*-methyl-Lys of H3, shows a flat surface lined mainly with hydrophobic residues. The opposite side instead presents mostly acidic side chains and backbones of carbonyl oxygen atoms and therefore, it is more hydrophilic.[103,104]

The tower domain protrudes away from the AOL domain and serves as a platform to link LSD1 to its binding partners, such as co-repressor element silencing factor CoREST.[26] LSD1 is able by itself to remove methyl and dimethyl groups on H3K4 *in vitro,* whereas for nucleosomal demethylation it requires CoREST.[105] Through the SANT2 domain of CoREST, LSD1-CoREST binds the DNA and exerts its demethylase activity on chromatin. In addition to this function, CoREST potentiates the demethylase activity on targeted histones and diminishes LSD1 proteosomal inactivation.[77,106,107]

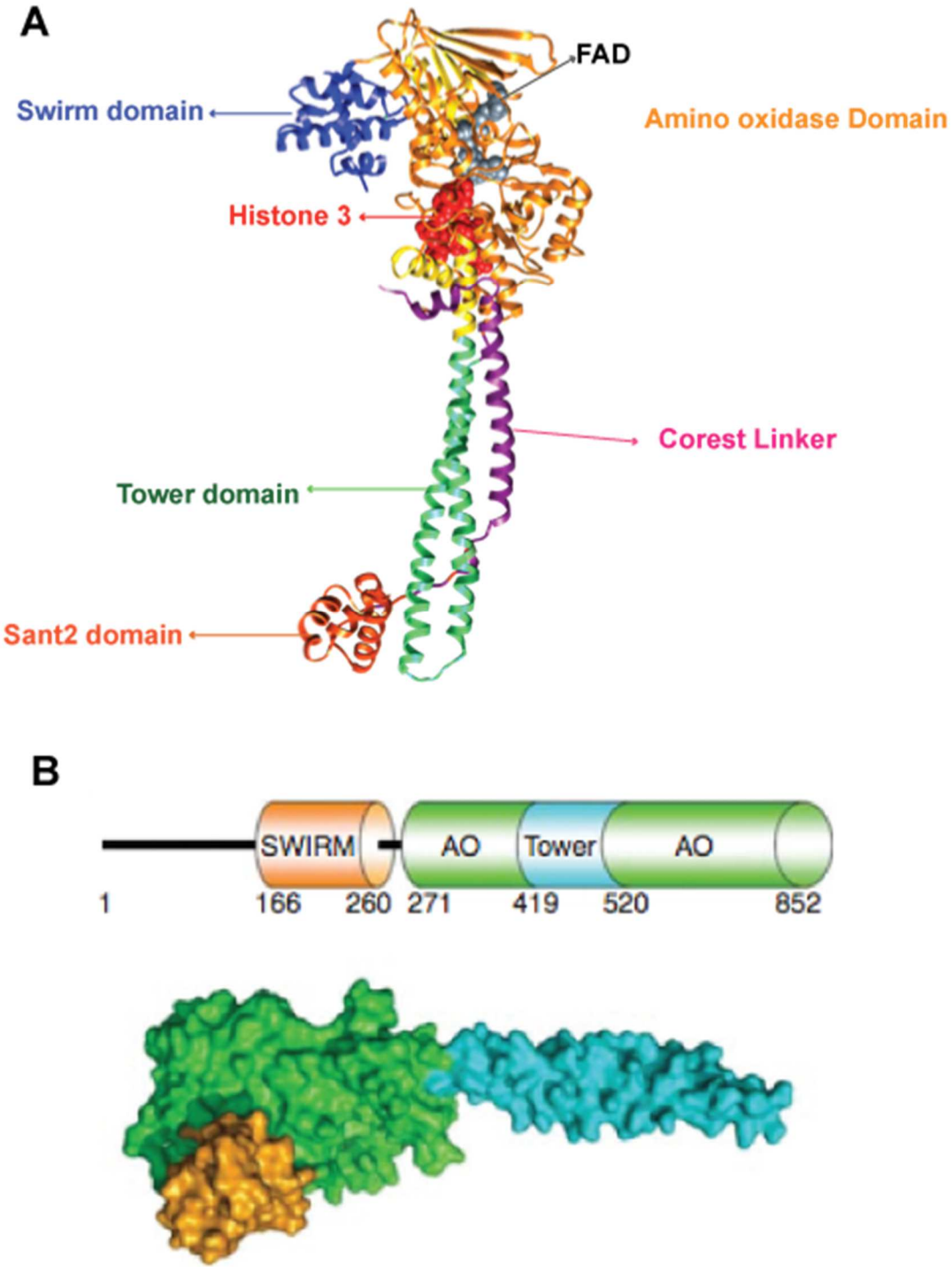

Figure 1.9: X-ray crystal structure of LSD1 with H3 and LSD1 domains.

(A) LSD1-CoREST X-ray structure, (PDB code: 2XUU); **(B)** Linear representation and surface structure of LSD1. Image **B** adapted from Lynch *et al.*[84]

The demethylation mechanism via LSD1 involves the reduction of FAD to FADH2 and oxidation of the methyl ε-amine of the methylated lysine, generating an iminium cation (Figure 1.10).[108,109] This is next hydrolysed to a carbinolamine that spontaneously degrades to formaldehyde and demethylated amine. The reaction results in a hydride transfer with the simultaneous reduction of FAD to FADH2 that is regenerated to its oxidised form by molecular oxygen, producing hydrogen peroxide (H_2O_2) as a side product. The requirement of protonated hydrogen for the electron transfer and imine intermediate formation, limits the LSD1 activity to mono and di-methylated lysine.[104,109,110]

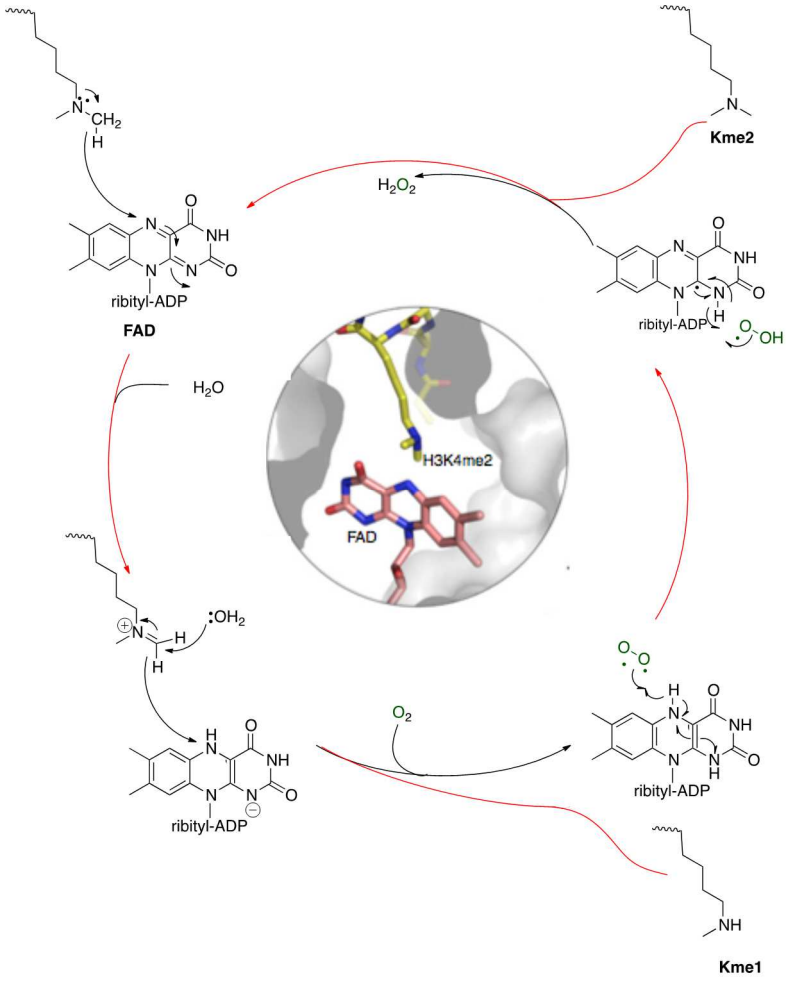

Figure 1.10: LSD1 demethylation mechanism on H3 substrate.

Although possessing high homology with other FAD-dependent enzymes, no catalytic cross-reactivity has been reported concerning LSD1, implying a high degree of specificity.[101] Furthermore, LSD1 does not show catalytic preferences for H3K4 mono or di-methyl-lysines, while the rates of demethylation are affected by the presence of

other PTMs along the H3.[104,108] For example, acetylation of H3K9 increases the LSD1 K_m by 6-fold, phosphorylation on H3S9 abolishes the demethylase activity *in vitro* and methylation at the H3K9 does not affect the catalysis rate.[104]

Beyond LSD1, a second isoform of lysine-specific demethylase belongs to this family of FAD-dependent KDMs and is termed **LSD2**. LSD2 (KDM2 of KDM1b or AOF1), is the only known mammalian homologue of LSD1.[70,111] Both proteins share a similar catalytic domain (around 31% homology) but differ at the N-terminal region. Like LSD1, LSD2 can only remove methyl groups on mono and di-methylated H3K4; differently from LSD1, it is found associated with coding region of the genome. Moreover, it does not require CoREST for its nucleosomal activity[70] and this could imply that LSD2 is involved in different transcriptional programs by associating with other coregulators.[98]

The hydrogen peroxide generated by the activity of the two flavoenzymes represents an important feature, as the reactive oxygen species are potentially dangerous for chromatin environment.[112] An intriguing hypothesis is that they might have a signalling role in cellular processes, retrieving other chromatin remodeling factors.[108,112,113]

1.4.2. Important LSD1 functions as a catalytic subunit in multi-component systems and its association with transcription factors

LSD1 is commonly found complexed with biomolecules or enzymes, taking part in multi-component systems that function coordinately as whole catalytic unit. Such protein complexes contain the essential elements for gene targeting and the simultaneous regulation of multiple epigenetic modifications. By influencing the substrate specificity, the localisation as well as the degree of activity of LSD1 within chromatin, these interactions confer to LSD1 catalysis on H3 diverse biological effects.[72,98]

As aforementioned, one of the critical binding partners for LSD1 nucleosomal demethylation is C-terminal domain of repressor element-1 silencing transcription factor (CoREST) and this is commonly found cooperating with LSD1 within multi-component systems.[106,110,114] CoREST consists of three major protein domains, which are the N-terminal domain ELM2, two SANT domains (SANT1 and SANT2) and a linker domain.[114] The region that encompasses ELM2 and SANT1 functions as a platform to link LSD1 to the HDAC family of deacetylases.[115] Hence CoREST asSTDbles deacetylases and demethylases enzymes, bridging together two epigenetic effectors to nucleosomal substrates. The LSD1-CoREST-HDAC complex operates as a double-blade razor eliminating first the acetyl groups from lysine residues via HDAC and then, the methyl groups from H3K4 via LSD1. The complex associates with several transcription factors and regulates important biological pathways.[97,98,116–121]

For example, it participates in hematopoietic differentiation by associating with B lymphocyte-induced maturation protein 1 (Blimp-1). Blimp-1 is a transcription factor with a pivotal role in embryo development and homeostasis of plasma cells. LSD1-HDAC-CoREST is recruited by Blimp-1 to silence the mature B-cell gene expression at the end of cell differentiation programs. In addition to Blimp-1, LSD1-CoREST-HDAC complex regulates erythropoiesis by associating with the transcription factor TAL1 (Figure 1.11).[119] Depending on the context, TAL1 acts as a transcriptional repressor or activator: while in normal cell physiology regulates the formation of B and T cells lineages, its aberrant activation is linked to T-cell lymphoblastic leukaemia onset and progression.[122] In erythroid stem cells progenitors, the transcriptional factor is engaged with LSD1 in maintaining cells in an undifferentiated state. When the cells became

differentiation-competent, LSD1 dissociates from TAL1 promoter and such event is accompanied by the activation of other PTMs, such as the phosphorylation of S173 and the recruitment of HMTs and HATs.[119,123] This translates in an increment of H3K4me2 and AcH3K9/K4 marks in mature cells.[123] The TAL1-LSD1 association is recovered at a later stage of cell-maturation and the activity of LSD1 on H3K4me1/me2 represses TAL1, contributing in arresting cell differentiation and proliferation programs.[119,122] Undoubtedly, eventual perturbations along the processes can result in abnormal cell growth or impaired cell differentiation that could lead to blood-related malignancies.

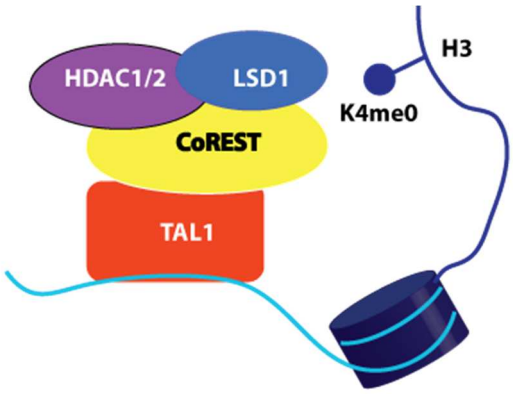

Figure 1.11: Association of LSD1-CoREST HDAC with TAL1.
TAL1 recruits LSD1 during different stages of erythropoiesis.

LSD1-CoREST-HDAC activity is involved in the regulation of the nervous system as demonstrated by its cooperation with nuclear receptor 2 (NR2E1-TLX, Figure 1.12).[79] TLX controls the metabolism and development of neuronal tissues[118,124] and LSD1, by associating with TLX, becomes a downstream target of the micro RNA miR-137: TLX in neuronal stem cells recruits LSD1 to the miR-137 genomic region to repress miR-137 primary precursor expression. Simultaneously, miR-137 antagonises LSD1 activity by removing it from its genomic *loci*, sustaining this way the miR-137 expression, which is associated with neuronal stem cells proliferation, neuronal and glial differentiation and migration.[125] In addition, co-immunoprecipitation of the TLX-LSD1 complex revealed that other proteins are likely to associate with the TLX-LSD1 as for example ZMYM2, GSE1 and ZMYM3.[118] Although the biological relevance of such proteins in neuronal maturation programs is unclear, it has been observed that ZMYM3 proteins also associates with Snail-1, which is another LSD1 binding partner and a master regulator

of the epithelial-to-mesenchymal transition (EMT).[98] Recently, Yokoyama and colleagues demonstrated that LSD1-CoREST-HDAC complex associates with TLX in retinoblastoma cells.[118] The complex was found responsible for the onset and the progression of the carcinoma by controlling the expression of genes linked to cell proliferation, as for example the tumour suppressor gene PTEN. As the retina is considered part of the central nervous system,[126] this work further evidentiate the importance of LSD1 for neuronal tissues homeostasis and pathogenesis.[118,127]

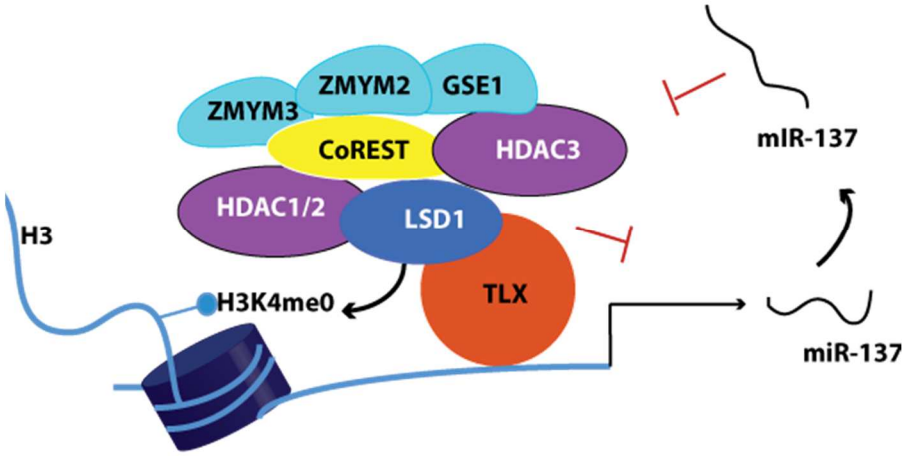

Figure 1.12: Association of LSD1-CoREST-HDAC with TLX.
The complex is recruited by TLX transcription factor and forms a negative feedback loop with microRNA in miR-137 in the control of neuronal differentiation.

LSD1 is found to take part in the NuRD (Mi-2) complex (Figure 1.13).[97] HDAC1, HDAC2, several histone-binding proteins, metastasis associated proteins MTA1, MTA2 and MTA3, methyl CpG binding domain protein and the chromodomain DNA-binding helicase CHD3 form the NuRD complex.[120] The MTA proteins display both ELM2 and SANT domains, sharing strikingly structural similarities with CoREST.[97] In a similar fashion as with CoREST, the LSD1 tower domain binds to the NuRD MTA (1-3) subunits. By exploiting the LSD1 demethylase activity on H3K4, NuRD amplifies its silencing activities on target genes promoters. The genes repressed by the LSD1-NurD complex are critically implicated in cell growth, survival and invasion.[97] One of the downregulated elements is TGFβ1, a key modulator of EMT in epithelial tumours.[97,128] By reducing the levels of TGFβ1, the LSD1-NuRD complex was shown to suppress breast cancer potential *in vivo*.[97] Notably, a subsequent study in HeLa cell extracts did

not identify LSD1 as a permanent subunit of NuRD, suggesting that such cooperation is potentially context-dependent.[129] Furthermore, the LSD1-NuRD complex was found to interact with KDM5B (JmjC KDMs). Within this complex, both the epigenetic erasers concertedly the demethylation on H3K4 and delete the chemokine CCL14 signalling pathway, which is linked to metastasis and angiogenesis.[130]

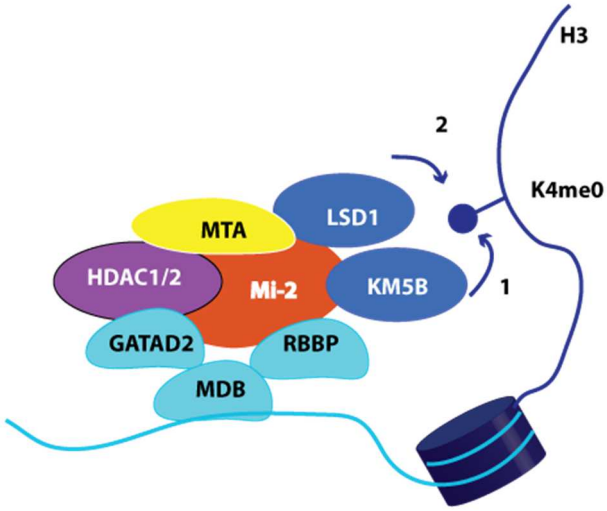

Figure 1.13: Association of LSD1 with NuRD complex.
LSD1 is recruited by the MTA subunit of the NuRD complex to enhance epigenetic silencing activities on target genes. In this context LSD1 suppresses EMT in breast cancer.

The C-terminal binding protein CtBP is heavily implicated in tumorigenesis and acts as repressor of mammalian genes by associating with several binding partners.[121,131–133] Many repressive functions of CtBP have been linked with LSD1-containing complexes.[121,134,135] The earliest and of foremost importance involves LSD1 as well as other PTMs as for example H3K9 methyltransferase and deacetylases; together the chromatin remodellers synchronise their activities for the repression of the E-cadherin gene, conferring to cells mesenchymal phenotype.[121]

Recently, it has been discovered that several SNAG-containing proteins are regulated by LSD1.[136,137] The SNAG domain consists of a pattern of conserved amino acids at the N-terminal, which reSTDbles H3.[117] This feature enables the SNAG-containing proteins to physically interact with LSD1 AOL domain. Among the SNAG-containing proteins, the zinc finger protein Snail-1 is the most studied for its salient roles in metastasis and cell migration roles in epithelial tumours by controlling the EMT.[117,137–141] By recruiting LSD1, Snail-1 reduces the level of mono-di-methylated H3K4 at its target genes,

promoting transcriptional repression (see Chapter 2). Hence LSD1 by associating with Snail-1, has a salient role in the control of the EMT.[117] Accordingly, it has been demonstrated that the inhibition of the LSD1-Snail-1 interaction reverts the status of silenced genes and re-establishes the epithelial phenotype in neuroblastoma and colon cancers cells without impairing cell proliferation.[117,142]

Long non-coding RNAs (lncRNAs) are an emergent class of LSD1 binding partners. LncRNAs are composed of non-coding genetic material and lack of a defined biological function.[143] The most studied lncRNA is the HOX antisense intergenic lncRNA (HOTAIR) and its overexpression in breast tumours is a marker of tumour aggressiveness.[143,144] It is characterised by two binding domains: one for the Polycomb repressive complexes 2 (PRC2) and one for LSD1 complexes.[27] PRC2 is a member of the PcG family proteins and has histone methyltransferase activity and primarily trimethylates histone H3K27 (an epigenetic mark associated with gene silencing). The binding of LSD1 complexes and PCR2 to the HOTAIR enables their coordinative activity in silencing tumour suppressor signalling pathways (Figure 1.14).[143]

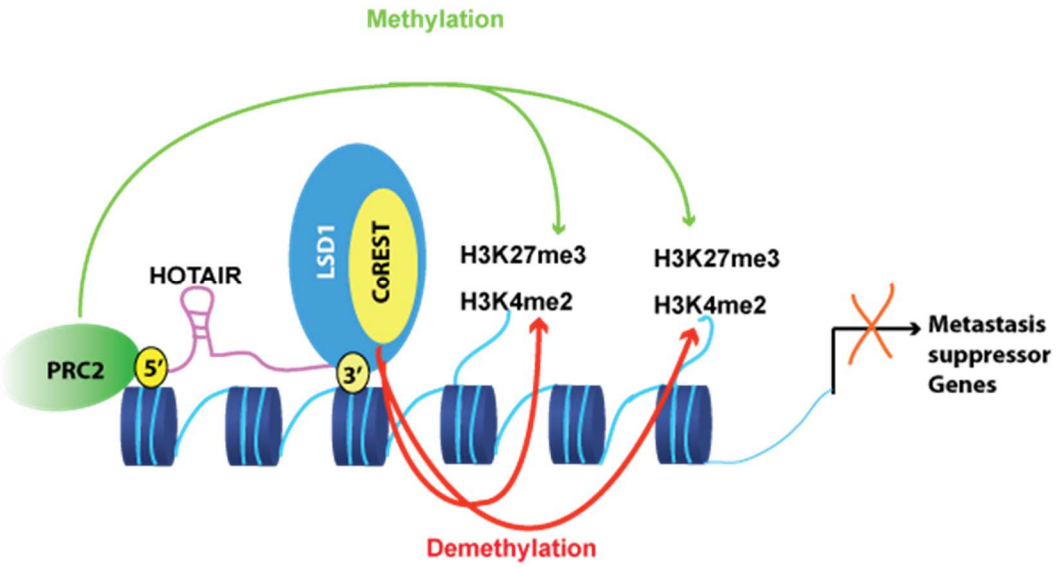

Figure 1.14: LSD1-CoREST association with lncRNA HOTAIR.

Unlike the LSD1 associations described so far, which correlate with transcriptional repression and gene silencing, LSD1 acts instead as a transcriptional activator in association with nuclear receptors (androgen and estrogen receptors, Figure 1.15).[145,146]

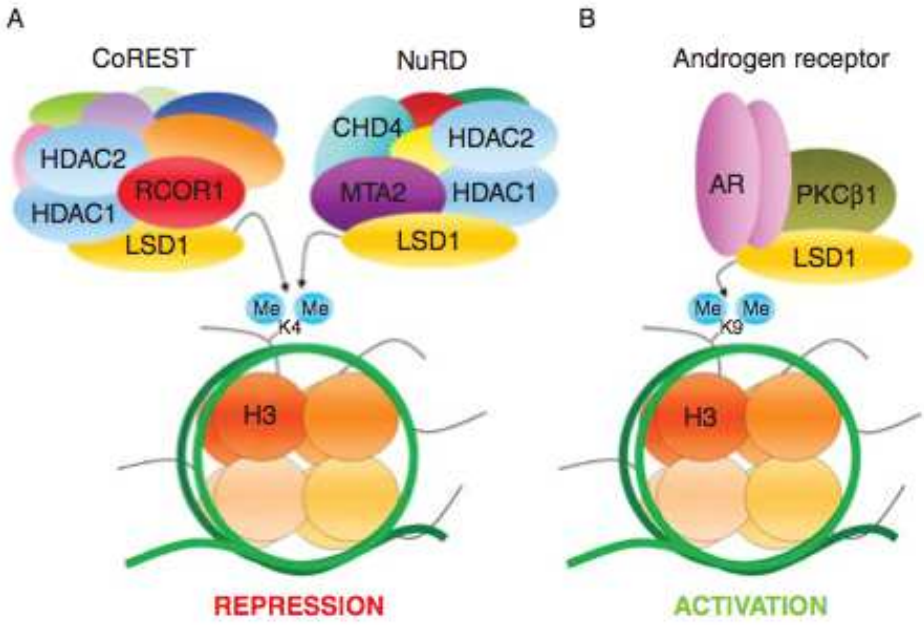

Figure 1.15: LSD1 in association with protein complexes and the repressive or activation effects on target genes when acting on H3K4me1/me2 or H3K9me1/me2.

By changing substrate specificity, the enzymatic activity of LSD1 can lead to transcriptional repression or activation. Adapted from Lynch *et al.*[84]

Nuclear receptors are transcription factors regulated by steroid hormones (estrogen and androgen) ligands.[147] The transcriptional activity of the nuclear receptor androgen receptor (AR) regulates the prostate functions by providing instructions for androgen hormones in both physiological and pathological conditions.[148] After hormonal binding, LSD1 forms a complex with the AR and translocates to the nucleus to co-localise at the androgen response elements promoters (AREs) (Figure 1.16). Through its catalytic activity on H3K9me1/me2, LSD1 promotes the transcriptional activation of targeted genes such as the prostate specific antigen (PSA).[93,149] Androgen regulated genes, such as PSA and *TMPRSS2:ERG* fusion gene, are expressed in hormone independent cancers, indicating that AR transcriptional activity has been reactivated despite castrate serum androgen levels.[81,150] These phenomena have been correlated to AR mutations or alternative splicing, increased intra-tumoural androgen synthesis, increased co-activator expression and activation of several kinases that may directly or indirectly sensitise AR to low levels of androgens. LSD1 pharmacological inhibition with pargyline or TCP in prostate cancer cells has shown a decrease of PSA and *Tmprss2* expression and

suppression of growth in hormone dependent and independent prostate cancer cell lines.[91,146,149–151] Additionally, it has been shown that LSD1 is *per se* able to induce AR-dependent transcription by regulating H3K9me1/me2 even in the absence of androgen.[91] Therefore, the LSD1-AR association constitutes a potential target for therapeutic effects in prostate cancers.

The reason why the association of LSD1 with AR induces changes in substrate specificity from H3K4 to H3K9 leading to gene activation instead of repression has not been fully understood. Metzger and colleagues proposed that the key event contributing to this switch is the association to LSD1-AR of kinase PKCβ1. Upon hormone binding, the kinase phosphorylates the H3T6 and such modification prevents the demethylation on H3K4.[152] On the other hand, high levels of androgen promote in post-castration models of prostate malignancies a negative feedback loop whereby AR recruits LSD1 at target promoters to mediate instead *AR* repression via H3K4me1-me2 demethylation.[81] Hence the dual roles of LSD1 in AR regulation, involving both transcriptional activities, mediated by demethylation of H3K9me1/me2 and transcriptional silencing, through H3K4me1/me2, still remains enigmatic.

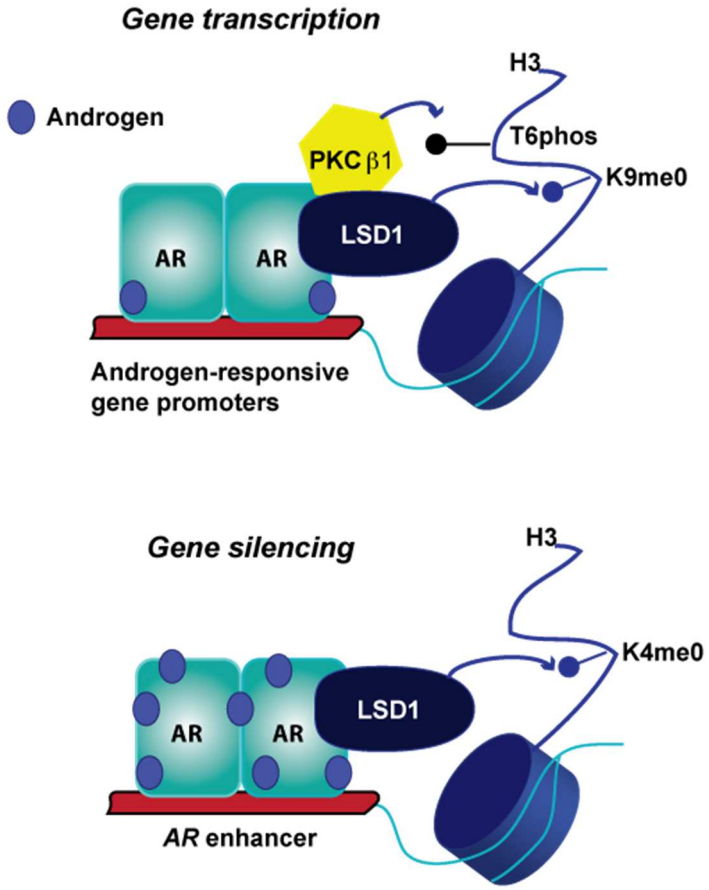

Figure 1.16: Effects of LSD1 activity in association with nuclear hormone receptor AR.
After hormonal stimuli, LSD1 demethylates H3K9me1 and H3K9me2, promoting gene transcription. Conversely, at high levels of circulating hormones, the AR recruits LSD1 to its promoter regions to repress transcription by demethylating H3K4me1/2.

Similarly to AR, the estrogen nuclear receptor ERα controls cellular processes in tissues targeted by estrogenic hormones and its dysregulation is implicated in the genesis and progression of tumours.[153] ERα is associated with LSD1 constitutively and in absence of estrogenic stimuli, LSD1 demethylates H3K4.[112] Upon hormonal induction, ERα recruits LSD1 to its target gene promoters to enable the transcription of signalling pathways regulated instead by H3K9 demethylation. In addition, also the ERα corepressor CAC1, the aberrant expression of which associates with resistance to paclitaxel, is found to interact with LSD1-ERα.[154] When CAC1 binds to LSD1-ERα, it decreases the occupancy of the complex to target genes *loci* and, by accumulating H3K9me1/2, decreases gene transcription (Figure 1.17).[154]

Noteworthily, the X-ray crystal structure of LSD1-CoREST bound to an H3 peptide, suggested that only the N-terminal residues 1-7 are capable to enter into the LSD1 enzymatic pocket, positioning the K4 in front of FAD for demethylation.[155] Therefore, according to this structural study, the demethylation on K9 is structurally incompatible and it is likely that nuclear hormone receptors AR and ERα are directly or indirectly involved in a transient structural modification to the LSD1 catalytic pocket that enables switching substrate specificity. In keeping with this, PELP1, a co-regulator of ERα with unknown activities, associates with LSD1-ERα and alters the demethylase substrate specificity from H3K4me2 to H3K9me2.[156] Moreover, a recent report from Cortez and coworkers implies that targeting LSD1-PELP1 partnership could be of therapeutic interest in breast cancer.[99] Similarly to PELP1 interaction, it has been revealed that the JmjC KDMs subfamily KDM4C cooperates with LSD1-AR complex, participating in the sequential removal of H3K9me3 residues and this might also contribute in changing substrate specificity.[157]

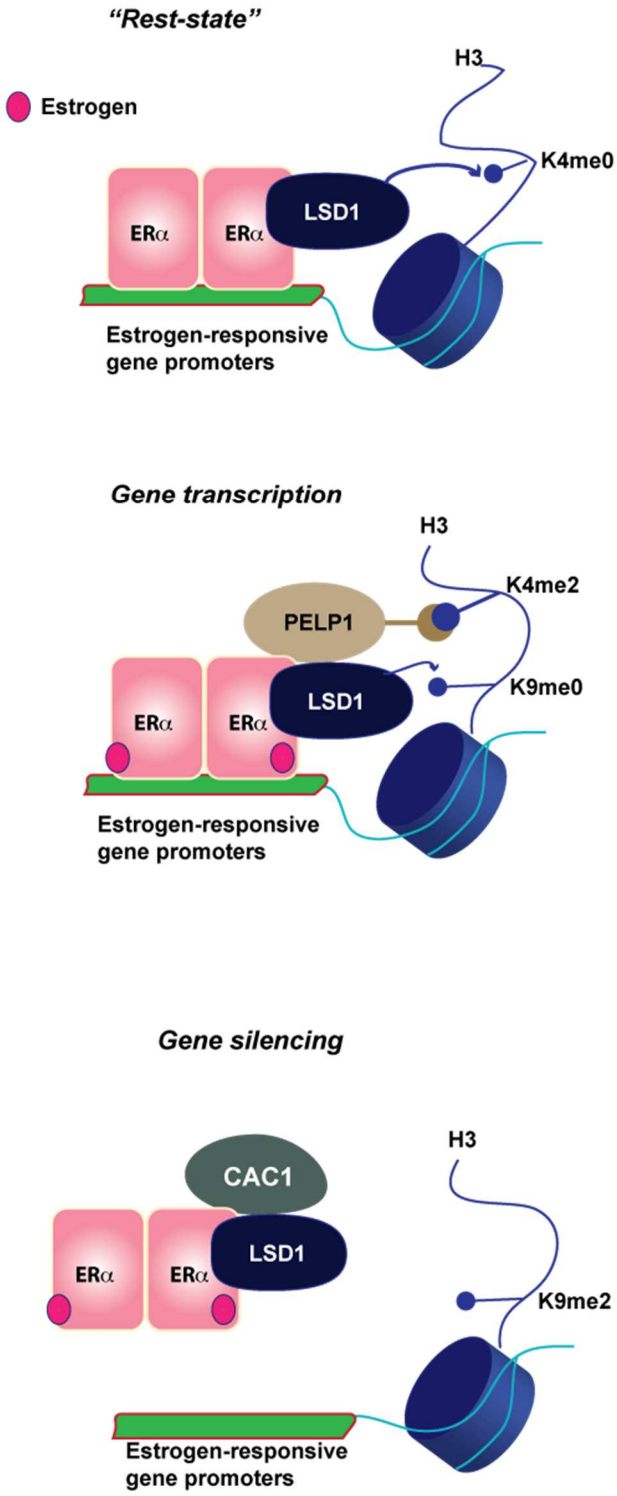

Figure 1.17: Effects of LSD1 activity in association with nuclear hormone receptor ERα.
LSD1 is constitutively associated with ERα. In the absence of estrogenic stimuli, the enzyme demethylates H3K4. After estrogenic stimulation, LSD1 initiates gene transcription following the removal of H3K9me1/2. When the protein CAC1 binds to LSD1-ERα, it prompts the removal of the complex from the target gene promoters silencing the LSD1-dependent activity by increasing the H3K9me1/2.

1.5. Reversible and irreversible inhibitors of LSD1

Given the multiple roles of LSD1 in pathobiology, several drug design efforts, including from our group, have focused on the development of LSD1 inhibitors.
These can be grouped into irreversible (covalent) and reversible inhibitors.

1.5.1. Irreversible inhibitors of LSD1

Initial attempts to target LSD1 were performed with known inhibitors of monoamine oxidases (MAO). LSD1 and MAO belong to the same FAD-dependent oxidase family and share a high level of sequence homology at their catalytic sites. Based on this information, initial studies of lead discovery were focused on the known monoamine oxidase inhibitors (MAOIs) and identified clorgyline and deprenyl as active molecules against LSD1.[158–160] Following the initial reports, irreversible MAOIs nialamide, clorgyline, deprenyl and pargyline were tested but failed to show inhibitory activity against LSD1. Simultaneously, phenelzine and tranylcypromine (TCP) were found to inhibit H3K4 demethylation of LSD1 at 200 µM and 100 nM concentrations respectively (Figure 1.18).[159]

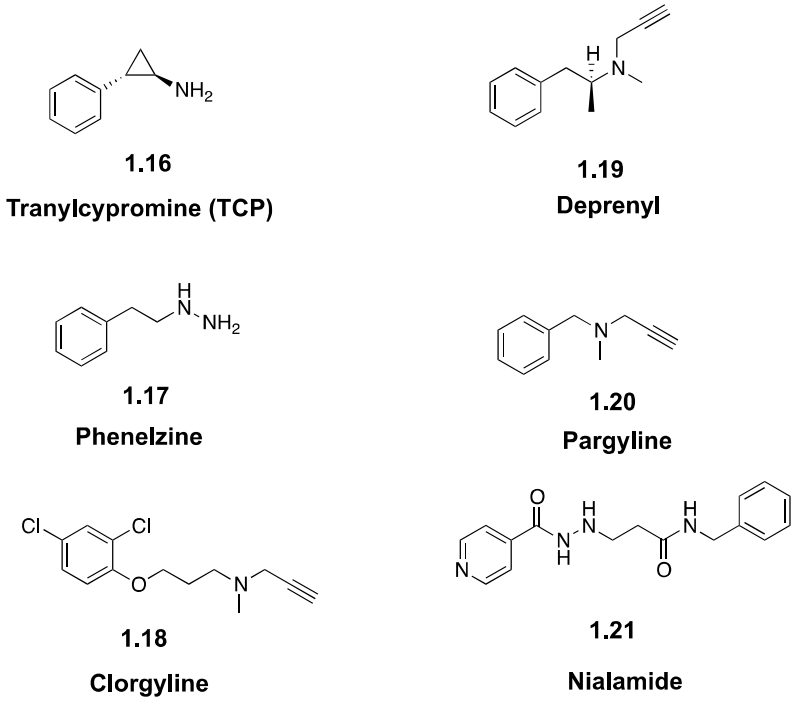

Figure 1.18: MAO inhibitors first tested against LSD1.

1.5.1.1. Mechanisms of irreversible inhibition

The first developed MAOIs covalently bind to the MAO enzymes or FAD, causing irreversible inhibition. Due to their role in the catabolism of dietary amines, the irreversible blockage of MAOIs might cause hypertensive problems (*cf.* cheese-effect*) if the diet is not controlled during their use.[161] The simplest example of irreversible inhibition is phenelzine, a member of hydrazine class of MAOIs. The hydrazine moiety was shown to form a covalent complex with FAD.[160]

TCP shows a more complicated irreversible binding that can occur by several different mechanistic pathways.[103,155,162]

Schmidt and coworkers initially proposed the C-C bond formation between TCP and FAD (Scheme 1.2, A), would occur through a single electron transfer (SET) to the C(4a) of the FAD.[162] Subsequent cleavage of one of the C-C bonds of the cyclopropyl ring would lead to the formation of a cinnamaldehyde adduct (b4, Scheme 1.2) through the formation of a benzylic radical. Alternatively, this could proceed through the radical intermediate attack on the flavin ring followed by ring opening and formation of an atropaldehyde adduct (c3, Scheme 1.2).[162]

* The *cheese effect* refers to a hypertensive crisis that the individual subject to MAOIs treatment experiments with the concomitant consumption of foods containing tyramine (i.e. cheese).[161]

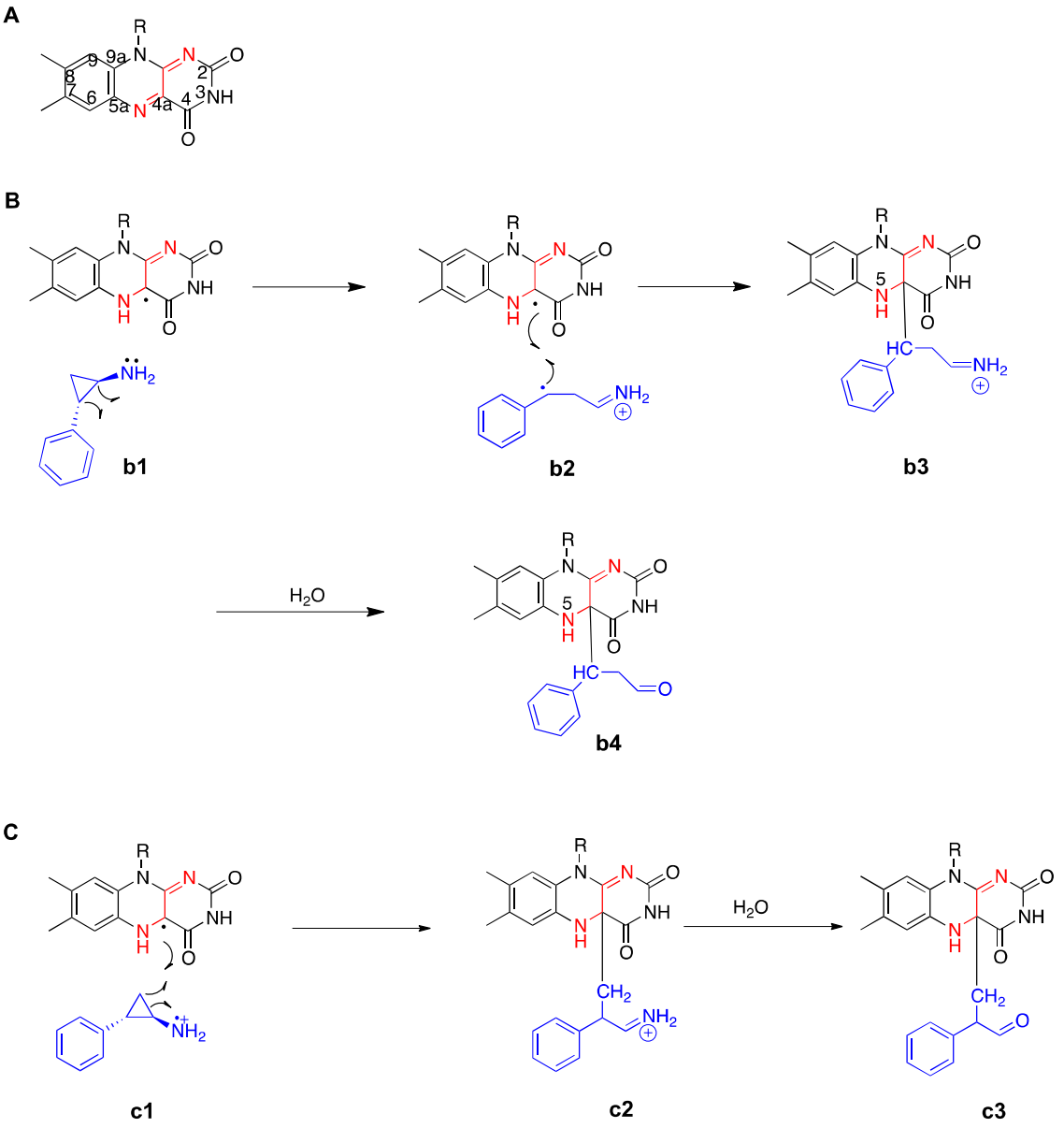

Scheme 1.2: Proposed models for TCP-FAD adduct formation, by Schmidt and colleagues.
(A) FAD ; (B) cinnamaldehyde adduct (b4) (**C**) atropaldehyde adduct formation (c3).

Later Yang and coworkers, suggested a SET mechanism from TCP to FAD that would [159] first generate an amine radical cation; ring opening of the cyclopropane would result in a stabilised benzylic radical and an iminium cation followed by C-C bond formation and imine hydrolysis that would lead to a 5-membered ring fused to C(4a) and N(5) of FAD.

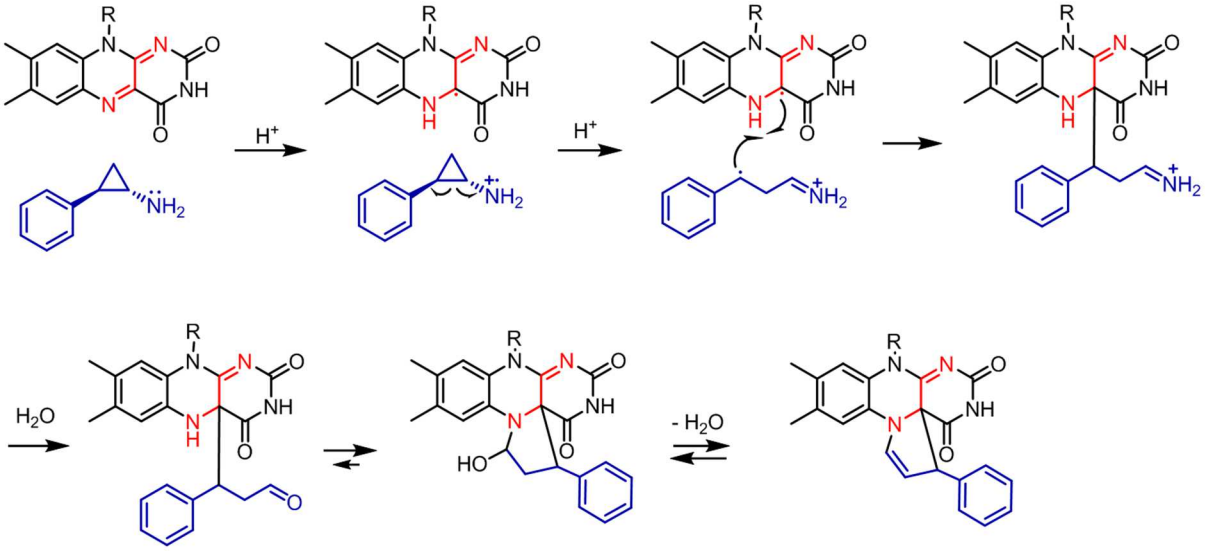

Scheme 1.3: Proposed models for TCP-FAD adduct formation in LSD1, known as five membered ring model, by Yang and colleagues.

R = ribityl-ADP.

Mimasu and coworkers resolved another crystal structure with improved resolution and suggested that the TCP-FAD adduct not only contains the C(4a) complex, which is the major adduct formed, but also incorporates an intermediate such as N^5 adduct (Scheme 1.4).[163]

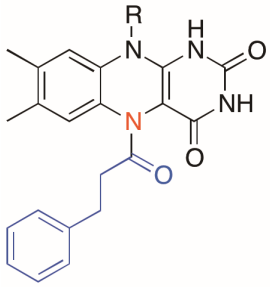

Scheme 1.4: N^5 adduct postulated by Mimasu and colleagues.

R=ribityl-ADP.

1.5.1.2. Phenelzine analogues

Phenelzine is one of the first compounds identified to inhibit LSD1 but only a few groups developed analogues due to their unselective inhibition.[160] A recent report describes a para-phenylbutyrylamide substituted phenelzine derivative termed bizine (**1.22**, Figure 1.19), as an active inhibitor of recombinant LSD1 (K_i 59 nM).[164]

Biological investigations on **1.22** demonstrated fluctuating levels of H3K4me2 at 0.4 µM (determined by Western blot) and moderate anti-proliferative activity in LNCaP cells (androgen dependent adenocarcinoma cell line) (IC_{50}>50 µM). Bizine was also evaluated successfully in protecting neurons from oxidative stress induced by homocysteic acid.[164,165]

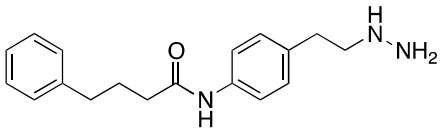

1.22

Figure 1.19: Bizine structure.

1.5.1.3. Tranylcypromine analogues

Tranylcypromine (***tra**ns*-2-phen**yl**-**cy**clo**pro**pyl-1-a**mine**, TCP) was firstly synthesised by Burger and Yost in 1948[166] and commercialized as an antidepressant (Parnate®).[167] Having a primary amine and a phenyl ring, it contains two stereocenters corresponding to the carbons at the cyclopropyl ring. It is clinically administered as a racemic mixture of two *trans* enantiomers 1*S*,2*R*-(+)-**1** and 1*R*,2*S*-(−)-**1**.[167] The 1*S*,2*R*-(+)-**1** enantiomer is identified to be ten times more potent than the (−)-enantiomer in *vivo*.[168] However, the oral intake of only the single (+)-**1** enantiomer of TCP caused severe side effects including weight loss, gastrointestinal disorders and agitation.[168] TCP inhibits LSD1 enzymatic activity *in vitro* with a K_i spanning from 477 µM to 2 µM.[66] Huge variations in the reported values highlights the variability of the assay conditions, detection methods and the constructs used for LSD1 expression.[66,169,170]

TCP is the most used scaffold for the synthesis of novel covalent inhibitors of LSD1. The development of more selective inhibitors was focused on the functionalization of the different elements of the TCP core and specifically the phenyl ring, amine group and the cyclopropane ring.

I) Tranylcypromine analogues with substitutions at the phenyl ring

A pioneering work from Gooden and colleagues revealed that TCP derivatives bearing a *para*-substituted aromatic rings were slightly more potent than the correspondent unsubstituted compound.[171] Within the series, 4-bromo and 4-methoxy TCP analogues displayed four to five-fold decrease of K_i compared to TCP. Following this study, Benelkebir *et al.* completed the enantioselective synthesis of a series of *para*-substituted TCP adducts (**1.23** and derivatives, Figure 1.20), with increased potency against LSD1 (K_i 3.7 µM) and anti-proliferative activity on LNCaP cells.[170]

Ueda and coworkers designed TCP-lysine hybrid structures (NCL1 and NCL2, **1.24** and **1.25** respectively, Figure 1.20), based on the X-ray crystal structure of FAD-propargyl-lysine adduct. In **1.24** and **1.25**, the Lys side chain was derivatised with the TCP phenyl ring via an ether bond; the amino and carbonyl group were substituted with benzyl and benzoyl structures to increase selectivity over MAO (the latter possess a smaller catalytic site), enhance potency (favour stronger interaction with the hydrophobic residues on the LSD1 catalytic cleft) and increase cellular uptake. The compounds were

active LSD1 blockers (K_i=2.5 µM and 1.5 µM respectively) and were also able to arrest cancer cell proliferation at µM concentration (6-67 µM range).[172] The effect of **1.24** was further examined in LNCaP cells, where the suppression of cell proliferation was associated with apoptosis and autophagy induction.[95] Additionally, in a xenograft model of prostate adenocarcinoma, the systemic administration of **1.24** (0.5-1.0 mg/kg), promoted the decrease of tumour volume without associated side effects.[95] The same research group also investigated on the activity of the single enantiomers of **1.24** and the separation via chiral chromatography led to compounds **1.27** and **1.28**, (Figure 1.20).[173] Enzymatic and biological evaluations revealed that **1.27** (1*S*, 2*R*)-NCL1 was four times more potent than **1.28** (1*R*, 2*S*)-NCL1 in enzymatic assays, whereas equal anti-proliferative activities were reported for both structures in neuroblastoma and kidney tumours cell lines.[172,173]

The library of TCP-Lys compounds was expanded further with the synthesis of **1.26**, which displays a supplementary modification at the TCP nitrogen and specifically, 1-acetyl-4-methyl-piperazine. The *N*-substitution promoted an enhanced enzymatic activity and increased the selectivity versus LSD1. The *N*-alkylated structure was in fact six times more potent (K_i=0.38 µM) compared to **1.25** (non-alkylated). Strangely, the increment in enzymatic potency did not translate into increased pharmacological effects, as **1.26** was equally potent to **1.25** in arresting the proliferation of SHSY5Y cells (neuroblastoma), but less active in HeLa (cervical) cells.

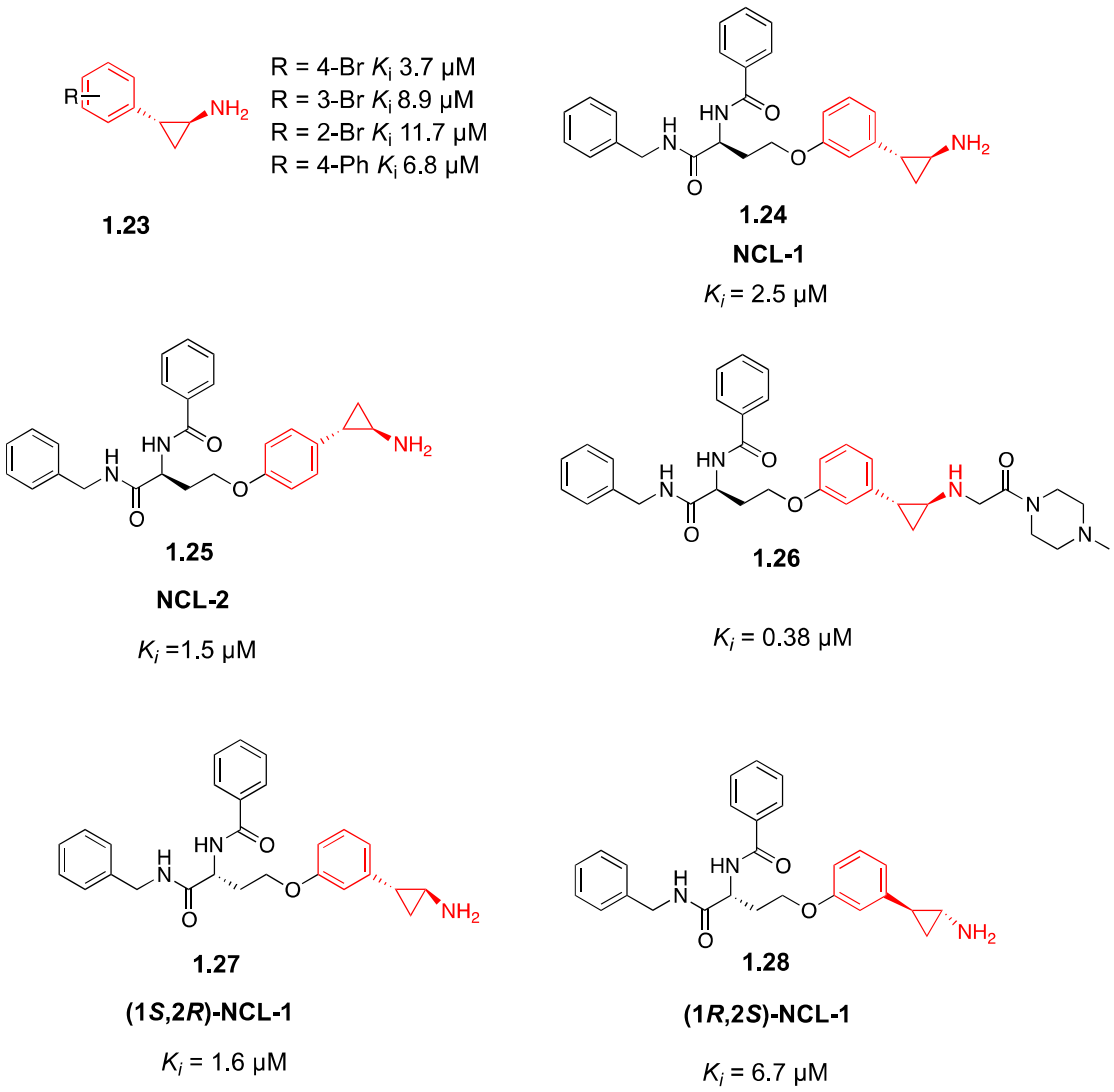

Figure 1.20: TCP based irreversible inhibitors substituted at the phenyl ring.
TCP core is highlighted in red.

A structure-based design led to the synthesis of *trans*-2-pentafluoro-phenylcyclopropylamine (2-PFPA) and a series of fluorinated TCP analogues.[174] The X-ray crystal structure of **1.29** (Figure 1.21) bound to the LSD1 catalytic site (PDB code: 2Z5U) revealed the presence of a large hydrophobic pocket. Such observations led to **1.30**, which has an additional phenyl ring in *ortho* position. The molecule **1.30** displayed enhanced enzymatic activity (K_i 0.99 µM) compared to **1.29,** supporting the crystallography data.

1.29

K_i = 8.9 µM

1.30

S2101

K_i = 0.99 µM

Figure 1.21: Fluorinated TCP derivatives.

Binda and coworkers generated a library of derivatives displaying bulky-branched substituents to the aromatic ring of *trans*-TCP. The structures present a *N*-carbobenzyloxy-(Z-) amino acid moiety in *para* at the TCP-phenyl ring and their biological evaluation revealed interesting properties (Figure 1.22).[175] The compounds were capable of hindering the growth of a broad panel of cancer cells at low concentrations (1-6 µM).[66,175] Moreover, compound **1.32** (Figure 1.22) induced differentiation in APL cells (acute promyelocytic leukaemia) as a single agent and synergistically with *trans* retinoic acid (ATRA).[66,175] The authors investigated also how TCP stereoconfiguration influences the biology. The results revealed no significant differences between the enzymatic activities of the two enantiomers (K_i of **1.33** *vs.* **1.34**, Figure 1.22) for LSD1 inhibition.[175] Conversely, the configuration was crucial for MAO B activity suppression, as the (+)-*trans* isomer was 20-fold more potent compared to the (−)-*trans* isomer. TCP derivatives with *cis* configuration displayed less affinity towards LSD1, LSD2 and MAO B.[175]

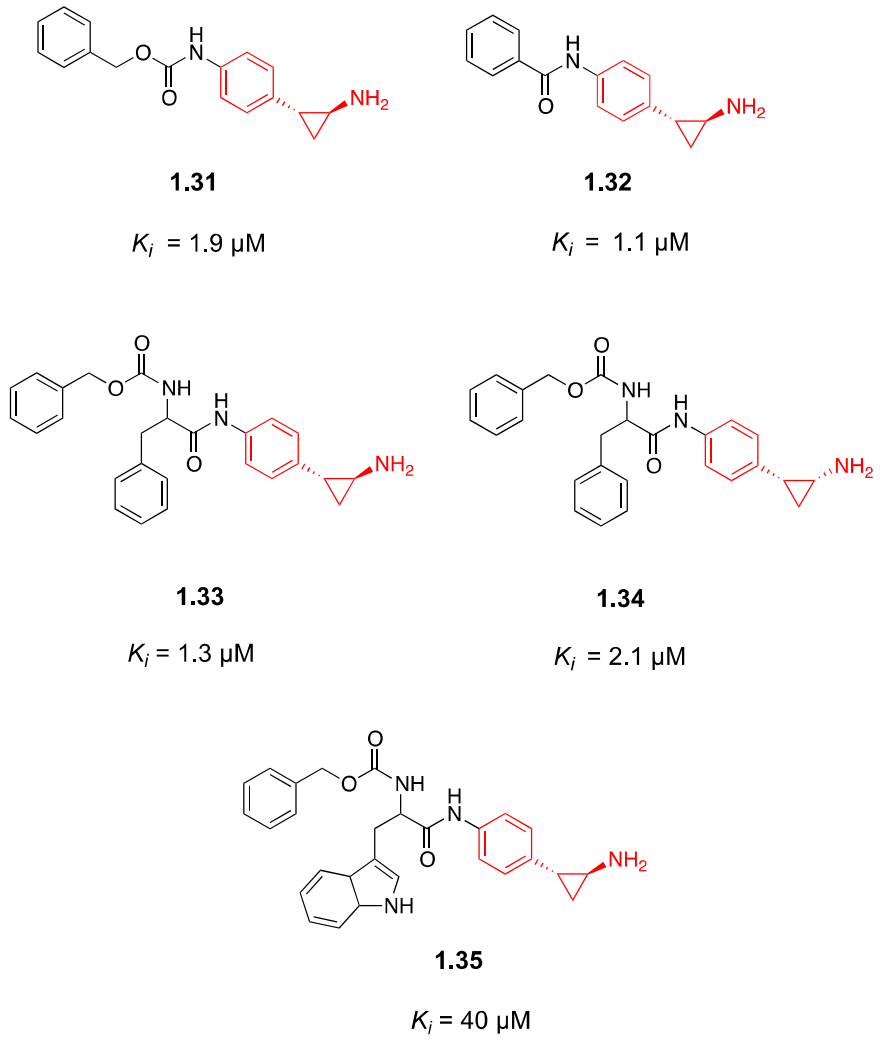

Figure 1.22: TCP analogues synthesised by Binda and colleagues.

Rotili *et al.* synthesised several pan-histone demethylase inhibitors by incorporating inhibitors of both the KDMs families in the same structure.[176] To do so, the TCP core was coupled with 4-carboxy-4'-carbomethixy-2,2'-bypiridine or 5-carboxy-8-hydroxyquinoline, which are known inhibitors of the JmjC KDMs.[176] Enzymatic evaluations revealed that the bi-functional structures suppressed concurrently LSD1 and a panel of JmjC demethylases, with similar potencies as the reference compounds.[176] Compounds **1.36** and **1.37** (Figure 1.23) were among the most potent, displaying also selectivity towards LSD1 over MAOs. Immunoblotting measurements supported the effective demethylases inhibition, as µM treatments induced a dose-dependent hypermethylation at H3K9me3 and increased expression of H3K4me2 in LNCaP and HT116 cells (HT116 is a colon cancer cell line). Additionally, µM concentrations of

1.36 and **1.37** (10-100 µM range) were more efficient in inducing apoptosis in colon and prostate carcinoma cells compared to unconjugated single agents.[176]

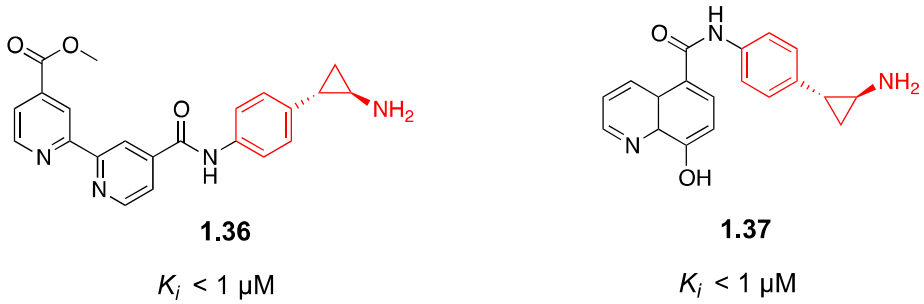

Figure 1.23: Pan-histone KDMs inhibitors.

II) Tranylcypromine analogues with substitutions at the phenyl ring and nitrogen

Evidence of potency and selectivity achieved through *para*-substitution on the phenyl ring of TCP has been further evidentiated in several patents disclosed by Oryzon Genomics and GlaxoSmithKline. In the former, a series of *N*-substituted (hetero) aryl cyclopropylamines were prepared and among them, ORY-1001 (**1.38**, Figure 1.24) was licensed to Roche and entered clinical trials in early 2014 for the treatment of AML.[56,71,177] In addition, Takeda[178] and GlaxoSmithKline[179] also have filed patents focusing on LSD1 irreversible inhibition. **GSK2879552** (**1.41**, Figure 1.24) has recently entered Phase I clinical trials targeting small cell lung cancer (SCLC).[179]

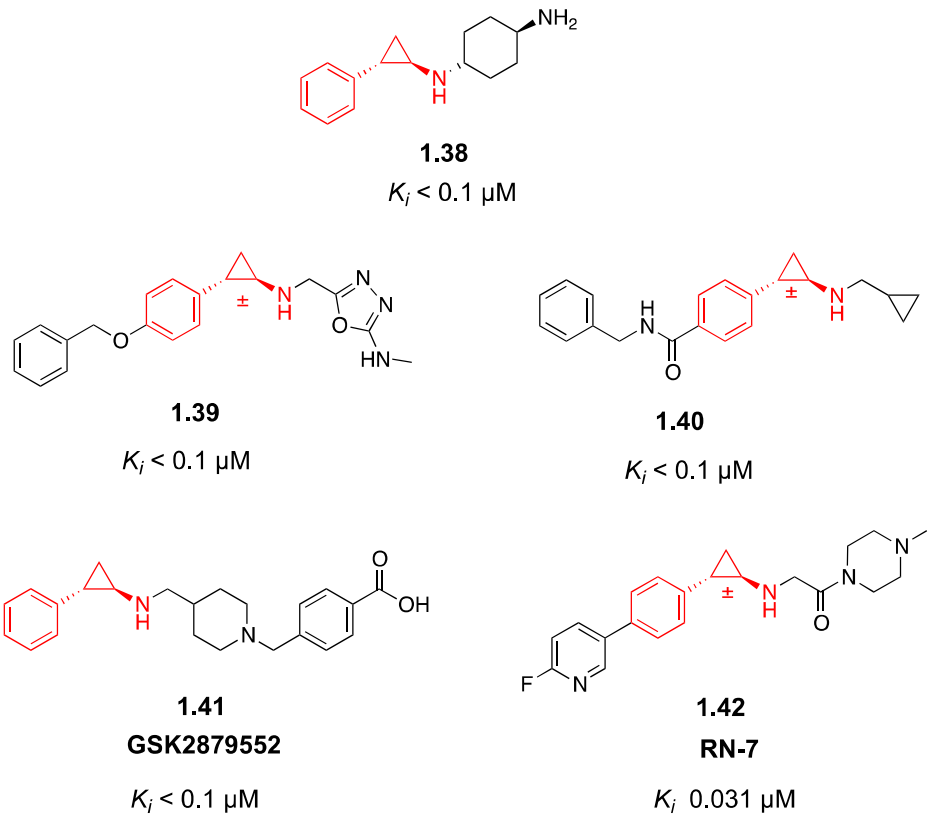

Figure 1.24: TCP derivatives with phenyl ring and nitrogen functionalisation.
1.38 and **1.39** Oryzon compounds (ORY-1001 **1.38**); **1.40** Takeda compound; **1.41** GSK compound; **1.42** brain penetrating TCP-derivative.

Compound **1.41** proved to be extremely powerful in a cell-free enzymatic assay (K_i 0.13 nM) and able to arrest AML and SCLC in *in vivo* models. Interestingly, although the compounds' activities are linked to LSD1 inhibition, **GSK2879552** treatment was not associated with a cellular increase of H3K4me2.[179]

Of note is a study built on the patented work of Guibourt *et al.*, investigating the activity of *N*-alkylated compounds in nervous system and memory formation.[33] Among them, RN-7 (**1.42,** Figure 1.24) was 300-fold more selective for LSD1 compared to TCP and systemic administration resulted in impaired memory consolidation in rodents, suggesting that LSD1 could also be involved in cognitive functions.[33]

III) Tranylcypromine analogues with substitutions at the at the cyclopropyl ring

Based on earlier reports of methyl-substituted cyclopropyl rings designed as MAOIs, Vianello and colleagues[180,181] researched on a library of *trans* isomers with hydrophobic and hydrophilic substituents at the α-position of the cyclopropyl ring.[180] Alkyl, benzyl and phenyl substitutions resulted in TCP analogues with increased LSD1 inhibition and selectivity over MAOs (Figure 1.25). Conversely, derivatives functionalised with hydrophilic substituents demonstrated reduced potency. The work also investigated how stereoconfiguration influences the binding of compounds bearing methyl, ethyl, phenyl and benzyl substituents. No substantial differences were reported among the structures (Figure 1.25).

Tranylcypromine derivatives substituted at the cyclopropyl ring

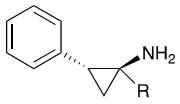

1.43 R = *trans* **Methyl** K_i = 1.72 µM

1.44 R = *trans* **Ethyl** K_i = 0.779 µM

1.45 R = *trans* **Phenyl** K_i = 0.161 µM

1.46 R = *trans* **Benzyl** K_i = 0.617 µM

1.47 R = *trans* **2-Naphthyl (CH$_2$)** K_i = 0.218 µM

1.48 R = *trans* **Ph-(CH$_2$)$_2$** K_i = 0.202 µM

Tranylcypromine derivatives substituted at the cyclopropyl and phenyl ring

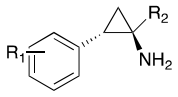

1.49 **R$_1$ = m - Br, R$_2$ = Ethyl** K_i 0.031 µM

1.50 **R$_1$ = m - Cl, R$_2$ = Ethyl** K_i 0.038 µM

Figure 1.25: Cyclopropyl-substituted TCP-derivatives.

Additional electron-donating or -withdrawing groups at the phenyl ring further extended the library (**1.49** and **1.50**, Figure 1.25). Within such modifications, the activity of compounds having electron-withdrawing groups at the phenyl was improved.[182]

1.5.1.4. Other irreversible inhibitors of LSD1

In addition to the TCP-based compounds, several studies focused on the search for novel scaffolds. One of these scaffolds that is worth mentioning is the **pargyline-lysine** based analogues by Schmitt *et al.*[151] Molecular modelling and chemical refinement led to compounds with higher activity on LSD1 than pargyline (**1.51** and **1.52**, Figure 1.26). Treatment of MCF7 (breast cancer) cells with compounds **1.51** and **1.52** (90 and 100 µM respectively) prompted cell proliferation arrest and increased the levels of H3K4me2.[151]

Several natural compounds are also reported as antagonists of LSD1 enzymatic activity. Abdulla *et al.*,[183] proposed that resveratrol is able to prevent LSD1 enzymatic activity in a concentration dependent manner. Sakane *et al.*[184] designed and tested a series of acyclic diterpenoids (**1.54**, Figure 1.26) based on the reported capacity of farnesol to suppress LSD1.

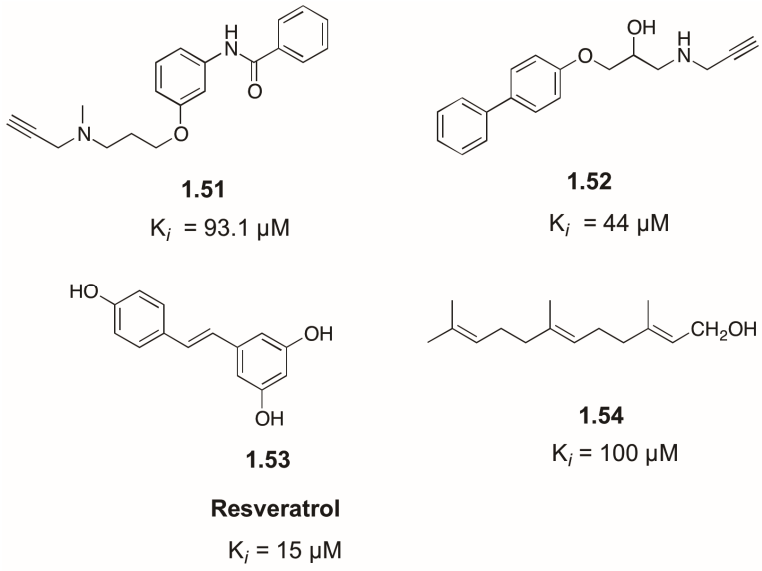

Figure 1.26: Non-TCP based irreversible inhibitors of LSD1.
1.51 and **1.52**, pargyline-lysine based inhibitors; **1.53** and **1.54** natural product inhibitors of LSD1.

Despite the scarce activity and lack of biochemical studies, the structures reported in these works are unrelated to known antagonists and their SAR could be further exploited for the synthesis of novel LSD1 inhibitors.

1.5.2. Reversible inhibitors of LSD1

As reported in earlier sections, numerous covalent inhibitors of LSD1 were successfully discovered with potential therapeutic applications. In contrast, research of reversible inhibitors was not equally successful.
The reversible inhibitors of LSD1 can be classified according to their chemical nature or discovery process.

1.5.2.1. Polyamine analogues

Polyamine oxidases constitute a family of FAD-dependent oxidoreductases that oxidase acetylated polyamines. Their metabolic pathway has been recently identified as a druggable target for neoplastic and infectious diseases.[185–187] The polyamine oxidases N^1-acetylpolyamine oxidase (APAO) and spermine oxidase (SMO) share 60% sequence homology with the LSD1 C-terminal domain and can be inhibited by molecules containing guanidine moieties, such as guazatine (**1.55**, Figure 1.27).[101,188]
In 2006, Bi and coworkers generated a series of (bis)guanidines and (bis)biguanides as antitrypanosomal compounds, targeting the parasitic trypanothione-disufide reductase.[189] Considering the high structural similarity of these compounds with guazatine, these were assessed as LSD1 inhibitors.[190] The polyamines **1.56** and **1.57** (Figure 1.27) were able to antagonise LSD1 activity in a non-competitive fashion at concentrations lower than 2.5 µM. The biological applications of such compounds were substantiated with cellular experiments and **1.56**-**1.57** were capable of modulating the expression of methylated histones (increase of H3K4me1 and H3K4me2, and decrease of H3K9me2 expression) as well as reverting silenced genes involved in tumour suppression of HCT116 cells. The synthesis of long chain oligoamines with rotational bond restrictions further extended this initial work and the decamines **1.58** and **1.59** (*cis*-*trans* isomers) were able to suppress LSD1 activity at 10 µM concentration.[191] Cellular evaluations in HCT116 cells revealed in addition that µM treatments with such compounds induced the re-expression of multiple silent genes like Wnt signalling pathway, frizzled-related protein family RP, and the GATA family of transcription factors.[191] In addition to these effects, **1.58** displayed synergy with DNMT inhibitor 5-

azacytidine in arresting cancer cell proliferation in a xenograft model for colon cancer without associated toxicity.[191]

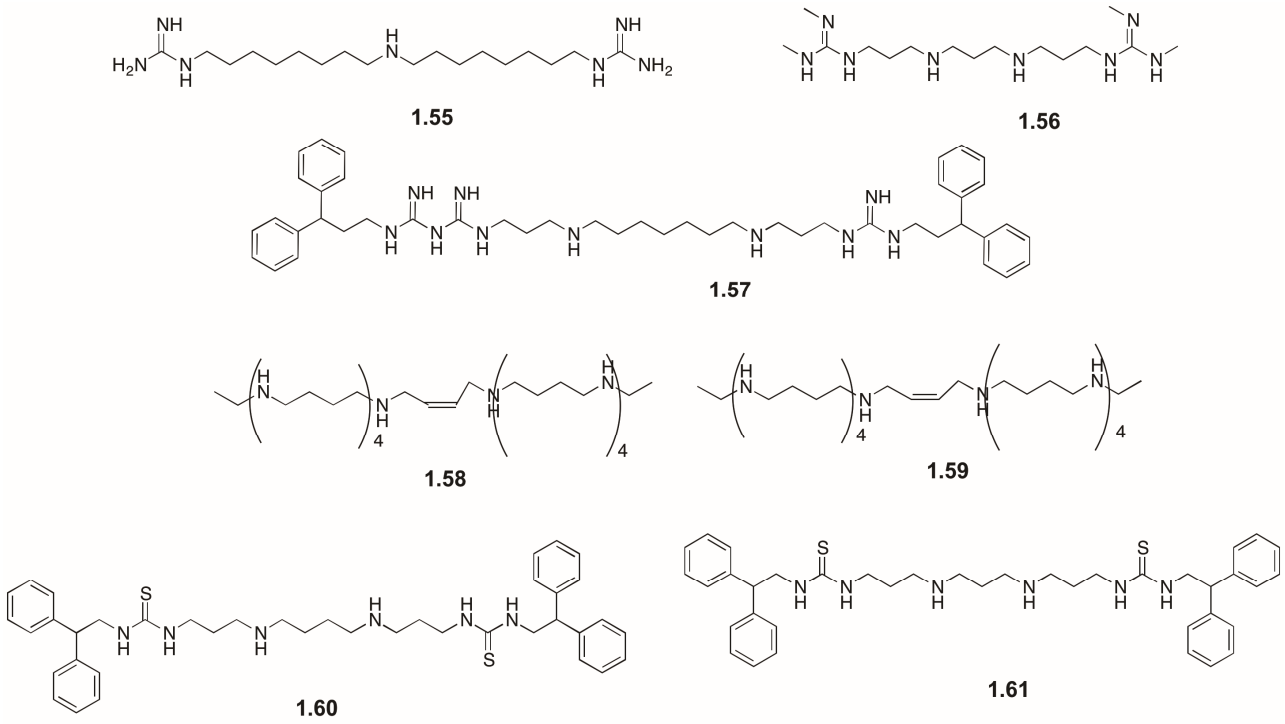

Figure 1.27: Polyamine based reversible inhibitors.

The repertoire of polyamine-based inhibitors of LSD1 was expanded with the insertion of (bis)urea and (bis)thiourea moieties.[192] Derivatives **1.60** and **1.61** (Figure 1.27), exhibited excellent potency in non-small cells lung carcinoma cells (l10.3 µM and 9.4 µM respectively), and selectivity for LSD1.[192]

Despite the promising results and the possible application of such compounds to a wide array of diseases, no structural studies so far defined the precise mechanism and therefore, more evidence is needed to link the observed pharmacology with LSD1 inhibition.[193]

1.5.2.2. Small molecule reversible inhibitors

The availability of numerous LSD1 X-ray crystal structures paved the way for numerous virtual screening efforts to discover LSD1 reversible inhibitors. The first study was performed by Wang *et al.*[194] and resulted in the identification of compound **1.62** (Figure 1.28), which demonstrated in *vitro* inhibition of LSD1 at 5.3 µM with selectivity over LSD2 and JARID1A (a JmjC KDM). The compound displayed in addition anti-proliferative activity in HeLa cells at µM concentrations.[194]

Another virtual screen led to the identification of *N*'-(1-phenylethylidene)-benzohydrazide-based structures as potential suppressors of LSD1.[195] Among them **SP-2509**, also called HCI2509 (**1.63**, Figure 1.28), revealed an interesting biological profile, being able to inhibit LSD1 enzymatically at 13 nM and arresting the growth of diverse cancer cells (breast, colon, prostate, melanoma, pancreatic and glioblastoma) at low µM range (IC_{50s} spanning from 0.3 to 3 µM).

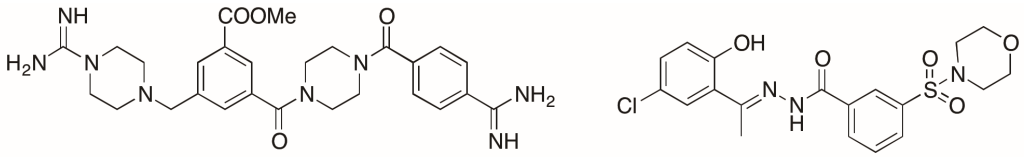

1.62
CB1007
K_i 5.3 µM

1.63
SP-2059
K_i 13 nM

Figure 1.28: Reversible inhibitors discovered with bioinformatic tools.

As reported by the authors, despite the surprising biology and the unconventional structure, **1.63** failed to demonstrate unambiguously target inhibition. The compound was unable to induce the expression of CD86, a cellular marker that correlates with LSD1 inhibition.[195,196] Moreover, immunoblotting experiments reported the increased expression of H3K4me2 only at 10 µM dose. The reason for these incongruities, as noted by Mould *et al*,[197] might arise from the interference of the hydrazide moiety with the biological assays.[198] The *N*'-(2-hydroxybenzylidene) hydrazide motif has been identified among the pan-assay interference compounds (PAINS). The presence of this moiety can often lead to fallacious results, which are attributed to interferences with the

assay conditions.[198] According to the mechanism shown in Scheme 1.6, such chemical entities hold a strong propensity for Michael addition reactivity via a quinoid tautomeric formation that is susceptible of nucleophilic attack from assay reagents or amino acid residues (i.e. cysteine).[199,200]

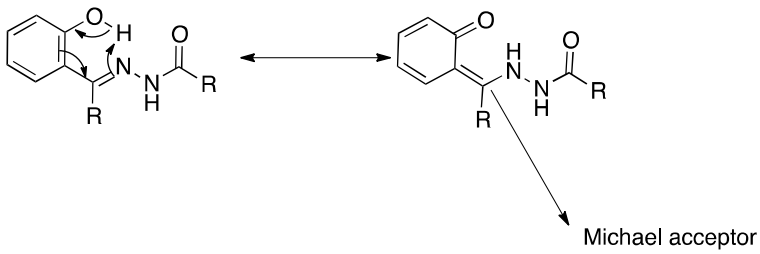

Scheme 1.~~46~~: Mechanism of intramolecular proton transfer for *N*'-(2-hydroxybenzylidene) hydrazide-containing compounds proposed for the formation of a quinoid tautomer form, which is susceptible of nucleophilic attack.

In addition, it has also been observed that such moiety can form cytotoxic complexes with transition metal ions.[201] Therefore the observed data for **1.63** could derive from an off-target pharmacology in lieu of LSD1 inhibition.[198] Biological assays with **SP-2509** in AML lines further evidentiate the sub-micromolar anti-cancer potential of the compound. Moreover, 1 µM treatment was sufficient to trigger the expression of the differentiation markers CD14 and CD11b.[202] In addition, the compound revealed a synergistic effect with HDACi in arresting AMLs growth and the treatment was non-toxic for normal blast cells.[202] Additional experiments with **SP-2509** in Ewing showed that the compound reverts the growth of the tumour in both *in vitro* and *in vivo* models.[203]

Fragment based screening on structure **1.64** (Figure 1.29), led to the identification of the aminothiazole core structure as a potential LSD1 antagonist. Consistently, the derived compounds **1.64a** and **1.64b** (Figure 1.29), revealed a 50-fold increase in activity in enzymatic assays compared to the initial fragment, displaying high selectivity for LSD1 over other FAD-dependent oxidases.[197,204] However, the enzymatic results did not correlate with cellular experiments and both **1.64a** and **1.64b** were devoid of cellular activities.

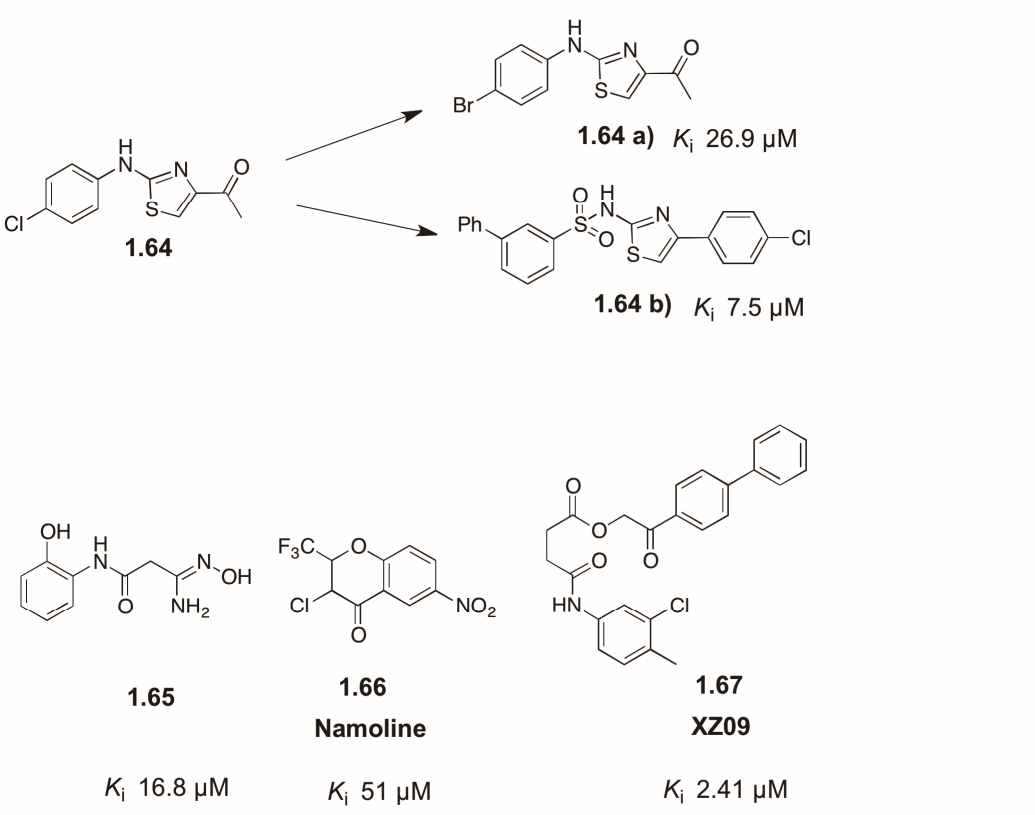

Figure 1.29: Reversible inhibitors discovered with bioinformatics tools or fragment based screen.

Hazeldine and colleagues performed another virtual screening on LSD1 catalytic site (PDB code: 2V1D) and their results identified low molecular weight amidoximes as potential scaffolds for LSD1 suppression.[205] Among them, compound **1.65** (Figure 1.29) showed anti-proliferative activity on Calu-6 cells and increased expression of silenced tumour suppressor genes.[205]

Searching for LSD1 blockers, Willmann and coworkers explored an informatic approach termed "proteins structure similarities search clustering" (PSSC) that enables the detection of structural similarities among different binding pockets.[93] Only the binding pocket of MAOs was found homologous to the LSD1 AOL domain. Thus, the group screened an extensive library of potent MAOIs[206] based on γ-pyrones structures against LSD1. The study led to the discovery of 3-chloro-6-nitro-2-(tri-fluoromethyl)-4H-chromen-4-one or namoline (**1.66**, Figure 1.29) that was able to suppress LSD1 enzymatic activity via a reversible mechanism (K_i=50 µM). Mass spectrometry experiments with a histone substrate showed increase in H3K4me2 at 20 µM and cytotoxicity assays revealed that namoline was capable of arresting LNCaP cells

proliferation at 100 µM dose. Although the systemic administration of namoline (0.02 g/kg) in prostate adenocarcinoma xenograft reduced the tumour volume, the treatment was associated with weight loss, which could be indicative of off-target toxicity.[93]

Identification of XZ09 (**1.67**, Figure 1.29) was accomplished through a constructed pharmacophore combined with docking methods.[207] The compound was capable of inhibiting selectively LSD1 at low µM concentrations (2.41 µM). [207]

Dulla *et al.,* designed several 3-amino-guanidine substituted phenyl-oxazole structures (**1.69-1.71**, Figure 1.30) by merging the key chemical features characterising different classes of LSD1 inhibitors in the same molecular structure.[208] Despite the low enzymatic potency (IC_{50} 10-16 µM) the compounds were able to arrest cancer cell proliferation of HeLa and MDA-MB-213 cells (breast) at a concentration as low as 1 nM. As noted by the authors, the exceptional cellular data might arise from a marked sensitivity to the treatment of the cancer lines tested or from off-target effects.[208] Noteworthy, treatment with **1.69-1.71** (10 µM, 72 h) induced apoptotic events in zebrafish (*Danio rerio*) embryos, without associated toxicity.[208]

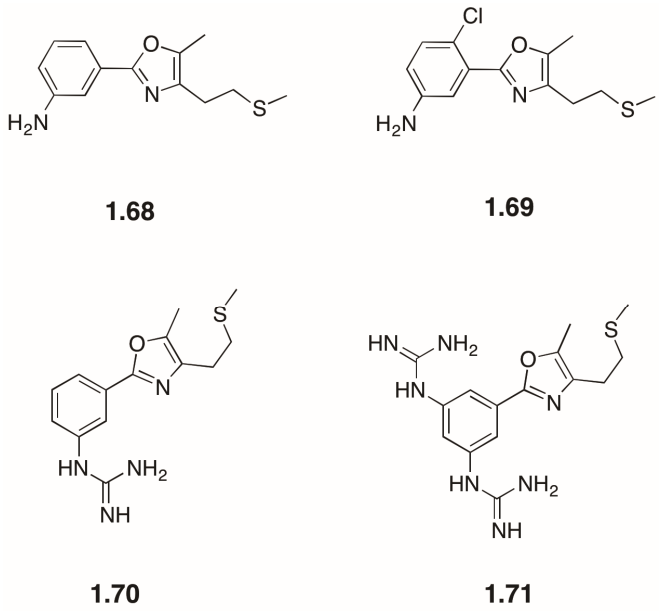

Figure 1.30: Phenyl-oxazole based reversible inhibitors.

In 2013 GlaxoSmithKline disclosed a reversible inhibitor of LSD1 with interesting biology (**1.72**, Figure 1.31). **GSK 354** is able to block LSD1 at 90 nM and displays a remarkable selectivity for LSD1 over other flavin oxidases.[197,204,209] Moreover, it suppresses cellular LSD1 at 1.4 µM, a determination based on the compound's capacity to trigger the expression of the CD86 marker. Currently, the amount of information on **GSK 354** is limited.

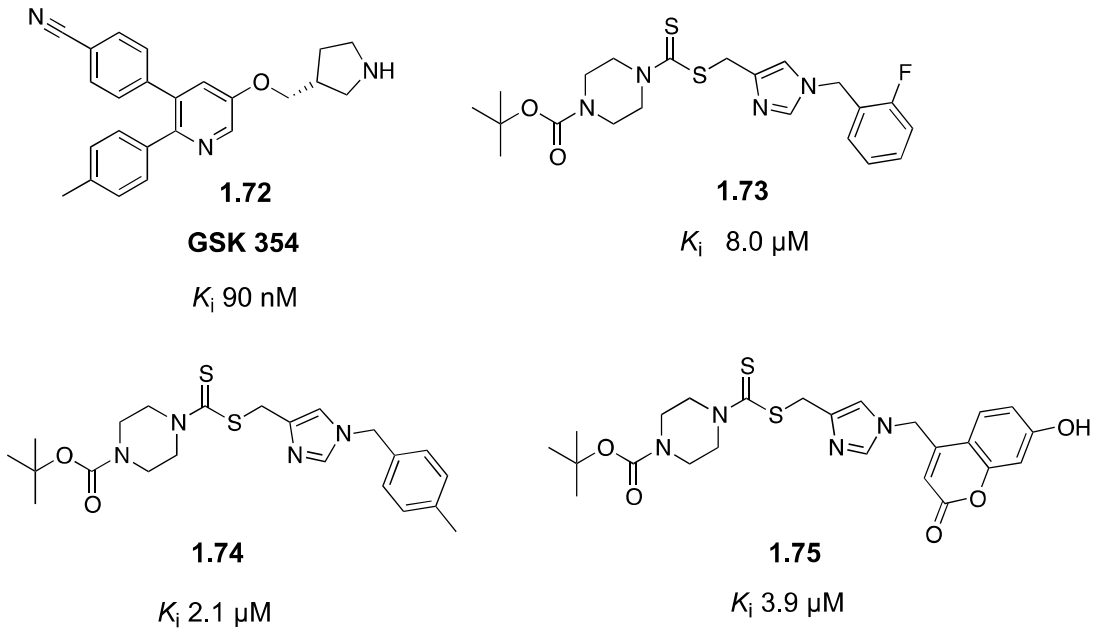

Figure 1.31: GSK and triazole-dithiocarbamate based reversible inhibitors.

Based on the pharmacological applications of heterocyclic azoles and thiocarbamate moieties as antimycotic, anti-neoplastic and antibacterial agents, Zhang *et al*. built a library of triazole-dithiocarbamate hybrids as potential LSD1 blockers (**1.73-1.75**, Figure 1.31).[210] The 1,2,3 triazole scaffold was easily obtained via Huisgen cycloaddition employing alkynes and azides.[211] The enzymatic activity, evaluated with a peroxidase coupled functional assay, revealed µM inhibition for selected structures.[212] In addition, compound **1.75** was evaluated successfully in a xenograft model of human gastric tumour.

1.5.2.3. Peptide based reversible inhibitors

The first substrate inhibitors were designed by taking advantage of the homology between LSD1 and MAOs and introducing flavin-reactive warheads into peptides derived from N-terminal H3.[158–160,213] The warheads included *N*-propargyl, cyclopropyl, aziridine, phenelzine, and TCP substituents (**1.76-1.83**, Figure 1.32). The peptide with a phenelzine moiety (**1.83**) was among the most potent LSD1 inhibitor (K_i 4.5 µM). The analogue **1.76**, displaying a propargyl-lysine warhead inhibited LSD1 enzymatic activity at 16.6 µM in a time and concentration dependent fashion.[213]

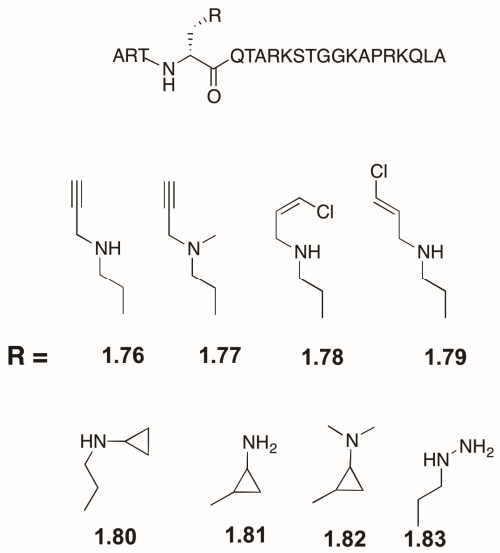

Figure 1.32: Structure of substrate analogues inhibitors of LSD1.
Top: H3 N-terminal 21-mer.

Our group reported recently a series of relatively low molecular weight peptides based on Snail-1 protein. As described in an earlier section, Snail-1 is found to bind LSD1-CoREST by the N-terminal region, acting as a DNA binding motif and on that account, we designed small peptide analogues of the Snail-1 N-terminal domain. The hexamer **PRSFLV** showed a K_i of 28 µM as well as anti-proliferative activity on THP-1 cells. The non-covalent inhibition was supported by numerous crystal structures of the peptide bound to the catalytic pocket of LSD1 (see Chapter 2).[214]

1.6. AIMS

Based on the evidence reviewed above, disentangling the functions of LSD1 could lead to design novel drug for several diseases.

In the research presented in this thesis, I aim to broaden the current knowledge on this important demethylase. In order to do so I firstly focused on the design reversible inhibitors of LSD1 by synthesising small peptides (MW < 600 Da) based on Snail-1 N-terminal sequence. Recent scientific literature has in fact shown that the Snail family of transcription factors interact with LSD1 via the N-terminal domain impeding the LSD1 demethylase function. Secondly I used Phage Display technology to explore a library of peptides that could lead to reversible LSD1 inhibitors.

The second part of the thesis focused on the search of irreversible inhibitors of LSD1, as they are potential antitumor therapeutic agents. I planned to investigate on the SAR of tranylcypromine: as a large hydrophobic pocket has been observed in the crystal structure of LSD1, analogues of TCP bearing substituents on the phenyl ring can represent an interesting target. To measure the efficacy of such analogues and enzymatic assay will be employed. Compounds that display a better activity will be tested on more complex biological system. I also aim to explore an activity based probes to label fluorescently LSD1. This will be achieved by synthesising a TCP analogue having an alkyne moiety. The molecule will be exploited as a bioorthogonal partner of an azide containing imaging tag.

This thesis constitutes a methodological framework to target LSD1 pharmacologically, providing several approaches through which reversible and irreversible inhibitors can be designed.

Chapter 2 - Protein recognition by short peptides: reversible inhibitors of the LSD1-CoREST complex

2.1. Introduction

One of the main limitations of LSD1 inhibition is the lack of selectivity of the currently available blockers, which are mostly based on covalent FAD modifiers. Reversible inhibition could reduce possible side effects associated with a long half-life and non-specific interactions. Some reversible inhibitors have been reported but possess low activity or are polycationic in nature.[188,215] As mentioned in the previous Chapter, Snail-1 is a recently discovered LSD1 binding partner and member of the SNAIL/SCRATCH family of transcription factors and is involved in cell differentiation and development processes. Here we report for the first time Snail-1-based short peptides (MW < 800 Da) that are able to inhibit LSD1 reversibly and at micromolar concentrations. Studies of the crystal structure of diverse active peptides sequences bound to the LSD1 catalytic site give further insight into LSD1 biochemistry.[214] Moreover, the findings shown here open further possibilities for the design of novel reversible inhibitors of LSD1.

2.1.1. LSD1-Snail-1 interaction

The interaction of LSD1 with the Snail family of transcription factors uncovered valuable information on the biology of this epigenetic target.[216] The Snail family of proteins is devoted to the inhibition of cell-specific epithelial genes associated with apoptosis and cell cycle progression.[140,141] Specifically, Snail-1 promotes the induction of the phenotypic change called epithelial-to-mesenchymal transition (EMT).[138] The EMT allows the conversion of cells from a static state (epithelial) to a mesenchymal state, whereby they acquire stem cell properties. EMT takes place in tissue formation during embryonic development, wound healing and tissue remodeling processes. In contrast, its aberrant regulation in epithelial tumours is associated with the acquisition of motile and invasive properties.[138,217,218] An exceptional characteristic of the EMT is its reversibility: when far away from the primary tumour, cells are not influenced by the initial chemical stimuli and can revert to the epithelial state through a process called

mesenchymal-to-epithelial transition (MET). The process of switching from EMT to MET is potentially regulated by epigenetic mechanisms.[164] In both physiological and pathological events, EMT is accompanied by the direct repression of E-cadherin transcription.[218] E-cadherin is a single span trans-membrane glycoprotein that sustains cell adhesion and polarity. Its down-regulation in epithelial tumours correlates with cancer metastasis and poor prognosis.[139]

In 2010, Tandem Array Purification (TAP) coupled with mass spectrometry studies revealed that Snail-1 recruits LSD1 for repression and such interaction is found to be co-localised in the nucleus of a number of cancer cell models.[117] Interestingly, the binding takes place through the N-terminal domain and particularly via a characteristic N-terminal sequence in Snail-1, termed SNAG (Figure 2.1 A). The alignment of the N-terminal sequences of several evolutionary related C2H2 zinc finger transcription factors such as Gfi1, Slug, Scratch, insulinoma-associated protein IA-1 (INSM1) and Ovo-like 1 (OVOL1) revealed that the SNAG sequence is conserved. This feature predicts that probably, many other) transcription factors of the SNAIL/Scratch family can associate to LSD1 (and possibly LSD2) following the same molecular mechanism targeted by LSD1. The SNAG sequence is important for protein stability and protein repressive activities. For example, in Snail-1 the abrogation of SNAG generates mutants unable to interact with LSD1.[219] In addition, it has been demonstrated that LSD1 is recruited at the E-cadherin gene promoters by Snail-1 where it demethylates H3K4me2 and promotes transcriptional silencing effects.[220] In human breast cancer cells, Snail-1 mutants lacking the SNAG-LSD1 interaction do not suppress the E-cadherin gene, suggesting that SNAG domain and LSD1 are both responsible for the E-cadherin repression.[221]

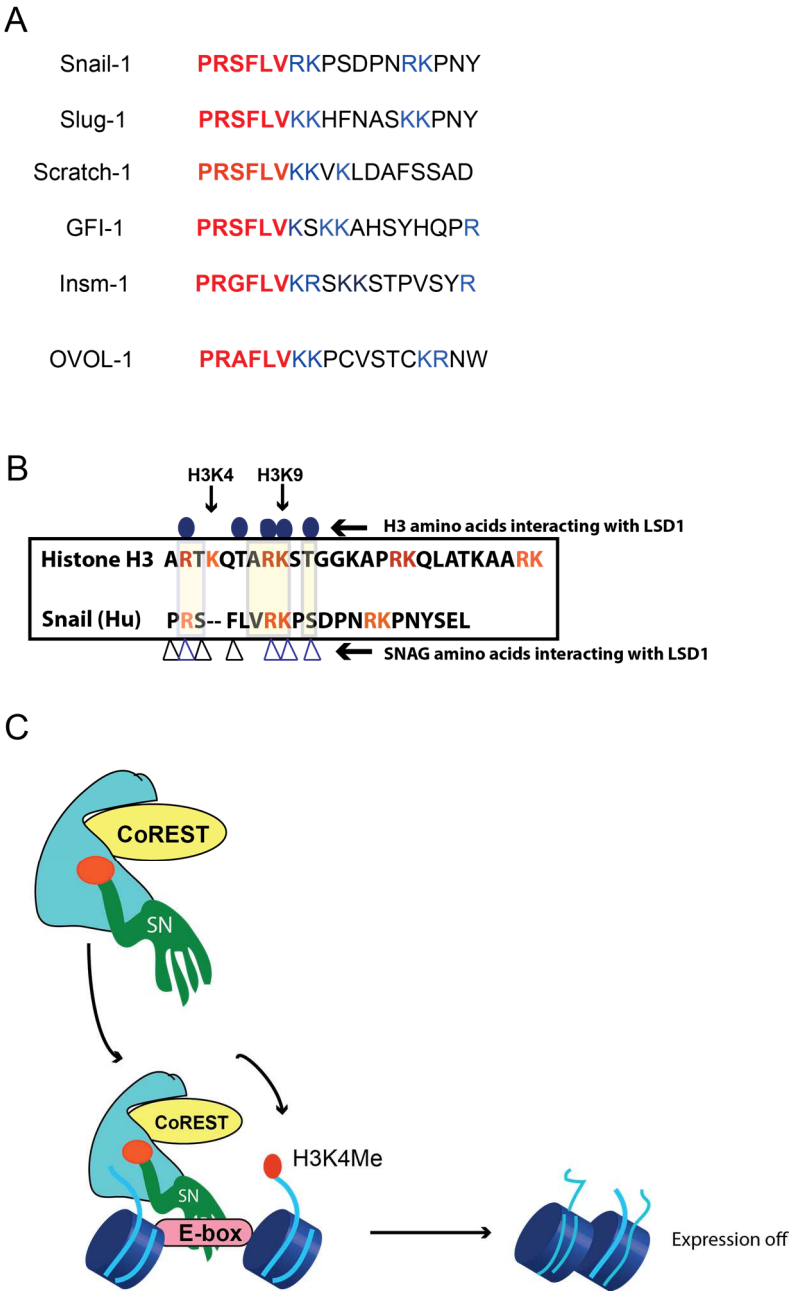

Figure 2.1: Snail-1-LSD1 interaction.

(A) Alignment of the N-terminal sequences of several evolutionary related CH2H2 zinc finger transcription factors. The conserved SNAG domain residues are in red and basic residues Arginine (R) and Lysine (K) in blue; (**B**) Alignment of Snail-1 and H3 N-terminal domain. R and K residues are shown in red and the conserved pattern of amino acid residues is highlighted in yellow. The blue dots (top) and triangle (bottom) indicate the H3/Snail-1 amino acid residues involved in the interaction with LSD1 catalytic pocket; (**C**) Schematic diagram illustrating the mechanism of Snail-1 (SN-green) –LSD1/CoREST (cyan) interaction: SNAG domain of Snail-1 (red dot) functions as a molecular hook to recruit and bind to LSD1-CoREST complex; the newly formed ternary complex is stabilised from proteosomal degradation. The complex is recruited to E-boxes of Snail-1 target genes such as E-cadherin. Here the H3 substrate competes with the SNAG domain for LSD1.Adapted from Lin *et al.* [117]

Single mutations at positions Pro1, Arg2, Ser3, Phe4, Arg7 and Lys8 are especially detrimental as they result in Snail-1 mutants that are unable to interact with LSD1. Interestingly, the amino acids Arg2, Arg7 and Lys9 are fundamental for H3 binding to the LSD1 catalytic pocket (Figure 2.1, B). Superimposition of H3 and Snail-1 sequences showed that in both the natural substrate and LSD1 binding partner, the side chains make the same interactions in the catalytic cleft.[117,136] Another feature that the N-terminal domains of H3 substrate and the Snail-1 have in common, resides in the α-helical conformation adopted by their first four amino acids when interacting with LSD1.[105] In addition, it has been shown that irreversible LSD1 suppressors, such as pargyline and H3 peptides bearing both methylated and unmethylated H3K4 sequences, are effective blockers of the SNAG-LSD1 interaction, implying that SNAG mimics the H3 sequence (Figure 2.1 B). Taken together, this information led to the hypothesis that Snail-1 binds to the LSD1 catalytic site and inhibits its enzymatic activity.[117] Baron *et al.*[111] showed that a 20-amino acid long peptide, corresponding to the N-terminus of Snail-1, effectively suppresses the LSD1-CoREST enzymatic activity at concentrations as low as 0.21 ± 0.07 μM. Likewise, also LSD2 binds the Snail-1 peptide, although with lower affinities.

The crystal structure of the Snail-1-LSD1-CoREST complex revealed that only the first N-terminal 9 residues of Snail-1 within the 20 amino acid long tested sequence were critical for binding, while the later amino acid residues were found disordered. Therefore, shorter peptides mimicking the structure of the conserved SNAG pattern may be useful tools to arrest the Snail-1-mediated initiation of EMT and cancer propagation by modulating LSD1 enzymatic activity. Given their lower molecular weight compared to the full SNAG domain, these could be investigated as leads for the discovery of LSD1 antagonists via reversible inhibition.

2.2. Experimental strategy

Following such preliminary data on Snail-1-LSD1 interaction, we decided to synthesise peptide sequences derived from the Snail-1 N-terminal domain and evaluate them as potential LSD1 binders. Three different strategies were followed: length scanning to probe the influence of chain length on binding affinity, alanine-scanning to evaluate the role of the side chains and single-point substitutions at the critical positions. The binding affinities of the synthetic peptides were measured in a competitive binding assay using recombinant human LSD1-CoREST complex and the histone H3 mono-methylated K4 peptide as substrate. When possible, the three-dimensional crystal structures of the LSD1-CoREST-peptide complexes were determined. The conformational propensities of the unbound peptide enSTDbles were probed by molecular dynamics and finally, the *in vitro* efficacy of selected peptides were examined in cell-based assays.

2.2.1. Synthesis of SNAG-like peptides

Solid-Phase Peptide Synthesis (**SPPS**) was used to synthesise the truncated Snail-1 N-terminal domain sequences.[222] SPPS is a technique based on the sequential addition of amino acids protected at the side chain and α-amino group to a polymeric insoluble matrix.

The synthesis requires:

I. **loading/attaching** the first amino acid (from the C-terminal end) onto the solid support;
II. **deprotection** of the N-α protective group from the first amino acid;
III. **coupling** reaction between the first amino acid and α-carboxyl of a second amino acid with formation of the peptide bond;
IV. **deprotection** of the N-α protective group of the second amino acid;
V. **cleavage** of the peptide from the resin (after the desired number of coupling/deprotection cycles) when the peptide is released from the solid support;

The general protocol for SPPS synthesis of a peptide bearing a C-terminal amide is illustrated in Figure 2.2.

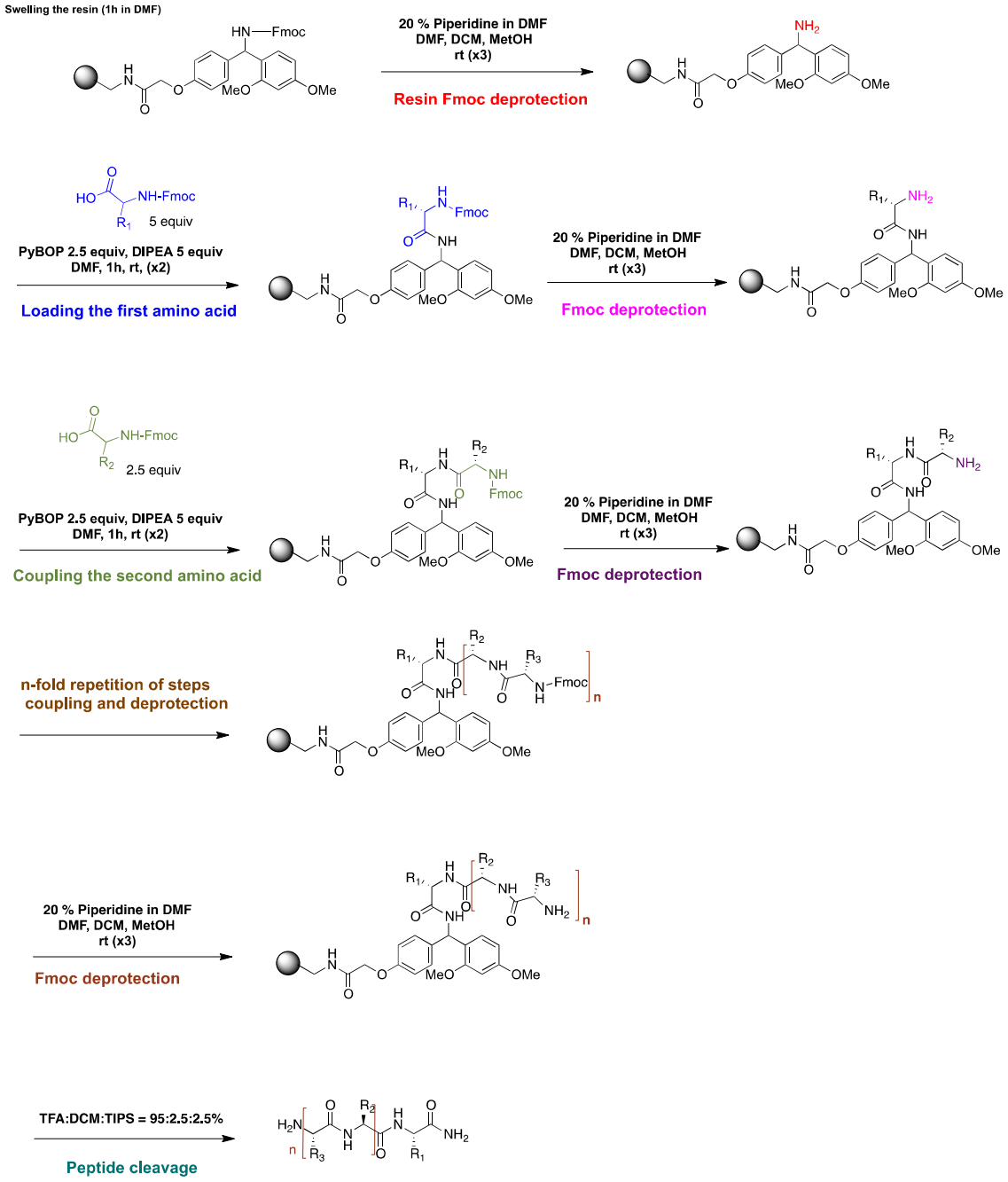

Figure 2.2: General procedure for SPPS using Rink Amide AM resin.

In SPPS, the peptide is asSTDbled from the C-terminal end to the N-terminal end with the α-carboxyl group of the last amino acid of the sequence anchored to the solid support. The use of a solid support is the main advantage of this technique as it enables the complete synthesis in a single reactor and facilitates the isolation of the product after each step (from excess of reagents or by-products). This results in reduced manipulation and waste material, together with a significant reduction of working times as the procedure can be automated.[223] A limitation of the SPPS is the possible synthesis of incomplete sequences (missing one or more residues or synthesis of truncated sequences) in addition to the correct one. As such side products have similar characteristics to the desired peptide the resulting purification can be difficult.

2.2.2. Loading step

The loading consists of the anchorage of the first amino acid to the solid support. The procedures for this critical step are chosen according to the resin linker used.[222,223]

The solid support for solid-phase consists of small beads of polystyrene (PS) copolymerized with 1% m-divinylbenzene or polyacrylamide. Other resins also contain up to 70% polyethylene glycol (PEG) attached through an ether link to the polymer. These materials swell abundantly in non-protic polar solvents such as *N*,*N*-dimethylformamide (DMF) and *N*-methyl-2-pyrrolidone (NMP) reaching a volume equal to 10 times the initial one.[224] Prior to the loading step, the resin is swollen in DMF for 1 h with constant agitation. Properly swollen resin allows for rapid diffusion of the reactants inside the granules and accommodation of the growing peptide chains.

The beads are derivatised with a wide variety of linkers and in this project the following types were used:

- **Wang resin**, possessing a hydroxybenzyl linker, which gives C-terminal acidic peptides (Figure 2.3, A);
- **Rink amide AM** and **NovaPEG rink amide** resin, possessing a trialkoxybenzhydrylamine linker, which produces C-terminal amide peptides (Figure 2.3 B-C).

When using Wang resin, the first amino acid is loaded through esterification of the acidic group of the C-terminal amino acid and the resins' alcohol. Specifically, in the peptide **PRSFLV**-$_{COOH}$ (**2.8,** Figure 2.11) the first amino acid Valine was loaded via symmetric anhydride formation, which involves two steps:

1) Formation of the symmetric anhydride with *N*,*N*'-diisopropylcarbodiimide (DIC) (Figure 2.4 A) in dichloromethane (DCM).
The mechanism involves the formation first of an *O*-acylurea intermediate (Scheme 2.1 1a-b). Next a further carboxylic acid molecule (Scheme 2.1 1c) interacts with the intermediate, generating the highly reactive symmetric anhydride and the soluble *N, N'*-diisopropylurea.
2) Esterification of the symmetric anhydride with 4-dimethylaminopyridine (DMAP), (Figure 2.4 B) with the hydroxyl of Wang resin linker.

The newly synthesized anhydride is quickly transferred to the reactor vessel that contains the resin. Here the anhydride (acyl donor) acetylates DMAP, forming an acylpyridinium cation (Scheme 2.1, 2a-b). The alcohol reacts with acetylated DMAP to form an ester (Scheme 2.1, 2b). The acetate from the anhydride acts as a base and removes the proton from the alcohol that subsequently functions as a nucleophile, forming a covalent bond with the acetyl group (Scheme 2.1, 2c). The acetyl on DMAP is then cleaved to regenerate the catalyst and newly formed ester (Scheme 2.1, 2d). In contrast, using Rink Amide AM, which provides amide-terminal peptides, the anchorage of the first amino acid to the resin beads is performed in the same way as the coupling step (see below), using an excess of reagents.

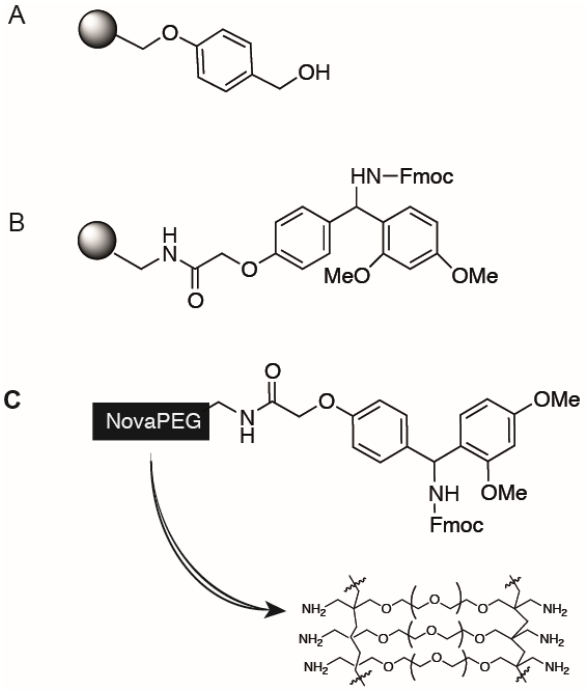

Figure 2.3: Structure of solid supports used in this project.

(A) Wang Resin; **(B)** Rink amide resin; **(C)** NovaPEG Rink amide resin and detailed structure of the PEG polymer.

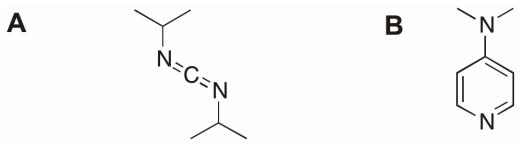

Figure 2.4: Structures of DIC and DMAP.

(A) DIC *N*,*N*'-Diisopropylcarbodiimide; **(B) DMAP**, *N*,*N*-4-Dimethylaminopyridine.

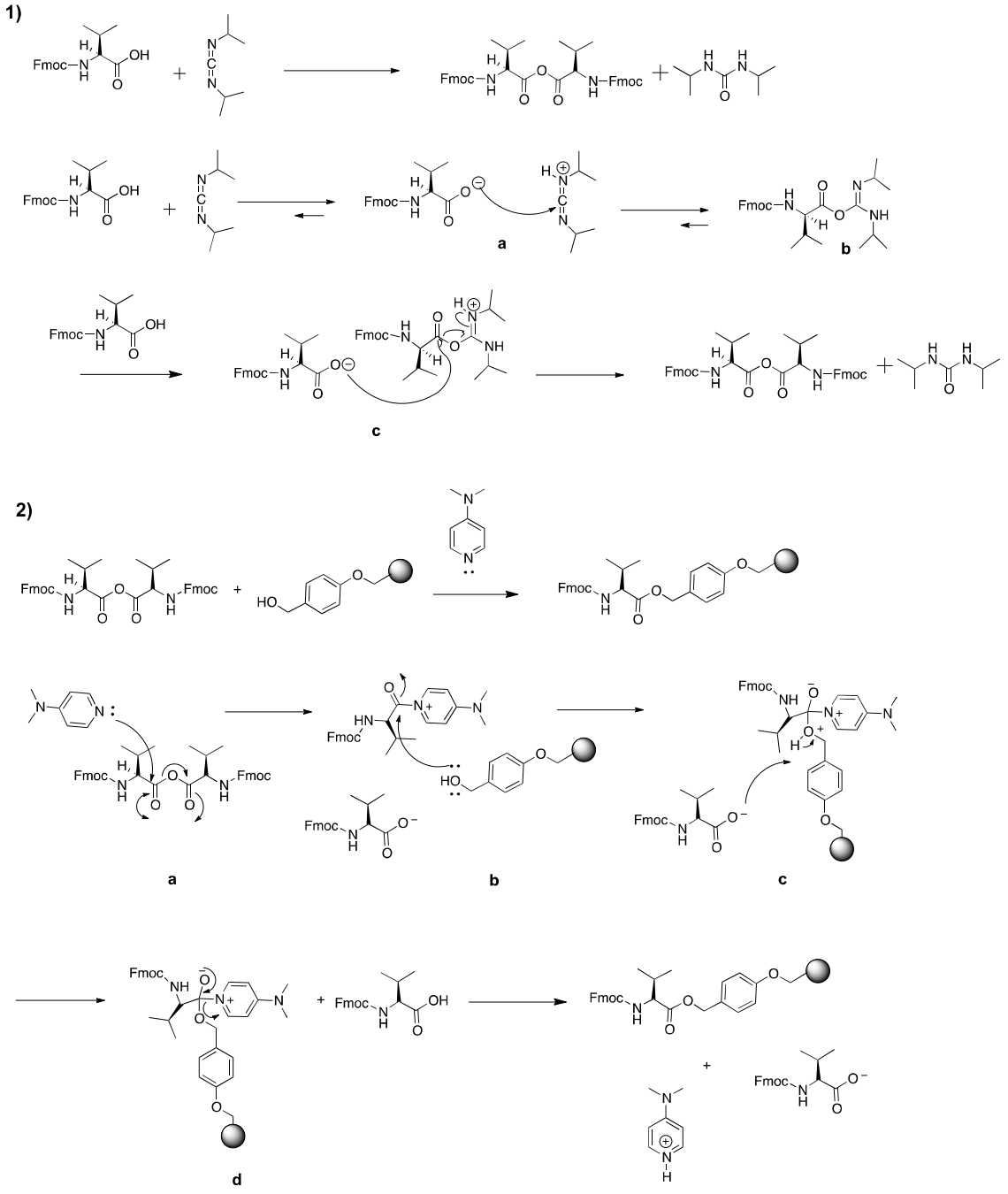

Scheme 2.1: Mechanism of Wang resin loading steps.

1. Symmetrical anhydride formation; **2.** DMAP esterification.

2.2.3. Fmoc-deprotection step

In SPPS, the protecting groups are either “permanent” or “temporary”. The “permanent” groups are removed only after the peptide is asSTDbled while the “temporary” ones are removed at intermediate stages.

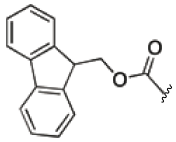

Figure 2.5: Structure of Fmoc protecting group.

During the synthesis, the removal of the N-α “temporary” protective group cannot affect the stability of the side chain (“permanent” protecting groups). The N-α protection used in this project is 9-fluorenylmethyloxycarbonyl (Fmoc, Figure 2.5), which is cleaved with mildly basic conditions and specifically 20% (v/v) of piperidine in DMF. The amino acid side chain protecting groups, such as *tert*-butyloxycarbonyl (Boc) and benzyl protecting group are all acid labile and removed at the end of the synthesis.

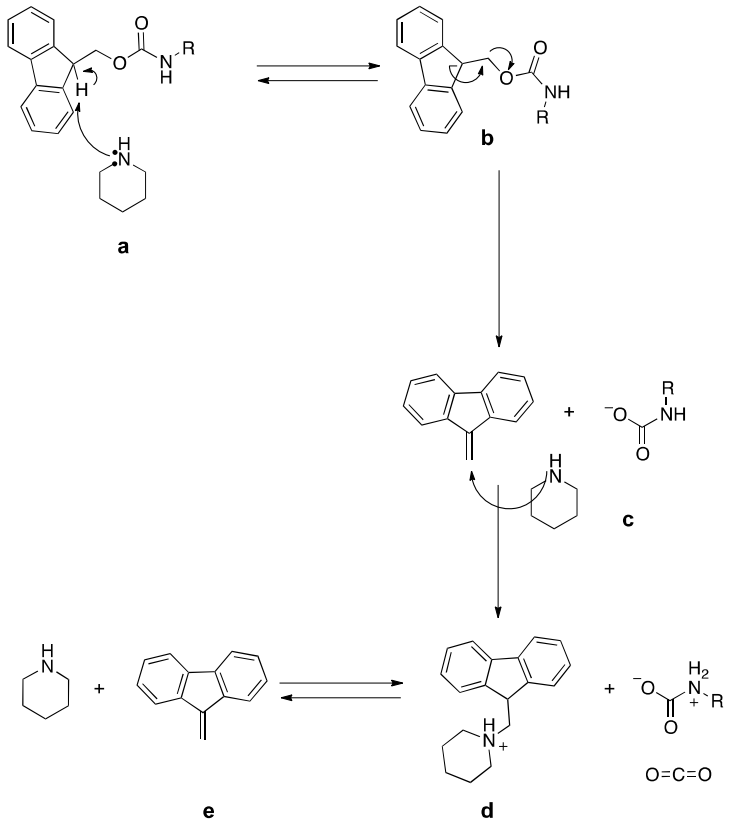

Scheme 2.2: Mechanism of Fmoc deprotection with piperidine.

The Fmoc deprotection mechanism involves the formation of dibenzocyclopentadienide by proton abstraction of piperidine (Scheme 2.2, a-b). The elimination reaction gives dibenzofulvene (Scheme 2.2, c) that is trapped by the excess of piperidine. The generated carbamic acid spontaneously decarboxylates and gives the N-terminal free amine (Scheme 2.2, d). To ensure the complete deprotection, 3 cycles of Fmoc deprotection were performed: one of 10 min and two of 5 min each, followed by multiple washes with DMF, DCM and MeOH in sequence, to remove side products and reagent excesses.

2.2.4. Coupling step

Chain elongation in SPPS occurs by condensation between the N-terminal end of the first anchored amino acid (to the resin or to another amino acid) and the C-terminal of a new one, forming an amide bond. All couplings were performed for 45 min with 2.5 equiv. (relative to resin loading) of coupling reagent, benzotriazo-1-yl-oxytripyrrolidinophosphonium hexafluorophosphate (PyBOP®) and 5 equiv. (relative to resin loading) of Hünig's base (DIPEA, *N*,*N*-Diisopropylethylamine). When using Rink amide AM resin, the first coupling was performed with doubled amount of equivalents of coupling reagents and to improve yields, the coupling step was repeated twice for each amino acid. The general coupling mechanism with PyBOP® proceeds as shown in the Scheme 2.3.

PyBOP® is a hydroxybenzotriazole-based phosphonium salt that reacts with the deprotonated acid (deprotonated by DIPEA) to generate an activated acylphosphonium specie (Scheme 2.3, a-b) and hydroxybenzotriazole (HOBt) (Scheme 2.3, c). Thereafter, HOBt reacts with the activated acid to produce a reactive benzotriazole (Bt) ester that undergoes aminolysis (Scheme 2.3, c-d) and formation of the amide bond. The excess of reagents is next removed at the end of coupling with repeated solvent washes (DMF, DCM).

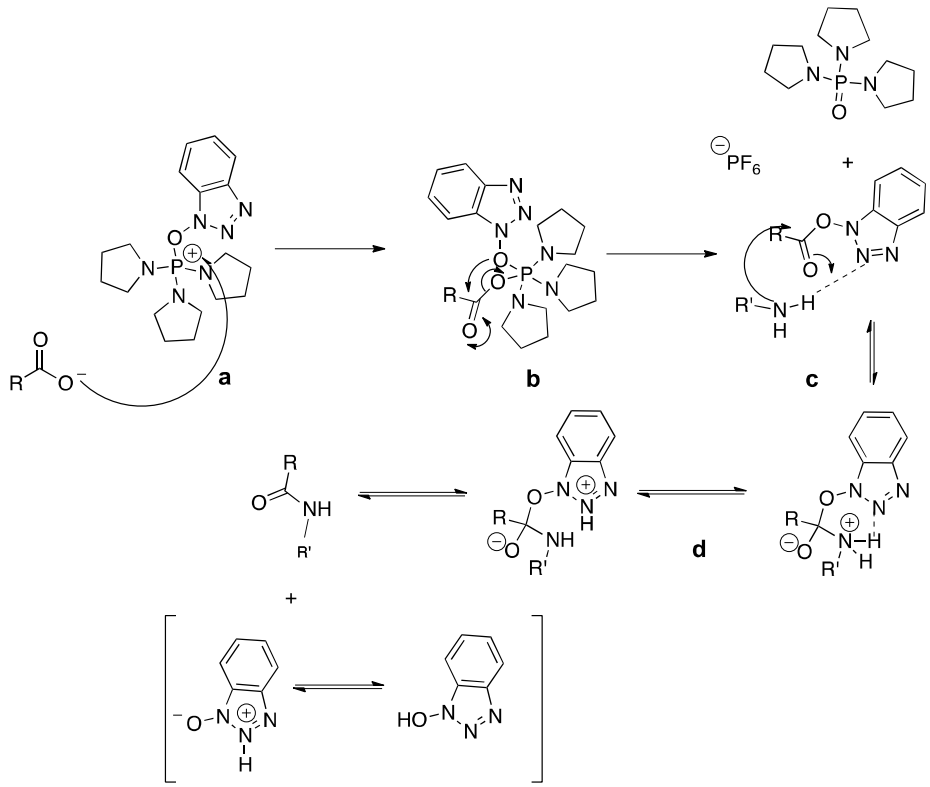

Scheme 2.3: Mechanism of coupling reaction using PyBOP®.

2.2.5. Cleavage step

After chain elongation, the peptide is released from the resin with the concurrent removal of the amino acid side chain protecting groups. This is achieved by employing a cleavage cocktail composed of strong acids and other components such as scavengers. The deprotection of the side chains with highly acidic conditions generates highly reactive species (such as carbocations), which can cause covalent modifications to susceptible unprotected residues.[225] The use in the cleavage cocktail of nucleophilic reagents, known as scavengers (reagents which have similar chemical properties to those of the species to be protected), together with the TFA (trifluoroacetic acid), greatly reduces such unwanted side reactions.

The composition of the cleavage cocktail depends on the amino acids present in the sequence and the type of protecting groups used for side chains protection. In the present work, we used the following side chain protecting groups: **Pbf** for Arg, **Trt** for Asn, Gln and His, **O-*t*Bu** for Asp and Glu, **Boc** for Lys and ***t*-Bu** for Ser, Thr and Tyr. Triisopropylsilane (TIPS) was used as carbocation scavenger for the acid deblocking of

side chain (Figure 2.6) and specifically a solution of TFA/TIPS/H_2O = 95 : 2.5 : 2.5.

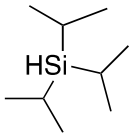

Figure 2.6: Structure of triisopropylsilane (TIPS).

2.2.6. Monitoring coupling and deprotection steps

Coupling and deprotection steps were monitored using Kaiser (or ninhydrin test) and chloranil test. [226–228] The ninhydrin test is a quantitative test that detects the presence of free primary amine groups by a reaction that gives a dark blue colour. If the couplings involved secondary amines, a chloranil test was used instead. This colorimetric test is based on the formation of dialkylaminovinyl derivatives of chloranil (tetrachloro-1,4-benzoquinone). When unprotected secondary amines are present, the beads acquire a dark green colour after heating.

2.2.7. Overcoming difficult sequences

During the elongation of the peptides with sequences **ARAFAA**, **LRSFLV**, **PKSFLV**, **PRLFLV**, **PLSFLV**, **PRAAAA** and longer amino acids (above 8 amino acids residues), we observed shrinkage of resin volume associated with difficult or incomplete coupling/deprotection steps. These phenomena were indicative that aggregation had occurred. In fact, along the synthesis, the amino acids interact via hydrogen bond formation: growing peptides acquire a β-sheet conformation bringing together chains and acting as supplementary cross-linkers between the growing peptides.[229] This makes it difficult for reagents to penetrate inside the beads and access the reactive groups. All the peptides mentioned contain Ala, Leu and Val amino acids that are known to have a higher propensity for aggregation.[224,229] To overcome this issue, we first used a *low loading* (LL) Rink amide AM resin (loading 0.13 mmol/g). Such resin possesses a smaller number of substitutions, which reduce the potential

hindrance generated by growing peptides attached to beads and consequently, the chance of inter-chain interactions. However, for longer sequences the use of LL resin was not advantageous as we still faced aggregation-related synthetic problems. To overcome this, we employed NovaPEG resin (Figure 2.3 C), which is exclusively composed of PEG units. Being amphiphilic in nature, this material has better swelling and mechanical properties and it is stable in a variety of solvents, a feature that facilitates the polymer handling during the reaction steps and washes.[224] In addition, for the synthesis of difficult sequences we employed a resin-capping procedure after systematic double coupling. Such step involves the acetylation (capping) of unreacted amino acids by reacting the resin for 10 min with a solution composed of 9:1 pyridine:acetic acid.

2.3. Enzymatic and structural evaluation of the SNAG-like derivatives binding to LSD1

The synthesis of SNAG-derivatives was followed up with the assessment of enzymatic activity performed by our collaborator Prof. Andrea Mattevi and his group at the Department of Biology and Biotechnology "Lazzaro Spallanzani" at the University of Pavia (Italy). They also carried out soaking experiments with the peptides and LSD1. When suitable diffraction quality crystals were obtained, X-ray structure determination of the protein-peptide ligand was done to gain insight into the binding interactions. The results from the enzymatic evaluation iteratively guided our synthesis and the succeeding modifications to the initial SNAG sequence. The peptides potency was assessed with an enzymatic assay monitoring hydrogen peroxide formation (a side product of LSD1 activity). The assay consisted in incubating recombinant LSD1-CoREST (residues 308-440, 1 μM), with varying peptide ligands (0-200 μM) and dimethylated H3K4 peptide substrate (2-30 μM). The absorbance changes were monitored at 515 nm and initial velocity values were fitted to equations describing competitive, uncompetitive and noncompetitive inhibition patterns. In all cases, the best fit was obtained with the equation describing a competitive inhibition and data are reported in the figures below as $K_i \pm$ STDV (n=5).

Table 2.1: Summary of SNAG-like peptides activity

	Sequence	K_i (µM ± STD, n=5)
2.1	**PRSF**	> 200
2.2	**PRSFLV**	28.4 ± 4.8
2.3	**PRSFLVRK**	2.0 ± 3.5
2.4	**PRSFLVRKP**	0.1 ± 59
2.5	**RSFLV**	> 200
2.6	**PRSFL**	120.0 ± 20
2.7	**Acetyl-PRSFLV**	48.0 ± 13.0
2.8	**PRSFLV$_{(COOH)}$**	60.2 ± 12.7
2.9	**ARSFLV**	157 ± 16.5
2.10	**PASFLV**	> 200
2.11	**PRAFLV**	6.4 ± 1.3
2.12	**PRSALV**	71.4 ± 15.1
2.13	**PRSFAV**	18.0 ± 5.4
2.14	**PRSFLA**	44.4 ± 5.5
2.15	**PLSFLV**	55.0 ± 11.0
2.16	**PKSFLV**	49.6 ± 8.2

2.17	**PRSMLV**	3.0 ± 2.7
2.18	**PRSYLV**	> 200
2.19	**PRLYLV**	29.1 ± 3.9
2.20	**PRSK(Cbz)LV**	12.4 ± 4.3
2.21	**LRSK(Cbz)LV**	6.6 ± 1.5
2.22	**PRSK(me2)LV**	19.7 ± 2.4
2.23	**PRSK(me2)VKRKP**	3.3 ± 0.8
2.24	**PRSK(me2)L**	> 200
2.25	**PRSFAA**	10.7 ± 1.1
2.26	**ARAFAA**	> 200
2.27	**PRAAAA**	27.7 ± 4.0
2.28	**PRSFQTV**	8.0 ± 0.32

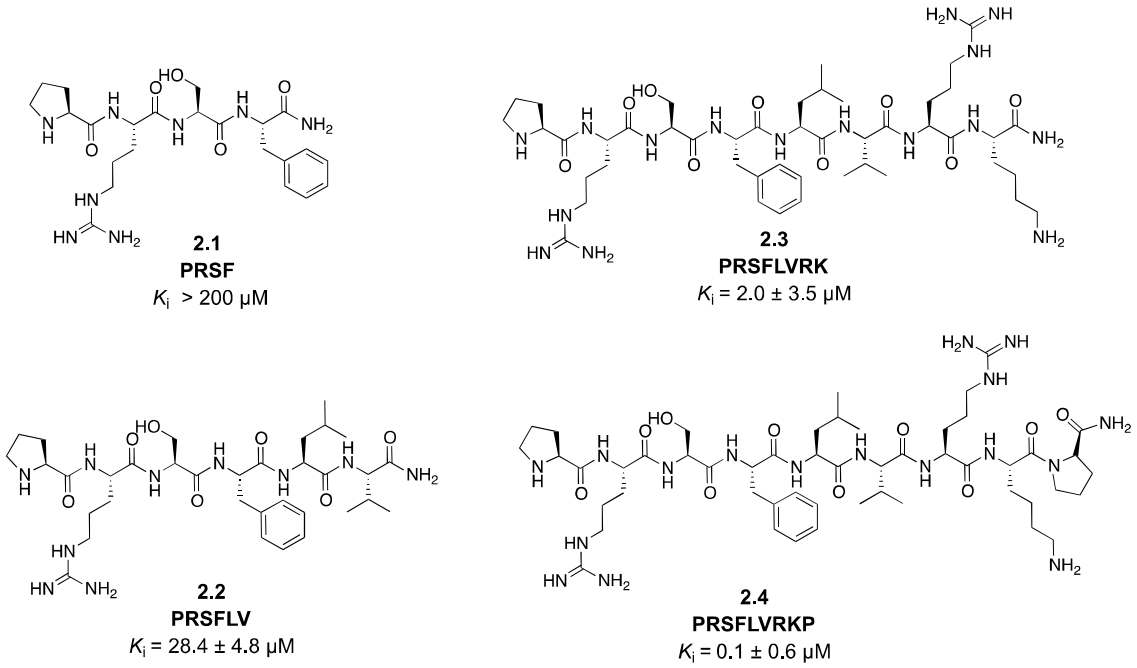

Figure 2.7: Structure of the first synthesised SNAG-like peptides.

K_i are reported as µM ± STDV (n = 5).

We first explored the activity of the 4-mer, 6-mer, 9-mer and 10-mer sequences corresponding to the N-terminal Snail-1 (Figure 2.7). According to the literature,[104,110] the first 4 residues (residues 1–4) of Snail-1 adopt a helical turn reSTDbling the histone 3 substrate and therefore, these could be sufficient for LSD1 binding. However, the tetrapeptide **PRSF** by itself (**2.1**) was found inactive (K_i > 150 µM), whereas the 6-amino peptide (**2.2**) exhibited a stronger binding (K_i of 28 µM). The sequence **PRSFLV** (**2.2)**, resulted a weaker binder compared to the 9-mer **2.4**, suggesting that residues 7-9 (thought non-essential) contribute actively to bind the LSD1 catalytic site. The 9-mer **PRSFLVRKP** contains most of the conserved N-terminal residues of Snail-1 and revealed a strong binding affinity for LSD1-CoREST. Albeit the high activity, the increased length of 9 amino acids made it less appealing than the 6-mer **PRSFLV** for further exploration of structure-activity relationships.

Crystallographic structures revealed that **PRSFLV** (PDB: 3ZMT) binds to the catalytic pocket of LSD1, indeed with an identical fashion to the first six amino acids of Snail-1. As shown in Figure 2.8, the **PRSFLV** sequence in complex with LSD1-CoREST perfectly overlaps the N-terminal end of Snail-1: the first four amino acids, retain the helical conformation with all backbone atoms bound in a solvent-inaccessible positions.

Furthermore, the side chains are mostly inaccessible to solvent with the exception of Arg2. In particular, Pro1 is fully encapsulated by the protein catalytic pocket. This is fully consistent with the observation that truncation of Pro1 drastically reduces activity, highlighting the significant almost essential contributions of this residue (see below).
Longer truncated Snail-1 peptides did not seem to promote a greater inhibition compared to the 6-mer or 9-mer, suggesting that LSD1-CoREST can effectively bind the 6-amino acid Snail-1 sequence, whose helical conformation and N-terminal group are snugly embedded by the active site cleft.

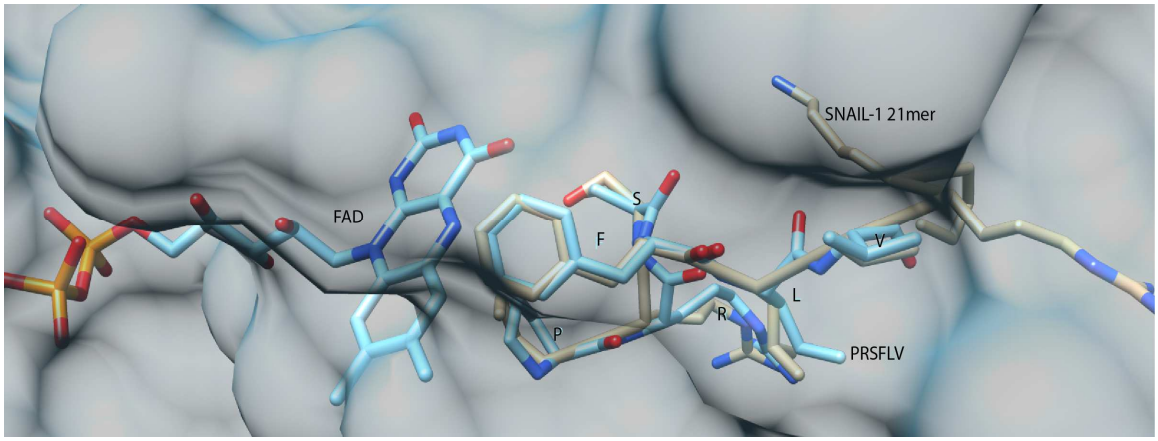

Figure 2.8: X-ray crystal structure of Snail-1 N-terminal 21-mer (light brown, PDB: 2Y48) and PRSFLV (cyan, PDB: 3ZMT) bound to LSD1-CoREST.
Nitrogen atoms are shown in blue and oxygen atoms in red. The amino acid side chains of the peptides adopt the same conformation. Amino acids in **PRSFLV** are labelled with their one letter code.

Intriguingly, the truncated N-terminal Snail-1 **PRSFLV** sequence and H3 bind to LSD1-CoREST in a helical conformation. Hence, the question whether peptides exist in nature already in this conformation or are shaped into secondary structure only after binding with the enzyme was raised. To address this inquiry, circular dichroism spectroscopy on four peptides corresponding to H3 21-mer, INSM1 20-mer, Snail-1 20-mer, and Snail-1 9-mer was carried out at the University of Pavia. The data, supported at a later time by computational studies, show that all of the peptides fold into their secondary structure only upon binding to LSD1.

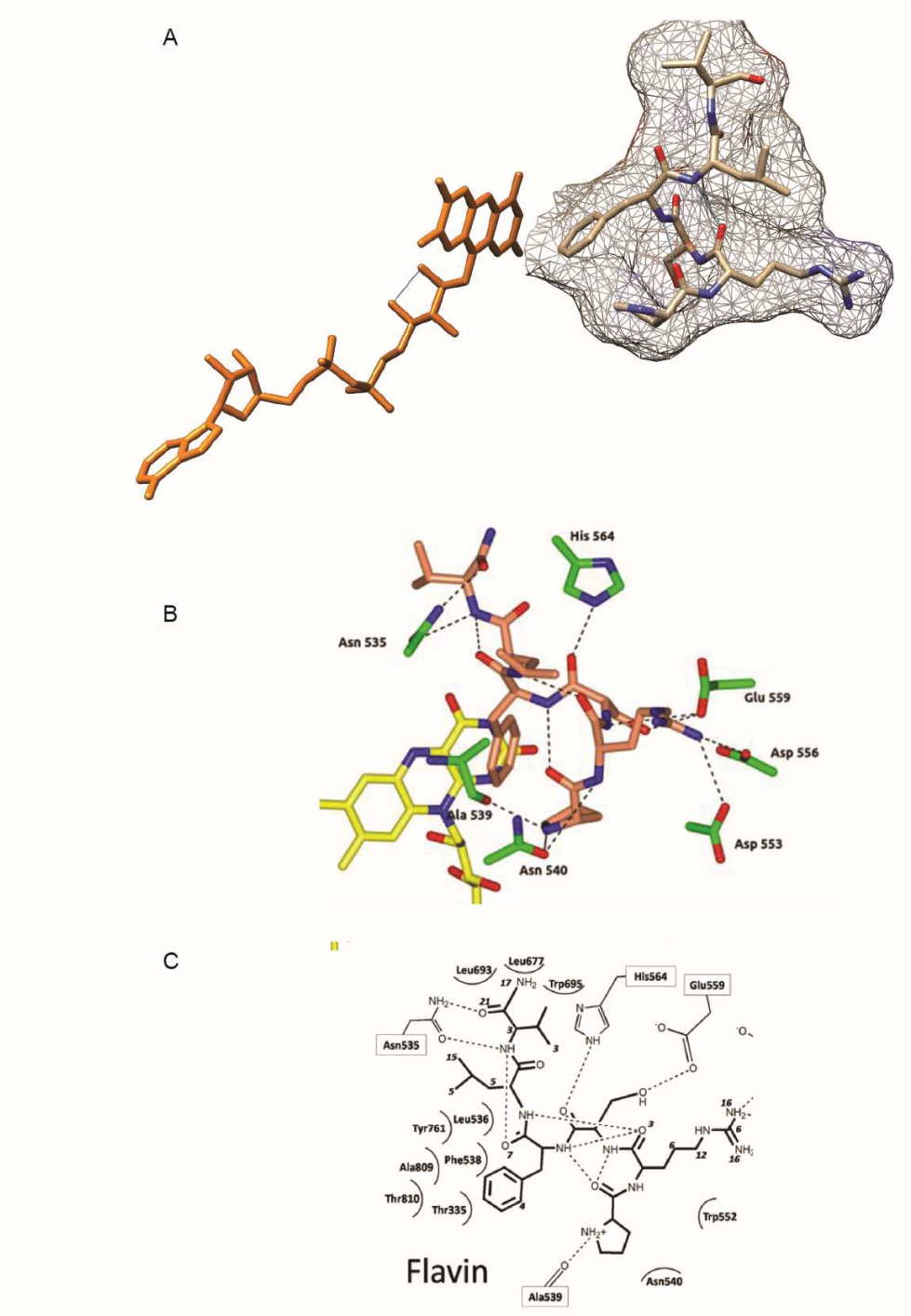

Figure 2.9: X-ray crystal structure of PRSFLV peptide bound to the LSD1 catalytic site.

(**A**) Electron density map (contoured at the 1.2σ level) of **PRSFLV** in the catalytic site calculated previous to its inclusion (**B**) Three-dimensional view of **PRSFLV** (the N-terminal hexapeptide of human Snail-1). Protein carbons are shown in green, FAD carbons in yellow, and peptide carbons in brown. H-bonds are shown as dashed lines (**C**) Schematic representation of the peptide-protein interactions. The atomic accessible surface areas are shown. Adapted from Tortorici *et al.*[214]

2.3.2. Peptide length and influence of N- and C-terminal functional groups

Further reductions in the number of amino acids to the active minimum length of **PRSFLV** scaffold were performed, to pursue the initial goal of reducing the molecular weight necessary for efficient reversible inhibition of LSD1. The peptide comprising the N-terminal 5-amino acids was found to retain binding but only with relatively low affinity (K_i of 120 µM). In contrast, **RSFLV** (**2.5**, Figure 2.10) turned out to be almost devoid of activity.

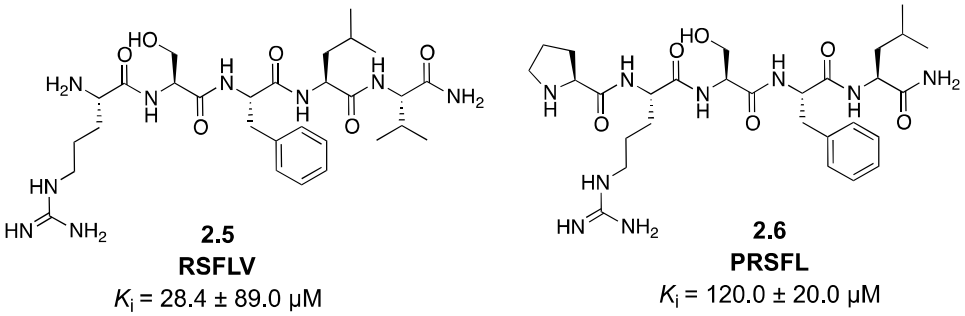

Figure 2.10: Length determination of active SNAG-derived peptides.
K_i are reported as µM ± STDV (n = 5).

Next, the C-terminal and N-terminal "states" were analysed to measure the importance of the free amine N-terminus and C-terminus amide. To this end, the activities of two **PRSFLV-**modified peptides **(2.7** and **2.8**, Figure 2.11) bearing respectively an acetylated N-terminus **(Acetyl- PRSFLV)** and a free C-terminal acid (**PRSFLV-COOH)** were prepared. Both **2.7** and **2.8** turned out to be weak inhibitors of LSD1 (K_i = 48.0 µM and 60.0 µM respectively)compared to **PRSFLV**.

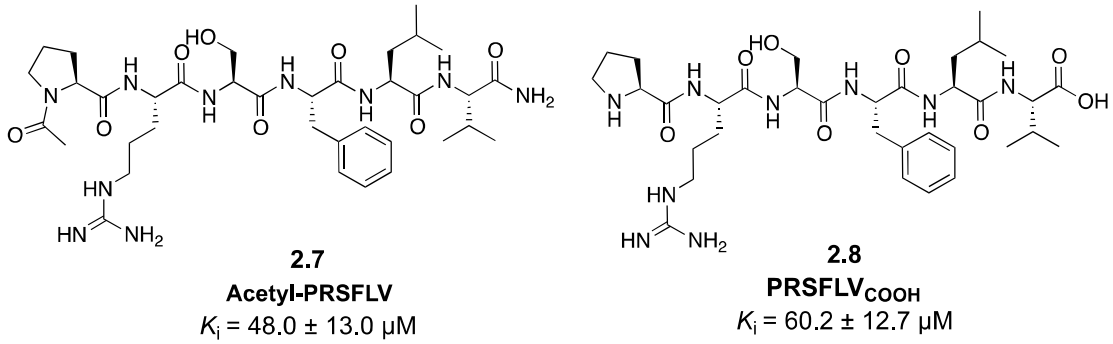

Figure 2.11: Modifications at the N- and C-termini of PRSFLV peptide.
K_i are reported as value ± STDV.

The identification of a minimal peptide length for efficient binding (μM range) guided us to ask the next logical questions: which side chains are important for peptide binding in the core of the cleft? Are there strict sequence restraints?

Alanine-scan mutagenesis allowed the evaluation of each individual residue contribution in the **PRSFLV** peptide's bioactivity. Each amino acid was substituted with alanine, the simplest residue after glycine, used in this technique given its small size and chemical stability.[230]

From the results achieved, Pro1 substitution with Ala1 was unfavourable for binding (**2.9**, Figure 2.12). Proline acts as an alpha helix initiator in protein secondary structure and can promote the helical turn of the bound sequence into the hydrophobic cleft of LSD1.[214] The observed crucial importance of Pro1 in our experiments substantiate the previous work of Saleque *et al.*,[219] where abrogation or Ala substitution of Pro1 in the SNAG-containing protein Gfi-1 (a protein that controls haematopoietic differentiation, Figure 2.1) resulted in protein inactivation.

The Ala substituted **PASFLV**, which lacks the polar residue Arg2 (**2.10**, Figure 2.12) was unable to bind LSD1, implying that polar residue in position 2 may establish favourable electrostatic interactions with the cluster of negatively charged residues in the LSD1 active site. The result was expected as all the related transcription factors and H3 present Arg in position 2 (Figure 2.1, A-B). In H3, Arg2 participates in intra-peptide hydrogen bonds with the carbonyl oxygens of Gly12, Gly13 and the side chain of Ser10. It also interacts with the carboxylate groups of Asp553, Asp556, and Glu379 of the LSD1 catalytic pocket.[110]

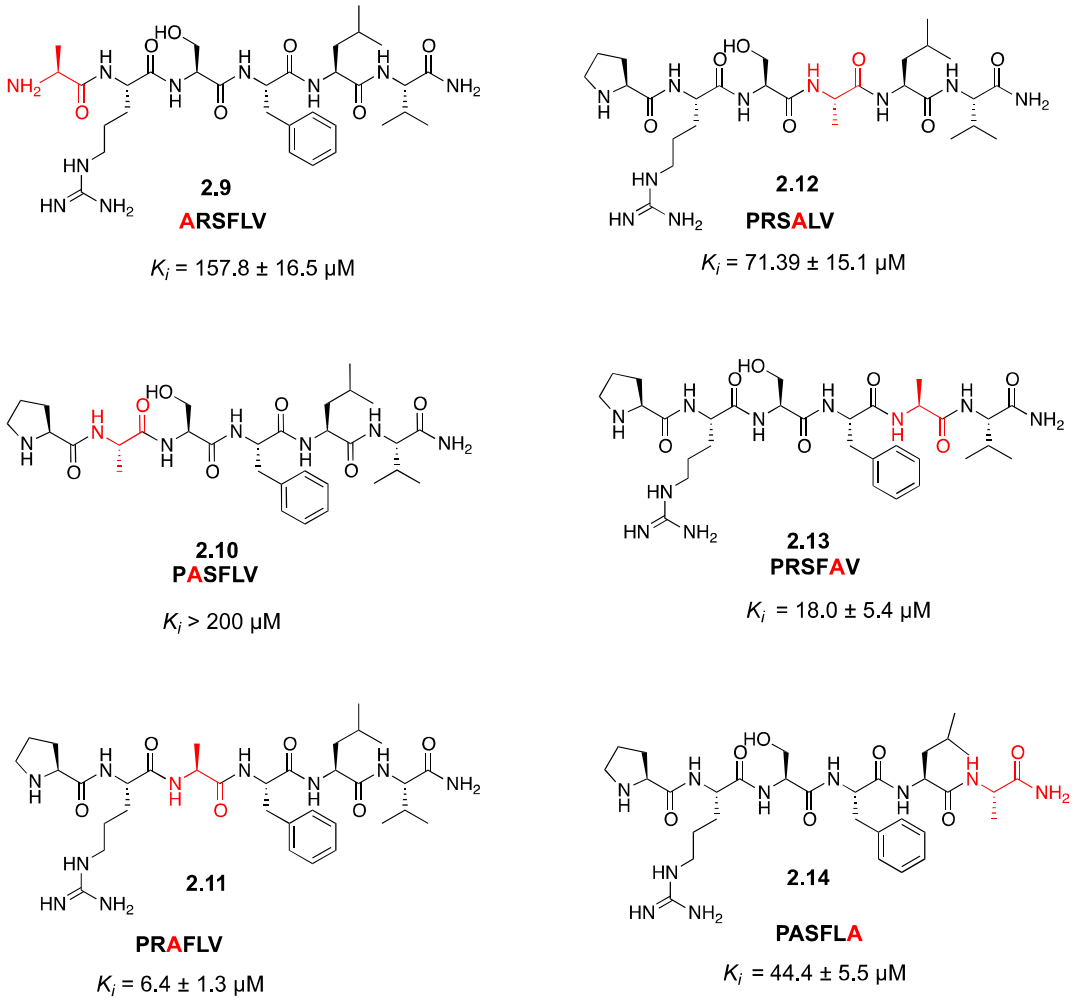

Figure 2.12: Ala-scanning on PRSFLV peptide.

The mutated positions on **PRSFLV** peptide are highlighted in red. K_i are reported as µM ± STDV (n = 5).

Reduced binding affinity has also been reported with an H3 peptide bearing methylated Arg2. Similarly to the H3 natural substrate, crystal structure analysis of the 6-mer **PRSFLV** revealed that the Arg2 side chain also interacts with a ring of Asp556 and Glu379 side chains in the catalytic site. Its aliphatic portion is involved in intra-peptide contacts with Leu5 and both events favour the sequence helical conformation.

To gain further insight on the importance of such position, we synthesised **PLSFLV** and **PKSFLV** (Figure 2.13), which have a hydrophobic residue and positively charged amino acid respectively, in position 2. Both the resulting compounds were less active than **PRSFLV** (K_i 55 and 49 µM, **2.15** and **2.16** Figure 2.13), further substantiating the importance of Arg2 presence.

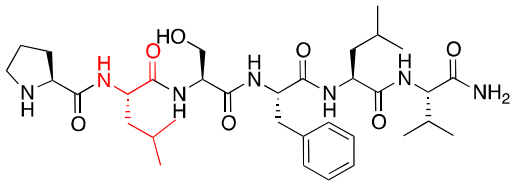

2.15

PLSFLV

K_i = 55.0 ± 11 μM

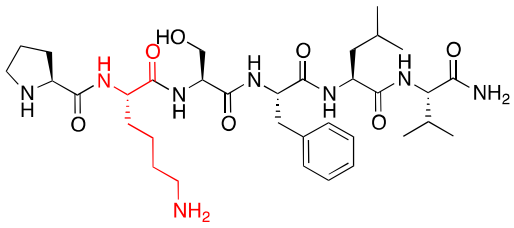

2.16

PKSFLV

K_i = 49.6 ± 8.2 μM

Figure 2.13: Side chain substitutions at the 2nd position of PRSFLV peptide.
K_i are reported as μM ± STDV (n = 5).

Collectively, these data indicate that the combination of conformational propensity, van der Waals interactions by the aliphatic groups and the "diffuse" positive charge of the guanidinium group, render Pro1-Arg2 crucial elements for efficient binding, which are selectively recognised by the active site cleft.

For **PLSFLV** and **PKSFLV** it was possible to obtain X-ray crystal structures (**PLSFLV**- PDB code: 3ZMV and **PKSFLV** PDB code: 3ZMU, Figure 2.14 and Figure 2.15 respectively).

Figure 2.14: X-ray crystal structure of SNAG-derived PLSFLV peptide bound to the LSD1 catalytic site.

Figure 2.15: X-ray crystal structure of SNAG-derived PKSFLV peptide bound to the LSD1 catalytic site.

Further analysis on **PLSFLV** peptide X-ray crystal structure revealed that this is also able to bind in an allosteric fashion to a different cleft of LSD1-CoREST (Figure 2.16).

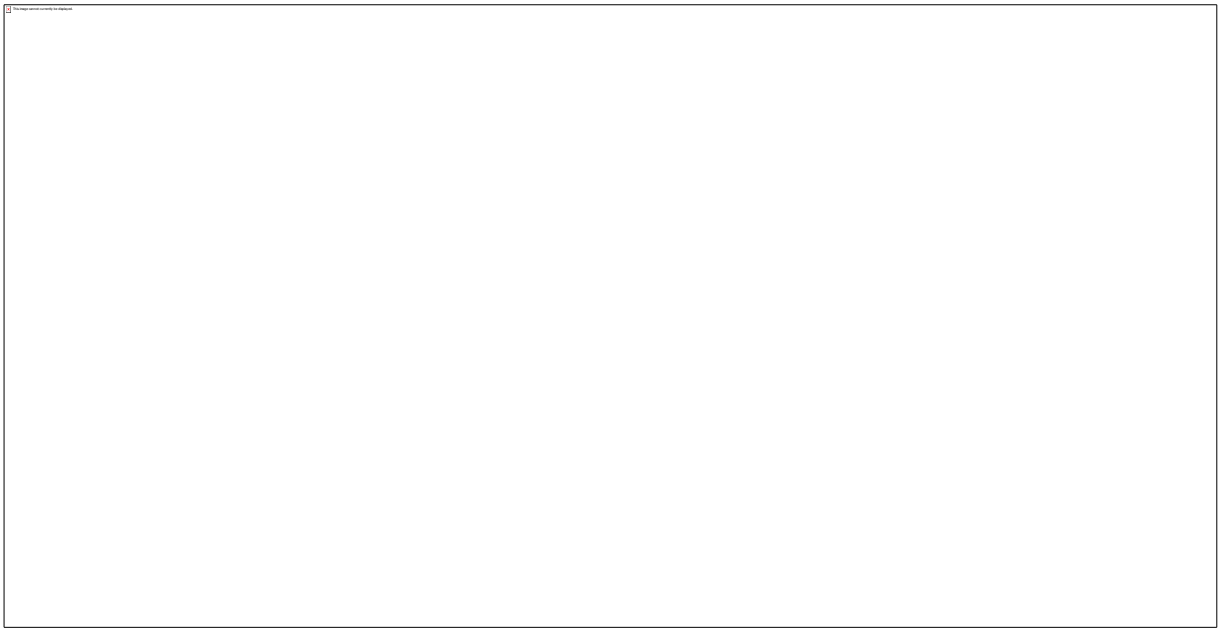

Figure 2.16: X-ray crystal structure of SNAG-derived PLSFLV peptide bound to LSD1 catalytic site and allosteric binding.

The peptide is bound to the catalytic site (circled in blue) and to a different cleft.

Based on this information, our collaborator Prof. Riccardo Baron and his group (University of Utah, Salt Lake City, Utah) explored other plausible druggable spaces in LSD1-CoREST. With computational studies and molecular dynamics simulation, five new possible binding regions were found (Figure 2.17).[231] These regions have a strong propensity for molecular binding and correspond to:

A. a region interfacing the SANT2/Tower domain (Figure 2.17 A);
B. a region interfacing SWIRM/AOL domain (Figure 2.17 B);
C. a region interfacing AOL/Tower interface (Figure 2.17 C);
D. a region encompassing the back of AOL domain (Figure 2.17 D);
E. a small pocket in the AOL domain (Figure 2.17 E);

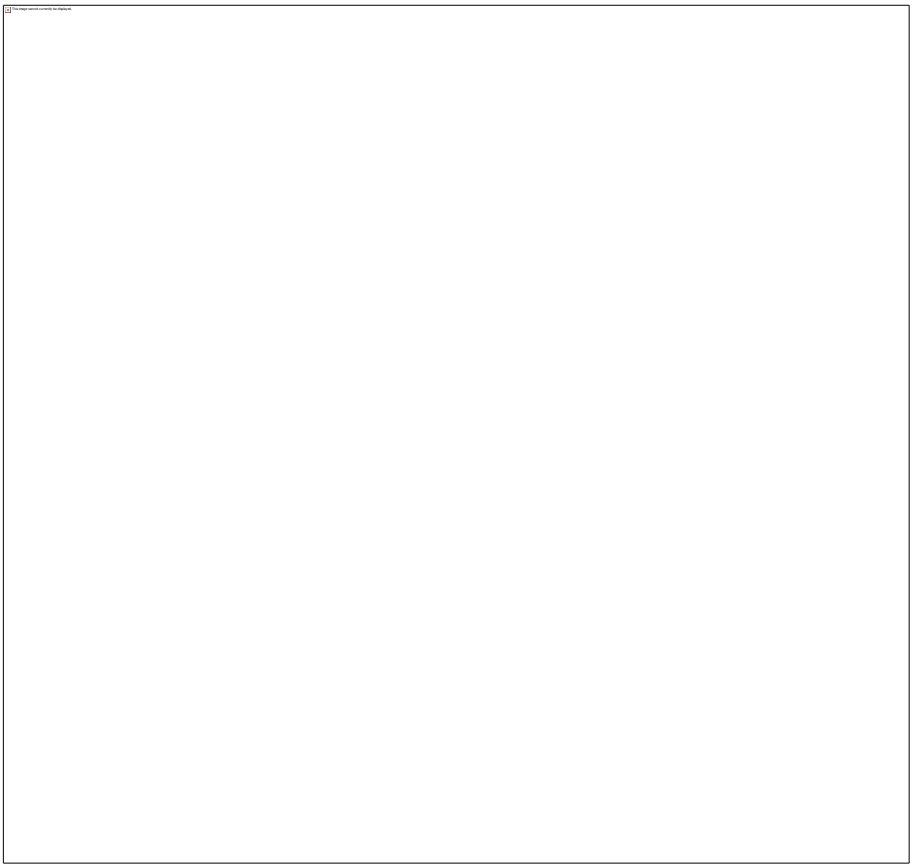

Figure 2.17: New druggable spaces of LSD1-CoREST.

These were highlighted using colored spheres and named based on their location: **SANT2/Tower interface (green, A)**, **AOL/Tower interface** (red, B), **SWIRM/AOL interface** (blue, C), **Peptide binding region** (yellow, D), and small **AOL pocket** (grey, E). LSD1 (orange), CoREST (cyan), and the H3-histone N-terminal tail (purple) are shown as cartoons **(B)** Table shows the residues of the new binding sites. Adapted from Robertson *et al.* [231]

In this context of extended potential binding sites, the peptide **PLSFLV** binds to the E region (Figure 2.17) and adopts an extended conformation enabling its backbone to interact with residues 317-323 of LSD1-CoREST (Figure 2.18), through hydrogen bonding. Phe4 and Val6 are also involved in van der Waals interactions with adjacent residues (Ala318, Thr319, Phe320 Leu329, Val747) of the LSD1 allosteric cleft.

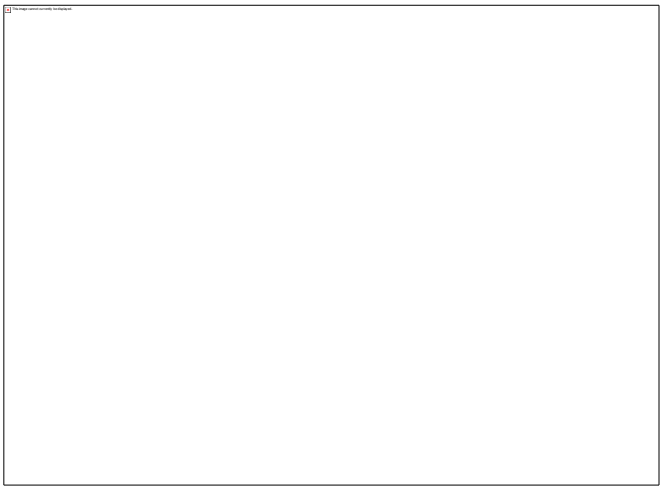

Figure 2.18: X-ray crystal structure of SNAG-derived PLSFLV peptide bound to the AOL small pocket. PLSFLV (Green) and LSD1 (brown) are highlighted (nitrogen atoms: blue; oxygen atoms: red) in the new LSD1-CoREST binding region (Figure 2.16, region D). The unbiased 2Fo-Fc electron density map (contoured at 1.2 σ level) was calculated prior to inclusion of the peptide in the refinement. The electron density of Pro-1 was not clear for Pro1 of the bound peptide was not visible in the electron density and thus not included in the model. See also Table 1 and Figure 8, region D. From Robertson *et al.* [231]

Differently from positions 1 and 2, positions 3-6 of **PRSFLV** are not as essential for binding as throughout our studies, the affinities to LSD1 were not critically influenced by the replacement at such positions with other residues.

The N-terminal alignment of Snail-1 with other transcription factors shows that the third position can accommodate various residues like Alanine (OVOL1) or Glycine (INSM1) (Figure 2.1 A). In addition, we reported that the mutation of Ser3 in **PRSFLV** was unable to affect the LSD1 suppression in the SNAG-derivative **PRAFLV** (**2.12,** K_i = 6.4 ± 1.3 µM, Figure 2.12).

In both Snail-1 and H3, the N-terminal 4th residue represents a critical amino acid for LSD1 activity: in H3 it normally accommodates lysine mono-methylated or di-methylated, whereas in Snail-1 wild type and truncated sequences, the phenyl ring of Phe4 points towards FAD, making direct contact with it. Accordingly, the substitution of Phe4 with Ala was disadvantageous for LSD1 inhibition (**PRSALV**, K_i = 71.4 ± 15.1 µM). Forneris *et al.*[110] reported a 30-fold increase in binding affinity for a H3 substrate bearing a methionine in position 4.

Based upon this observation, we synthesised **PRSMLV**, which showed similarly to the H3 modified peptide an improved binding affinity towards LSD1 (K_i of 3 µM). The

non-polar nature of methionine promotes possibly the interaction with FAD allowing a tighter binding to the demethylase.[110,214] Methionine was next substituted with the bulkier hydrophobic residue tryptophan in **PRSWLV**. The change was however unfavourable for binding (K_i >100 µM).

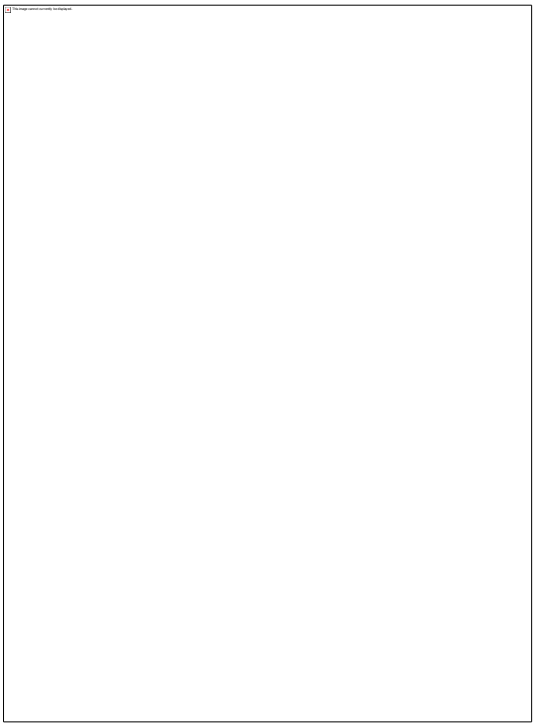

Figure 2.19: Side chain substitutions at the 4th position of PRSFLV peptide.
K_i are reported as µM ± STDV (n = 5).

As the 3rd position can accommodate different amino acids and the side chain of position 4 needs to establish interaction with the flavin ring, **PRLYLV** was synthesised next. This sequence possesses a Leu residue in position 3 (a hydrophobic residue like Ala) and in position 4 tyrosine. X-ray crystal structure analyses (PDB code: 3ZN1) revealed that like Phe4, the phenyl ring of Tyr points towards the FAD cofactor and the sequence showed relative affinity towards LSD1 (K_i 29 µM, **2.21** Figure 2.20).

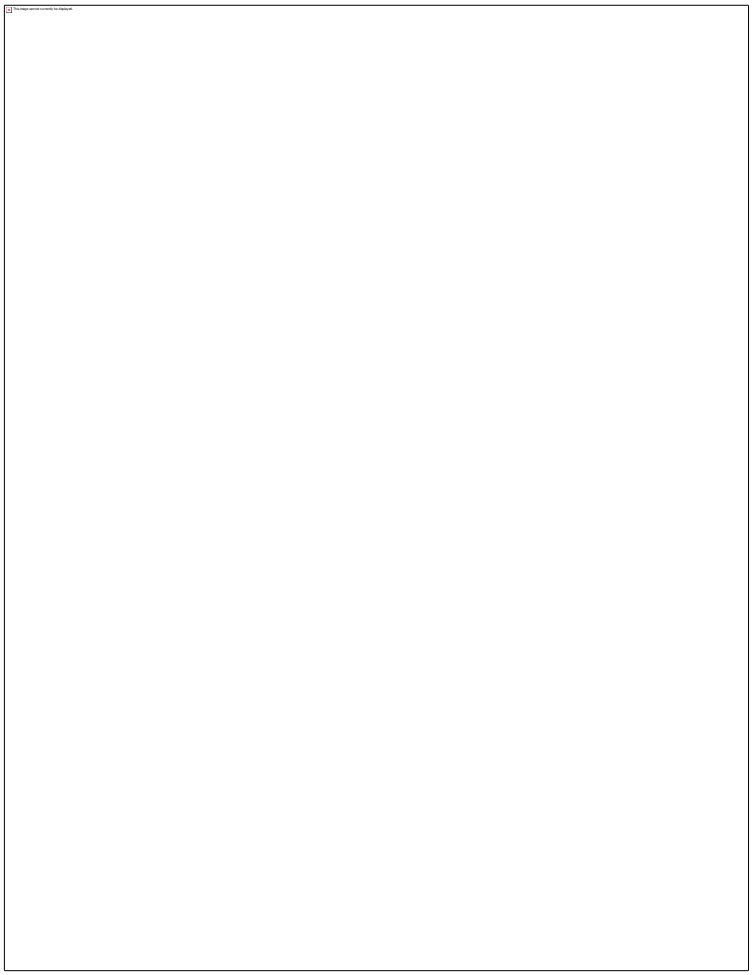

Figure 2.20: Side chains substitutions to the 3rd and 4th positions of PRSFLV peptide.

(A) Side chain similarities between Ala-Leu and Phe-Tyr; **(B) PRLYLV** structure.

K_i are reported as µM ± STDV (n = 5).

Figure 2.21: X-ray crystal structure of SNAG-derived PRLYLV peptide bound to LSD1 catalytic site.
The tyrosine residue in 4th position makes contact with Flavin ring similar to Phe4.

We next developed sequences with a longer side chain in position 4, in order to examine the effects of structures having a residue with higher propensity of interaction with FAD. For this purpose, we chose to replace the Phe4 of **PRSFLV** scaffold with the commercially available N-ε-Cbz-L-Lys, a lysine residue bearing a carboxybenzyl protecting group (Cbz) and prepared **PRSK(Cbz)LV**.

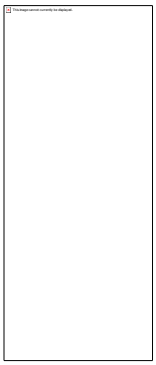

Figure 2.22: Chemical structure of carboxybenzyl (Cbz) protected lysine.

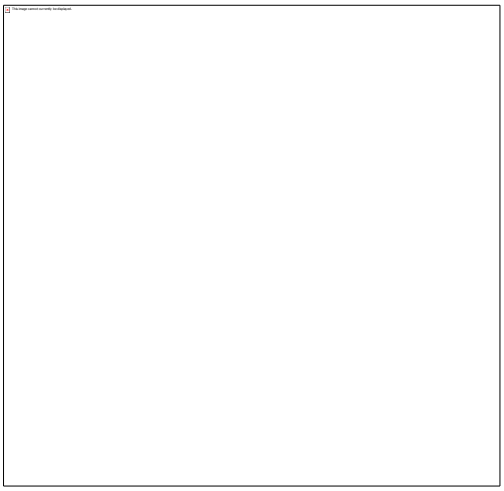

Figure 2.23: Side chain substitution at the 4th position of PRSFLV peptide with carboxybenzyl containing lysine.

K_i are reported as value ± STDV (n = 5).

The mutated sequence **PRSK(Cbz)LV** also proved to be a good inhibitor of LSD1 (K_i = 12.4 µM). To further evaluate the effects on the activity of the Cbz group, we synthesised **LRSK(Cbz)LV**. In that way, we would have gained a further insight if the improved activity generated by Cbz could balance the absence of Pro1. Such sequence showed a five-fold increase in inhibitory activity compared to **PRSFLV** peptide, balancing effectively the lack of Pro1.

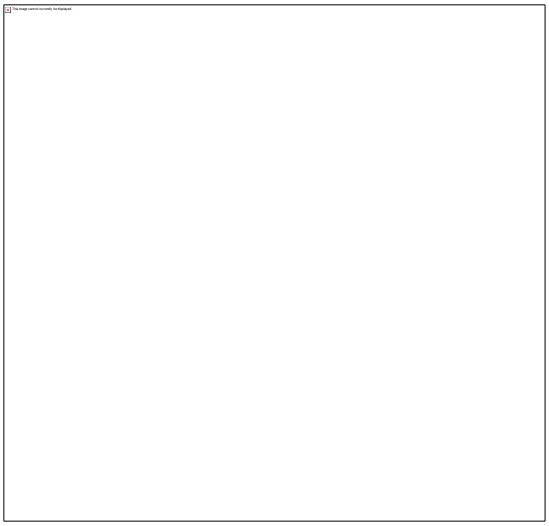

Figure 2.24: Side chain substitutions at the 1st and 4th positions of PRSFLV peptide.

K_i are reported as µM ± STDV (n = 5).

As Phe4 occupies the same position as the mono and di-methylated Lys4 in the natural substrate, we hypothesised that a peptide containing this modification in position 4th, could act as a substrate. Interestingly, the sequence **PRSK(me2)LV** instead of being a substrate, resulted in an effective LSD1 inhibitor with high affinity towards the enzyme (K_i = 19.7 ± 2.4 μM).

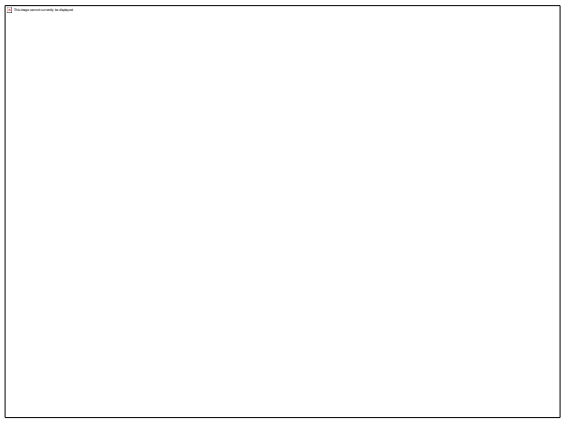

Figure 2.25: PRSFLV mutant possessing a di-methylated Lysine in 4th position.
K_i are reported as μM ± STDV (n = 5).

PRSK(me2)LV was also evaluated against **LSD2**, the human homologue of LSD1 and here it also acted as an inhibitor and not as substrate (K_i = 2.5 ± 0.4 μM). Intrigued by this result, we synthesised **PRSK(me2)LVRKP** as the unmethylated 9-mer of Snail-1 binds tightly to the LSD1 catalytic cleft and thus it was possible that the di-methylated 9-mer could act as an inhibitor. **PRSK(me2)L** sequences from the N-terminal of Snail-1 was also synthesised to prove whether the di-methylated lysine could improve the binding affinity towards the enzyme. Surprisingly the di-methylated 9-mer also acted as an inhibitor and not a substrate as expected, whereas the di-methylated 5-mer was inactive. This implies that the environment of H3 is fundamental for the demethylase activity of LSD1. Unfortunately no crystal structures of the di-methylated peptides were achieved.

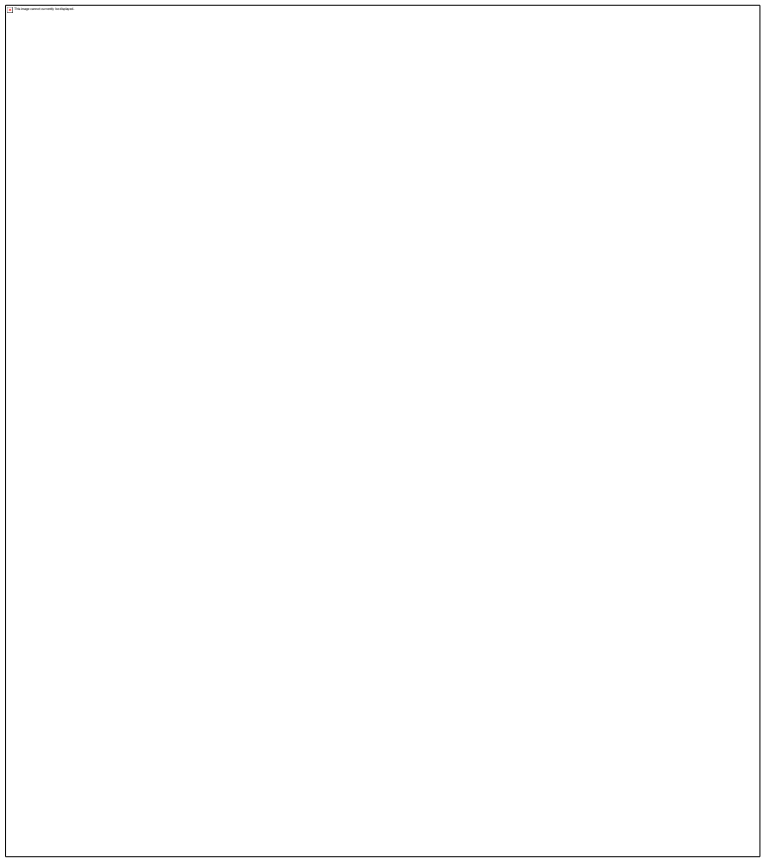

Figure 2.26: 9-mer and 5-mer mutants of PRSFLV peptide bearing a methylated Lys in 4th position.
K_i are reported as μM ± STDV (n = 5).

The last two positions in **PRSFLV** peptide are occupied by leucine and valine and Ala-scan mutagenesis generated two inhibitors of LSD1, **PRSFAV** and **PRSFLA**, which exhibited respectively two-fold increase and a slight decrease in activity (**2.13** and **2.14**, Figure 2.13).

For **PRAFAV** it was possible to obtain an X-ray crystal structure and the analysis showed that the hydrophobic amino acid Ala perfectly overlaps with the Val residue of the SNAG 6-mer **PRSFLV** (Figure 2.27).

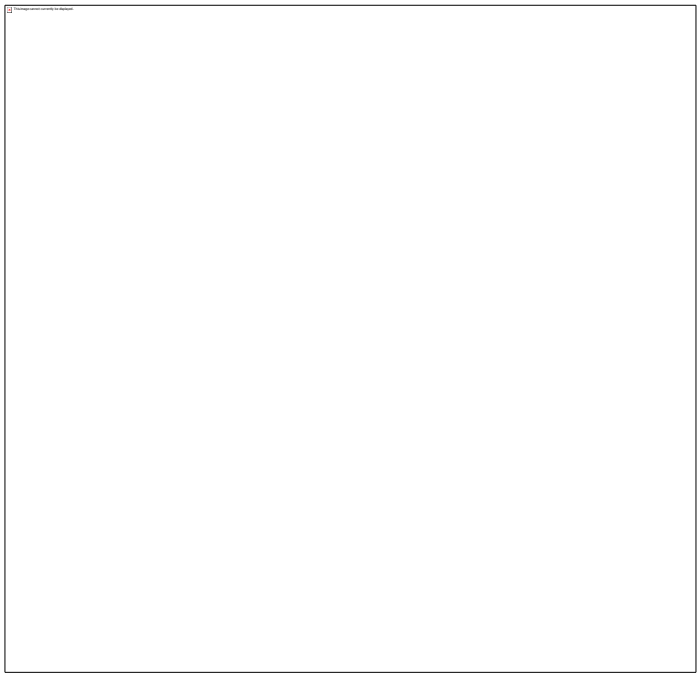

Figure 2.27: X-ray crystal structures of peptides PRSFLV and PRSFAV (PDB: 3ZMZ).
PRSFLV is shown in white, **PRSFAV** mutant is shown in light brown, oxygen atoms in red and amines in blue. The sequences show the same binding mode as **PRSFLV** to the catalytic site of LSD1.

Figure 2.28: Side chain substitutions at the 5th and 6th positions of PRSFLV peptide.
K_i are reported as µM ± STDV (n = 5).

To evaluate Val6 contribution to the binding, we generated a mutant possessing two Alanine residues at position 5 and 6, corresponding to **PRSFAA** (**2.25**, Figure 2.28). Analysis of the X-ray crystal structure revealed a perfect overlap between the Snail-1

native sequence and the **2.25** (Figure 2.29). In addition, the enzymatic evaluations confirmed the affinity for LSD1 catalytic site (K_i = 10.7 ± 1.1 µM). The data conveyed once more the little contribution of positions 3-6 to **PRSFLV** binding activity.

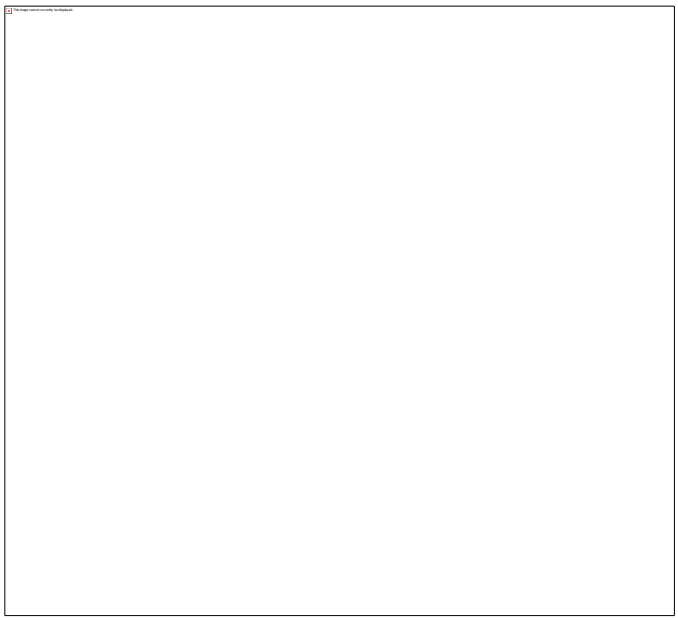

Figure 2.29: X-ray crystal structures of peptides PRSFLV and PRSFAA (PDB: 3ZN0).
PRSFLV is shown in white, **PRSFAA** mutant is showed in light brown, oxygen atoms in red and amines in blue. The sequences show the same binding mode into the catalytic site of LSD1.

Thereafter, we examined further the importance of Pro1 and the ancillary roles of the side chains of residues 3-6 in binding LSD1, with the synthesis of two supplementary structures with multiple Ala residues and namely **ARAFAA** and **PRAAAA** (**2.26** and **2.27**, respectively, Figure 2.30). **ARAFAA** was unable to block LSD1 while **PRAAAA** revealed to suppress LSD1 activity at 28.0 µM, displaying an almost identical affinity for LSD1 as **PRSFLV**.

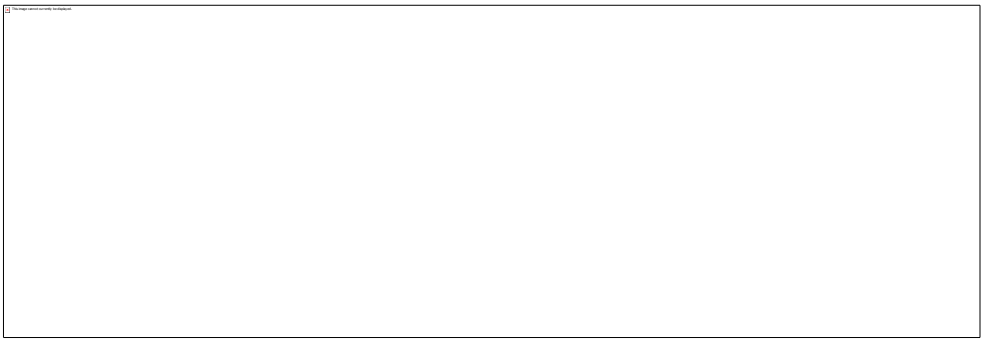

Figure 2.30: Poly-alanine sequences

K_i are reported as µM ± STDV (n = 5).

.

2.3.3. Snail-1 and H3 binding modes compared

Overall, the data suggested that Pro1 is the critical residue for binding to LSD1 as the various prepared mutants containing other residues at that position revealed weaker affinities for the epigenetic target. In contrast to this observation, H3 contains an Ala in the first position. This explains the poor binding of short H3 peptides to LSD1 (Table 2.1). This notion finds further support from the properties exhibited by the Snail1-H3 hybrid sequence (**PRSFQTV**). This molecule was designed with the idea that, in addition to the Pro1-Ala substitution, another main difference between the first amino acids (N-terminal) of Snail-1 (**PRSFLVR**) and **H3 (ARTKQTAR)** is the insertion of Gln5-Thr6 of H3 in place of Leu5 of Snail-1. However, we found that **PRSFQTV** (**2.27**, Figure 2.31) binds to LSD1-CoREST with a K_i of 8.0 µM. This, combined with Ala-scanning experiments, indicates that Pro1-Ala substitution is indeed the main factor that weakens the binding of the N-terminal residues of H3 compared to Snail-1, making short H3 peptides of 8 or 12 amino acids able to only weakly associate to LSD1.[104,110]

Figure 2.31: Peptide PRSFQTV, hybrid sequence Snail-1-H3.
K_i are reported as μM ± STDV (n = 5).

Another important aspect is that although the Snail-1 6-amino acid peptide can bind to LSD1 and exert biological activity, the additional residues 7-9 also contribute to binding. No further contribution is given by the subsequent amino acids of the N-terminal portion of the protein (Table 2.1). This is entirely consistent with the sequence comparisons, because Snail-1-SCRATCH transcriptions factors are highly conserved sequences in their 9 N-terminal residues. Their sequences diverge after this initial strictly conserved segment.[141] This is not the case of the H3 N-terminal tail, whose binding can take place (though weakly) also for peptides that lack the first 4 N-terminal amino acids and substantially depends also on residues after Arg8 (Table 2.1). Accordingly, mutations of Gly12 and Gly13 to Ala have been shown to essentially abolish peptide binding to LSD1-CoREST; such a Gly-Gly motif is absent in the Snail-1 sequence and probably crucial to establish the folded conformation of the LSD1-bound H3 peptide.[104] Thus, on one hand the presence of Ala1 (instead of Pro1) diminishes the contribution to binding of the very first N-terminal stretch of the H3 peptide but, on the other hand, this is partly compensated by the contribution given by the more distant residues in positions 10-20 along the sequence. Indeed, the crystal structure shows that the residues 9-16 are engaged in a network of intra- and inter-molecular H-bond interactions, which critically depend on the amino acid sequence.

Table 2.2: Histone 3 and Snail-1 N-terminal sequences and their enzymatic evaluation as inhibitors of LSD1 enzymatic activity.
From references[104,110]

Peptide	Sequence	K_i (µM ± STDV, n = 3)
H3 1–21	ARTKQTARKSTGGKAPRKQLA	1.8 ± 0.6
H3 1–12	ARTKQTARKSTG	199.0 ± 22.0
H3 6–21	TARKSTGGKAPRKQLA	87.0 ± 29.0
SNAIL1 1–20	PRSFLVRKPSDPNRKPNYSE	0.2 ± 0.1
INSM1 1–20	PRGFLVKRSKKSTPVSYRVR	0.2 ± 0.1

2.4. Biological evaluation of SNAG-like sequences

To investigate whether a live cell would uptake and/or respond to the SNAG-like peptides, we tested the cell viability in SK-MEL-28 (melanoma), A549 (lung) and HL-60 and THP-1 (acute myeloid leukaemia) cells. Biological testing of similar peptides was unreported so far and we hoped to identify active sequences albeit the absence of a cell penetrating sequence, which could have enhanced the cellular uptake.
The SK-MEL-28 cell line is a fast growing melanoma model, whereby Snail-1 is over-expressed. The cells were treated with different concentrations of **PRSFLV** (10 µM, 25 µM, 50 µM, 100 µM, 200 µM and 500µM) and **TCP** (500 µM).

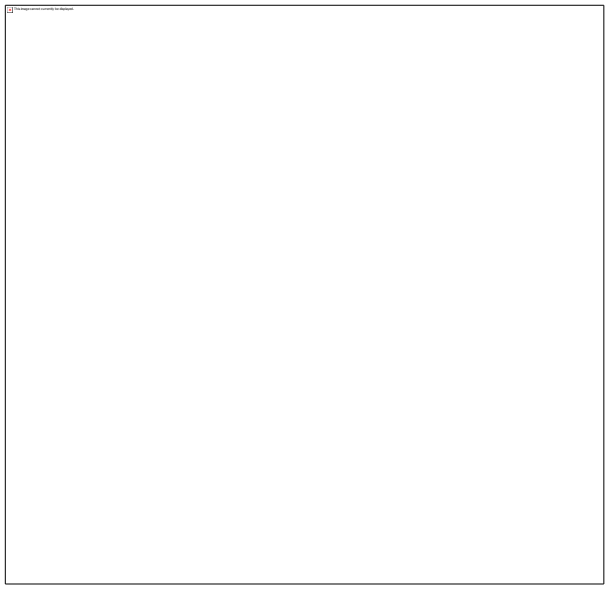

Figure 2.32: Effects of SNAG-like derivative PRSFLV on SK-MEL-28 cells proliferation (72 h) measured with MTT assay.

Absorbance (570 nm) results were normalised to pre-treatment levels. Statistical significance was determined with one-way ANOVA corrected for multiple comparisons using Dunnett's test. Data are shown as means ± STD (n=5); *p < 0.05, ** p < 0.01, *** p < 0.001.

As reported in Figure 2.32, there is an evident trend linking peptide concentration to cell viability. At 500 and 200 μM the presence of **PRSFLV** hindered cell viability, while at 100, 50, 25, 10 μM it seems that the peptide promotes instead SK-MEL-28 proliferation. Yet 50 μM was inconsistent with the general observed trends. In addition, TCP treatments were unable to modulate cell viability at the tested concentrations. In order to verify whether these results depended upon the peptide or the cell line, we repeated the cell proliferation assay using A549 cells (small cell lung cancer). There is evidence that this cancer line is correlated to LSD1 overexpression.[232]

In A549 cells we also tested the activity of **PRSMLV,** the potent SNAG-derivative bearing a methionine in position 4th that showed great binding affinity towards LSD1 (K_i = 3.0 μM) and **LRSK(CbZ)LV** peptide. As shown in Figure 2.33, only the peptide **LRSK(CbZ)LV** was able to significantly modulate cell growth.

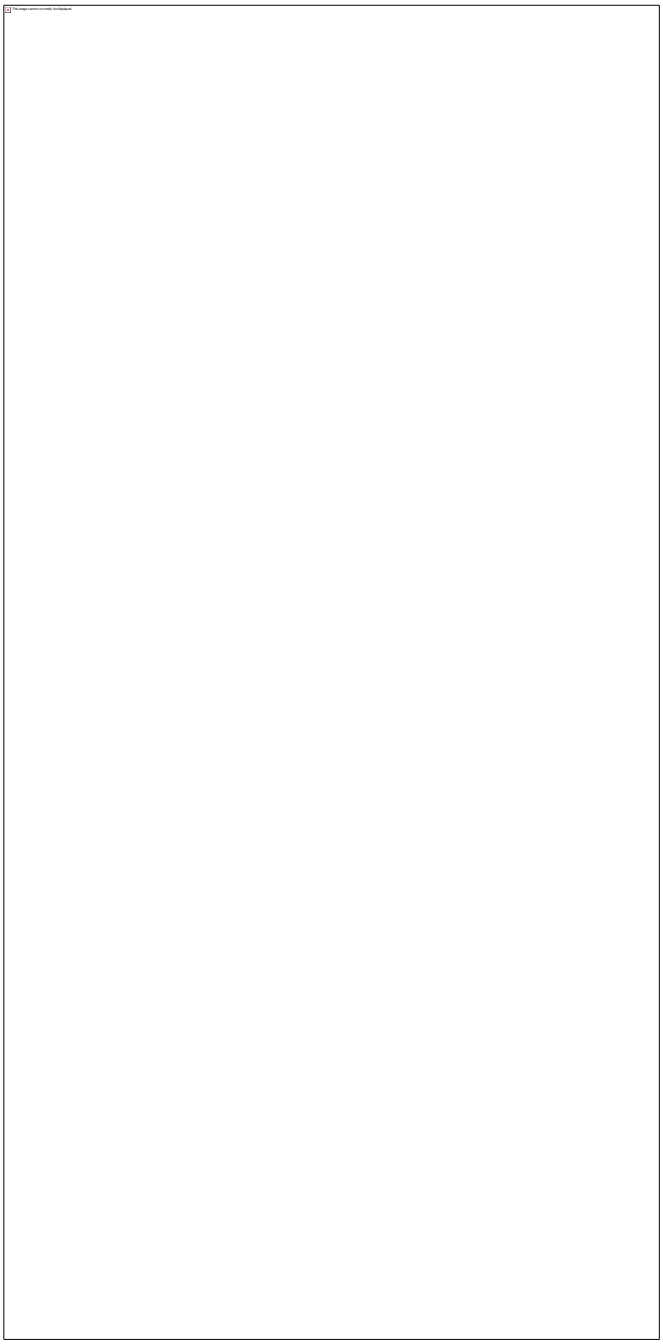

Figure 2.33: Effects of SNAG-like derivatives on A549 cells proliferation (72 h) measured with MTT assay. **(A) PRSFLV (B) PRSMLV (C) LRSK(Cbz)LV.** Absorbance (570 nm) results were normalised to pre-treatment levels. Statistical significance was determined with one-way ANOVA and corrected for multiple comparisons using Dunnett's test. Data are shown as means ± STD (n=5); *p < 0.05, **p < 0.01, ***p < 0.001.

To further explore the anti-proliferative activities of SNAG-derivatives, we tested selected sequences in AMLs (Acute myelocytic leukaemia) and specifically in THP-1 and HL-60 cell lines. In this tests, we also used as a positive control the TCP analogue **MC2584**, (Figure 2.34)[175] prepared by our collaborators in University La Sapienza, Rome, that showed anti-proliferative effects in APL cells (Acute promyelocytic leukaemia NB4 cells)

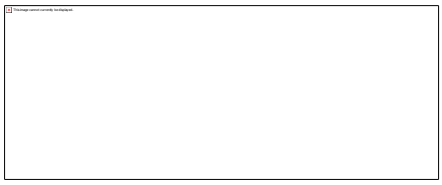

Figure 2.34: A TCP analogue with marked anti- APL activity.

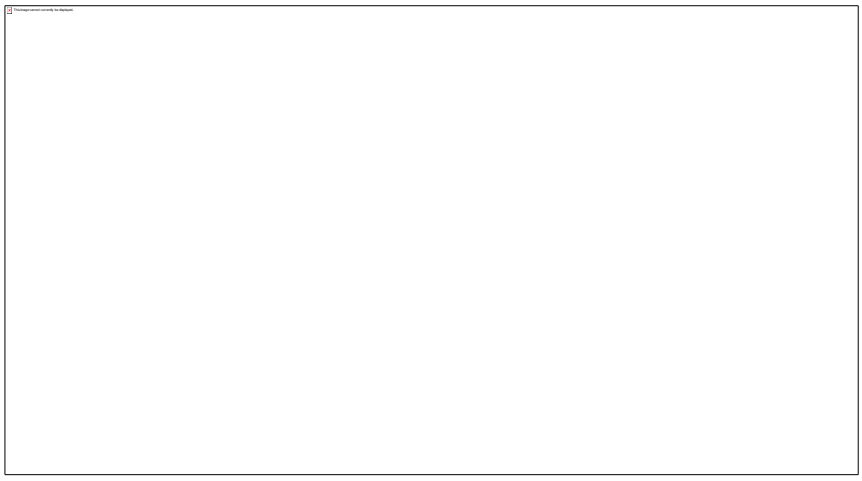

Figure 2.35: Effects of SNAG-like derivatives PRLYLV, LRSK(Cbz)LV, PRSMLV and PLSFLV on HL-60 and THP-1 cells proliferation (72 h) analysed with MTS assay

The absorbance values were normalised to pre-treatment levels (vehicle control). Statistical significance was determined with one-way ANOVA and corrected for multiple comparisons using Dunnett's test. Data are shown as means ± STD (n=5); *p < 0.05, ** p < 0.01, *** p < 0.001.

Peptides **PRLYLV**, **PRSMLV** and **LRSK(Cbz)LV** significantly reduced cell proliferation at 1 mM concentration (72 h treatment). The cellular suppression of LSD1 was also confirmed by Western blot. Data showed an increment of H3K4me2 after 4 h treatment with 1 mM of **PRSMLV** and **PLSFLV** peptides.

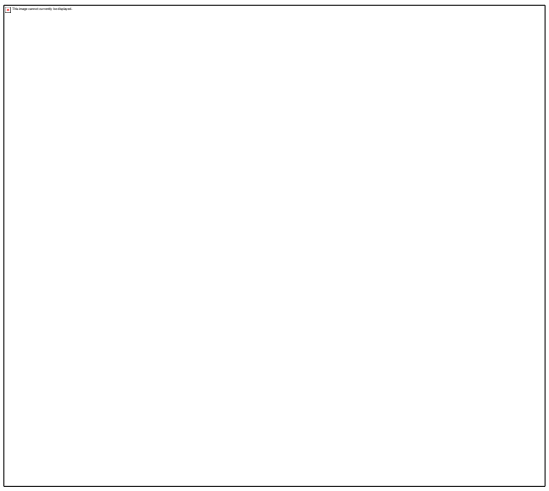

Figure 2.36: Western bolt analysis of the effects of SNAG-derivatives PRSMLV and PLSFLV peptides on the expression of H3K4me2 in treated HL-60 total cell lysate.

Taken together, these results suggest that targeted Snail-1/LSD-1 inhibition causes decreased proliferation in different cell lines and may provide novel therapeutics for a number of different cancers including leukaemia and prostate cancer. The biggest limitation to the biological evaluation is the high concentration at which the peptides activity is appreciable. In addition, their short length also implies that they may be nonspecific and it is not possible to conclude whether these peptides crossed the cell membrane or instead triggered cell surface receptors leading to activation of pro-apoptotic or pro-survival signalling pathways. However, the peptides show downstream effects such as increased levels of H3K4me2 in leukaemia cell lines.

2.5. Conclusions

In this work we synthesised small LSD1 reversible inhibitors based on the previous observation of LSD1-Snail-1 interaction. The designed small ligands were μM inhibitors of LSD1 enzymatic activity and their effective binding was supported by numerous X-ray crystal structures. By targeting LSD1, the peptides were able to modulate the activity of AML cells. Since previous studies have shown how Snail-1 recruits LSD1 for demethylation at its target genes via the SNAG domain, it could seem counterintuitive that Snail-1 also inhibits LSD1 enzymatic activity. The

present study provides a possible explanation to this paradox: the SNAG domain recruits LSD1 but then releases it to the H3 tail. We found in fact that the first 6-residues of Snail-1 are sufficient for binding to LSD1, whereas the residues 10-20 do not contribute to enhance the affinity. On the other hand, the residues 10-20 of H3 establish multiple interaction with LSD1, allowing H3 to displace the SNAG domain from the active site of LSD1.

Hence the discovery of small LSD1/CoREST peptide ligands lays the foundation for a deeper understand of the LSD1 interaction with the Snail family of binding partners as well as the structure-based development of further analogues with improved drug-like properties.

Chapter 3 - Targeting LSD1 with Phage display technology

3.1. Introduction

The successful synthesis of small peptides acting as reversible inhibitors of LSD1 prompted us to investigate other non-covalent LSD1 antagonists. **Phage display technology** was utilised to screen the binding affinities of a large number of peptides towards LSD1. This technique offers a powerful and highly specific alternative to rational design and virtual screening to explore peptide-LSD1 interactions.

Many examples in the literature describe Phage display-derived peptides that interacted successfully with the surface of proteins,[233] antibodies[234] and receptors;[235] such screens led to the discovery of peptide sequences and proteins that are at the later stages of drug development.[236–238]

The widespread use of this technology for peptide selection is justified by its simplicity, its specificity and the stability of the phage particles.[239] These characteristics enable the application of the phage display to a wide array of biological surfaces including *in vivo* screening for the isolation of peptides targeting specific cell-surface biomarkers.[240] For example, Cwirla *et al*. demonstrated the specificity of peptide libraries by screening a library of 3×10^8 recombinant peptides, displayed on a phage vector, towards a well-known antibody.[234] Specifically, the authors screened the phage library against the antibody 3-E7, which binds to the N-terminal sequence of opioid peptides through the motif Tyr-Gly-Gly-Phe, crucial for antibody recognition. The sequencing of 51 clones derived from this study revealed that most of the isolated sequences presented a N-terminal Tyr-Gly motif.[234] The same authors identified peptides binding to thrombopoietin[235] and erythropoietin[241] receptors by screening libraries displayed on phage vectors and plasmids. These two studies led to the synthesis of extremely potent peptidomimetics with affinities for the receptors comparable to the natural substrates (0.5 nM).

Mintz *et al.* utilised a library of peptides for panning towards antibodies produced in prostate cancer patient serum. Analysis of peptide sequences displayed by phage bound to purified immunoglobulins led to the identification of a recurrent sequence correlating

with poor prognosis patients. Subsequent molecular studies on such sequences identified a striking correlation of the displayed peptide with the expression protein Grp78.[242] The study evidentiated the successful use of Phage display for systematic high-throughput fingerprinting of circulating proteins in cancer patients and the potential of the technique for the application in diagnostics.

Besides the phage display, other displaying platforms have been used for protein-protein interaction research.[239,240] These are mRNA, ribosome, DNA and cell display (Figure 3.1). Among them Phage display is the most utilised screening platform.[240] The distinct feature shared by all these molecular platforms resides in the ability of physically linking the genotype to the phenotype. This characteristic enables the rapid identification of the displayed peptide chains harboured on their surface.

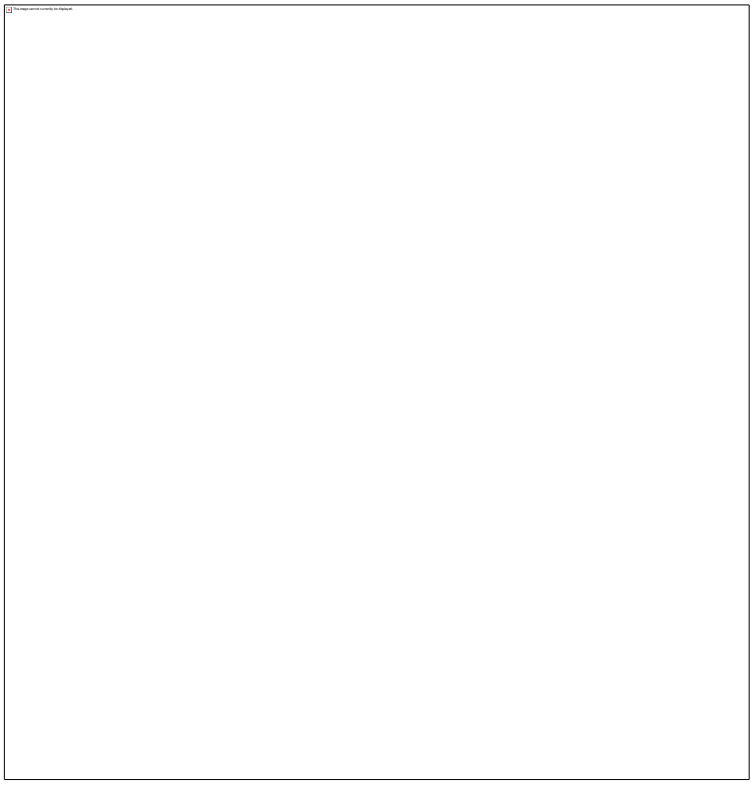

Figure 3.1: Peptide display platforms.

Adapted from Sergeeva *et al.* [240]

Only one study so far describes the application of phage display libraries for the identification of peptides binding to epigenetic targets. In this work, Leurs *et al.* screened three phage displaying libraries, against both LSD1 and JmjC families of demethylases.[243] The study led to the identification of six novel peptide sequences. Among them, the ones targeting LSD1 do not share similarities with LSD1 natural substrate H3 or any known LSD1-binding partner. The hits discovered, however, displayed only weak inhibition *in vitro* for the targeted demethylases. To optimise the peptide affinity for the cognate targets, the authors applied several modifications to the original phage-derived sequence, by removing and/or exchanging amino acid residues. The aspartate and asparagine residues, which are known to destabilise the peptides in solution, were substituted with alanine or glutamate residues and such modifications led to a dramatically increase of peptide binding affinities. The efforts of this research were next addressed mostly towards the JmjC KDMs. Subsequent studies on their binding mechanism were achieved by employing mass spectrometry techniques.[244]

The current project explores the potential of Phage display technique using a library of 12-mer peptides for the identification of new LSD1 ligands able to antagonise the demethylase activity. The data gathered from the selection could be eventually used to design additional drug-like molecules based on phage display-derived scaffolds.

3.2. Phage display

3.2.1. The phage vector

In Phage display, the "display" is achieved through association of short DNA sequences, encoding for oligopeptide chains, into viral DNA by common recombinant DNA techniques. Standard microbiological procedures are then used to maintain and propagate the phage.[245] The viral recombinant vectors are bacteriophages, able to replicate in bacteria and present the ability of harbouring DNA sequences of foreign species, as for example human DNA or synthetic DNA fragments.[239,245]

To propagate phages, the most commonly employed host is the bacterium *Escherichia coli* (*E. coli*).[245]

Three types of bacteriophages have been described: filamentous, lambda and T7. The family of filamentous phage is composed by three genetically and phenotypically equivalent strains: M13, f1 and fd. M13 is the best characterised and the most used as phage display vector.[246,247]

M13 possesses a single stranded DNA, composed of 6407 nucleotides. There are nine genes that encode for eleven proteins and these are grouped on the basis of their biological function:[245,246]

- pII, pV, pX which are DNA replication proteins;
- pIII, pVI, pVII, pVIII, pIX which are capsid proteins;
- pI, pIV and pXI are proteins associated with phage asSTDbly;

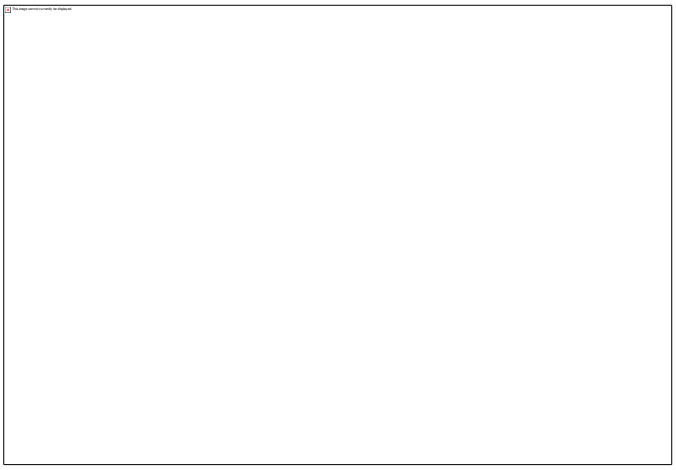

Figure 3.2: Schematic representation of a phage vector.
Adapted from Løset *et al.* [248]

At one tip of each virion particle there are five copies each of protein pVII and pIX (genes VII and IX), whereas at the other end there are 5 copies each of protein pIII (minor coat) and pVI (genes III and VI, respectively).[239] Three domains, linked to each other through glycine rich spacers, compose the minor coat of pIII (N1, N2 and CT).[249,250] The first domain is required during the infection as it allows the single strand DNA to accommodate into the bacterial cytoplasm; the second domain is responsible for binding the bacterial F-pilus by establishing disulfide bridges. The third domain, CT, is responsible for the terminal asSTDbly of the phage particle and the phage release from the host cells.[249,250]

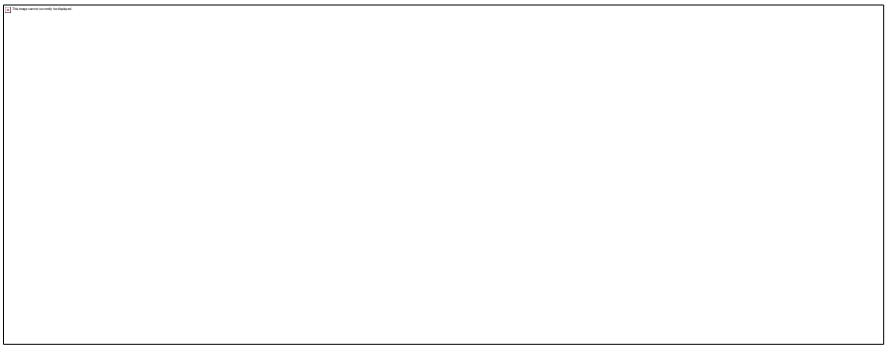

Figure 3.3: Ff-phage minor coat protein pIII scheme of organisation and sequence localisation.
D stands for domain and in brackets are reported the number of amino acid contained in each domain.
Adapted from Holliger et *al.* [251]

When the virus replicates in the host, the inserted DNA also replicates. Therefore, each peptide-phage clone in the library carrying the foreign DNA sequence can multiply in the bacterial host, producing identical progeny phages.[252,253] Such phage clones compose a phage-display "library". Each clone, by carrying a unique foreign DNA insert, displays a different peptide on its surface.[252]

The phage vector initiates the infection by attaching its N-terminal domain of pIII minor coat to the bacteria's F-pilus and entering the host cell (Figure 3.3).[251] The minor coat is then disasSTDbled and the single stranded DNA enters the bacterial cytoplasm. Successively, the *E. coli* machinery synthesises a virus's complementary DNA strand and in this way, a double stranded replicative form of DNA is formed and used by the host machinery as a template to generate phage proteins. Conversely to the lytic phages such as T7, after infection and replication, filamentous phages do not lyse the cells, being able to be released without lysing the host cell membranes. This feature favours this class of phages for display technique applications as the isolation process do not requires purifications steps from the genetic material resulting from bacterial lysis.[246]

The inserted DNA can be localised into the phage's pIII, pVIII and pVI and the segments harboured into the first two proteins are synthesised with the N-terminal signal peptides attached and directing into the membrane.[252] Being inserted in the inner membrane of the host cells, the signal peptide is cleaved, leaving the synthesised protein to span the cytoplasmic membranes: in this orientation the amino-terminal is found in the cytoplasm (*outside* the virion particle) whereas the C-terminal is encountered in the periplasm (*inside* the virion particle).[239] This way, the peptide sequence is linked genetically to the endogenous amino acids of the coat protein making a hybrid "fusion" protein.[253] The recombinant sequence at the N-terminal is followed by a short characteristic sequence at the C-terminal. For example, the library of phage used in the present study, corresponds to a combinatorial library of random dodecapeptide fused into pIII minor coat protein of the M13 phage (PhD-12^{TM} from New England Biolabs) with a characteristic sequence (factor Xa protease cleavage). The factor Xa protease cleavage at the C-terminal is composed by the tetrapeptide Gly-Gly-Gly-Ser (X_{12}GGGS, X=random sequences). The factor Xa protease cleavage sequence enables the recombinant peptides to be "dangled" off the pIII (Figure 3.4) and to interact with the target.

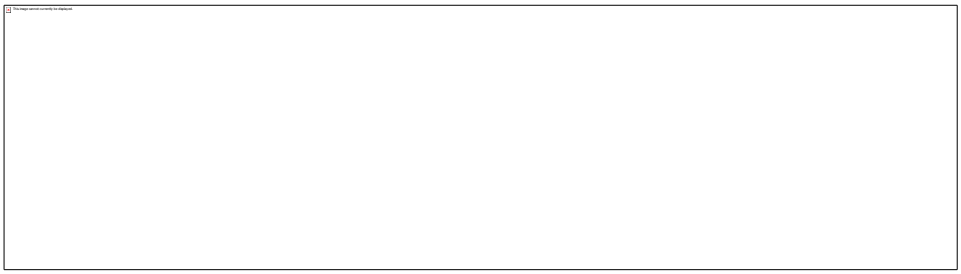

Figure 3.4: Schematic representation of PhD-12™ from New England Biolabs.
X= randomised sequence (12 amino acids); GGGS corresponds to the linker sequence.

Having a free N-terminus, the peptides displayed possess a considerable flexibility to interact with the target and have similar characteristics to peptides in solution. The choice for the library peptides' length was determined on the basis of the results obtained in Chapter 2, where LSD1 inhibitors were found to vary from 6 to 20 amino acids in length.

3.2.2. The phage display cycle and the selection process

The main goal of any display technique is the progressive reduction of the initial number of phages contained in the library to a smaller one, in which only the "fittest" for the cognate target will be included.

Screens with phage display technique involve several steps and after an initial selection, high affinity clones are amplified to achieve a library with phages with increased suitability for the target. The amplified phages are subjected to iterative rounds of panning to select further a pool of high affinity binding sequences. A general scheme of the panning procedure is shown in Figure 3.5.

The selection process is governed by two factors: yield and stringency.[239] The yield governs the population of phage that exhibits the desired target behaviour, sustaining the selection process, while stringency discriminates between high and low affinity clones. The yield is important for the first rounds of panning as high stringency in these steps could involve the risk of losing a wide phage population containing, potentially, high affinity binders. On the other hand, stringency can help throughout the selection process during the subsequent rounds of panning.

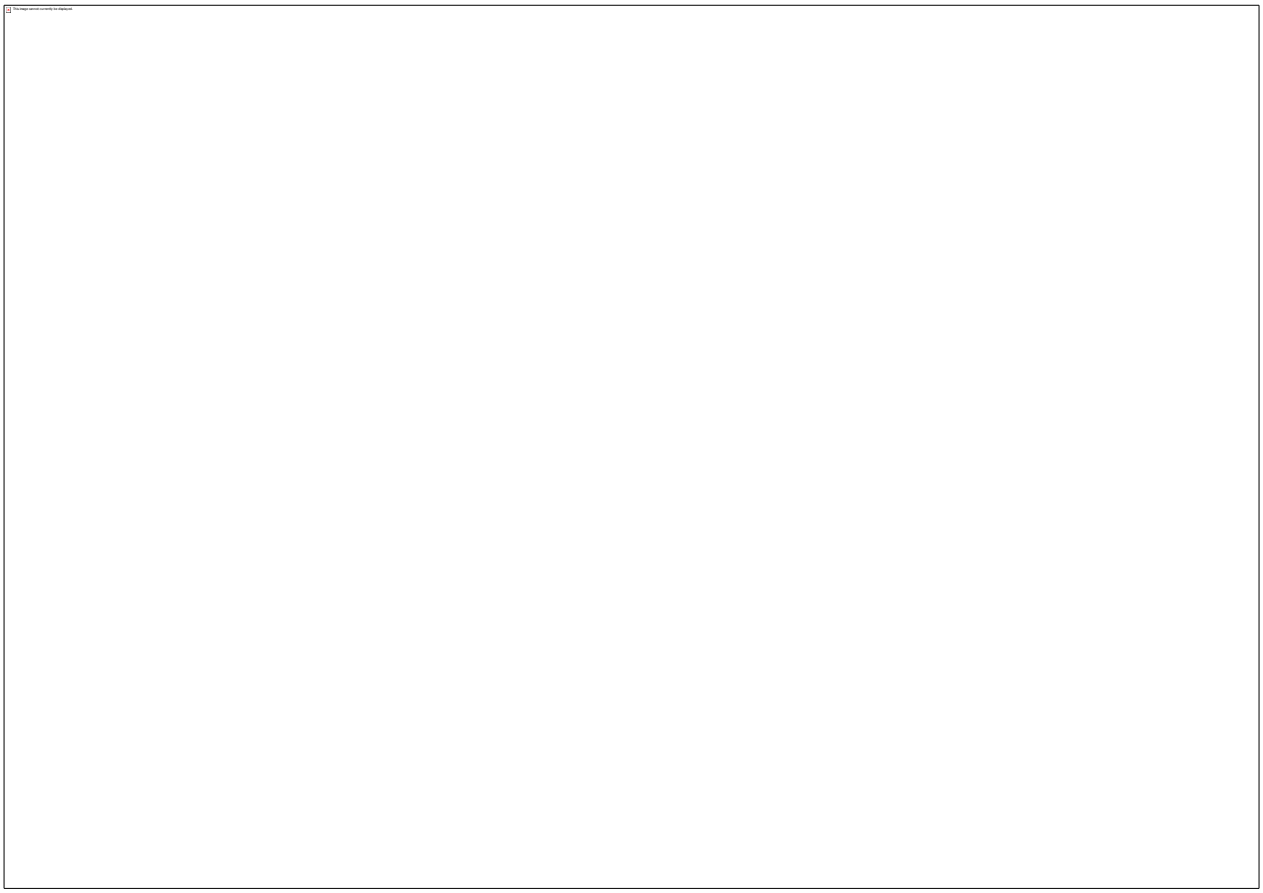

Figure 3.5: Schematic representation of a biopanning cycle.
Adapted from Ullman *et al.* [254]

3.2.3. Biopanning cycle

The biopanning cycle starts with the incubation of the target with the phage library. This process, common to all display platforms, is controlled by the affinity of the oligopeptides displayed on the phage coat for a given target.

Normally, polystyrene-based surfaces are employed to immobilise the target (protein/enzyme).[255] Alternatively, in a two-step selection, the target displaying an affinity tag is firstly exposed to the oligopeptides library in *solution*; next, the target-phage complex is captured by a surface enriched with elements with affinity for the target tag.

In the described project, His-tagged LSD1 was incubated with the library in solution and nickel containing magnetic beads were employed to immobilise the target-phage complex by application of a magnetic.[256] The solution panning has many advantages over the immobilised methods as it requires less amount of target to be used and avoids the target denaturation upon absorption onto the polystyrene beads. Moreover, this panning procedure enables the protein/enzyme target to maintain its natural orientation.[257] It has been reported that the immobilisation on polystyrene-based surfaces can lead to unfavourable orientations to establish interactions with the displayed oligopeptides.[257] During the panning, high affinity clones are captured by the target surface whereas low affinity or unbound phages are washed away with solutions containing detergent (Tween® 20). The bound phages are then recovered with specific elution strategies using high-salt acidic solutions or known ligands. The eluted phages are next amplified by infecting a low-density fresh *E. coli* culture to yield a large crop of progeny clones composed by affinity binders. After each panning/amplification step, the number of phages recovered is monitored with the blue plaque-forming assay (also called titering).[258] In this assay, each virus is displayed in an agar plate as a small blue dot and each dot corresponds to one plaque-forming unit (pfu). The formation of the blue plaques is enabled by the presence in the M13 vector of the lacZ gene encoding for β-galactosidase (β–gal), and two reagents used for the preparation of the agar plate. These are 5-bromo-4-chloro-3-indolyl-p-D-galactoside (X-gal) and isopropyl-p-D-thiogalactopyranoside (IPTG). Phage infected bacteria and IPTG prompt the production of the β–gal that hydrolyses the X-gal creating the blue plaques.

The panning and amplification cycles are repeated several times and the process leads to an enrichment of the phage library towards the target's tightest bound sequences. After several biopanning cycles (normally 4-5), there will be a point when the entire phage population will have nearly the same binding affinity,[239,245] and at this stage phage DNA is sequenced and the peptide harboured onto its surface identified. The binding affinities of each clone are then measured by enzyme-linked immunoassorbent assay (ELISA) or other tests.

3.2.3.1. Elution

In biopanning, the elution step is of high importance since it enables the recovery of high affinity binders. Commonly used elution buffers consist of solutions that weaken the receptor-phage interactions without impairing phage infectivity. These are high salt-acidic buffers (0.1 M glycine-HCl, pH 2.2) or high affinity ligands, which competitively displace bound phages. The competitive elution is often used to reduce the background of non-specifically bound sequences.[253,259] Since the elution with a competitive ligand is a two-stage process, the binding kinetics need to be taken into account. The competitive ligand elution requires first the natural dissociation of the clone from the catalytic site and secondly its re-occupation by the competitive inhibitor. Consequently, each step will have a specific association and dissociation rate constants (K_{on}/K_{off}).[239] High affinity phages will have a reduced K_{off} and thus, with shorter elution time, these will not be eluted. On the other hand, prolonged exposures can potentially elute, without discrimination, both high affinity and low affinity clones.[245]

3.3. Expression and purification of full length human recombinant His-tag LSD1

For the phage display experiments and the enzymatic evaluation of the phage display-derived peptides, we used human recombinant His-tagged (full-length) LSD1. To measure the ability of phage display derived peptides to suppress LSD1 catalytic activity a hydrogen-peroxidase-coupled assay was performed (Amplex®Red).

3.3.1. LSD1 expression and purification

LSD1 was expressed and purified under direct supervision of Dr. Patrick Duriez at the University of Southampton Cancer Research UK centre.

The process for His-tagged LSD1 expression and purification is common to standard protocols for protein expression. This involves the introduction of a plasmid promoter containing an expression vector into a host cell; the host cell then rapidly multiplies producing high quantities of DNA encoding for the target protein; the lysis of the host enables the release of the genetic material, which is next purified by chromatography.[260] After isolation, qualitative and quantitative tests are performed. All these steps were optimised for LSD1 and what follows is a description of the used protocol.

3.3.1.1. Plasmid vector

A plasmid is a DNA double stranded circular molecule that once incorporated into a host DNA acquires the ability of replicating independently from chromosomal DNA.[260] Plasmids are widely used in molecular biology as they can accommodate DNA fragments and such modified plasmids are called vectors. Plasmid vectors are commonly used in molecular biology techniques being applied in cloning, transferring and gene manipulation processes.[260] Once the vectors have been inserted in the host cell they regulate the host machinery to replicate the inserted DNA fragments in large quantities. The vector used to insert the gene encoding for human-LSD1 is pET15b, a plasmid composed by 5708 bp carrying at the N-terminal a stretch of 6 histidine (His) residues. These N-terminal residues allow the purification of the target protein by nickel affinity chromatography. The vector having a gene encoding for antibiotic resistance,

restricts the propagation of only host cells carrying the plasmid encoding for LSD1. Dr. Yang Shi, from Harvard Medical School, Boston, donated the plasmid pET15b-LSD1 to the laboratory of Dr. Duriez.

3.3.1.2. Induction and Growth

The DNA fragment encoding for LSD1 expression in the engineered pET vector is a lac operon and its transcription is triggered by the presence in the culture media of isopropyl-β-D-thiogalactopyranoside (IPTG).[261]

The DNA fragment encoding for LSD1 expression in the engineered pET vector is a lac operon and its transcription is triggered by the presence in the culture media of isopropyl-β-D-thiogalactopyranoside (IPTG).[261]

The pET vector normally contains three elements: a gene that encodes for antibiotic resistance, a lacI gene from the lac operon that codes for the lac repressor (LacI) and the gene of interest. This is inserted just after the T7 promoter DNA sequence, the Lac operator DNA sequence and the ribosome-binding site (at the start of the mRNA transcript). The induction process begins with the LacI falling of the operator DNA sequence placed in front of the gene of interest; subsequently the T7 RNA polymerase is introduced and recognise the T7 promoter without the presence of the repressor (LacI). After these two events the transcription of the gene of interest can begin. Commercially available *E.coli* strains have been engineered to have a gene encoding for T7 RNA polymerase under a modified lac operon system. This is called DE3 or BL21 and has instead of a T7 promoter sequence in front of the lac operator sequence, a lac promoter sequence that native *E.coli* RNA polymerase is able to bind. When the LacI falls of the lac operator sequence of DNA in the host chromosome, the T7 of the RNA polymerase of the gene of interest can be translated and transcribed.[260,261]

LacI senses the presence of lactose and when lactose binds to LacI, induces a protein conformational change that renders the protein unable to bind to the operator DNA sequence. Being a mimic of lactose, IPTG also induce such conformational change, reducing the affinity for DNA; however, IPTG does not take part in any bacterial metabolic pathway and therefore, its concentration will remain constant for all the expression process. When LacI can no longer bind to the operator, native *E.coli* RNA

polymerase starts the transcription of the T7 RNA polymerase gene engineered into its chromosome and, when the protein is expressed binds to the T7 promoter sequence upstream to the gene of interest on the plasmid insert and the transcription of the protein of interest starts.

E. coli (BL21 CodonPlus-RIPL) harbouring the pET15b-LSD1 was cultured for 16 h at 37 ˚C and after that time cells were harvested by centrifugation and lysed.

3.3.1.3. Lysis

To extract the crude genetic material containing the protein of interest, a lysis step was performed. The pelleted bacteria cells were lysed with a solution containing detergents to enhance the bacterial lysis (Triton X), specific enzymes and protease inhibitors to prevent the LSD1 degradation by bacterial enzymes and DNase I, to break down the released double stranded DNA. The genetic material and cell debris were then discarded with a centrifugation step and the supernatant containing the target protein purified.

3.3.1.4. Purification

The purification of LSD1 was accomplished in three stages. In the first stage the crude extract was eluted through a nickel based column (affinity purification). This type of column exploits specific covalent binding interaction between the column material, decorated with Ni^{2+}, and the 6-histidine residues in the protein N-terminal domain. The affinity interactions between the Ni^{2+}-His, enable His-tagged LSD1 to be retained from the bacterial lysate. Gel electrophoresis (i.e. SDS-PAGE) was next used to separate the proteins recovered from this initial purification step and identify the fractions containing LSD1. Such fractions displayed a band at 80 kDa after Coomassie blue staining; these were combined and subjected to a second step of purification, which involved the use of gel filtration.[260] This step separates soluble macromolecules from small molecules and removes remaining salts and buffer reagents derived from earlier purification steps. The fractions collected were re-assessed with gel electrophoresis and the ones in which LSD1 was detected asSTDbled and further purified with Q-Sepharose™ column (anion exchange column). The material composing such column displays negatively charged

anions (counter-ions). Negative charged molecules bind to the resin by displacing the resin's counter-ion.[262,263] The protein is eluted from the resin with increasing concentration of salted buffer (NaCl) and increased pH. The negative ions in the salt buffer displace the protein by competing with it for binding to the resin, whereas the decrease in pH enables an increased positive charge on the protein, allowing its elution from the column.[262] When the pH of the elution buffer reached the LSD1 isoelectric point (~ 6), the fractions were collected and a last electrophoresis step was performed to isolate the pure fractions. LSD1 obtained was then concentrated and quantified.

3.3.1.5. Analysis of the pure protein

We quantified the pure LSD1 by Bradford assay. This spectroscopic quantitative assay is based on the absorbance shift of the dye Coomassie blue at acidic pH upon binding to specific protein amino acid residues (arginine, histidine, phenylalanine, tryptophan and tyrosine residues) and hydrophobic interactions.[264] After quantitative evaluation, the protein was aliquoted and kept at -80 ˚C. Benelkebir *et al.* previously studied the kinetics of LSD1 and the K_m (Michaelis constant) was determined to be 21 µM, using a peroxidase-coupled assay and as substrate the H3K4me2 peptide (21 amino acid long) at pH = 7.5.[170] The K_m, is defined as "the substrate concentration at which the reaction is half of the V_{max}" (the system maximum velocity achieved at substrate saturating concentrations). The determination of this parameter is important to define the concentration of substrate (H3K4me2) to use in the enzymatic assays. The protein activity was measured with Amplex®Red by incubating LSD1 with TCP and measuring the residual enzymatic activity, which should fall in the range 30-15 µM.

3.4. Amplex®Red assay

The Amplex®Red assay was used to determine the ability of phage-derived sequences to inhibit LSD1 demethylase activity on H3K4me2.

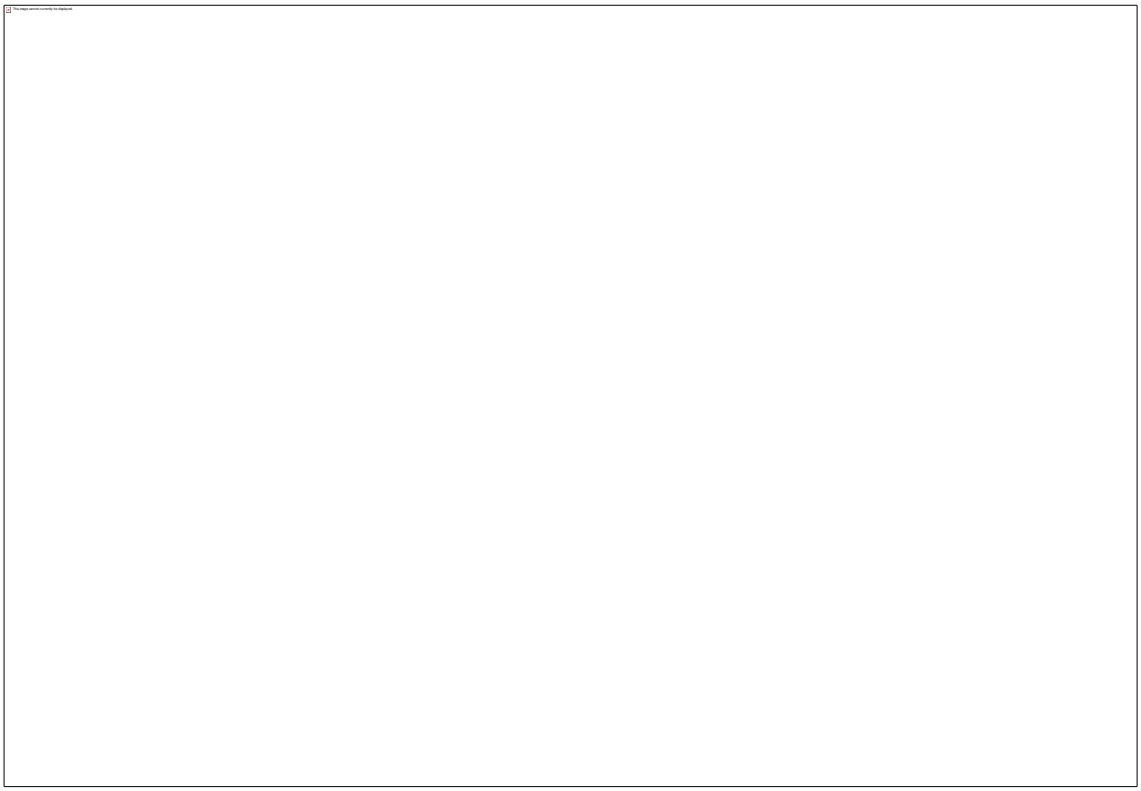

Figure 3.6: Mechanism of demethylation and Amplex®Red assay.

(A) LSD1 promotes the catalytic demethylation of di-or mono-methylated Lys 4 on Histone 3 (H3K4) through a Flavin dependent oxidative mechanism. The histone 3 binds to the FAD, which oxidizes the H3K4 side chain with its prosthetic group. Concurrently, reduction of oxygen to hydrogen peroxide takes place. The formed imine intermediate is then hydrolysed generating the demethylated H3 and formaldehyde. (**B**) FAD reduction and regeneration and peroxide release**.** (**C**) Peroxidase-base coupled assay: the horseradish peroxidase uses ADPH (Amplex®Red) as an electron donor during the reduction of hydrogen peroxide to oxygen. This leads to the conversion of ADPH to ADP (resorufin), which is highly coloured and its fluorescence is measurable.

In such an assay, the purified LSD1 is combined with the test peptides derivatives (or other potential inhibitors) and then incubated with H3K4me2 peptide natural substrate (sequence ARTK(me2)QTARKSTGGKAPRKQLA) in the presence of FAD. The read out of the assay is the colorimetric reaction of Amplex®Red with hydrogen peroxide (H_2O_2), the by-product of LSD1 demethylation. The fluorescence is immediately detected (530 nm excitation and emission at 590 nm).

The activity of the inhibitor is evaluated by comparing the fluorescence values obtained under test conditions (LSD1+substrate+inhibitor) with control conditions, which corresponds to the maximum catalytic activity (LSD1+substrate−inhibitor). The enzyme assay is normally repeated in triplicate using TCP or known LSD1 non-covalent inhibitors as positive controls.

3.5. Phage display strategies used in panning against the LSD1 catalytic site

To screen peptides displayed on a phage library against LSD1, a total of four rounds of solution biopanning were performed (Figures 3.7-3.9).

To circumvent the selection of phages that are not specifically bound to the target, a pre-selection step or negative selection step was introduced after a first round.

The first two rounds were performed while maintaining a low degree of stringency in order to enrich the library with specific LSD1 binders, without discriminating between high affinity (phages positioned near or inside the LSD1-AOD domain) and low affinity ones (bound to other surfaces). Following two rounds, a competitive elution was employed to improve the selection for peptides that were tightly bound to the LSD1 catalytic site (Figure 3.9).

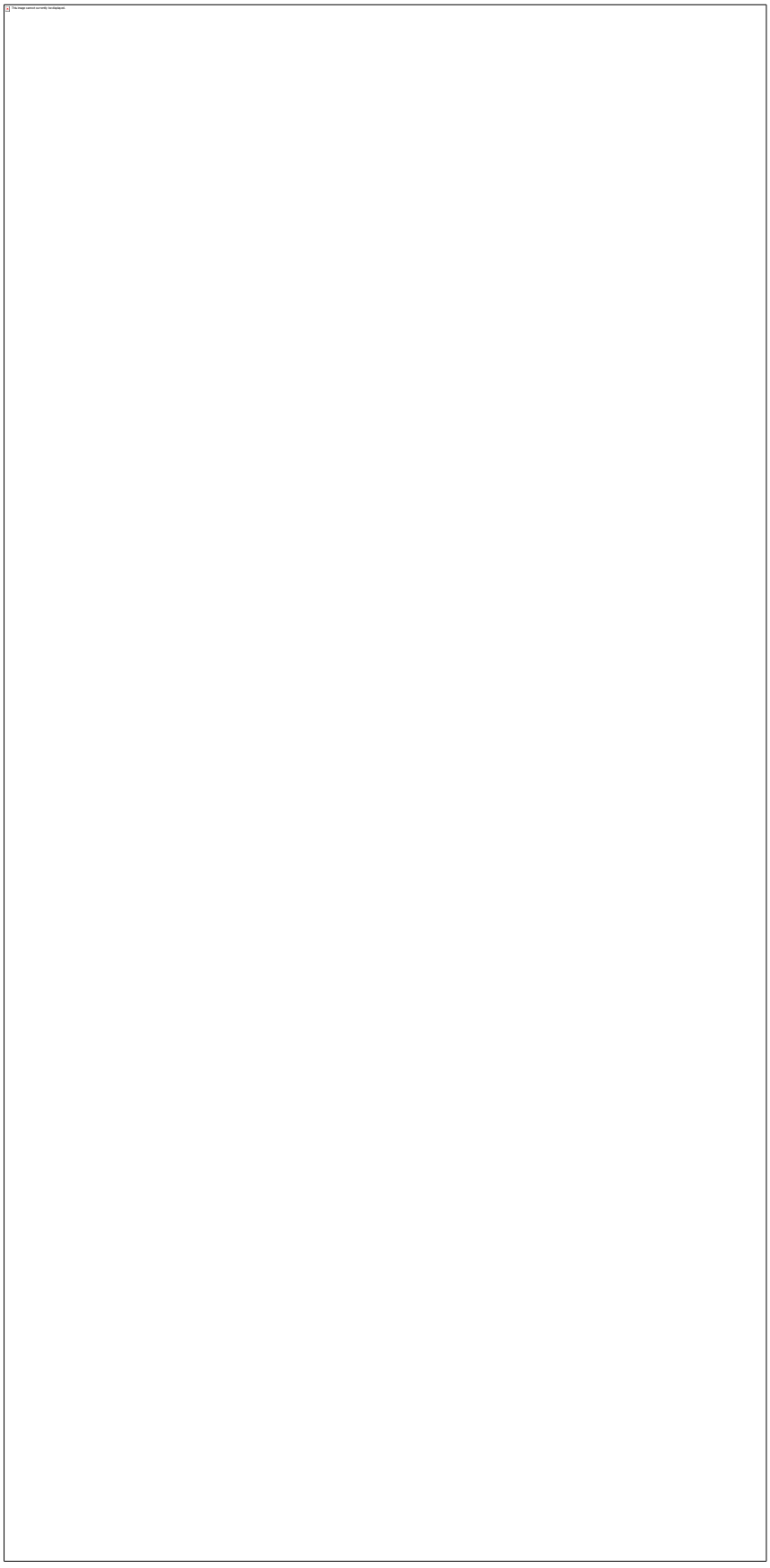

Figure 3.7: Scheme illustrating the different biopanning steps in ROUND 1..

Figure 3.8: Scheme illustrating the different panning steps in ROUND2.

Figure 3.9: Scheme illustrating the different biopanning steps in ROUND 3-4 of.

In these last two rounds, a solution of 1 mM of a known water-soluble LSD1 peptide ligand **PRSFLVRKP** (Figure 3.9) was used in order to elute LSD1-captured phages. The high affinity of **PRSFLVRKP** (K_i 0.136 µM) for LSD1 catalytic site and the saturating concentration of the specific ligand would enable the elution of phages therein localised. Three elutions of 10 min each were performed and the period of elution was selected according to the standard incubation times used to antagonise LSD1 in enzymatic evaluations.[170]

After 4 rounds of selection to enrich for higher affinity peptides, a last step of phage propagation preceded individual phage characterization through DNA extraction and sequencing. The peptides obtained from the study were then synthesised by Solid Phase Peptide Synthesis and the activity of the native sequences evaluated with a peroxidase coupled assay (Amplex®Red).

3.6. Results

3.6.1. Protein expression

The reported method for LSD1 expression was optimised in the laboratory of Dr. Duriez and has been shown to be reproducible. The full length human recombinant His-tag LSD1 obtained with such described procedures has been used in all stages of panning experiments and enzymatic assays throughout the course of the PhD.

The Figures 3.10 and 3.11 report two images of the electrophoresis showing the gradual purification of LSD1.

Analysis of the target state was also carried out during the panning by electrophoresis to verify the LSD1 stability during the experiments.

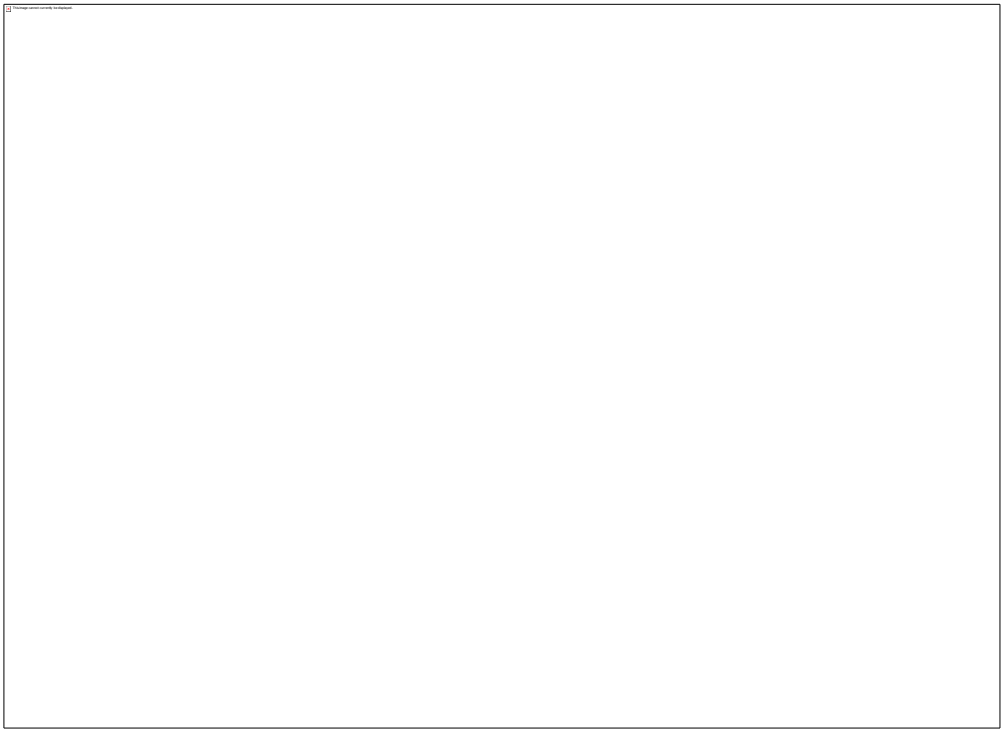

Figure 3.10: Coomassie Blue stained polyacrylamide gel of affinity purified LSD1 protein.
The image shows the SDS-PAGE results of first and second steps of purification after protein extraction. Bands identifying LSD1 are inside rectangle boundary (80 kDa).

Figure 3.11: Coomassie Blue stained polyacrylamide gel of LSD1 after anion exclusion column.
Bands identifying LSD1 are inside rectangle boundary (80 kDa).

3.6.2. Phage display results

The number of phages yielded in each round of panning and amplification was determined with the blue plaque forming assay as described earlier.

The selection process was monitored by calculating the output/input ratio (Table 3.1 and Figure 3.12). The output is the number of phages recovered after each amplification step per mL of solution used for the elution steps, while the input is the number of phages used for the panning step.

Table 3.1: Output/input ratio obtained in the four rounds (R) of panning against LSD1 catalytic site.

G_e1-2-3 represent the glycine eluates 1-2-3 whereas P_e1-2-3 the competitive elution.

	R 1		***R 2***		***R 3***		***R4***	
Input (pfu/mL)	**1×10^{11}**		**1×10^{11}**		**1×10^{11}**		**1×10^{11}**	
Output /input (pfu/mL)	G_e1	1.4×10^{-6}	G_e1	4.6×10^{-6}	P_e1	1.4×10^{-5}	P_e1	2.4×10^{-5}
	G_e2	1.5×10^{-6}	G_e2	1.27×10^{-5}	P_e2	7.8×10^{-5}	P_e2	3.5×10^{-5}
	G_e3	2.3×10^{-5}	G_e3	1.23×10^{-4}	P_e3	8.5×10^{-5}	P_e3	1.5×10^{-4}

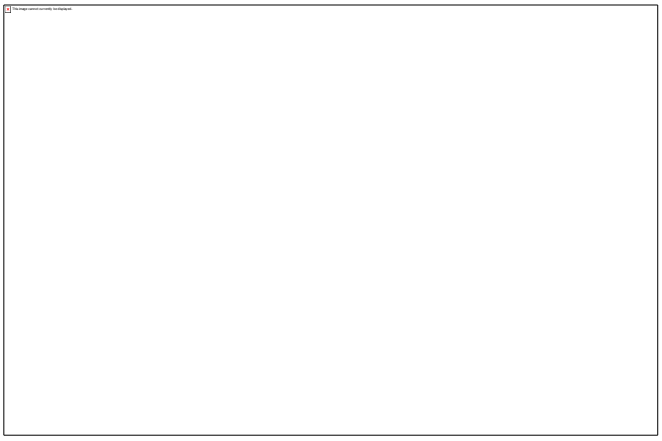

Figure 3.12: Enrichment of displaying peptides targeting LSD1.

The trends observed in the four rounds of panning revealed a progressive selection for higher affinity phage binders. As shown in Figure 3.12, after the first round we observed a surprising loss of peptide diversity, equal to 99%. The used PhD-12^{TM} library contains in 10 µL (10×10^{11} pfu), 1.2×10^{6} different peptides (10 copies of the same peptide) and by recovering only 23.000 peptides we removed the initial great heterogeneity of displayed sequences. This result could have been driven from the limited presence in the library of peptides capable to interact with LSD1. After a second round of panning, the input/output ratio increased, indicating an enrichment of affinity phage. A competitive elution was next used in round 3 and 4 and, after a slight decrease in yield (round 3 compared to round 2) we registered an increase in phage number. The decrease was proportional to the greater degree of stringency applied in round 3. Notably, the last elution step for each elution made, using either glycine or peptide in the process of elution, resulted in the highest titer of phages. A possible explanation could be a higher K_{off} of peptides with affinities for LSD1 and as a consequence, these were released with a slower rate from the target.

Following four rounds of panning, six clones from the amplified round 4 were harvested and their DNA sequenced (Table 3.2).

Table 3.2: Peptide sequences displayed by the sequenced clones after cleavage.

Clone	*Peptide sequence*
3.1	RKQHAIPLIWPA
3.2	RKQHAIPLIWPA
3.3	GGTKAPRLEHGP
3.4	NPHTHTHGAFVS
3.5	RKQHAIPLIWPA
3.6	RKQHAIPLIWPA

The sequencing revealed that four out of the six clones sequences displayed the same peptide. The enrichment for a specific sequence motif is a recurrent theme in phage display screening and often associated with the increase of fitness of the selected clones for the target.[239]

None of the sequences showed homology with known non-covalent inhibitors of LSD1, reported in Chapter 2 and a search with Basic Local Alignment Search Tool (BLAST,

NCBI, Bethesda, USA) was unable to identify proteins with structural similarities to known LSD1 binding partners. These results were quite unexpected as commonly, screening combinatorial libraries by affinity selection leads to ligands with a certain grade of homology with primary structures interacting with the target.[265]

Peptide **3.4** bears three His residues and the emergence of such amino acids is often correlated with the association of His-rich displayed peptides to the transition metal Ni^{2+}, chelated on the beads employed to capture the protein-phage complex. As histidine-rich clones are not always generated by target-unrelated selection processes,[266,267] peptide **3.4** along with peptides **3.1** and **3.3**, was synthesised and screened. The peptides were prepared via Fmoc-SPPS on a Rink Amide resin to yield sequences with free N-terminus and a C-terminal amide, mimicking the peptides state displayed on the pIII phage protein.

The ability of the purified synthetic peptides to inhibit LSD1 was next examined with Amplex®Red peroxidase-coupled assay. The concentrations used for the screening were the following: 800 µM, 400 µM, 200 µM, 100 µM, 50 µM, 25 µM, 12.5 µM, 6.25 µM and 3.13 µM. SNAG-derived **PRSFLV** peptide was used as a positive control (Table 3.3 and Figure 3.13).

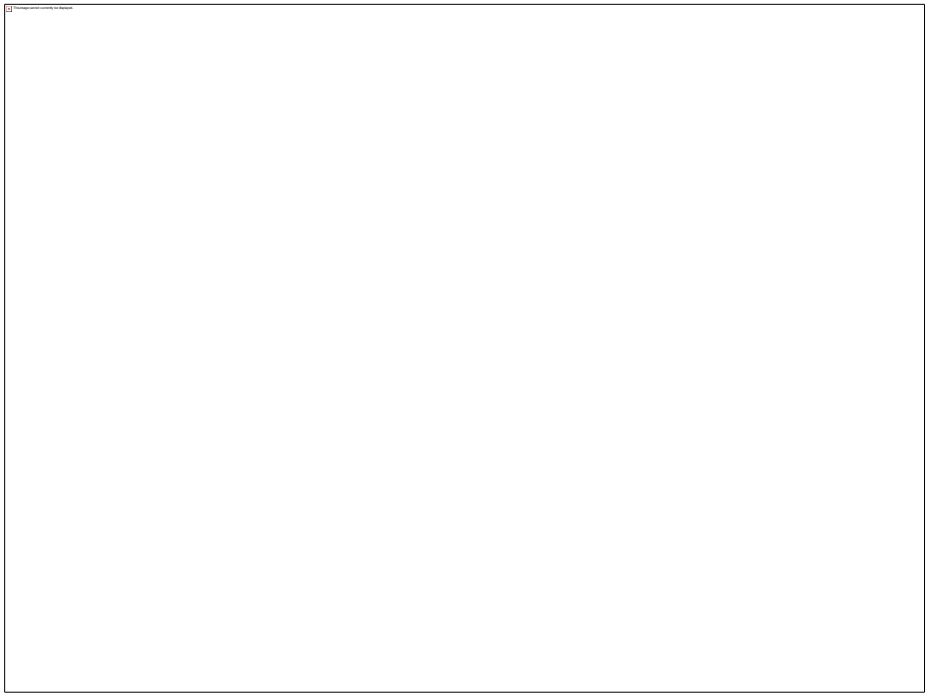

Figure 3.13: Dose-response curves generated with Amplex®Red enzymatic assay testing phage displayed derived peptides.

X-axis is in logarithm of concentration (M, Molar); Y-axis is the % of relative fluorescent unit (RFU) compared to 100% activity (LSD1+substrate, - inhibitor). Data were fitted with nonlinear regression model and are shown as mean ± STD (n=3).

Table 3.3: IC_{50}s values obtained with enzymatic evaluation of phage derived peptides measured with Amplex®Red.

Enzymatic results are expressed as % RFU normalised to pre-treatment level (LSD1 + Substrate, no inhibitor) ± STD (n=3).

Peptide	Sequence	IC_{50} (µM ± STD, n = 3)
3.0	**PRSFLV**	18.4±1.6
3.1	**RKQHAIPLIWPA**	332.7±3.2
3.3	**GGTKAPRLEHGP**	> 800
3.4	**NPHTHTHGAFVS**	> 800

The peptide **RKQHAIPLIWPA (3.1)** inhibits LSD1 at high concentration and was the only peptide showing activity. Despite being inactive at the tested concentrations, the dose-response curve obtained with **3.3** revealed a dose-dependent decrease in demethylase activity. The same concentration-dependent trend was not observed in the case of **3.4**.

3.7. Discussion

The present study was designed to discover non-covalent peptides with affinity to LSD1 by phage display using a 12-mer linear library of random combinatorial peptides; a total of four rounds of panning were performed using full-length human recombinant His-tagged LSD1 and six clones were sequenced.

The selection process was monitored by the estimation of the output/input ratio. Results showed an initial drastic exclusion of the peptides originally present in the PhD-12™ library. In the subsequent rounds of panning we observed a substantial increase of recovered phages. To select for high binders (i.e. phage bound to LSD1 catalytic pocket), we inserted in the elution buffer of rounds 3 and 4, a known peptide ligand, capable of competitively displacing phage bound to the LSD1 active site.

Sequencing results of six randomly selected clones revealed that four out of six clones displayed the same peptide sequence. As suggested by the literature, the recurrence of homologous peptides is either associated with the appropriate selection of affinity phage[239] or it is attributed to propagation related events.[267] Propagation related events occur when certain phages propagate at a faster rate than others and consequently predominate.[267] It has been reported that some displayed sequences can decrease the phage infectivity and consequently, slowing down the phage release from the host cell; another factor contributing to a decrease in diversity is associated with the incompatibility of certain peptides to be displayed on the phage surface.[268]

Nonetheless, within the isolated peptides, the sequence **3.1** was the only one promoting inhibition of LSD1 demethylase activity at 300 µM and normally, faster propagating clones are generally unlikely to have affinity to the target.

Literature evidence reports that moderate affinity peptides are more likely to be selected than high affinity ones.[233,246,269] The strongest affinity peptides can be underrepresented or absent in the chosen library, factors that probably have driven the selection to weaker

binders. Screening other displaying libraries of phage like Ph.D.™-7, can be suggested to exploit further the potential of this technique for the discovery of non-covalent LSD1 inhibitors with more desired characteristics. In keeping with this, the Ph.D.™-12 library manual reports that the increased length of the randomised sequence in the 12-mer library, may enable the target to select sequences via multiple weak binding contacts instead of a few strong contacts; this could have been the case for LSD1 and therefore it would be useful to assess shorter length libraries.

It has been shown that, besides the interaction with the active site, selected peptides can also interact with the target via allosteric modulation.[265] In keeping with this, it has been reported that LSD1 displays supplementary druggable spaces.[231] Therefore these could have been targeted by the displayed peptides and **3.1** could have interacted with other surfaces of LSD1, binding away from the catalytic domain.

The poor activity exerted by **3.1** can also be attributed to the loss of multivalency in the synthetic peptide compared to the corresponding phage. Each phage displays in fact from 3 to 5 copies of each peptide in the pIII protein.[270] Thus the interactions with LSD1 exerted by the multimers during the panning could have differed from the monomeric activity promoted by the synthetic peptides.[271]

Despite the inability to inhibit LSD1 at low concentrations, the dose-response curves of **3.3** indicate a dose-dependent decrease in demethylation, implying that higher concentrations could have contributed potentially to a greater effect.

Peptide **3.4** showed a histidine motif and such sequences, as previously mentioned, are considered target-unrelated hits.[266] Histidine can form a strong coordination bond through the nitrogen of the imidazole ring (electron donor) and the positive Ni^{2+}. During the panning steps, nickel-containing beads have been used for affinity purification and a negative selection step has been introduced in the second round of panning to avoid the selection of such clones.[266,267] Thus, the presence of the motif was considered a coincidence and the peptide was synthesised and tested. However, among all the screened sequences, it is the one that impairs LSD1 demethylase activity the least. The selection of such a clone that most likely derives from the presence of nickel-coated-beads could be avoided by the addition of a preventive pre-selection-step at the beginning of round 3 and 4. Furthermore, it has been estimated that displayed peptides need to have a $K_{off} > 50$ µM to sustain the vigorous washing steps prior to the elution.[272]

Although this is likely to increase the selectivity towards the target, it can equally decrease the number of high affinity binders from the other. A possible strategy to weaken the selection pressure and particularly in targeting LSD1, could have been the reduction in the amount of Tween® (detergent) used during the washing steps in the first rounds of panning. This foresight could have potentially contributed to a less marked loss of phage diversity in round 1.

In rounds 3 and 4 we used a competitive elution in order to increase the selectivity for phages that interact with the LSD catalytic site. As explained before, in this type of elution the rates of association and dissociation from the catalytic site may affect the outcome of the selection process. The elution process is governed by the exposure time of phage-LSD1 complex to the competitor and therefore, shorter exposure could not elute all phages localised in the catalytic site, while longer exposures may elute all phages without discriminating between high and low affinity ones. For this project, we have chosen only one time point (10 min), based on the standard time-course used for enzymatic inhibition of LSD1 antagonist. Perhaps, we should have used different incubation times (5-20 min for example) along round 3 and round 4, to better manage the association and dissociation rate constants (K_{on}/K_{off}) and monitor the selection process by determining the number of recovered phages during each time interval.

To increase peptide-binding efficiency in the post-selected sequences, a strategy reported by some authors is the inclusion of the C-terminal linker sequence GGGS the synthetic peptides.[243,273] However, as the known LSD1 binders interact with the catalytic site via the N-terminal domain, adding residues to the C-terminal domain is unlikely to lead to any improvement to the binding affinities of the synthetic peptides towards LSD1.

3.8. Conclusions

The present study was designed to determine if a peptide screen on a Phage display system could unravel potent, non-competitive inhibitors of LSD1. It represents the first study, which used as eluent a soluble peptide ligand for LSD1. Three peptides were identified from this study and among them the sequence RKQHAIPLIWPA displayed some activity against LSD1 demethylase. This pioneering work can be considered a starting point for the use of this potent technique to explore new non-covalent LSD1 inhibitors.

Chapter 4 - Synthesis of irreversible inhibitors of LSD1 targeting acute myeloid leukaemia

4.1. Introduction

Acute myeloid leukaemia (AML) is a tumour of the myeloid line of blood cell. The genesis of the diseases is still unclear and recently the pathology onset has been associated with epigenetic dysregulations.[84,274] Given the reversibility of the epigenetic modifications, epigenetic modulators have been identified as possible strategic targets for AML therapy, whereby therapeutic interventions are still limited.[67,84,197] LSD1 has crucial roles in both normal hematopoiesis and myeloproliferative disorders via its activity on mono- and di-methylated H3K4 residues and its association with multiple protein complexes such as CoREST,[77] Blimp-1[116] and TAL1.[119]

The activity of LSD1 is usually suppressed irreversibly and several research groups, starting with TCP as a lead, have generated potent and selective molecules (reviewed in Chapter 1). The majority of the drug design efforts have been based on the functionalisation of the TCP scaffold and specifically, on the addition of bulky branched side chains to the phenyl ring.[275] The X-ray crystal structure of the TCP-FAD adduct[159] suggests that the phenyl ring is positioned in a large hydrophobic pocket and besides the contacts with the methyl groups of T335 and T810 through van der Waals interactions, it establishes poor connections with the surrounding surface. This implies that LSD1 catalytic site can accommodate large groups at this position and consequently, these can influence the drugs' final effects.

Moreover, as the MAO catalytic site is smaller compared to that of LSD1, this type of substitution has also shown to increase selectivity *versus* LSD1 over MAO.[162]

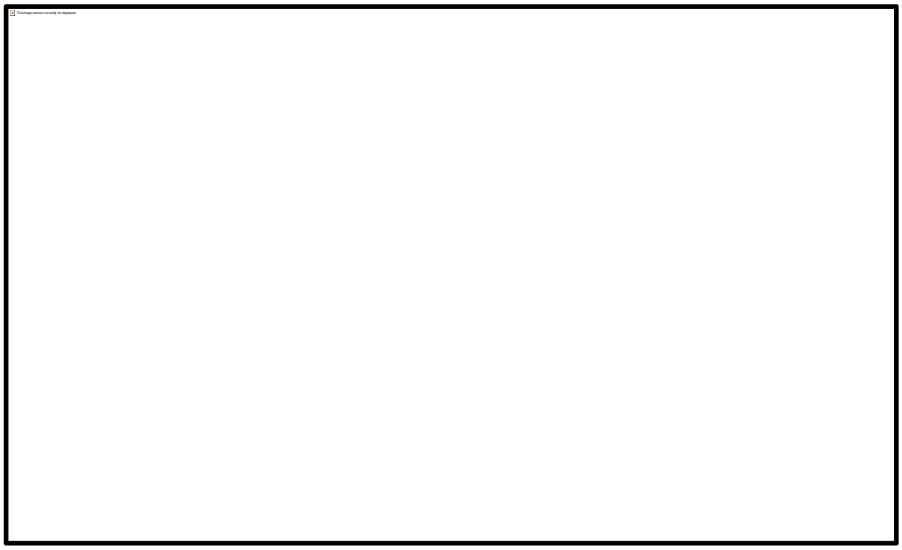

Figure 4.1: TCP-FAD adduct in the hydrophobic catalytic pocket of LSD1.
PDB code: 2XUN; red areas represent hydrophobic surfaces whereas blue areas represent hydrophilic surfaces.

Therefore, TCP analogues presenting large branched groups at the phenyl ring of the TCP scaffold could act as LSD1 inhibitors with increased potency and selectivity. An opposing approach to decorating the phenyl ring is the functionalisation of the TCP nitrogen atom. This strategy has led to the generation of two potent LSD1 inhibitors that recently entered Phase I clinical trials, namely GSK2879552 by GlaxoSmithKline[276] and ORY-1001 by Oryzon[56] (Figure 4.2). The former used for the treatment of relapsed/refractory small cell lung cancers and the latter, for relapsed or refractory acute leukaemia.

Figure 4.2: TCP, GSK2879552 and ORY-1001 molecular structures.

In this study, we aimed to develop a new series of LSD1 covalent inhibitors.

Since TCP is clinically used as a racemic mixture of the two *trans* enantiomers that bind equally well to LSD1, we preferred a non-enantioselective route to our inhibitors. The phenyl ring was decorated with bulky substituents via an efficient synthetic method to increase the enzymatic potency of the lead TCP (K_i 21 μM). Given the recent findings correlating LSD1 with myeloproliferative disorders and the limited therapies for such disease, the enzymatically active compounds were evaluated in leukaemia cell models.

Figure 4.3: General structure of our novel TCP analogues.

4.1.1. Roles of LSD1 in normal hematopoiesis and leukaemia

AML accounts for 34% of adult leukaemia in the UK and long-term survival rates continue to be poor (approximately 30-40%). Although complete remission is achieved after standard chemotherapies employing high doses of anthracycline and cytarabine, patients suffer from frequent relapses of treatment-refractory disease.[277,278] As a consequence, 20% of AML patients do not survive more than 5 years[279,280] and according to the National Cancer Intelligence Network, no improvements on these survival rates in the last two decades have been registered. This unfavourable situation implies a strong need for new therapeutics.

AML is caused by impaired hematopoiesis, which is a complex process whereby hematopoietic stem cells (HSC) differentiate into mature blood cells. The differentiation process ensures a constant blood production during lifetime, giving rise to all the lymphoid and myeloid lineage. The latter give rise to neutrophils, eosinophils, basophils, monocytes and macrophages, megakaryocites, platelets and erythrocytes. Ineffective hematopoiesis leads to an excessive production of immature blood cells, termed blasts, that accumulate in the bone marrow.[281] Such situation is characteristic of myeloproliferative tumours and suppression of hematopoiesis and bone marrow failure are the major consequences of the pathology.[197,278]

In the differentiation process, both methylation and acetylation patterns determine the cell fate decisions by influencing the expression of specific genes in specific cell types. Such patterns are, at least in part, controlled by LSD1 activity.[29,49,281] Given the LSD1 association with multiple protein complexes, the molecular roles of LSD1 in normal hematopoiesis are far for being fully understood.[84] LSD1 is highly expressed in hematopoietic stem cells and participates in normal hematopoiesis.[84] This has been demonstrated by examining the effects of LSD1 knockdown. The lack of LSD1 in murine models has been associated with disruption of granulocytes and red blood cells terminal differentiation, which correlated with the reduction of platelets number and lethal anaemia.[282,283] Similar effects were observed after LSD1 pharmacological suppression[67] and LSD1 deletion in cell lines experiments.[219] Dent *et al.* demonstrated that bone marrow transplantation in a murine model with LSD1 deficient cells was ineffective in producing T and B cells in the recipient mice, emphasising its role also in lymphocytes developement.[69]

At the molecular level, LSD1 participates in hematopoiesis via its association with multiple transcription factors. For example, it cooperates with the transcriptional repressor Blimp-1 to mediate the repression of genes leading to mature B cells.[116] Disruption of the interaction between LSD1 and the growth factors Gfi1 and Gfi1b perturbs hematopoietic differentiation of both normal progenitors and leukaemogenic cells.[219] The LSD1-TAL1 association was also described to regulate cell differentiation programs in both physiological and pathological contexts.[119]

While LSD1 plays a critical role in the normal hematopoiesis, its over-expression is linked to the genesis and the fatal prognosis of AML patients.[84,284] In pre-clinical studies, LSD1 was shown to sustain the oncogenic potential of leukaemic stem cells in a murine model of human myeloid leukaemia (MLL-AF9). Moreover, in the same study, TCP derivatives triggered the differentiation process.[67] Accordingly, Schenk and coworkers showed that the exposure of HL-60 and U937 AML cell lines (which are insensitive to the differentiation therapy with *trans* retinoic acid-ATRA) to TCP-ATRA combined treatments retrieved the cells expression of the differentiation markers CD11b and CD14. Additionally, the treatment was proven to be non-toxic for normal, fast reproducing HSC cells.[86] Therefore, LSD1 inhibitors could be employed as differentiating agents for leukaemia treatment.

As LSD1 has simultaneous roles in normal blood cell development and myeloproliferative disorders, one of the majors concerns with the pharmacological interventions using LSD1 suppressors remains the possible disruption of terminal differentiation of normal blood stem cells.[285] Nevertheless, the current therapies for leukaemia also promote transient cytopenia and anaemia and these consequences are managed efficiently.[197] In addition, cytopenia induced by LSD1 inhibition appears to be reversible, supporting LSD1 as a promising therapeutic target for AML.[67]

Synthetic approach

Several methods have been reported for the generation of the TCP core.[171,172,174,175] Generally, these procedures involve the formation of the cyclopropyl ring by either ylide initiated Michael addition or transition metal catalysed cyclopropanation with diazo-compounds as sources of carbenes.

For the synthesis of our library of TCP analogues we adopted the procedures shown in Scheme 4.1.

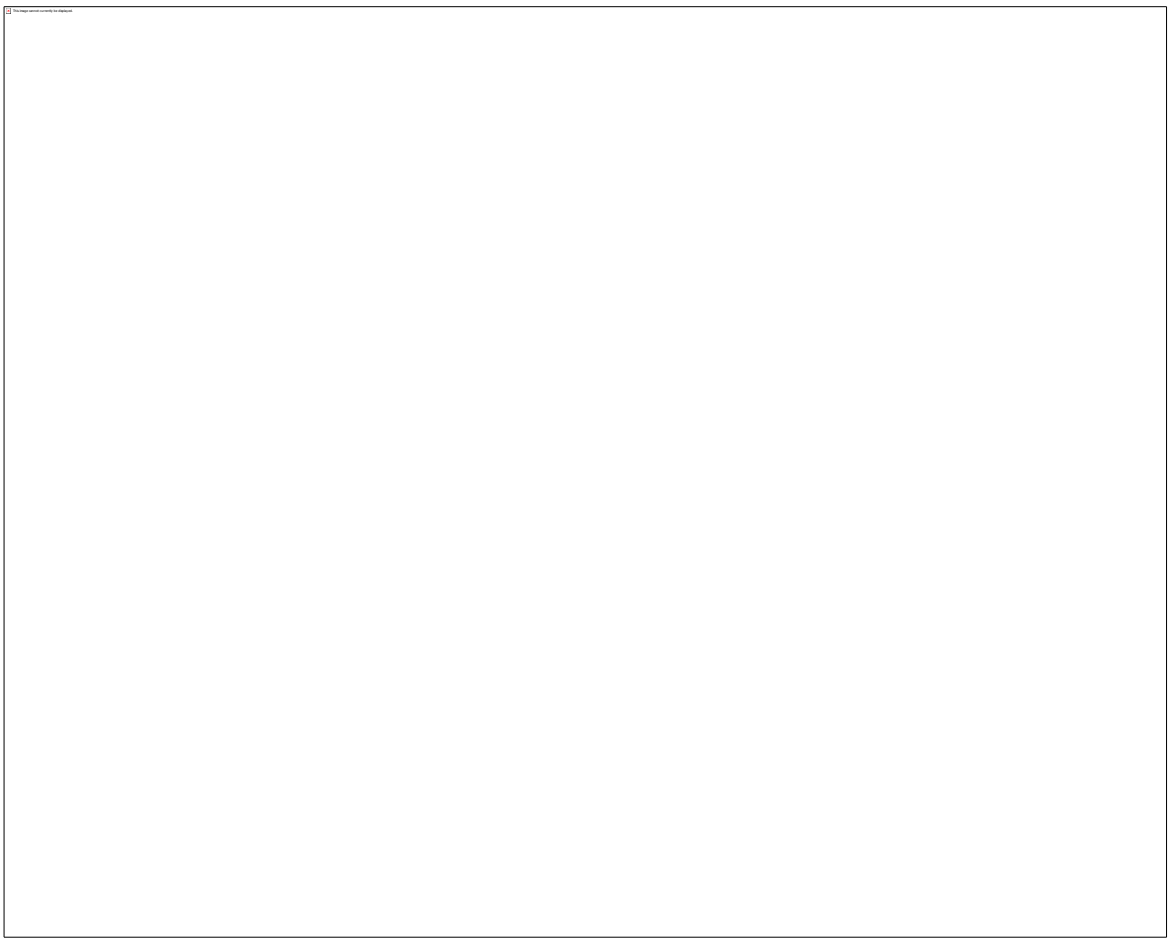

Scheme 4.1: Synthetic strategy adopted for the generation of novel TCP derivatives.

In this approach, commercially sourced 4-formyl benzaldehyde **4.1** was esterified with anhydrous MeOH and acetyl chloride to give **4.2**. As we expected to decorate at a later stage of the synthesis the phenyl ring of TCP with bulky groups, we carefully chose the protective groups so that the conditions used for the removal of these to get the TCP core were compatible with the stability of the initial methyl ester protection.

To achieve a stereoconfiguration equivalent to TCP, corresponding to the *trans* isomers of 2- phenylcyclopropylamine (racemate of (−) and (+) enantiomers, 50:50 mixture of 1*S*,2*R* (+) and 1*R*,2*S* (−)), we followed two steps from one of the recent Oryzon patents by Guibourt and colleagues.[177] Firstly, we converted the aldehyde of **4.2** to olefin via Horner-Wadsworth-Emmons reaction to obtain the (*E*) *tert*-butyl acrylate derivative **4.3**. Secondly, to achieve the *trans* tert-butyl cyclopropanecarboxylate derivative, of formula **4.4**, we performed Johnson-Corey-Chaykovsky cyclopropanation.

The Horner–Wadsworth–Emmons reaction is a variant of the Wittig reaction and one of the most used methods for the preparation of alkenes.[286] It involves the use of phosphonate-stabilised ylides (phosphonate carbanions) generated by deprotonation with moderately strong bases, such as potassium *tert*-butoxide (KO*t*-Bu). The formed ylide is a strong nucleophile and attacks the electrophilic C-atom of the aldehyde generating an oxyanion ring. The intermediate creates an unstable four-membered oxaphosphetane intermediate. Decomposition of the oxaphosphetane ring by disruption of the C-P and C-O σ bonds leads to the formation of the C=C π bond of the alkene and a phosphate ester as a side product (Scheme 4.2).[286] The use of a stabilised ylide ensures the *E*-selectivity of the resultant olefin.[286]

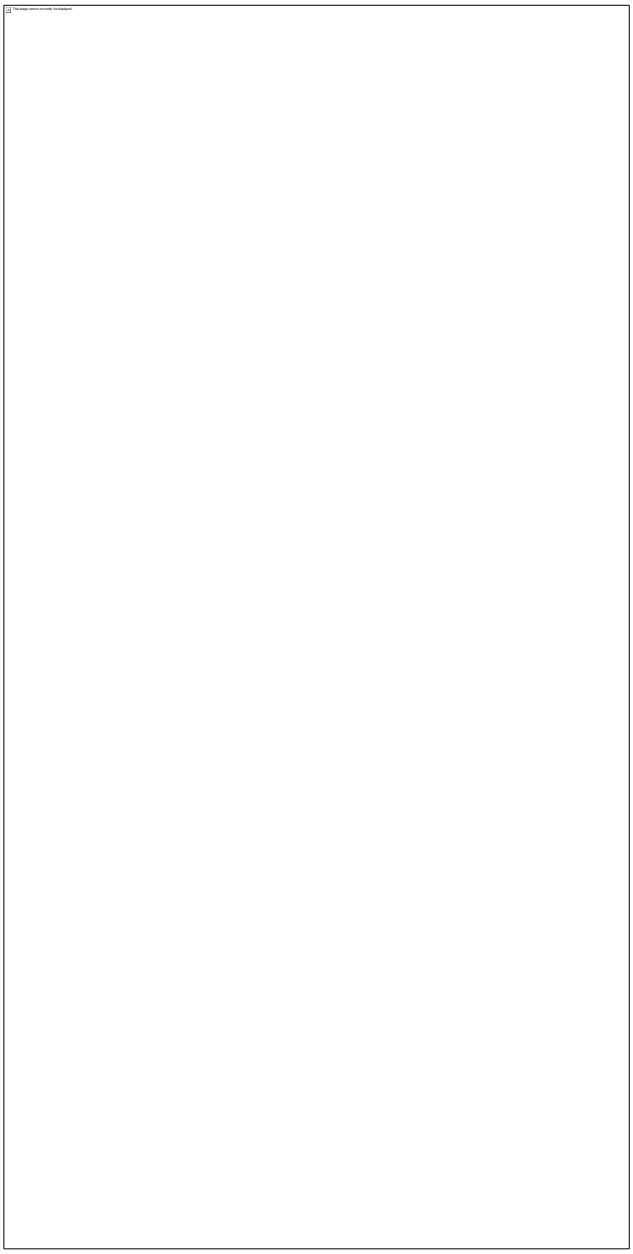

Scheme 4.2: Horner–Wadsworth–Emmons mechanism.

The analysis of the NMR spectrum of **4.3** confirmed the successful *E*-olefination. The calculated *J*-coupling for the hydrogen at 6.43 ppm is 16 Hz, which is typical of vicinal *trans* hydrogens.

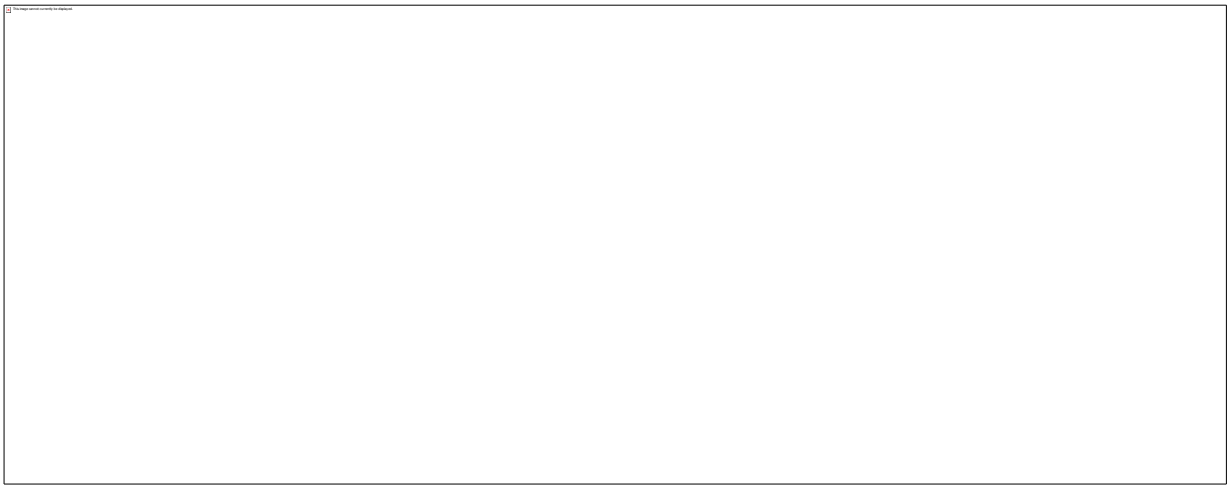

Figure 4.4: NMR spectrum of 4.3 (^{1}H NMR, $CDCl_3$).
The doublet at 6.43 ppm has a *J* value of 16.0 Hz, typical of vicinal *trans* hydrogens.

In the Oryzon patent is reported the use of triethyl phosphonoacetate for the conversion to the acrylate, leading to the formation of an ethyl acrylate derivative. Instead, we employed *tert*-butyl diethyl phosphonoacetate to achieve the *tert*-butyl protected acrylate. This is because we protected the carboxylic acid in *para* position at phenyl ring with a methyl ester. The use of *tert*-butyl diethyl phosphonoacetate enabled the removal of the *tert*-butyl-protected acrylate in acidic conditions, in which the methyl ester protection is stable. In contrast, using triethyl phosphonoacetate would have required deprotection in basic conditions in the following synthetic steps (see below), with inevitable removal of the initial methyl ester protection.

The cyclopropanation following the Johnson-Corey-Chaykovsky method was used in both the works of Guibourt *et al.*[177] and Ueda *et al.*[172]

After deprotonation of trimethylsulfoxonium iodide ($Me_3S(O)^+I^-$, the methyl donor) with sodium hydride (NaH) in DMSO, the generated ylide (dimethyloxosulfonium methylide, Corey-Chaykovsky reagent) was added to the alkene to form the cyclopropyl ring of the TCP core (**4.4**).

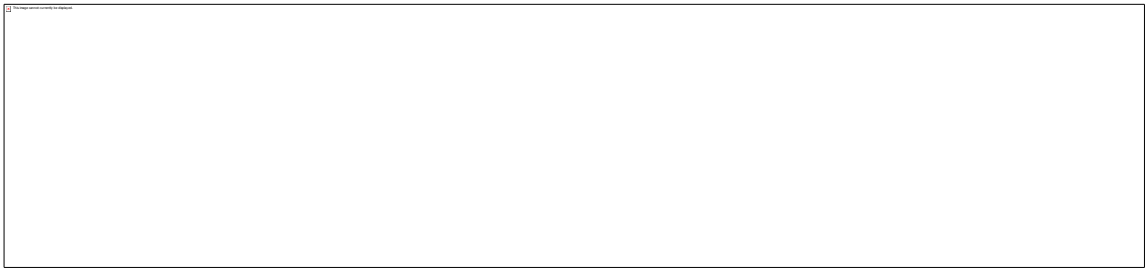

Scheme 4.3: Ylide-initiated Michael addition.

Johnson-Corey-Chaykovsky cyclopropanation is usually non-specific and both (*E*) and (*Z*) olefins give *trans*-cyclopropanes.[287] The *trans* configuration of 4-methyl arylcyclopropyl-*tert*-butyl ester **4.4** was confirmed by the $^{1}H–^{1}H$ coupling constants of the cyclopropyl moiety (J_{ab}=4.2-4.5 Hz).

We next hydrolysed *tert*-butyl protecting group of **4.4** with TFA and triethylsilane in DCM and achieved the carboxylic acid with formula **4.5**. The acid was converted to acyl azide with diphenylphosphoryl azide (DPPA) and the acyl azide rearranged to isocyanate by Curtius rearrangement. The formed isocyanate intermediate can further react with nucleophiles in solution and in this case, the product was scavenged with *tert*-butanol, being the reaction solvent. This afforded the *tert*-butyloxy (Boc) carbamate derivative with formula **4.6**. The Curtius rearrangement was utilised successfully by Ueda and colleagues and by our group for the generation of several TCP analogues.[170,172]

The methyl ester protection at the *para* position of the TCP core was next removed with basic conditions using LiOH in water-THF and the obtained Boc-amino-phenyl cyclopropyl benzoic acid **4.7** was coupled to several substituted amines using 1-Ethyl-3-(3-dimethylaminopropyl) carbodiimide (EDCI) and HOBt as coupling reagents with Hünig's base (Scheme 4.4).[288] The coupling step afforded the amide intermediates **4.8a-s** (Scheme 4.1). Final hydrolysis of the Boc protecting group in acidic conditions (HCl 6 N) completed the synthesis of the targeted compounds **4.9-4.27**.

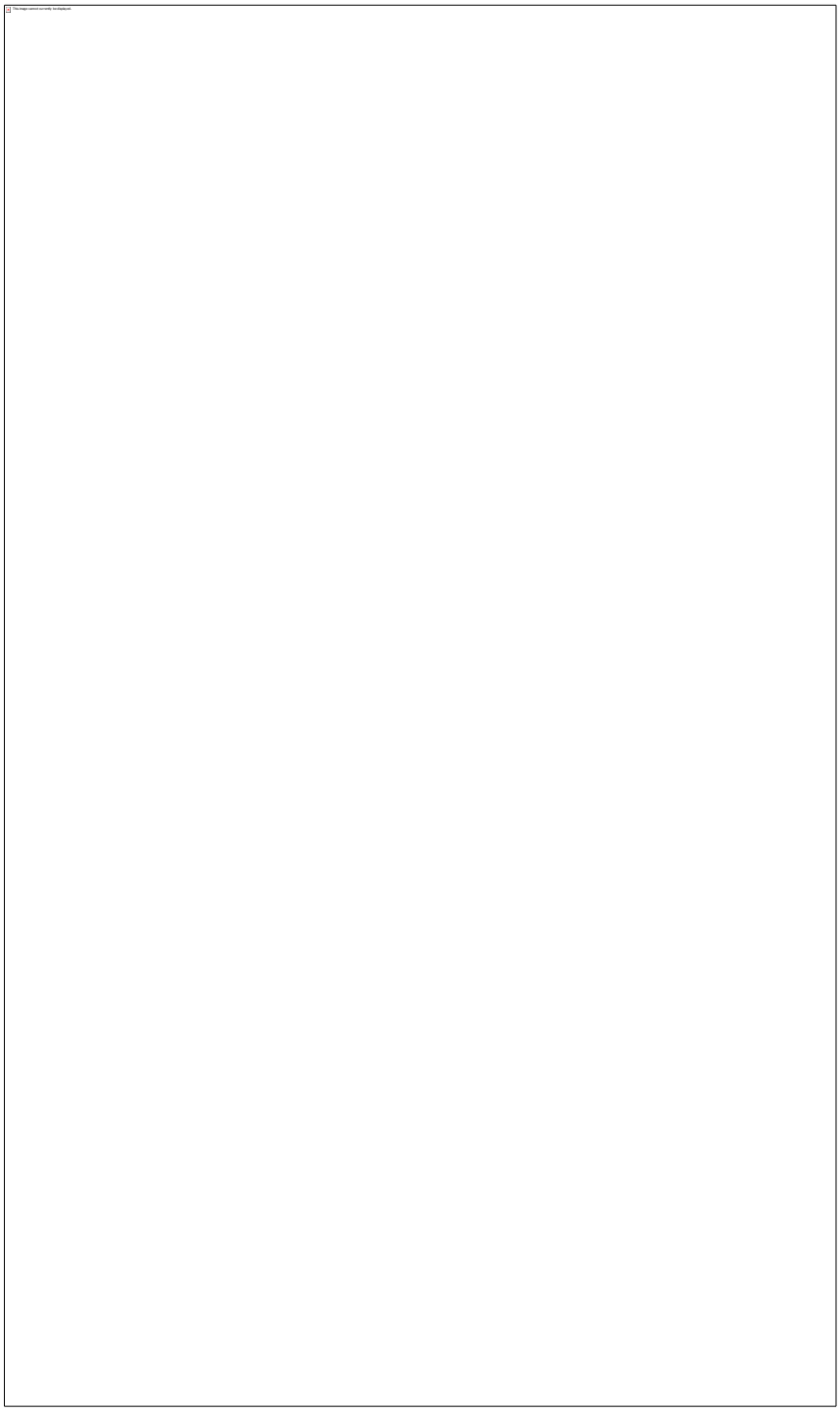

Scheme 4.4: Coupling reaction mechanism.

Figure 4.5: Library of new TCP derivatives.

The Boc-protected precursors of **4.22**, **4.23**, **4.24**, **4.25** and **4.27** were very difficult to purify. Particularly, the use of HCl (6 N) for the deprotection of intermediates **4.8-n** and **4.8-o** substituted in para with 1-(2-pyridyl) piperazine and 1-(2-pyrimidyl) piperazine was unsuccessful and only deprotection with weaker acidic conditions enabled the amine albeit in a very low yield (13%). During the course of this study, a Takeda patent was published with similar amide analogues of TCP and these were obtained with an equivalent synthetic procedure.[178] Among them, compound **4.10** features in the company work; all the other compounds represent instead novel chemical entities.

4.2. Enzymatic evaluation of novel LSD1 inhibitors

To measure the ability of **4.9**-**4.27** in inhibiting LSD1 enzymatic activity, we performed a peroxidase-coupled assay (Amplex®Red).

The compounds activity was firstly measured at 50 and 10 µM and if such treatment produced detectable inhibition, a dose-response experiment was carried out in order to determine the half maximal inhibitory concentration (IC_{50}). To this end, five to nine concentration points for each compound were evaluated in triplicate and the fluorescence results fitted in a sigmoid dose-response curve (Table 4.1).

Table 4.1: Results obtained with the enzymatic evaluation of TCP derivatives 4.9-4.27.

Results are expressed as % RFU normalised to pre-treatment level (LSD1 + Substrate, no inhibitor) ± STD (n=3).

Compound	IC_{50} (μM±STD, n=3)
TCP	21
4.9	20.0±0.3
4.10	0.3±0.01
4.11	0.4 ± 0.04
4.12	0.7±0.01
4.13	17.4±0.9
4.14	0.6±0.01
4.15	2.4±0.1
4.16	5.8±0.5
4.17	1.3±0.3
4.18	0.9±0.2
4.19	> 50
4.20	32.0±0.3
4.21	21.4±0.7
4.22	1.5±0.2
4.23	1.8±0.5
4.24	0.5±0.1
4.25	0.9±0.1
4.26	0.5±0.04
4.27	1.8±0.3

Selected examples of the sigmoidal dose-response curves obtained with the enzymatic evaluations are shown in Figure 4.6.

Figure 4.6: Dose-response curves showing the effects of TCP derivatives on LSD1 enzymatic activity.
(A) TCP; (B) 4.10; (C) 4.11; (D) 4.14 (E) 4.26; (F) 4.27.
The X-axis is in logarithm of concentration (M, Molar); the Y-axis is the % of relative fluorescent unit (RFU) compared to 100% activity (LSD1 + substrate, no inhibitor). Data were fitted with nonlinear regression and are shown as means ± STD (n=3).

Overall, enzymatic evaluations revealed an increased ability of the substituted analogues to inhibit LSD1 demethylase activity compared to TCP scaffold, being **4.10**, **4.11** and **4.14** among the most potent analogues.

Compounds that were more potent than TCP (IC_{50} enzymatic assay < 21 µM, namely **4.10**, **4.11**, **4.12**, **4.13**, **4.14**, **4.15**, **4.16**, **4.17**, **4.18**, **4.21**, **4.23**, **4.24**, **4.25**, **4.26** and **4.27**) were further evaluated in biological assays.

4.3. Biological evaluation of novel LSD1 inhibitors in cell models of leukaemia

4.3.1. Cell viability

To test weather the inhibition of the enzymatic activity of LSD1 in a cell-free assay could be translated in pharmacological effects in cells, active compounds were tested in six AML cellular models and namely HL-60, MV4-11, KASUMI, U937, OCI-AML3 and THP-1 cell lines. These AML lines are representative of three AML subtypes according to the FAB classification, which ranks AMLs based on their differentiation status, being M1 the least and M6 the most differentiated class.[289]

Table 4.2: FAB classification of the AML cell lines used.

M2	M4	M5
KASUMI1	OCI-AML3	MV4-11
HL-60		THP-1
		U937

After incubation with the LSD1 inhibitors, cell survival was quantified using CellTiter-Glo®, a luminescent reagent that detects the presence of metabolically active cells by measuring the quantity of adenosine triphosphate (ATP) in the system (Figure 4.7).

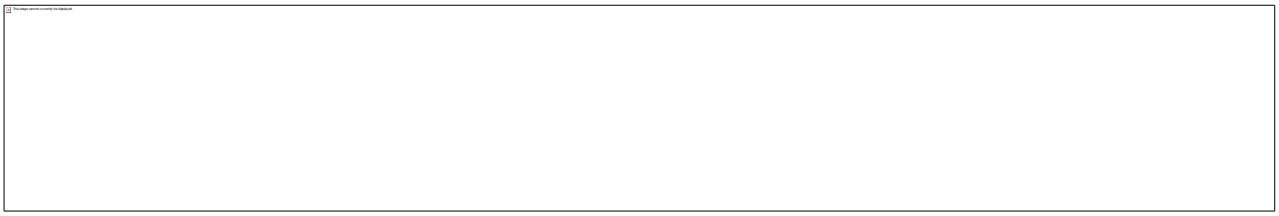

Figure 4.7: CellTiter-Glo® luminescence.
The luciferase contained in Ultra-Glo™ uses the luciferin as substrate in the presence of ATP, releasing bioluminescence. Adapted from the manufacturer manual.[290]

The first set of experiments was performed to estimate the anti-proliferative activity of TCP in the AML cell lines and define the appropriate experimental conditions (concentrations and course of treatment) to evaluate the activities of the novel TCP-derived analogues. To do so, cells were treated with five concentrations (1 µM, 3 µM, 10 µM, 30 µM and 100 µM) and cultured for 48 h and72 h (Figure 4.8).

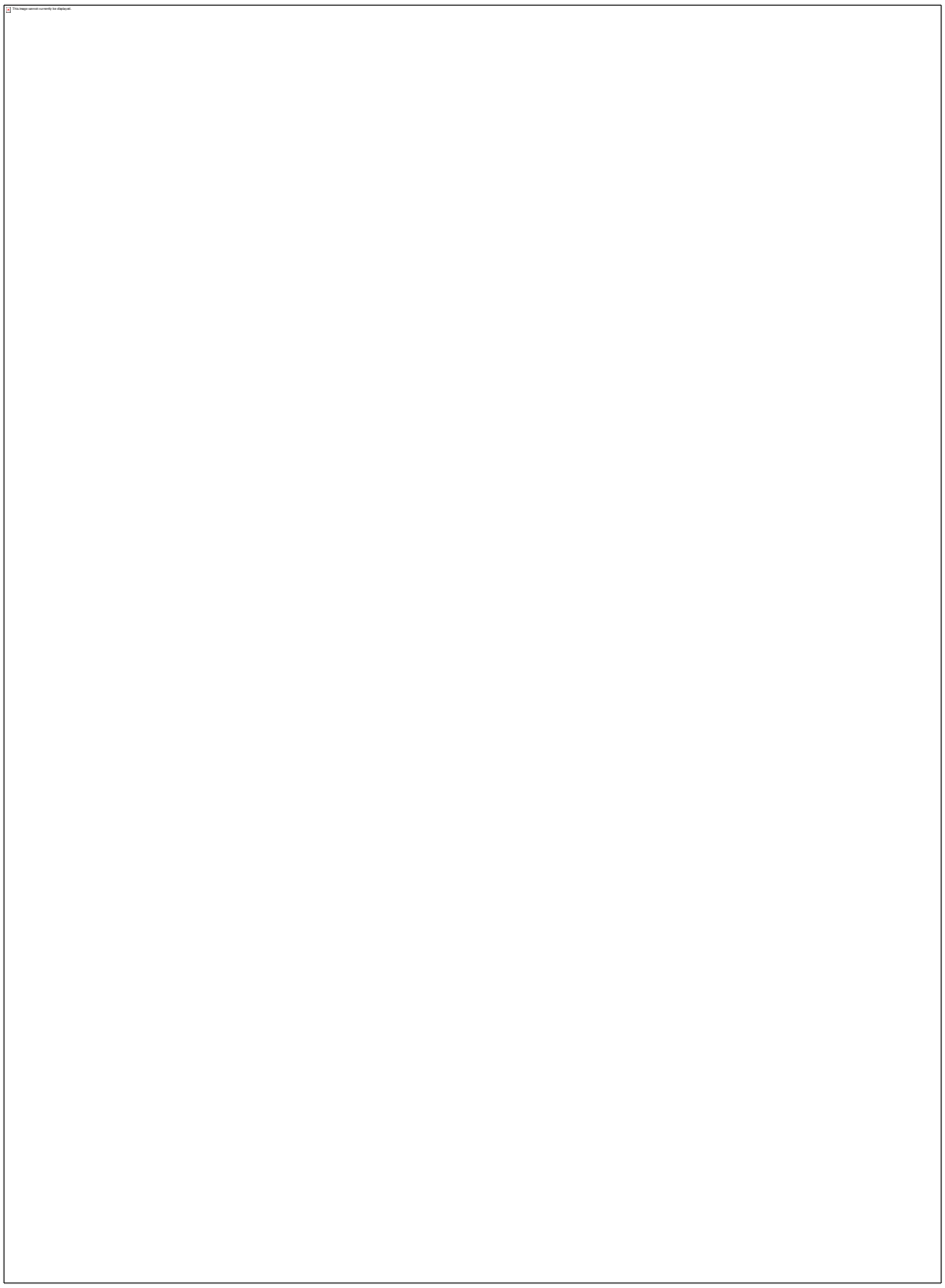

Figure 4.8: Effects of TCP on the proliferation of AMLs (48 h and 72 h).

Survival (RLU) was normalised to pre-treatment levels (untreated cells). Statistical significance was determined with two-way ANOVA and corrected for multiple comparisons using Dunnett's test. Data are shown as means ± STD (n=5); *p < 0.05, **p < 0.01, ***p < 0.001, ****p < 0.0001.

TCP treatments revealed to hinder the viability of KASUMI, HL-60, MV4-11 and OCI-AML3 cells at 3-10 µM, while U937 and THP-1 were not significantly affected. Generally, marked effects were registered following 72 h exposure.

The anti-proliferative activities of **4.10** and **4.11**, which demonstrated exceptional abilities in suppressing LSD1 enzymatically, were next evaluated. The compounds were first tested at two concentrations (1 µM and 100 nM). As the enzymatic inhibition of such compounds increased by 50-fold compared to TCP, cellular activity was predicted to fall in this range of concentrations. Viable numbers were measured after 24 h, 48 h, 72 h and 120 h with CellTiter-Glo® (Figure 4.9 and 4.10).

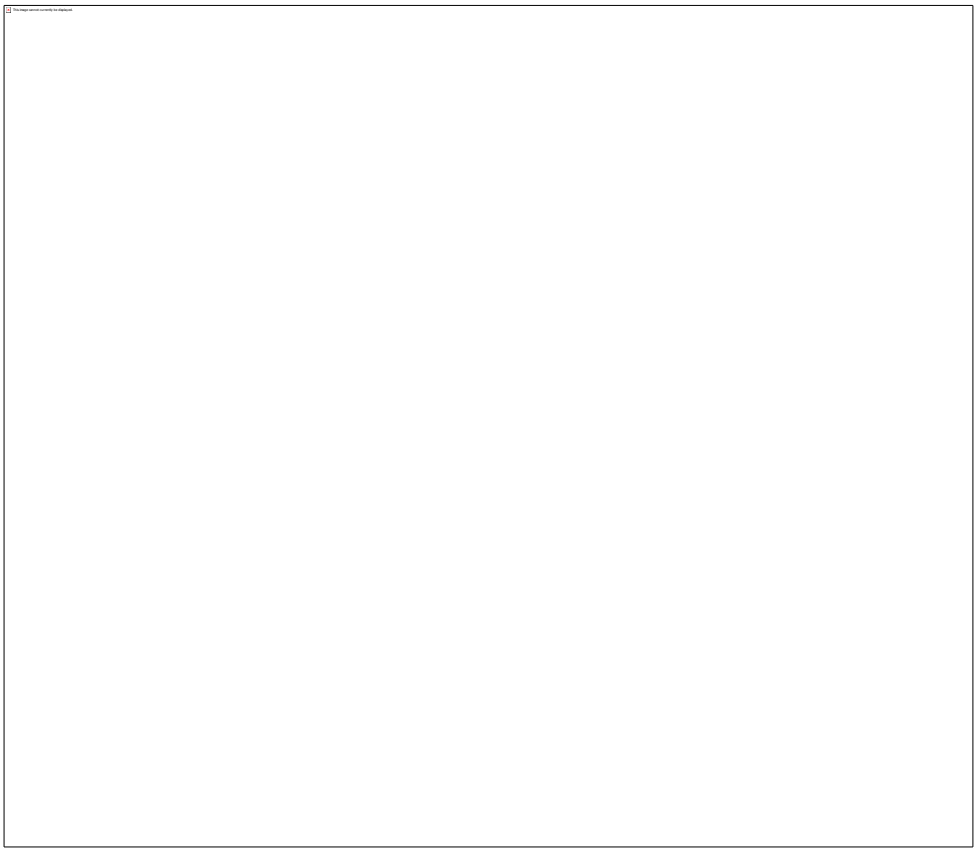

Figure 4.9: Effects of TCP analogue 4.10 (100 nM and 1 µM; 24 h, 48 h, 72 h and 120 h) on the proliferation of AMLs.

Survival (RLU) was normalised to pre-treatment levels for each cell line. Statistical significance was determined with one-way ANOVA and corrected for multiple comparisons using Dunnett's test. Data are shown as means ± STD (n=5); *p < 0.05, **p < 0.01, ***p < 0.001, ****p < 0.0001).

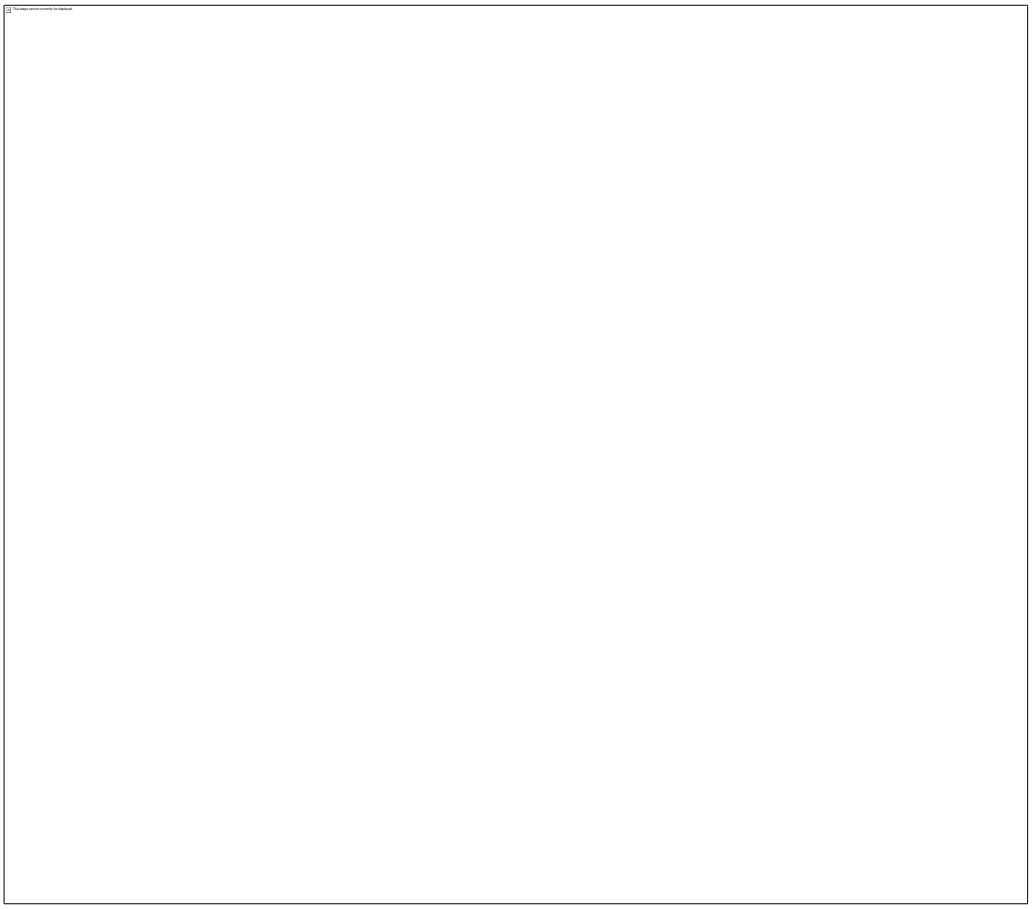

Figure 4.10: Effects of TCP analogue 4.11 (100 nM and 1 µM; 24 h, 48 h, 72 h and 120 h) on the proliferation of AMLs.

Survival (RLU) was normalised to pre-treatment levels for each cell line. Statistical significance was determined with one-way ANOVA and corrected for multiple comparisons using Dunnett's test. Data are shown as means ± STD (n=5); *p < 0.05, **p < 0.01, ***p < 0.001, ****p < 0.0001).

This preliminary evaluation confirmed the enhanced anti-proliferative activity of the novel compounds compared to the scaffold TCP. The effects exerted by **4.10** and **4.11** resulted similar. A substantial drop in cell proliferation was generated after prolonged exposures (48-120 h) and the most significant effects were detected in HL-60, THP-1, KASUMI and MV4-11 cells, whereby survival was significantly decreased at 1 µM. Interestingly, after short-time incubation (24 h and 48 h) an increment in cell proliferation was observed, mostly evident in OCI-AML3. The registered data are in agreement with the increased expression of LSD1 in poorly differentiated AMLs reported in the literature. LSD1 is greatly expressed in cells ranked in the FAB-M1 subtype[84] and HL-60 and KASUMI belong to the FAB-M2 subtype, also characterised by poor differentiated blasts. A high reduction in cell viability was also reported for

MV4-11 cells, ranked in the M5 subtype and characterised in contrast, by cells with a more differentiated status.

After assessment of **4.10** and **4.11**, the anti-leukaemic activity of the remaining compounds, belonging to the new library of TCP derivatives, was examined in similar experimental conditions. Although the most evident decrease in cell proliferation was recorded at 120 h, prolonged incubation can lead to cell stress and depletion of medium nutrients. For these reasons, the effects of **4.12-4.25** were evaluated following 72 h treatment and at the previously reported concentrations (1 μM and 100 nM, Figures 4.11-4.21). As compounds **4.26** and **4.27** have been synthesised later on to further extend the library, these were not included in the first tests.

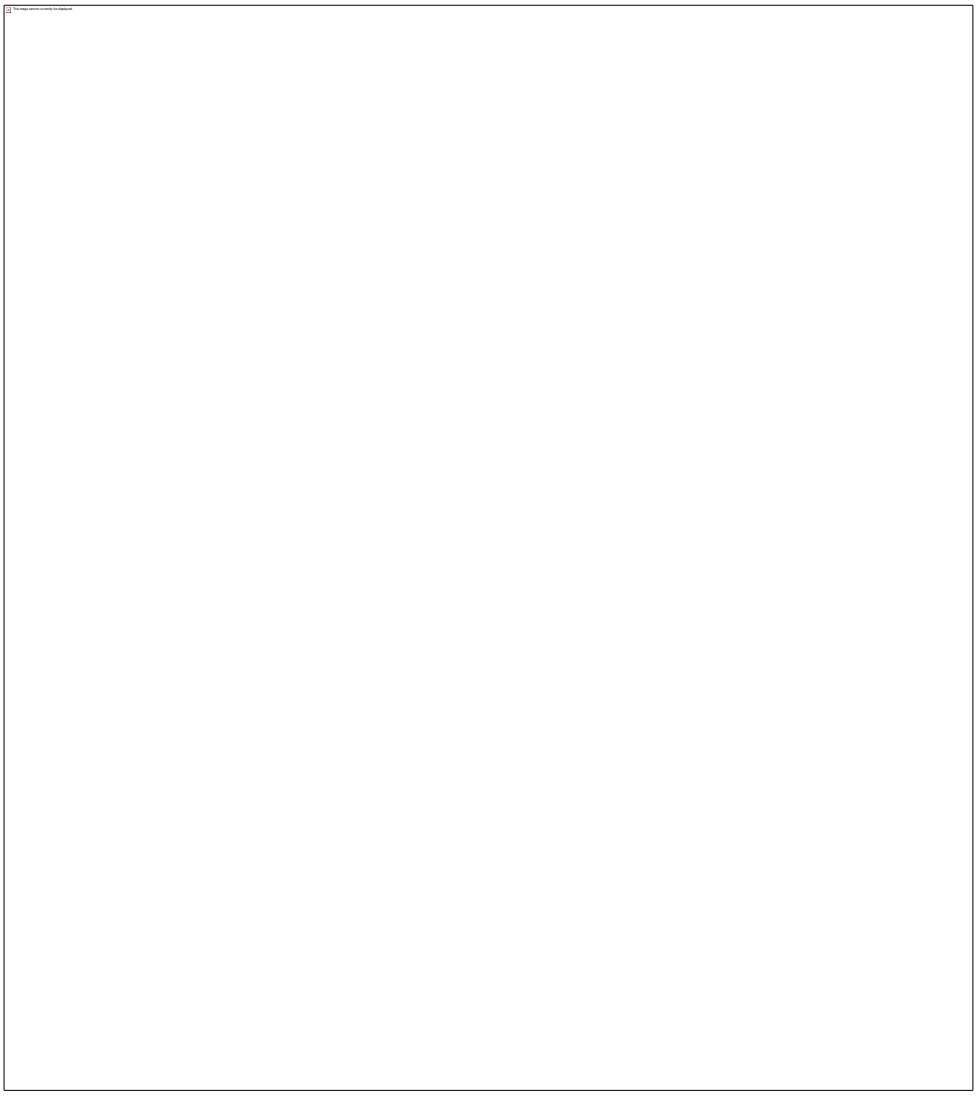

Figure 4.11: Effects of TCP analogue 4.12 (100 nM and 1 µM, 72 h) on the proliferation of AMLs.
Survival (RLU) was normalised to pre-treatment levels for each cell line. Statistical significance was determined with one-way ANOVA and corrected for multiple comparisons using Dunnett's test. Data are shown as means ± STD (n=5); *p < 0.05, **p < 0.01, ***p < 0.001, ****p < 0.0001.

Figure 4.12: Effects of TCP analogue 4.13 (100 nM and 1 µM, 72 h) on the proliferation of AMLs.
Survival (RLU) was normalised to pre-treatment levels for each cell line. Statistical significance was determined with one-way ANOVA and corrected for multiple comparisons using Dunnett's test. Data are shown as means ± STD (n=5); *p < 0.05, ** p < 0.01, ***p < 0.001, ****p < 0.0001.

Figure 4.13: Effects of TCP analogue 4.14 (100 nM and 1 µM, 72 h) on the proliferation of AMLs.

Survival (RLU) is normalised to pre-treatment levels for each cell line. Statistical significance was determined with one-way ANOVA and corrected for multiple comparisons using Dunnett's test. Data are shown as means ± STD (n=5); *p < 0.05, **p < 0.01, ***p < 0.001, ****p < 0.0001.

Figure 4.14: Effects of TCP analogue 4.15 (100 nM and 1 µM, 72 h) on the proliferation of AMLs.
Survival (RLU) was normalised to pre-treatment levels for each cell line. Statistical significance was determined with one-way ANOVA and corrected for multiple comparisons using Dunnett's test. Data are shown as means ± STD (n=5); *p < 0.05, **p < 0.01, ***p < 0.001, ****p < 0.0001.

Figure 4.15: Effects of TCP analogue 4.16 (100 nM and 1 µM, 72 h) on the proliferation of AMLs.
Survival (RLU) was normalised to pre-treatment levels for each cell line. Statistical significance was determined with one-way ANOVA and corrected for multiple comparisons using Dunnett's test. Data are shown as means ± STD (n=5); *p < 0.05, **p < 0.01, ***p < 0.001, ****p < 0.0001.

Figure 4.16: Effects of TCP analogue 4.17 (100 nM and 1 µM, 72 h) on the proliferation of AMLs.
Survival (RLU) was normalised to pre-treatment levels for each cell line. Statistical significance was determined with one-way ANOVA and corrected for multiple comparisons using Dunnett's test. Data are shown as means ± STD (n=5); *p < 0.05, ** p < 0.01, *** p < 0.001, ****p < 0.0001.

Figure 4.17: Effects of TCP analogue 4.18 (100 nM and 1 µM, 72 h) on the proliferation of AMLs.
Survival (RLU) was normalised to pre-treatment levels for each cell line. Statistical significance was determined with one-way ANOVA and corrected for multiple comparisons using Dunnett's test. Data are shown as means ± STD (n=5); *p < 0.05, ** p < 0.01, *** p < 0.001, ****p < 0.0001.

Figure 4.18: Effects of TCP analogue 4.21 (100 nM and 1 µM, 72 h) on the proliferation of AMLs.
Survival (RLU) was normalised to pre-treatment levels for each cell line. Statistical significance was determined with one-way ANOVA and corrected for multiple comparisons using Dunnett's test. Data are shown as means ± STD (n=5); *p < 0.05, ** p < 0.01, *** p < 0.001, ****p < 0.0001.

Figure 4.19: Effects of TCP analogue 4.23 (100 nM and 1 µM, 72 h) on the proliferation of AMLs.
Survival (RLU) was normalised to pre-treatment levels for each cell line. Statistical significance was determined with one-way ANOVA and corrected for multiple comparisons using Dunnett's test. Data are shown as means ± STD (n=5); *p < 0.05, ** p < 0.01, ***p < 0.001, ****p < 0.0001.

Figure 4.20: Effects of TCP analogue 4.24 (100 nM and 1 µM, 72 h) on the proliferation of AMLs.
Survival (RLU) was normalised to pre-treatment levels for each cell line. Statistical significance was determined with one-way ANOVA and corrected for multiple comparisons using Dunnett's test. Data are shown as means ± STD (n=5); *$p < 0.05$, ** $p < 0.01$, *** $p < 0.001$, ****$p < 0.0001$.

Figure 4.21: Effects of TCP analogue 4.12 (100 nM and 1 µM, 72 h) on the proliferation of AMLs.
Survival (RLU) was normalised to pre-treatment levels for each cell line. Statistical significance was determined with one-way ANOVA and corrected for multiple comparisons using Dunnett's test. Data are shown as means ± STD (n=5); *p < 0.05, ** p < 0.01, *** p < 0.001, ****p < 0.0001.

With the exception of compound **4.21**, which was devoid of activity, all the tested compounds caused a significant decrease of AMLs viability at the selected concentrations. In accordance with the data obtained with the previous evaluations of TCP, **4.10** and **4.11** the cell lines resulting most sensitive to anti-LSD1 treatments were KASUMI, HL-60, THP-1 and MV4-11 cells.

To further characterise the active new compounds, IC_{50}s were determined by exposing AMLs to a broader range of concentrations (10 µM, 3 µM, 1 µM, 0.3 µM, 0.1 µM, 0.03 µM, 0.01 µM, 0.003 µM and 0.001 µM) and the survival rates measured after 72 h incubation.

Figure 4.22: Dose-response curves showing the effects of 4.10 on AMLs proliferation (72 h).

The X-axis is in logarithm of concentration (M, Molar); Y-axis is the % of RLU (relative luminescence unit) compared to 100% activity (vehicle control, DMSO). Data are shown as means ± STD (n=5).

Figure 4.23: Dose-response curves showing the effects of 4.11 on AMLs proliferation (72 h).
The X-axis is in logarithm of concentration (M, Molar); Y-axis is the % of RLU (relative luminescence unit) compared to 100% activity (vehicle control, DMSO). Data are shown as means ± STD (n=5).

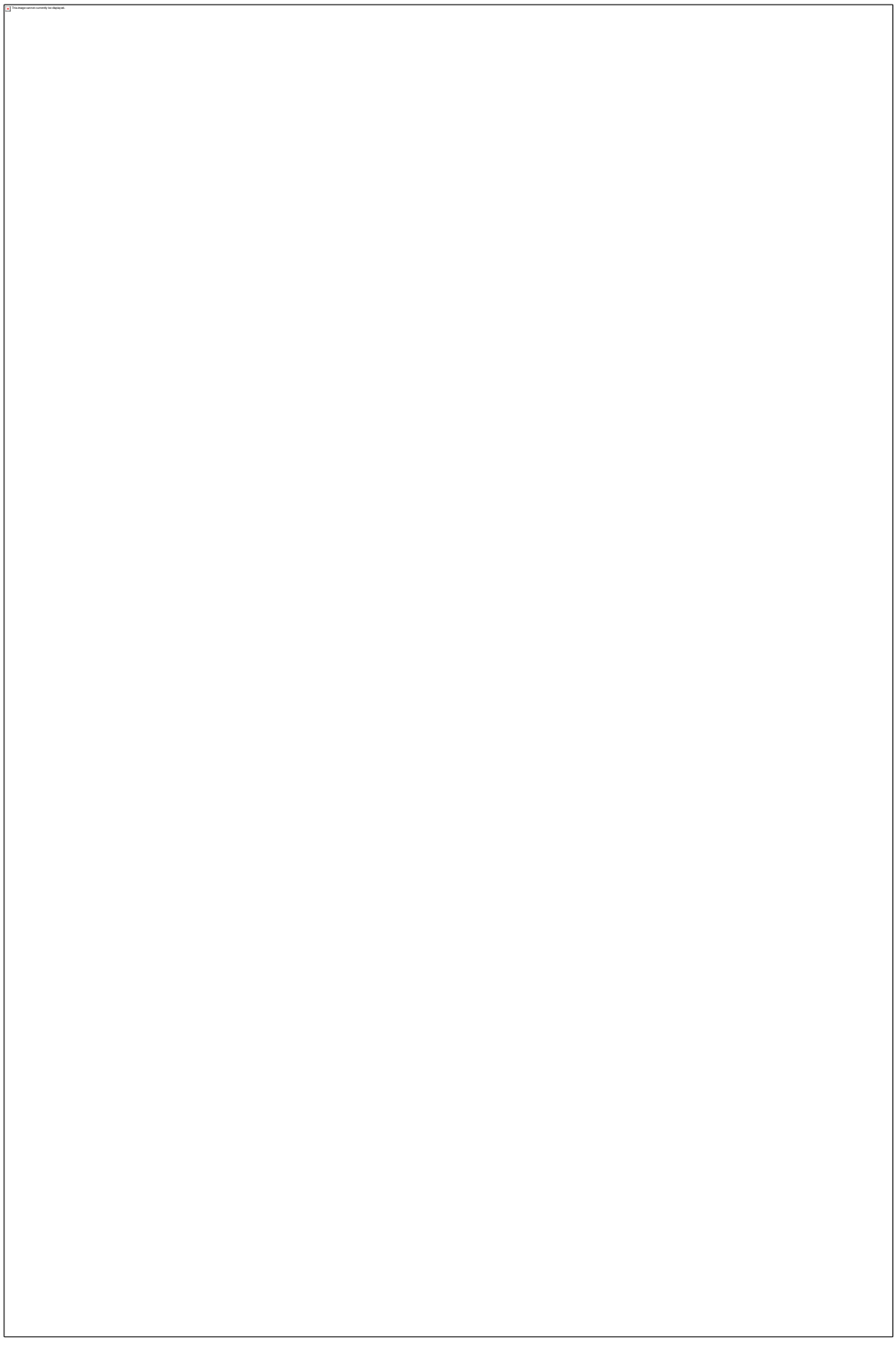

Figure 4.24: Dose-response curves showing the effects of novel TCP-derivatives on AMLs proliferation (72 h). The X-axis is in logarithm of concentration (M, Molar); Y-axis is the % of RLU (relative luminescence unit) compared to 100% activity (vehicle control, DMSO). Data are shown as means ± STD (n=5).

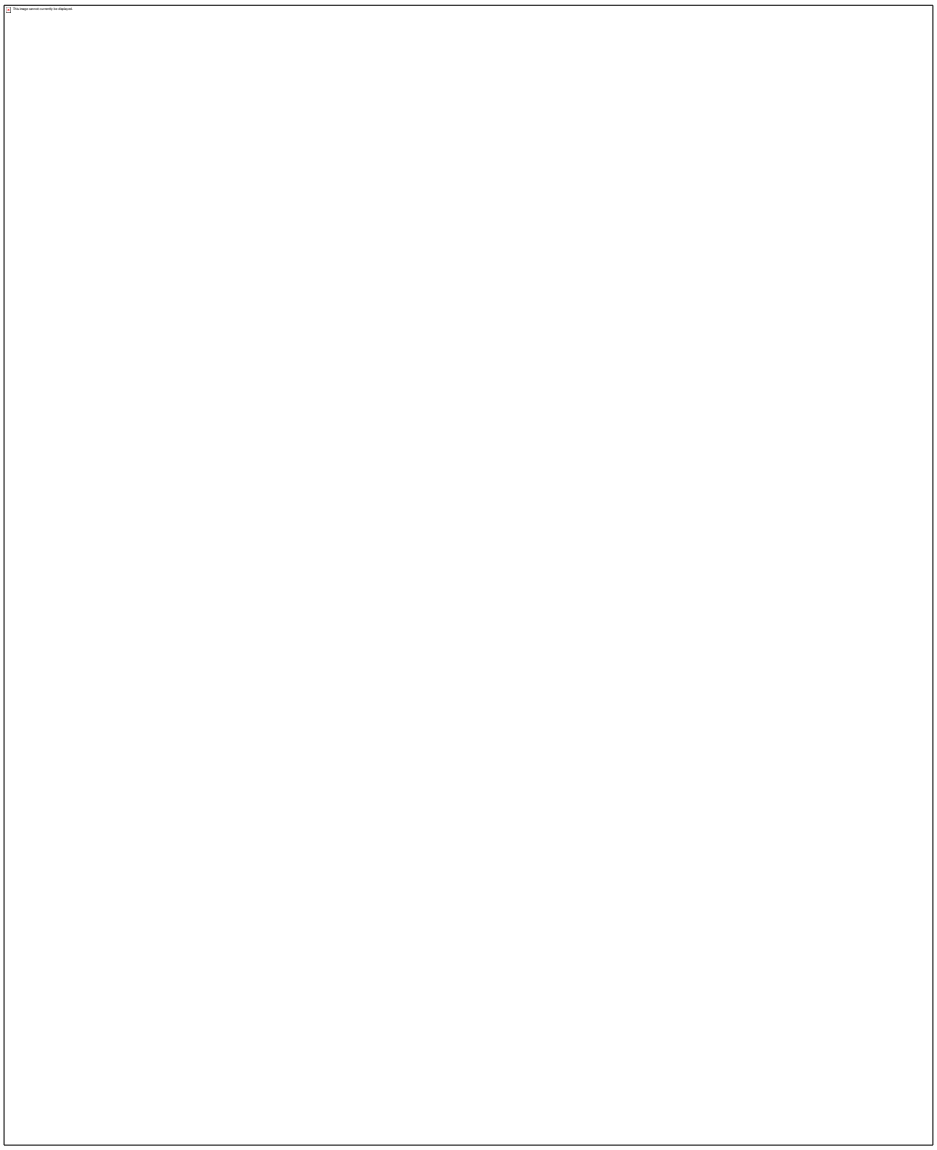

Figure 4.25: Dose-response curves showing the effects of novel TCP-derivatives on AMLs proliferation (72 h). The X-axis is in logarithm of concentration (M, Molar), Y-axis is the % of RLU (relative luminescence unit) compared to 100% activity (vehicle control, DMSO). Data are shown as means ± STD (n=5).

Table 4.3: *In vitro* anti-proliferative results of novel TCP-analogues on AMLs.
Values are reported in μM ± STD (n=5).

	IC_{50} (μM ± STD, n=5)					
Compound						
	KASUMI	**U937**	**HL-60**	**OCI-AML3**	**THP-1**	**MV4-11**
TCP	32±1.8	> 100	84±15.0	89±13.0	81±3.9	63±8.4
4.10	0.03±0.03	1.6±0.09	1.7±0.14	1.8±0.08	0.1±0.08	0.18±0.07
4.11	0.7±0.03	1.2±0.02	0.09±0.01	0.06±0.04	0.2±0.02	0.19±0.4
4.14	0.4±0.01	0.6±0.01	0.6±0.01		1.0±0.10	0.1 ± 0.08
4.15	0.4±0.27	0.6±0.08				1.2±0.01
4.16	0.3±0.01					0.1±0.02
4.17	0.06±0.008				0.4±0.1	0.2±0.07
4.18	0.02±0.001					0.2±0.02
4.23	2.3±0.4		0.6±0.3			
4.25						0.2 ± 0.07
4.26			0.1±0.02	0.2±0.01		
4.27			0.3±0.01			

Results revealed that after 72 h treatment, the new TCP derivatives were able to arrest cell proliferation and particularly, **4.10** and **4.11** were active in the entire panel of analysed AMLs. Interestingly, the dose-response curves revealed that none of the new analogues produced a 100% inhibition of cells proliferation.

4.3.2. Evaluations of activity persistence

A washout experiment was carried out next to verify the covalent inhibition.[291] This consists of cells/protein/enzymes being treated with the tested inhibitor for a short period of time and then in clearing the inhibitor from the system by washout. The residual activity of the washed-out treatment is measured and compared to a continuous treatment (without washout). For covalent blockers, the washed out samples should demonstrate the persistence of the activity.[291] In such experiments cells were treated with 100 µL of media containing 200 nM of analogues **4.10**, **4.11** and **4.14** or left untreated for a period of 6 hours. After the short exposure, medium containing the drug was removed (washout) and replaced by inhibitor-free medium. Following 72 h culturing, survival rates in washout samples were measured and the values obtained compared with the survivals rates of continuous treatment (72 h treatment without a pre-exposure followed by drug-containing medium removal).

The direct comparison between pulsed (washout) *versus* continuous treatment (Figure 4.26), confirmed that compounds **4.10**, **4.11** and **4.14** indeed act in an irreversible fashion as the anti-proliferative effects were maintained despite the washout.

Figure 4.26: Washout experiments with TCP derivatives 4.10, 4.11 and 4.14.

Results were obtained with CellTiter-Glo® and RLU was normalised to control (untreated). Statistical significance was determined with one-way ANOVA and corrected for multiple comparisons using Dunnett's test. Data are shown as means ± STD (n=5).

4.3.3. Evaluation of post-treatment H3K4me2 expression levels by immunoblotting

We next evaluated the H3K4me2 expression levels in KASUMI cells treated with TCP derivative **4.11** by immunoblotting.

Treated cells (200 nM concentration) were cultured for 2 h, 4 h, 6 h, 48 h and 72 h. Cell lysates were separated by 14% SDS-polyacrylamide gel electrophoresis (SDS-PAGE) and blotted membranes were probed for H3K4me2 and H3 (total).

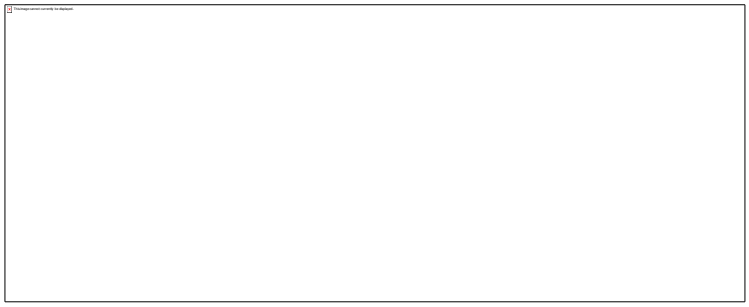

Figure 4.27: Western blot analysis of the methylation state of H3 after treatment of KASUMI cells with compound 4.11 (200 nM) for different time points. The blots indicated the H3K4me2 levels (top) compared to H3 (total, loading control - bottom).

Data revealed that 200 nM treatment with **4.11** were sufficient to promote an increase of H3K4me2 over time, strikingly correlating the compounds activities with LSD1 inhibition. The highest levels of expression were detected after 48 and 72 h of incubation, while shorter exposures were in contrast unable to produce significant modulation of H3K4me2 expression. The result evidentiated the slow course of action of the new TCP analogues, which was already observed in cell viability assays.

4.3.4. CD86 evaluations

By RNA sequencing and analysis of the THP-1 cell line upon treatment with an inhibitor of LSD1, Somervaille's group has recently described the transcriptome that correlates with LSD1 inhibition.[196] The group found that one of the most up-regulated genes was CD86. This cluster of differentiation belongs to the immunoglobulin family and operates as a linker for the co-inhibitory immune response of the CTL4 and CD28 receptors.[292,293] The CD86 marker is expressed by antigen-holding property cells, such as macrophages, dendritic cells and monocytes.[292] It is currently used as a biological marker to demonstrate cellular LSD1 inhibition.[196]

To evaluate a potential increase of CD86 expression triggered by the novel LSD1 inhibitors, THP-1 cells were incubated with **4.10** and **4.11** (200 nM) and after the appropriate treatment course (24 h, 48 h, and 72 h) the cells surface was stained with CD86 antibody (Ab) conjugated with a fluorophore (fluorescein isothiocyanate FITC). Cells were next analysed by flow cytometry (Figures 4.28 and 4.29).

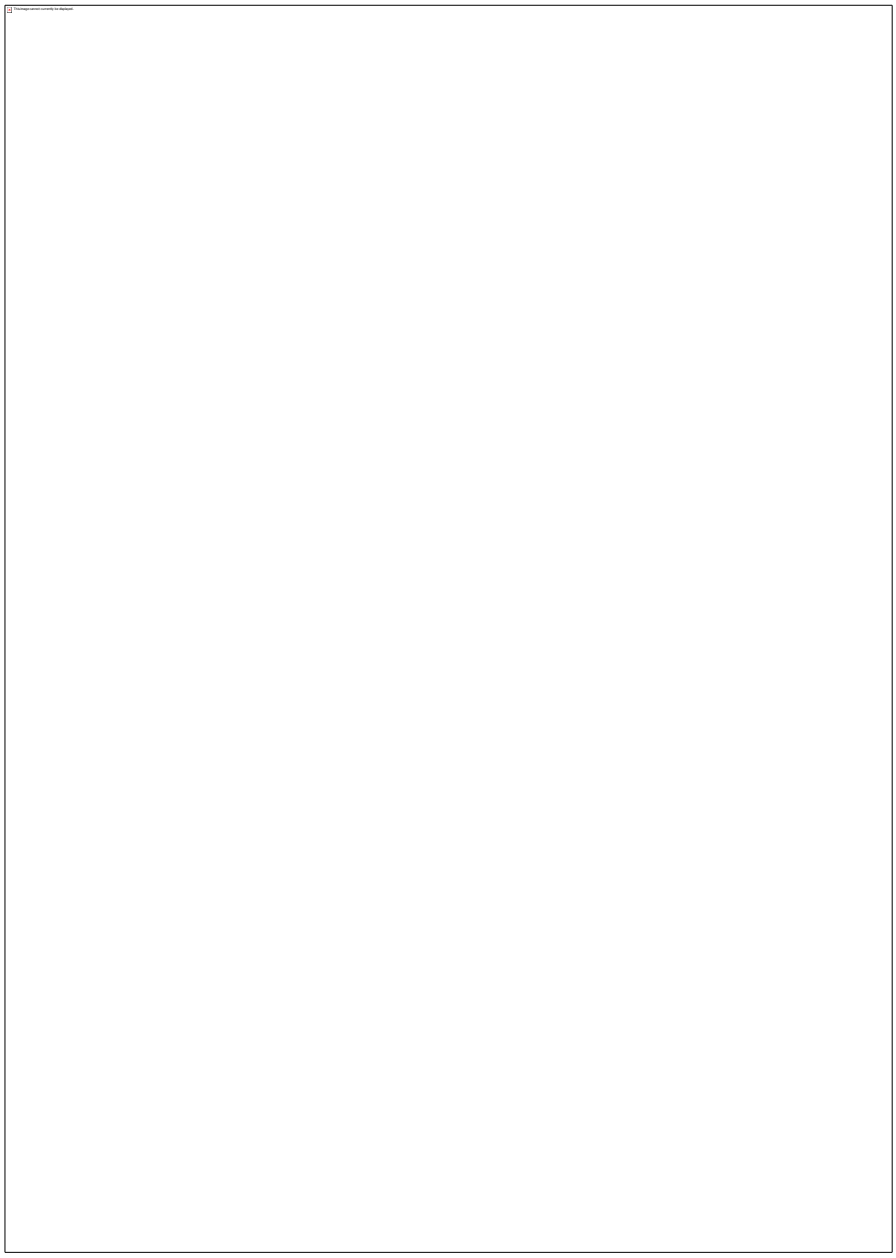

Figure 4.28: Effects of 4.10 (200 nM, 24 h, 48 h and 72 h) on the expression of CD86 in THP-1 cells.
(A) 24 h treatment; **(B)** 48 h treatment; **(C)** 72 h treatment; **(D)** statistical analysis. Cells were gated based on forward scatter (FSC) and side scatter (SSC) parameters. In the X-axis are reported the mean fluorescence increase of treated cells stained with CD86-FITC conjugated Ab and the fluorescent increase of the control (untreated cells- IgG Isotype-FITC). In the Y-axis is reported the cell count. Graphs **D-E** shows the results graphically summarised for three independent experiments. Statistical significance was determined with two-way ANOVA and corrected for multiple comparisons with Bonferroni's test. Values are expressed as means % of increase ± STD (n=3); ****$p < 0.0001$.

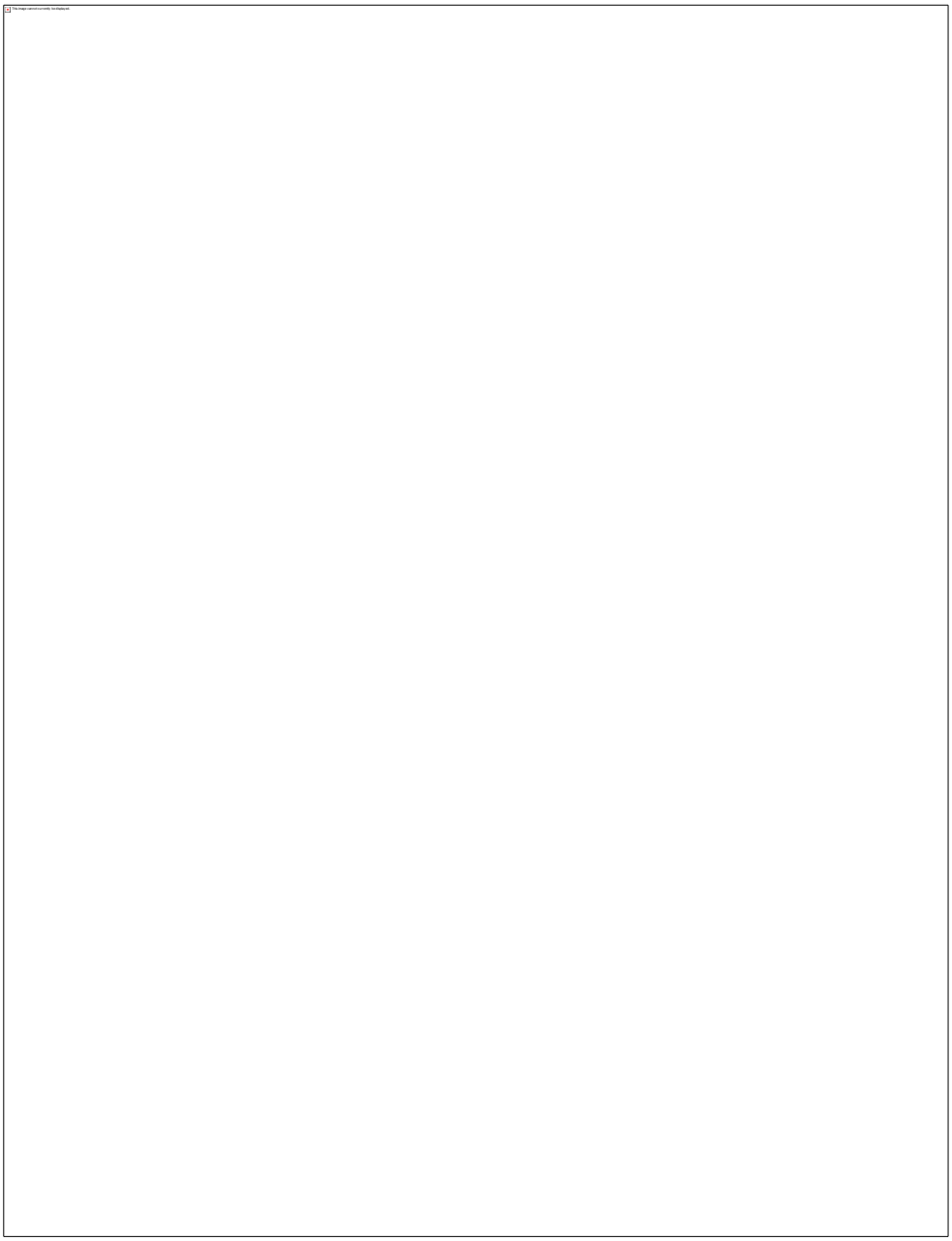

Figure 4.29: Effects of 4.11 (200 nM, 24 h, 48 h and 72 h) on the expression of CD86 in THP-1 cells.
(A) 24 h treatment; **(B)** 48 h treatment; **(C)** 72 h treatment; **(D)** statistical analysis. Cells were gated based on FSC and SSC parameters. In the X-axis are reported the mean fluorescence increase of treated cells stained with CD86-FITC conjugated Ab and the fluorescent increase of control (untreated cells- IgG Isotype-FITC). In the Y-axis is reported the cell count. Graphs **D-E** shows the results graphically summarised for three independent experiments. Statistical significance was determined with two-way ANOVA and corrected for multiple comparisons with Bonferroni's test. Values are expressed as means % of increase ± STD (n=3); ****$p < 0.0001$.

Following 24 h treatment, only a small percentage of cells incremented the CD86 expression. The effects become more evident with time as after 48 h and 72 h incubation with **4.10** and **4.11**, the CD86 expression increased by 70-90% in all the analysed samples (Table 4.4). The data prompted us to investigate if **4.10** and **4.11** were capable to induce CD86 expression in other cell lines (MV4-11, OCI-AML3 and KASUMI cells, Figure 4.30-4.31).

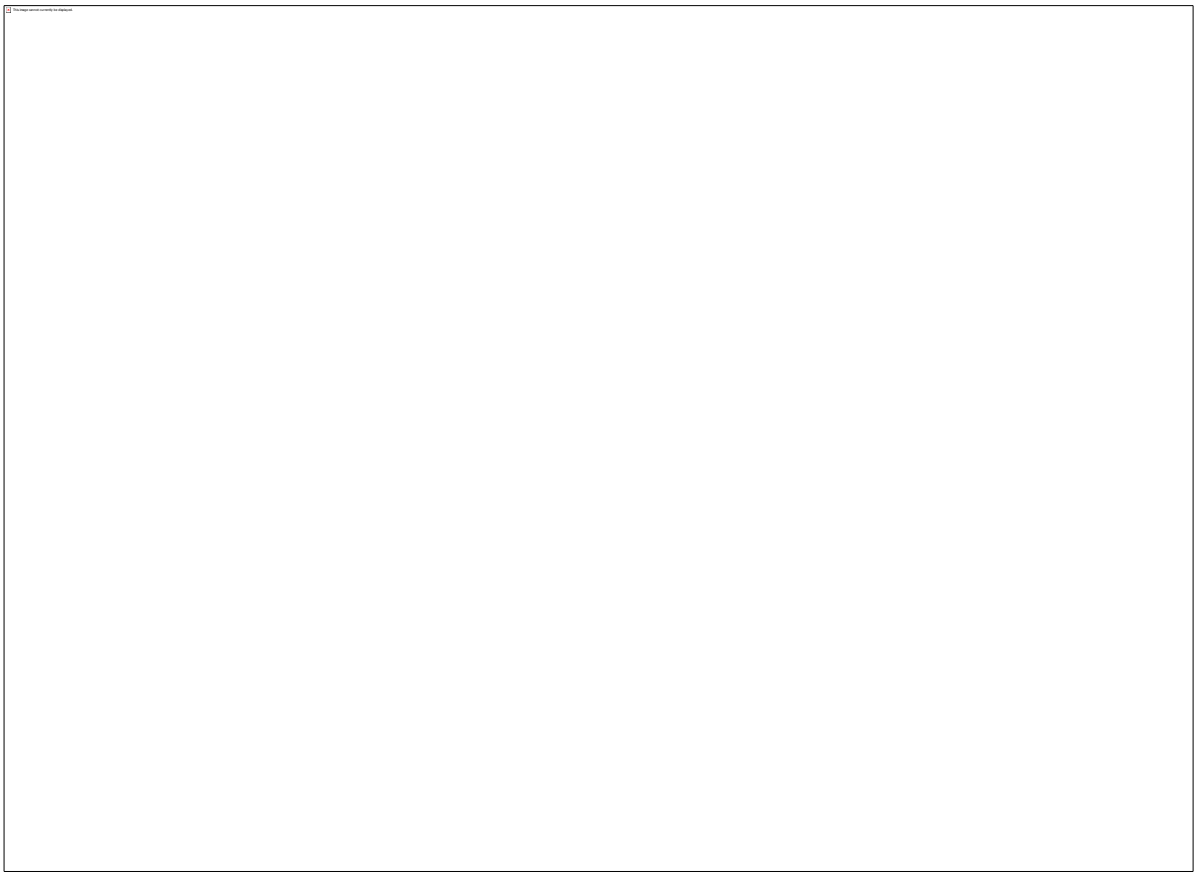

Figure 4.30: Effects of 4.10 and 4.11 (200 nM, 48 h and 72 h) on the expression of CD86 in MV4-11 cells.
(A-B) Results following 48 h and 72 h treatments with **4.10**; **(D-E)** results following 48 h and 72 h treatments with **4.11**; **(C-F)** statistical analysis; cells were gated based on FSC and SSC parameters. In the X-axis are reported both the mean fluorescence increase of treated cells stained with CD86-FITC conjugated Ab and the fluorescent increase of control (untreated cells- IgG Isotype-FITC). In the Y-axis is reported the cell count. Statistical significance was determined with two-way ANOVA and corrected for multiple comparisons with Bonferroni's test. Values are expressed as means % of increase (compared to control) ± STD (n=3); **p < 0.01; ****p < 0.0001.

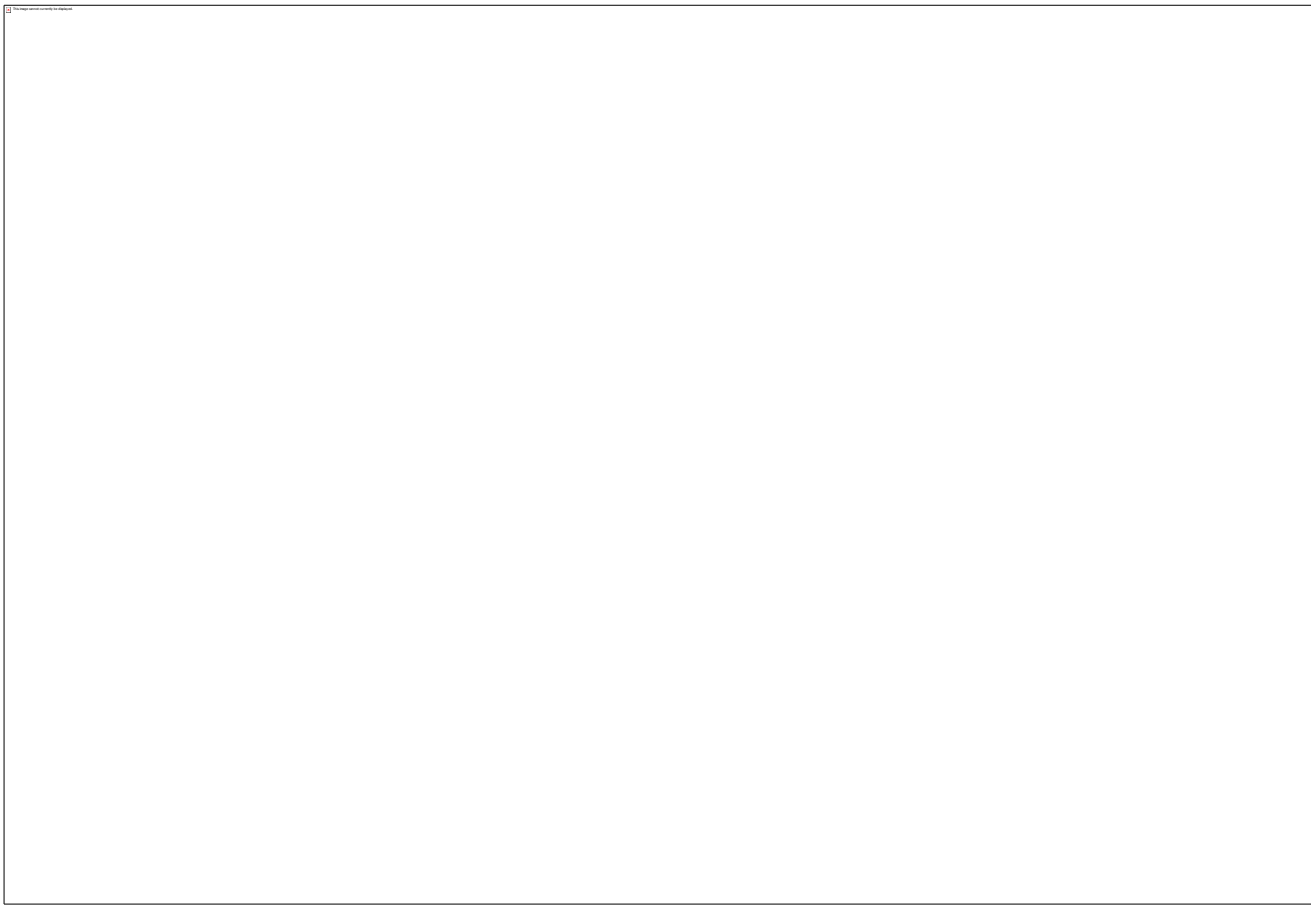

Figure 4.31: Effects of 4.10 and 4.11 (200 nM, 48 h and 72 h) on the expression of CD86 in OCI-AML3 and KASUMI cells.

(A-B) Results following 48 h and 72 h treatments with **4.10** in OCI-AML3 **(A)** and KASUMI **(B)**; **(D-E)** Results following 48 and 72 h treatment with **4.11** in OCI-AML3 **(D)** and KASUMI **(E); (C-F)** statistical analysis; cells were gated based on FSC and SSC parameters. In the X-axis are reported both the mean fluorescence increase of treated cells, stained with CD86-FITC conjugated Ab and the fluorescent increase of control (untreated cells- IgG Isotype-FITC). In the Y-axis is reported the cell count. Statistical significance was determined with two-way ANOVA and corrected for multiple comparisons with Bonferroni's test. Values are expressed as means % of increase (compared to control) ± STD (n=3); ****$p < 0.0001$.

Given that also **4.14** revealed interesting biological results in enzymatic and cellular evaluations, we decided to test whether the 2-thiophenethylamine substituted analogue was equally able to induce the CD86 expression in MV4-11, THP-1, KASUMI and OCI-AML3 cells at nM concentrations (200 nM).

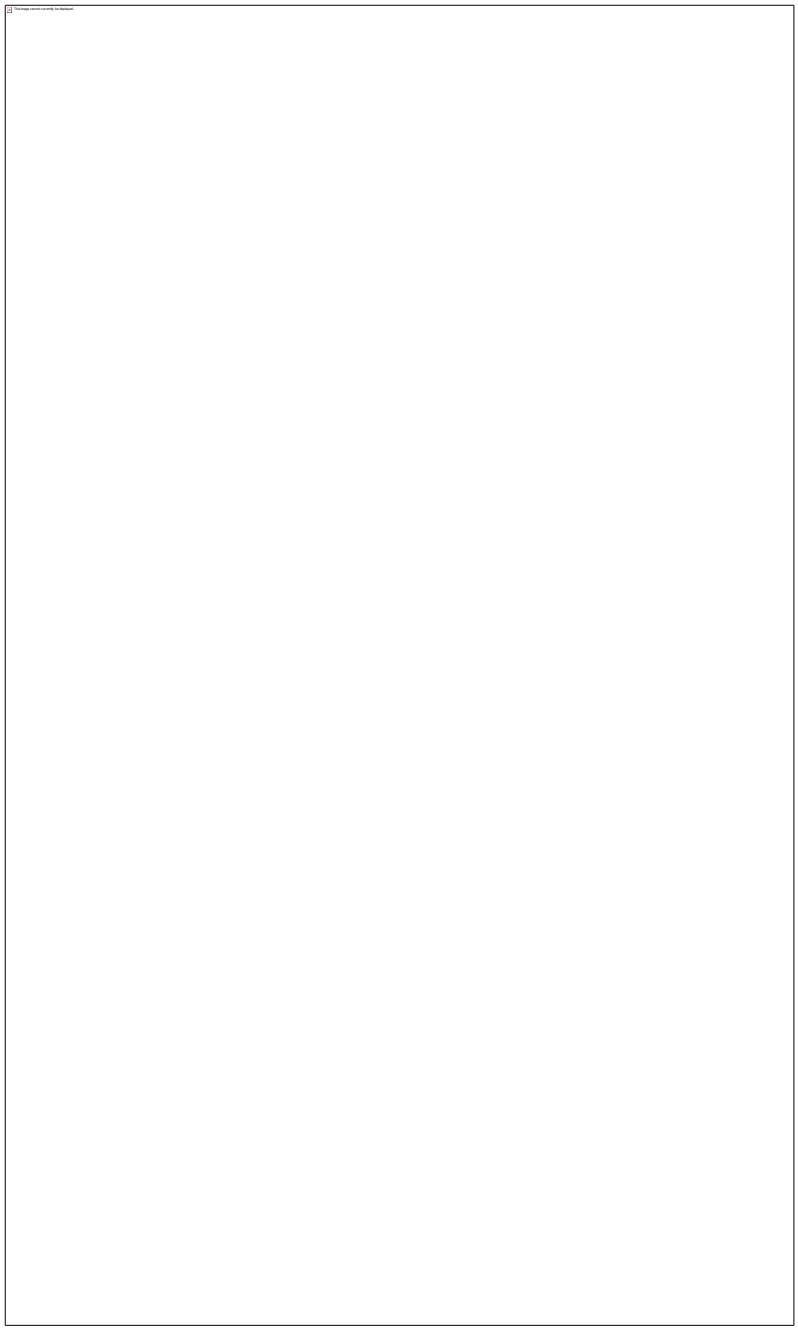

Figure 4.32: Effects of 4.14 (200 nM, 72 h) on the expression of CD86 in THP-1, MV4-11, KASUMI and OCI-AML3 cells.

Cells were gated based on FSC and SSC parameters. In the X-axis are reported both the mean fluorescence increase of treated cells stained with CD86-FITC conjugated Ab and the fluorescent increase of control (untreated cells-IgG Isotype-FITC). The Y-axis is the cell count. Statistical significance (plot E) was determined with two-way ANOVA and corrected for multiple comparisons with Bonferroni's test. Values are expressed as means % of increase (compared to control) ± STD (n=3); ****$p < 0.0001$.

Table 4.4 summarises the data gathered with CD86 evaluations in THP-1, MV4-11, OCI-AML3 and KASUMI cell lines with **4.10**, **4.11,** and **4.14** following 24 h, 48 h and 72 h treatments (200 nM).

Table 4.4: Increase (%) of CD86 expression induced by TCP derivatives 4.10, 4.11 and 4.14 in AML cell lines (200 nM, 24 h, 48 h, 72 h).

Results are expressed as % of increase normalised to pre-treatment level (DMSO-vehicle control) ± STD (n=3); nt: not tested.

Compound (200 nM)	Cell line	24 h	48 h	72 h
4.10	**THP-1**	29.0±5.7%	80.3±4.2%	92.9±1.2%
4.11		18.5±1.7 %	70.3±8.2%	92.4±3.3%
4.14		nt	nt	40.3±1.9%
4.10	**MV4-11**	nt	41.8±0.7%	79.5±3.2%
4.11			38.9±1.7%	81.2±2.5%
4.14			nt	94.1±0.3%
4.10	**OCI-AML3**	nt		65.5±4.3%
4.11				69.8±5.7%
4.14				78.3±3.7%
4.10	**KASUMI**	nt		81.7 ± 3.1%
4.11				73.8±3.4%
4.14				69.0±1.7%

The overall analyses imply that the novel inhibitors **4.10**, **4.11** and **4.14** are capable to induce the expression of the CD86 marker in AML cell lines. Specifically, treatment with **4.10** and **4.11** showed a marked effect on THP-1 and MV4-11 cells, while **4.14** promoted only a 40% increase THP-1 and pronounced effects in MV4-11 cells. Similar results were observed for the three TCP-analogues in OCI-AML3 and KASUMI cells. The registered induction of CD86 expression substantiate further that the biological effects of the compounds correlate with LSD1 inhibition. Moreover, as the CD86 is present in the surface of macrophages, dendritic cells and monocytes, the post-treatment induction of such marker in tumorigenic cells is likely to correlate with a potential differentiating mechanism of action. To verify this initial information, the levels of CD11b and CD14 were analysed in AMLs treated with nM concentrations of **4.10** and **4.11**.

4.3.5. CD11b and CD14 evaluations

CD11b and CD14 are glycoproteins situated on the myeloid cell surface with antigen properties. They are exclusively expressed in mature leucocytes and undifferentiated cells lack their expression.[86,294] Consequently their expression levels are examined to estimate the differentiating properties of pharmacological agents.[295–297]

In the following experiments, AMLs (U937, MV4-11, KASUMI, HL-60, THP-1, OCI-AML3) were treated with 200 nM of **4.10** or **4.11** and following 48 h incubation, the levels of CD11b and CD14 were examined by flow cytometry (Figures 4.33-4.44).

Figure 4.33: Effects of 4.10 (200 nM, 48 h) on the expression of differentiation markers CD14 and CD11b in U937 cells.

FSC and SSC profiles were applied for the initial gating by selecting cell size and distribution and remove cell debris. Plots **A, B**, **C** show the Isotype controls. Plots **D**, **E**, **F** show the experimental conditions. Plots **A** and **D** show the gated population: in the X-axis is reported the mean fluorescence increase for FITC-CD14 Ab; in the Y-axis is reported the mean fluorescence increase for PE-CD11b Ab. Plots **B** and **C** (black histograms) report the fluorescence increase of Isotype controls (untreated cells); **E** shows the fluorescence increase of the monocytic marker CD14; **F** shows the fluorescence increase of the myeloid marker CD11b. Numbers shown in each box are the % of cells expressing CD14 or CD11b. (**G**) Shown are results graphically summarised for three independent experiments. Statistical significance was determined with two-way ANOVA and corrected for multiple comparisons with Bonferroni's test. Values are expressed as means % of CD14-CD11b increase ± STD (n=3); ****$p < 0.0001$.

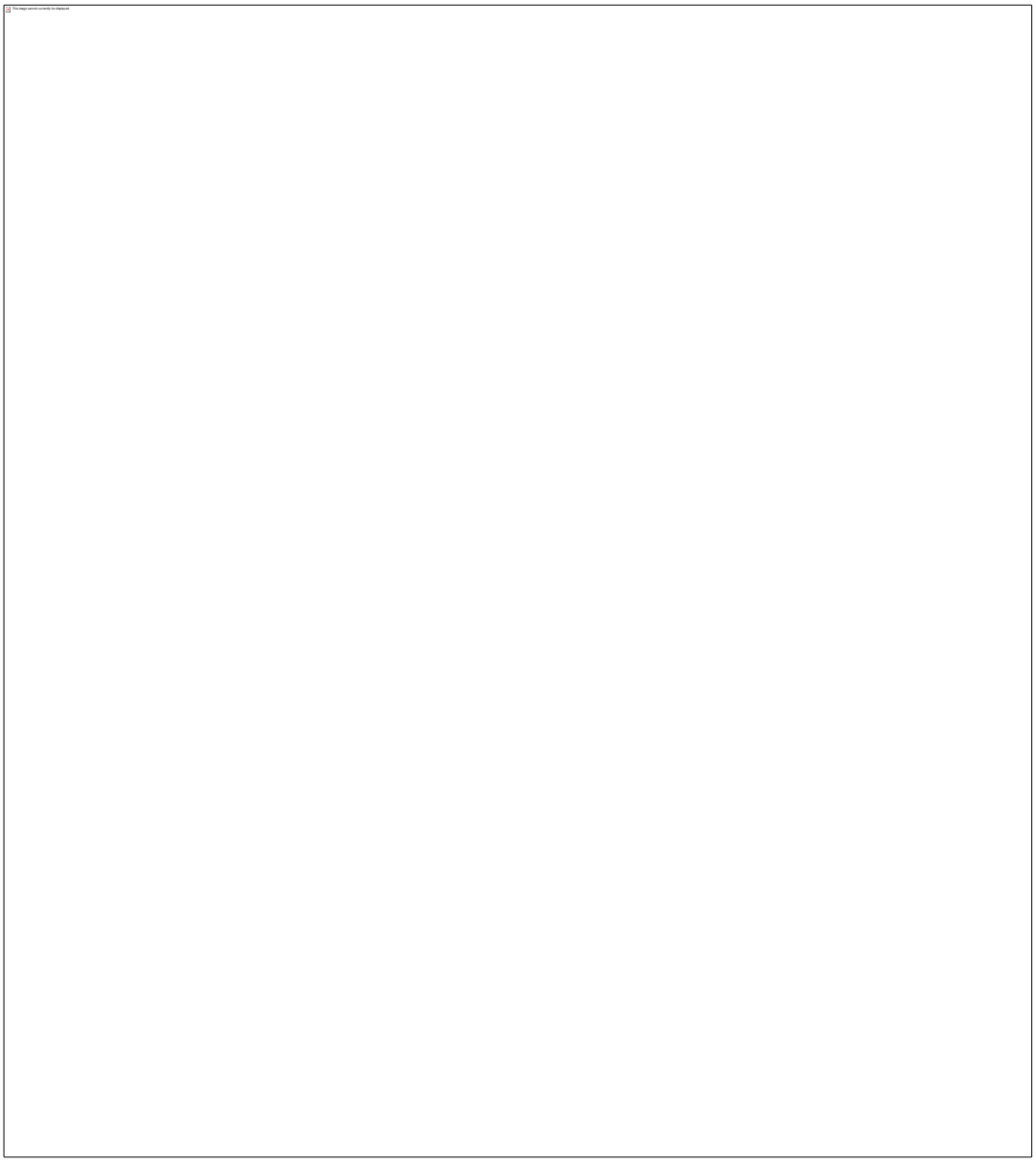

Figure 4.34: Effects of 4.11 (200 nM, 48 h) on the expression of differentiation markers CD14 and CD11b in U937 cells.

FSC and SSC profiles were applied for the initial gating by selecting cell size and distribution and remove cell debris. Plots **A, B**, **C** show the Isotype controls. Plots **D**, **E**, **F** show the experimental conditions. Plots **A** and **D** show the gated population: in the X-axis is reported the mean fluorescence increase for FITC-CD14 Ab; in the Y-axis is reported the mean fluorescence increase for PE-CD11b Ab. Plots **B** and **C** (black histograms) report the fluorescence increase of Isotype controls (untreated cells); **E** shows the fluorescence increase of the monocytic marker CD14; **F** shows the fluorescence increase of the myeloid marker CD11b. Numbers shown in each box are the % of cells expressing CD14 or CD11b. (**G**) Shown are results graphically summarised for three independent experiments. Statistical significance was determined with two-way ANOVA and corrected for multiple comparisons with Bonferroni's test. Values are expressed as means % of CD14-CD11b increase ± STD (n=3);***$p < 0.01$;****$p < 0.0001$.

Figure 4.35: Effects of 4.10 (200 nM, 48 h) on the expression of differentiation markers CD14 and CD11b in HL-60 cells.

FSC and SSC profiles were applied for the initial gating by selecting cell size and distribution and remove cell debris. Plots **A, B**, **C** show the Isotype controls. Plots **D**, **E**, **F** show the experimental conditions. Plots **A** and **D** show the gated population: in the X-axis is reported the mean fluorescence increase for FITC-CD14 Ab; in the Y-axis is reported the mean fluorescence increase for PE-CD11b Ab. Plots **B** and **C** (black histograms) report the fluorescence increase of Isotype controls (untreated cells); **E** shows the fluorescence increase of the monocytic marker CD14; **F** shows the fluorescence increase of the myeloid marker CD11b. Numbers shown in each box are the % of cells expressing CD14 or CD11b. (**G**) Shown are results graphically summarised for three independent experiments. Statistical significance was determined with two-way ANOVA and corrected for multiple comparisons with Bonferroni's test. Values are expressed as means % of CD14-CD11b increase ± STD (n=3); *** $p < 0.001$.

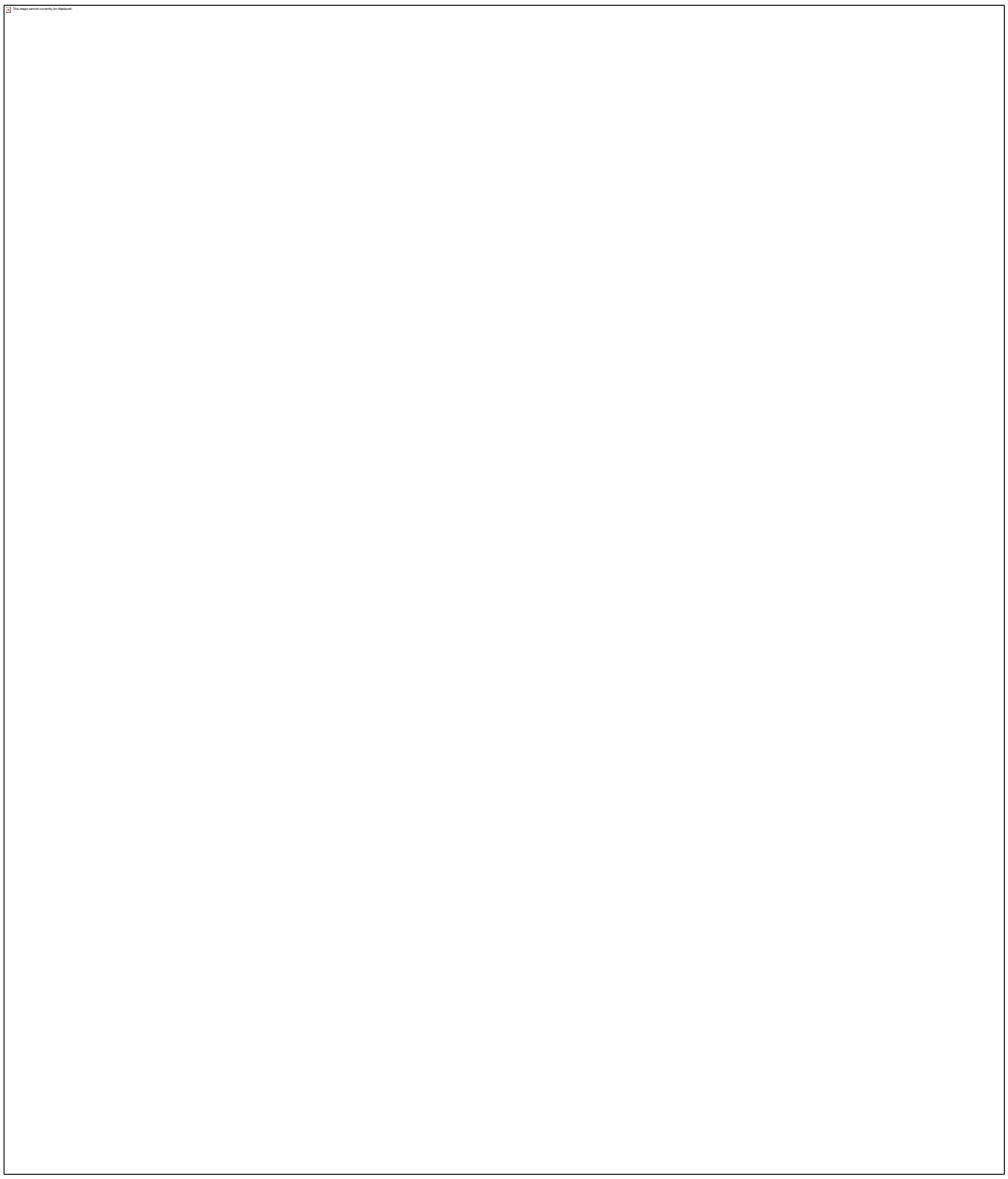

Figure 4.36: Effects of 4.11 (200 nM, 48 h) on the expression of differentiation markers CD14 and CD11b in HL-60 cells.

FSC and SSC profiles were applied for the initial gating by selecting cell size and distribution and remove cell debris. Plots **A, B**, **C** show the Isotype controls. Plots **D**, **E**, **F** show the experimental conditions. Plots **A** and **D** show the gated population: in the X-axis is reported the mean fluorescence increase for FITC-CD14 Ab; in the Y-axis is reported the mean fluorescence increase for PE-CD11b Ab. Plots **B** and **C** (black histograms) report the fluorescence increase of Isotype controls (untreated cells); **E** shows the fluorescence increase of the monocytic marker CD14; **F** shows the fluorescence increase of the myeloid marker CD11b. Numbers shown in each box are the % of cells expressing CD14 or CD11b. (**G**) Shown are results graphically summarised for three independent experiments. Statistical significance was determined with two-way ANOVA and corrected for multiple comparisons with Bonferroni's test. Values are expressed as means % of CD14-CD11b increase ± STD (n=3); *$p < 0.05$, ***$p < 0.001$.

Figure 4.37: Effects of 4.10 (200 nM, 48 h) on the expression of differentiation markers CD14 and CD11b in THP-1 cells.

FSC and SSC profiles were applied for the initial gating by selecting cell size and distribution and remove cell debris. Plots **A, B**, **C** show the Isotype controls. Plots **D**, **E**, **F** show the experimental conditions. Plots **A** and **D** show the gated population: in the X-axis is reported the mean fluorescence increase for FITC-CD14 Ab; in the Y-axis is reported the mean fluorescence increase for PE-CD11b Ab. Plots **B** and **C** (black histograms) report the fluorescence increase of Isotype controls (untreated cells); **E** shows the fluorescence increase of the monocytic marker CD14; **F** shows the fluorescence increase of the myeloid marker CD11b. Numbers shown in each box are the % of cells expressing CD14 or CD11b. (**G**) Shown are results graphically summarised for three independent experiments. Statistical significance was determined with two-way ANOVA and corrected for multiple comparisons with Bonferroni's test. Values are expressed as means % of CD14-CD11b increase ± STD (n=3); ****$p < 0.0001$.

Figure 4.38: Effects of 4.11 (200 nM, 48 h) on the expression of differentiation markers CD14 and CD11b in THP-1 cells.

FSC and SSC profiles were applied for the initial gating by selecting cell size and distribution and remove cell debris. Plots **A, B**, **C** show the Isotype controls. Plots **D**, **E**, **F** show the experimental conditions. Plots **A** and **D** show the gated population: in the X-axis is reported the mean fluorescence increase for FITC-CD14 Ab; in the Y-axis is reported the mean fluorescence increase for PE-CD11b Ab. Plots **B** and **C** (black histograms) report the fluorescence increase of Isotype controls (untreated cells); **E** shows the fluorescence increase of the monocytic marker CD14; **F** shows the fluorescence increase of the myeloid marker CD11b. Numbers shown in each box are the % of cells expressing CD14 or CD11b. (**G**) Shown are results graphically summarised for three independent experiments. Statistical significance was determined with two-way ANOVA and corrected for multiple comparisons with Bonferroni's test. Values are expressed as means % of CD14-CD11b increase ± STD (n=3); **$p < 0.01$.

Figure 4.39: Effects of 4.10 (200 nM, 48 h) on the expression of differentiation markers CD14 and CD11b in OCI-AML3 cells.

FSC and SSC profiles were applied for the initial gating by selecting cell size and distribution and remove cell debris. Plots **A, B**, **C** show the Isotype controls. Plots **D**, **E**, **F** show the experimental conditions. Plots **A** and **D** show the gated population: in the X-axis is reported the mean fluorescence increase for FITC-CD14 Ab; in the Y-axis is reported the mean fluorescence increase for PE-CD11b Ab. Plots **B** and **C** (black histograms) report the fluorescence increase of Isotype controls (untreated cells); **E** shows the fluorescence increase of the monocytic marker CD14; **F** shows the fluorescence increase of the myeloid marker CD11b. Numbers shown in each box are the % of cells expressing CD14 or CD11b. (**G**) Shown are results graphically summarised for three independent experiments. Statistical significance was determined with two-way ANOVA and corrected for multiple comparisons with Bonferroni's test. Values are expressed as means % of CD14-CD11b increase ± STD (n=3); **p < 0.01.

Figure 4.40: Effects of 4.11 (200 nM, 48 h) on the expression of differentiation markers CD14 and CD11b in OCI-AML3 cells.

FSC and SSC profiles were applied for the initial gating by selecting cell size and distribution and remove cell debris. Plots **A, B**, **C** show the Isotype controls. Plots **D**, **E**, **F** show the experimental conditions. Plots **A** and **D** show the gated population: in the X-axis is reported the mean fluorescence increase for FITC-CD14 Ab; in the Y-axis is reported the mean fluorescence increase for PE-CD11b Ab. Plots **B** and **C** (black histograms) report the fluorescence increase of Isotype controls (untreated cells); **E** shows the fluorescence increase of the monocytic marker CD14; **F** shows the fluorescence increase of the myeloid marker CD11b. Numbers shown in each box are the % of cells expressing CD14 or CD11b. (**G**) Shown are results graphically summarised for three independent experiments. Statistical significance was determined with two-way ANOVA and corrected for multiple comparisons with Bonferroni's test. Values are expressed as means % of CD14-CD11b increase ± STD (n=3); ****$p < 0.0001$.

Figure 4.41: Effects of 4.10 (200 nM, 48 h) on the expression of differentiation markers CD14 and CD11b in KASUMI cells.

FSC and SSC profiles were applied for the initial gating by selecting cell size and distribution and remove cell debris. Plots **A, B**, **C** show the Isotype controls. Plots **D**, **E**, **F** show the experimental conditions. Plots **A** and **D** show the gated population: in the X-axis is reported the mean fluorescence increase for FITC-CD14 Ab; in the Y-axis is reported the mean fluorescence increase for PE-CD11b Ab. Plots **B** and **C** (black histograms) report the fluorescence increase of Isotype controls (untreated cells); **E** shows the fluorescence increase of the monocytic marker CD14; **F** shows the fluorescence increase of the myeloid marker CD11b. Numbers shown in each box are the % of cells expressing CD14 or CD11b. (**G**) Shown are results graphically summarised for three independent experiments. Statistical significance was determined with two-way ANOVA and corrected for multiple comparisons with Bonferroni's test. Values are expressed as means % of CD14-CD11b increase ± STD (n=3); **$p < 0.01$.

Figure 4.42: Effects of 4.11 (200 nM, 48 h) on the expression of differentiation markers CD14 and CD11b in KASUMI cells.

FSC and SSC profiles were applied for the initial gating by selecting cell size and distribution and remove cell debris. Plots **A, B**, **C** show the Isotype controls. Plots **D**, **E**, **F** show the experimental conditions. Plots **A** and **D** show the gated population: in the X-axis is reported the mean fluorescence increase for FITC-CD14 Ab; in the Y-axis is reported the mean fluorescence increase for PE-CD11b Ab. Plots **B** and **C** (black histograms) report the fluorescence increase of Isotype controls (untreated cells); **E** shows the fluorescence increase of the monocytic marker CD14; **F** shows the fluorescence increase of the myeloid marker CD11b. Numbers shown in each box are the % of cells expressing CD14 or CD11b. (**G**) Shown are results graphically summarised for three independent experiments. Statistical significance was determined with two-way ANOVA and corrected for multiple comparisons with Bonferroni's test. Values are expressed as means % of CD14-CD11b increase ± STD (n=3); **p < 0.01, ****p < 0.0001.

Figure 4.43: Effects of 4.10 (200 nM, 48 h) on the expression of differentiation markers CD14 and CD11b in MV4-11 cells.

FSC and SSC profiles were applied for the initial gating by selecting cell size and distribution and remove cell debris. Plots **A, B**, **C** show the Isotype controls. Plots **D**, **E**, **F** show the experimental conditions. Plots **A** and **D** show the gated population: in the X-axis is reported the mean fluorescence increase for FITC-CD14 Ab; in the Y-axis is reported the mean fluorescence increase for PE-CD11b Ab. Plots **B** and **C** (black histograms) report the fluorescence increase of Isotype controls (untreated cells); **E** shows the fluorescence increase of the monocytic marker CD14; **F** shows the fluorescence increase of the myeloid marker CD11b. Numbers shown in each box are the % of cells expressing CD14 or CD11b. (**G**) Shown are results graphically summarised for three independent experiments. Statistical significance was determined with two-way ANOVA and corrected for multiple comparisons with Bonferroni's test. Values are expressed as means % of CD14-CD11b increase ± STD (n=3); ****$p < 0.0001$.

Figure 4.44: Effects of 4.11 (200 nM, 48 h) on the expression of differentiation markers CD14 and CD11b in MV4-11 cells.

FSC and SSC profiles were applied for the initial gating by selecting cell size and distribution and remove cell debris. Plots **A, B**, **C** show the Isotype controls. Plots **D**, **E**, **F** show the experimental conditions. Plots **A** and **D** show the gated population: in the X-axis is reported the mean fluorescence increase for FITC-CD14 Ab; in the Y-axis is reported the mean fluorescence increase for PE-CD11b Ab. Plots **B** and **C** (black histograms) report the fluorescence increase of Isotype controls (untreated cells); **E** shows the fluorescence increase of the monocytic marker CD14; **F** shows the fluorescence increase of the myeloid marker CD11b. Numbers shown in each box are the % of cells expressing CD14 or CD11b. (**G**) Shown are results graphically summarised for three independent experiments. Statistical significance was determined with two-way ANOVA and corrected for multiple comparisons with Bonferroni's test. Values are expressed as means % of CD14-CD11b increase ± STD (n=3); ****$p < 0.0001$.

Table 4.5: Increase (%) of CD14 and CD11b expression induced by TCP derivative 4.10 in AMLs (200 nM, 48 h).

Results are expressed as % of increase normalised to pre-treatment level (DMSO-vehicle control) ± STD (n=3).

Cells line treated with 4.10 (200 nM) 48h	CD14 increase (% ± STD, n=3)	CD11b increase (% ± STD, n=3)
U937	24.2±1.5	94.2±1.2
HL-60	20.8±3.0	68.3±11.8
OCI-AML3	69.7±12.3	70.4±13.9
MV4-11	83.0±1.51	70.4±1.5
KASUMI	2.7±0.7	17.9±3.5
THP-1	97.0±0.9	93.6±5.3

Table 4.6: Increase (%) of CD14 and CD11b expression induced by TCP derivative 4.11 in AMLs (200 nM, 48 h).

Results are expressed as % of increase normalised to pre-treatment level (DMSO-vehicle control) ± STD (n=3).

Cell lines treated with 4.11 (200nM, 48 h)	CD14 increase (% ± STD, n=3)	CD11b increase (% ± STD, n=3)
U937	14.1±0.9	90.6±2.6
HL-60	29.1±4.7	66.1±11.0
OCI-AML3	84.4±5.6	72.5±9.3
MV4-11	80.5±2.8	72.9±4.4
KASUMI	3.8±0.1	23.4±0.9
THP-1	97.1±1.2	98.4±0.4

As anticipated with the examination of CD86 expression, the compounds' ability to trigger cell differentiation was confirmed by the effects registered with CD14 and CD11b experiments. The compounds were able to increase CD14 and CD11b expression in leukaemia after 48 h and at a dose of 200 nM. Equal activities were

obtained with **4.10** and **4.11**. However, results revealed that **4.10** was unable to promote a significant increment of the monocytic marker CD14 in KASUMI and HL-60 line, whereas a moderate increase was registered after treatment with **4.11** in the same cells. Therefore such data imply an incomplete differentiation for HL-60 and KASUMI cells. In the case of KASUMI, the lack of CD14 expression was accompanied with a drop in cell count (Figure 4.41 and 4.42). Notably, the post-treatment induction of the differentiation markers was significant also in U937 and OCI-AML3 cells, which demonstrated a lower sensitivity to **4.10** and **4.11** treatments in cytotoxicity assays.

4.3.6. Effects on normal hematopoietic stem cells

The CD34 marker is a differentiation stage-specific leucocyte antigen present in immature hematopoietic cells.[298,299] Leukaemic blasts or differentiating cells do not express such markers and the CD34 expression decreases during the maturation process. Because of its features, this marker is commonly used in leukaemia studies to determine the toxicity of anti-AML agents.[86,300] If the treatment results in toxicity, cells cease to express CD34.[86,300]

As previously mentioned, the pharmacological deletion of LSD1 has been correlated with toxic effects for normal dividing blood cells.[67,84] Therefore, to examine the potential toxicity associated with **4.10** and **4.11**, post-treatment expression $CD34^+$ was evaluated by flow cytometry. In order to do so, $CD34^+$ expressing blasts derived from patient bone marrow biopsies were exposed to increasing concentrations of **4.10** and **4.11** (0.001 µM-10 µM concentrations range) or left untreated, and cultured for 48 and 72 h. Cells stained with CD34 Ab were analysed by flow cytometry (Figure 4.45).

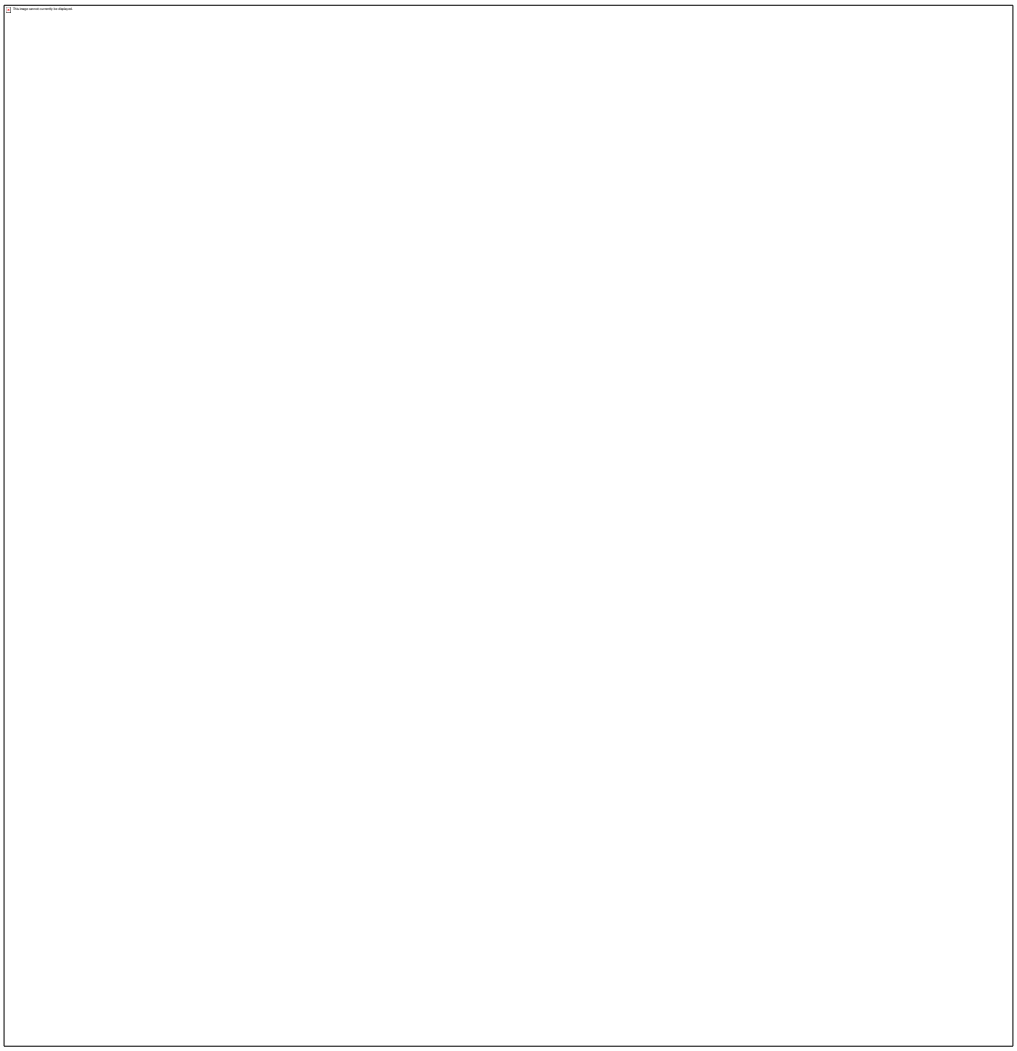

Figure 4.45: Healthy CD34$^+$ HSC counts after treatment with increasing concentrations of 4.10 and 4.11 for 48 h and 72 h.

Statistical significance was determined with one-way ANOVA and corrected for multiple comparisons with Dunnett's test. Data are shown as means ± STD (n=3).

Results revealed that the numbers of CD34$^+$ cells remained unchanged in treated samples (compared to untreated) during all the time courses. Even at high dose (10 µM), CD34 expressing cells were insensitive to the treatment. Hence, based on this result, the LSD1 pharmacological suppression exerted by **4.10** and **4.11** is not associated with toxicity for normal dividing cells nor induced differentiation in non-leukaemic stem cells; the results confirm the specificity and pre-clinical safety of the examined TCP-derivatives.

4.4. Evaluation in human prostate adenocarcinoma cells

Further investigations were carried out on LNCaP prostate adenocarcinoma lines by our collaborators in Southampton, by Dr. Simon Crabb's group. As said before, LSD1 is able to associate with AR to demethylate the repressive marks of mono- and dimethyllysine on H3K9.[146,149,150]

For cell viability experiments, cells were exposed to increasing concentrations of the TCP derivatives and the cell viability measured after 72 h (Table 4.7).

Table 4.7: Results of enzymatic assay and viability preliminary experiments in LNCaP cells.
Values are expressed in µM ± STD (n=3 for enzymatic evaluations, n=2 for LNCaP evaluations).

Compound	IC_{50} enzymatic (%RFU ± STD µM, n= 3)	IC_{50} LNCaP inhibition
TCP	21 µM	2.5 mM
4.10	0.3±0.01	515.2±112.2 µM
4.11	0.4±0.04	520.3±60.4 µM
4.14	0.6±0.01	206.3±12.3 µM
4.15	2.4±0.1	162.2±3.7 µM
4.17	1.3±0.2	543.7±132.4 µM
4.18	0.9±0.1	94.0±110.9 µM

The preliminary evaluation of LSD1 inhibitors revealed an enhanced activity of the new analogues in hindering LNCaP cell proliferation compared to TCP. Surprisingly, compounds **4.10** and **4.11** were among the least active in the prostate cell line, inhibiting cell proliferation at 500 µM, whereas **4.18** presenting a bromine substituent on the benzylamine ring, revealed a higher anti-proliferative activity. Compounds **4.14** and **4.15** were also relatively good inhibitors in arresting cell proliferation (206.3 µM and 162.2 µM) compared to TCP. Further experiments are being performed with **4.10**, **4.11, 4.14, 4.18**, **4.22** and **4.23** to examine the downstream molecular markers of LSD1 inhibition in prostate cell lines.

4.5. Discussion

The aim of the present study was to synthesise irreversible inhibitors of LSD1 based on TCP molecular structure. By using a simple synthetic approach, we generated a total of eighteen new compounds, decorated at the phenyl ring with bulky substituents all with interesting biology. Cell-free enzymatic evaluation confirmed the enhanced potency of the new analogues, as these were 50-fold more potent compared to TCP. The enzymatic evaluations were strengthened by cellular experiments, whereby the compounds produced intriguing effects.

The simplest compound, the amino-oxoethyl substituted analogue **4.19**, showed similar enzymatic activities to TCP. The benzylamine (**4.10)** and the phenethylamine **(4.11)** derivatives were the strongest LSD1 inhibitors.

The addition of further hindering substituents, in **4.12** (dibenzylamine substituted) and **4.13** (4-phenylbenzylamine substituted), also positively contributed to improve LSD1 inhibition. Despite the strong similarity between **4.12** and **4.13,** the former is 40-fold more potent than the latter; this may arise from the presence of one more rotatable bond in **4.12** that can potentially confer an increased mobility to the benzyl rings that can adjust in the catalytic cleft of LSD1.

Bioisosteric substitution of the phenethyl ring of **4.11** with thiophenethyl, leads to compound **4.14.** Given that the vinylene (-CH=CH-) group is a ring equivalent of the divalent sulfur in the thiophene ring, compound **4.14** displayed a similar biological profile to **4.11**.

Replacement of benzyl and phenethyl with non-aromatic rings was less favourable for the activity. Cyclohexanemethyl (**4.15**) and cylohexaneethyl (**4.16**) substituted analogues suppressed LSD1 enzymatic activity at higher concentrations (2.5 μM and 5.4 μM respectively) compared to the aromatic **4.10** and **4.11**. The result emphasises the importance of the aromatic rings at that position, which can potentially promote stronger interactions with the flat hydrophobic LSD1 catalytic site. Cellular experiments with **4.15** and **4.16** revealed similar anti-proliferative effects in KASUMI, U937 and MV4-11 cells.

Thereafter, we decorated the benzyl ring of **4.10** with different substituents in *para* position and specifically with bromine (**4.17**), fluorine (**4.18**), chlorine, (**4.19**), methoxy (**4.20**) and nitro (**4.21)** groups. In some cases, the presence of such substituents critically

influenced the binding activity of the small molecules. The fluorine substituted **4.17** retained both enzymatic (1.3 µM) and cellular activities. Also the bromine substitution did not alter the drug's pharmacology, as **4.18** blocked LSD1 demethylase at nM concentrations and hindered the proliferation of KASUMI and MV4-11 cell lines equally well. Moreover, additional cell viability assays performed in prostate adenocarcinoma LNCaP cells revealed that **4.18** was able to arrest cancer cell proliferation at lower concentrations compared to the potent anti-leukaemia agents **4.10** and **4.11**. Bromine substitution increases the molecule lipophilicity and the greater effects in LNCaP cells of such analogue could be related to the electronic changes conferred by the halogen.

Substitution with chlorine (**4.29**) resulted instead in a reduced anti-LSD1 effect, as no enzymatic inhibition was detected at 50 µM. Chlorine is an electron-withdrawing substituent and it increases the molecule's global acidity and lipophilicity by decreasing the pKa. Consequently, this modification can compromise the original non-substituted benzyl ring interactions with the target cleft.

The strong electron-donating methoxy, annexed at the benzyl ring in **4.20**, displayed an unfavourable binding profile with its enzymatic activity fading to 32 µM. The NO_2 *para*-substitution in **4.21** also exerted an unfavourable effect towards the LSD1 inhibition. The nitro group is a strong electron-withdrawing group and its presence dramatically decreases the lipophilicity. This change in properties have potentially led the molecule to interact with less hydrophobic regions of the LSD1 cleft. Although some enzymatic potency was maintained, **4.21** failed to impair cell proliferation. Hence, collectively these data suggest that marked electron-withdrawing and electron-donating groups are unfavourable for the interactions with LSD1 catalytic pocket.

Nitrogen containing aryl moieties are commonly found in drugs[301] and to direct further SAR, the effects of pyridyl-piperazine (**4.22**) and pyrimidyl-piperazine (**4.23**) substitutions were analysed. The biological profile was found to be similar for both substitutions as **4.22** and **4.23** were equally able to impede LSD1 demethylation at ~1 µM concentration. AMLs viability was also effectively reduced with nM treatments with such compounds. These results prompted us to further exploit such structural modification and we expanded the library with molecules **4.24-4.27**. Compounds **4.24** and **4.25** have, in addition to piperazine, a sulfonamide component. Sulfonamides are

known to have anti-cancer potential,[302,303] hence their insertion in the library. The evaluation of **4.24** and **4.25** demonstrated that sulfonyl-containing molecules are suitable to fit the LSD1 enzymatic cleft.

The piperazine component was further investigated with compounds **4.26** and **4.27**, which have a supplementary *ortho* substituted phenyl ring with a fluorine or nitrile group, introduced to maximise the structural diversity of the library. Both modifications generated potent LSD1 inhibitors with strong anti-proliferative properties in all the tested cell lines.

To fully characterise the biological behaviour of the new TCP derivatives, compounds **4.10**, **4.11** and **4.14** were selected for further analyses given their high enzymatic potential in contrasting LSD1 demethylase, the high synthetic yield and the easy purification compared to other compounds. The cellular evaluations started with the examination of **TCP** in MV4-11, HL-60, THP-11, U937, KASUMI and OCI-AML3 cells. **TCP** was able to hinder cell proliferation after 72 h of incubation and marked decrease in cell viability was registered at 30 µM. Compounds **4.10** and **4.11** were next analysed in the leukaemia cells at lower concentrations (1-100 nM) and four different time courses (24 h, 48 h and 72 h). After 24 h, treatments were ineffective in arresting cell growth whereas marked decrease of cell viability was observed after 48 h, 72 h and 120 h in all the analysed cell lines. This delayed effect might be partially due to the positive charge present in the molecules. Positive charges may hinder the penetration of these compounds inside the cell membrane. However, this slow activity could also represent a physiological effect of pharmacological action on cellular LSD1. In keeping with this, other studies reported similar treatment course to achieve significant reduction of cell proliferation via LSD1 inhibition.[174,175,304]

To verify that the observed activities were driven by an irreversible mechanism, a washout experiment was employed with compounds **4.10**, **4.11** and **4.14**.[291,305] Results confirmed that the biological data are promoted by covalent inhibition as after washout, **4.10, 4.11** and **4.14** retained the anti-proliferative behaviour.

Immunoblotting evaluations in KASUMI cells treated with 200 nM of **4.11** for different time courses (2 h, 4 h, 6 h, 48 h and 72 h), showed a time dependent accumulation of the H3K4me2 expression, which was most marked following 48 h and 72 h. As several studies indicate that LSD1 inhibition promotes the reactivation of myeloid-

differentiation associated genes,[86] the induction of differentiation markers was assessed by flow cytometry.

The marker CD86, for which the induced expression is directly linked with the LSD1[196] inhibition, was evaluated first. Treatments with 200 nM of **4.10, 4.11** or **4.14** for 24 h, 48 h and 72 h demonstrated a marked increase in CD86 expression in THP-1, MV4-11, OCI-AML3, HL-60, KASUMI and U937 cells. Once more, the compounds biological effects were time-dependent as short exposures (24 h) were unable to increase significantly the CD86 expression. In contrast, prolonged incubations (48-72 h) promoted a marked induction of the examined parameter.

To further characterise the differentiating potential of the drugs, the cellular levels of CD11b and CD14 expression were measured after treatments with **4.10** and **4.11**. Results revealed that 48 h incubation with 200 nM of benzyl and phenethyl substituted TCP derivatives strongly induced the expression of CD11b and CD14 markers in leukaemia cell lines. The expression of the maturation-associated myeloid surface marker CD11b implies that treated cells are differentiating along the monocytic/macrophagic pathways. In addition, cells that demonstrated less sensitivity to the LSD1 inhibitors in cytotoxicity assays, such as U937 and OCI-AML3, also displayed a marked increase of CD11b. The strong increase in differentiation markers justifies the initial results observed during cytotoxicity evaluations in OCI-AML3, whereby following 24 h exposure a significant increase in cell growth was registered. Moreover, none of the tested derivatives revealed a 100% inhibition of cell survival rates. In the light of these data, a possible explanation for the partial inhibition is that the compounds did not cause cell death, but differentiation instead. Therefore the CD data clarify why the dose-response curves were not reaching zero proliferation even at high concentrations. Noteworthly, the reagent used to measure cell survival (CellTiter-Glo®) quantifies cellular ATP production and does not discriminate between differentiating and tumorigenic cells.

The treatment with **4.10** (200 nM, 48 h) resulted only in a moderate increase of human monocytic endotoxin receptor CD14 in U937 and low response in HL-60 and KASUMI cells. This implies a partial differentiation of the analysed samples. KASUMI and HL-60 cells belong to the M2 class and are myeloblastic leukaemia models characterised by a very poorly differentiated status.[296,306] Likely, increased exposure time and drug

concentrations could have led to a significant CD14 increase. Also, several studies reported a special pathway for HL-60 cells terminal differentiation in regard to CD14 expression. It is in fact showed that HL-60 cells, after exposure to maturation inducer agents, were less able to express CD14 compared to other AML lines.[296,306] Additionally, Palis *et al.* reported that HL-60's ability to differentiate can be affected by the number of passages during cell culture procedures.[307] Taken together, the data obtained for HL-60 cells could depend on the cell line rather than solely being an effect of **4.10**. Unlike HL-60 cells, in KASUMI the limited response concurs with a reduction in cells count and such effect was observed in three independent replicates.

To evaluate the haematological toxicity associated with LSD1 suppression, the effects of **4.10** and **4.11** were examined in normal hematopoietic stem cells expressing $CD34^+$. Human hematopoietic non-malignant $CD34^+$ exposed for 48 h and 72 h with concentrations up to 10 μM of **4.10** and **4.11**, did not show sensitivity to the treatment, accrediting the specificity of such LSD1 inhibitors for tumorigenic cells and their safety for normal HSC.

An interesting observation resulting from this study was the great effect of TCP derivatives on MV4-11 cell line. Genetically, MV4-11 cells are characterised by overexpression of the Fms-like tyrosine kinase 3 mutation (FLT-3).[308] In normal hematopoietic cells, FLT-3 acts as a growth factor by stimulating the hematopoietic cell progenitors to differentiate and increase the number of B and T cells. In AML context, FLT-3 suffers two types of mutations; one is the internal tandem mutation of the juxtamembrane region (ITD) and the other is point mutation tyrosine kinase (TKD). FLT-3, ITD and TKD mutations concur to promote ligand independent activation of the receptor, leading to the blast cell survival over their normal counterpart.[309] Thus, accordingly to the results obtained in MV4-11, it is conceivable to hypothesise that LSD1 is somehow linked with the FLT-3 mutation and its pharmacological inhibition could revert the sustenance of blast cell survival through the disruption of FLT-3-ITD-TKD activity. Although until now there is no scientific evidence reporting LSD1 direct involvement wit FLT-3, Shih *et al*. associated the reduced methylation marks with FLT-3 ITD mutation.[309]

Derivatives were also evaluated in LNCaPs. The compounds presented an enhanced anti-proliferative activity compared to TCP, which arrested cell proliferation only at 2.5 mM.

Unfortunately, during the course of this work, the company Takeda filed a patent for LSD1 inhibitors with similar structures to the ones reported here and structure **4.10** is included in such work.

4.6. Conclusions and future work

In this project a series of TCP analogues containing a substituted cyclopropyl core have been designed and synthesised. The used synthetic route enabled the generation of nineteen new analogues in seven steps.

A fluorometric assay was used to test the enzymatic activity and eight compounds proved to antagonise LSD1 demethylation at nM concentrations. The data confirmed that analogues with bulkier substituents at the TCP core greatly impair the LSD1 catalytic activity and the substituents nature critically influences the drugs final effects. Strong electron withdrawing and electron-donating groups generated weak analogues, whereas sulfonyl-containing moieties resulted in favourable substitutions for the interaction with the target.

The link between the compounds activity and LSD1 inhibition was strongly supported by the analyses of downstream molecular markers for LSD1 inhibition, as the accumulation of H3K4me2 and CD86 expression.

Biological evaluations were carried out in an extended panel of leukaemia cell models and the analogues showed a 1000-fold enhanced biological activity compared to TCP scaffold. Compound **4.10** and **4.11** have proved to trigger cell differentiation at nM concentrations as demonstrated by the analysis of CD14 and CD11b post-treatment expression levels in six *in vitro* models of AML. The compounds have also been evaluated in LNCaP cells showing enhanced activity compared to TCP in arresting the cancer proliferation. In addition, the compounds were non-toxic for fast-reproducing normal cells, hence selective for cancer cells.

Being drug-like analogues, the compounds could be assessed in *in vivo* models for leukaemia as single agents or in combination with other AML inhibitors or other epigenetic drugs.

Chapter 5 - Evaluation of synthetic intermediates as potential inhibitors of LSD1

5.1. Introduction

The established mechanism for the LSD1 inactivation with TCP-like compounds rely on the formation of a covalent adduct between the NH_2 group of TCP and the FAD isoalloxazine ring. This irreversible modification impedes the FAD-dependent LSD1 demethylase activity on targeted histones.[175] Accordingly, compounds bearing a protected amine group are prevented to form the covalent adduct with the FAD ring. The primary amine is necessary for the covalent modification, involving electron reduction of LSD1-bound-FAD complex and homolytic cleavage of the cyclopropyl ring with the formation of a five-membered ring stable adduct.[98,159,175] During the evaluation of TCP derivatives reported in Chapter 4, two synthetic *tert*-butyloxycarbonyl protected (Boc-NH_2) intermediates revealed, surprisingly, potent anti-proliferative activities.

Compounds **5.1** and **5.2** (Figure 5.1 A) were synthesised through the Horner-Wadsworth-Emmons reaction of 4-methyl formylbenzoate, Johnson-Corey-Chaykovsky cyclopropanation, Curtius rearrangement and amide formation following the procedures described in Chapter 4. These correspond to the protected precursors of TCP analogues **4.11** and **4.14**. In a cell viability experiment with LNCaP cells, **5.1** and **5.2** showed an exceptional ability to hinder cell proliferation at nM concentrations (IC_{50} **5.1** = 260 nM, and IC_{50} **5.2** = 650 nM, Figure 5.1). Notably, a much lower activity in the same cell lines was observed for the free amine counterparts **4.11** and **4.14** (Chapter 4 and Figure 5.1 B).

Figure 5.1: Effects of TCP derivatives 4.11 and 4.14 and their Boc-protected *precursors* 5.1 and 5.2 on LNCaP cells proliferation.

(A) Molecular structure of **5.1**, **5.2** (Boc-protected compounds) and **4.11**, **4.14** (free amines); **(B)** IC_{50}s values determined with cellular evaluation of **5.1** and **5.2** in LNCaP cells. Results are expressed as means (µM) ± STD (n=2); **(C)** Dose- response curves showing the effects of **5.1** (left) and **5.2** (right) in LNCaP cells. The X-axis is in logarithm of concentration (M, Molar); Y-axis is the % of RLU (relative luminescence unit) normalised to baseline (100 % activity, vehicle control - DMSO). Data were fitted by nonlinear regression analysis.

To test whether the results obtained with **5.1** and **5.2** were linked to LSD1 inhibition, we evaluated their enzymatic ability in arresting LSD1 demethylase activity with Amplex®Red peroxidase-coupled assay. However, the compounds were enzymatically inactive in the cell-free assay (data not shown).

The experiment was repeated with the following conditions: **1)** increasing the concentration of inhibitors (up to 250 µM); **2)** increasing the incubation time of LSD1+inhibitor (overnight, 72 h and 96 h). In all the cases, **5.1** and **5.2** were unable to arrest the substrate demethylation.

To support the data obtained in prostate cancer cells, the anti-proliferative activities of **5.1** and **5.2** were evaluated in AML cell lines. Cell viability of KASUMI, MV4-11, OCI-AML3, HL-60, THP-1 and U937 cells, treated with increasing concentrations of **5.1** and **5.2** (10 µM, 3 µM, 1 µM, 0.3 µM, 0.1 µM, 0.03 µM, 0.01µM, 0.003 µM and 0.001 µM, 72 h) was measured with CellTiter-Glo®.

High anticancer potency was revealed for both the compounds in the AMLs (Figure 5.2, Figure 5.3 and Table 5.1).

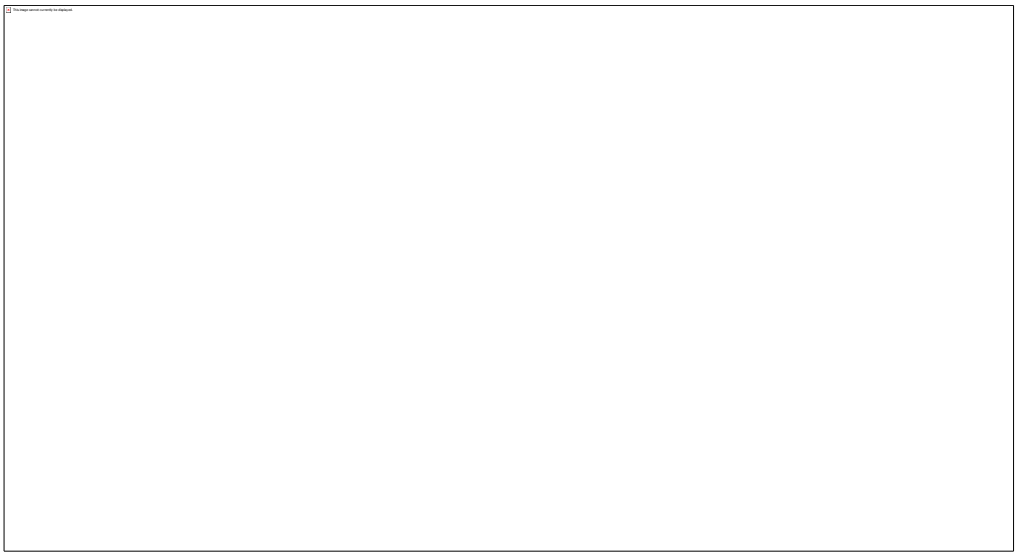

Figure 5.2: Dose-response curves showing the effects of *N*-protected TCP derivative 5.1 on AMLs proliferation (72 h).

The X-axis is in logarithm of concentration (M, Molar); Y-axis is the % of RLU (relative luminescence unit) normalised to baseline (100 % activity, vehicle control - DMSO). Data were fitted by nonlinear regression analysis. Data are shown as mean ± STD (n=5).

Figure 5.3: Dose-response curves showing the effects of *N*-protected TCP derivative 5.2 on AMLs proliferation (72 h).

The X-axis is in logarithm of concentration (M, Molar); Y-axis is the % of RLU (relative luminescence unit) normalised to baseline (100 % activity; vehicle control- DMSO). Data were fitted by nonlinear regression analysis. Data are shown as means ± STD (n=5).

Table 5.1: Enzymatic and anti-proliferative activity (IC_{50} values) of TCP analogues 4.11 and 4.14 and their respective *N*-protected *precursors* 5.1 and 5.2.

Values obtained in enzymatic and cell viability experiments are reported in µM ± STD (n=3 for enzymatic, n=5 for cellular evaluations); ** Tested at two concentrations (100 nM and 1 µM).

Assay	**4.11**	**4.14**	**5.1**	**5.2**
Enzymatic	0.5±0.42	0.6±0.83	> 250	> 250
Cell viability				
MV4-11	0.2±0.1	0.1±0.8	0.5±1.1	0.6±0.7
HL-60	0.06±4.2	0.2±3.6	0.4±1.2	0.5±0.4
THP-1	0.2±2.1	1.0±0.1	0.2±4.3	0.6±0.5
U937	1.2±2.1	0.6±0.1	0.4±0.4	0.6±0.2
OCI-AML3	0.06±4.2	-**	0.4±1.7	0.5±0.7
KASUMI	0.7±0.3	0.6±8.2	0.5±1.3	0.7±0.1

As shown in Figures 5.2-5.3 and Table 5.1, Boc-protective intermediates **5.1** and **5.2** were able to arrest AMLs proliferation at low μM range, mirroring the cellular results obtained with the free amine counterparts. Interestingly, unlike the latter, the treatments with **5.1** and **5.2** produced a 100% inhibition of cell survival.

Given the compounds unusual structural feature and their capacity to act as potent anti-proliferative agents in both prostate and AMLs, we decided to explore further the *N*-protected TCP analogues.

At the beginning of the study, three mechanisms were hypothesised to justify the biological data for **5.1** and **5.2**:

I. The Boc-compounds function as *pro-drugs*. The *N*-protecting group could facilitate the compounds cellular uptake by masking the positively charged free amine and increasing lipophilicity. Once inside the cells membrane, these could be possibly converted to the irreversible inhibitors by the cells metabolic machinery.

II. The observed activity is based on an LSD1-unrelated mechanism.

III. The compounds act through an LSD1-dependent mechanism without impairing LSD1 demethylase activity.

In order to establish which of the three hypothesised mechanisms is more likely to occur, we took the following steps.

First, we assessed the compounds in other cancer cell lines to investigate on their anti-proliferative potential.

Second, to verify if the biological observations depend exclusively on the *N*-protection or if other structural features contribute to the drugs' effects, other TCP-related compounds bearing a Boc-protecting group were evaluated. Additionally we investigated the activities of similar *N*-protecting groups.

Third, we employed biological experiments (time-course, washout and downstream evaluation of LSD1-dependent biological markers) to fully profile the compounds in leukaemia cells and eventually confirm or revoke the LSD1 implication in the compounds' pharmacology.

5.2. Towards the molecular mechanism of action of Boc-protected TCP derivatives

5.2.1. Further cytotoxicity assays in prostate and haematological cancer cell lines

To further research on the abilities of **5.1** and **5.2** to suppress tumour growth, we performed supplementary evaluations on prostate and haematological cancers cell lines. Prostate cell lines PC3 and DU145 which possess moderate (DU145) and high (PC3) metastatic potential compared to LNCaP line, were exposed to increasing concentrations of **5.1**, its free amine derivative **4.11** and **5.3**, corresponding to **GSK-LSD1** (Figure 5.4).[179] The latter is one of the most potent and selective inhibitors of LSD1 reported to date with a K_i of 16 nM and proved capacity of arresting small cell lung cancer (a solid tumour) proliferation at nM concentrations (2-240 nM). As GSK-LSD1 is currently used as a positive control for LSD1 studies, we decided to include the molecule in the cytotoxicity assays to compare its activity with our anticancer agents in prostate adenocarcinoma cells.[179]

Figure 5.4: Molecular structure of GSK-LSD1.

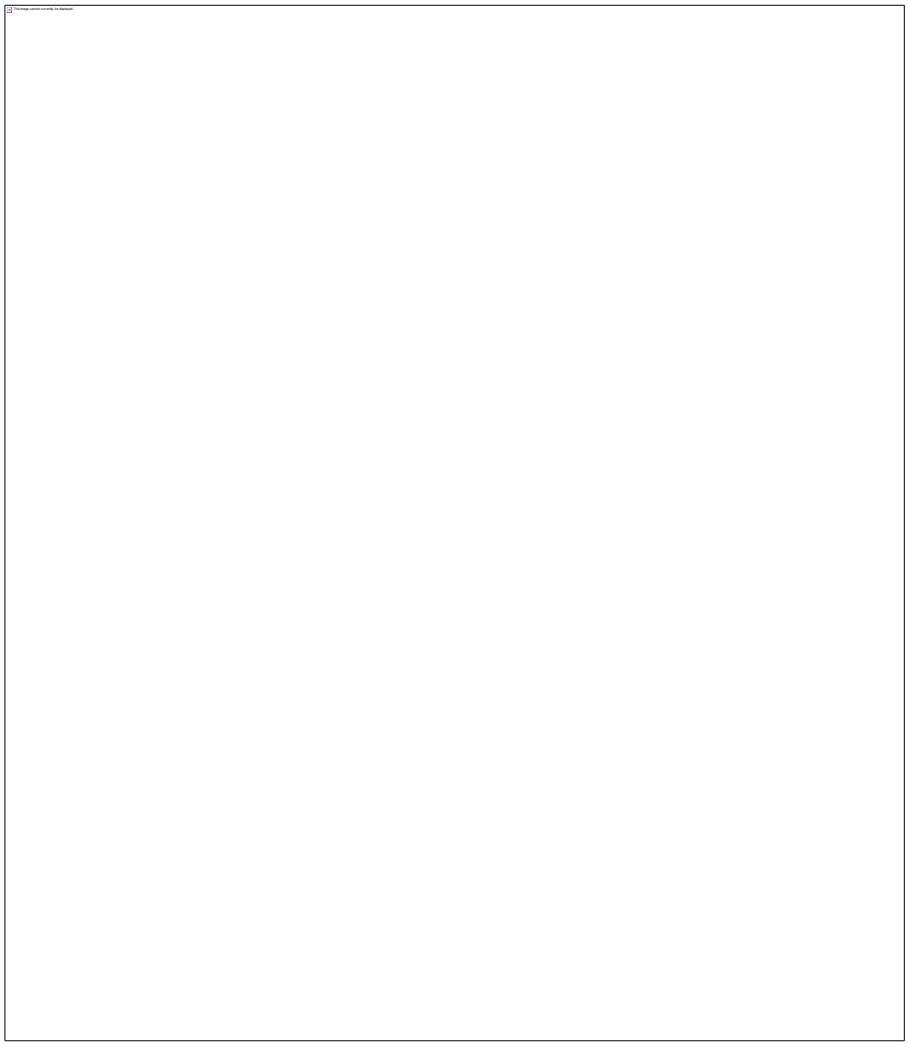

Figure 5.5: Cell viability results in PC3 (A) and DU145 (B) cells, assessed by MTT assay (72 h).
Cells were treated for 72 h with different concentrations of **GSK-LSD1** (black bars), **4.11** (orange bars) and **5.1** (white bars). Results are expressed as a % of cell viability (compared to control - untreated cells). Data are shown as means ± SD (n=6).

The results (Figure 5.5) obtained, further proved the anti-proliferative activity of **5.1**. In both PC3 and DU145 cells, **5.1** treatments **(**5 µM, 72 h) reduced cell viability by 80%. Remarkably, the compound displayed increased efficacy compared to its free amine counterpart **4.11**, (orange bars) and **GSK-LSD1** (**5.3**, black bars).

Compounds **5.1** and **5.2** were next evaluated in multiple myeloma (MM) cell lines, a type of haematological cancer interesting the plasma cells of the bone marrow.[310] In MM cells, U266, LP-1, RPMI-8266 and H929 cells, the compounds were tested only at a single dose (500 nM) for 24 h, 48 h and 72 h. The concentration was decided based on

the results obtained in AML cell lines (IC_{50}s falling in the range 200-700 nM, Table 5.1). The chosen concentration however, was unable to cause significant effects.

Despite the negative results, the data imply that the compounds' pharmacology is not simply associated with a non-specific toxic mechanism.

Having gained supplementary evidence that **5.1** and **5.2** promoted the arrest of cell proliferation and apparently, without correlating with unspecified harmful effects, we prepared additional compounds to establish the structural features that are determinant for the biological data.

5.2.2. Synthesis of diverse *N*-protected TCP-like compounds and their biological evaluation

To verify whether the *tert*-butyloxycarbonyl protection is the key element for the marked anti-proliferative behaviours of **5.1** and **5.2**, we synthesised Boc-protected TCP and the *precursor* of the TCP amide analogue **4.10**, for which we report potent biological activities in AMLs (**5.4** and **5.5**, respectively, Figure 5.6). The compounds were then tested on AMLs and LNCaPs. If the Boc protection was solely responsible for the increase in cytotoxicity, especially in the prostate tumour cells, both **5.4** and **5.5** would be able to suppress tumour proliferation.

The concentration used for testing **5.4** and **5.5** were selected in accordance to the results reported for the respective free amines (**TCP** and **4.10**). To test **5.4**, we used a range of 3 mM-1 µM whereas to test **5.5**, we used a range of 10-0.001 µM for AMLs experiments and a range of 1 mM - 1 µM for LNCaPs experiments. Post-treatment viable numbers were measured after 24 h, 48 h and 72 h treatment.

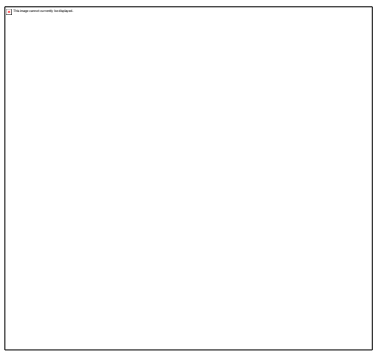

Figure 5.6: Boc-protected compounds 5.4 and 5.5 molecular structure.

5.4 Boc-protected-TCP, **5.5** Boc-protected TCP-derivative substituted with benzylamine.

Surprisingly, neither **5.4** nor **5.5** showed activity, suggesting that the presence of Boc-protection is not the only element defining the anti-tumour properties. Such evidence also partially refutes the first hypothesised mechanism. Namely, if the activities observed with **5.1** and **5.2** were generated by a *pro-drug*-like mechanism, **5.4** and **5.5** would have exhibited the same biological properties as their free amine homologues **TCP** and **4.10**.

Besides that, compounds **5.1** and **5.5** share a high structural similarity, which makes the data even more interesting. The contrasting results could be attributed to the different *para* substitutions at the TCP phenyl ring being a phen**ethyl**amine for **5.1** and **benzylamine** for **5.5** (Figure 5.7).

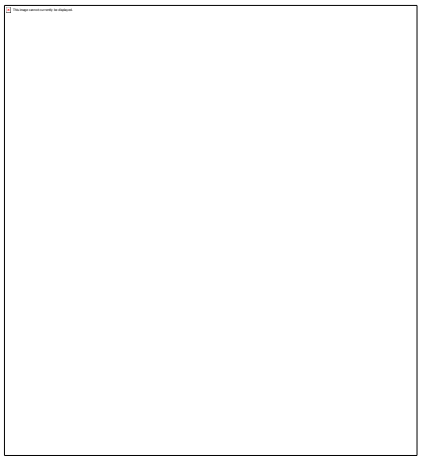

Figure 5.7: Structures of *N*-protected TCP derivative 5.1, 5.2 (active) and 5.5 (inactive).

Notably, both **5.1** and **5.2** contain the same **ethyl** carbon chain between the TCP-phenyl ring and the thiophenyl or phenyl moiety (Figure 5.7). To assess if the structural similarity between the active compounds correlates with the cellular effects, a supplementary structure was generated by coupling the 4-(*tert*-butoxycarbonyl) amino) cyclopropyl) benzoic acid (**4.16**, Chapter 4) with tryptamine (Scheme 5.1). The activities of **5.6** were then evaluated in HL-60 and THP-1 and LNCaPs.

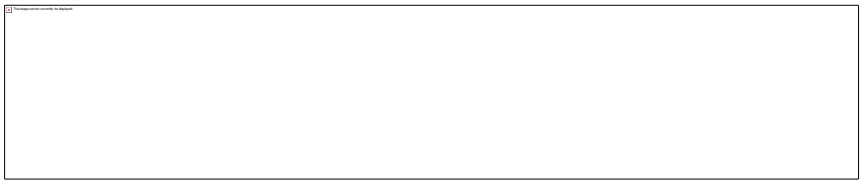

Scheme 5.1: **Coupling of 4-(*tert*-butoxycarbonyl)- amino) cyclopropyl) benzoic acid 4.6 with tryptamine.**

Figure 5.8: Dose-response curves showing the effects of *N*-protected TCP derivative 5.6 on HL-60 and THP-1 cells proliferation (72 h).

The X-axis is in logarithm of concentration (M, molar); Y-axis is the % of RLU (relative luminescence unit) normalised to baseline (100 % activity = vehicle control, DMSO). Data were fitted by nonlinear regression analysis and are shown as means ± STD (n=5).

Following 72 h treatment with **5.6**, cell viability results revealed a dose-dependent decrease of cell proliferation in AMLs (IC_{50} HL-60 = 1.17 ± 0.2 µM and IC_{50} THP-1 = 0.91 ± 0.1) and LNCaPs (0.45 ± 3.2 µM).

In the light of these results, the presence of an ethyl carbon chain in the substituted amine is probably a key element to achieve biological activity with *N*-protected derivatives. However, this must be confirmed, given the small number of molecules tested.

Thereafter, two further compounds bearing a similar *N*-protecting group, namely the *N*-ethyl carbamate, were synthesised (**5.7** and **5.8**, Figure 5.9).

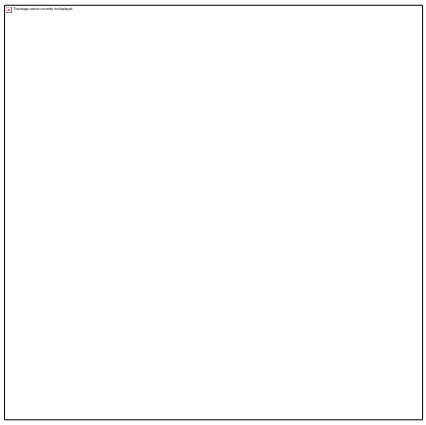

Figure 5.9: *N*-ethyl carbamate protected compounds 5.7 and 5.8.

These were prepared by adapting the Curtius rearrangement[311] protocol and scavenging the generated isocyanate with ethanol instead of *tert*-butanol.

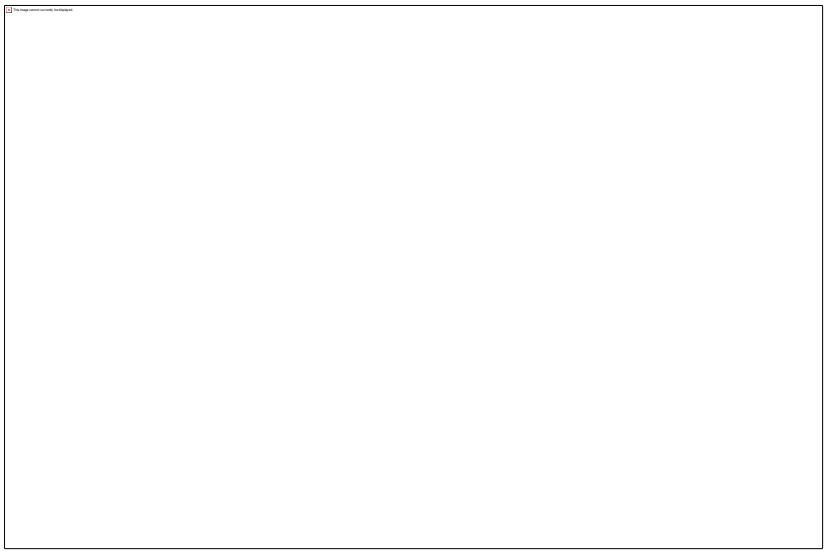

Scheme 5.2: Synthesis of *N*-ethyl carbamate TCP derivatives.

The ability of the *N*-ethyl carbamate derivatives to interfere with LSD1 demethylase was evaluated with the Amplex®Red assay and, similarly to the Boc-compounds, **5.7** and **5.8** were devoid of enzymatic activity. Notwithstanding, these prevented AMLs growth at concentrations similar to the ones observed for the Boc derivatives **5.1**, **5.2** and **5.6** (Figure 5.10-5.11 and Table 5.2).

Figure 5.10: Dose-response curves showing the effects of *N*-protected TCP derivative 5.7 on AMLs proliferation (72 h).

The X-axis is in logarithm of concentration (M, Molar), Y-axis is the % of RLU (relative luminescence unit) normalised to baseline (100 % activity = vehicle control, DMSO). Data were fitted by nonlinear regression analysis and are shown as means ± STD (n=5).

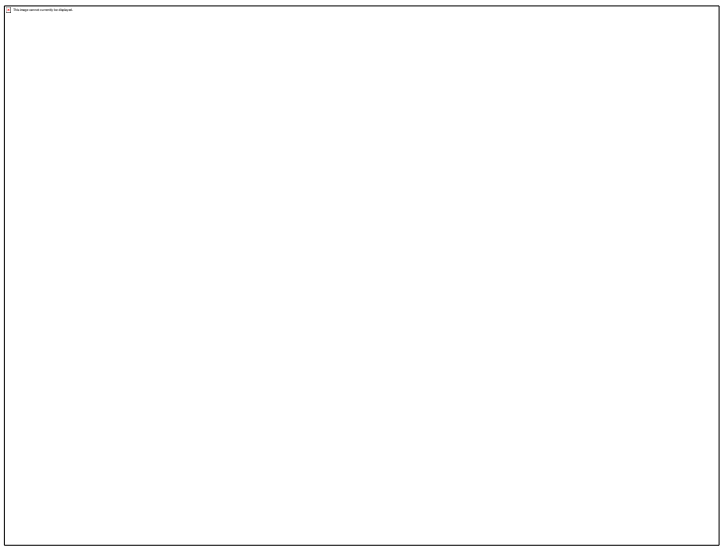

Figure 5.11: Dose-response curves showing the effects of *N*-protected TCP derivative 5.8 on AMLs proliferation (72 h).

The X-axis is in logarithm of concentration (M, Molar); Y-axis is the % of RLU (relative luminescence unit) normalised to baseline (100 % activity = vehicle control, DMSO). Data were fitted by nonlinear regression analysis and are shown as means ± STD (n= 5).

Table 5.2: *In vitro* cytotoxicity results of 5.7 and 5.8 in AMLs proliferation (72 h).
Results are reported in μM ± STD (n=5); nt: not tested.

Compound	MV4-11	HL-60	OCI-AML3	U937	THP-1
5.7	1.3±2.7	0.4±7.45	1.4±0.5	0.3±2.8	nt
5.8	0.5±1.5	0.7±5.21	0.5±0.4	nt	0.3±1.2

Therefore, the biological evaluations confirmed the lack of enzymatic activity for all the *N*-protected TCP derivatives and suggested that the presence of the *N*-protection is not the only putative factor for the pharmacological effects. Based on the preliminary observation, we selected **5.1** and **5.8** for supplementary studies as representatives for the *N*-protected class of compounds. What follows is the description of the supplementary biological evaluations we have made attempting to characterise the effects of the synthetic intermediates.

5.3. Biological profiling of *N*-protected derivatives

In order to refute or substantiate a correlation between the suppression of LSD1 activity and the cellular effects, and to further characterise the pharmacology of the *N*-protected compounds we conducted several experiments with leukaemia cells. These consisted in a study of the kinetics required for the activity, a washout experiment to define if the observed data derive from a covalent inhibition and evaluated the expression levels of downstream markers associated with LSD1 inhibition and differentiation (H3K4me2, CD86, CD11b and CD14).[101,196] Finally, we examined the potential toxic effects of **5.1** on non-malignant HSC cells expressing $CD34^{+}$.[86,312]

5.3.1. Time-course evaluation

To define the time-course required for the protected compounds to trigger effects, **5.1** was incubated with THP-1 (100 nM and 1 µM) and cell viability was measured after 24 h, 48 h and 72 h (Figure 5.12). The concentrations for the experiment were kept the same as for the free amine, to allow a directed comparison between the data of **5.1** and **4.11**.

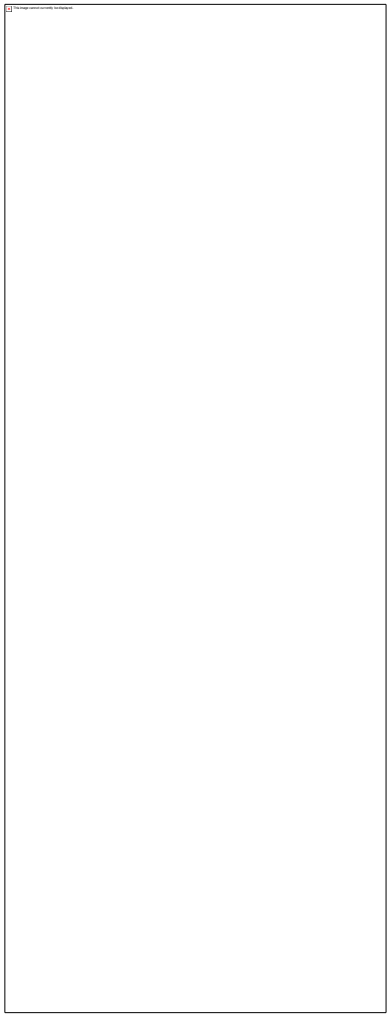

Figure 5.12: Effects of compound 5.1 (100 nM and 1 µM) on the proliferation of THP-1 cells (24 h, 48 h and 72 h).

Survival (RLU) is normalised to pre-treatment levels. Statistical significance was determined with one-way ANOVA and corrected for multiple comparisons using Dunnett's test. Data are shown as means ± STD (n=5); *** $p < 0.001$ **** $p < 0.0001$.

The data indicate a fast course of action for **5.1** (Figure 5.12), as a significant decrease in cell survival was observed after only 24 h treatment. With prolonged exposures the reduction was even more pronounced, reaching nearly 100% inhibition at 72 h and 1 µM concentration.

The results differ from the time course observed with free amine, which required longer incubation time (72 h) to exhibit inhibitory effects. Compound **4.11**, the free amine counterpart of **5.1** was unable to reduce significantly the cell viability after short incubation (Figure 5.13).

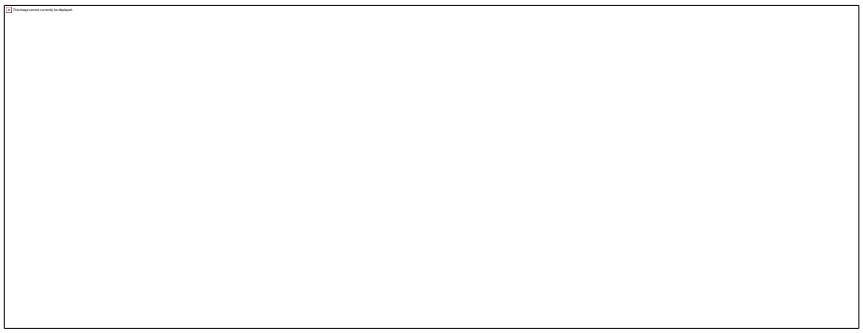

Figure 5.13: Cytotoxicity effects of 4.11 and 5.1 (100 nM -1 µM) after 24 h treatment in THP-1 cells.
Survival (RLU) is normalised to pre-treatment levels. Statistical significance was determined with one-way ANOVA and corrected for multiple comparisons using Dunnett's test. Data are shown as means ± STD (n=5); *** $p < 0.001$ **** $p < 0.0001$.

5.3.2. Evaluation of activity persistence

To determine if the reported effects are due to irreversible inhibition, the persistence of the anti-proliferative behaviour of **5.1** was evaluated with a washout experiment.[305] AMLs (MV4-11, THP-1, KASUMI, HL-60, U937 and OCI-AML3 were stimulated with **5.1** (200 nM) or left untreated for 6 h, followed by washout of inhibitor-containing medium. Compounds residual activity was next measured after 72 h.

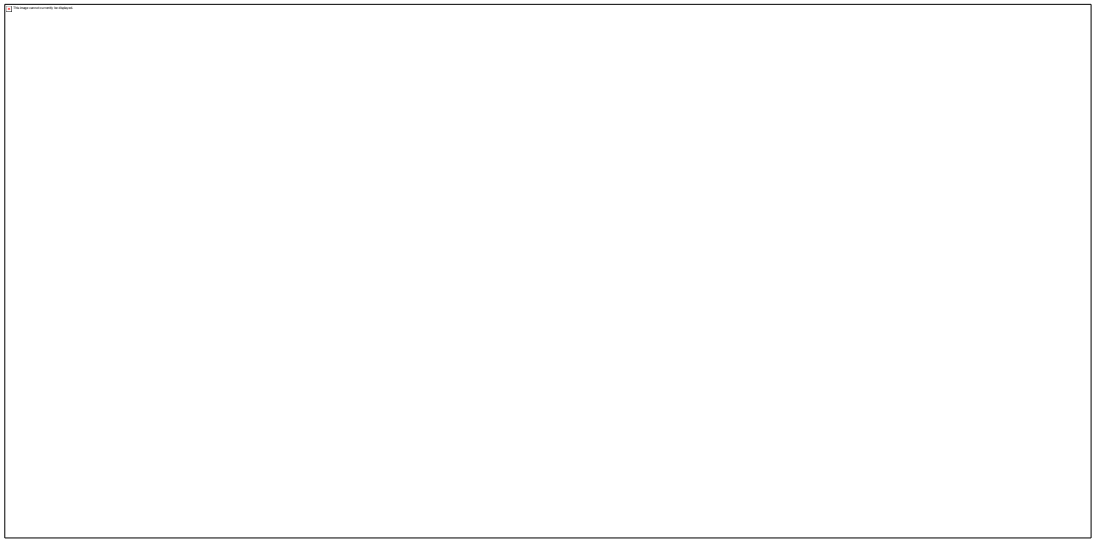

Figure 5.14: Washout experiments with 5.1 on AML cell lines.
Results were obtained with CellTiter-Glo® and RLU was normalised to control (untreated). Statistical significance was determined with two-way ANOVA and corrected for multiple comparisons using Bonferroni's test. Data are shown as means ± STD (n=5).

Results indicate an irreversible binding as **5.1** was able to maintain over time the anti-proliferative properties despite the washout. The direct comparison between continuous (black bars) and pulsed treatment (green bars), did not produce a significant variation in cell count. In contrast, if the activity was generated by a reversible mechanism, **5.1** after being cleared from the system, would not have been able to generate the observed anti-tumorigenic activities.[291]

5.3.3. Evaluation of H3K4me2 expression by immunoblotting

A Western blot analysis of the H3K4me2 levels was next employed to establish whether the biological data are generated by an LSD1-dependent mechanism. KASUMI cells were incubated with 200 nM of **5.1** or left untreated and cultured for 2 h, 4 h, 6 h, 48 h and 72; blotting membranes of separated proteins were probed for H3K4me2 and H3 (total).

Figure 5.15: Western blot analysis of the methylation state of H3 after treatment of KASUMI cells with compound 5.1 (200 nM) for different time points. The blots indicated the H3K4me2 levels (top) compared to H3 (total, loading control - bottom)..

Data revealed a progressive increase of di-methylated H3 over time and, as the H3K4 demethylation is directly linked with LSD1 inhibition, we cannot exclude the involvement of LSD1 in the pharmacological activities of **5.1**.

In addition, the increase of the methylation mark is significant after only 6 h of incubation; in contrast, at equivalent experimental conditions (same cell line and same concentrations), the free amine counterpart **4.11** promoted an increase of H3K4me2 after 48 h of treatment. Therefore, the data further substantiate the faster onset of activity by **5.1**.

5.3.4. CD86 expression

As previously mentioned, the increased expression of CD86 is a direct consequence of LSD1 inhibition.[196] To corroborate the evidence designating a possible involvement of LSD1 in the observed activities, we evaluated the post-treatment induction of the CD86 in THP-1 cells with both Boc and ethyl carbamate derivatives. The incubation time was selected according to the previous experiments. Given that 6 h were sufficient to induce H3K4me2 expression and 24 h were sufficient to arrest cell proliferation, CD86 expression was measured after 24 h treatment with **5.1**, **5.2** and **5.8**.

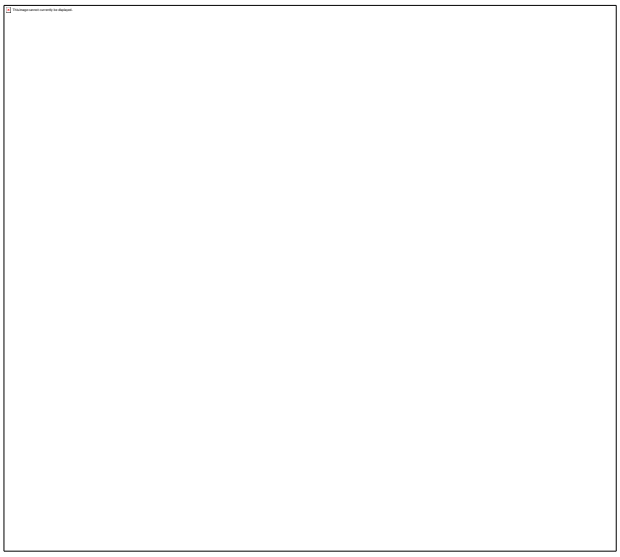

Figure 5.16: Effects of *N*-protected TCP-derivatives 5.1, 5.2 and 5.8 (200 nM, 24 h), on the expression of CD86 in THP-1 cells.

(A) 5.1, (B) 5.4 (C) 5.8, (D) statistical analyses of three independent experiments with similar results.

Cells were gated based on FSC and SSC parameters. X-axis represents the fluorescence increase (compared to control) generated by cells expressing CD86. Statistical significance was determined with two-way ANOVA and corrected for multiple comparisons with Bonferroni's test. Values are expressed as means % of increase (compared to control) ± STD (n=3); ****p < 0.0001.

Table 5.3: Increase (%) of CD86 expression induced by *N*-protected TCP derivatives 5.1, 5.2 and 5.8 (200 nM, 24 h) in THP-1 cells.

Results are expressed as % of increase compared to pre-treatment level (vehicle control) ± STD (n=3).

Compound	CD86 (%) (Compared to control, ± STD, n=3)
Control	8.7±2.1
5.1	61.0±1.5
5.2	72.5±8.2
5.8	46.7±2.9

After only 24 h treatments, the protected derivatives were able to trigger the expression of CD86. The registered augment was slightly less marked compared to the free amine counterparts. In addition, treatments with **5.8** (thiophenethylamine TCP-derivative *N*-protected as the ethyl carbamate) promoted a less pronounced increase (46.7±2.9%) compared to Boc-protect compound. The CD86 evaluations further suggest that LSD1 is the possible target of the *N*-protected compounds.

5.3.5. CD14 and CD11b expression

To determine whether the protected compounds affect the myelocytic differentiation markers, we measured the levels of CD14 and CD11b in AML cell lines after treatment with **5.1** and **5.8.** THP-1 and MV4-11 cells treated with 200 nM of **5.1** or **5.8** were cultured for 24 h. Whole cells stained with fluorescent antibodies were then analysed by flow cytometry (Figure 5.17-5.18 and Table 5.4).

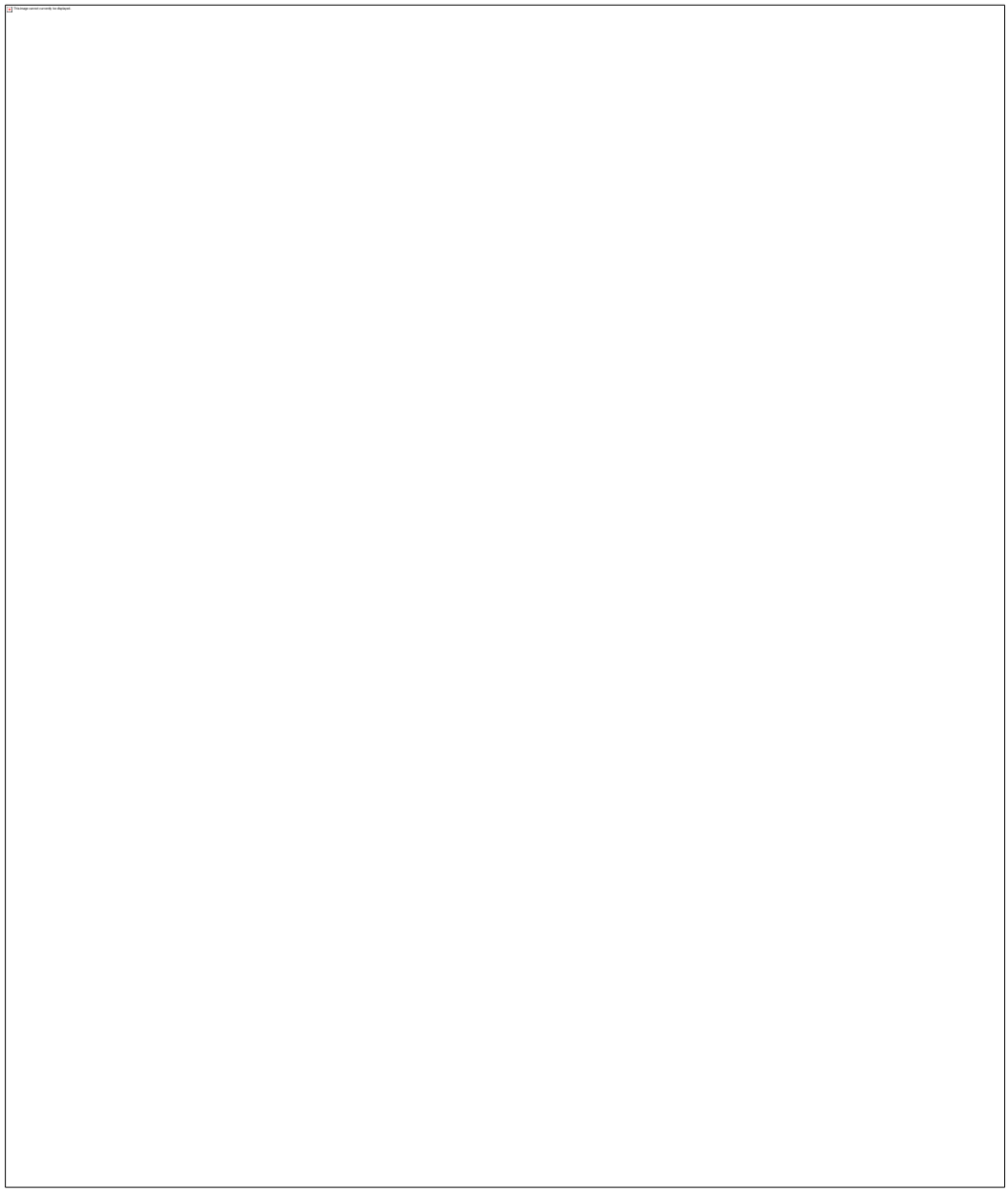

Figure 5.17: Effects of *N*-protected TCP derivative 5.1 (200 nM, 24 h) on the expression of differentiation markers CD14 and CD11b in THP-1 cells.

FSC and SSC profiles were applied for the initial gating by selecting cell size and distribution and remove cell debris. Plots **A, B**, **C** show the Isotype controls. Plots **D**, **E**, **F** show the experimental conditions. Plots **A** and **D** show the gated population: in the X-axis is reported the mean fluorescence increase for FITC-CD14 Ab; in the Y-axis is reported the mean fluorescence increase for PE-CD11b Ab. Plots **B** and **C** (black histograms) report the fluorescence increase of Isotype controls (untreated cells); **E** shows the fluorescence increase of the monocytic marker CD14; **F** shows the fluorescence increase of the myeloid marker CD11b. Numbers shown in each box are the % of cells expressing CD14 or CD11b. (**G**) Shown are results graphically summarised for three independent experiments. Statistical significance was determined with two-way ANOVA and corrected for multiple comparisons with Bonferroni's test. Values are expressed as means % of CD14-CD11b increase ± STD (n=3); *** $p < 0.001$, ****$p < 0.0001$.

Figure 5.18: Effects of *N*-protected TCP derivative 5.8 (200 nM, 24 h) on the expression of differentiation markers CD14 and CD11b in MV4-11 cells.

FSC and SSC profiles were applied for the initial gating by selecting cell size and distribution and remove cell debris. Plots **A**, **B**, **C** show the Isotype controls. Plots **D**, **E**, **F** show the experimental conditions. Plots **A** and **D** show the gated population: in the X-axis is reported the mean fluorescence increase for FITC-CD14 Ab; in the Y-axis is reported the mean fluorescence increase for PE-CD11b Ab. Plots **B** and **C** (black histograms) report the fluorescence increase of Isotype controls (untreated cells); **E** shows the fluorescence increase of the monocytic marker CD14; **F** shows the fluorescence increase of the myeloid marker CD11b. Numbers shown in each box are the % of cells expressing CD14 or CD11b. (**G**) Shown are results graphically summarised for three independent experiments. Statistical significance was determined with two-way ANOVA and corrected for multiple comparisons with Bonferroni's test. Values are expressed as means % of CD14-CD11b increase ± STD (n=3); ****$p < 0.0001$.

Table 5.4: Increase (%) of $CD14^+$ and $CD11b^+$ expression induced by *N*-protected TCP derivatives 5.1 and 5.8 (200 nM, 24 h) in THP-1 and MV4-11 cells.

Results are expressed as % of increase compared to control Ab* ± STD (n= 3).

Ab*: Human IgG-FITC and IgG-PE; Ab**: Human anti-CD14-fluorescein (FITC) and anti-CD11b-phycoerythrin (PE).

	CD14-CD11b (%) ±STD (n=3)	
Conditions	**$CD14^+$**	**$CD11b^+$**
THP-1+Ab*	22.3±0.5	8.0±1.0
THP-1+5.1+Ab**	78.5±10.2	91.5±4.4
MV4-11+Ab*	8.5±1.4	7.7±1.4
MV4-11+5.8+Ab**	67.7 ± 2.5	83.0±1.9

Mirroring the results in both the AML cell lines, **5.1** and **5.8** equally promoted the expression of the monocytic and myeloid markers CD14 and CD11b. This implies that, *N*-protected compounds promote a fast differentiation, phenocopying the effect seen with their free amine counterparts. The differentiation is also associated with a decrease in cell count (plots E and F, Figures 5.17 and Figure 5.18) and such reduction is more noticeable after treatment with compound **5.8**.

5.3.6. CD34^{+} evaluation

To estimate the myelotoxicity, bone marrow cells expressing CD34 derived from AML patients, were exposed to increasing concentrations of **5.1** during 72 h. Subsequently, cells were stained with appropriate antibody-FITC conjugated (anti-CD34 mouse monoclonal antibody to human FITC conjugated) and cells expressing CD34 counted by flow cytometry. As previously described, the CD34 marker is a differentiation stage-specific leucocyte antigen and examining the number of CD34 expressing cells upon pharmacological treatments can give an evaluation of a drug toxicity.[298,299]

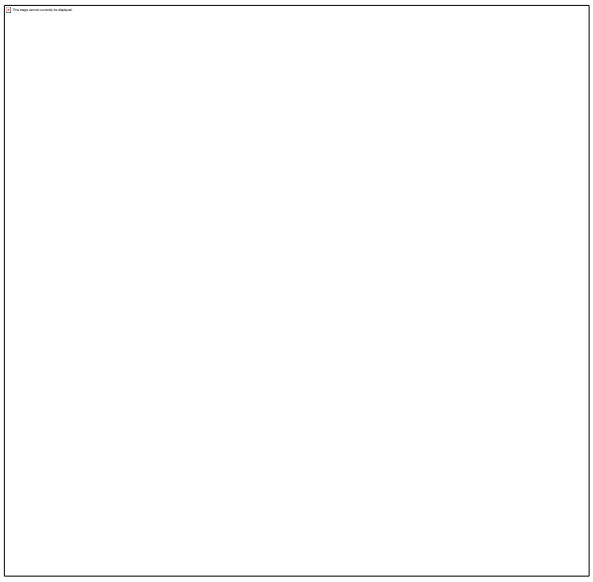

Figure 5.19: Healthy CD34+ expressing HSC treated with increasing concentrations of *N*-protected TCP derivatives 5.1 (72 h).

Data are shown as means ± STD (n=3). Statistical significance was determined with one-way ANOVA and corrected for multiple comparisons with Dunnett's test; *p < 0.05.

As reported in Figure 5.19, normal HSC cells were less sensitive to **5.1** treatments than tumorigenic cells. A significant decrease of CD34^{+} expressing cells was registered only at 1 µM and 10 µM doses, while the compound is able to arrest cancer cell proliferation at concentrations < to 1 µM. Moreover the results are based on 72 h incubation and, as reported by previous experiments, **5.1** present a faster course of action in tumorigenic cells.

5.4. Discussion

The present study was designed to examine the effects of synthetic intermediates of TCP analogues with *N*-protected carbamates. The compounds showed remarkable biological effects in arresting human leukaemia and prostate adenocarcinoma cells despite lacking LSD1 inhibition in cell-free assay. At the beginning of the study, we hypothesised that the compounds could act as *pro-drugs*. However, results did not substantiate this supposition. Amides and carbamates are not labile in cells, and these have proven to possess a faster course of action than the free amines. Such kinetic is highly unlikely if metabolic activation is involved. Moreover, if a *pro-drug* mechanism was likely to occur, both **5.4** and **5.5**, corresponding respectively to Boc-protected TCP and Boc-protect benzyl derivative **4.10**, would have been able to inhibit AML and LNCaPs proliferation. However, the compounds were devoid of activity upon protection.

A structural observation among the *N*-protected TCP synthetic intermediates revealed that all the active molecules show a common feature. In compounds **5.1** and **5.2,** the TCP core has been substituted in *para* at the phenyl ring with an **ethyl-**containing amine, specifically phen**ethy**lamine and thiophen**ethyl**amine. This feature represents the only difference between the active **5.1** and inactive **5.5**. Supplementary biological evaluation with the Boc protected **5.6**, substituted with tryptamine at the phenyl ring (*para*), evidentiated the ability of the agents holding this characteristic to suppress cell proliferation at low µM range. Albeit the positive results with **5.6**, the presence of the ethyl linker as a determinant factor for the activity cannot be confirmed without testing additional compounds.

The *N*-ethyl carbamate protected compounds also decreased cell viability of AMLs lines and at similar concentrations as the *N*-*tert*-butyloxycarbonyl compounds. In addition, we proved that the affects of **5.1** are irreversible, as after a shorter exposure (6 h) followed by washout, the compound maintained the anti-cancer potential.

To further profile the mechanism of action, Western blotting and flow cytometry experiments were employed. Western blot analyses of KASUMI cells treated during 6 h with **5.1**, revealed a marked increase in H3K4me2, which is a direct cellular consequence of the LSD1 pharmacological inhibition. The data however, contrast with the lack of enzymatic activity measured by the Amplex®Red assay.

Treatment with nM concentrations of **5.1**, **5.2** and **5.8** (200 nM, 24 h) induced an increment of CD86 marker in THP-1 cells, further correlating the pharmacological effects with LSD1 suppression. Similar concentrations were also able to trigger the differentiation marker CD11b and CD14 in MV4-11 and THP-1 cells, mirroring the effects of the free amine counterparts described in Chapter 4. Cytotoxic effects were evaluated next in HSC expressing CD34 and **5.1** treatments correlated with toxicity at 1 µM and 10 µM. Yet, the concentrations generating the observed anti-cancer and differentiation activities were much lower (200-900 nM) and therefore, normal cells are less sensitive to the treatments compared to the tumorigenic counterparts.

Overall results indicate a possible LSD1-dependent mechanism and in accordance with this, recent experiments by Lynch *et al*. suggest the phenotypic effects and therapeutic benefits of TCP and analogues are independent of their inhibition of histone demethylation.[313] Instead, their key function is to block LSD1 binding to Gfi1 transcriptional repressor. Gfi1 is a crucial regulator of the myeloid differentiation transcription programme and is required for maintaining stem cell competence.[314] It is a transcription repressor involved in hematopoiesis and oncogenesis that regulates neutrophil differentiation, promotes proliferation of lymphoid cells, and it is required for granulocyte development.[314,315] In both mice and humans with Gfi1 mutations, myeloid progenitor cells fail to differentiate to mature neutrophils, causing the accumulation of monocytes and abnormal cells that blend features of monocytes and granulocytes. As previously reported, Gfi1 contains a N-terminal SNAG domain[137] that binds to LSD1 and functions as scaffolding for the asSTDbly of several complexes with histone-modifying enzymes like HDAC1 and HDAC2 and the corepressor CoREST to suppress the expression of target genes implicated in multi-lineage blood cell development.[219] Interestingly, depletion of either Gfi1 or LSD1 (by silencing or pharmacological inhibition) has the same effect on haematopoiesis.[67] These findings could suggest a similar mechanism for the Boc-compounds, which could disrupt the Gfi1-LSD1 interaction without affecting LSD1 demethylase activity. However, if on one hand the lack of enzymatic activity and the induction of the cell differentiation markers fit with Lynch and colleagues findings, on the other hand **5.1** proved to increase H3K4me2 expression in cellular context.

It must be considered that the activity of LSD1 demethylation is a multiple coordinate process involving the association of LSD1 with positive and negative regulatory factors like HDACs, CoREST and BHC80 partners.[77] Unlike the cell-free enzyme assay, the high potency observed in cells could be an effect of LSD1 association with other regulatory protein complexes, whereby the demethylase activity of LSD1 could be regulated by other intracellular factors such as CoREST and HDACs for instance.[114,120,316]

Whether the effects of compounds **5.1**, **5.2**, **5.6**, **5.7** and **5.8** depend on transcriptional or post-transcriptional modifications, the *N*-protected compounds are linked with growth inhibition, loss of viability and differentiation process which are inversely correlated with LSD1 activity.

These results raise many other questions and further biological assays are needed to characterise the mechanism of action.

5.5. Conclusions and future work

The experiments in this chapter were designed to elucidate the mechanism underlying the activity of a small series of Boc-protected TCP like compounds. Regardless of the exact mechanism of action, the compounds have proven to inhibit LSD1 mediated processes in cells.

The increase of H3K4me2 confirms the involvement of LSD1 as controller of cell proliferation and the data suggest that the binding of LSD1 at its catalytic site is not the sole cause of cell proliferation inhibition. Future work will involve optimisation of the series and further biological experiments will be carried on to clarify their mechanism of action and advance one compound into an *in vivo* efficacy model for AML, either as a monotherapy or in combination with current standard of care chemotherapeutic agents.

Chapter 6 - Exploring activity based probes for LSD1 labelling

6.1. Introduction

LSD1 activity tightly regulates gene transcription in both normal and diseases states. Due to its dynamic behaviour, it is difficult to monitor LSD1 within proteomes. Generally, the traditional genomic and proteomic profiling methods for the evaluation protein activities, such as the analyses of expression levels and examination of protein modifications, are indirect and unable to provide information about enzymes catalytic activity promoting the measured effects.[317–319] Moreover, such molecular methods cannot identify protein post-translational modifications or protein association in complexes within the cellular environment.[319–321] To overcome the limitations of traditional methods, activity-based protein profiling (ABPP) technique has been designed to provide a chemoproteomic tool for the characterisation of the protein/enzymes functional regulation in their natural context.[319] ABPP utilises chemical and protein based molecules called activity based probes (ABP), which are able to bind covalently to target enzymes through the enzyme's activity. These molecules consist generally of two elements (Figure 6.1): **1)** a reactive group (warhead) which interacts specifically with the desired target and **2)** a reporter tag, which enables the detection and isolation of the probe-labelled protein/enzyme (biotin and fluorophores).[321,322]

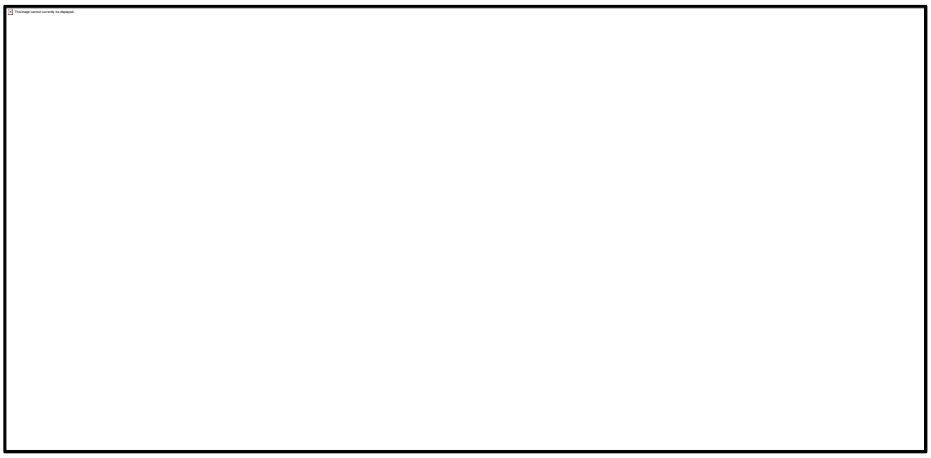

Figure 6.1: Traditional design of ABP.
Adapted from Heal *et al.* [323]

Due to their high specificity, the probes can be applied to complex proteomes such as tissue lysates, whole cells or even organisms.[317]

The use of activity based probes has been successfully applied to the characterisation and asSTDbly of functional understanding of proteins involved in cancer, signalling pathway and host-virus infection as well as many others.[320] The use of these tools is still limited to proteins or enzymes with well-known activities as cysteine proteases, serine hydrolases[320] and the potential application of ABP for the examination of epigenetic modifications has not been widely investigated. To analyse the proteins interacting with tri-methylated H3K4, Li et *al*. developed a modified peptide able to associate with proteins interacting with H3K4me3.[324] Such peptide corresponds to a modified H3K4me3 N-terminal 15-mer, having a benzophenone replacing Ala-7 and a terminal alkyne moiety. Upon UV irradiation, the formed benzophenone radicals and the conjugation to the alkyne, via click chemistry, of an azide-rodhamine fluorophore, the proteins interacting with the tri-methylated histone 3 were visualised in complex proteomes.[324] No studies so far addressed the design of ABP for LSD1 labelling.

As LSD1's functions still need to be fully characterised, it is worthwhile to explore a method to fluorescently label LSD1.

A recent work reported on the use of ABP for studying MAO A and MAO B, the FAD dependent family oxidases homologous of LSD1.[325] The MAOs have been labelled *in situ* by analogues of deprenyl (a known MAOI). These analogues displayed an alkyne

moiety that was conjugated with an azide containing a fluorophore. The probes were successfully employed to label both purified enzyme and complex proteomes as mouse and human-derived tissues.[325]

As the enzymatic activity of LSD1 and MAOs are similar, this work inspired us to synthesise a water-soluble molecular probe for LSD1, to interrogate the biomolecular interactions and the effects associated with the enzyme activity and inhibition in both *in vitro* and *in vivo* assays.

6.2. Reporter tags

Biotin and fluorophores are the most used reporter tags for labelling purposes. Biotin is crucial for protein isolation. An ABP carrying a Biotin tag, facilitates both the protein visualisation with streptavidin-conjugated reporters on protein blots, and the isolation by purification with immobilised streptavidin agarose beads.[318] However, the use of Biotin has many inconvenience, including endogenous biotinylation of biomolecules, long blotting procedures for visualisation and incomplete cell penetration due to Biotin's hydrophilic nature.[326,327] Fluorophores are a valid alternative to Biotin and represent the current trend in ABP design. The commonly used fluorophores are rhodamine and boron-dipyrromethene (BODIPY).[327] Protein labelled with fluorophores are readily visualised by direct in-gel scanning under a fluorescent scanner avoiding blotting procedures and purification steps. Furthermore, the hydrophobic character of fluorophores also makes the fluorescent ABP more cell permeable and their application in *in vivo* experiments.[318] The choice of the reporter tag greatly influences the structure and the physico-chemical features of the irreversible inhibitor. Although the fluorophores are hydrophobic in nature and smaller than Biotin, these can hamper in some cases the cell distribution and the ABP selectivity for the target. To overcome these limitations, a "tag-free" (tandem) approach was established.[321] By this method, the reporter tag is conjugated to the ABP after its covalent binding to the targeted enzyme.[321] The most common procedure to connect the tag to the inhibitor, which was also used in this project, consists to the copper catalysed click reaction (CC, click chemistry). This procedure is enabled by the introduction of two bioorthogonal reactive partners: an azide and an alkyne, in both ABP warhead and tag, which react specifically to each other in aqueous media. Through CC, these two chemical species are conjugated via copper catalysed 1,3-dipolar cycloaddition to form a stable 1,4 substituted triazole. Since both azide and alkyne are unique, stable and unreactive chemical specie with natural occurring groups, they can be safely used in a biological context (Figure 6.2).

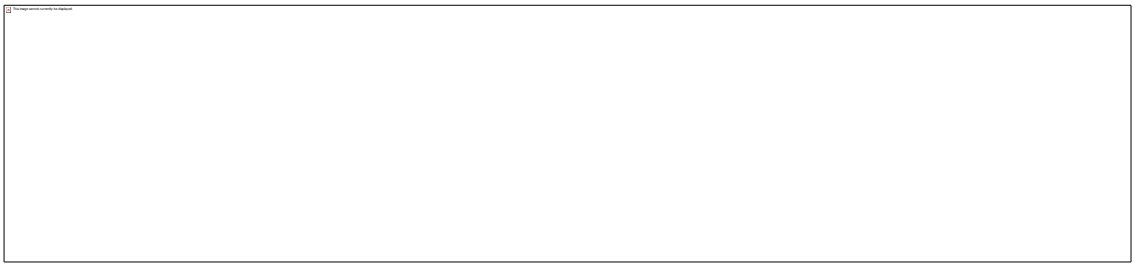

Figure 6.2: Illustration of tag-free ABPP approach.

Specimens to be labelled (protein/enzyme/cells) are first treated with tag-free azide or alkynes modified probes, which are then conjugated *in situ* with complementary alkyne/azide tags via click chemistry.

Other labelling methods that have been used to conjugate a fluorophore to the ABPs include strain promoted click chemistry,[328] Staudinger ligation[329] and Diels-Alder ligation.[326] The first one is widely investigated as it excludes the use of cuprous ions to catalyse the conjugation that can result harmful to living systems. The copper ions can in fact catalyse atmospheric oxygen reaction forming reactive oxygen species (ROS).[330]

6.2.1. Click chemistry mechanism

The copper-catalysed click chemistry (Scheme 6.1) begins with the coordination of the alkyne to the Cu(I) species (1), forming Cu-acetylide specie (2). In the second step (B), the azide binds to the Cu^{+} through the nitrogen and replaces one of the ligands, forming the intermediate 3. The distant nitrogen of the azide (3) attacks then the C-2 of the acetylide, leading to the formation of a six-membered copper (III) metallocycle (4). Ring contraction (D) leads to the formation of the triazolyl-copper derivative that precede the protonolysis of 5, releasing the triazole product.[211,331]

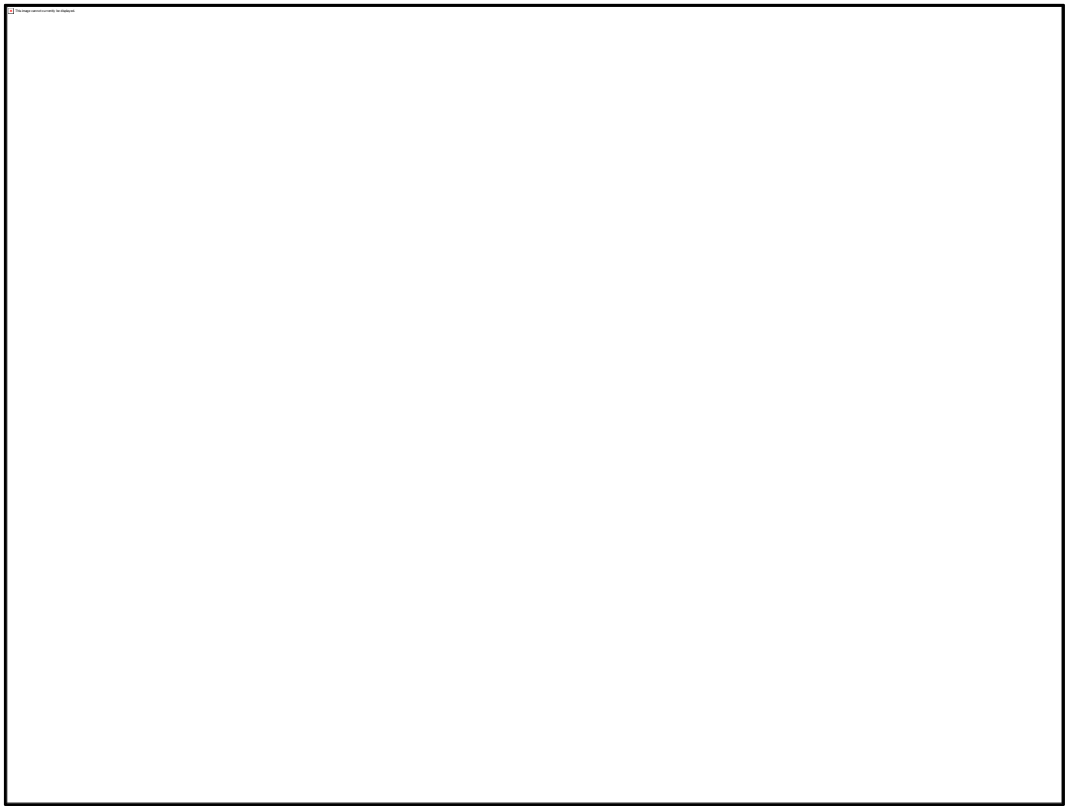

Scheme 6.1: Proposed mechanism for copper assisted CC.
Adapted from Himo *et al*.[331]

The copper catalyst is generally prepared *in situ* by reduction of Cu(II) salts. Copper sulphate pentahydrate ($CuSO_4.5H_2O$), is the most widespread source of cuprous ions for CC[211] and is usually reduced by sodium ascorbate. Other reducing agents have been successfully employed. Tris(2-carboxyethyl)phosphine (TCEP) (Figure 6.3-A) is often used in bio-conjugation as it also protects cysteine residues of proteins from oxidative coupling.[332]

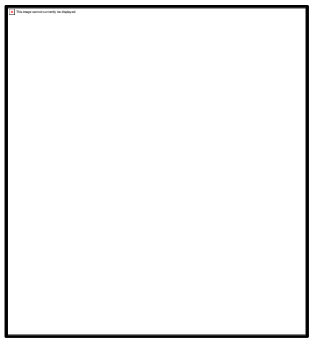

Figure 6.3: (A) TCEP, (B) TBTA molecular structures.

Since copper ions can easily undergo redox reactions if not properly chelated, the click chemistry requires the presence of an accelerating ligand to maintain a sufficient quantity of Cu^{+} in solution and in the right oxidation state. Among the known ligands, tris-(benzyltriazolylmethyl) amine (TBTA), (Figure 6.2-B) has been successfully used in bioconjugation.[321,325,333] TBTA has a tetradentate ability to bind copper, enveloping it in a way that no free binding sites are left for destabilising interactions.[333]

6.3. ABPs investigated in this project

In this study, we investigated two molecules as click chemistry reagents for labelling LSD1: (±)-*trans*-2-(4-(hex-5-yn-1-yloxy)phenyl)cyclopropanamine (**6.7**) and (±)-*trans*-2-(4-(prop-2-yn-1-yloxy)phenyl)cyclopropanamine (**6.8**, Figure 6.4).

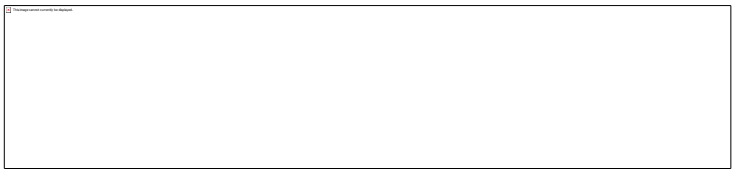

Figure 6.4: Molecular structures of the probes investigated as ABPs for LSD1 labelling.

Both molecules feature a TCP core, which is indispensable for LSD1 covalent inhibition. To the TCP structure, we introduced an alkyne appendix to allow the conjugation with an azide containing imaging tag via CC. The TCP core in **6.8** is connected to the alkyne moiety by a smaller carbon (propargyl) linker compared to **6.7** (hexynyl) and was provided by a collaborator from Münster University. The probe was originally designed to generate a molecular probe for MAO's labelling.

The synthetic route adopted to obtain probe **6.7** (Scheme 6.2), consisted in the nucleophilic substitution of 4-hydroxybenzaldehyde (**6.1**), which was reacted in DMF at reflux with 6-chlorohexyne, for 3 days. The remaining steps (from structure **6.2** to **6.7**), and specifically Horner-Wadsworth-Emmons reaction of **6.2**, Johnson-Corey-Chaykovsky cyclopropanation, Curtius rearrangement and amide formation, were performed according to the procedures described in Chapter 4.

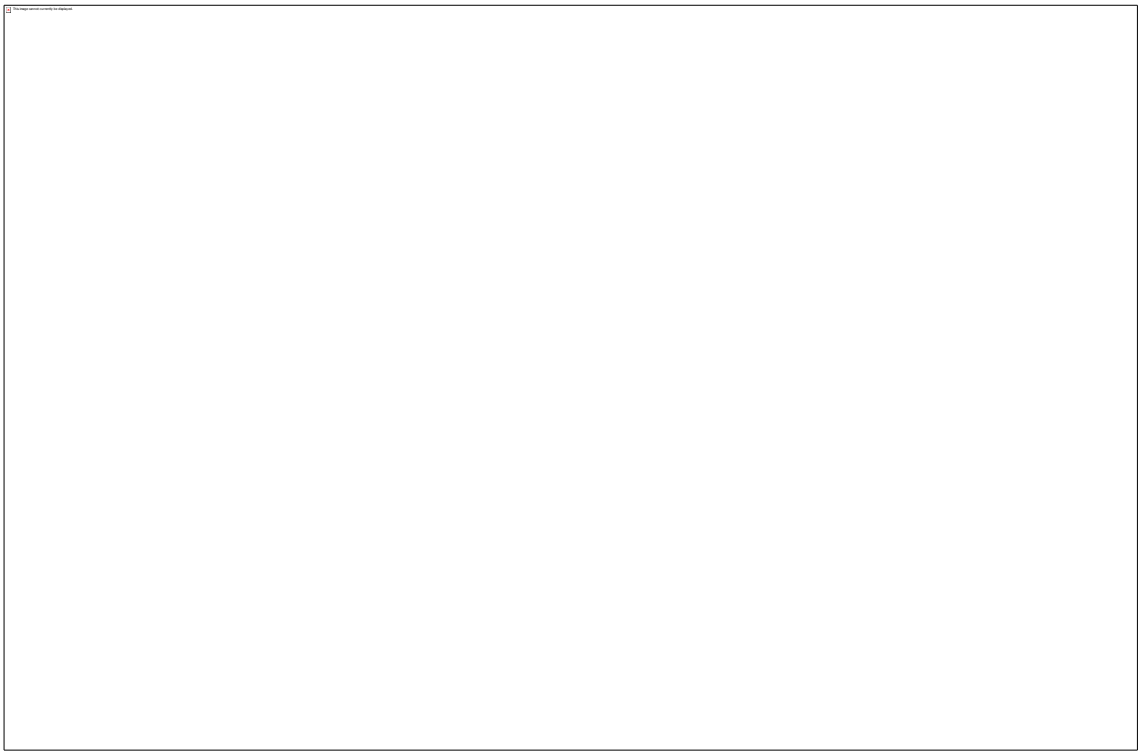

Scheme 6.2: Synthesis of ABP 6.7.

Thereafter, **6.7** and **6.8** were reacted in both enzymatic and cells experiments with the red-fluorescent tetramethylrhodamine-azide (TAMRA-azide, Figure 6.5).

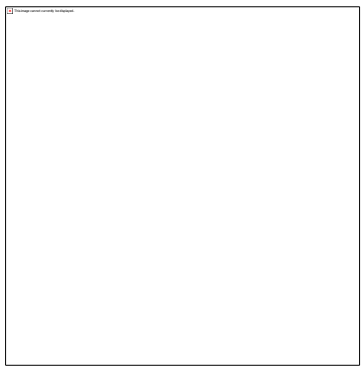

Figure 6.5: Structure of TAMRA-azide.

Given its ability to distribute evenly in cells cytoplasm and nucleus, the rhodamine fluorophore has been selected to label LSD1.[324,325,334]

Labelling LSD1 with **6.7** and **6.8** would follow the sketch shown in Figure 6.6. The compounds would occupy the LSD1 catalytic site forming a covalent adduct with the FAD. The alkyne tail, protruding from the phenyl ring would conjugate with the

TAMRA-azide under the CC conditions using TCEP, TBTA and $CuSO_4$ as source of copper. The labelled LSD1 would be then visualised with in-gel fluorescence scanning.

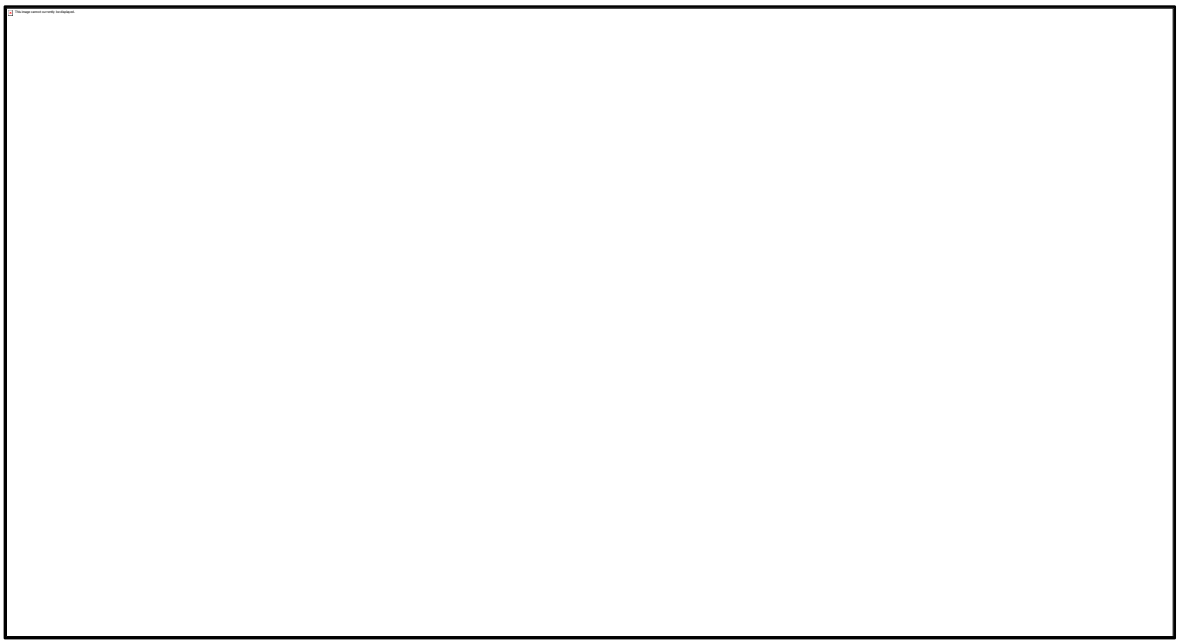

Figure 6.6: Mechanism for fluorescently labelled LSD1 with ABPs 6.7 and 6.8.

6.4. Biological evaluation

Before embarking into labelling experiments, enzymatic evaluation of **6.7** and **6.8** was carried out to verify if the incorporation of the alkyne interfered with the anti-LSD1 properties of TCP.

To this end, nine points concentration of ABPs **6.7** and **6.8** (50 µM, 25 µM, 12.5 µM, 6.13 µM, 3.1 µM, 1.6 µM, 0.8 µM, 0.4 µM and 0.2 µM) were incubated with purified recombinant LSD1 and the residual activity measured with Amplex®Red-peroxidase coupled assay using TCP as a positive control (Figure 6.7 and Table 6.1).

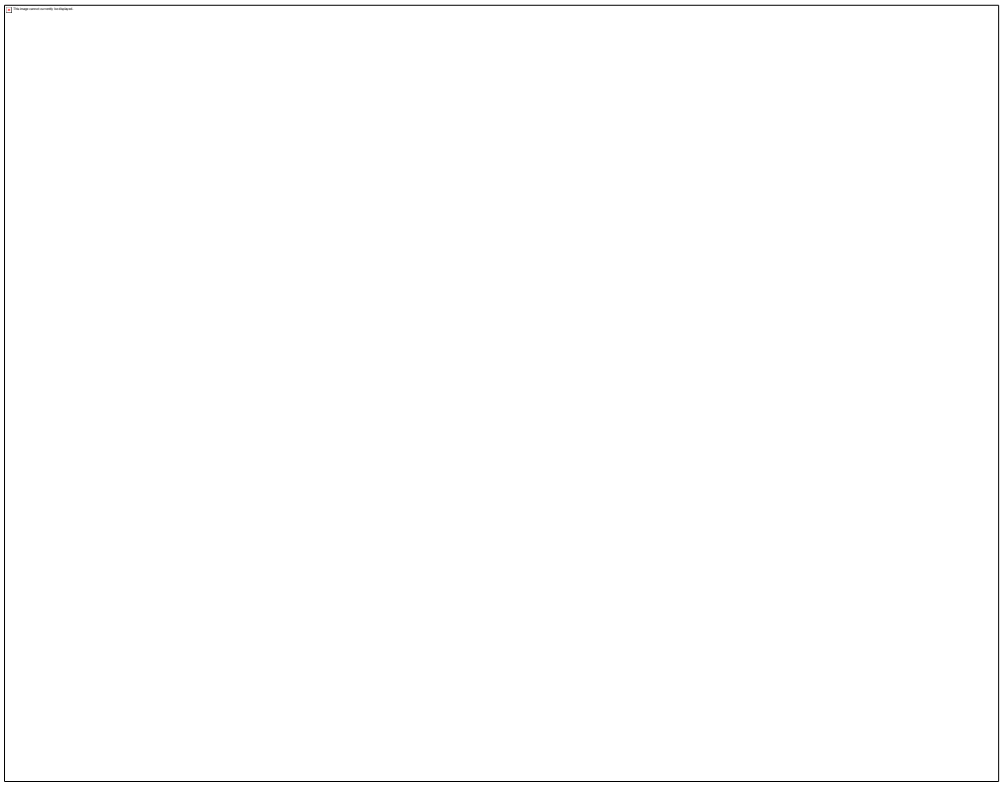

Figure 6.7: Dose-response curves showing the enzymatic activity of probes 6.7 (A), 6.8 (B) and TCP (C).
The X-axis is in logarithm of concentration (M, Molar); the Y-axis is the % of relative fluorescent unit (RFU) compared to 100% activity (LSD1 + substrate). Data were fitted with nonlinear regression and are shown as means ± STD (n=3).

Table 6.1: IC_{50}s values determined with enzymatic evaluation of 6.7 and 6.8 as LSD1 inhibitors.
Enzymatic results are expressed as % RFU normalised to pre-treatment level (LSD1 + Substrate, no inhibitor) ± STD (n=3).

Compound	IC_{50} (µM ± STD, n=3)
TCP	21±2.4
6.7	1.3±1.0
6.8	3.3±1.3

Enzymatic results proved that the incorporation of the alkyne moiety in **6.7** and **6.8** did not interfere with LSD1 inhibition and actually enhanced the TCP potency. The probe **6.7** was also assessed as anti-MAO A and B agent and similarly to what observed in LSD1, the introduction of the alkyne moiety in *para* to the TCP core promoted an increased potency, impeding MAO activities at µM range (Table 6.2). Therefore **6.7** could be potentially employed as an ABP to fluorescently label LSD1 and MAO.

Table 6.2: IC_{50}s values determined with enzymatic evaluation of 6.7 as MAOI.
Values are shown as means (µM) ± STD (n=3).

Compound	IC_{50} MAO A (µM±STD, n=3)	IC_{50} MAO B (µM ±STD, n=3)
TCP	14.4±0.7	1.9±0.6
6.7	2.4±0.8	0.4±0.06

Since the scope of this project included labelling cellular LSD1, the ability of the probe to modulate cell viability was also examined. Compounds were tested in HL-60 cells at eight different concentration points (30 µM, 10 µM, 3 µM, 1.0 µM, 3 µM, 0.1 µM, 0.03 µM, 0.001 µM, and 0.0003 µM) and following 72 h treatment, viable numbers were measured with CellTiter-Glo® (Table 6.3).

Table 6.3: IC_{50}s values obtained with cytotoxicity evaluation of 6.7 and 6.8 in HL-60 cells.
Values are shown as means (µM) ± STD (n=3).

Compound	IC_{50} HL-60 (µM±STD, n=5)
TCP	84±15.0
6.7	1.20±0.8
6.8	1.74±0.3

Cell viability results revealed the ability of both **6.7** and **6.8** to modulate cell growth of HL-60 cells at µM range. ABPs **6.7** and **6.8** were also tested in MV4-11 and THP-1 cells at 10 µM and 1 µM, significantly decreasing the cell proliferation at 1 and 10 µM in both the cell lines.

6.5. LSD1 labelling experiments

Given the favourable biological properties of **6.7** and **6.8**, we proceeded to assess their ability to fluorescently label LSD1, following the two step labelling procedure reported by Krysiak et *al.*[325] A preliminary proof-of-concept experiment was carried out to estimate the potency of the ABP, by examining the quantity of protein and probe required for CC and LSD1 visualisation. To this end, purified recombinant LSD1 (16.5 µg and 3.5 µg concentration) was incubated with **6.7** and **6.8.** The probes were used in excess compared to the IC_{50} in order to saturate the enzymatic pocket and enabling, potentially, a better visualisation of the labelled protein. ABPs **6.7** or **6.8** and LSD1 were allowed to interact for 1 h at room temperature and next, TAMRA-azide was conjugated via CC. To visually detect the labelling events, SDS-PAGE and in-gel scanning were employed (Figure 6.8).

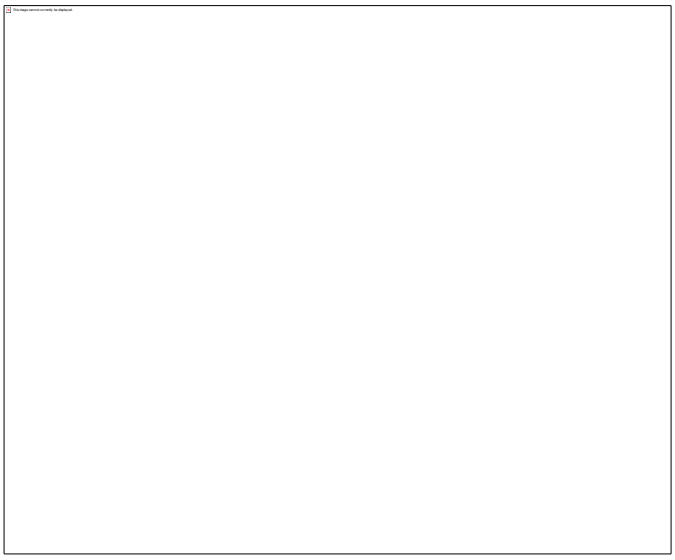

Figure 6.8: In-gel fluorescent scanning results of LSD1 labelling with 6.7 and 6.8 conjugated via CC with TAMRA.

Fluorescence was recorded with ImageQuant™ LAS 4000 Image Analyzer with a Fujinon VRF43LMD3 Lens and a 575DF20 filter at 573 nm.

Imaging results strikingly demonstrated the successful application of **6.7** and **6.8** as click reagents to label LSD1. However, the quantity of protein determined the quality of the labelling procedure as with reduced amount of enzyme (3.5 µg), lower intensity signals were detected. Additionally, no substantial differences were recorded between the two probes.

Prompted by these results, we further evaluated the ability of the probes to compete for LSD1 catalytic site and labelling the enzyme with an *in situ* labelling competition experiment. To this end, ABP **6.7** (10 µM) was incubated with LSD1 (16.5 µg) for 1 h, along with the LSD1 inhibitors **4.10** or **4.11** (200 nM), whereby the activity was widely described in Chapter 4. After incubation, TAMRA-azide was introduced by click chemistry to the alkyne moiety of **6.7**.

Figure 6.9: Molecular structure of LSD1 inhibitors used in a competition assay with ABPs 6.7 and 6.8.

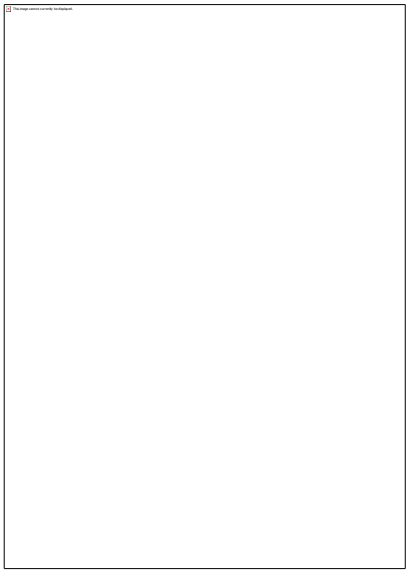

Figure 6.10: Results of in *situ* competitive assay using in-gel fluorescent scanning of ABP 6.7 with LSD1 inhibitors 4.10 and 4.11.

(A) Experimental conditions; (B) Loading control (Comassie blue staining); (C) Fluorescence intensity evaluation with ImageJ (compared to control = recombinant LSD1 only); in the X-axis are reported the different conditions used and Y-axis are reported the measured fluorescent intensity.

In-gel scanning revealed that **6.7** competed with LSD1 inhibitors **4.10** and **4.11** for the enzyme catalytic site. The simultaneous incubation of the probe with the potent LSD1 suppressors generated in fact a 20% decrease in signal (Figure 6.10) compared to the fluorescence intensity produced by **6.7** alone (corresponding to 100% fluorescence).
Similar results were obtained competing **6.8** and **4.11** simultaneous incubation (Figure 6.11).

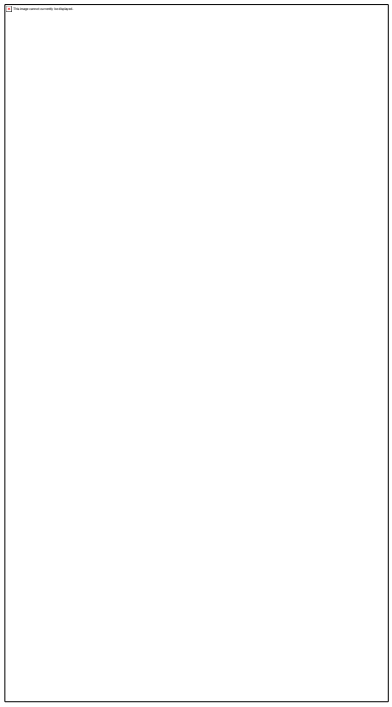

Figure 6.11: Results of in *situ* competitive assay using in-gel fluorescence scanning of ABP 6.8 with LSD1 inhibitor 4.11.

(A) Experimental conditions; (B) Loading control (Comassie blue staining); (C) Fluorescence intensity evaluation with ImageJ (compared to control = recombinant LSD1 only); in the X-axis are reported the different conditions used and Y-axis are reported the measured fluorescent intensity.

We next assessed the ability of **6.7** and **6.8** to label the LSD1 in complex proteomes. For such experiments, we used AMLs lines.
HL-60 cells were stimulated with 5 µM or 10 µM of probes **6.7** and **6.8** for 24 h and 72 h. To avoid interference of lyses buffers components with the CC conditions, cells were lysed by sonication. The amount of protein was adjusted for each CC reaction to 2 mg/mL and TAMRA-azide was added to the cells lysate along with ligand (TBTA) and the reducing agents (TCEP). The mixture was allowed to react for 1 h in the presence of

catalytic amounts of Cu^{+}. Electrophoresis of soluble and insoluble lysate fractions was next performed.[325] However no fluorescent signal was detected with such procedure.
After a first unsuccessful attempt, we next increased the CC reaction time in cell lysates from 1 h to 12 h and 24 h. Anyhow, even upon prolonged reaction times, we were unable to visualise the labelled enzyme. Similar conditions were also experimented using THP-1 and MV4-11, two AMLs lines whereby both **6.7** and **6.8** demonstrated anti-proliferative activities. Unfortunately, also in this occasion, the CC reaction did not yield a significant result.

6.6. Discussion

In this project, the aim of synthesising a molecular probe for LSD1 labelling has been partially achieved. The ABP **6.7** was successfully applied as a CC reagent to label purified LSD1 with a rhodamine chromophore. Another ABP, **6.8**, containing a small tether (propargyl linker) between the TCP core and the bioorthogonal CC partner alkyne, was also able to efficiently label the LSD1. As the molecules demonstrated to interact with both LSD1 and MAO families of oxidases, the optimisation of the labelling protocols with such ABPs, could provide a valuable way for fluorescently visualise both families of enzymes.
The fluorescently labelling abilities of **6.7** and **6.8** were next exploited in an *in situ* competitive assay. The probes were incubated with LSD1 along with the LSD1 inhibitors **4.10** and **4.11**. The results obtained proved the ability of the probes to compete for LSD1 catalytic site as a decrease in fluorescence was detected, suggesting that **4.10** and **4.11** occupation of the catalytic pocket, prevented the LSD1 interaction with the ABPs.

Disappointingly, the probe failed to label LSD1 in a complex biological system as whole cells.
These conclusions held true after adjusting the initial CC protocol used by Krysiak *et al.* for MAOs labelling with alkyne containing Deprenyl derivatives.[325,334] However, with longer reaction times, longer time-course treatment with the ABPs as well as using different AMLs lines, the click chemistry reaction with TAMRA azide did not proceed in our case, to any visualising extent. The cell lines used express only endogenous

LSD1 and thus the amount present were probably not sufficient to be visualised with the used ABP's. The inefficiency of the CC in cells specimens could reside in many factors and first of all the used chromophore. Although TAMRA-azide properties of evenly distribution in cells and efficiently diffuse into cytosol and nucleus have been widely proved in unpermebilised cells,[327] the results reported here suggested a potential inability of the fluorophore to diffuse across the cells membranes and reach its click partner. The chromophore could have associate with different intracellular organelles and accumulate in other cell compartments,[335–339] limiting the quantity needed to perform CC. The use of different commercially available fluorophores-azide and light microscopy observation of fixed cells could have been employed to evaluate the extent of these hypothesised events in influencing the ABP potency. To perform the CC we used TBTA as ligand and TCEP as a reducing agent. TBTA was used at substoichiometric amounts in relation to the Cu^{+} concentrations (0.1:1 mM), due to its poor solubility.[321,325] Therefore to increase the CC yield and enable the fluorescence visualisation we could have increased the TBTA concentration or employed other available ligands, such as the water-soluble tris (3-hydroxypropyltriazolylmethyl) amine (THPTA).[321,333] Furthermore, although TCEP is commonly used as a valuable reducing agent in bioconjugations,[321,340] it can reduce the azide conjugated with the chromophore to amine and therefore interfere with the CC reaction yield.[341]

6.7. Conclusions and future work

In conclusion, two molecular probes were evaluated as alkyne reactive partners in CC reaction for LSD1 labelling.

Both the tested probes were able to inhibit LSD1 enzymatically at µM range and cell evaluations prove their ability to hinder cellular proliferation. Both probes were able to label pure His-tagged human recombinant LSD1 when conjugated with click chemistry with an azide containing reporter rag (TAMRA-azide), partially fulfilling the aims of the project. *In situ* labelling competitive experiments were also accomplished. Unfortunately, we were not able to visualise LSD1 in cell lysate and further work will be carried out to optimise these pioneering experiments.

Using cells overexpressing exogenous LSD1 could increase the amount of LSD1 and increment the chance of successfully label the target protein. Light microscopy analysis of the fate of the reporter tag in cell lysate could help to identify more suitable fluorophores for LSD1 visualisation in AMLs. Using different ligands instead of TBTA and other reducing agents could also improve the CC yield and potentially enable a better visualisation of the labelled enzyme.

Notwithstanding, these molecules are the first ABP specific for labelling LSD1, opening new venues for LSD1 labelling studies.

Chapter 7 - Towards the discovery of novel inhibitors of LSD1

7.1. Introduction

In this project, resulting from multiple collaborations, compounds of different natures were evaluated as potential inhibitors of LSD1. The molecules were first assessed in an enzymatic assay using Amplex®Red.[170] Having LSD1 a salient role as an oncogene,[342] the anticancer potential of enzymatically active inhibitors was examined in cancer cells.

7.2. Evaluation of TCP analogues from a library of active phenylcyclopropylamines

A series of substituted phenylcyclopropylamines was the first series of compounds to be tested (Figure 7.1). These were synthesised by Prof. Günter Haufe group at the University of Münster and display substituents at the TCP core. The majority of them also have a fluoro group at the cyclopropyl ring.

Figure 7.1: Library of phenylcyclopropyl amines MAOIs tested as LSD1 inhibitors.

The compounds were first tested with Amplex®Red at 50 µM and 10 µM and molecules proving to suppress LSD1 at such doses were tested in a broader range of concentrations in order to determine the IC_{50}s from dose-response curves (Table 7.1).

Table 7.1: IC_{50}s values obtained with enzymatic evaluation of fluorinated TCP measured with Amplex®Red assay.

Enzymatic results are expressed as % RFU normalised to pre-treatment level (LSD1 + Substrate, no inhibitor) ± STD (n=3).

Structure	LSD1 enzymatic activity (IC_{50} µM±STD *n=3*)
7.1 (TCP)	21
7.2	> 50
7.3	6.8±1.3
7.4	> 50
7.5	>50
7.6	> 50
7.7	1.2±0.1
7.8	> 50
7.9	1.5±2.8
7.10	> 50
7.11	> 50
7.12	> 50
7.13	> 50
7.14	> 50
7.15	6.7±0.3
7.16	4.1±0.03
7.17	8.2±0.8
7.18	9.2±0.05
7.19	8.4±0.3
7.20	>50

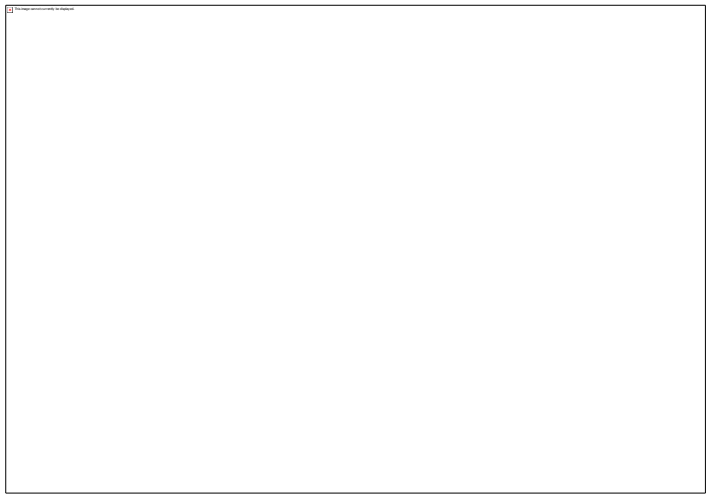

Figure 7.2: Dose-response curves determined with Amplex®Red assay.

The X-axis is the logarithm of concentration (M, Molar); the Y-axis is the % of relative fluorescent unit (RFU) compared to 100% activity (LSD1 + substrate, no inhibitor). Data were fitted with nonlinear regression and are showed as means ± STD (n=3); TCP was used as a positive control.

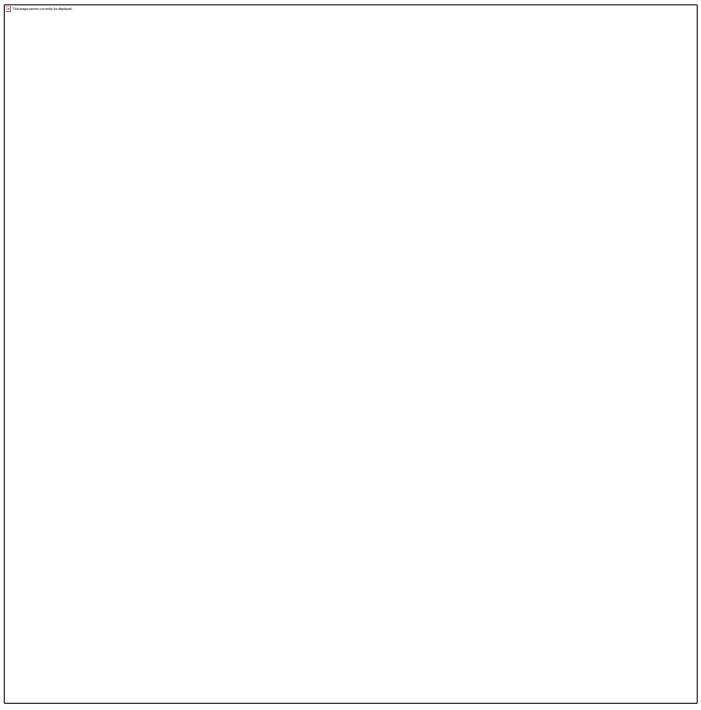

Figure 7.3: Dose-response curves determined with Amplex®Red assay.

The X-axis is the logarithm of concentration (M, Molar); the Y-axis is the % of relative fluorescent unit (RFU) compared to 100% activity (LSD1 + substrate). Data were fitted with nonlinear regression and are data are showed as means ± STD (n=3). TCP was used as a positive control.

Compounds **7.3**, **7.5**, **7.7**, **7.15**, **7.16**, **7.18** and **7.19** were more active than TCP, implying that compounds with *trans* configuration and bearing fluoro at the cyclopropyl ring, have enhanced activity compared to phenylcyclopropylamines with *cis* configuration.

Compound **7.2**, with a hindering benzyl on the cyclopropyl nitrogen was devoid of activity. The substituents at TCP scaffold greatly influenced the drugs effect on LSD1 enzymatic inhibition. Phenyl substitutions in *meta* potentiated the activity: the fluorinated phenylcyclopropylamines containing NO_2 was able to inhibit LSD1 activity at low µM range (IC_{50}s < 10 µM) and *meta* substituted molecules with strong donor groups (-OMe and -F) displayed the best activities within the series. Surprisingly, **7.16**, albeit having a *cis* configuration, demonstrated to contrast the enzyme demethylation at low concentrations. Derivatives with CF_3 and F_5S substituents at the phenyl ring also revealed to actively suppress LSD1.

Thereafter, the enzymatically active compounds **7.7**, **7.9**, **7.15**, **7.16**, **7.18** and **7.19** were selected for cellular evaluations. The time course and concentrations were chosen according to the biological results obtained with our LSD1 inhibitors. HL-60, THP-1, MV4-11, OCI-AML3 and KASUMI cells were treated with increasing concentration the inhibitors (0.001 µM, 0.003 µM, 0.1 µM, 0.3 µM, 1 µM, 3 µM, 10 µM and 30 µM). Following 72 h treatment, cell survival rates were detected with CellTiter-Glo®.

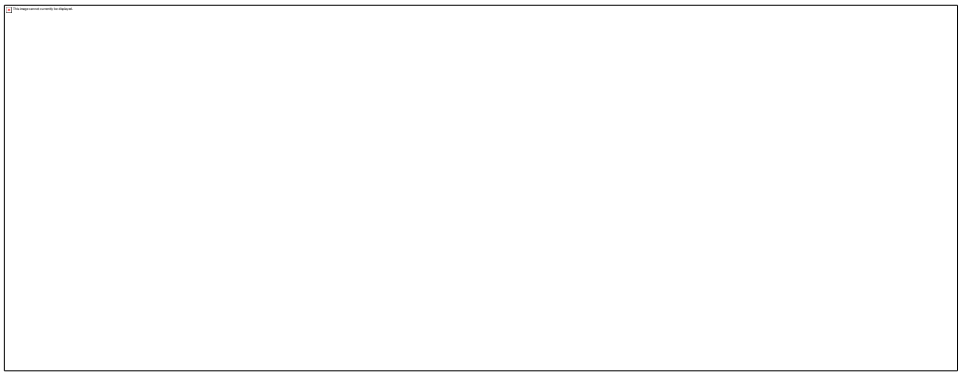

Figure 7.4: Dose-response curves showing the effects of fluorinated phenylcyclopropylamines 7.3 on AMLs proliferation (72 h).

The X-axis is in logarithm of concentration (M, Molar), Y-axis is the % of RLU (relative luminescence unit) compared to 100% activity (vehicle control, DMSO). Data are shown as means ± STD (n=5).

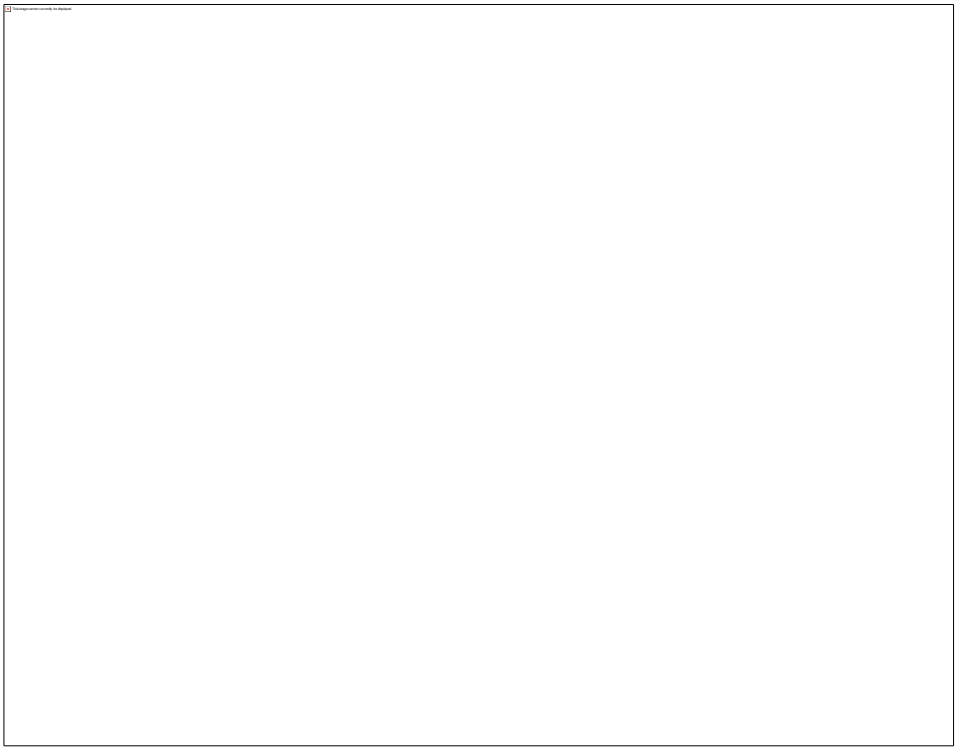

Figure 7.5: Dose-response curves showing the effects of fluorinated phenylcyclopropylamines 7.7 on AMLs proliferation (72 h).

The X-axis is in logarithm of concentration (M, Molar), Y-axis is the % of RLU (relative luminescence unit) compared to 100% activity (vehicle control, DMSO). Error bars correspond to STD (n=5).

Figure 7.6: Dose-response curves showing the effects of fluorinated phenylcyclopropylamines 7.15 on AMLs proliferation (72 h).

The X-axis is in logarithm of concentration (M, Molar), Y-axis is the % of RLU (relative luminescence unit) compared to 100% activity (vehicle control, DMSO). Data are shown as means ± STD (n=5).

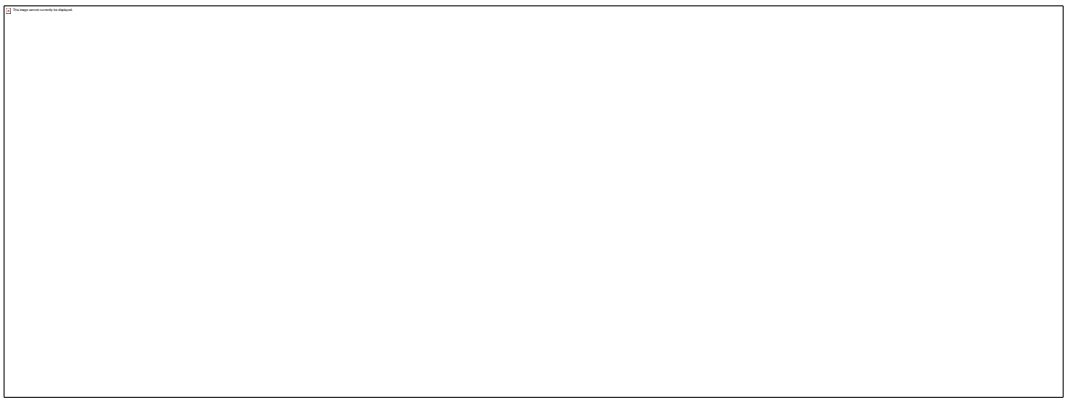

Figure 7.7: Dose-response curves showing the effects of fluorinated phenylcyclopropylamines 7.16 on AMLs proliferation (72 h).

The X-axis is in logarithm of concentration (M, Molar), Y-axis is the % of RLU (relative luminescence unit) compared to 100% activity (vehicle control, DMSO). Data are shown as means ± STD (n=5).

Table 7.2: IC_{50}s values obtained with cytotoxicity evaluation of fluorinated phenylcyclopropylamines on AMLs proliferation.

Values are reported in µM ± STD (n=5); nt: not tested.

	Compounds						
Cell line	**7.3**	**7.7**	**7.15**	**7.16**	**7.17**	**7.18**	**7.19**
OCI-AML3	>30	nt	1.0±3.2	nt	>30	nt	>30
MV4-11	>30	1.9±0.3	4.9±0.4	8.2±0.4	nt	>30	nt
KASUMI	nt	3.4±0.2	nt	nt	>30	nt	>30
THP-1	>30	8.5±0.3	1.6±0.3	7.0±0.2	>30	nt	>30
HL-60	18.6±1.7	nt	3.9±0.4	nt	nt	>30	nt

The results obtained in cellular experiments strengthen the data observed with the enzymatic assay. Compounds **7.7**, **7.15** and **7.16**, which were able to suppress the activity of recombinant LSD1 at low concentrations were the most potent anti-AML agents. However, the Nitro substituted derivative **7.3**, displayed only moderate activity in HL-60 cells, whereas fluorinated TCP derivative containing CF_3 and F_5S **7.17-19** despite being more active than TCP in the cells-free assay, were unable to modulate cells growth at the tested concentrations.

To verify whether the anti-proliferative effects were linked to LSD1 suppression, we examined the downstream expression levels of molecular markers associated with LSD1 pharmacological inhibition. We chose to perform the experiments with **7.7**, which hindered MV4-11 cell line proliferation at low concentrations. This AML model is representative of the FLT-3 mutation, associated with poor prognosis of AML patients and drug-resistance.[308,309] Immunoblotting of MV4-11 cells treated with **7.7** (0.3 µM, 1 µM, 3 µM, and 6 µM) proved a concentration dependent accumulation of methylated histone (Figure 7.8). In addition, we measured the expression levels of CD86 and after 48 h incubation (3 µM), flow cytometry results revealed an increase in the analysed parameter by 98.4%, further substantiate that the pharmacological effects are LSD1-dependent.

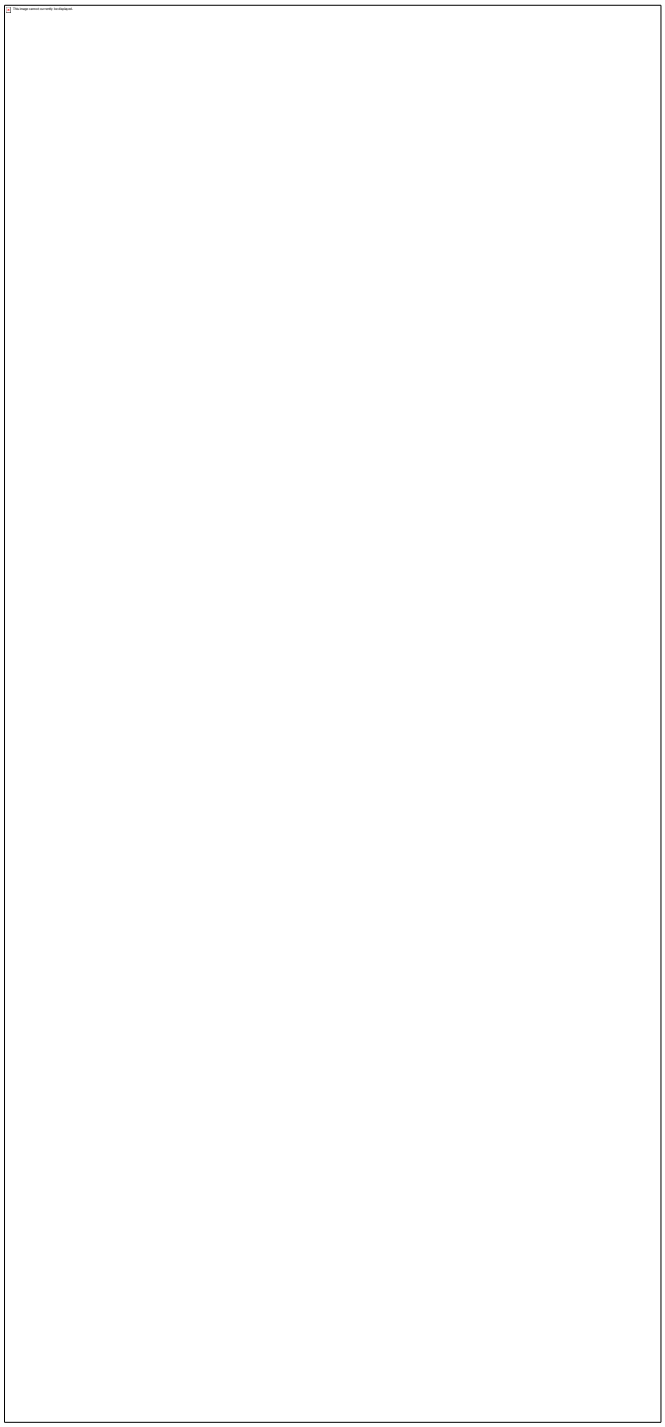

Figure 7.8: Molecular effects of fluorinated tranylcypromine 7.7 on MV4-11 cells.

(A) Western blot: cells were treated with increasing concentrations of **7.7** and protein separated with 14% polyacrylamide gel. Blotting membranes were probed for anti-H3K4me2, H3 (total) and β-actin (control); **(B)** CD86 induction: cells were gated based on FSC and SSC parameters. In the X-axis is reported the mean fluorescence increase of treated cells stained with CD86-FITC conjugated antibody and the fluorescent increase of the control (untreated cells). The Y-axis is the cell count. **(C)** Statistical significance for CD86 evaluations determined with Student's t-test; values are expressed as means % of increase (compared to control) ± STD (n=3); ****$p < 0.0001$.

7.3. Evaluation of *Cis*-cyclopropylamines

A total of four *cis*-cyclopropylamines provided by Prof. Sven Mangelinckx group at the Ghent University, Belgium, were also tested as possible LSD1 inhibitors (Figure 7.9). The compounds were synthesised based on docking studies as potent MAO inhibitors and are racemic *cis*-cyclopropylamine with an alkoxy group at the 2-position of the cyclopropyl ring, replacing the more common phenyl substituent.[343]

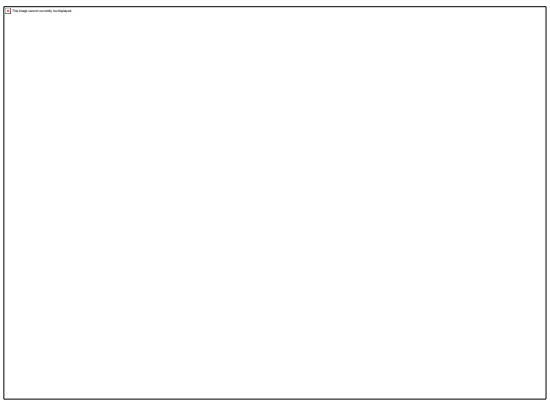

Figure 7.9: *Cis*-cyclopropylamines molecular structure.

The compounds however were inactive at the maximum tested concentration (50 µM). Despite that, **7.21** and **7.24** proved to bind covalently to MAOs and hinder the monoamine oxidases activity at nM concentrations. In addition, the compounds inactivate preferentially MAO B. Enzymatic and computational studies revealed in fact that **7.24** is four times more selective towards MAO B (5 nM) and over 20-fold more potent than TCP. Lacking the activity on LSD1, the compound structure can be used as a lead to design selective MAO B inhibitors to be employed as antidepressant.[343]

7.4. Evaluation of a library of pargyline analogues

In 2005, pargyline, a known MAO inhibitor, was utilised in linking LSD1 activity to AR-dependent gene activation.[146] Based on this study, Culhane *et al*. generated a peptide, corresponding to the N-terminal H3, having the Lys in position 4, modified with a propargyl moiety (Scheme 7.1).[213] Such structures were extremely active as LSD1 inhibitor. Subsequent MS and NMR studies[158] revealed the mechanism underlying the demethylase inhibition by the peptide; this would start with the oxidation of the amine to the propargylic iminium ion, which undergoes Michael addiction to the N^5 of the flavin ring, forming a stable adduct.

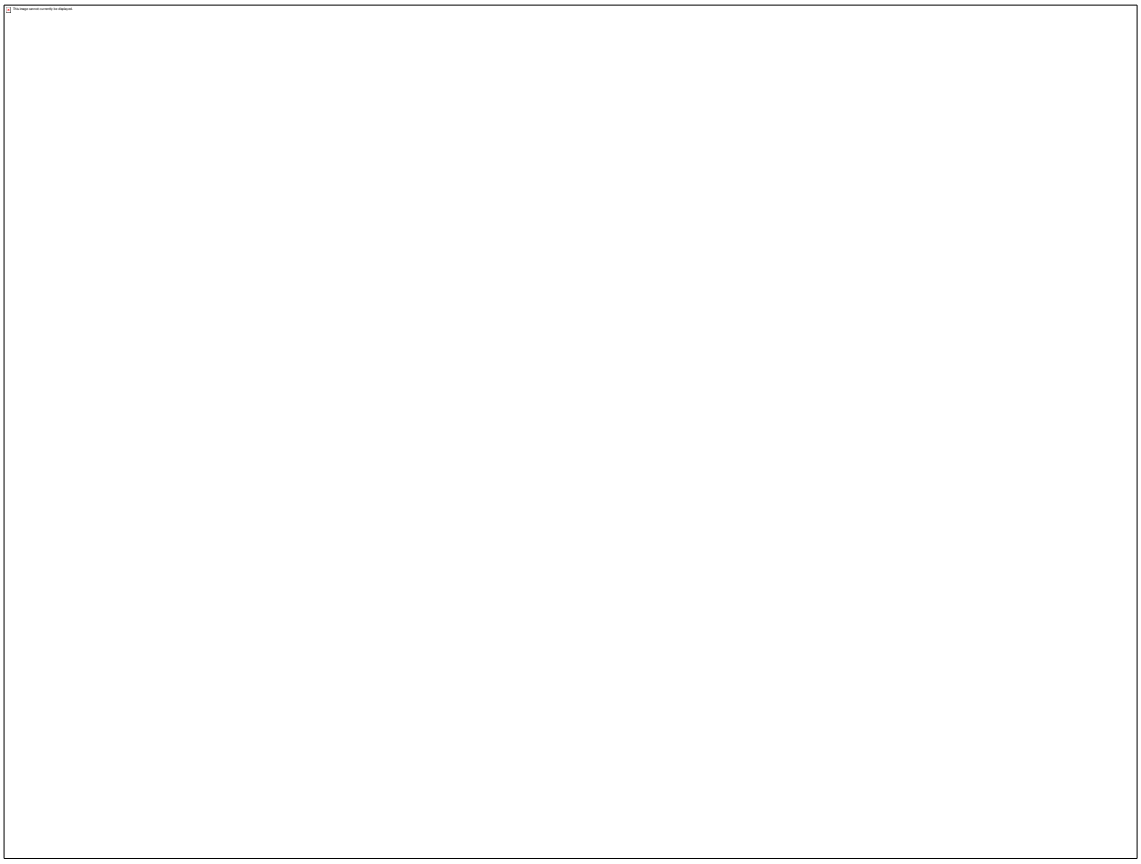

Scheme 7.1: Mechanism based inhibition of modified H3 N-terminal peptide (7.25) containing a propargyl moiety.

Adapted from Culhane *et al.*[213]

In keeping with these works and with the goal of finding new suitable scaffolds for LSD1 inhibition, we tested a series of propargylamine derivatives (Figures 7.10).

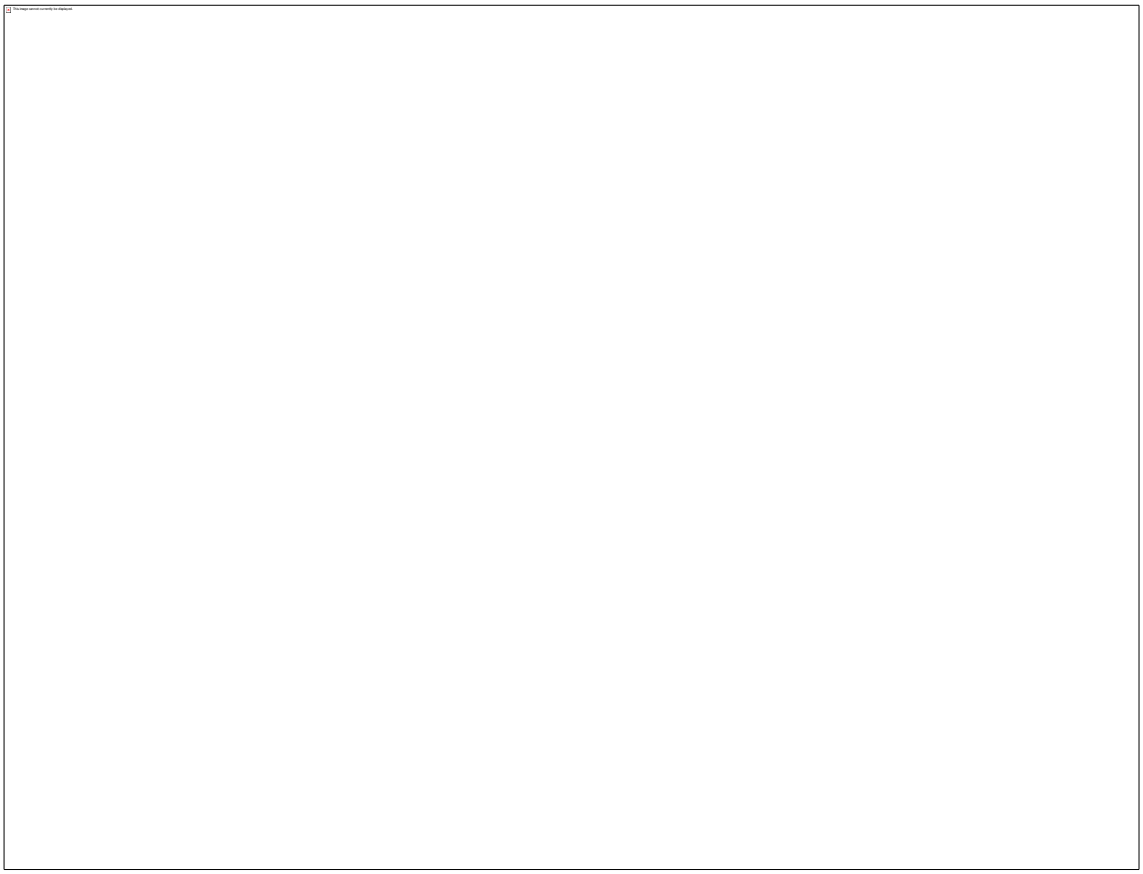

Figure 7.10: Pargyline analogues tested as LSD1 inhibitors.

Within this series, only compound **7.33** displayed enzymatic activity at 30 µM. However, this was devoid of anti-proliferative potential in AML cell lines.

7.5. Conclusions

In this project we evaluated 49 compounds with diverse chemical nature as LSD1 inhibitor. Several compounds belonging to a series of TCP analogues designed as MAOIs efficiently suppress the LSD1 activity in a cell-free assay (µM concentrations) and actively inhibit the proliferation of AML cell lines. For this series, the stereochemistry appears to be crucial as the compounds with *trans* configurations were more efficient than the *cis*. Micromolar concentrations of compound **7.7** were able to increase cellular levels of H3K4me2 and induce the expression of CD86 in MV4-11, linking the pharmacological profile with the LSD1 inhibition.

Cis-cyclopropylamines and pargyline analogues were in contrast unable to hinder LSD1 enzymatic activity at the maximal dose of 50 µM. Nonetheless, the *cis*-cyclopropylamine **7.4** revealed to be a potent MAOI and the structural features will be exploited for the design of novel antidepressant.

General conclusions and final remarks

The research conducted here broadened the current knowledge on the epigenetic target LSD1. The study encompassed two phases: a first one where we researched on potential reversible inhibitors and a second one on irreversible inhibitors of LSD1.

Based on previous studies on the SNAG-domain of Snail-1, we synthesised truncated peptide analogues of this LSD1 binding partner. By length scanning, ala-scanning and single-point mutations to the critical amino acid of SNAG we generated a series of peptides with interesting biological activity. The work extended the knowledge on LSD1 protein recognition and LSD1 binding mode with the SNAG-family of proteins. In addition, several X-ray tri-dimensional crystal structures of the synthetic peptides bound to the LSD1 catalytic pocket supported the work. This could be further exploited for virtual screening and docking studies. The peptides arrest cancer cell proliferation and modulate the LSD1-dependent transcriptional pathways such as H3K4me2 levels in AMLs and TMPRSS2, mimicking the activities of covalent inhibitors. The findings of the first part of the work were then combined to Phage display technology to research onto novel non-covalent-inhibitors based on PRSFLVRKP peptide. Such peptide demonstrated high affinity to the LSD1 catalytic site and therefore, it was used as a competitor of a Phage display library of peptides. Three peptides were identified with this technique and albeit these displayed poor activity in a cell-free assay, the information acquired could be used as a starting point to carry onto the application of Phage display technology to target LSD1.

The second part focused on the search of novel irreversible inhibitors of LSD1. Based on the structure of TCP we developed an efficient synthetic method for the generation of multiple structural analogues. Eighteen new TCP derivatives were generated, displaying hindering elements at the phenyl ring. Their ability to suppress LSD1 was evaluated with a fluorometric assay and the results revealed an improved activity compared to the TCP scaffold. The active analogues were next evaluated in an extended panel of acute myeloid leukaemia cells where they showed nM potency in arresting cancer cells growth and promoting cell differentiation. In addition, selected molecules displayed enhanced potency compared to TCP in arresting the proliferation of prostate adenocarcinoma cells. Surprisingly, in the course of this study, synthetic intermediates of TCP analogues presented exceptional cellular effects. Being protected at the nitrogen

of TCP cyclopropyl ring, the compounds lacked the enzymatic activity but were potent anti-cancer agents in prostate and leukaemia tumours. From this initial observation, we made additional *N*-protected synthetic intermediates to have a further insight on such unexpected pharmacology. The data gathered substantiated an LSD1 mediated process involved in the observed effects; however, more research is required to further clarify the exact mechanism of action.

We also explored activity based probes to label fluorescently LSD1 by synthesising a TCP analogue with an alkyne moiety. The molecule was exploited as a bioorthogonal partner of an azide containing imaging tag. We were pleased to verify that the ABP successfully labelled recombinant LSD1. However, we were unable to fluorescently label LSD1 in whole cells. Further work is needed in such area to optimise the visualisation of cellular LSD1.

Collectively, this thesis constitutes a valuable methodological framework to target LSD1 pharmacologically, providing several approaches through which reversible and irreversible inhibitors can be designed. Additionally, it further supports the role of LSD1 in cell growth in a spectrum of cancer cell lines bolstering the hypothesis that selective LSD1 inhibitor might represent an effective therapeutic tool in the future.

Chapter 8 - Experimental procedures

8.1. General procedures for Chemistry

All chemicals were purchased from Sigma Aldrich, Lancaster Synthesis GmbH, Alfa Aesar, and Novabiochem. All Fmoc-amino acids, solvents and reagents for peptide synthesis were purchased from AGTC.

Resins were purchased from Millipore AGTC.

All anhydrous solvents were purchased as Aldrich®sure/seal bottles. All solvents were reagent grade and, when necessary, purified and dried by standard methods. TLC was used to monitor the reaction and performed on aluminium-backed silica gel coated plates (Merck DC, Alufolien Kieselgel 60 F_{254}) with spots visualized by UV-light (λ 254 nm) or stained with dyes (potassium permanganate solution or ninhydrin), followed by heating. Organic solutions were dried over anhydrous $MgSO_4$ prior to product concentration. Product concentration after reactions and extractions involved the use of a rotary evaporator operating at reduced pressure of ca. 20 Torr and the term *in vacuo* refers to solvent concentration at reduced pressure. Products were normally purified with column flash chromatography using silica gel (MN Kieselgel 60, 40-63 μm, 230-400 mesh ASTM).

NMR spectra were recorded on a Bruker AC 400 spectrometer at 400 MHz for ^{1}H NMR and 100 MHz for ^{13}C NMR; Spectral data were reprocessed with Bruker Topspin 3.2 software or MESTRENOVA. The spectra were calibrated to the residual deutereted solvent peak ($CDCl_3$, CD_3OD, DMSO-*d*6). The chemical shifts are reported in δ (ppm) units followed by brackets containing spectra details in this order: multiplicity (s: singlet, d: doublet, t: triplet, q: quartet, m: multiplet, br: broad), coupling constants (reported in Hz), number of protons (from integration). ^{13}C HNMR were reported with chemical shifts.

High-resolution mass spectra (HRMS) were acquired through the EPSRC National Mass Spectrometry Service Centre, Swansea. Melting points were determined with a STUART Melting point SMP10. Infra-red (IR) spectra were determined with Perkin Elmer, Spectrum GX, FT-IR system. The spectra were analysed with Spekwin 32 and reported as absorptions as wavelengths in cm^{-1}.

When necessary, gross purification was performed with Biotage Isolera Four using a 12 g C18 cartridge and a gradient from 95:5 water: methanol → 5:95 water: methanol with 0.05% TFA additive over 50 minutes and a flow rate of 50 mL/min. Collection was monitored by UV at 214 and 254 nm.

RP-HPLC analyses were performed with an Agilent Technologies 1200 series chromatograph with an Agilent Technologies ZORBAX Eclipse XDB-C18 (5 µm, 4.6×150 mm) column. Gradient used: 95:5 water: methanol with 0.05% TFA additive to 5:95 water: methanol over 15 min returning to 95:5 water: methanol over 5 min at a flow rate of 1 mL/min. Small scale purification was achieved with STDi prep RP-HPLC on a Agilent Technologies 1200 series chromatograph using an Agilent Technologies ZORBAX Eclipse XDB-C18 (5 µm, 9.4×250 mm) column with a flow rate of 4 mL/min (same gradient as above).

MALDI-ToF was performed on a Shimadzu Biotech MALDI-TOF spectrometer (Kratos), using as a matrix composed α-cyano-4-hydroxycinnamic acid in HPLC-grade methanol (5 mg/500 µL) used in a proportion of 1:1 with the tested peptide. Automated synthesis was performed on a 24-reactor block SYRO Multiple Peptide Synthesizer (Syro I, Multisyntech GmbH), equipped with a vortexing unit (Multisyntech, Witten, Germany).

8.2. General procedures for Biology

Unless otherwise stated, all the reagents were purchased from commercial sources as Sigma Aldrich (Poole, UK) and Fisher Scientific (Loughborough, UK). Centrifuge used were RC-M150 GC, RC-5B UltraPro80, Sorvall GmbH, Hamburg and 5451C Mini spin plus, Eppendorf AG, Hamburg. The raw data collected were normalised to controls and IC_{50}s and statistical significance were determined using GraphPad Prism 6 software (San Diego, CA).

8.2.1. Cell culturing

The diverse AML cell lines used for the biological evaluations were obtained from DMSZ (German Collection of Microorganisms and Cell Cultures) and European Collection of Cell Cultures. They were authenticated by DNA-fingerprinting. Prof. Kristian Bowles, UEA Medical Centre, Norwich, UK, provided the library of AML cell lines. The cell lines were used at low passage number for a maximum of 6 months post-resuscitation and tested regularly for mycoplasma infection.

AML cell lines (THP-1, HL-60, MV4-11, KASUMI, OCI-AML3, and U937) were cultured in RPMI 1640 medium (GIBCO) supplemented with 10% Foetal Calf Serum (FCS, GIBCO) and 5% of 2 mM L-glutamine and penicillin/streptomycin (P/S, Fisher). Cells were grown at 37 ˚C with 5% CO_2. Cells concentration was maintained at 25×10^4 cells/mL.

8.3. Experimental procedures for Chapter 2

8.3.1. Solid phase peptide synthesis (SPPS)

8.3.1.1. Swelling resin (Wang, Rink AM, NOVA-peg)

Dry resin (100-600 mg) was placed in a SPPS reactor with a sintered filter and covered with DMF. The resin was shaken in an orbital shaker for 45 min and if necessary deprotected with a solution of 20% pyridine in DMF (v/v%).

8.3.1.2. Resin loading

Wang resin was loaded with the symmetrical anhydride procedure followed capping of unreacted amino acids. To this end, the resin was reacted for 10 min with a solution composed of 9:1 pyridine:acetic acid.
Rink Amide resin was loaded with the first amino acid (5 equiv.), PyBOP (5 equiv.) and DIPEA (10 equiv.), which were added to the deprotected resins and allowed to react in DMF for 45 min with constant agitation. The resin loading with rink amide was repeated twice to ensure complete loading.

8.3.1.3. PyBOP® coupling and deprotection

Chain elongation was achieved using 2.5 equiv. of protected amino acid with respect to resin loading. Amino acids were dissolved in DMF and PyBOP® (2.5 equiv.) DIPEA (5 equiv.) were used as coupling agents. The reaction mixture was allowed to react for 45 min 45 min followed by washing off the resin with DMF. The coupling reaction was repeated twice for each amino acid. Removal of Fmoc groups was achieved using 20% piperidine in DMF over 10 min followed by washing with DMF. The deprotection step was repeated to ensure completion (2 additional times, each one 5 min, for a total of 3 times). Once chain elongation was completed, the resin was dried down using DCM followed by DCM:MeOH 1:1 and dried by application of vacuum. Coupling and

deprotection steps were monitored with colorimetric tests such as ninhydrin (Kaiser) or chloranil.

8.3.1.4. Kaiser test and chloranil tests

Kaiser test

After 5 washes with EtOH, a small amount of resin beads were used to verify the absence of free amine by adding 3 drops of each Kaiser test solution to the beads, followed by heating. The blue colour appearance indicated the presence of free amine and therefore the incomplete coupling.

Kaiser test solutions

Solution A: 2% KCN/H_2O (v/v);

Solution B: 5% ninhydrin (w/v) 98% pyridine (v/v) in Ethanol;

Solution C: 4:1 phenol (w/v) in EtOH;

Chloranil test

After 5 washes with DMF, a small amount of resin beads were used to verify the absence of free amine by adding 3 drops Chloranil test solution to the beads followed by heating. The green colour appearance indicated the presence of free amines.

Chloranil test solutions

Solution A: 2% Chloranil in DMF (w/v);

Solution B: 2% acetaldehyde in DMF (v/v);

8.3.1.5. Automated synthesis

Automated peptide synthesis was employed for the generation of peptides **2.3**, **2.4**, **2.5**, **2.6** and **2.7** using Fmoc-*t*Bu strategy and PyBOP/DIPEA as coupling reagents. Fmoc deprotection was achieved with 20% piperidine solution in DMF (v/v%).

General scheme for automated peptide synthesis is shown in Table 8.1

After completion, the completed peptide was removed from the automated synthesiser and the resin beads washed from any residual DMF with multiple DCM washes. Global deprotection and purification were performed next as described below.

Cycle	Steps	Conditions	Time
1	***Swelling***	DMF shaking (5 mL)	1 h
2	***Loading***	First amino acid (5 equiv.) PyBOP (5 equiv.) DIPEA (10 equiv.)	3 h; the loading is repeated twice
	Washing	DMF (5 mL×3)	5 min; the washes are repeated three times
	Fmoc removal	Piperidine (20%) Solution in DMF (2 mL)	15 min; the cleavage is repeated twice
	Washing	DMF (5 mL)	5 min
3	***Coupling***	Second amino acid PyBOP (2 equiv.) DIPEA (2.5 equiv.) DMF (2 mL)	1 h; the coupling is repeated twice
	Washing	DMF (5 mL)	5 min; the washes are repeated three times
	Fmoc removal	Solution of piperidine (20% in DMF)	15 min; the cleavage is repeated twice
	Washing	DMF (5 mL)	5 min; the washes are repeated three times
	The Cycle 3 is repeated until the last amino acid of the desired sequence is loaded		
	Manual washing	DCM	4 min

Table 8.1: **Protocol for automated peptide synthesis with Syro I.**

8.3.1.6. Global deprotection and resin cleavage

Global deprotection and resin cleavage were achieved by treating the resin with a cleavage cocktail composed by TFA:DCM:TIPS 95:2.5:2.5 for 3 h with constant agitation. The TFA solution containing the crude peptide was filtered off and the resin washed with neat TFA (2 mL). The TFA contained in the crude was removed by rotary evaporation and the residue precipitated in Et_2O. The excess of Et_2O was decanted and the peptide recovered by filtration. The peptide was dissolved in H_2O with drops of acetic acid if necessary and lyophilised.

8.3.1.7. Peptide purification

Analytical RP-HPLC was employed to determine the purity of the product after synthesis and between purification steps. Gross purification was performed on a Biotage Isolera Four using a 12 g C18 cartridge and a gradient from 95:5 water:methanol → 5:95 water:methanol with 0.05% TFA additive over 50 minutes and a flow rate of 20 mL/min. Collection was monitored by UV at 214 and 254 nm. Fractions were then reassessed by analytical RP-HPLC. Fractions suspected of containing the target peptide were recovered by lyophilisation, their mass determined using MALDI-TOF and purified further using STDi-preparative RP-HPLC on a Agilent Technologies 1200 series chromatograph using an Agilent Technologies ZORBAX Eclipse XDB-C18 (5 µm, 9.42×50 mm) column with a flow rate of 4 mL/min. Final identity of peptides was confirmed by RP-HPLC and MALDI.

8.3.1.8. Preparation of symmetric anhydride

Fmoc-Valine-OH (0.404 g, 1.19 mmol, 10 equiv.) was dissolved in dry DCM and a minimum amount of DMF (drops). Subsequently, DIC (0.092 mL, 0.595 mmol, 5 equiv.) was added dropwise at 0 ˚C. The mixture was allowed to stir for 30 min and then the solvents evaporated *in vacuo*. The symmetrical anhydride was then dissolved in DMF (minimum amount) and added to 70 mg of swollen Wang resin (in DMF) for 20 min (loading 1.7 mmol/g). The mixture was allowed to shake for 4 h. After that time, the solution was drained and the resin transferred to a vessel for peptide synthesis.

8.3.1.9. Acetylation at the N-terminus

(Proline acetylation – structure 2.7)

A solution of acetic anhydride (5 drops) and pyridine (100 µL) in DMF was added to the resin. The resin was shaken for 30 min and then washed several times to remove excess of reagents.

8.3.1.10. Dimethylation of *N,N* Fmoc-lysine-OH[344]

To a solution of Fmoc-lysine-OH (1 g, 2.3 mmol), 37 % formaldehyde solution (0.84 mL, 21.71 mmol) and AcOH (0.36 mL) in 1,4-dioxane, $NaBH_4$ (0.7 g, 18.62 mmol) was added in portions at 0 ˚C. After half of the $NaBH_4$ was added, another portion of 37% formaldehyde (0.84 mL, 21.71 mmol) was added to the reaction mixture. The pH of the reaction mixture was maintained at 3-6 by the addition of AcOH (drops). The reaction mixture was then warmed to room temperature and stirred overnight. The mixture was diluted with H_2O (6 mL) and the pH adjusted to 6. The organic solvents were removed *in vacuo* and the aqueous phase extracted with DCM 10 times. The combined organic phases were dried over MgSO4, filtered and concentrated in vacuum to give a yellow oil (0.87 g, 87% yield). The modified amino acid was purified by Biotage Isolera as described in the General procedures and then used in the synthesis of **2.22** and **2.23**: ^{1}H NMR (DMSO-d_6) δ 7.87 (d, *J*=7.5 Hz, 2H CH), 7.72-7.67 (m, 2H), 7.40 (t, *J*=7.0 Hz, 2H CH), 7.30 (t, 2H, *J* = 7.3 Hz, CH), 7.22 (d, 1H, *J* = 7.5 Hz, NH), 4.26-4.17 (m, 3H, OCH_2, CH), 3.79-3.86 (m, 1H, H_α), 2,44 (t, 2H, *J* = 7.5 Hz, H_ε) 2.30 (s, 6H, $N(CH_3)_2$), 1.73-1.54 (m, 2H, H_β), 1.50 -1.37 (m, 2H, H_δ), 1.33-1.27 (m, 2H, H_γ); ^{13}C NMR (DMSO-d_6) δ 173.7 (C=O), 156.2 (C=O), 143.8 (C), 140.7 (C), 127.6 (CH), 127.1 (CH), 125.2 (CH), 120.1 (CH), 65.6 (CH_2), 56.0 (CH), 53.7 (CH_2), 46.6 (CH), 41.8(CH_3), 30.1 (CH_2), 23.1 (CH_2), 22.7 (CH_2).

The spectroscopic data are consistent with that[344] reported in the literature.

8.3.1.11. Peptide characterization

	Sequence	Yield	MALDI-TOF (*m/z*)
2.1	**PRSF**	32 %	Expected 504.58, Found 505.35 $[M+H]^+$, 527.34 $[M+Na]^+$.
2.2	**PRSFLV**	20 %	Expected 717.87, Found 718.49 $[M+H]^+$.
2.3	**PRSFLVRK**	19 %	Expected, 1001.63 Found 1002.06 $[M+H]^+$, 1024.06 $[M+Na]^+$.
2.4	**PRSFLVRKP**	21 %	Expected 1098.34, Found 1099.04 $[M+H]^+$, 1121.03 $[M+Na]^+$.
2.5	**RSFLV**	35 %	Expected 520.62, Found 520.59.
2.6	**PRSFL**	34 %	Expected 617.63, Found 618.50 $[M+H]^+$.
2.7	**Acetyl-PRSFLV**	21%	Expected, 758.44, Found 760.43 $[M+H]^+$.
2.8	**PRSFLV$_{(COOH)}$**	22%	Expected 717.42, Found 719.06 $[M+H]^+$.
2.9	**ARSFLV**	34 %	Expected 691.83, Found 691.40 $[M+H]^+$.
2.10	**PASFLV**	32 %	Expected: 632.76, Found 654.09 $[M+Na]^+$.
2.11	**PRAFLV**	38 %	Expected: 701.87, Found 702.12, 703.15 $[M+H]^+$.
2.12	**PRSALV**	44 %	Expected 641.77, Found 641.19.
2.13	**PRSFAV**	15 %	Expected 675.79, Found 675.75.
2.14	**PRSFLA**	21 %	Expected 689.82, Found 689.4.1
2.15	**PLSFLV**	14 %	Expected found 673.83, Found 675 $[M+H]^+$, 697 $[M+Na]^+$, 712.99 $[M+K]^+$.

2.16	**PKSFLV**	31 %	Found 712.16, Found 713.19 $[M+ H]^+$.
2.17	**PRSMLV**	38 %	Expected 701.89, Found 701.97.
2.18	**PRSYLV**	40%	Expected 733.87, Found 733.76; 755.54 $[M+Na]^+$; 771.73 $[M+K]^+$.
2.19	**PRLYLV**	21 %	Expected 759.95 Found 759.78, 781.78 [M+Na]; 797.81 $[M+K]^+$.
2.20	**PRSK(Cbz)LV**	36 %	Expected 831.50, Found 832.70.
2.21	**LRSK(Cbz)LV**	21%	Expected 847.53, Found 848.75 $[M+H]^+$, 870.93 $[M+Na]^+$, 886. 94 $[M+K]^+$.
2.22	**PRSK(me2)LV**	18%	Expected 752.49, Found 752.78.
2.23	**PRSK(me2)VKRKP**	17%	Expected 1106.74, Found 1100.16.
2.24	**PRSK(me2)L**	28 %	Expected 626.42, Found 627.53 $[M+H]^+$.
2.25	**PRSFAA**	24 %	Expected 647.74, Found 648.02 $[M+H]^+$.
2.26	**ARAFAA**	12 %	Expected 604.34, Found 605.19 $[M+ H]^+$.
2.27	**PRAAAA**	15 %	Expected 554.33, Found 555.36 $[M+H]^+$.
2.28	**PRSFQTV**	25 %	Expected 703.81, Found 703.77.

8.3.2. Biological studies

Prof. Andrea Mattevi's group at Biocristallography laboratory, Department of Biology and Biotechnology "Lazzaro Spallanzani" at University of Pavia, Italy performed the LSD1 inhibition assay. Compound **MC2584** used for AML cell lines evaluation was provided by Prof. Antonello Mai at University La Sapienza, Rome, Italy. The LNCaP prostate cancer work was conducted at University of Southampton in the laboratory of Dr. Simon Crabb. The AMLs work was performed in the laboratory of Dr. Maria O'Connel, University of East Anglia, Pharmacy department.

8.3.3. Enzymatic studies

The LSD1 enzyme assay consists of a peroxidase-coupled assay, which monitors hydrogen peroxidase production (a side product of LSD1 demethylation) in the presence of different concentrations (2-100 μM range) of mono-methylated H3K4 peptide substrate with the inhibitor under analysis (global range 1-300 μM, depending on the inhibitors' level of activity). The data gathered were fitted to a Michaelis-Menten model for competitive inhibition and a value for the dissociation constant K_i was calculated for each peptide

Snail-1 analogues were soaked in solution with crystals of LSD1-CoREST complex for 3 h, then instantly frozen at a temperature of 100 K. X-ray scanning and multiple computer software were employed to generate a crystal structure with a resolution of 3.0 Å.

8.3.4. Cell-based studies

Anti-proliferative activity on different cancer cell lines

The anti-proliferative activity of SNAG-like peptides **PRSFLV** (**2.2**), **PRSMLV** (**2.17**), **PRLYLV** (**2.19**), **LRSK(Cbz)LV** (**2.21**), and **PLSFLV** (**2.15**) were assessed in SK-MEL28, A549 and THP-1 and HL-60 cells.

- **SK-MEL28 and A549**

SK-MEL28 and A549 cells were cultured in RPMI1640 medium with 10% Foetal Calf Serum (FCS), 2 mM L-glutamine and penicillin/streptomycin (P/S) and grown at 37 ˚C in an atmosphere of 5% CO_2. Cells were seeded at a density of 4500 cells/well in a 96 well plate with complete growth medium for 12 hours to achieve optimum cell adherence. The media was then removed and SKMEL-28 cells were treated with different concentrations of **PRSFLV** (500 µM, 200 µM, 100 µM, 50µM, 25 µM), dissolved in Phosphate buffered saline (PBS). **PRSFLV**, **PRSMLV** and **LRSK(Cbz)LV** were added to A549 cells, previously dissolved in growth media at different concentrations (2 mM, 1.5 mM, 1 mM, 750 µM, 500 µM, 250 µM, 125µM, 62 µM, 31 µM and 15 µM). After 72 h, the medium containing the treatment was removed from the plates and 200 µL of fresh pre-warmed growth media was added to each well. A solution of MTT reagent (50 µL, 2 mg/mL) was added and after 2 hours incubation, removed and replaced with 200 µL of DMSO and 25 µL of Sorensen's glycine buffer (0.1 M glycine, 0.1 M NaCl, pH 10.5). For each condition 5 experimental replicates were carried out. The absorbance of each well was read at 570 nm. Collected raw data were analysed using GraphPad Prism 6 to calculate means and the standard deviation.

- **THP-1 and HL-60**

THP-1 and HL-60 cell lines were cultured in RPMI 1640 medium (GIBCO) supplemented with 10% Foetal Calf Serum (FCS, GIBCO) and 5% of 2 mM L-glutamine and penicillin/streptomycin (P/S, Fisher). Cells were grown at 37 ˚C with 5% CO_2. Cells concentration was maintained at 25×10^4 cells/mL.

Anti-proliferation assay was carried out using MTS reagent (CellTiter96® Aqueous One Solution, Cell Proliferation Assay). THP-1 and HL-60 cells were plated in 96 well plates at a concentration of 5×10^4 cells/well and 3×10^4 cells/well respectively and immediately treated with 1 μL of peptide diluted in growth media at the following final concentrations: 2 mM, 1 mM, 500 μM, 250 μM, 125 μM, 62 μM, 31 μM and 15 μM. Peptides **PRSMLV**, **LRSK(Cbz)LV**, **PRLYLV** and compound **MC2586** were evaluated in THP-1 cells. Peptides **LRSK(Cbz)LV**, **PRLYLV** and **PLSFLV** were evaluated in HL-60 cells. After 72 h of incubation with the compounds, 10 μL of pre-warmed MTS reagent was added to each well and after 3 h of incubation, the absorbance was measured at 492 nm on a BMG PolaSTAR OPTIMA plate reader (BMG Labtech). Each experimental condition was repeated five times. Data were analysed using GraphPad Prism 6. Western blot analysis experimental methods are reported in the methods session of Chapter 4 (page 298).

8.4. Experimental procedures For Chapter 3

All chemicals and reagents were of the highest quality and obtained from Sigma Aldrich (Poole, UK), Fisher Scientific (Loughborough, UK) unless stated otherwise. All procedures including biopanning, amplification and titration, were followed according to the procedures detailed in the manufacturer's manual.

8.4.1. Phage-Display

8.4.1.1. Phage library

The phage library Ph.D.™-12 was purchased from New England Biolabs (Ipswich, Massachusetts, USA). The combinatorial library of 10^{13} pfu per mL consists of approximately 1.28×10^{9} random 12 amino acid sequences displayed on the pIII minor coat protein of the M13 filamentous phage. These were introduced to phage DNA by electroporation and once amplified can give raise to approximately 100 copies of each sequence. The general motif of a displayed peptide is X_{12}GGGS where X represents any amino acid and GGGS is a short amino acid spacer that links the C-terminus of the peptide to the N-terminus of the pIII protein.

8.4.1.2. Bacterial host maintenance for phage propagation

M13 was supplied with New England Biolabs library kit. It is s a male specific coliphage that propagates in the ER2738 strain of *E. coli* (F^+; TET^R). M13 possess a mini transposon conferring antibiotic resistance and selectivity towards *E. coli* population bearing F-pilus. *E. coli* culture was prepared by streaking a small quantity of ER2738 glycerol stock in 10 mL of LB medium (10 g of Bacto-Tryptone, 5 g of yeast extract and 5 g NaCl per 1 L of ddH_2O) and incubating overnight at 37 ˚C. For phage propagation, 2 mL of this culture were added to 18 mL of fresh LB broth in a sterile 250

mL erlenmeyer flask and further propagated for 4.5 h at 37 ˚C in an orbital shaker (Stuart S150, Staffordshire, UK, 150 rpm).

8.4.1.3. Phage cycle – panning and purification

Four rounds of biopanning were performed. In the first round of biopanning, 2 µL of magnetic beads (MagneticHis^{TM}Ni-Promega UK) were washed with TBST 0.1% (3×1mL, 50 mM Tris buffered saline, 150 mM NaCl, pH 7.5 + 0.1% Tween- Fisher Scientific UK). Blocking buffer (0.1 M $NaHCO_3$ water solution, pH 8.6) was added and incubated on ice for 1 h with gentle rocking (Stuart STR6, London, UK). In the meantime, 20 µL of LSD1 protein full length (10 nM) in TBST 0.1% (170 µL) was incubated with 10 µL Ph.D.™-12 library for 20 min at rt. The blocking buffer was removed from beads with TBST 0.1% washes (1 mL×4). Protein and library were subsequently incubated with the washed beads for 20 min with gentle rocking. After that time, beads were washed 10 times with TBST 0.5% (1 mL×3, 50 mM Tris buffered saline, 150 mM NaCl, pH 7.5 + 0.5% Tween) and the phage-bound was eluted (1 mL, 0.1 M glycine, pH 2.2, 10 min, × 3 times), and neutralised with 150 µL Tris-HCl (1 M, pH 9.1). The eluates were titered to quantify the phage on LB/IPTG/X-gal plates using the blue plaque-forming assay.

The glycine eluate 3 was then amplified in 1:100 diluted *E. coli* ER2738 overnight. To purify the phage, the culture was centrifuged (Hermle Z326K, Wehingen, Germany, 17320 ×g, 4 ˚C, 10 min) to pellet the ER2738 cells. The resulting supernatant was removed and centrifuged again (17320 ×g, 4 ˚C, 2 min), and 80% of the resulting supernatant was removed and treated with 1/6th of its volume with PEG/NaCl (20% (w/v) polyethylene glycol-8000, 2.5 M NaCl) then incubated at 4 ˚C overnight. After overnight precipitation the resulting suspension was centrifuged (17320 ×g, 4 ˚C, 10 min) to pellet the phage. The supernatant was removed and discarded and the pellet was re-centrifuged briefly. Any residual supernatant removed. The phage pellet was then suspended in 1 mL of TBS (50 mM Tris-HCl (pH 7.5), 150 mM NaCl), transferred to a micro-centrifuge tube, and centrifuged (18620 ×g, 4 ˚C, 5 min). The supernatant was removed and 1/6th volume PEG-NaCl was added and precipitated on ice for 1 h. The resulting suspension was centrifuged (18620 ×g, 4 ˚C, 10 min) and any residual

supernatant removed. The resulting phage pellet was re-suspended in 0.2 mL TBS. The phage was again quantified by titering on LB/IPTG/X-gal plates.

In the second round a negative selection was performed. The amplified phage 55,5 μL (1×10^{11} pfu) was pre-incubated with the beads in the absence of target. The supernatant from this step was then reacted with the target in a positive selection as above and beads changed. For the third and fourth round the phage was eluted with a specific LSD1 binder, **PRSFLVRKP** (1 mg/mL solution 10 min×3). The remainder of the round was completed as before.

8.4.1.4. Phage DNA extraction and sequencing

Six individual, well-separated plaques were removed from a titering plate with a sterile pipette tip. The isolated plaque was added immediately to a tube of 10 mL overnight culture of *E.coli* ER2738, diluted 1:100. The tubes were incubated in an orbital shaker at 37 ˚C for 4.5 h. After amplification, the tubes were centrifuged (17320 ×g, 1 min), and 500 μL of the phage-containing supernatant was recovered. PEG-NaCl (200 μL, 20% PEG-8000, 2.5 M NaCl) was added to the supernatant and incubated at rt for 20 min. The resulting suspension was centrifuged to pellet the phage (18620 ×g, 4 ˚C, 10 min). Any remaining supernatant was discarded. The pellet was next suspended in 100 μL of Iodide buffer (10 mM Tris-HCl pH 8.0, 1 mM EDTA, 4 M NaI) and 250 μL of EtOH were added before incubation at rt to precipitate single stranded phage DNA. The resulting precipitate was centrifuged (14,000 rpm, 10 min, 4 ˚C) and the supernatant removed and discarded. The resulting DNA pellet was washed with EtOH (0.5 mL, 70%, stored at -20 ˚C) re-centrifuged briefly and any residual supernatant discarded, then dried *in vacuo*. The pellet was suspended in ddH_2O (30 μL). The ssDNA was then sent for sequencing to Source Biosciences (Cambridge UK). 4Peaks (A. Griekspoor and Tom Groothuis, mekentosj.com) was used to process the chromatograms. ExPASy translate tool was used to deduce the amino acid sequences of the phage displayed peptides. A BLAST search was performed for identification of homologies between the obtained peptides and known proteins.

8.4.1.5. Phage plaque formation assay

Reagents

- **IPTG/X-gal Stock:** To 25 mL DMF, 1.25 g of IPTG (isopropyl-β-D-thiogalactoside) and 1 g X-gal (5-bromo-4-chloro-3- indolyl-β-D-galactoside) were added. The DMF solution was aliquoted and stored at -20 ˚C.
- **LB/IPTG/X-gal Plates:** In 1 L of LB medium 15 g of agar were added and the solution autoclaved. After cooling, 1 mL of IPTG/X-gal was added and 20 mL of media dispensed in a petri dish. Plates were stored at 4 ˚C.
- **Top Agar:** 10 g Bacto-Tryptone, 5 g yeast extract, 5 g NaCl and 7 g of electrophoresis grade agarose were mixed in 1 L of ddH_2O and autoclaved. The agar was dispensed into aliquots and once solidified it was stored at rt and melted in a microwave as needed.

Top agar was melted in a microwave until dissolved and 3 mL were dispensed in a sterile centrifuge tubes (as many as the phage dilutions). LB/IPTG/X-gal plates were warmed at 37 ˚C. Phages were next serially diluted (1:10) in LB broth (10^1-10^4 for eluates and 10^8-10^{11} for amplified eluates) and 10 µL added to sterile eppendorf tubes. To each tube of phage, 200 µL of an overnight culture of ER2738 were added. The infected cells were transferred one at the time to centrifuge tubes containing the melted Top agar cooled. After brief vortexing, these were poured onto the pre-warmed LB plates and spread evenly with a gentle rotation. The plates were incubated at 37 ˚C overnight. The day after, the formed single blue plaques were counted and the number obtained multiplied by the dilution factor for that plate, in order to achieve the phage titer in plaque-forming units (pfu) per 10 µL.

8.4.1.6. LSD1 expression and purification

Cloning of LSD1 Protein expression and purification[†]

The plasmid pet15b-His-tagged full length human LSD1 was kindly provided by Fei Lan in Dr. Yang Shi lab (Harvard University, Boston) and was expressed in *E. coli* BL21 RIPL Codon Plus (DE3) (Stratagene). The protein expression was induced with 0.1 mM IPTG (isopropyl-β-D-thiogalactopyranoside) for 16 h at 37 ˚C. Bacteria culture was then centrifuged at 6,500 rpm for 10 min at 4 ˚C. After discarding the supernatant, the bacteria pellet was lysed in 40 mM Tris-HCl pH 8.0, 300 mM NaCl, 0.2 % Triton X-100, 5% glycerol, 10 µg/mL DNase I and 10 mM $MgCl_2$ in the presence of complete EDTA-free protease inhibitors (Roche). The lysate was sonicated on ice then centrifuged at 15,000 rpm for 20 min at 4 ˚C. The supernatant was applied to a 6.4 mL Ni^{2+} column (Sigma) in binding buffer (40 mM Tris-HCl pH 8.0, 300 mM NaCl and 5% glycerol) and eluted using a linear gradient up to 250 mM imidazole in binding buffer on an AKTA Prime FPLC system. To identify the fraction containing LSD1, SDS-PAGE was performed with BIO-RAD electrophoresis system (12% polyacrylamide gel) stained with Coomassie Brilliant Blue (BIORAD). The fractions containing His-LSD1 were pooled, concentrated on a 30 kDa MWCO Amicon filter. LSD1 was then applied to a size exclusion column (HiLoad 26/60 Superdex 200, GE HealthCare) equilibrated in 20 mM Tris-HCl pH 8.0, 150 mM NaCl, 0.5 mM EDTA, 1 mM DTT and 5% glycerol. The fractions containing LSD1 were pooled and diluted 1:5 into 20 mM Tris-HCl (pH 8.0), 5% glycerol before being applied to a Q-sepharose™ column (Sigma). LSD1 was eluted with a 5-30% linear gradient using 20 mM Tris-HCl pH 8.0, 5% glycerol and 1 M NaCl. The fractions containing purified LSD1 were pooled together. Protein concentration was determined by Bradford assay (BIORAD). Protein was aliquoted (100 µL) and stored at -80˚C.

[†] Protocol provided by Dr. Patrick Duriez, Cancer Research UK, University of Southampton.

8.4.2. Enzymatic assay

8.4.2.1. Amplex®Red solutions

- **Preparation of Amplex®Red**

The reactive Amplex®Red was freshly made for each reaction well and the 50 µL added were composed of:

- 1 µL of 10 U/mL of horseradish peroxidase reconstituted in Reagent Buffer (InVitrogen)
- 48.5 µL of 50 mM Potassium Phosphate buffer
- 0.5 µL of Amplex®Red (InVitrogen) previously reconstituted in DMSO

For each reaction well, 50 µL of such solution were added.

- **Preparation of Amplex® Red Stop solution**

One vial of Amplex®Red Stop reagent (InVitrogen) was dissolved in 1.45 mL of EtOH and gently vortexed until dissolution. An equal amount of EtOH containing the stop solution and ddH_2O were mixed together and 30 µL of such mixture were added to each reaction well.

8.4.2.2. Protocol for Amplex®Red

Inhibitor's stocks were prepared in DMSO and then diluted in 50 mM Potassium phosphate buffer pH 7.5 (1:1 mix of monobasic and dibasic). The desired concentration (10 µL of drug 5× final concentration) was added to a GREINER 96 well non-binding white plate followed by 30 µL of pure human recombinant His-tag-LSD1 protein diluted in 50 mM Potassium phosphate buffer at 0.00461 mg/mL concentration. The protein and the tested inhibitor were incubated at rt with gentle rocking for 10 min. After that time, 10 µL of peptide substrate corresponding to the first 21 amino acid of human histone 3 di-methylated on lysine 4 (sequence ARTK(me2)QTARKSTGGKAPRKQLA, Peptide Synthetic, PPR Ltd) were then added at a concentration of 150 µM (30 µM final concentration) and incubated for 20 min at rt with gentle rocking. Subsequently, 50 µL of Amplex®Red/HRP mixture were added to

each reaction well and incubated at rt with gentle shaking. After 30 min of incubation, the reaction was quenched by adding 20 µL of Amplex®Red Stop Solution (InVitrogen) to each reaction well. The fluorescence was read on a BMG Cell star microplate reader (Ex: 530 nm; Em: at 590 nm). Raw data were collected and analysed with GraphPad Prism 6. The results were expressed as the relative fluorescence unit (RFU) compared to 100% of enzymatic activity (LSD1 + substrate, no inhibitor). Data were fitted with nonlinear regression and are shown as means ± STD, n=3).

8.4.3. Peptide synthesis

To synthesise peptide **3.1**, **3.3** and **3.4**, **SPPS** was employed using Fmoc/*t*-Bu strategy and PyBOP/DIPEA as coupling reagents. Procedures for resin swelling, loading, coupling and deprotection, global deprotection and cleavage, purification steps are described in Chapter 2.

8.4.4. Peptide characterisation

3.1: RKQHAIPLIWPA, yield 37 %
Maldi-TOF (*m/z*): Expected 1428.728, Found: 1430.71, 1431.73 $[M+H]^+$,1453.78 $[M+Na]^+$, 1468.81 $[M+K]^+$.

3.3: GGTKAPRLEHGP, yield: 35 %
Maldi-TOF (*m/z*): Expected: 1218.36; Found: $[M+H]^+$1219.50.

3.4: NPHTHTHGAFVS, yield: 42 %
Maldi-ToF (*m/z*): Expected 1303.383, Found: 1304.1305.09 $[M+H]^+$, 1326.15 $[M+Na]^+$, 1327.14 $[M+H^++Na^+]$, 1342.13 $[M+K]^+$, 1343.12 $[M+H^++K^+]$.

Maldi-TOF Spectra

PRSFLVRKP

Peptide 3.1

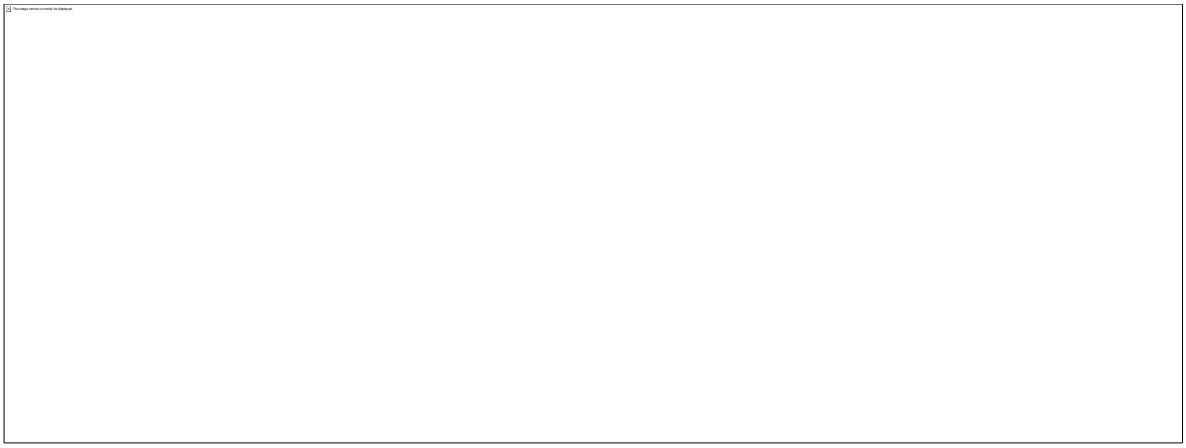

Peptide 3.3

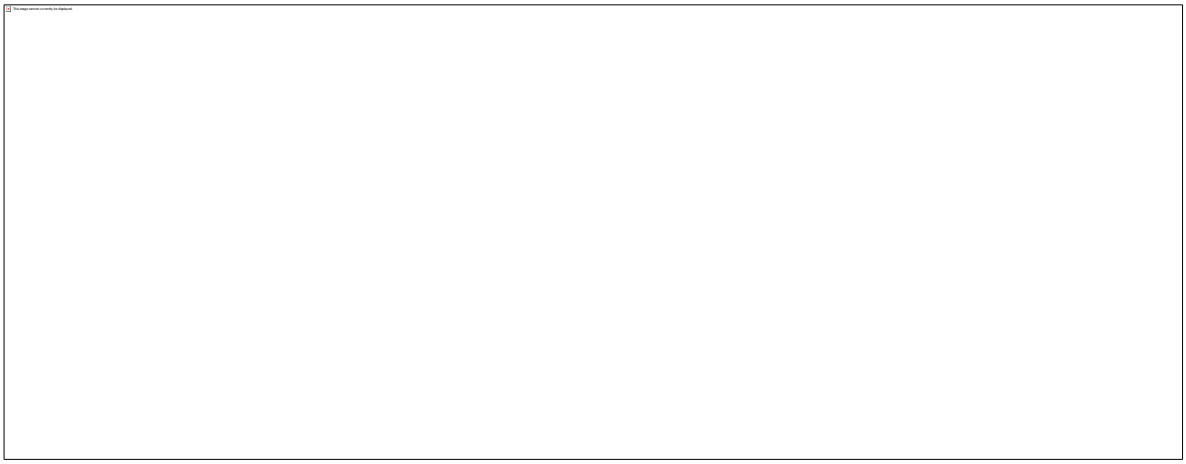

Peptide 3.4

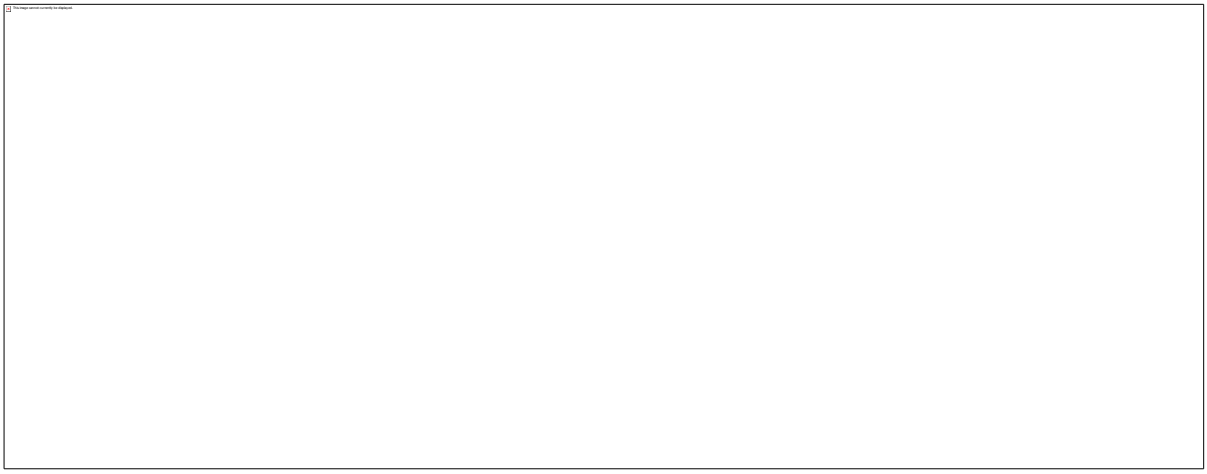

8.5. Experimental procedures Chapter 4

8.5.1. Synthesis of irreversible inhibitors TCP analogues

4.2
Methyl 4-formylbenzoate[345]

4-Formylbenzoic acid (**4.1**) (10.0 g, 66.0 mol, 1.0 equiv.) was dissolved in anhydrous MeOH (100 mL) with cooling (-5 ˚C) and acetyl chloride (24.1 g, , 21.2 mL, 0.33 mol, 5.0 equiv.) was added dropwise over a period of 10 min. After 30 min, the reaction mixture was warmed to rt and stirred overnight. The volatiles were removed *in vacuo* and the residue dissolved in EtOAc (70 mL), washed with 1 N NaOH, (100 mL×3) followed by sat. $NaHCO_3$ (50 mL × 3), H_2O (50 mL×3) and brine (50 mL×3). The organic phase was dried over $MgSO_4$ and filtered. The solvent was removed *in vacuo* and the desired product **4.2** was obtained (9.8 g, 91%) as a crystalline white solid that was used without further purification: R_f = 0.4, (petroleum ether/EtOAc 3:7): mp 180 ˚C; IR 1716, 1684, 1428 cm^{-1}; ^1H NMR ($CDCl_3$) δ 3.91 (s, 3H), 7.94 (d, *J* = 8.5 Hz, 2H), 8.19 (d, *J* = 8.3 Hz, 2H), 10.00 (s, 1H); ^{13}C NMR ($CDCl_3$) δ 52.6, 129.6, 130.3, 135.2, 139.3, 166.2, 191.7; HRMS (ESI) *m/z* calcd. for $C_9H_9O_3$ $[M+H]^+$ 165.0546, found 165.0545.

The spectroscopic data are consistent with that[345] reported in the literature.

4.3
(*E*)-Methyl 4-(3-(*tert*-butoxy)-3-oxoprop-1-en-1-yl)benzoate

To a solution of KO*t*-Bu (7.3 g, 64.6 mmol, 1.1 equiv.) in dry THF (100 mL) *tert*-butyl dietyl phosphonacetate (16.3 g, 15.4 mL, 64.6 mmol, 1.1 equiv.) was slowly added (dropwise) at -5 ˚C for a period of 15 min. The mixture was stirred for 1 h while mantaining the same temperature. Compound **4.2** (9.8 g, 58.7 mmol, 1 equiv.), dissolved in dry THF (40 mL), was then added dropwise to the mixture with vigorous stirring at -5 ˚C for a period of 20 min. Th reaction mixture was then warmed to rt and stirred overnight. After that time, the reaction mixture was poured into iced H_2O (100 mL) and extracted with EtOAc (100 mL×5). The organic phases were combined (500 mL) and washed with sat. $NaHCO_3$ (100 mL), H_2O (100 mL) and brine (100 mL) and dried over $MgSO_4$; evaporation of the solvent *in vacuo* released **4.3** (14.9 g, 98%) as a white crystalline solid that was used without further purification: R_f =0.64 (petroleum ether/ EtOAc 2:8); mp 64 ˚C; ^{1}H NMR ($CDCl_3$) δ 1.52 (s, 9H), 3.90 (s, 3H), 6.43 (d,J = 16.0 Hz, 1H), 7.53-7.59 (m, 3H), 8.04 (d,*J* = 8.0 Hz, 2H). ^{13}C NMR ($CDCl_3$) δ 28.2, 52.3, 80.9, 122.6, 127.8, 130.1, 131.2, 139.0, 142.1, 165.8, 166.5; HRMS (ESI) *m/z* calcd for $C_{15}H_{19}O_4$ $[M+H]^+$ 263.1278, found 263.1278.

The spectroscopic data are consistent with that[346] reported in the literature.

4.4
(±)-*trans*-4-methyl[2-(*tert*-butoxycarbonyl) cyclopropyl)]benzoate[178]

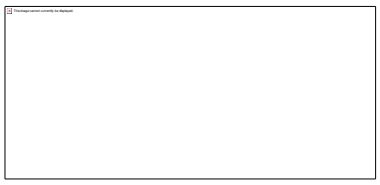

Trimethylsulfoxonium iodide (15 g, 68.1 mmol, 1.2 equiv.) was added in small portions to a suspension of NaH (2.27 g, 68.1 mmol, 60 wt% in mineral oil, 1.21 equiv.) in dry DMSO (60 mL). The solution was stirred for 45 min. The olefin **4.3** (14.9 g, 56.8 mmol, 1 equiv.) dissolved in DMSO (60 mL), was then added dropwise to the formed ylide and the reaction stirred overnight at rt. After completion, the reaction mixture was poured into iced water (100 mL) and extracted with EtOAc (70 mL×10). The organic phases (700 mL) were combined and washed with sat. $NaHCO_3$ (200 mL), H_2O (200 mL) and brine (200 mL) and dried over $MgSO_4$. Purification of the crude yellow oil by silica gel column chromatography (petroleum ether/ EtOAc 8.9:1.9) afforded **4.3** (3.7 g, 23%) as a white crystalline solid; R_f=0.66 (petroleum ether /EtOAc 8:2); mp 40 ˚C; IR 1715, 1609, cm^{-1}; ^1H NMR ($CDCl_3$) δ 1.26 (ddd,*J* = 4.8, 6.4, 8.5 Hz, 1H), 1.46 (s, 9H), 1.57 (m, 1H), 1.88 (ddd, *J* = 4.4, 5.5, 8.6 Hz, 1H), 2.4 (ddd, *J* = 4.1, 5.4, 9.5 Hz, 1H), 3.9 (s, 3H), 7.1 (d, *J* = 8.3 Hz, 2H), 7.9 (d, *J* = 8.4 Hz, 2H); ^{13}C NMR ($CDCl_3$) δ 16.5, 24.6, 24.8, 27.1, 50.9, 79.8, 124.9, 127.6, 128.7, 145.07, 165.8, 171.0; HRMS (ESI) *m/z* calcd. for $C_{16}H_{24}O_4N$ $[M+NH_4]^+$ 294.1700, found 294.1704.

This compound is reported in the literature[178] although characterisation data was not provided.

4.5
(±)-*trans*-[2-(4-(methoxycarbonyl)phenyl]cyclopropanecarboxylic acid[178]

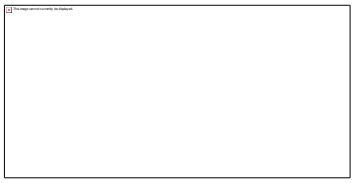

Trifluoroacetic acid (19.7 g, 13.2 mL, 0.17 mol, 13 equiv.) and triethylsilane (3.86 g, 5.3 mL, 33.25 mmol, 2.5 equiv.) were added to a solution of **4.4** (3.7 g, 13.4 mmol, 1 equiv.) in DCM (40 mL). The reaction mixture was stirred at rt and monitored by TLC. After completion, the reaction mixture was co-evaporated with acetonitrile (15 mL×3) to give **4.5** (2.1 g, 72%) as a white crystalline solid that was used without further purification: mp 123 ˚C; IR 3307, 1716, 1608, 1476.5, cm^{-1}; ^{1}H NMR (CD_3OD) δ 1.43 (ddd, *J*=4.6, 6.5, 8.5 Hz, 1H), 1.60 (ddd, *J* = 4.6, 5.3, 9.4 Hz, 1H), 1.92 (ddd, *J* = 4.1, 5.4, 8.5 Hz, 1H), 2.51 (ddd, *J* = 4.0, 6.3, 9.2 Hz, 1H), 3.90 (s, 3H), 7.25 (d, *J*=8.4 Hz, 2H), 7.93 (d, *J* = 8.44 Hz, 2H); ^{13}C NMR (CD_3OD) δ 17.9, 25.6, 26.9, 52.5, 127.1, 129.4, 130.7, 147.6, 168.7, 176.4; HRMS (ESI) *m/z* calcd. for $C_{12}H_{11}O_4$ $[M-H]^-$ 219.0663, found 219.0659.

This compound is reported in the literature[178] although characterisation data was not provided.

4.6
(±)-*trans*-4-methyl-2-[(*tert*-butoxycarbonyl)amino]cyclopropyl benzoate[178]

The acid **4.5** (2.1 g, 9.5 mmol, 1.0 equiv.), diphenylphosphoryl azide (2.86 g, 2.27 mL, 10.5 mmol, 1.1 equiv.) and triethylamine (1.44 g, 1.98 mL, 14.3 mmol, 1.5 equiv.) were combined in *tert*-butanol (11 mL) under argon, heated at reflux and allowed to react for 72 h. After that time, the reaction mixture was cooled to rt, diluted with EtOAc (20 mL) and washed with saturated Na_2CO_3 solution (20 mL×3). The organic layer was separated and the aqueous layer further extracted with EtOAc (20 mL). The organic layers were combined (40 mL), washed with sat. $NaHCO_3$ (10 mL), H_2O (10 mL) and brine (10 mL) and dried over $MgSO_4$. Concentration *in vacuo* afforded a yellow oil which was purified by silica gel column chromatography (Hexane/EtOAc 8:2) affording **4.5** (1.6 mg, 42%) as a white crystalline solid: R_f=0.57 (Hexane /EtOAc 8:2); mp 45 ˚C; ^{1}H NMR ($CDCl_3$) δ 1.20-1.24 (m, 2H), 1.43 (s, 9H), 2.07 (td, *J* = 3.1, 7.6 Hz, 1H), 2.70-2.78 (m, 1H) 3.9, (s, 3H), 7.15 (d, *J* = 8.5 Hz, 2H), 7.9 (d, *J* = 8.4 Hz, 2H); ^{13}C NMR ($CDCl_3$) δ 14.8, 26.3, 28.0, 28.1, 28.4, 55.3, 113.8, 127.8, 130.6, 132.7, 157.9; 168.7; HRMS (ESI) *m/z* calcd. for $C_{15}H_{18}N_1O_4$ $[M-H]^-$ 276.1241, found 276.1243.

This compound is reported in the literature[178] although characterisation data was not provided.

4.7

(±)-*trans*-4-2-[(*tert*-butoxycarbonyl) amino)cyclopropyl]benzoic acid[178]

To a suspension of **4.6** (1.6 g, 5.7 mmol, 1 equiv.) in THF:H_2O: (3:1 ratio), LiOH (0.4 g, 17.32 mmol, 3 equiv.) was added and the reaction heated to 50 ˚C and stirred for 3 h. The reaction progress was monitored by TLC and after completion, the reaction mixture was diluted with water (10 mL) and acidified to pH 1-2 with sat. $KHSO_4$. The aqueous layer was extracted with EtOAc (20 mL×3) and the combined organic layers (60 mL) were washed with sat. $NaHCO_3$ (10 mL), H_2O (10 mL) and brine H_2O (10 mL) and dried over $MgSO_4$. Solvent concentration *in vacuo* afforded **4.7** (1.3 g, 82%) as a white solid. The product was used in the following step without further purification: IR 3314, 2873, 1681, 1453 cm^{-1}; ^1H NMR (CD_3OD) δ 1.21-1.25 (m, 1H), 1.43 (s, 9H), 2.04 (td, *J* = 3.9, 7.9 Hz, 1H), 2.69-2.65 (m, 1H), 7.19 (d, *J* = 8.3 Hz, 2H), 7.91 (d, *J* = 8.3 Hz, 2H); ^{13}C NMR (CD_3OD) δ 17.1, 25.8, 28.7, 35.0, 80.3, 126.9, 129.4, 130.7, 148.5, 158.9, 169.9; HRMS (ESI) *m/z* calcd. for $C_{17}H_{25}NO_4$ $[M+H]^+$ 273.1961, found 273.1962.

This compound is reported in the literature[178] although characterisation data was not provided.

Coupling procedure (4.8a-s)

To a stirring suspension of the acids **4.7** in DCM, 2 equiv. of DIPEA were added and the mixture stirred until obtaining a clear solution. Subsequently, HOBt (0.2 equiv.) and EDCI (1.5 equiv.) were added and stirred for 30 min. The desired amine **(a-s**, Table 4.8, 1.2 equiv.) was added to the stirring mixture and the reaction further stirred at rt overnight. After that time, the reaction mixture was diluted with DCM and washed with 2 N HCl and 1 N NaOH. The organic layers were combined, washed with sat. $NaHCO_3$, H_2O and brine and dried over $MgSO_4$. Concentration *in vacuo* afforded amides **4.8a-s.**

Compound	Amine	Yield
4.8-a	Glycynamide hydrochloride	42%
4.8-b	benzylamine	67%
4.8-c	phenethylamine	63%
4.8-d	dibenzylamine	56%
4.8-e	4-phenylbenzylamine	58%
4.8-f	2-thiophenethylamine	51%
4.8-g	cyclohexanemethylamine	52%
4.8-h	cylohexaneethylamine	57%
4.8-i	4-fluorobenzylamine	59%
4.8-j	4-bromobenzylamine	61%
4.8-k	4-chlorobenzylamine	56%
4.8-l	4-methoxybenzylamine	51%
4.8-m	4-nitrobenzylamine	56%
4.8-n	1-(2-pyridyl) piperazine	36%
4.8-o	1-(2-pyrimidyl)piperazine	43%
4.8-p	1-tosylpiperazine	65%
4.8-q	1-(methylsulfonyl)piperazine	56%
4.8-r	1-(2-fluorophenyl)piperazine	45%
4.8-s	2-(piperazin-1-yl)benzonitrile	53%

Table 8.2: Amine used in the coupling reaction for the generation of intermediates 4.8-a-s.

Boc-deprotection (4.9-4.27)

The amides (**4.8a-s**) were dissolved in HCl (6 N) in THF with cooling and the reaction monitored by TLC. Amides **4.8-b**, **4.8-c**, **4.8-e**, **4.8-f** were deprotected with 4 N HCl, whereas amide **4.8-m**, **4.8-n**, **4.8-o, 4.8-q**, **4.8-r, 4.8-s** were deprotected with 3 N HCl. After completion, the deprotected amines were diluted with acetonitrile and concentration *in vacuo* afforded the deprotected amines that were washed with diethyl ether. Compounds **4.9-4.27** were then analysed by HPLC and purified by RP-HPLC. Gross purification was performed on a preparative RP-HPLC gradient from 95:5 water: methanol → 5:95 methanol: water with 0.05% TFA additive over 30 minutes and a flow rate of 20 mL/min. Collection was monitored by UV at 214 and 254 nm. The collected fractions were assessed by analytical RP-HPLC and the ones suspected to have the desired compound diluted in water (5 mL), lyophilised and fully characterised.

4.9

4-(±)-*trans*-2-aminocyclopropyl)-*N*-(2-amino-2-oxoethyl)- benzamide hydrochloride

Yield 15%, yellow oil; ^{1}H NMR (CD_3OD) δ 1.38-1.42 (m, 1H), 1.47-1.52 (m, 1H), 2.43-2.48 (m, 1H), 2.91-2.94 (m, 1H), 3.74 (s, 1H), 4.02 (s, 1H), 4.08, (s, 1H), 7.31 (dd, *J* = 2.7, 8.0 Hz, 2H), 7.85 (t, *J* = 7.60 Hz, 2H); ^{13}C NMR (CD_3OD) δ 14.6, 22.3, 32.3, 42.3, 127.5, 128.9, 133.5, 144.3, 169.2, 172.8; HRMS (ESI) *m/z* calcd. $C_{12}H_{16}N_3O_2$ $[M+H]^+$ 234.1237, found 234.12068. Purity 96%. For this compound was not possible to achieve a good IR spectra due to the low yield.

4.10

4-((±)-*trans*-2- aminocyclopropyl)-*N*-benzylbenzamide hydrochloride[178]

Yield 71%, yellow crystalline solid; mp 200 ˚C; IR 3336, 3289, 3075, 1674, 1437 cm^{-1}; ^{1}H NMR (CD_3OD) δ 1.36-1.42 (m, 1H), 1.46-1.51 (m, 1H), 2.46 (ddd, *J* = 3.3, 6.6, 9.9 Hz, 1H), 2.90-2.92, (m, 1H), 4.6 (s, 2H), 7.11-7.19 (m, 3H), 7.22-7.35 (m, 4H), 7.81 (d, *J* = 8.2 Hz, 2H); ^{13}C NMR (CD_3OD) δ 14.3, 22.4, 32.2, 44.4, 127.5, 128.2, 128.5,129.7, 129.5, 134.1, 140.2, 143.9, 169.6; HRMS (ESI) *m/z* calcd. for $C_{17}H_{19}N_2O_1$ $[M+H]^+$ 267.1492, found 267.1495; Purity 99%.

This compound is reported in the literature[178] although characterisation data was not provided.

4.11

4-(±)-*trans* -2-aminocyclopropyl)-*N*-phenethylbenzamide hydrochloride

Yield 67%, yellow solid; mp 180 ˚C; IR 3283, 1637, 1545 cm^{-1}; $^{1}HNMR$ (CD_3OD) δ 1.36-1.42 (m, 1H), 1.48 (ddd, *J* = 4.2, 6.7, 10.3 1H), 2.42 (ddd, *J* = 3.5, 6.3 Hz, 10.3 1H), 2.90 (t, *J* = 7.7 Hz, 3H), 3.58 (t, *J* = 7.2 Hz, 2H), 7.17-7.20 (m, 1H), 7.24-7.29 (m, 6H) 7.72 (d, *J* = 7.7 Hz, 2H); $^{13}CNMR$ (CD_3OD) δ 14.3, 22.4, 32.3, 36.3, 42.6, 127.3,127.4, 128.6, 129.5, 129.9, 134.3, 140.6, 143.8, 169.7; HRMS (ESI) *m/z* calcd. for $C_{18}H_{21}N_2O$ $[M+H]^+$ 281.1648, found 281.1648. Purity 96%.

4.12

4-(±)-*trans*-2-aminocyclopropyl)-*N*,*N*-dibenzylbenzamide hydrochloride

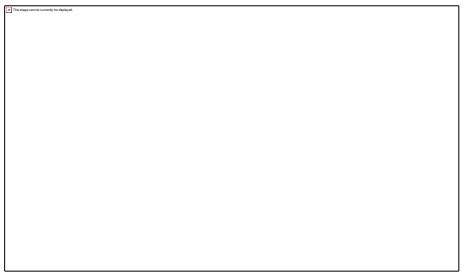

Yield 52%, yellow solid; IR 3214, 1645.7, 1620, 1452 cm^{-1}; ^{1}HNMR (CD_3OD) δ 1.37-1.38 (m, 1H), 1.49-1.56 (m, 1H), 2.43 (ddd, *J* = 3.2, 6.4, 9.8 Hz, 1H), 2.96-2.90 (m, 1H), 4.43 (br s, 2H), 4.66 (br s, 2H), 7.12 (br s, 2H), 7.24-7.30 (m, 7H), 7.32-7.39 (m, 5H), 7.43-7.50 (m, 2H); ^{13}CNMR (CD_3OD) δ 14.1, 22.3, 32.3, 53.7, 127.6, 128.0, 128.2, 128.7, 129.8, 129.9, 135.5, 142.2, 174.2; HRMS (ESI) *m/z* calcd. for $C_{24}H_{25}N_2O_1$ $[M+H]^+$, 357.1961, found 357.1960. Purity 99%.

4.13

N-([1,1'-biphenyl]-4-ylmethyl)-4- (*± trans* -2 -aminocyclopropyl) benzamide hydrochloride

Yield 34% yellow solid; IR 3402, 3045, 1715, 1632, 1540 cm^{-1};
^{1}H NMR (CD_3OD) δ 1.38-1.43 (m, 1H), 1.46-1.50 (m, 1H), 2.43 (ddd, *J*=3.5, 6.3, 10.2 Hz, 1H), 2.92 (ddd, *J* = 3.7, 7.9, 11.6 Hz, 1H), 4.61 (s, 2H), 7.26-7.29 (m, 2H), 7.30-7.34 (m, 1H), 7.39-7.45 (m, 4H), 7.56-7.60 (m, 4H), 7.83 (d, *J* = 8.4 Hz, 2H); ^{13}C NMR (CD_3OD) δ 14.3, 22.4, 32.2, 44.1, 127.4, 127.8, 128.0,128.2, 128.7, 128.9, 129.7, 134.0, 139.2, 141.3, 142.0, 143.8, 169.6. Purity 95%.

4.14

4-(±)-*trans* -2-aminocyclopropyl)-*N*-(2-(thiophen-2-yl)ethyl)benzamide hydrochloride

Yield 47%, yellow solid; mp 218 ˚C; IR 3318, 2775, 2977, 1626, 1505 cm^{-1}; ^{1}H NMR (CD_3OD) δ 1.37-1.42 (m, 1H), 1.48 (ddd, *J* = 4.56, 6.7, 10.2 Hz, 1H), 2.43 (ddd, *J* = 3.6, 6.0, 9.0 Hz, 1H), 2.90-2.94 (m, 1H), 3.13 (t, *J* = 7.0 Hz, 2H), 3.61 (t, *J*=7.0 Hz, 2H), 6.88 (dd, *J* = 1.0, 3.4 Hz, 1H), 6.91-6.94 (m, 1H) 7.20 (dd, *J* = 1.0, 4.8 Hz, 1H), 7.25 (d, *J*=8.4 Hz, 2H), 7.75 (d, *J* = 8.4 Hz, 2H); ^{13}C NMR (CD_3OD) δ 14.3, 22.4, 30.1, 32.2, 42.7, 124.7, 126.3, 127.4, 127.8, 128.6, 134.1, 142.5, 143.7, 169.7. Purity 97%. For this compound it was not possible to obtain HRMS data.

4.15

4-(±)-*trans*-2-aminocyclopropyl)-*N*-(cyclohexylmethyl)benzamide hydrochloride

Yield 58%, yellow solid; mp 198 ˚C; IR 3335, 1712, 1696, 1459 cm^{-1}; ^{1}H NMR (CD_3OD), δ 0.94-1.03 (m, 2H), 1.18-1.31 (m, 4H), 1.33-1.44 (m, 1H), 1.48-1.52 (m, 1H), 1.58-1.69 (m, 2H), 1.71-1.82 (m, 3H), 2.41-2.49 (m, 1H), 2.88-2.92 (m, 1H) 3.20 (d, *J* = 6.9 Hz, 2H), 7.26 (d, *J* = 8.2 Hz, 2H), 7.76 (d, *J* = 8.2 Hz, 2H); ^{13}C NMR (CD_3OD) δ 14.3, 22.4, 26.9, 27.6, 32.3, 39.2, 39.4, 47.2, 127.4, 128.6, 134.3, 143.6, 169.8; HRMS (ESI) *m/z* calcd. for $C_{17}H_{25}N_2O$ $[M+H]^+$, 273.1961, found 273.1962. Purity 97%.

4.16

4-(±)-*trans*-2-aminocyclopropyl)-*N*-(2-cyclohexylethyl)benzamide hydrochloride

Yield 33%, yellow solid; mp 79 ˚C; IR 3318, 1632, 1539, 1449 cm^{-1}; ^{1}HNMR (DMSO-*d*6) δ 0.84-0.96 (m, 2H), 1.08-1.31 (m, 5H), 1.36-1.44 (m, 2H), 1.45-1.51 (m, 1H), 1.64-1.80 (m, 5H), 2.43 (ddd, *J* = 3.5, 5.5, 10.1 Hz, 1H), 2.81-2.89 (m, 1H), 3.22-3.29 (m, 2H), 7.25 (d, *J* = 8.3 Hz, 2H), 7.75 (d, *J* = 8.3 Hz, 2H), 8.39 (t, *J* = 6.0 Hz, 1H), 8.64 (br s, 2H); ^{13}CNMR (CD_3OD) δ 14.3, 22.4, 27.4, 27.6, 32.2, 34.3, 36.8, 37.9, 38.8, 127.4, 128.6, 134.3, 143.6, 169.6; HRMS (ESI) *m/z* calcd. for $C_{18}H_{27}N_2O$ $[M+H]^+$ 287.2118, found 287.2119. Purity 98%.

4.17

4-((±)-*trans*-2-aminocyclopropyl)-*N*-(4-fluorobenzyl)benzamide hydrochloride

Yield 45%, yellow solid; mp 98 ˚C; IR 335, 2486, 1620, 1516, 1458 cm^{-1}; ^{1}H NMR (CD_3OD) δ 1.37-1.42 (m, 1H), 1.49 (ddd, *J* = 4.7, 7.0, 10.2 Hz, 1H), 2.43 (ddd, *J* = 3.6, 6.5, 10.0 Hz, 1H), 2.89-2.96 (m, 1H), 4.53, (s, 2H), 7.0 (t, *J*=8.7 Hz, 2H), 7.26 (d, *J*=8.2, 2H), 7.36 (m, 2H), 7.81 (d, *J*=8.3 Hz, 2H); ^{13}C NMR (CD_3OD) δ 14.3, 22.4, 32.3, 43.8, 116.2, 127.5, 128.5, 130.4, 133.9, 136.3, 143.9, 163.5 (d, J_{F-C}=220 Hz), 169.6; HRMS (ESI) *m/z* calcd. for $C_{17}H_{18}F_1N_2O$ $[M+H]^+$ 285.1398, found 285.1402. Purity 96%.

4.18

4-((±)-*trans* -2-aminocyclopropyl)-*N*-(4-bromobenzyl)benzamide hydrochloride

Yield 65 %, white solid; mp 97 ˚C; IR 3320, 3035, 2665, 1637, 1533, 14893 cm^{-1}; ^{1}HNMR (CD_3OD) δ 1.37-1.42 (m, 1H), 1.46-1.51 (m, 1H), 2.44 (ddd, *J* = 3.2, 6.3, 9.7 Hz, 1H), 2.90-2.93 (m, 1H), 4.52 (s, 2H), 7.26 (d, *J* = 8.0 Hz, 4H), 7.47 (d, *J* = 8.3 Hz, 2H), 7.83 (d, *J* = 8.3 Hz, 2H); ^{13}CNMR (CD_3OD) δ 14.4, 22.4, 32.3, 43.9, 121.8, 127.5, 128.8, 130.5, 132.6, 133.9, 139.6, 144.00, 169.7; HRMS (ESI) *m/z* calcd. for $C_{17}H_{18}BrN_2O$ $[M+H]^+$ 345.0597, found 345.0602. Purity 98%.

4.19

4-((±)-*trans*-2-aminocyclopropyl)-*N*-(4-chlorobenzyl)benzamide hydrochloride

Yield 15%, yellow solid; mp 102 ˚C IR 3301, 2354, 1637, 1556, 1515 cm^{-1}; ^{1}HNMR (CD_3OD) δ 1.36-1.41 (m, 1H), 1.48 (ddd, *J* = 4.2, 6.7, 10.2 Hz, 1H), 2.43 (ddd, *J* = 3.1, 6.2, 9.9 Hz, 1H), 2.90-2.94 (m, 1H), 4.5 (s, 2H), 7.27 (d, *J* = 8.3 Hz, 2H), 7.32 (s, 4H), 7.81 (d, *J* = 8.3 Hz, 2H); ^{13}CNMR (CD_3OD) δ 14.7, 22.8, 32.4, 43.9, 123.4, 127.4, 128.8, 129.7, 130.2, 132.9, 139.0, 144.1, 172.1; HRMS (ESI) *m/z* calcd. for $C_{17}H_{18}ClN_2O$ $[M+H]^+$ 301.1102, found 301.1102. Purity 94%.

4.20

4-((±)-*trans*-2-aminocyclopropyl)-*N*-(4-methoxybenzyl)benzamide hydrochloride

Yield 52%, yellow solid; mp 123 ˚C; IR 3364, 1672, 1528 cm^{-1}; ^{1}HNMR (CD_3OD) δ 1.36-1.41 (m, 1H), 1.49 (ddd, *J* = 4.6, 6.7, 10.5 Hz, 1H), 2.44 (ddd, *J* = 3.4, 6.3, 9.8 Hz, 1H), 2.91, (ddd, *J* = 4.0, 7.9, 11.7 Hz, 1H), 3.76 (s, 3H), 4.48 (s, 2H), 6.87 (d, *J* = 8.6 Hz, 2H), 7.25 (d, *J* = 8.4 Hz, 2H), 7.26 (d, *J* = 8.4 Hz, 2H), 7.79 (d, *J* = 8.1 Hz, 2H); ^{13}CNMR (CD_3OD) δ 14.3, 22.4, 32.3, 43.9, 55.7, 114.9, 127.5, 128.7, 129.8, 132.2, 134.1, 143.9, 160.4, 169.5; HRMS (ESI) *m/z* calcd. for $C_{18}H_{21}N_2O_2$ $[M+H]^+$ 297.1598, found 297.1595. Purity 98%.

4.21

4-((±)-*trans*-2-aminocyclopropyl)-*N*-(4-nitrobenzyl)benzamide hydrochloride

Yield 17%, brown solid; IR 3283, 1643, 1591, 1516 cm^{-1}; ^{1}H NMR (CD_3OD) δ: 1.38-1.44 (m, 1H), 1.45-1.49 (m, 1H), 2.43 (ddd, *J* = 3.3, 6.5, 9.8 Hz, 1H), 2.91-2.95 (m, 1H), 4.68 (s, 2H), 7.31 (d, *J* = 7.6 Hz, 2H), 7.58 (d, *J* = 8.8 Hz, 2H), 7.77 (d, *J* = 7.6 Hz, 2H), 8.2 (d, *J* = 8.8 Hz, 2H); ^{13}C NMR (CD_3OD) δ 14.4, 22.4, 32.3, 43.9, 124.6, 127.6, 128.8, 129.3, 133.6, 144.2, 148.1, 148.5, 169.7; HRMS (ESI) *m/z* calcd. for $C_{17}H_{18}N_3O_3$ $[M+H]^+$ 312.1343, found 312.1343. Purity 94%.

4.22

4-((±)-*trans* -2-aminocyclopropyl)phenyl)4-(pyridin-2-yl)piperazin-1-yl)methanone hydrochloride

Yield 13%, orange oil; IR 3358, 1603, 1545, 1435 cm^{-1}; ^{1}HNMR (CD_3OD) δ 1.37-1.43 (m, 1H), 1.51 (ddd, *J* = 4.4, 6.6, 11.1 Hz, 1H), 2.48 (ddd, *J* = 3.5, 6.3, 10.0 Hz, 1H), 2.93 (ddd, *J* = 4.4, 7.6, 11.2 Hz, 1H), 3.8 (br s, 8H), 7.06 (t, *J* = 6.5 Hz, 1H), 7.32 (d, *J* = 8.0 Hz, 2H), 7.42 (d, *J* = 9.2 Hz, 1H), 7.48 (d, *J* = 8.0 Hz, 2H), 8.0 (dd, *J* = 1.24, 7.9 Hz, 1H), 8.05 (dt, *J* = 1.6, 8.5 Hz, 1H); ^{13}CNMR (CD_3OD) δ 14.3, 22.4, 32.2, 44.8, 47.2, 114.3, 127.8, 128.8, 131.1, 134.5, 137.5, 142.8, 145.7, 153.7, 172.6; HRMS (ESI) *m/z* calcd. for $C_{19}H_{23}N_4O$ $[M+H]^+$ 323.1866, found 323.1869. Purity 95%.

4.23

4-(±)-*trans*-2-aminocyclopropyl-phenyl)-(4-(pyrimidin-2-yl)piperazin-1-yl)methanone hydrochloride

Yield 22 %, red oil; IR 3353,1678, 1632, 1551 cm^{-1}; ^{1}H NMR (CD_3OD) δ 1.39-1.45 (m, 1H), 1.47 (ddd, *J* = 4.5, 6.9, 10.1 Hz, 1H), 2.44 (ddd, *J* = 3.6, 6.4, 10.2 Hz, 1H), 2.92-2.96 (m, 1H), 3.53 (br s, 2H), 3.82 (br s, 4H), 3.94 (br s, 2H), 6.66 (t, *J* = 4.7, Hz, 1H), 7.29 (d, *J* = 8.2 Hz, 2H), 7.42 (d, *J* = 8.3 Hz, 2H), 8.35 (d, *J* = 4.8 Hz, 2H); ^{13}C NMR (CD_3OD) δ 14.2, 22.4, 32.1, 40.4, 41.7, 111.8, 127.7, 128.6, 135.2, 142.3, 159.1, 162.8, 172.45; HRMS (ESI) *m/z* calcd. for $C_{18}H_{22}N_5O$ $[M+H]^+$324.1819, found 324.1824. Purity 95%.

4.24

4-((±)-*trans*-2-aminocyclopropyl)phenyl)(4-(phenylsulfonyl) piperazin-1-yl)methanone hydrochloride

Yield 25%, white solid; IR 3392, 1637, 1652, 1551 cm^{-1}; ^{1}H NMR (CD_3OD) δ 1.33-1.38 (m, 1H), 1.45-1.50 (m, 1H), 2.41-2.43 (m, 1H), 2.45 (s, 3H), 2.87-2.89 (m, 1H), 3.00 (br s, 4H), 3.56 (br s, 2H), 3.77 (br s, 2H), 7.22 (d, *J* = 7.6 Hz, 2H), 7.30, (d, *J* = 7.6 Hz, 2H), 7.44 (d, *J* = 7.8 Hz, 2H), 7.65 (d, *J*=7.9 Hz, 2H); ^{13}C NMR (CD_3OD) δ 14.2, 21.5, 22.3, 32.2, 44.2, 47.2, 127.7, 128.6, 128.9, 130.9, 133.8, 134.5, 142.4, 145.6, 172.2; HRMS (ESI) *m/z* calcd. for $C_{21}H_{26}N_3O_3S$ $[M+H]^+$ 400.1689, found 400.1687. Purity 97%.

4.25

4-(±)-*trans*-2-aminocyclopropyl)phenyl(4-(methylsulfonyl)piperazin-1-yl)methanone hydrochloride

Yield 37%, white solid; IR 3387, 1614, 1562 cm^{-1}; $^{1}HNMR$ (CD_3OD) δ 1.37-1.42 (m, 1H), 1.47 (ddd, *J* = 4.5, 6.8, 10.3 Hz, 1H), 2.42 (ddd, *J* = 3.6, 6.6, 10.2 Hz, 1H), 2.87 (s, 3H), 2.89-2.93 (m, 1H), 3.26 (br s, 4H), 3.57 (br s, 2H), 3.8, (br s, 2H), 7.28 (d, *J* = 8.2 Hz, 2H), 7.41 (d, *J* = 8.3 Hz, 2H); $^{13}CNMR$ (CD_3OD) δ 14.2, 22.4, 32.0, 34.8, 46.7, 68.0, 127.8, 128.6, 134.7, 142.4, 172.3; HRMS (ESI) *m/z* calcd for $C_{15}H_{24}N_3O_3S$ [M+H]+ 324.1380, found 324.1380. Purity 99%.

4.26

4-((±)-*trans*-2-aminocyclopropyl) phenyl)4-(2-fluorophenyl)piperazin-1-yl)methanone hydrochloride

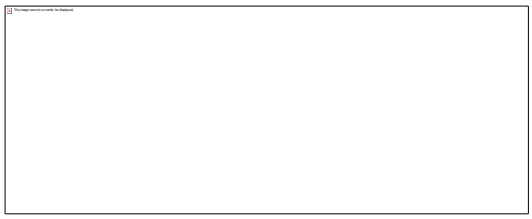

Yield 44%, yellow solid; IR 3387, 1603, 1505, 1470 cm^{-1}; ^{1}H NMR (CD_3OD) δ 1.37-1.42 (m, 1H), 1.44 -1.49 (m, 1H), 2.42 (ddd, *J* = 3.2, 6.3, 9.7 Hz, 1H), 2.89-2.93 (m, 1H), 3.16 (br s, 4H), 3.66 (br s 2H), 3.94 (br s 2H), 7.03-7.13 (m, 4H), 7.28 (d, *J* = 7.6 Hz, 2H), 7.42 (d, *J* = 7.8 Hz, 2H); ^{13}C NMR (CD_3OD) δ 14.5, 22.4, 32.4, 54.9, 68.0, 117.7, 122.3, 126.6, 127.9, 128.4, 128.9, 134.3, 135.9, 142.6, 156.6 (d, J_{F-C} = 245.8 Hz), 172.19; HRMS (ESI) *m/z* calcd. for $C_{20}H_{23}F_1N_3O$ $[M+H]^+$ 340.1820, found 340.1821. Purity 96%.

4.27

2-(4-(4-(±)-*trans*-2-aminocyclopropyl)benzoyl)piperazin-1-yl)benzonitrile hydrochloride

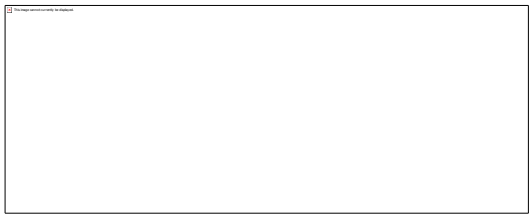

Yield 39%, white solid; IR 3353, 2856, 2221, 1632, 1562 cm^{-1}; ^{1}H NMR (CD_3OD) δ 1.38-1.42 (m, 1H), 1.44-1.51 (m, 1H), 2.40-2.45 (m, 1H), 2.92 (ddd, *J* = 4.2, 8.0, 11.0 Hz, 1H), 3.18 (br s, 2H), 3.56-3.59 (m, 1H), 3.64-3.68 (m, 3H), 3.71-3.74 (m, 2H), 3.95 (br s, 1H), 7.14 (t, *J* = 7.4 Hz, 1H), 7.19 (d, *J* = 8.2 Hz, 1H), 7.29 (d, *J* = 8.0 Hz, 2H), 7.43 (d, *J* = 8.0 Hz, 2H), 7.57-7.61 (m, 1H), 7.65 (dd, *J* = 2.07, 9.06 Hz, 1H); ^{13}C NMR (CD_3OD) δ 14.2, 22.4, 32.2, 43.7, 62.2, 107.7, 119.1, 120.6, 124.0, 127.7, 128.7, 135.1, 135.3, 135.4, 142.3, 156.6, 172.3; HRMS (ESI) *m/z* calcd. for $C_{21}H_{23}N_4O$ $[M+H]^+$, 347.1866, found 347.1869. Purity 96%.

8.5.2. Biology evaluation Chapter 4

All the AML work was conducted under supervision of Dr. Stuart Rushworth at the Biomedical Research Centre, University of East Anglia. Dr. Stuart conducted the $CD34^+$ cells preparation whereas I performed the flow cytometry evaluations. LNCaP viability measurements following LSD1 inhibitors treatment was performed by Dr. Simon Crabb's research group at the University of Southampton, Cancer Research UK. The procedures for LNCaP cells culturing and cell viability are reported in Chapter 2.

8.5.2.1. Cell viability experiments

For cytotoxicity assays, 100 µL of cells suspension was plated at a density of 5×10^4 cells/mL in 96 well plates. Drugs (250 mM stock) were dissolved to the appropriate concentration in RPMI complete medium (10×final concentration) and 10 µL of each concentration was immediately added to the plated cells. Each condition was repeated five times. After treatment, cells were cultured for the reported amount of time. Cell viability was then measured using CellTiter-Glo® (Promega, Southampton, UK) by adding 100 µL of the reagent to each well. After 10 min of incubation at rt, 100 µL of cell suspension + reagent were transferred into a white GREINER 96 well plate to eliminate stray light. Bioluminescence was recorded in a BMG Cellstar microplate reader. The raw data collected were normalised to control (vehicle control).

For the initial evaluation with TCP, the concentrations used were:

1 µM, 3 µM, 10 µM, 30 µM and 100 µM. Cells were cultured for 48 h and 72 h. After the appropriate interval, viable cells were analysed with CellTiter-Glo®. Luminescence values were normalised to pre-treatment levels and statistical significance was determined with two-way ANOVA and corrected for multiple comparisons using Dunnett's test.

For two-dose analyses, enzymatically active compounds were tested after 72 h treatment, while compounds **4.10** and **4.11** were tested at 24 h, 48 h, 72 h and 120 h. Cell viability was then measured using CellTiter-Glo®. Statistical significance was determined as above.

To obtain dose-response curves, cells were treated with the appropriate compounds at 10 µM, 3 µM, 1 µM, 0.3 µM, 0.1µM, 0.03 µM, 0.01 µM,0.003 µM and 0.001 µM concentrations. luminescence values were normalised to pre-treatment levels and data fitted with a nonlinear regression model using GraphPad Prism 6.

8.5.2.2. Washout experiment

In a 96 well plate, 100 µL of THP-1, HL-60, MV4-11, KASUMI, OCI-AML3 and U937 cells suspension were plated at a density of 5×10^4 cells/mL and treated with 10 µL of LSD1 inhibitors (200 nM final concentration) **4.10**, **4.11** and **4.14** or left untreated. Cells were allowed to grow for 6 h and after that time, inhibitor-containing medium was removed by centrifugation and replaced with fresh media (inhibitor-free). Cells were further cultured for 72 h and then viable numbers measured using CellTiter-Glo®. Viability values obtained were normalised to pre-treatment levels (vehicle control) and data obtained during continuous and pulsed treatment were statistically analysed. Statistical significance was determined with one-way-ANOVA and corrected for multiple comparisons using Dunnett's test.

8.5.2.3. SDS-PAGE and Immunoblotting

Solutions and buffers

- **10% APS:** 23 mg ammonium persulfate crystal were dissolved in 230 µL ddH_2O. The solution was stored at 4 ˚C.
- **4% (w/v) SDS:** 4 g of SDS were dissolved in 90 mL of ddH_2O with gentle stirring and brought to a final volume of 100 mL with ddH_2O.
- **10% (w/v) SDS**: 10 g of SDS were dissolved in 90 mL of ddH_2O with gentle stirring and brought to a final volume of 100 mL with ddH_2O.
- **1.5 M Tris-HCl, pH 8.8**: 27.23 g of Tris-base (18.15 g/100 mL) were dissolved in 80 mL of ddH_2O. The pH was adjusted to 8.8 with 6 N HCl. Total volume was brought to 150 mL with ddH_2O and the solution stored at 4 ˚C.
- **0.5 M Tris-HCl, pH 6.8:** 6 g of Tris-base were dissolved in 60 mL of ddH_2O with gentle stirring. pH was adjusted to 6.8 with 6 N HCl. Total volume was brought to 100 mL with ddH_2O and the solution stored at 4 ˚C.
- **1×TBS:** 6.05 g of Tris Base and 8.76 g of NaCl were dissolved in 800 mL of ddH_2O. The pH was adjusted to 7.5 with 1 M HCl. The volume was brought to 1 L with ddH_2O. TBS was kept at 4 ˚C.
- **20×TBST:** 48.4 g of Tris-base, 160 g NaCl, 62 mL of 5 M HCl, 20 mL Tween® 20, were dissolved in 1 L of ddH_2O (final volume). The pH was adjusted to 8.6 with 6 N HCl and the solution was stored at rt.
- **5×SDS running buffer (1 L):** 30.0 g of Tris-base, 140 g of glycine and 5 g of SDS were dissolved in 1 L of ddH_2O. The pH was adjusted to 8.3 and the solution stored at 4 ˚C.
- **1×SDS transfer buffer (1 L):** 3.0 g of Tris-base, 14.4 g of Glycine were dissolved in 900 mL of ddH_2O. Then, 100 mL of MeOH were added before use. Transfer buffer was used at 4 ˚C and prepared fresh for each experiment.
- **2×SDS loading buffer:** 1.52 g of Tris-base, 20 mL of glycerol, 2.0 g SDS, 2.0 mL β-mercaptoethanol and 1 mg Bromphenol Blue were added to 40 mL of ddH_2O. The pH was adjusted to pH 6.8 with 1N HCl. After gentle stirring, the volume was brought to 100 mL. The solution was stored at 4 ˚C.

- **14% SDS polyacrylamide gel (resolving gel), recipe for two gels:**

4.2 mL ddH_2O, 7.47 mL 30 % acrylamide (BIORAD), 160 µL of 10% SDS, 160 µL 10% APS and 16 µL Tetramethylethylenediamine (TEMED) were mixed and gently vortexed. For each polyacrylamide gel we used ± 5 mL of gel mix.

- **5% Stacking gel for each gel:** 2 mL of 30% acrylamide mix, 3 mL of 0.5 M Tris-HCl (pH 6.8), 0.12 mL of 10% (w/v) SDS and 6.76 mL of ddH_2O were mixed and gently vortexed.
- **Stripping buffer (1 L):** 15 g of glycine, 1 g of SDS and10 mL of Tween 20® were disolved in 1 L of ddH_2O. The pH was adjusted to 2.2 with 1 N HCl.

Antibodies

Antibodies for immunoblotting were purchased from Cell Signalling (anti-H3K4me2 #9725) or Abcam (anti-H3 ab100938, and Goat anti-Rabbit IgG (HRP) ab97080). The antibodies from Cell signalling were diluted to 1:1000 in 3% Bovine serum albumin (BSA) dissolved in TBST (w/v); the antibodies from Abcam were diluted 1:5000 (primary) or 1:10000 (secondary) in 3%BSA dissolved in TBST.

Cell preparation

KASUMI cells suspension was plated in a 24 well plate at a concentration of 25×10^5 cells/mL (1 mL /well). Stock of **4.11** (1 µL, 200 µM), prepared in complete RPMI medium, was added to the plated cells for a final concentration of 200 nM. Cells were cultured for 2 h, 4 h, 6 h, 48 h and 72 h. After the appropriate time-course, the cell culture plate with the treated cells was placed on ice and cells harvested. The wells were washed repeated with cold PBS to ensure the collection of all the cells in the well. Cells were then centrifuged at 16,000 rpm for 20 min at 4 ˚C and maintained on ice through the procedure. The cells pellet was re-centrifuged briefly to discard any remaining supernatant. To each sample, 50 µL of 1×SDS loading buffer were added and after a gentle mix, the samples were sonicated 3 times for 10-15 seconds each at level 3 in an ultrasonic bath SW3H (Fisher). Cellular proteins were maintained at -20 ˚C until electrophoresis and heated in a heating block for 10 min at 95 ˚C prior to use. After heating, samples were centrifuged at 16,000 rpm in a microcentrifuge for 1 min.

Gel electrophoresis

Protein lysates were separated by electrophoresis using a sodium dodecyl sulfate-polyacrylamide gel (SDS-PAGE) on a mini (8.6×6.7 cm) format SDS-PAGE gel (BIORAD) along with 8 µL of molecular weight marker (Fisher) that served as the ladder. Gel electrophoresis was run at 80 V for 20 min for stacking gel and 150 V (constant) for the resolving gel (60-70 min).

Immunoblotting

After electrophoresis, gels were placed in 1×transfer buffer for 10 min and proteins were transferred from the gel to a polyvinylidene difluoride (PVDF) membrane (GE healthcare) with 0.2 µm pore size. Prior to the use, the membrane was soaked for 1 min in MeOH and then equilibrated for 5 min in transfer buffer. The protein transfer was carried out on ice at 300 mA for 100-120 min, in a BIORAD Trans-Blot® system with continuous stirring. After the transfer, the blotting membrane was washed briefly with TBST and blocked for 1 h at rt with 3% BSA (w/v%) in TBST and incubated overnight with the primary Ab. The membrane was washed with TBST repeatedly for a total of five washes (five minutes/wash) to remove excess primary Ab and this was followed by an incubation with secondary Ab conjugated with horse-readish peroxidase. Detection was performed with Chemoluminescent substrate (Western Pico Super ECL reagent, Pierce) 2 mL per membrane and the bands of interest were visualised on an ImageQuant™ LAS 4000 Image Analyser.

Stripping for re-probing

For loading control, the membrane was re-probed for H3 (total), after a stripping procedure following Abcam protocol.

Stripping procedure

The stripping buffer (20 mL×membrane) was incubated with the memebrane for 10 min (twice). The membrane was then washed for 10 min with PBS (twice) and five minutes with TBST (twice). The membrane was blocked with 3% BSA and the remaining steps were performed as described above.

8.5.2.4. Flow-cytometry

Flow cytometry was performed in a BD Accuri™ C6 Flow Cytometer and data analysed using BD Accuri™ C6 Software version 1.0.264.15. Antibodies for CD86, CD14, CD11b and CD34 or Isotype controls were purchased from Myltenyi Biotec.

CD86 expression

Cells were plated at a concentration of 25×10^4 cells/mL (1 mL) in a 24 well plate. The plated cells were treated with 1 µL of 200 µM stock of **4.10**, **4.11** and **4.14** prepared in complete RPMI media to achieve a final concentration of 200 nM, or left untreated (vehicle control). Cells were further cultured for 24 h, 48 h and 72 h. After the appropriate time-course, 250 µL of treated and untreated cell samples were centrifuged for 4 min at 1000 rpm in a pre-cooled centrifuge (4 ˚C). The supernatant was discarded and cell pellet was washed twice with filtered PBS (0.2 µm filter), and re-centrifuged. Any remaining supernatant was discarded. To the treated samples, 2 µL of anti-CD86 fluorescent isothiocyanate (FITC) conjugated Ab (clone FM95) diluted in 100 µL of PBS were added whereas to the untreated sample, 2 µL of FITC-conjugated human IgG diluted in 100 µL of PBS were added. Samples were incubated with the Abs for 20 min in the dark at 4 ˚C and washed with ice cold PBS to remove excess Abs. Samples were centrifuged at 1000 rpm for 4 min in a pre-cooled centrifuge (4 ˚C). Washing was repeated twice and any remaining supernatant discarded. To each pellet, 100 µL of filtered PBS were then added and the fluorescence examined by flow cytometry. The % of fluorescence increase compared to control (untreated cells, stained with , IgG1 control) was recorded in three independent experiments and analysed using GraphPad Prism 6. Statistical significance was determined with two-way ANOVA and corrected for multiple comparisons with Bonferroni's test.

CD11b-CD14 expression

Cells were plated at a concentration of 25×10^4 cells/mL (1 mL) in a 24 well plate. The plated cells were treated with 1 µL of 200 µM stock of **4.10** or **4.11**, prepared in complete RPMI media (final concentration of 200 nM) or left untreated. Cells were cultured for 48 h. Next, 250 µL of each sample was centrifuged for 4 min at 1000 rpm in a pre-cooled centrifuge (4 ˚C). The supernatant was discarded and the cell pellet was washed twice with filtered PBS and re-centrifuged. Cells were then co-stained with 2 µL of anti-CD14 (FITC- conjugated) and 2 µL of anti-CD11b (phycoerythrin -PE conjugated) diluted in 100 µL of PBS. Untreated samples were co-stained with irrelevant antibodies (Isotype controls, FITC-conjugated mouse IgG or PE conjugated) also diluted in 100 µL of PBS. Samples were incubated for 20 min in the dark and excess Abs were washed with ice cold PBS. Samples were centrifuged at 1000 rpm for 4 min in a pre-cooled centrifuge (4 ˚C). Washing was repeated twice and any residual supernatant discarded. To each sample, 100 µL of filtered PBS was added and the fluorescence analysed by flow cytometry. The % increase in fluorescence compared to control (untreated cells, stained with Isotype controls) was recorded in three independent experiments and analysed using GraphPad Prism 6. Statistical significance was determined with two-way ANOVA and corrected for multiple comparisons with Bonferroni's test.

CD34+ expression

Hematopoietic $CD34^+$ cells were isolated from AML patient's volunteers following informed consent. $CD34^+$ cells were isolated from bone marrow mononucleate cells using human $CD34^+$ MicroBead selection kit (Miltenyi Biotec). $CD34^+$ cells were incubated with increasing concentration of **4.10** and **4.11** and the cells were further cultured for 48 h and 72 h. $CD34^+$ cells were treated as above and stained with anti CD34 FITC conjugated antibody (clone 8G12). The number of cells expressing the CD34 surface marker were counted using BD Accuri™ C6 Software. For $CD34^+$ experiments, at least 3 different donor samples were used to obtain the results presented. Cell type was confirmed by microscopy and flow cytometry. Statistical significance was determined with one-way ANOVA and corrected for multiple comparisons with Dunnett's test.

8.6. Experimental procedures Chapter 5

Procedures for the synthesis of compounds are the same as the ones reported for Experimental procedures in Chapter 4.

5.1
tert-butyl-(±)-*trans*-2-(4-phenethyl carbamoyl)phenylcyclopropyl carbamate

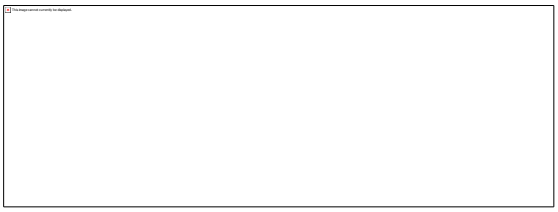

Yield: 63%, white solid; IR 3393, 3376, 1701, 1681, 1516 cm^{-1}; ^{1}HNMR ($CDCl_3$) δ 1.17-1.20 (m, 2H), 1.44 (s, 9H), 2.05 (td, *J*=3.0, 7.7 Hz, 1H), 2.68-2.77 (m, 1H), 2.92 (t, *J*=7.0 Hz, 2H), 6.73 (q, *J*=7.2 Hz, 2H), 4.87 (br s, 1H), 6.08 (br s, 1H), 7.13 (d, *J*=8.1 Hz, 2H), 7.21-7.24 (m, 3H), 7.39-7.34 (m, 2H), 7.58 (d, *J*=8.4 Hz, 2H); ^{13}CNMR ($CDCl_3$) δ 16.8, 22.1, 28.5, 33.1, 35.8, 41.2, 80.8, 125.39, 125.5, 125.8, 127.6, 127,76, 131.21, 137.9, 143.6, 156.7, 166.2; HRMS *m/z* calcd for $C_{23}H_{29}N_2O_3$ $[M+H]^+$ 381.2173, found 381.2173. Purity 98%.

5.2
tert-butyl (±)-*trans*-2-(4-(2-thiophenethyl carbamoyl)phenylcyclopropyl carbamate

Yield 51%, white solid; mp; 94 ˚C; IR: 3358, 3334.72, 1685, 1448.65 cm^{-1}; ^{1}HNMR ($CDCl_3$) δ 1.61-1.19 (m, 2H), 1.43 (s, 9H), 2.02-2.05 (m, 1H), 2.68-2.76 (m, 1H), 3.06 (t, *J*= 6.4 Hz, 2H), 3.62 (q, *J*=6.4 Hz, 2H), 4.93 (br s, 1H), 6.33 (br s, 1H), 6.83-6.87 (m, 1H), 6.95 (dd, *J*=3.4, 4.9 Hz, 1H), 7.10-7.16 (m, 3H), 7.61 (d, *J*=8.3 Hz, 2H); ^{13}CNMR ($CDCl_3$) δ 15.5, 23.9, 27.5, 28.9, 31.8, 40.12, 78.6, 122.9, 124.3, 125.3, 125.8, 125.9, 131.0, 140.2, 143.6, 155.1, 166.13; HRMS *m/z* calcd $C_{21}H_{27}N_2O_3S$ $[M+H]^+$ 387.1737, found 387.1737. Purity 99%.

5.4
tert-butyl-(±)-*trans*-2-phenylcyclopropyl) carbamate

Yield 72%, white solid; ^{1}HNMR ($CDCl_3$) δ**:** 1.12-1.19 (m, 2H), 1.45 (s, 9H), 2.03 (ddd, *J*=2.9, 6.3, 9.4 Hz, 1H), 2.71-2.74 (m, 1H), 7.12 (d, *J*=8.04 Hz, 2H), 7.17 (d, *J*=7.2 Hz, 2H), 7.23-7.27 (m, 1H).

The spectroscopic data are consistent with that[175] reported in the literature.

5.5
tert-butyl-(±)-*trans*)-2-(4-(benzylcarbamoyl) phenyl)cyclopropyl carbamate)

Yield 67%, white solid; ^{1}HNMR ($CDCl_3$) δ 1.20-1.24 (m, 2H), 1.46 (s, 9H), 2.06-2.11 (m, 1H), 2.74-2.79 (m, 1H), 4.65 (d, *J* = 6.4 Hz, 2H), 6.40 (br s, 1H), 7.8 (d, *J* = 8.7 Hz, 2H), 7.29-7.35 (m, 1H), 7.46-7.39 (m, 4H), 7.14 (d, *J* = 7.8 Hz, 2H); ^{13}CNMR ($CDCl_3$) δ 14.4, 16.9, 23.0, 28.7, 44.1, 68.0, 126.5, 127.0, 127.7, 128.0, 129.0, 132.0, 138.4, 144.9, 156.2, 167.1. ES^+ MS *m/z* 367 $[M+H]^+$.

The compound is reported in the literature,[178] although characterisation data are not provided. For the compound was not possible to achieve the HRMS data.

5.6
tert-butyl (±)-*trans*-2-(4-(2-(1*H*-indol-3-yl) ethyl)carbamoyl)phenylcyclopropyl carbamate

Yield 47%, pale yellow solid; mp 120 ˚C; IR 3372, 3314, 1528 cm^{-1};

^{1}HNMR ($CDCl_3$) δ 1.14-1.19 (m, 2H), 1.45 (s, 9H), 2.00-2.06 (m, 1H), 2.65-2.66 (m, 1H), 3.05 (t, *J*=7.04 Hz, 2H), 3.75 (q, *J* = 6.5 Hz, 2H), 6.31 (br s, 1H), 6.9 (br s, 1H), 7.06 (d, *J* = 7.8 Hz, 2H), 7.11 (t, *J* = 7.0, 1H), 7.19 (t, *J* = 7.0, 1H), 7.36 (d, *J* = 8.3 Hz), 7.5 (d, *J* = 8.3 Hz, 2H), 7.62 (d, *J* = 7.8 Hz, 1H), 8.4 (br s, 1H); ^{13}CNMR ($CDCl_3$) δ 14.5, 16.6, 21.0, 25.2, 28.5, 40.3, 80.0, 111.4, 112.9, 118.6, 119.6, 122.2, 122.4, 126.3, 127.0, 127.4, 132.4, 136.5, 144.7, 156.3, 167.3; HRMS *m/z* calcd. $C_{25}H_{30}N_3O_3$ $[M+H]^+$ 420.2282, found 420.2284. Purity 98%.

4.6a

Methyl 4-(±)-*trans* -2-((ethoxycarbonyl) amino)cyclopropyl)benzoate

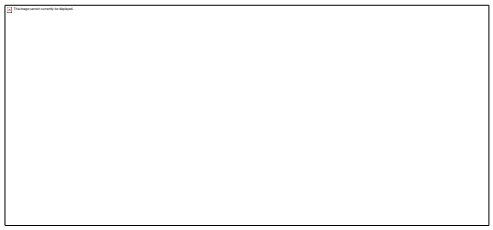

Yield 57%; white solid; IR 3324, 1718, 1684, 1614, 1522 cm^{-1}; ^{1}H NMR ($CDCl_3$) δ 1.22-1.29 (m, 5H), 2.11 (ddd, *J* = 3.2, 6.5, 9.4 Hz, 1H), 2.75-2.82 (m, 1H), 3.90 (s, 3H), 4.13 (q, *J* = 7.0 Hz, 2H), 4.97 (br s, 1H), 7.17 (d, *J* = 8.3 Hz, 2H) 7.93 (d, *J* = 8.3, 2H); ^{13}C NMR ($CDCl_3$) 14.6, 16.8, 33.3, 41.1, 52.2, 61.7, 126.3, 127.8, 129.5, 146.0, 155.8, 166.7; ES^+ MS *m/z* 264 $[M+H]^+$.

The compound is reported in the literature,[178] although characterisation data are not provided. For this compound was not possible to achieve HRMS data.

4.7a

4-(±)-*trans*-2-(ethoxycarbonyl-amino) cyclopropyl)benzoic acid

Yield 64%; white solid; IR 3318, 3012, 1730, 1533 cm^{-1}; ^{1}H NMR (CD_3OD) δ 1.21-1.28 (m, 5H), 2.1 (ddd, *J* = 3.2, 7.0, 10.8 Hz, 1H), 2.74-2.78 (m, 1H), 4.13 (q, *J* = 7.0 Hz, 2H), 4.08 (q, *J* = 7.0 Hz, 2H), 7.21 (d, *J* = 8.4 Hz, 2H) 7.93 (d, *J* = 8.4 Hz, 2H); ^{13}C NMR (CD_3OD) δ 14.6, 16.8, 34.2, 42.1, 61.7, 127.2, 128.7, 129.7, 130.6, 148.6, 159.7, 168.4; HRMS *m/z* calcd. for $C_{13}H_{16}N_1O_4$ $[M+H]^+$ 250.1074, found 250.1077.

The compound is reported in the literature,[178] although characterisation data are not provided.

5.7
ethyl-(±)-*trans*-2-(4-(phenethylcarbamoyl)phenyl)cyclopropylcarbamate

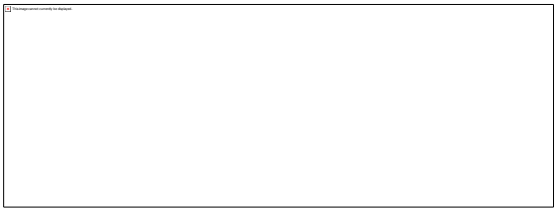

Yield: 54%, white solid; IR: 3312, 3191, 1689, 1637, 1545, 1510 cm^{-1}; ^{1}H NMR ($CDCl_3$) δ 1.20-1.27 (m, 5H), 2.07-2.11 (m, 1H), 2.72-2.76 (m, 1H), 2.92 (t, *J* = 6.9 Hz, 2H), 3.69 (q, *J* = 6.9, Hz, 2H), 4.12 (q, *J* = 6.9 Hz, 2H), 7.14 (d, *J* = 7.9 Hz, 2H), 7.19-7.24 (m, 3H), 7.28-7.34 (m, 2H), 7.58 (d, *J* = 7.8 Hz, 2H); ^{13}C NMR ($CDCl_3$) δ 14.6, 16.4, 25.2, 33.1, 35.7, 41.1, 61.0, 126.6, 126.7, 126.9, 128.7, 128.8, 132.4, 138.8, 144.4, 157.1, 167.2; HRMS *m/z* calcd. for $C_{21}H_{25}N_2O_3$ $[M+H]^+$ 353.1860, found 353.1860. Purity 98%.

5.8
ethyl(±)-*trans*-2-(4-(2-(*th*iophenethyl)carbamoylphenyl)cyclopropyl carbamate

Yield 49%; white solid; IR 3318, 3214, 1689, 1655, 1551, 1510 cm^{-1}; ^{1}H NMR ($CDCl_3$) δ 1.20-1.23 (m, 5H), 2.06-2.10 (m, 1H), 2.70-2.74 (m, 1H), 3.13 (t, *J* = 6.5 Hz, 2H), 3.69 (q, *J* = 7.04 Hz, 2H), 4.11 (q, *J* = 6.5 Hz, 2H), 6.85 (dd, *J* = 0.9, 3.3 Hz, 1H), 6.94 (dd, *J* = 3.4, 5.1 Hz, 1H), 7.13-7.17 (m, 3H), 7.61 (d, *J* = 8.1 Hz, 2H); ^{13}C NMR ($CDCl_3$) δ 14.6, 16.4, 25.2, 29.9, 33.1, 41.3, 61.0, 124.1, 125.5, 126.6, 127.0, 127.1, 132.3, 141.3, 141.5, 157.1, 167.2; HRMS *m/z* calcd. $C_{19}H_{23}N_2O_3S$ $[M+H]^+$ 359.1424, found 359.1425. Purity 98%.

8.6.1. Biological evaluation

General procedures for biological experiments are reported in Chapter 4.

Enzymatic assay protocol is reported in Chapter 3, whereas the procedures for cell viability using CellTiter-Glo®, washout, Western blot, CD11b-CD14, CD86 and CD34 analyses are reported in Chapter 4.

Cell viability on prostate cancer lines was performed in the laboratory of Dr. Wafa Al-Jamal at University of East Anglia, Pharmacy department. Cell viability on myeloma cell lines were performed at Biomedical Research Centre, University of East Anglia in the laboratory of Prof. Kristian Bowles.

8.6.1.1. Cell viability on prostate cancer lines (MTT assay)

Briefly, LNCaP, PC3 and DU145 cells were trypsinised, stained with Trypan Blue (0.4 %, 1:1) and counted using a hemocytometer. Cells were then seeded in 96-well plates (LNCaP 1.5×10^4 cells/well, PC3 and DU145 9×10^3 cells/well) in complete medium 24 h prior incubation. The following day, **4.11** stock (100 mM) diluted in complete medium was added to the cells. Untreated cells were used as a 100 % viability control. After 72 incubation, cells were incubated with MTT solution at 0.84 mg/mL final concentration for 2 h. Formazan crystals were dissolved in 200 µL DMSO and absorbance was read at 560 nm using FLUOstar Omega [BMG Labtech (UK)] plate reader. Six replicates per condition were used. The results were expressed as the % of cell viability (average ± SD) and normalised to control cells (pre-treatment levels).

8.7. Experimental procedures Chapter 6

6.2

4-(hex-5-yn-1-yloxy) benzaldehyde[347]

To solution of 4-hydroxybenzaldehyde **6.1** (5 g, 40.9 mmol, 1 equiv.) in anhydrous DMF (60 mL), 6-chloro-hex-1-yne (7.1 g, 7.4 mL, 61.4 mmol, 1.5 equiv.), KI (3.4 g, 20.5 mmol, 0.5 equiv.) and K_2CO_3 (11.3 g, 81.8 moles, 2 equiv.) were added with stirring. The mixture was heated at 80 ˚C and stirred for 3 days. After cooling to rt, the reaction mixture was diluted in EtOAc (375 mL) washed with H_2O (175 mL× 3) and brine (125 mL×3). The organic layers were combined and dried over $MgSO_4$. After filtration, the organic layers were concentrated *in vacuo* and precipitated in diethyl ether and hexane to give **6.2** (7.2 g, 35.6 mmol, 87%) as a white crystalline solid: ^{1}H NMR ($CDCl_3$) δ 1.70-1.77 (m, 2H), 1.92-1.99 (m, 3H), 2.30 (td, *J*=2.5, 6.5 Hz 2H), 4.08 (t, *J*= 6.7 Hz, 2H), 6.99 (d, *J*=8.5 Hz, 2H), 7.83 (d, *J*=8.6 Hz, 2H), 9.88 (s, 1H); HRMS (ESI) *m/z* calcd. for $C_{13}H_{15}O_2$ $[M+H]^+$ 203.1067, found 203.1065;
The spectroscopic data are consistent with that[347] previously reported.

6.3

(*E*)-ethyl 3-(4-(hex-5-yn-1-yloxy) phenyl) acrylate[177]

Triethyl phosphonoacetate (8.1 g, 7.2 mL, 36.2 mmol, 1.1 equiv.) was added dropwise over 15 min to a stirring suspension of KO*t*-Bu (4.06 g, 36.2 mmol, 1.1 equiv.) in anhydrous THF (100 mL) at -5 ˚C; the mixture was stirred for 45 min. After that time, **6.2** (7.2 g, 33.2 mmol) previously dissolved in anhydrous THF (35 mL), was added dropwise to the stirring reaction. The reaction was warmed to rt and allow stirring for

further 16 h. After completion, the reaction mixture was poured into iced H_2O (100 mL) and extracted with EtOAc (100 mL×3). The organic layers were combined, and washed with sat. $NaHCO_3$ (100 mL), H_2O (100 mL) and brine (100 mL) and dried over $MgSO_4$. Concentration *in vacuo* afforded **6.3** (9.7 g, 98%) as a white solid. The compound was used in the next step without further purification: ^{1}H NMR ($CDCl_3$) δ 1.33 (t, *J*=7.5 Hz, 3H), 1.68-1.75 (m, 2H), 1.68-1.93 (m, 2H), 1.97 (t, *J*=2.48 Hz, 1H), 1.33 (td, *J*=2.1, 7.0 Hz, 2H), 4.0 (t, *J*=6.3 Hz, 2H), 4.24 (q, *J*=7.2, 2H), 6.3 (d, *J*=16.4 Hz, 1H), 6.8 (d, *J*=8.7 Hz, 2H), 7.45 (d, *J*=8.7 Hz, 2H), 7.63 (d, *J*=16.0 Hz, 1H); ^{13}C NMR ($CDCl_3$) δ 14.4, 18.1, 24.9, 28.2, 60.3, 67.4, 68.7, 83.9, 115.4, 116.0, 127.1, 129.7, 144.3, 160.7, 167.4; HRMS (ESI) ***m/z*** calcd. for $C_{17}H_{21}O_3$ $[M+H]^+$ 273.1485, found 273.1487.

6.4

(±)-*trans*-ethyl2-(4-(hex-5-yn-1-yloxy)phenyl)cyclopropanecarboxylate[172]

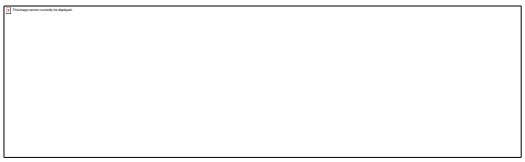

Trimethyl sulfoxomium iodide (11.7 g, 53.3 mmol, 1.2 equiv.) was added in small portions to a suspension of NaH (2.13 g, 53.3 mmoles, 60% in mineral oil, 1.21 equiv), in dry DMSO (45 mL) and the stirred for 45 min. The olefin **6.3** (9.6 g, 44.4 mmol, 1 equiv.) was then added dropwise with mixing and the reaction stirred at rt overnight. After completion, the reaction mixture was poured into iced H_2O (70 mL) and extracted with EtOAc (70 mL×10). The organic phases (700 mL) were combined and washed with sat. $NaHCO_3$ (200 mL) H_2O (200 mL), brine (200 mL) and dried over $MgSO_4$. Purification with silica gel column chromatography (Hexane/EtOAc, 8:2) afforded **6.3** as a white solid (4.9 g, 39%):^{1}H NMR ($CDCl_3$) δ 1.23-1.29 (m, 3H), 1.52-1.57 (m, 1H), 1.67-1.74 (m, 2H), 1.81 (ddd, *J*=4.1, 5.4, 8.1 Hz, 2H), 1.85-1.92 (m, 2 H), 1.96 (t, *J*=2.84 Hz, 1H), 2.27 (td, *J*=2.8, 7.4 Hz, 2H), 2.48 (ddd, *J*=4.3, 6.8, 9.5 Hz, 1H), 3.95 (t, *J*=6.0 Hz, 2H), 4.16 (q, *J*=7.1 Hz, 2H),6.80 (d, *J*=8.3 Hz, 2H), 7.0 (d, *J*=8.3 Hz, 2H); ^{13}C NMR ($CDCl_3$) δ 14.3, 16.7, 18.1, 23.6, 25.0, 25.8, 28.2, 60.6, 67.3, 68.6, 84.0,

114.5, 127.4, 131.8, 157.7, 174.02; HRMS (ESI) *m/z* calcd. for $C_{18}H_{23}O_3$ $[M+H]^+$ 287.1642, found 287.1645.

6.5
(±)-*trans*-2-(4-(hex-5-yn-1-yloxy)phenyl)cyclopropanecarboxylic acid

Compound **6.4** (4.9 g, 17.1 mmol) was taken up in aqueous NaOH (2 M, 8 mL) and MeOH (8 mL). The reaction was monitored by TLC and after 3 h, the solution was acidified with 2 N HCl and the salt filtration afforded compound **6.4** (4.3 g, 98%), as a white solid. The compound was used in the following step without purification: IR 3283, 1701, 1513 cm^{-1}; ^1H NMR (CD_3OD) δ 1.10-1.15 (m, 1H), 1.38-1.43 (m, 1H), 1.63-1.61 (m, 3H), 1.82-1.90 (m, 1H), 2.19-2.27 (m, 3H), 2.32 (ddd, *J*=4.3, 6.1, 9.5 Hz, 1H), 3.9 (t, *J*=6.4 Hz, 2H), 6.8 (d, *J*=8.5 Hz, 2H), 7.02 (d, *J*=8.5 Hz, 2H). ^{13}C NMR (CD_3OD) δ 16.8, 18.9, 25.9, 26.4, 26.9, 29.5, 68.5, 69.7, 84.7, 115.5, 120.3, 128.1, 134.1, 143.2, 158.9; HRMS (ESI) *m/z* calcd. for $C_{16}H_{17}O_3$ $[M-H]^-$ 257.1183, found 257.1181.

6.7
(±)-*trans*-2-(4-(hex-5-yn-1-yloxy)phenyl)cyclopropanamine

The acid **6.5** (4.3 g, 16.6 mmol, 1 equiv.), diphenylphosphoryl azide (5.0 g, 3.93 mL, 16.6 mmol, 1.1 equiv.) and triethylamine (2.5 g, 3.5 mL, 24.9 mmol, 1.5 equiv.) were combined in *tert*-butanol (50 mL) under argon, heated at reflux (80 ˚C) and allowed to react for 72 h. After that time, the reaction was cooled to rt and then diluted with EtOAc (70 mL) and washed with saturated Na_2CO_3 solution (100 mL×2). The organic layer was separated and the aqueous layer further extracted with EtOAc (70 mL). The

organics layers were combined (140 mL), washed with sat. $NaHCO_3$, (100 mL), H_2O (100 mL) and brine (100 mL) and dried over $MgSO_4$. The crude product was concentrated *in vacuo* to afford a browm oil which was purified by colum chromatography (Hexane/EtOAc, 8:2). Intermediate **6.6** (2.6 g, 8 mmol, 49%) was obtained as a pale yellow solid and treated with 4 N HCl aqueous (7 mL) overnight with cooling. The deprotected amine was co-evaporated with acetonitrile and purified by preparative RP-HPLC. Purification afforded **6.7** as a pale yellow solid (1.6 g, 78%): IR 3297, 2348,1600, 1512, 1454 cm^{-1}; ^1H NMR (CD_3OD) δ 1.22-1.29 (m, 1H), 1.30-1.37 (m, 1H), 1.63-1.71 (m, 2H), 1.82-1.90 (m, 2H), 2.20-2.26 (m, 3H), 2.30 (ddd, *J*=3.5, 6.5, 10.2 Hz, 1H), 2.75 (ddd, *J*=3.5, 4.2, 7.1 Hz, 1H), 3.96 (t, *J*=6.3 Hz, 2H), 6.85 (d, *J*=8.5 Hz, 2H), 7.07 (d, *J*=8.5 Hz, 2H); ^{13}C NMR (CD_3OD) δ 13.5, 18.9, 22.1, 26.4, 29.7, 31.8, 68.8, 70.4, 84.7, 115.7, 128.6, 131.6, 159.9; HRMS (ESI) *m/z* calcd. for $C_{15}H_{20}NO$ $[M+H]^+$ 230.1539, found 230.1539. Purity 95%.

8.7.1. Biology and in vitro click chemistry

The procedure for the enzymatic assay with Amplex®Red and cytotoxicity evaluation were performed according to the procedures described for Chapter 4 in this section. MAO enzymatic evaluation was performed in the laboratory of Prof. Haüfe at the University of Münster.

8.7.2. *In situ* labelling of purified human recombinant His-LSD1

8.7.2.1. Cycloaddition reaction, protein electrophoresis and in-gel fluorescence scanning[325]

Human recombinant His-tagged LSD1 stock (0.38 mg/mL) was diluted to 16.5 µg, 3.5 µg in 50 mM Potassium phosphate buffer pH 7.5 (1:1 mix of monobasic and dibasic) in a final volume of 44 µL. The protein was incubated with 10 µL of probe **6.7** or **6.8** (dissolved in phosphate buffer pH 7.5) at concentration of 5 µM and 10 µM for 1 h at rt. After that time, TAMRA-azide (ThermoFisher) (1 µL/reaction, 5 mM stock in DMSO) was added to each sample, followed by 1 mM TCEP (1 µL/reaction, 50 mM stock in dd

H_2O), and 100 µM TBTA (3 µL/reaction, 1.7 mM stock in DMSO:*tert*-BuOH 1:4 (v/v)). Samples were vortexed and 1 mM of $CuSO_4$ (1 µL/reaction, 50 mM stock in H_2O) was added to initiate the 1,3-cycloaddition reactions giving the total reaction volume of 50 µL. Samples were allowed to react at rt for 1 h in a centrifuge (350 rpm). The reaction was quenched with 50 µL 2 × SDS loading buffer and samples denaturated for 5 min at 95 ˚C on a heating block. Labelled protein samples (50 µL sample) were loaded on a 10% polyacrylamide gel along with 10 µL of ladder (PageRuler™ Prestained NIR Protein Ladder) and fluorescence was recorded with ImageQuant™ LAS 4000 Image Analyzer with a Fujinon VRF43LMD3 Lens and a 575DF20 filter. Gels were then subjected to Coomassie Brilliant Blue (Fisher) staining to verify equivalent protein loading.

8.7.2.2. Competition assay

Human recombinant His-tagged LSD1 stock (0.38 mg/mL) was diluted to 16.5 µg, in 50 mM Potassium phosphate buffer pH 7.5 (1:1 mix of monobasic and dibasic) and incubated with probes **6.7** or **6.8** (10 µM) and 200 nM of LSD1 inhibitors **4.10** or **4.11.** After that time, Cycloaddition reaction (using TAMRA-azide) protein electrophoresis and in-gel fluorescence scanning were performed as above.

8.7.2.3. Labelling experiments with AML cells[325]

THP-1, HL-60 and MV4-11 were plated at a concentration of 5×10^6 on Petri dishes (150×25 mm) with complete RPMI 1640 media, 10% FCS, 1% L-glutamine (2mM) and 1% Pens/Strep. Probes **6.7** and **6.8** were diluted at a concentration of 5 µM or 10 µM and added to the plated cells. Cells were allowed to culture for 24 or 72 h (37˚C, 5% CO_2). After that time, cells were transferred on a centrifuge tube and centrifuged at 15000 rpm for 4 min at 4 ˚C. The pellet was washed twice with PBS to remove the excess of probe and any supernatant remaining discarded. To the pelleted cells, 10 mL of PBS was added and cells centrifuged for 1 h at 4 ˚C. Cell pellet was suspended in 500 µL of PBS and lysed by sonication. Soluble and insoluble fractions were separated by centrifugation at 15000 rpm 30 min 4 ˚C. Insoluble pellets were suspended in 500 µL

PBS by sonication under ice cooling. Protein concentration was measured (BCA kit, Thermo Fisher) and adjusted to 2 mg/mL with PBS. The samples (44 µL probe-bound cell lysate) were subjected to CC and SDS-PAGE as described above.

Amplex®Red was used to measure the compounds activity. The details of the experiment are reported in Chapter 3.

.

8.8. Experimental procedures for Chapter 7

The enzymatic evaluations and cell culturing procedures were performed according to the description reported in Chapter 3 and Chapter 4 sections.

Cytotoxicity assay

For cytotoxicity assays, 100 µL of AMLs suspension was plated at a density of 5×10^4 cells/mL in 96 well plates. Drugs (250 mM stock) were dissolved to the appropriate concentration in RPMI complete medium (10× final concentration) and 10 µL of each concentration (0.001 µM, 0.003 µM, 0.1 µM, 0.3 µM, 1 µM, 3 µM, 10 µM and 30 µM) was immediately added to the plated cells. Each condition was repeated five times. After 72 h treatment, cell viability was measured using CellTiter-Glo® (Promega, Southampton, UK) by adding 100 µL of the reagent to each well. After 10 min of incubation at rt, 100 µL of cell suspension + reagent were transferred into a white GREINER 96 well plate to eliminate straight light. Bioluminescence was recorded in a BMG Cellstar microplate reader. The raw data collected were normalised to control (vehicle control) and dose-response curve determined with GraphPad 6.

CD86

1 mL of cell suspension (density 1×10^6) was plated in a 24 well plate and treated with 3 µM of 7.2. Cells were stimulated for 48 h at 37 ˚C in an atmosphere of 5% CO_2. After that time, cells were harvested in ice pelleted at 300 ×g for 10 min at 4 ˚C and the supernatant discarded. The pellet was re-suspended in 100 µL of cold PBS (Phosphate buffer saline, Fisher) and 10µL of CD86-FITC antibody (Miltenyi Biotec) was added. The cells incubated in the dark at 2 ˚C for 10 min. The antibody was then washed with 2 mL of cold PBS and centrifuged at 300 ×g for 10 min at 4 ˚C. The supernatant was aspirated completely and then 1 mL of PBS was added. Samples were analysed by flow cytometry (Becton Dickinsons FACSCalibur I)
Raw data were collected and standard deviation was measured. Result were expressed as the mean of the different experiments and analysed with GraphPad Prism 6.

Western blot

MV4-11 cells suspension was plated in a 24 well plate at a concentration of 25×10^5 cells/mL (1 mL /well). Stock of **7.7** was prepared in complete RPMI medium and was added to the plated cells for final concentrations of 0.3 µM, 1 µM, 3 µM and 6 µM. Cells were cultured for 72 h and then processed as described in Chapter 4. Blotting membranes were probed for H3K4me2, H3 (total) and β-actin (4 µL in 20 mL of 3%BSA). Visualisation was performed as described in Chapter 4.

Appendix

1. NMR spectra

^{1}H NMR SPECTRUM of 4.2

Chemical shift (ppm)

^{1}H NMR SPECTRUM of 4.3

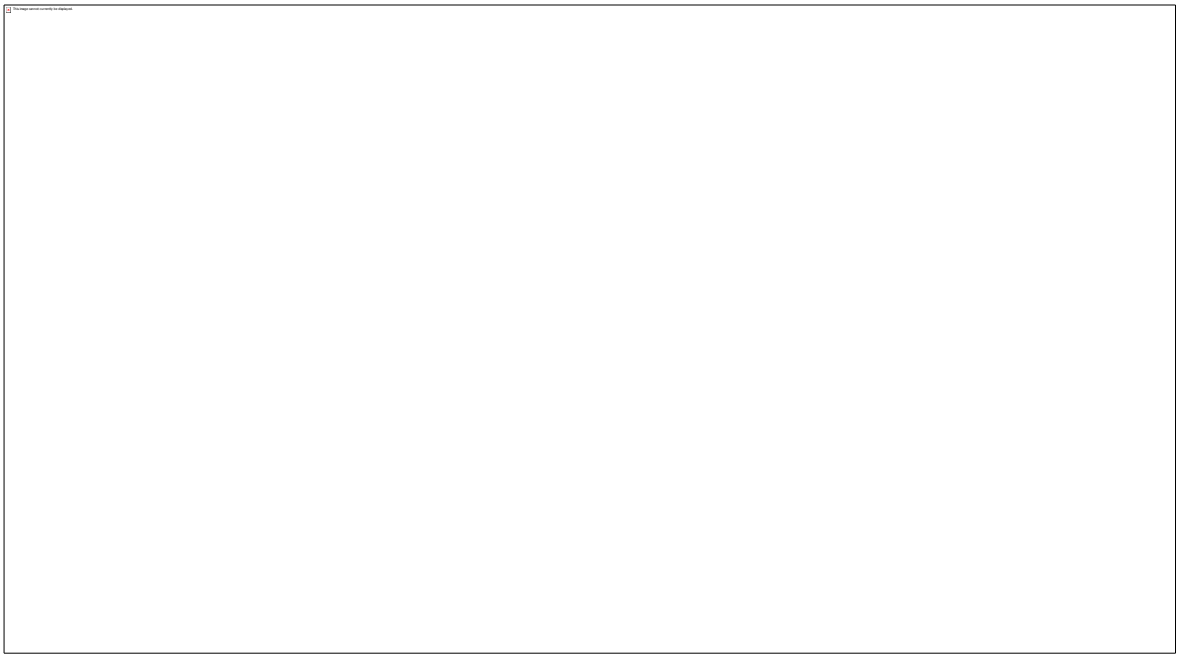

Chemical shift (ppm)

^{1}H NMR and ^{13}C NMR SPECTRA of 4.4

Chemical shift (ppm)

Chemical shift (ppm)

^{1}H NMR and ^{13}C NMR SPECTRA of 4.5

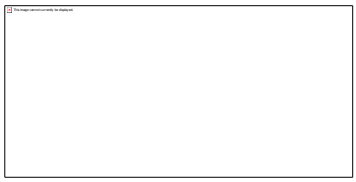

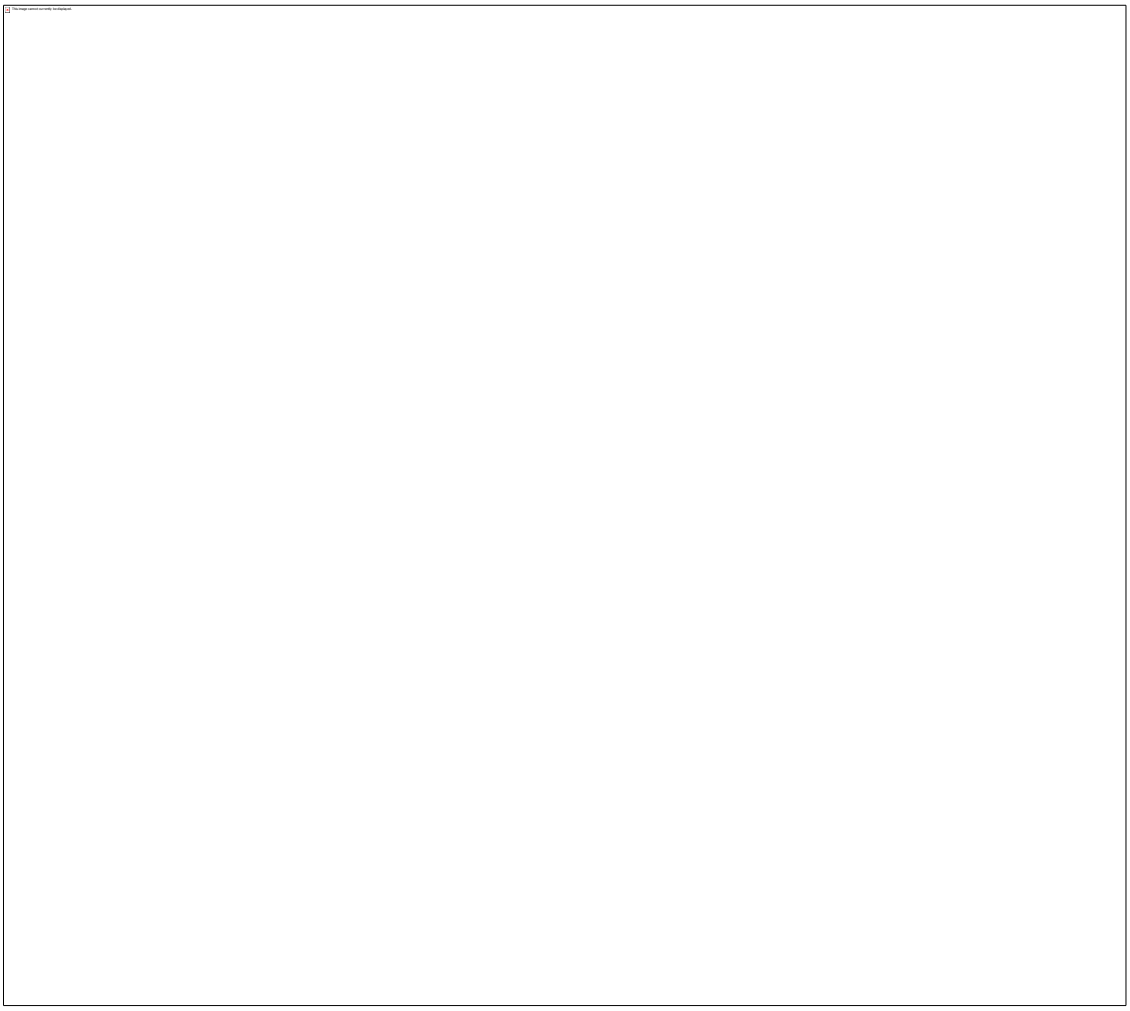

^{1}H NMR SPECTRUM of 4.6

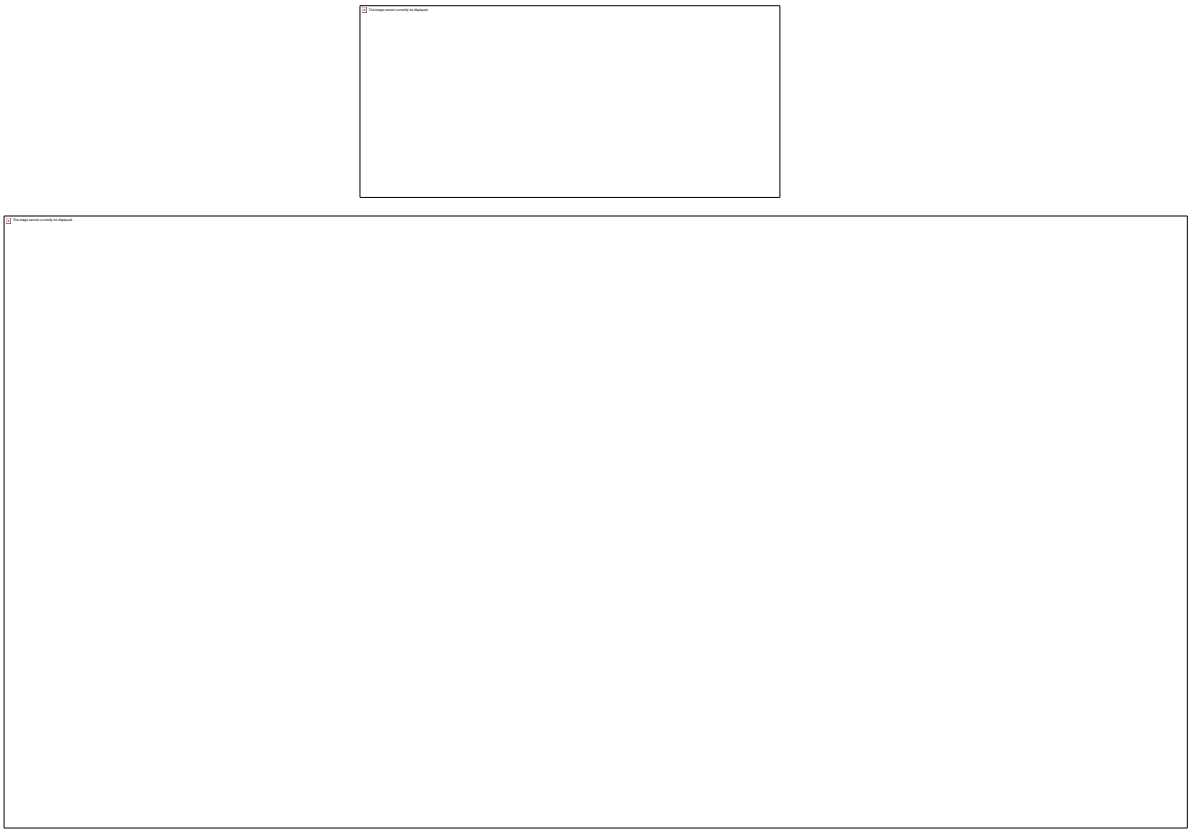

Chemical shift (ppm)

^{1}H NMR and ^{13}C NMR SPECTRA of 4.7

Chemical shift (ppm)

Chemical shift (ppm)

^{1}H NMR and ^{13}C NMR SPECTRA of 4.9

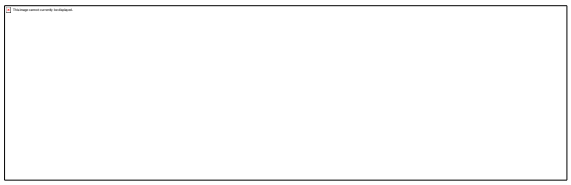

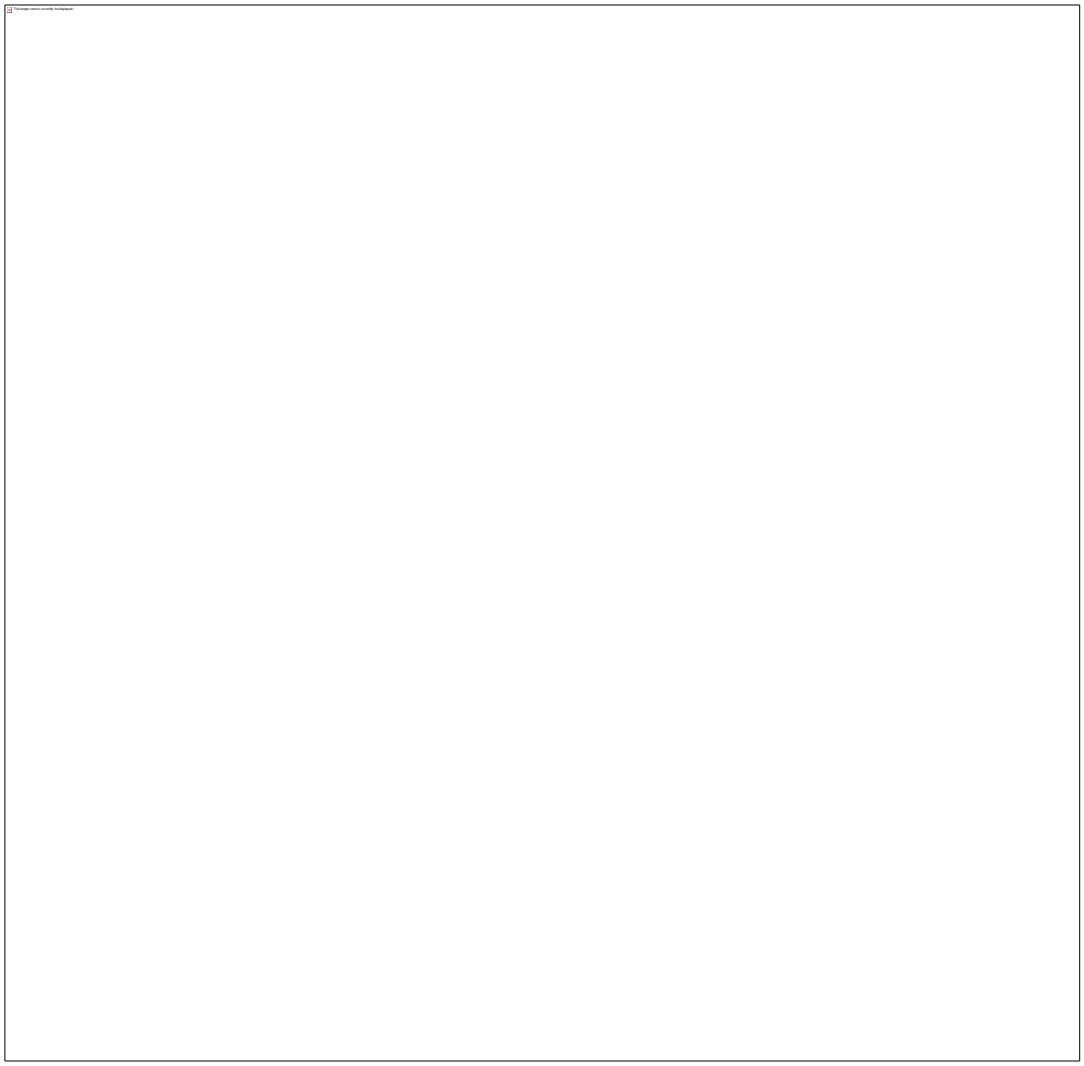

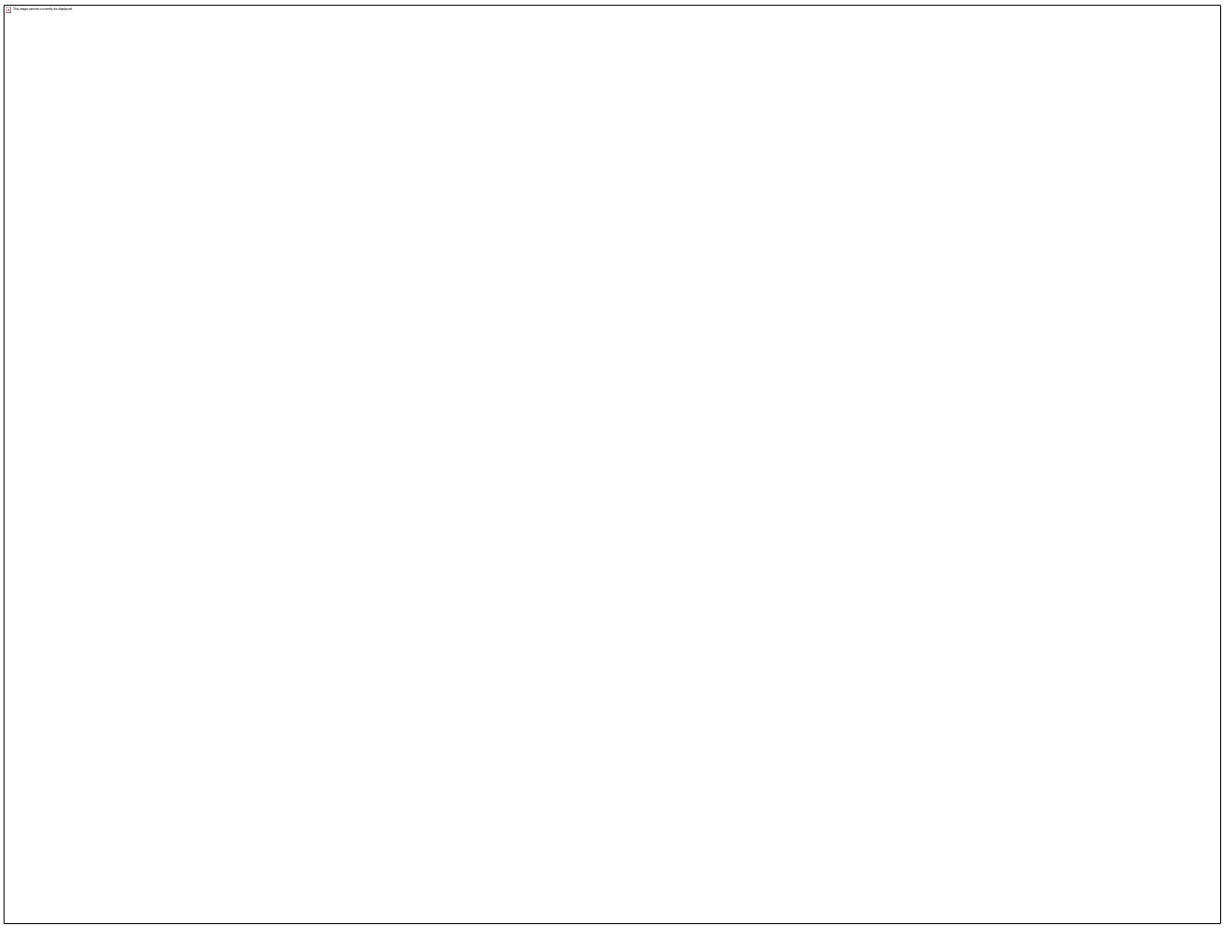

^{1}H NMR and ^{13}C NMR SPECTRA of 4.10

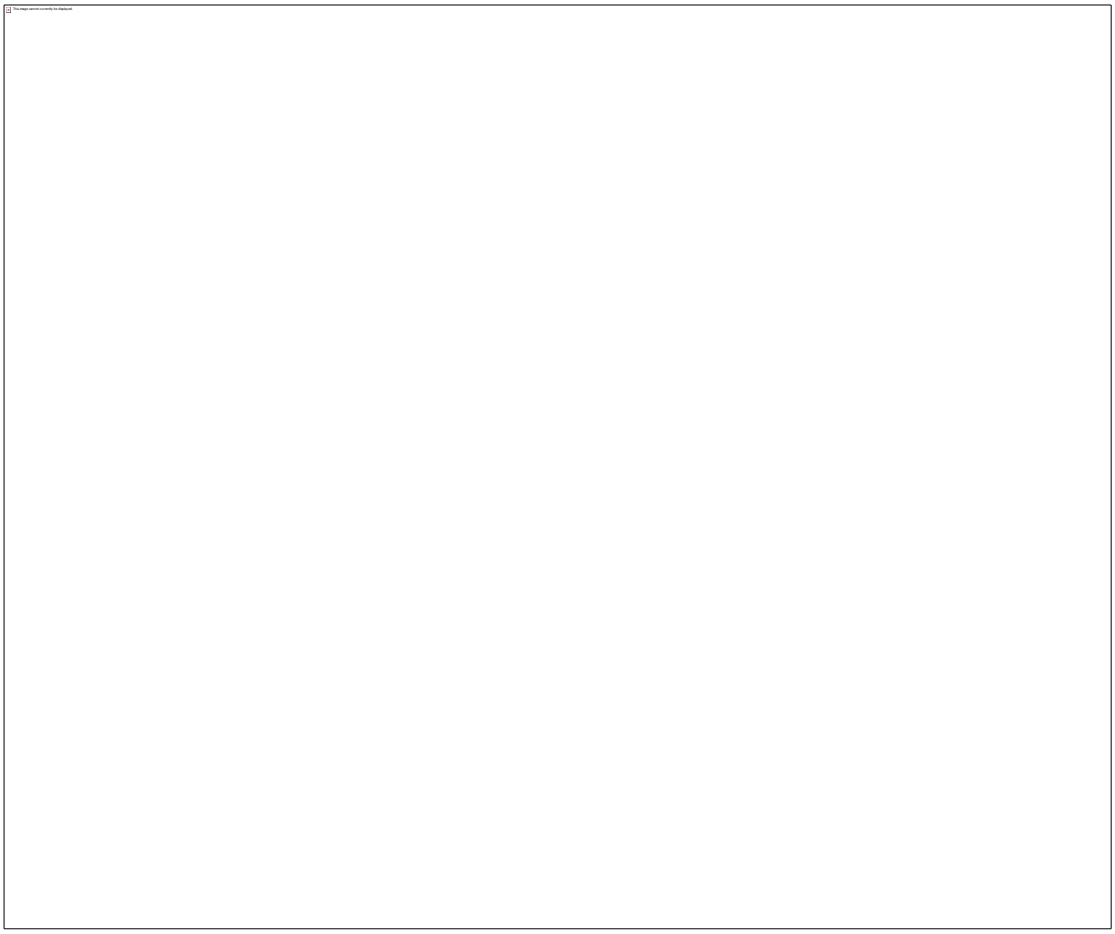

^{1}H NMR and ^{13}C NMR SPECTRA of 4.11

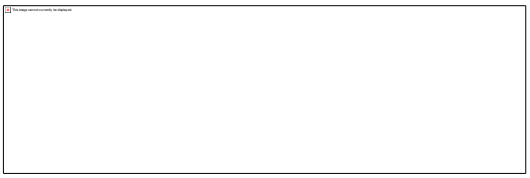

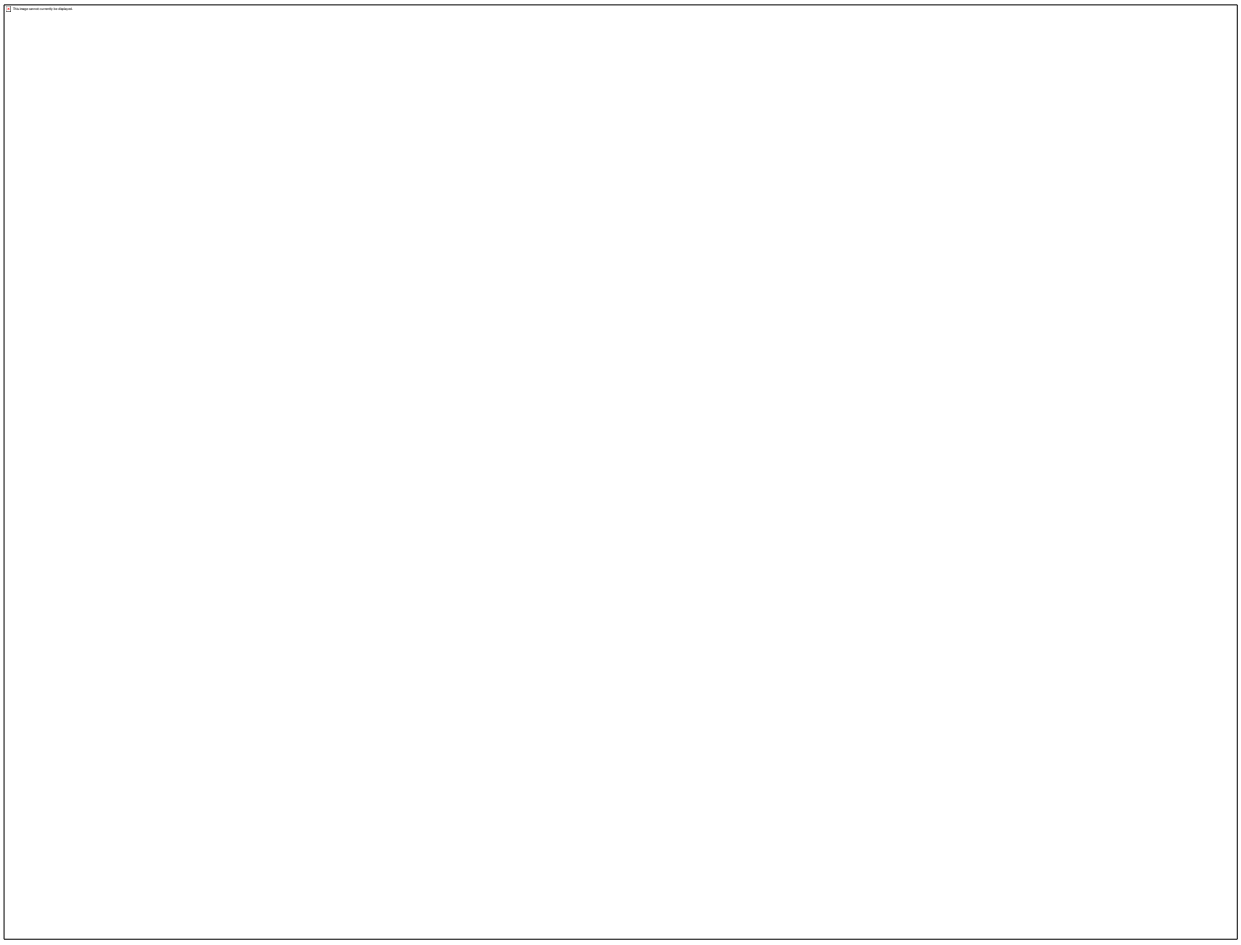

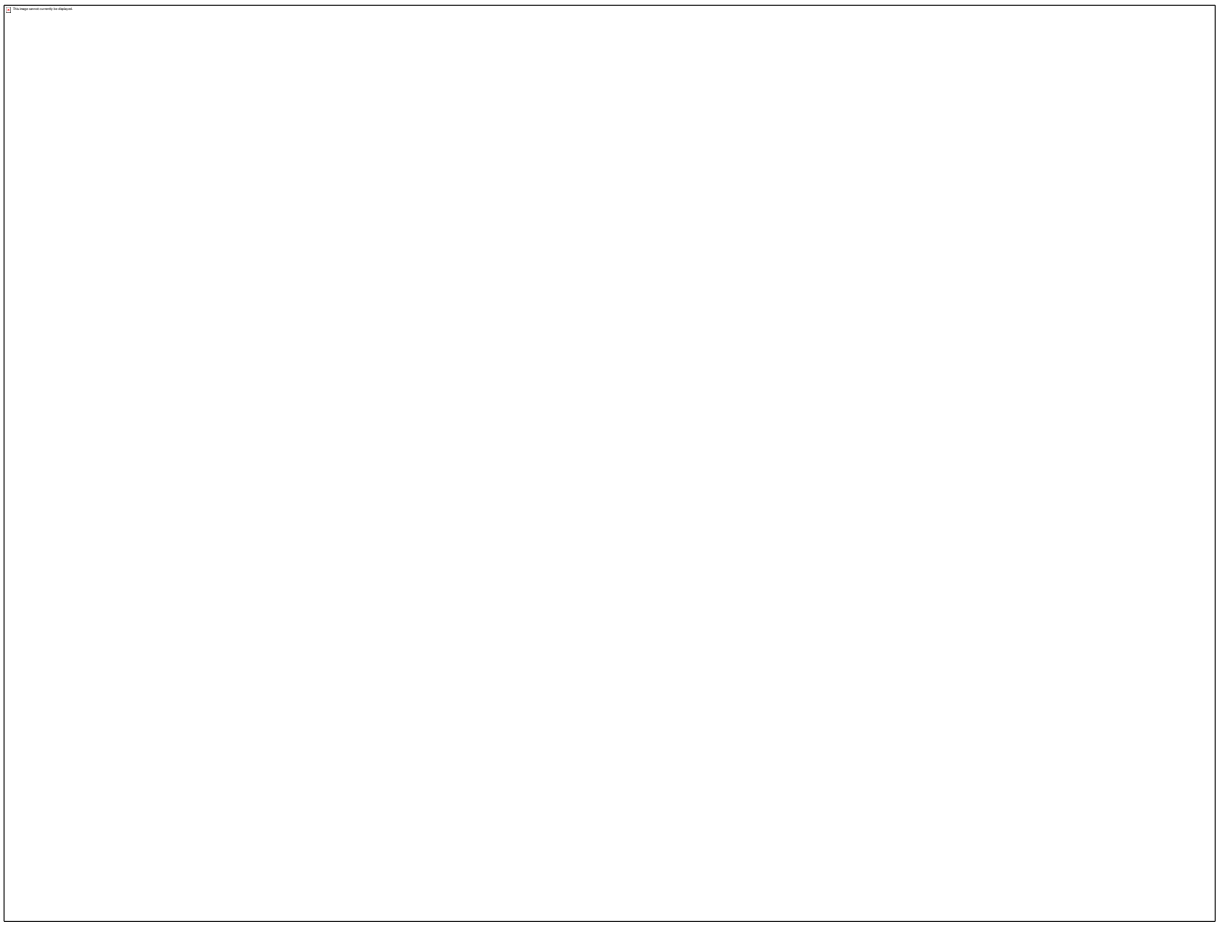

^{1}H NMR and ^{13}C NMR SPECTRA of 4.12

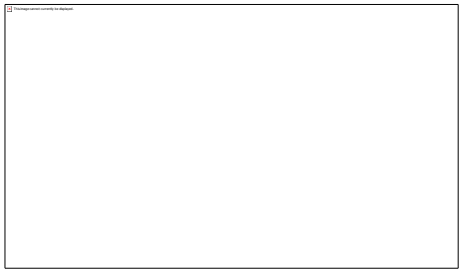

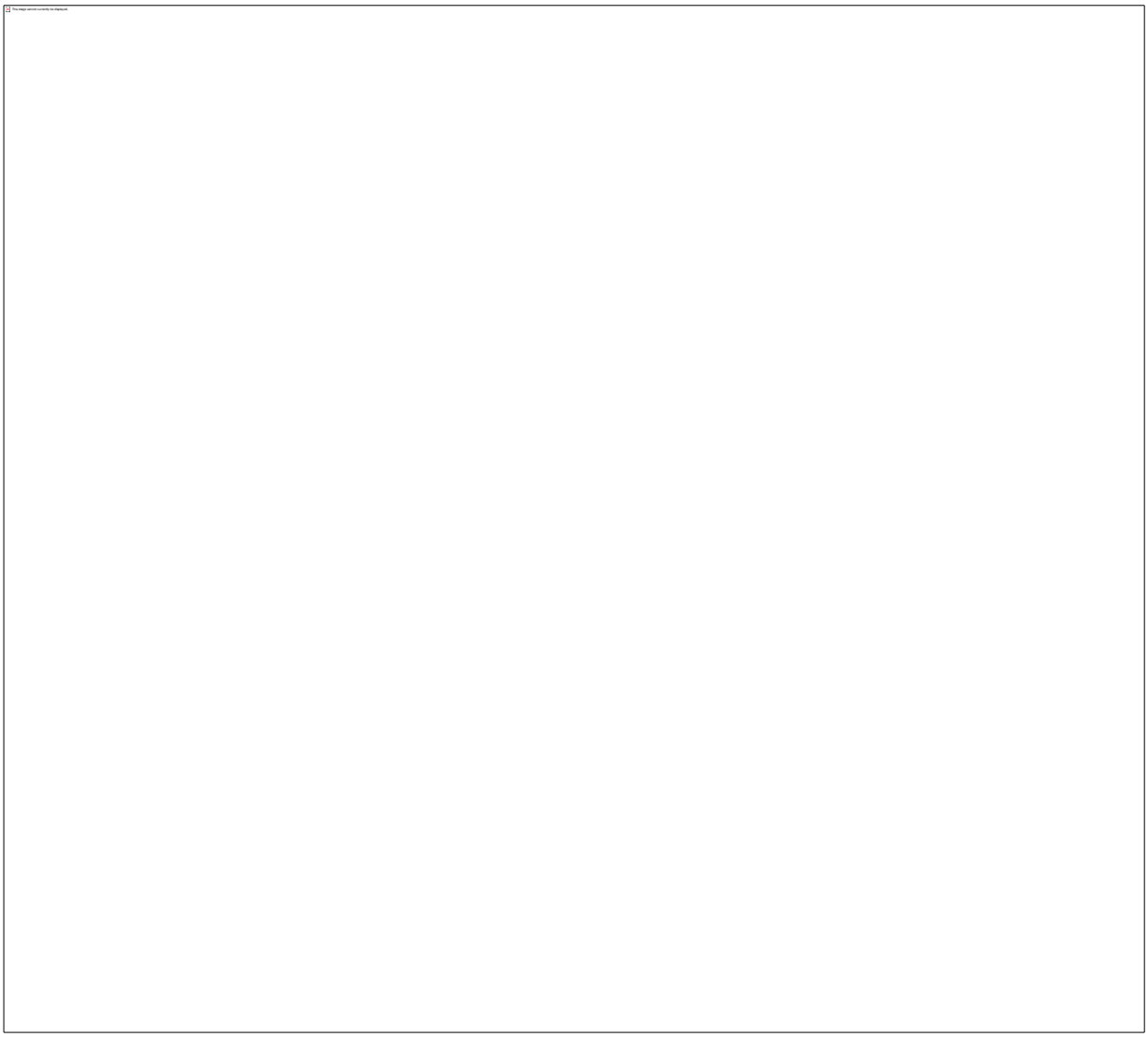

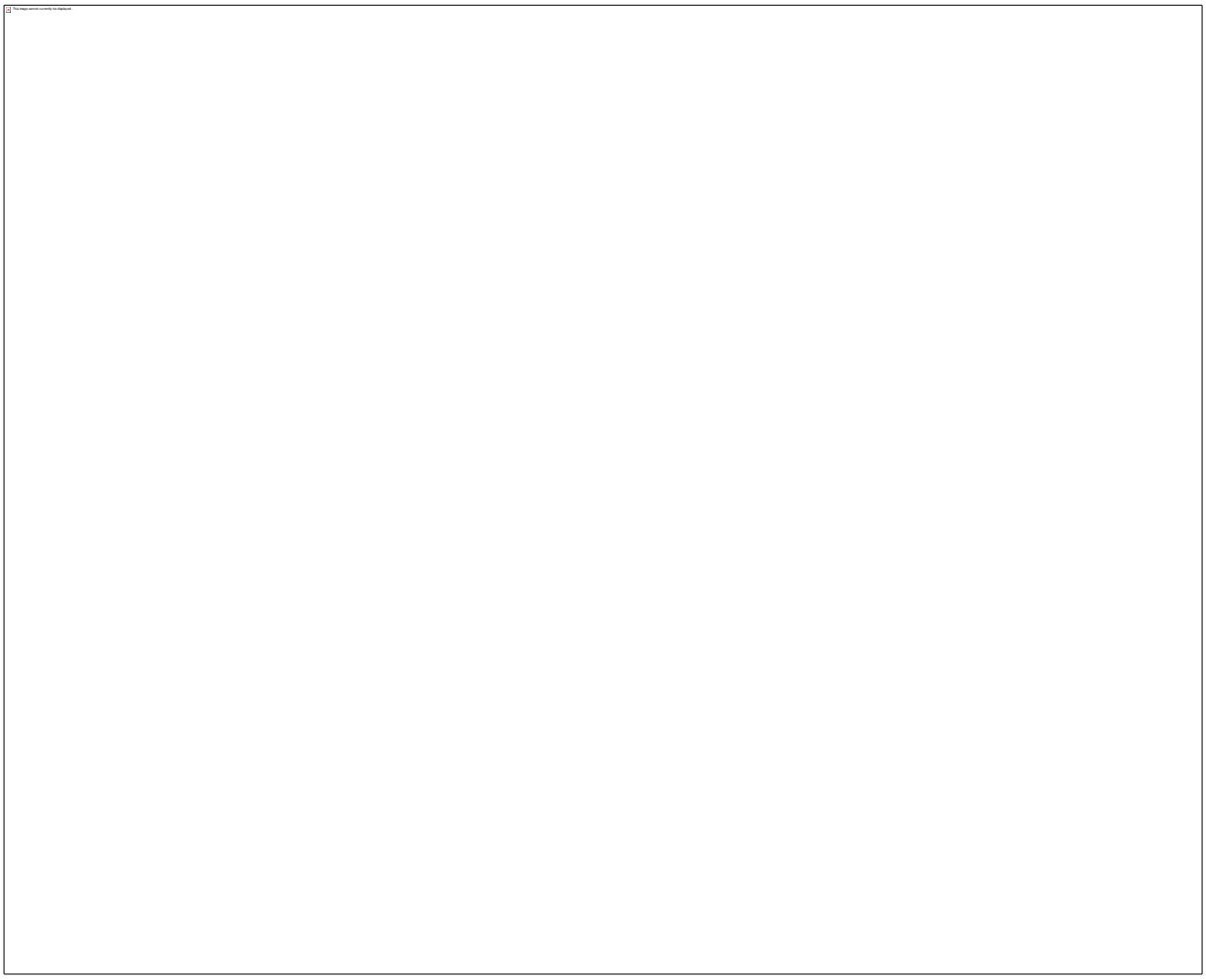

^{1}H NMR and ^{13}C NMR SPECTRA of 4.13

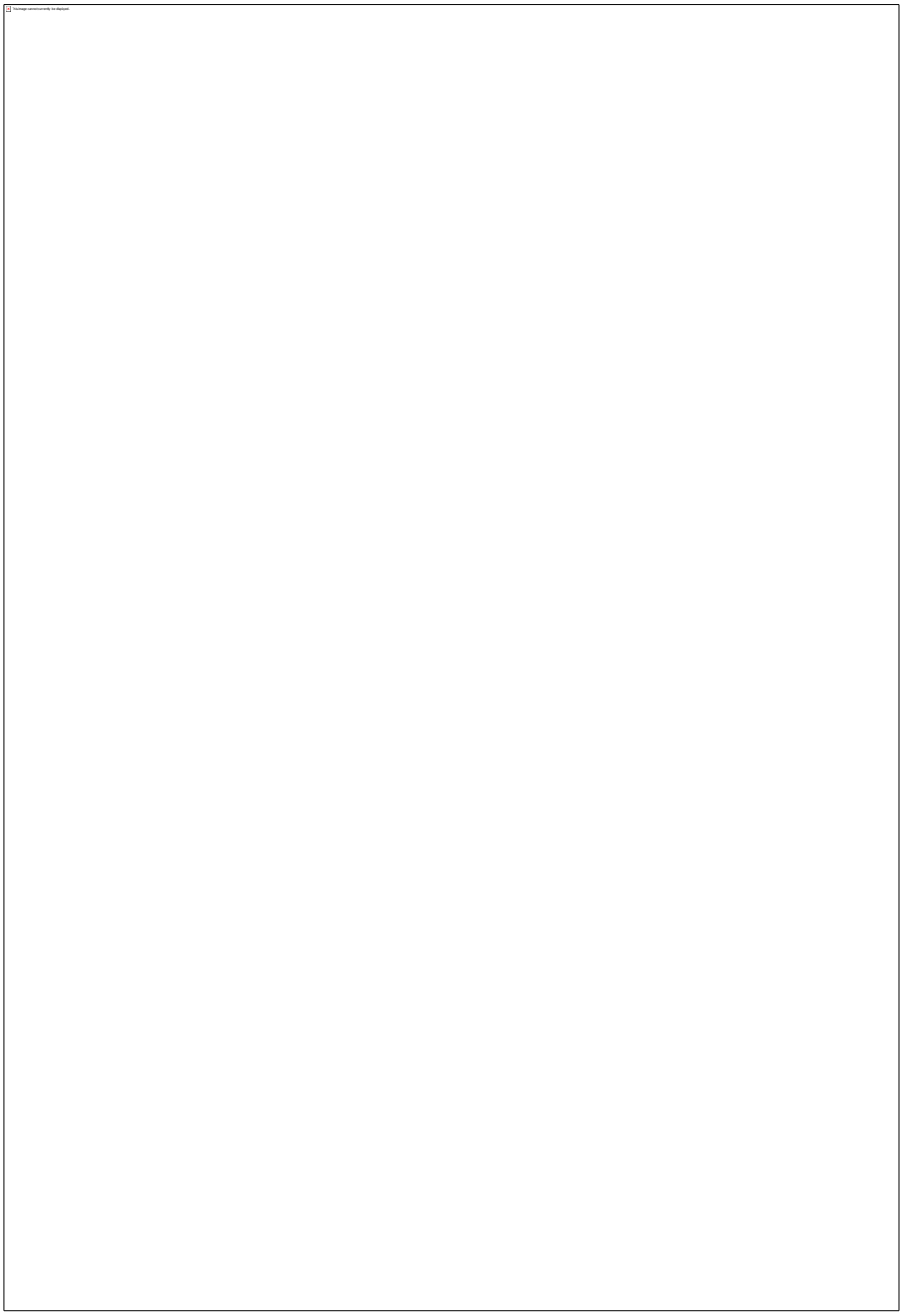

^{1}H NMR and ^{13}C NMR SPECTRA of 4.14

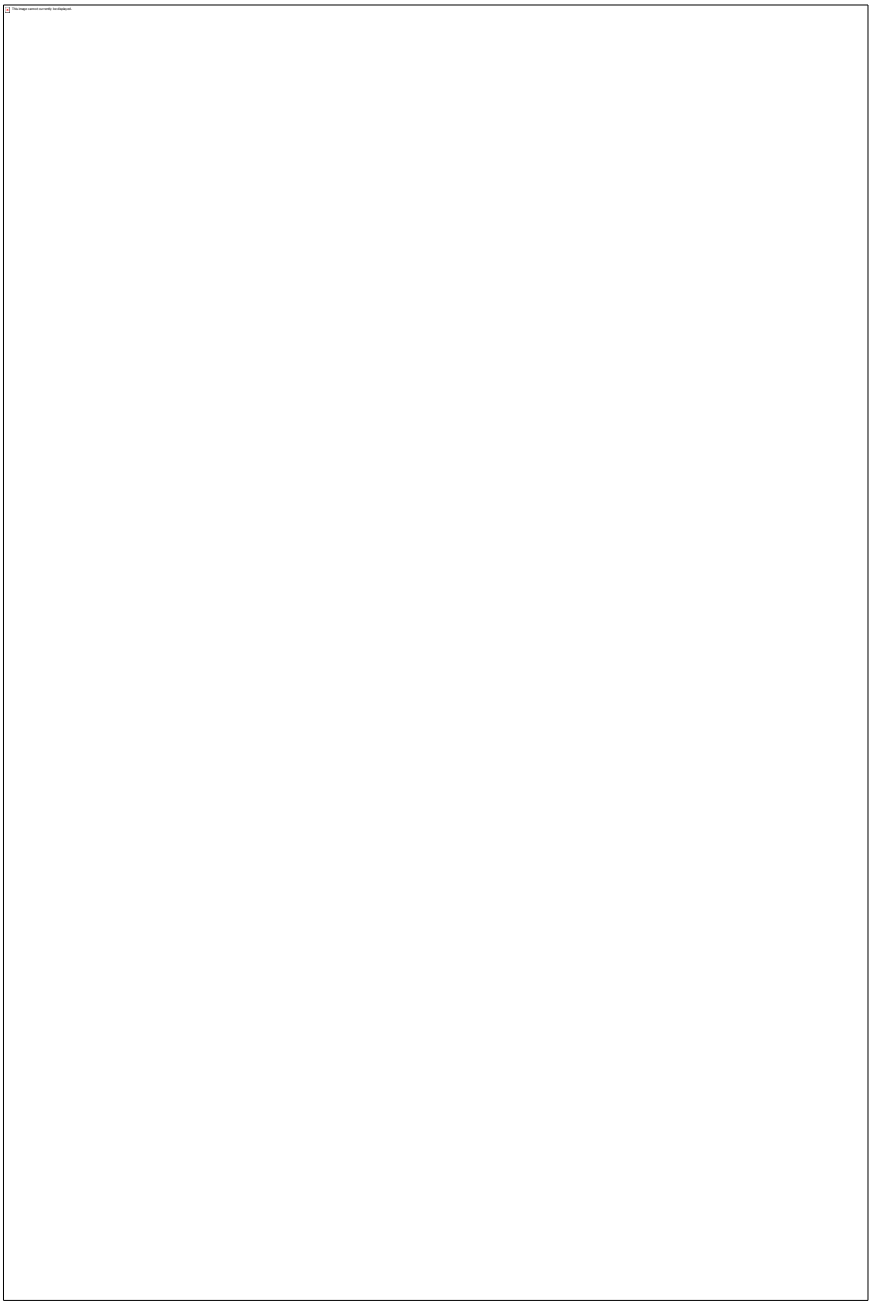

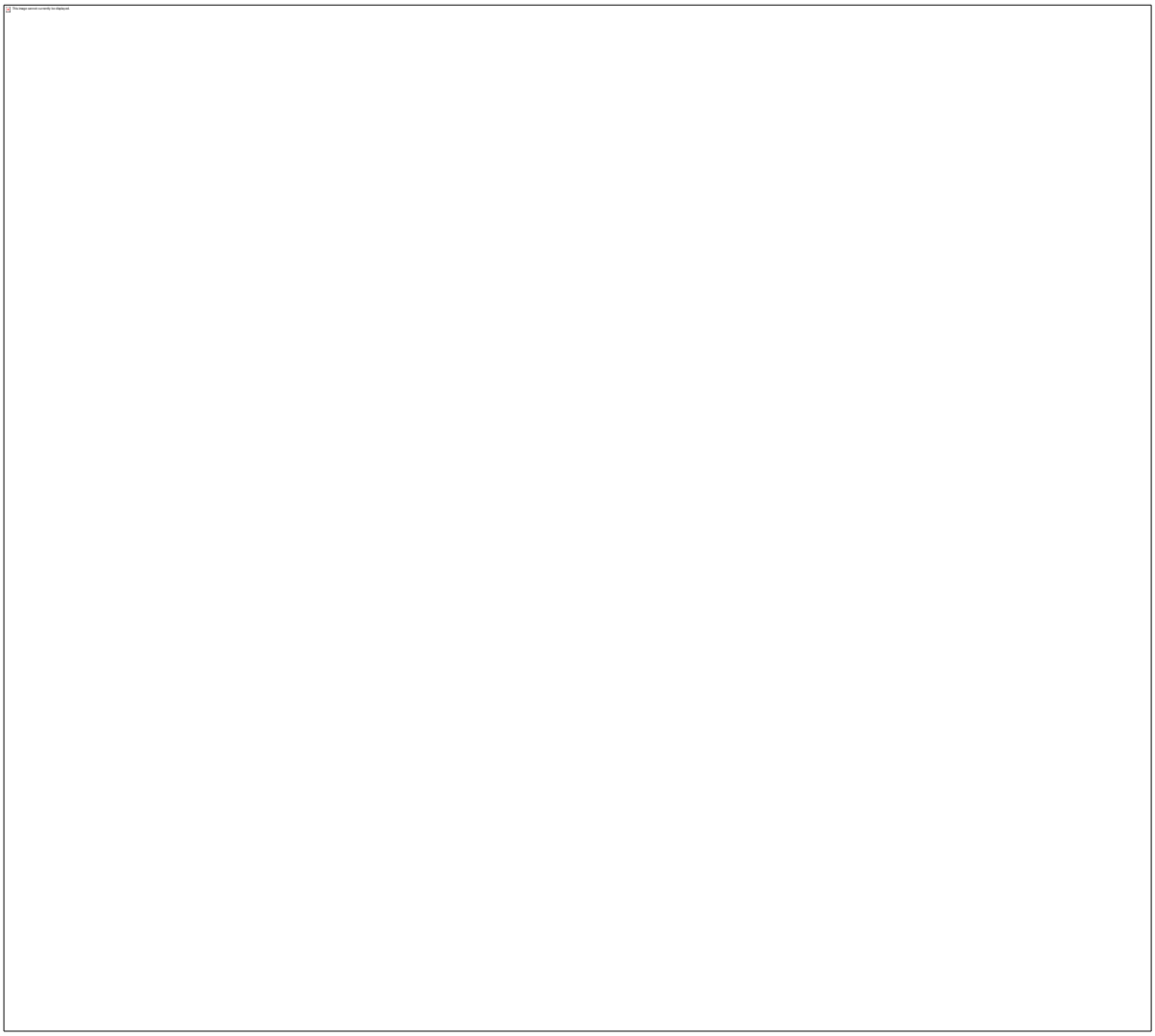

^{1}H NMR and ^{13}C NMR SPECTRA of 4.15

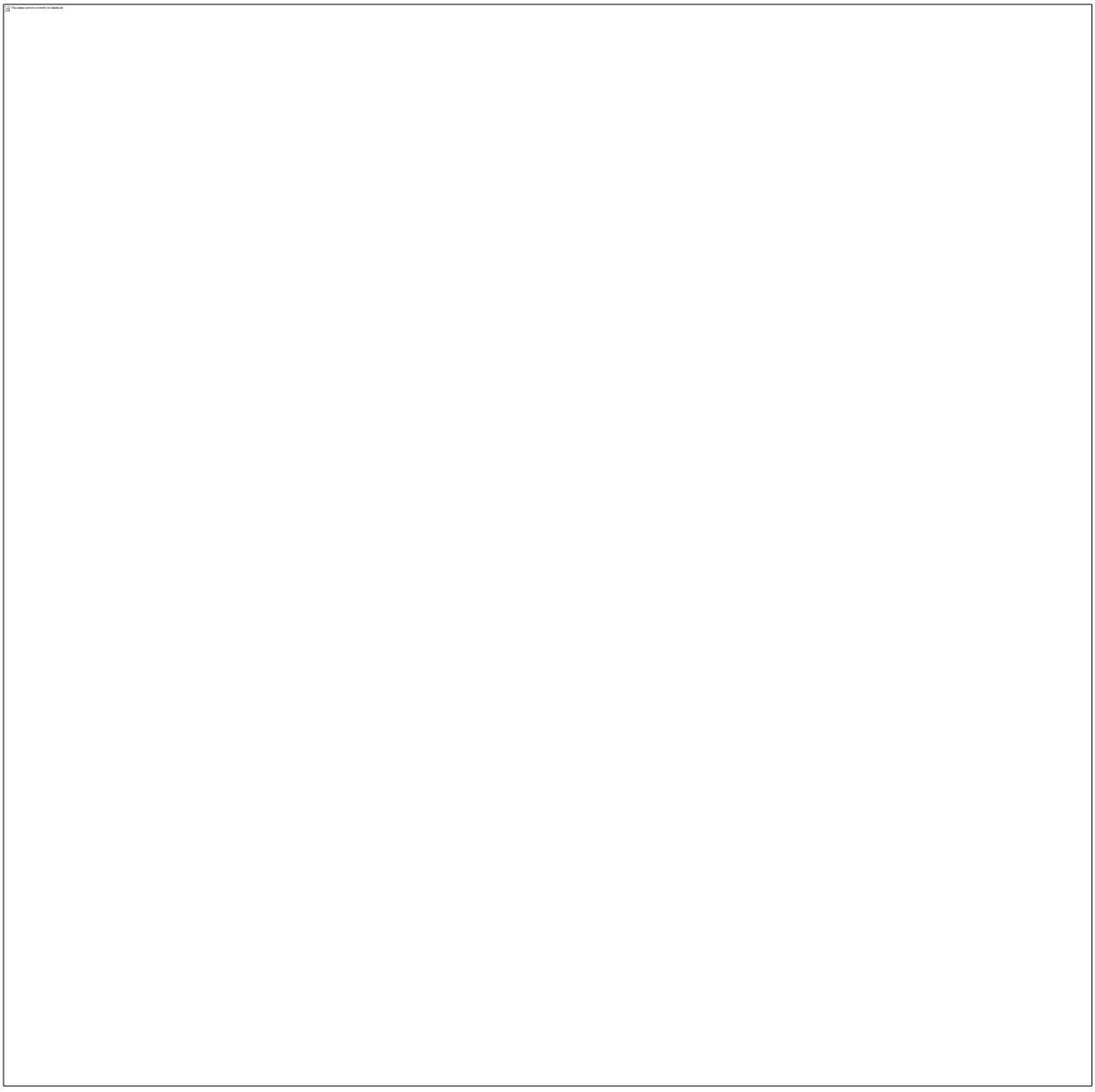

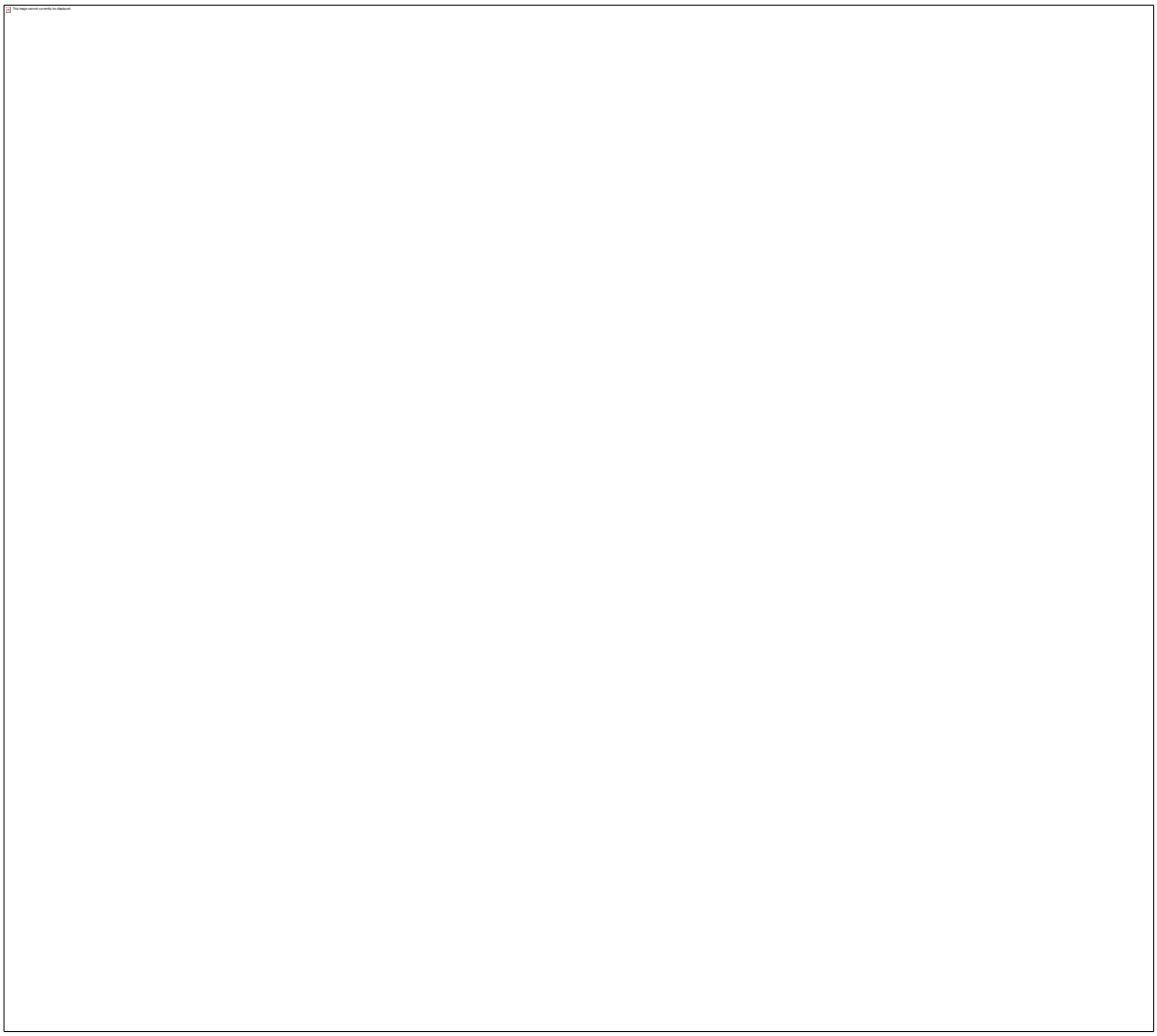

^{1}H NMR NMR and ^{13}C NMR SPECTRA of 4.16

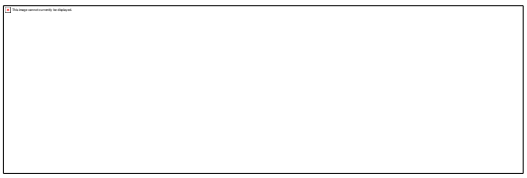

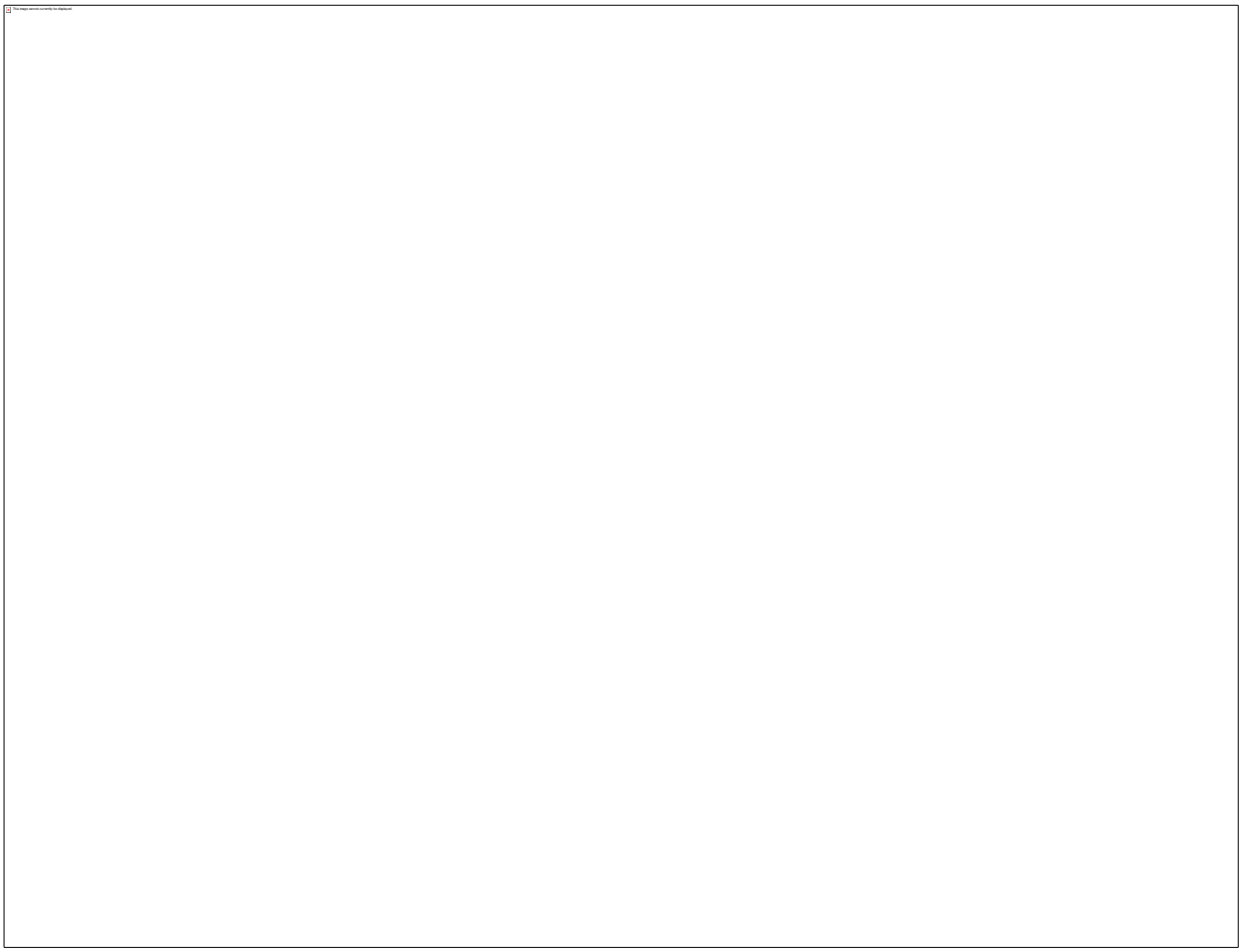

^{1}H NMR and ^{13}C NMR SPECTRA of 4.17

^{1}H NMR and ^{13}C NMR SPECTRA of 4.18

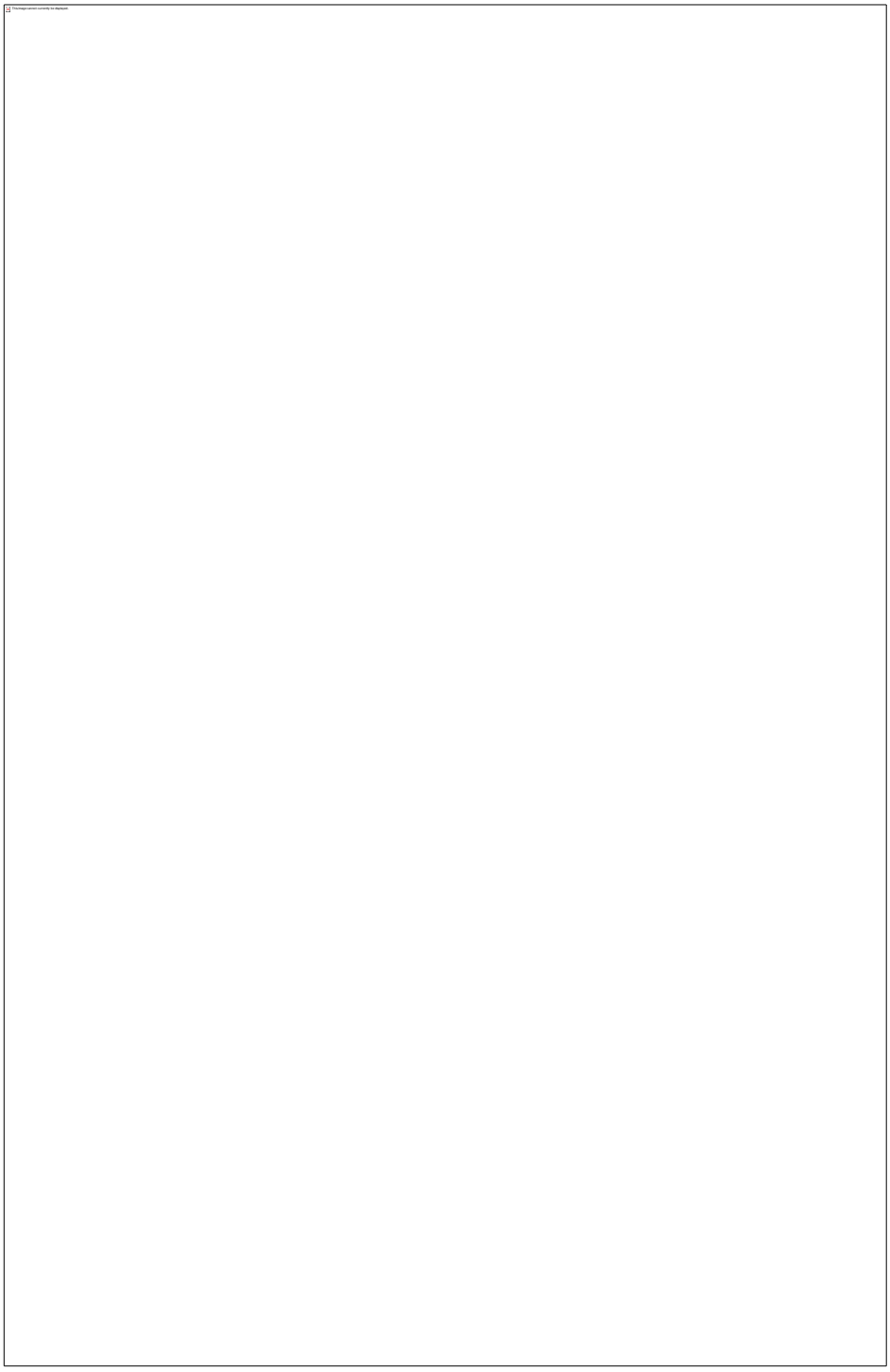

^{1}H NMR and ^{13}C NMR SPECTRA of 4.20

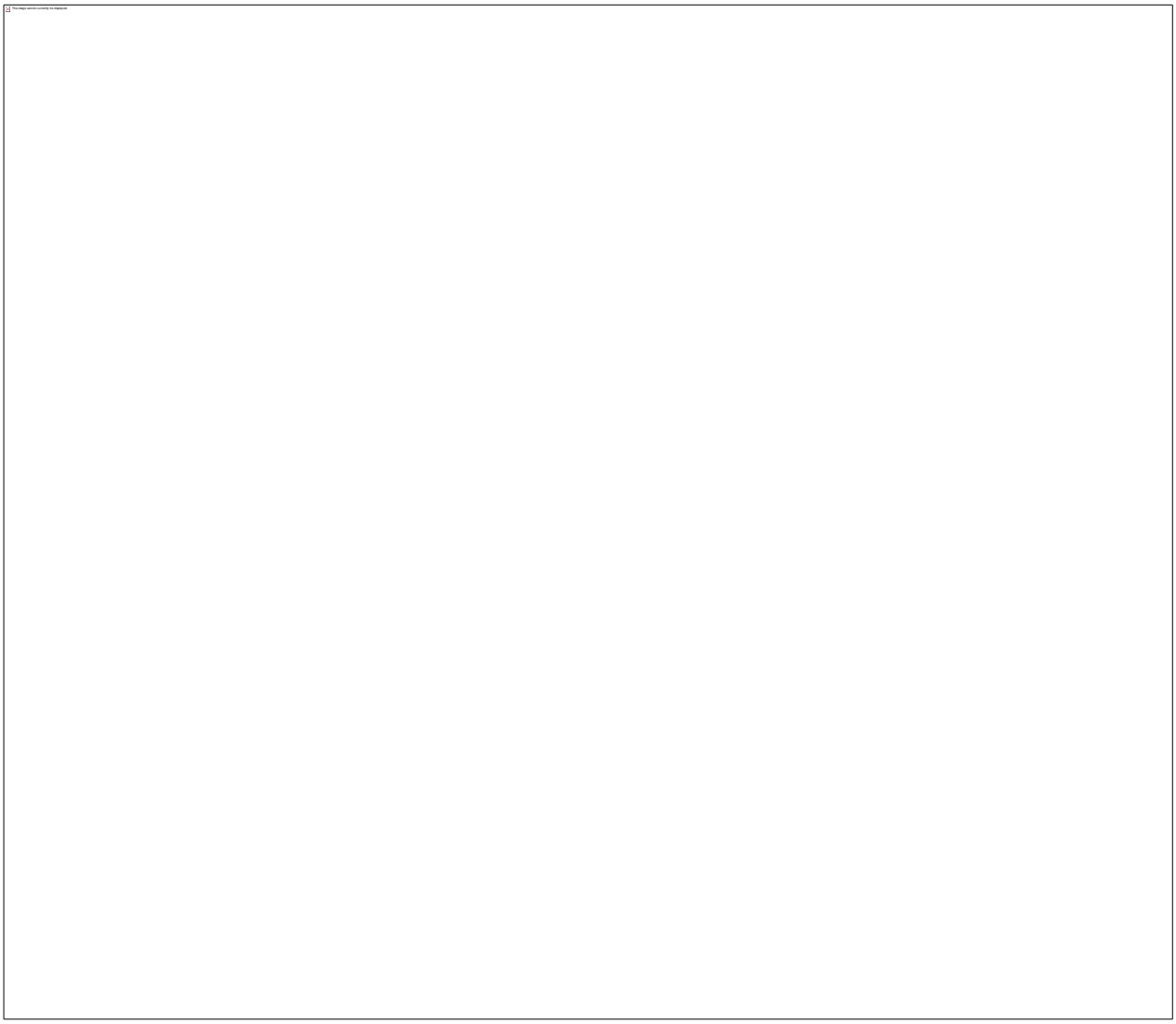

^{1}H NMR and ^{13}C NMR SPECTRA of 4.21

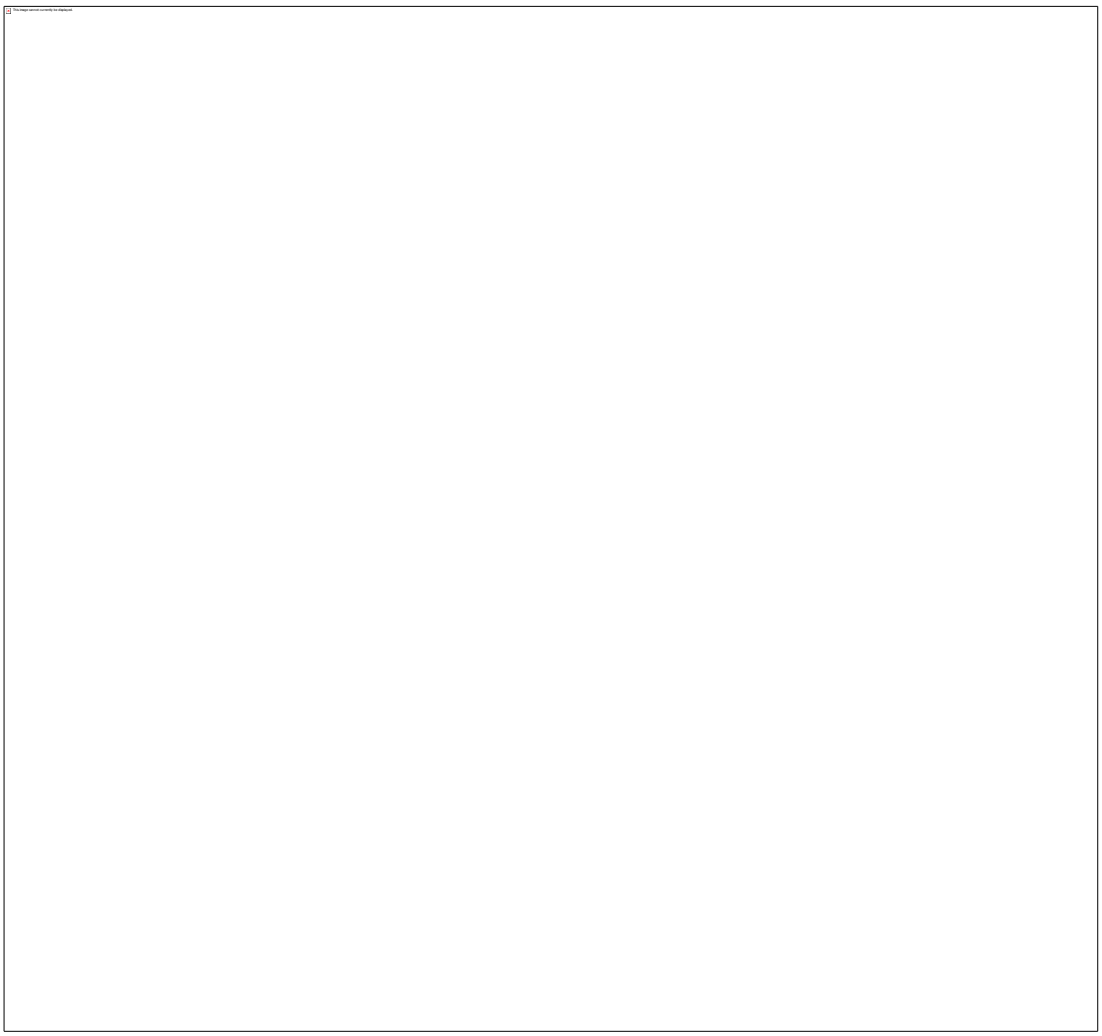

^{1}H NMR and ^{13}C NMR SPECTRA of 4.22

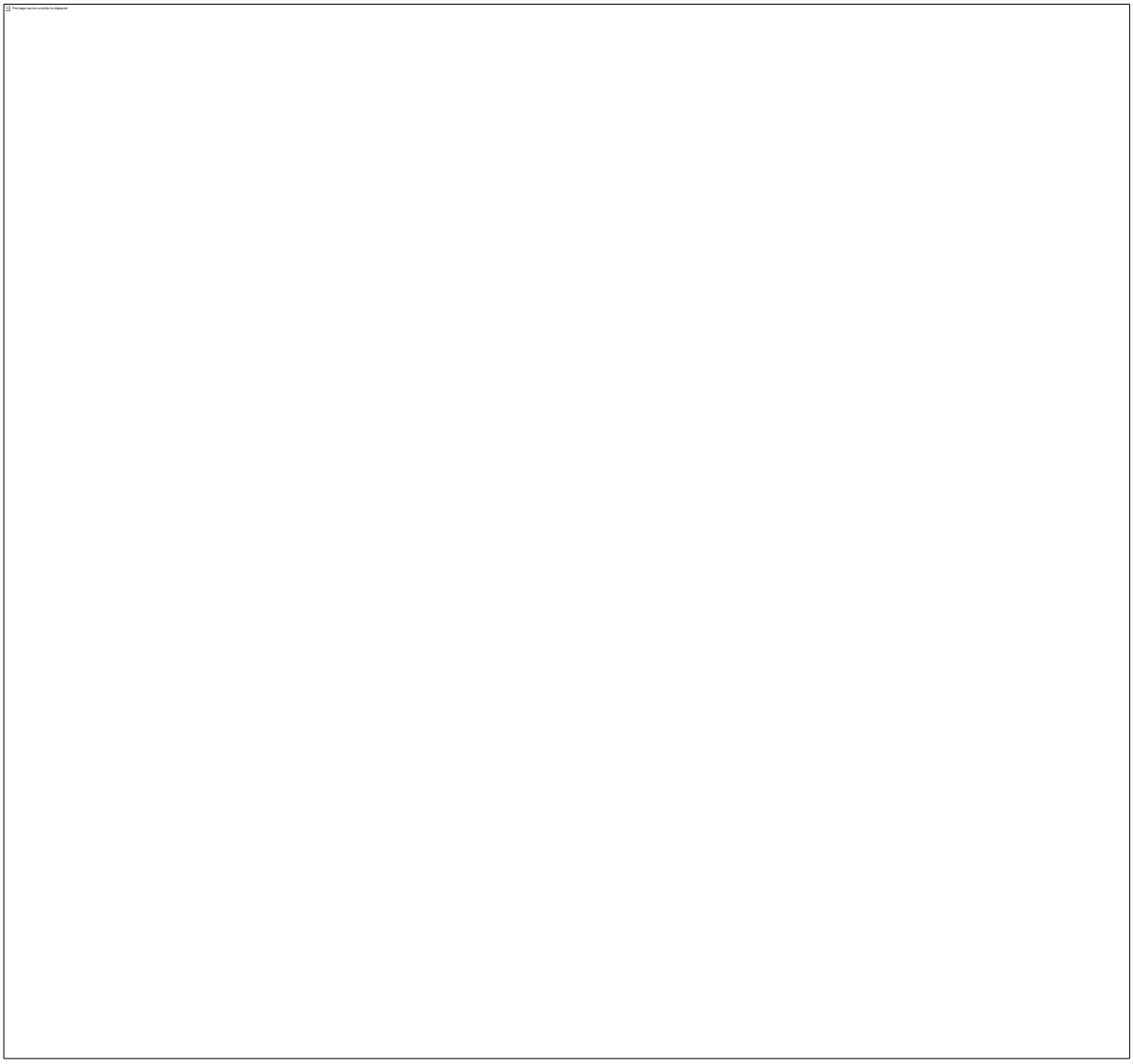

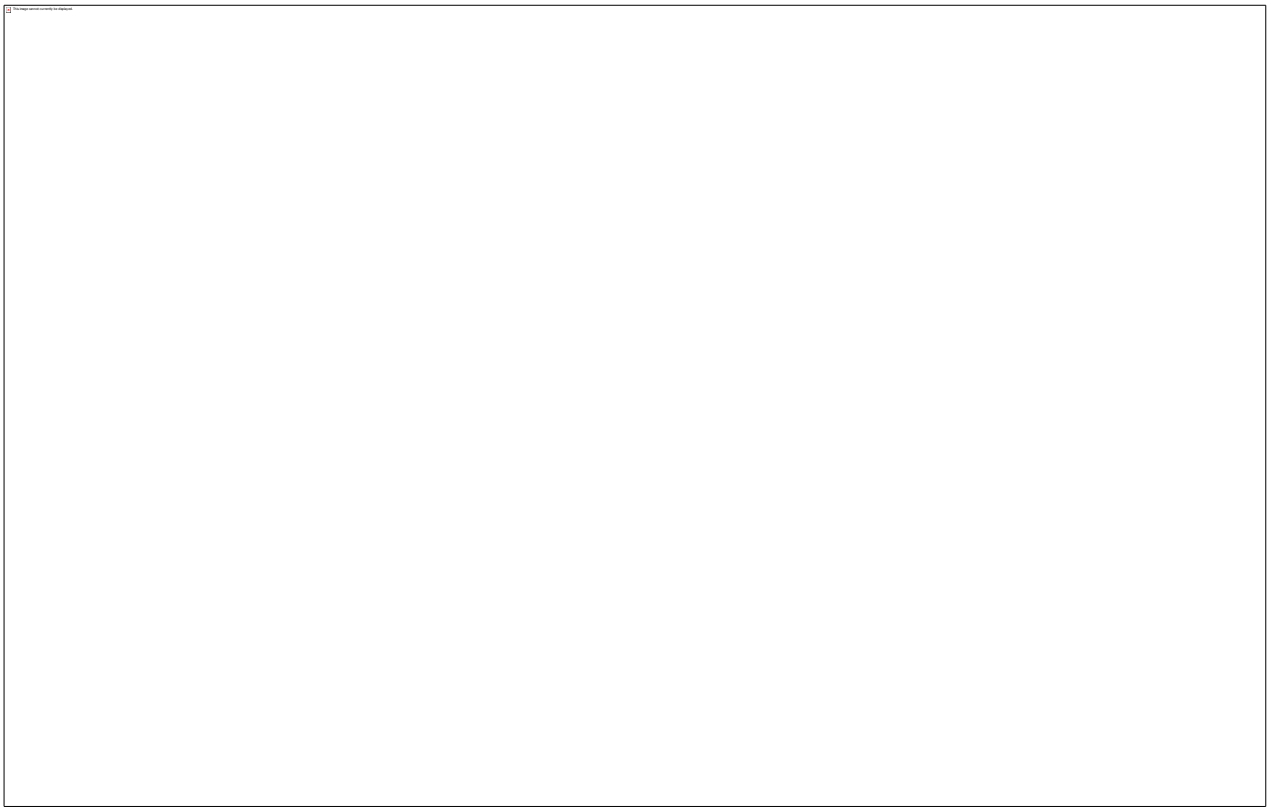

^{1}H NMR and ^{13}C NMR SPECTRA of 4.23

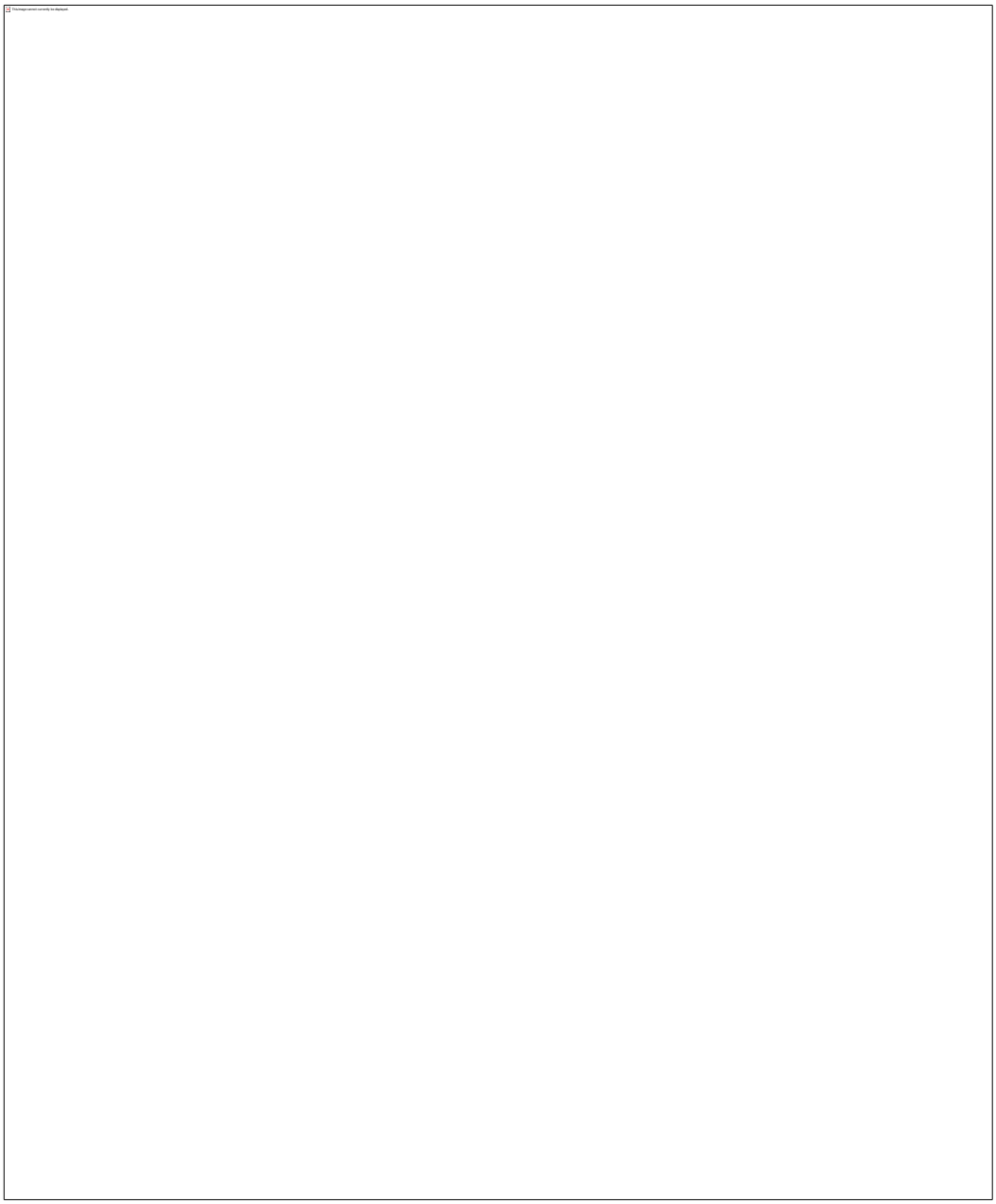

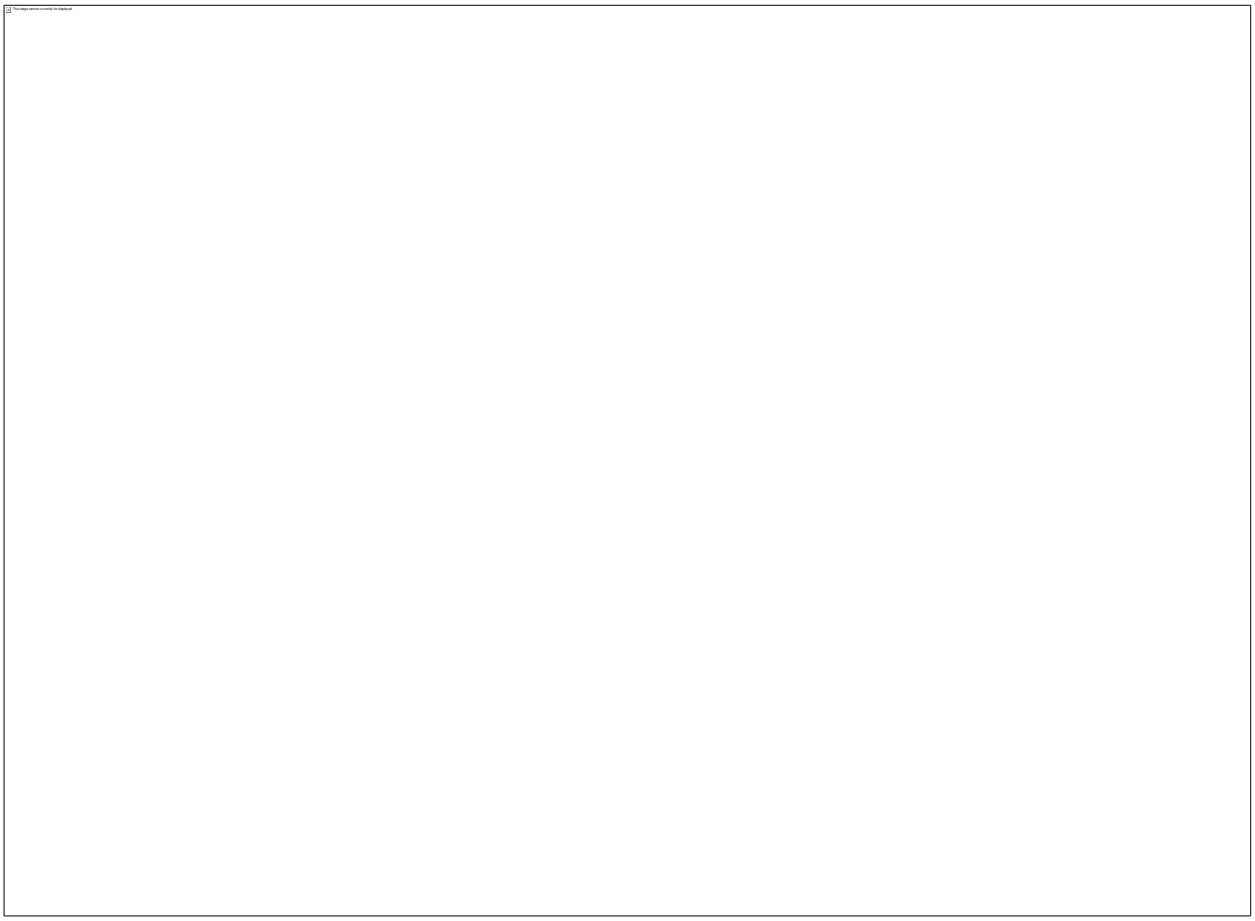

^{1}H NMR and ^{13}C NMR SPECTRA of 4.24

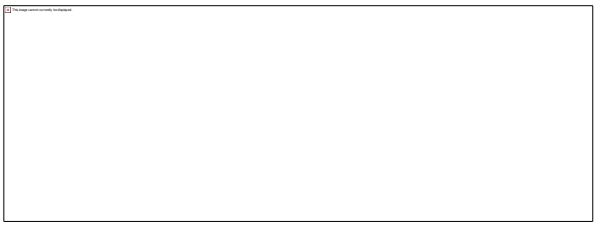

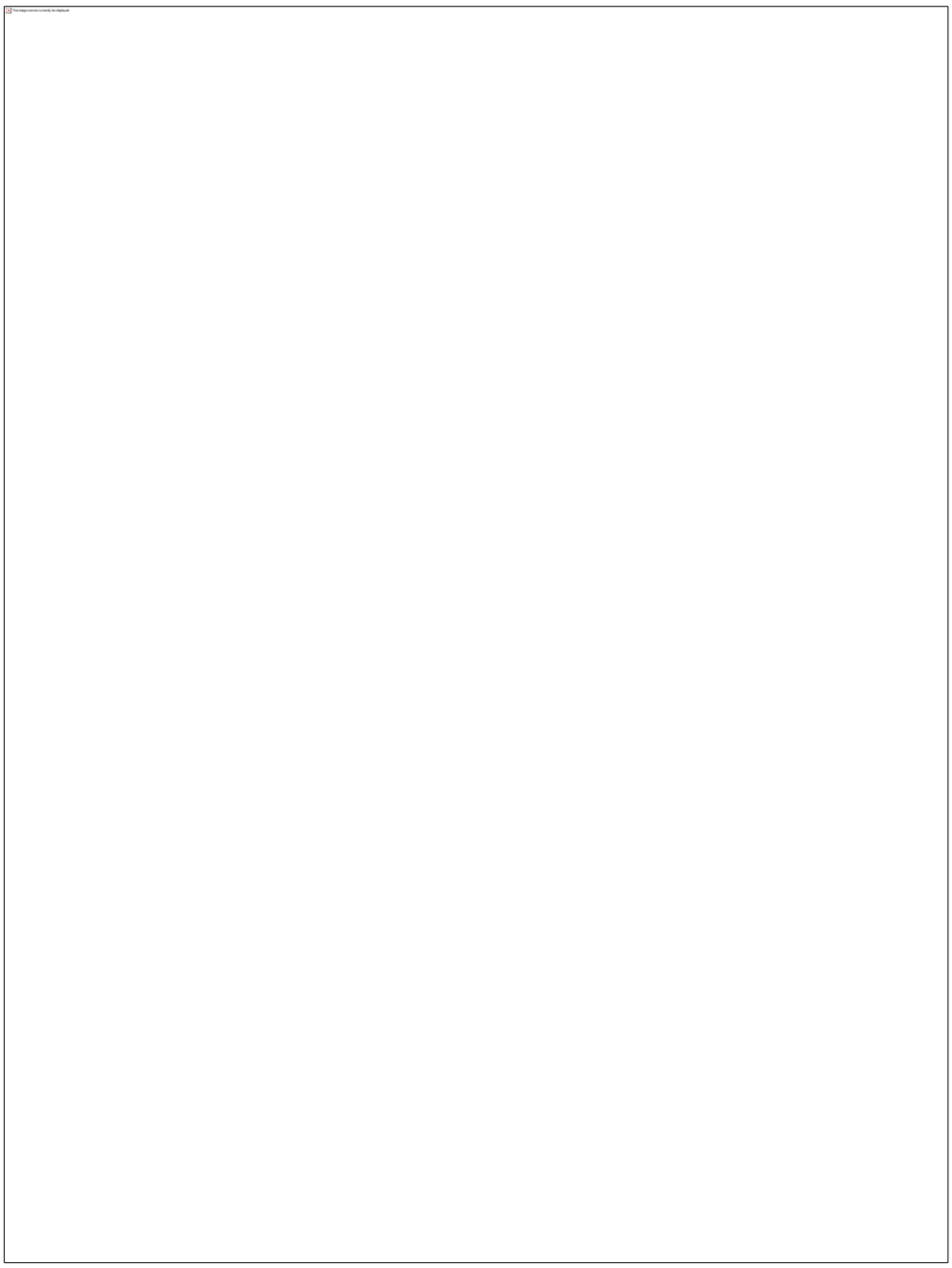

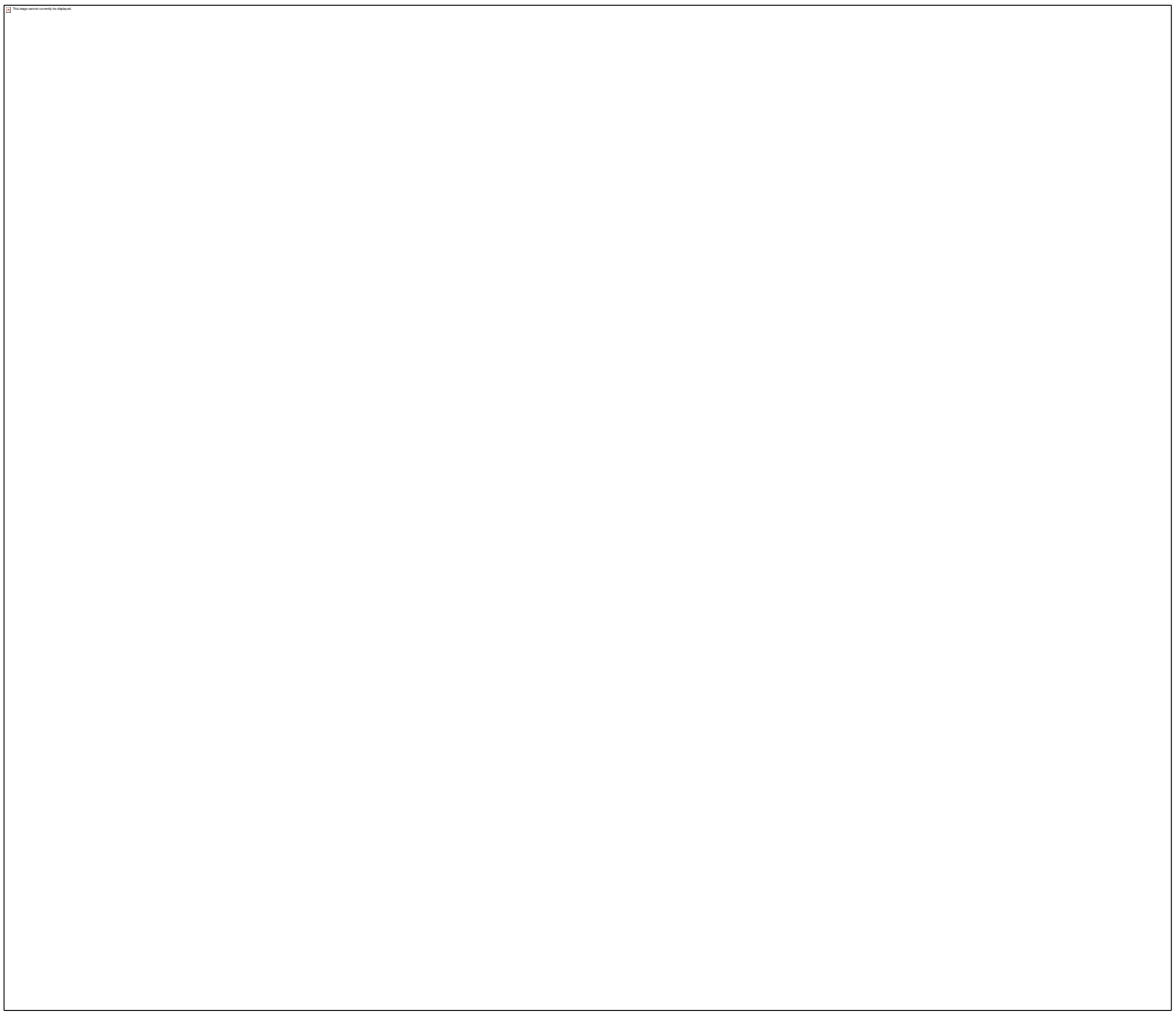

^{1}H NMR and ^{13}C NMR SPECTRA of 4.25

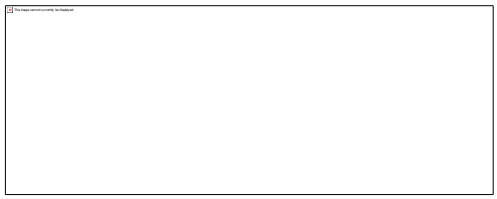

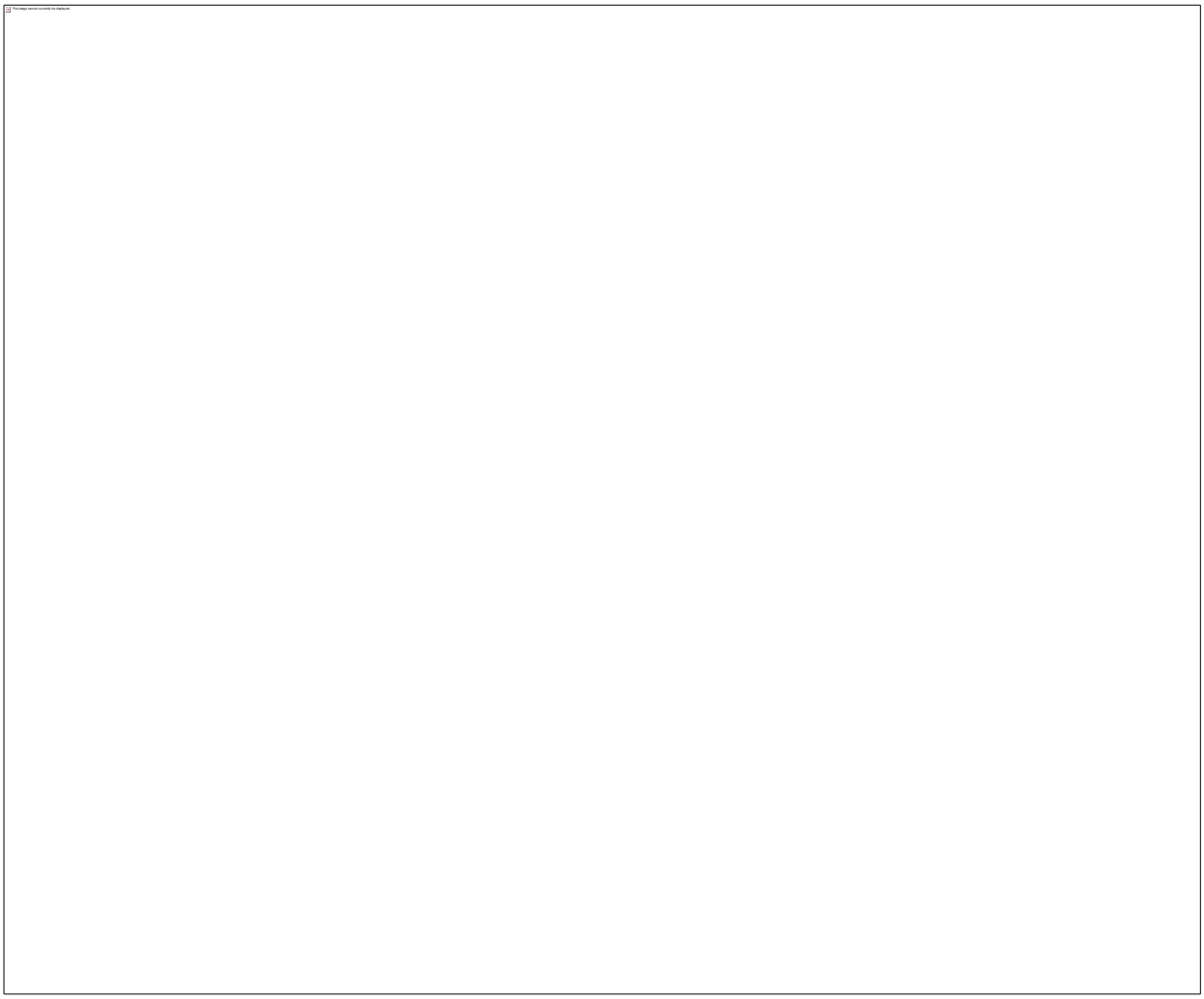

^{1}H NMR and ^{13}C NMR SPECTRA of 4.26

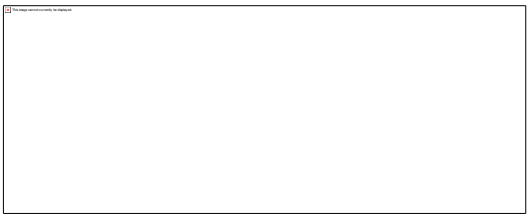

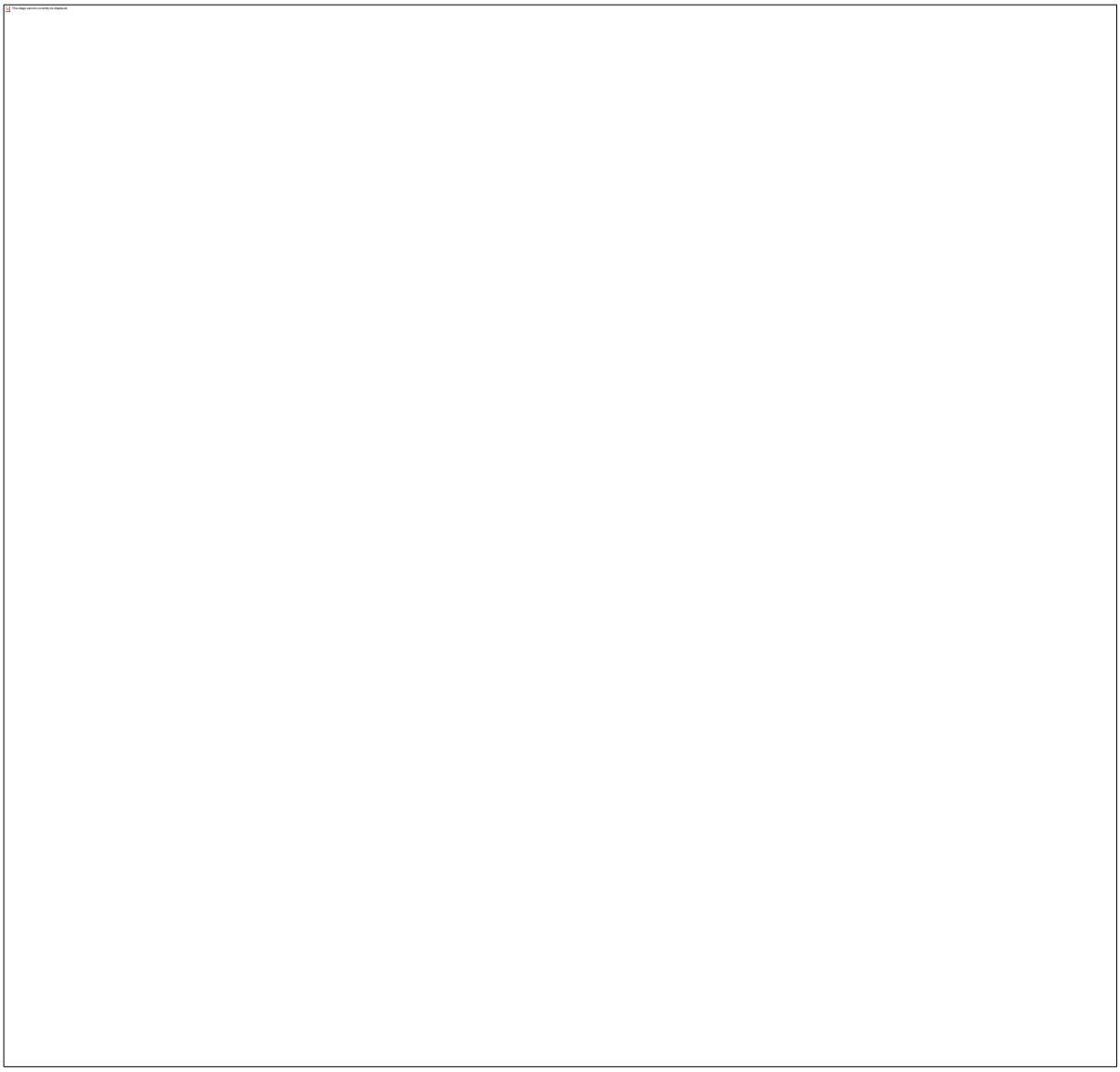

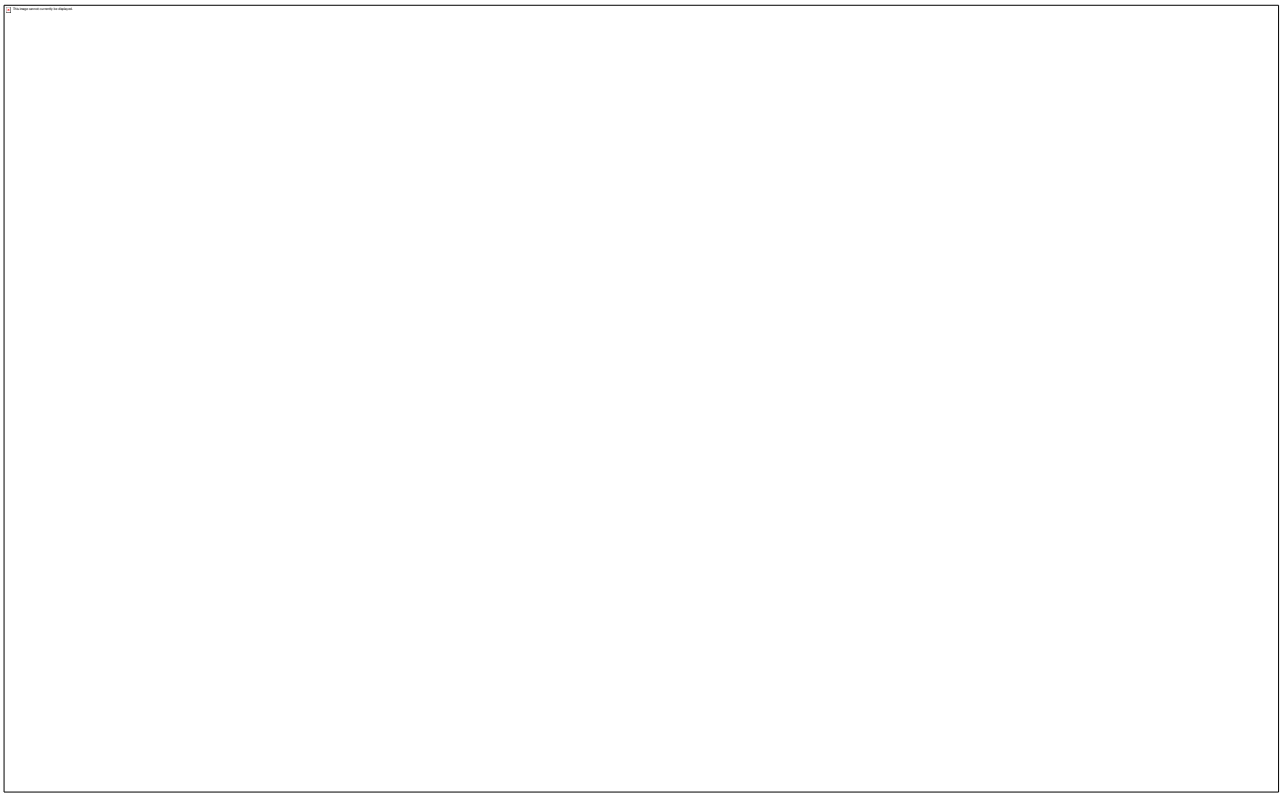

^{1}H NMR and ^{13}C NMR SPECTRA of 4.27

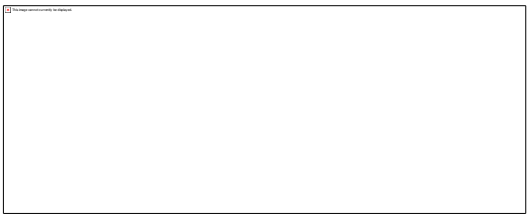

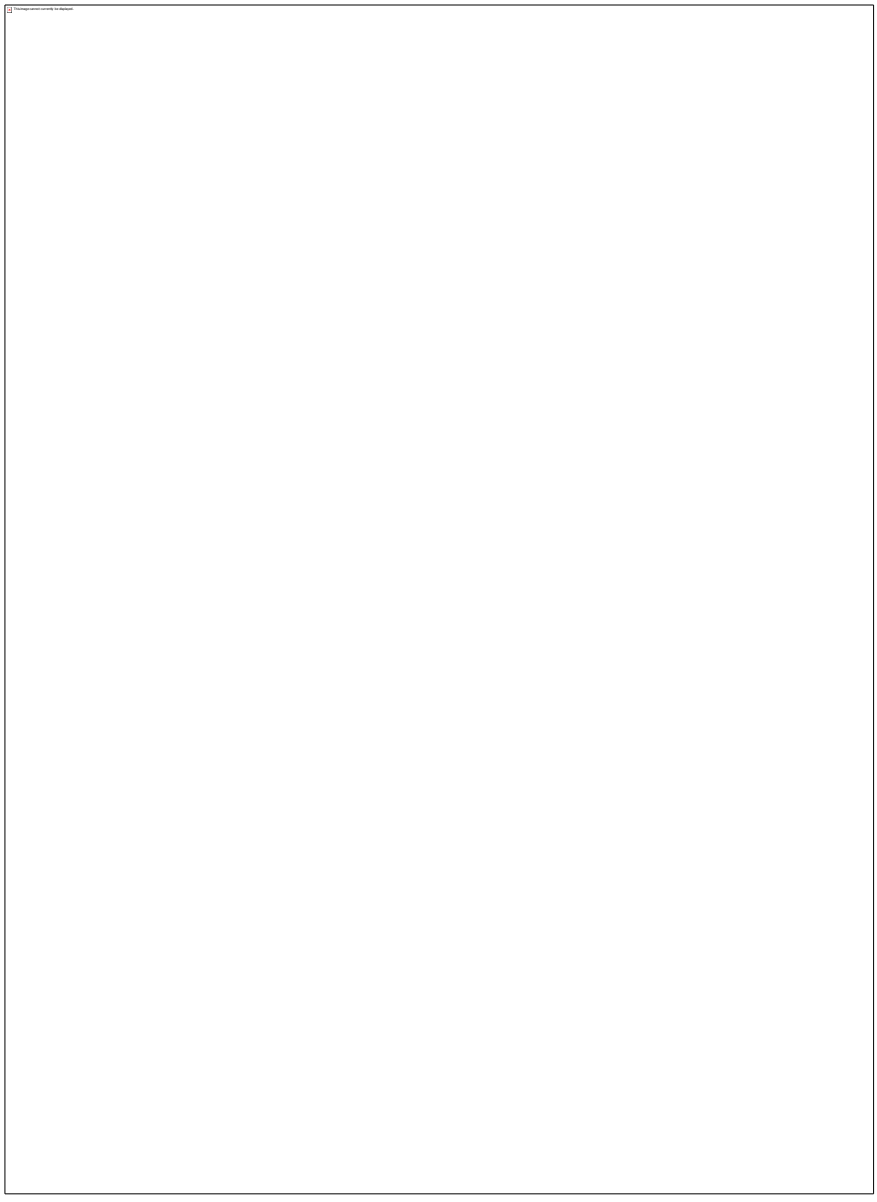

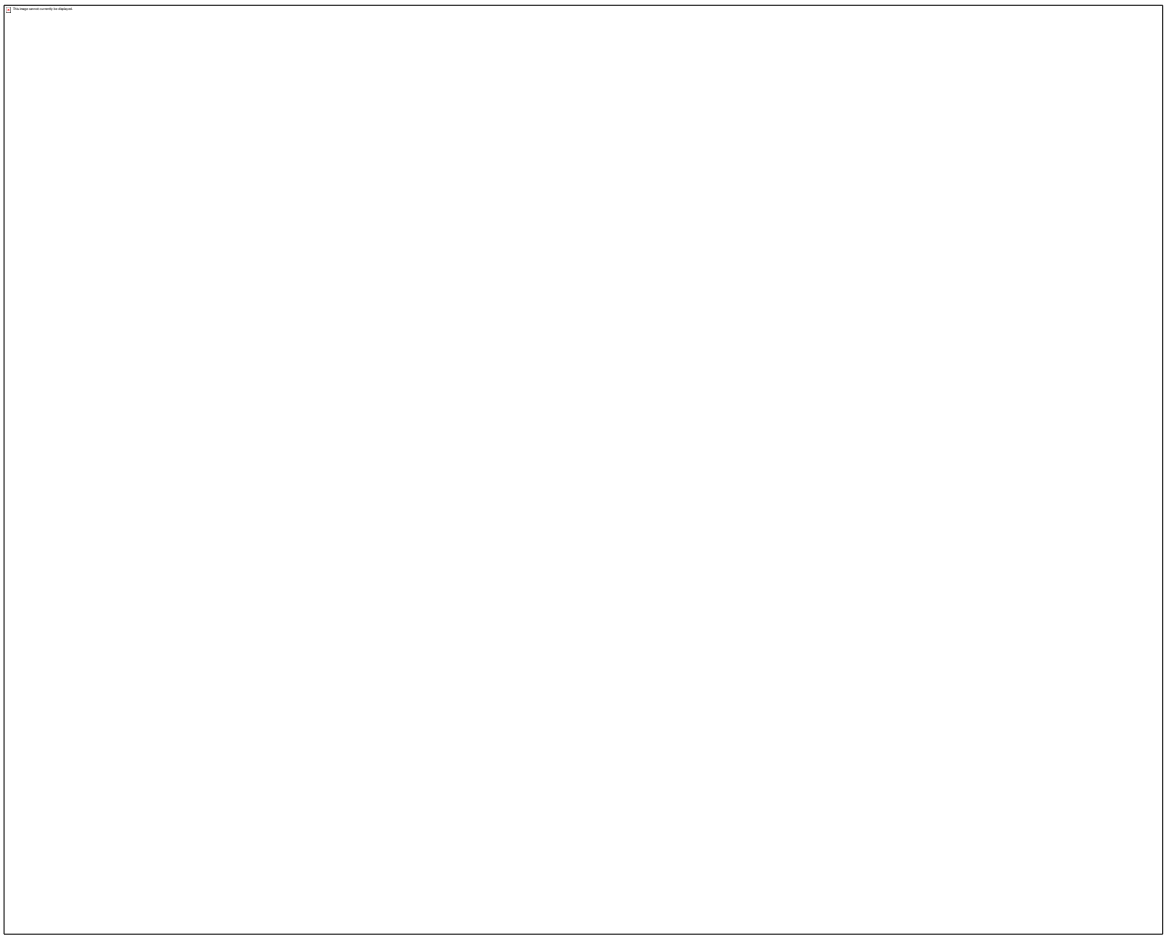

^{1}H NMR SPECTRUM of 5.1

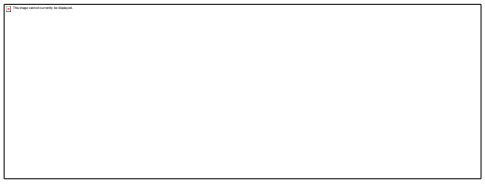

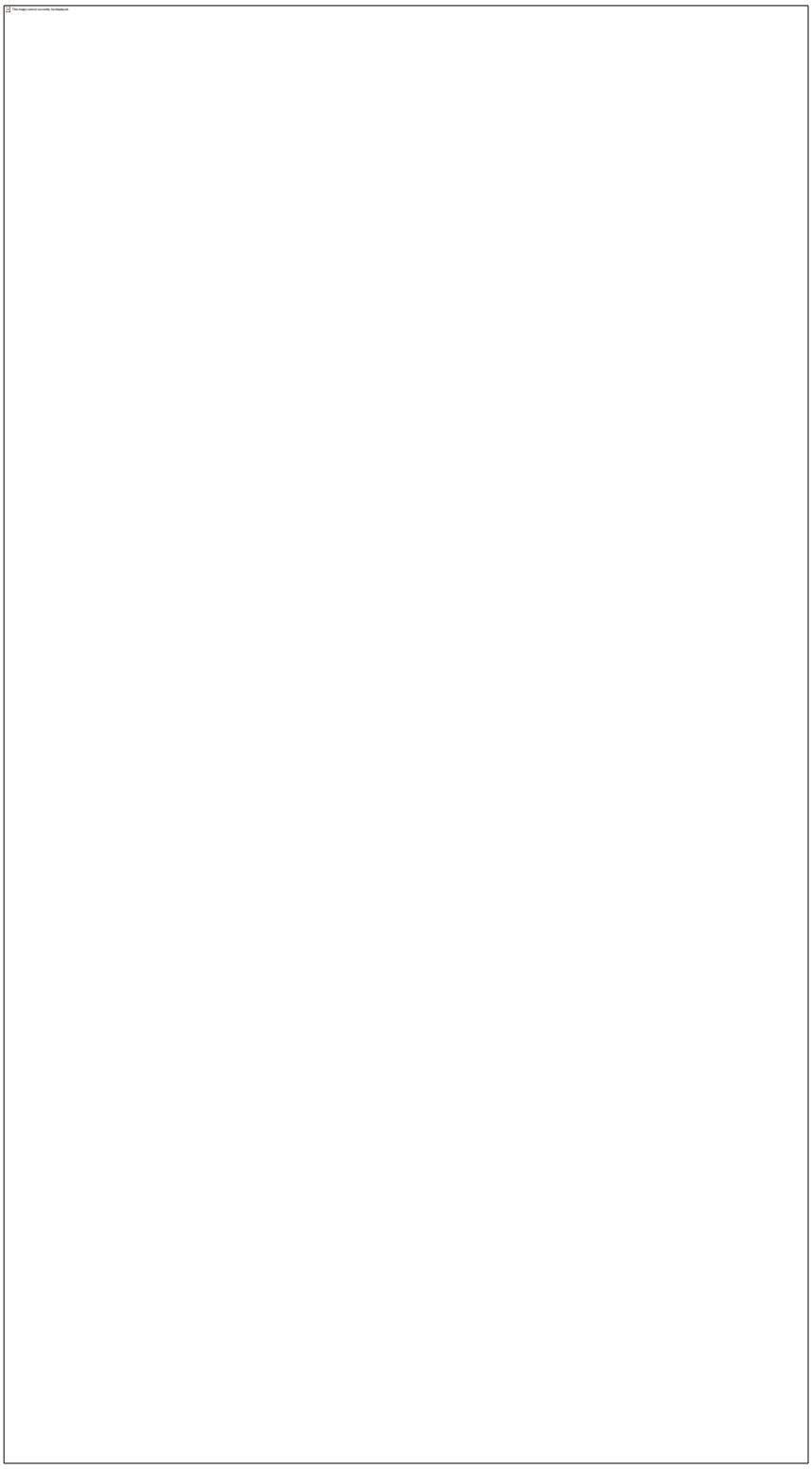

^{1}H NMR and ^{13}C NMR SPECTRA of 5.2

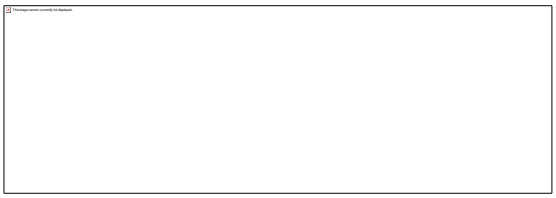

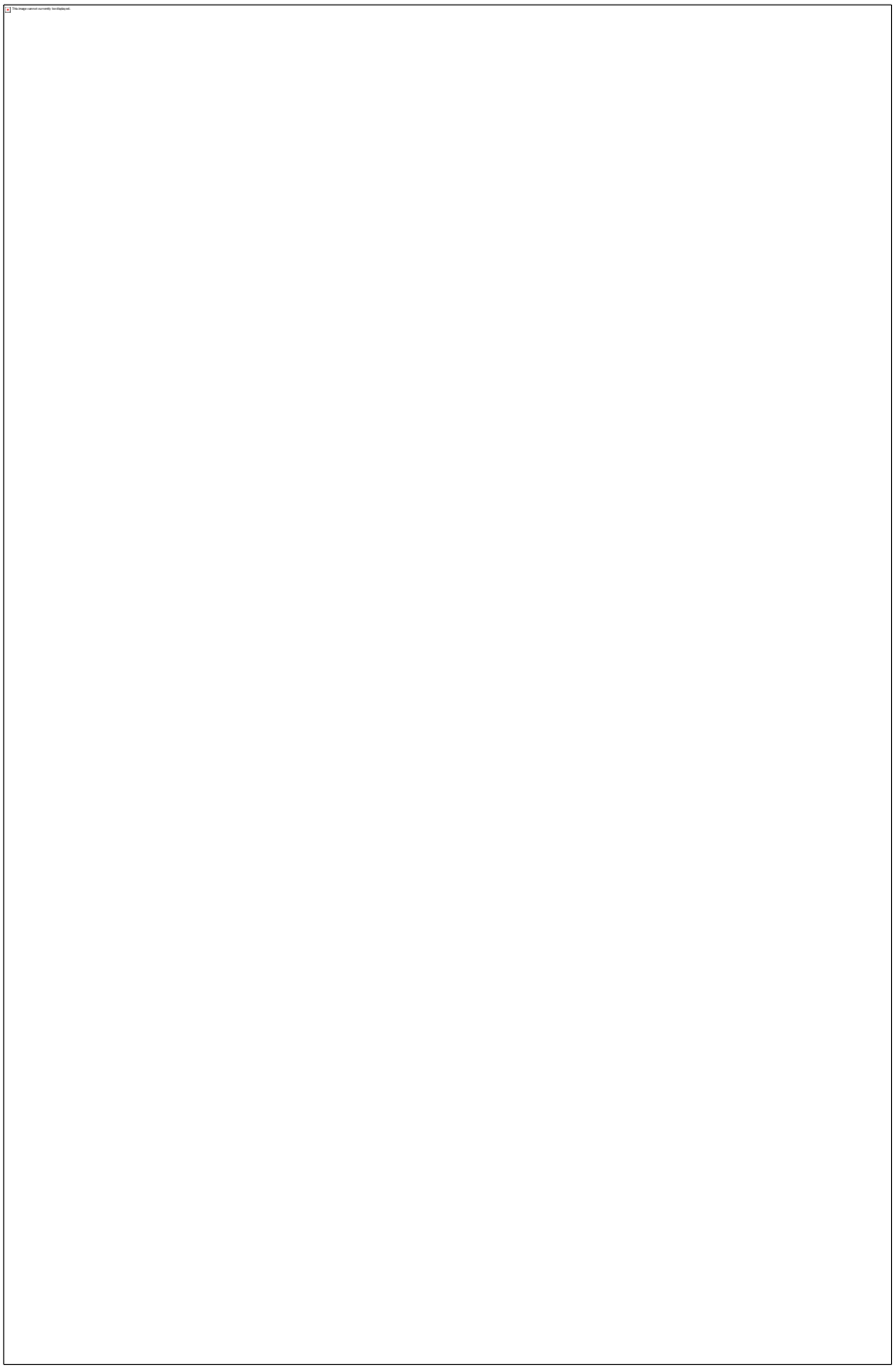

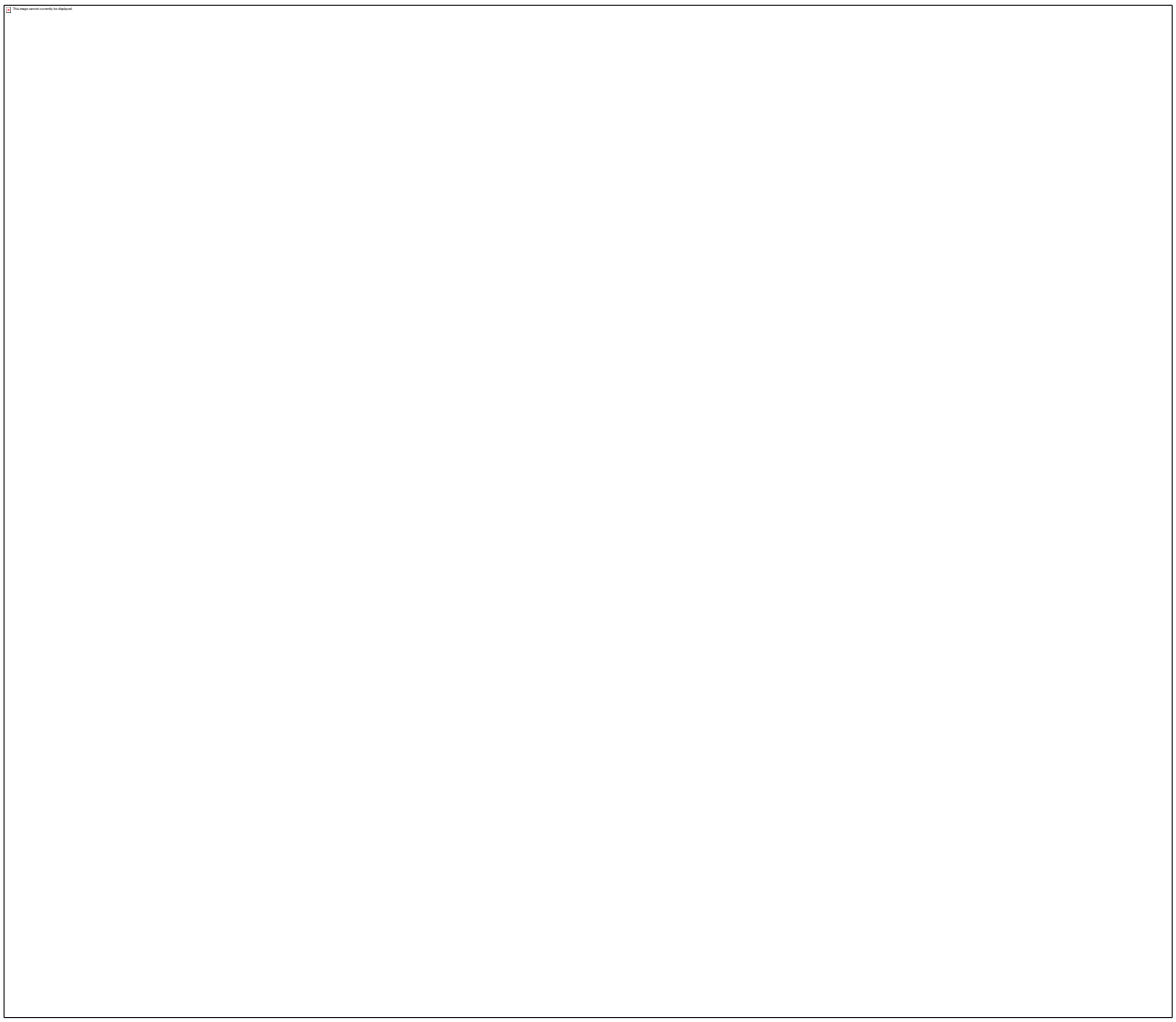

^{1}H NMR SPECTRUM OF of 5.5

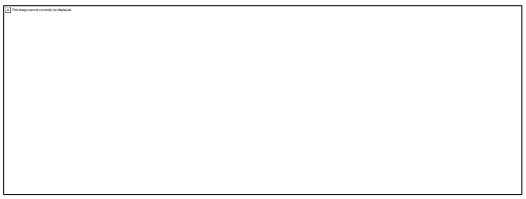

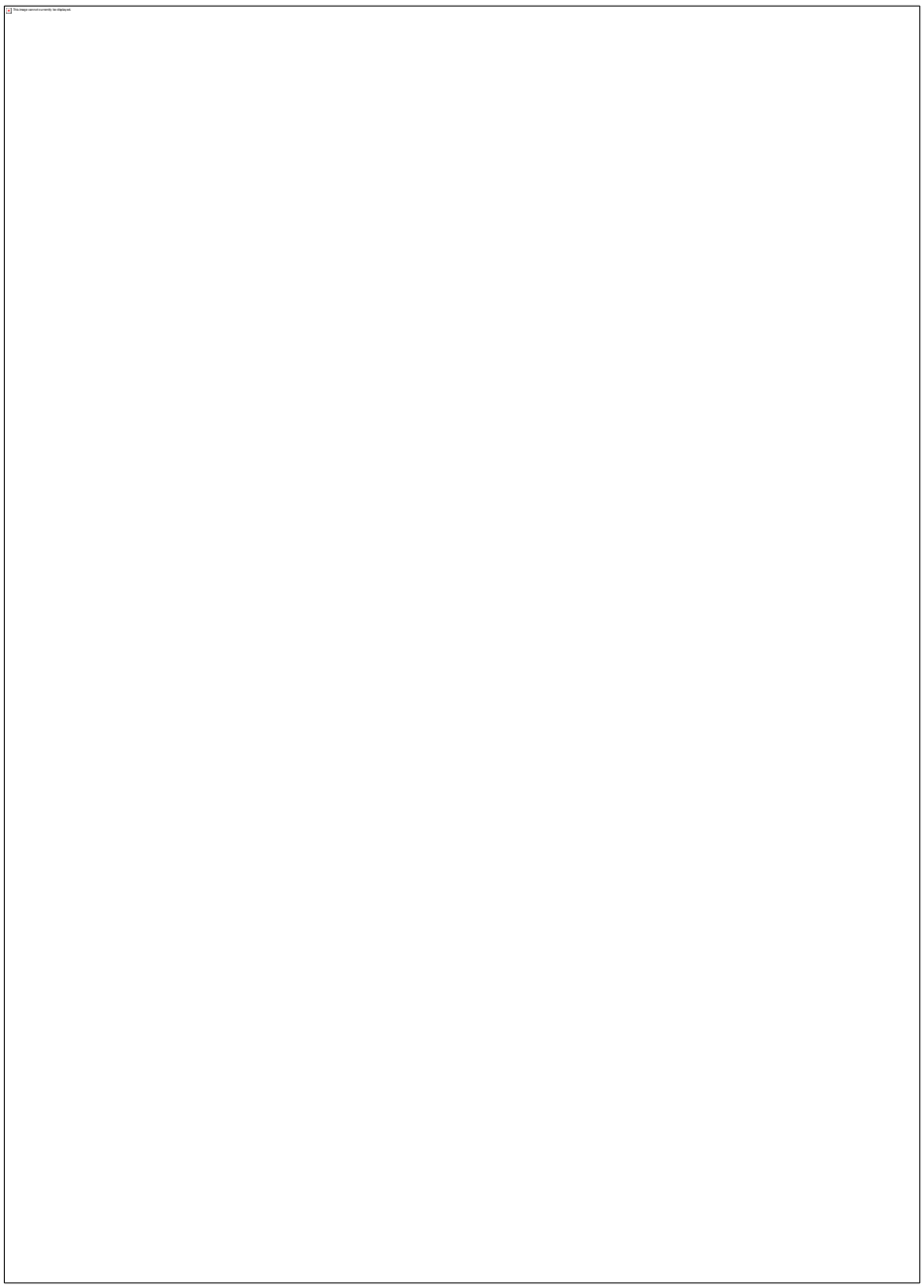

^{1}H NMR and ^{13}C NMR SPECTRA of 5.6

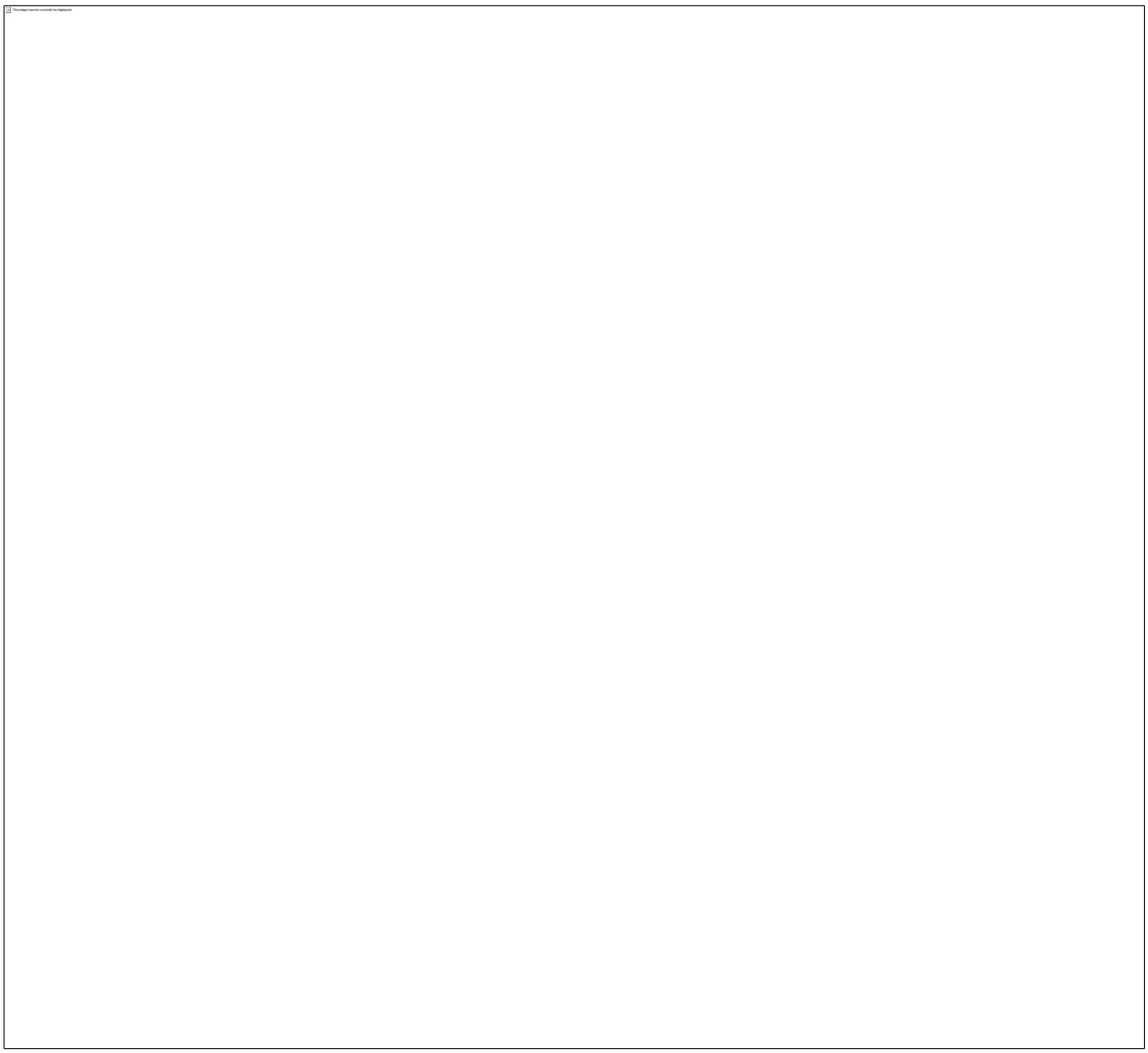

^{1}H NMR SPECTRUM of 4.6a

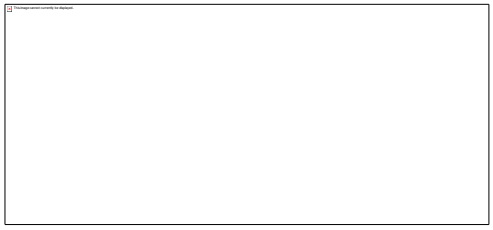

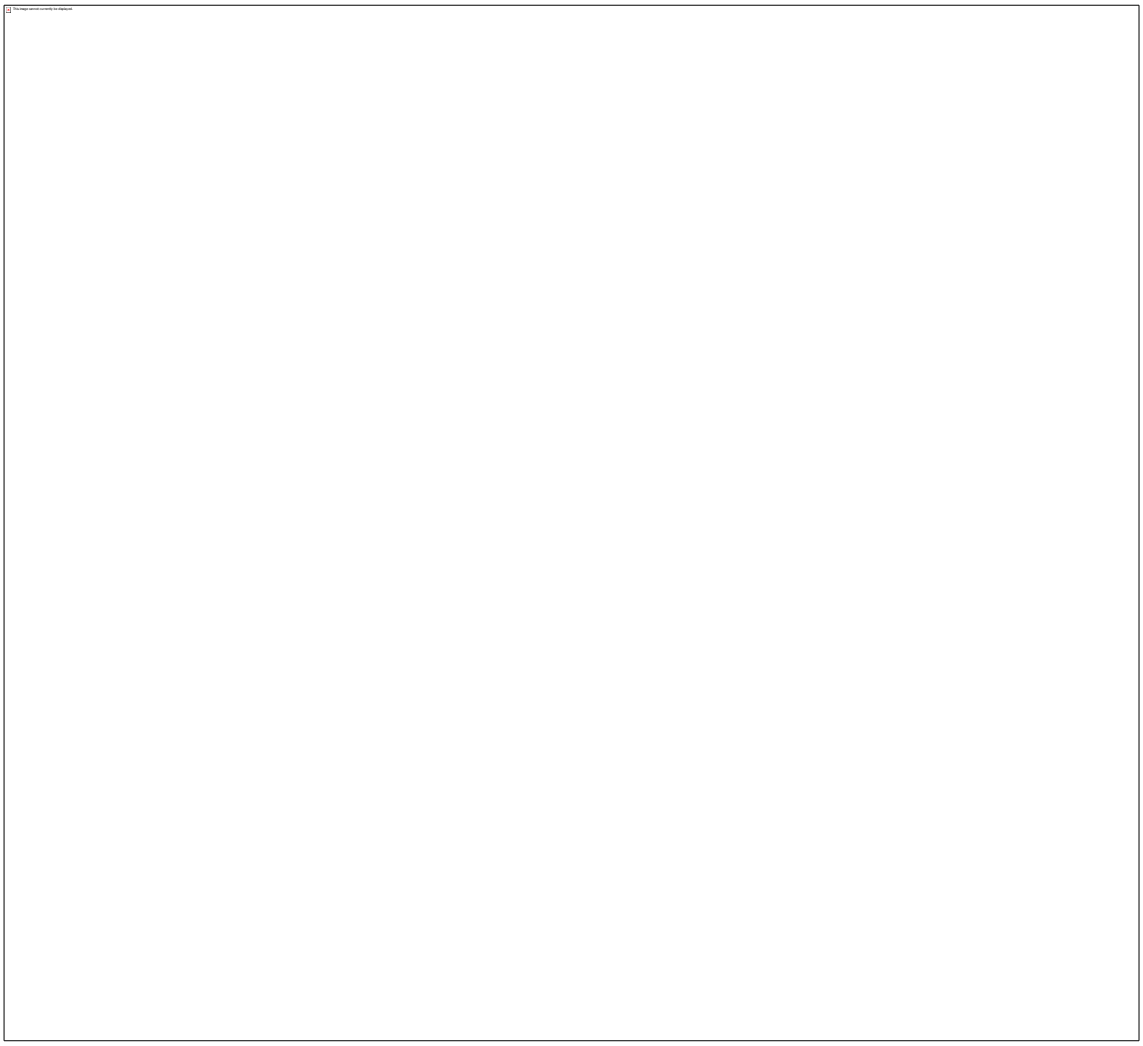

^{1}H NMR and ^{13}C NMR SPECTRA of 5.7

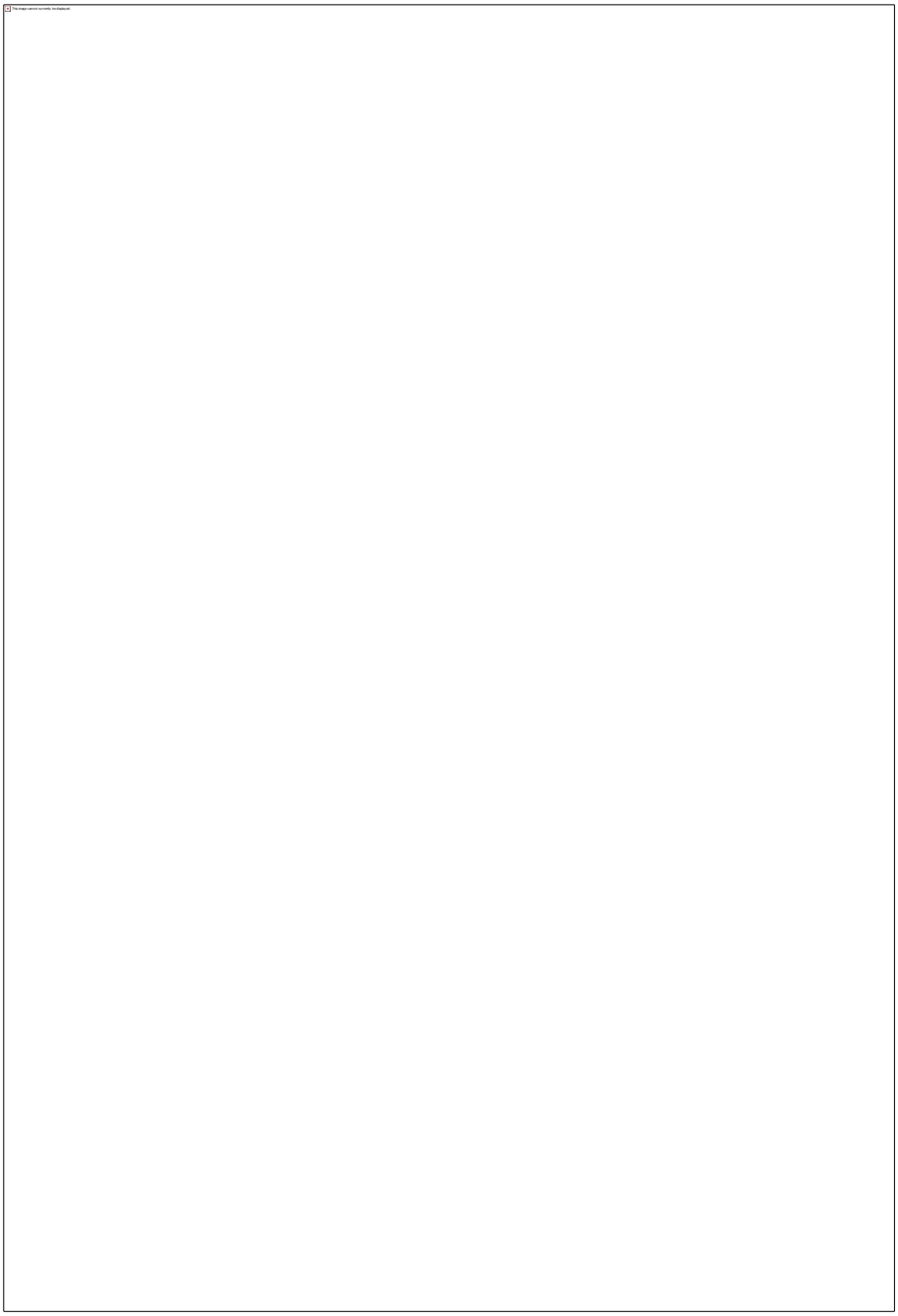

^{1}H NMR and ^{13}C NMR SPECTRA of 5.8

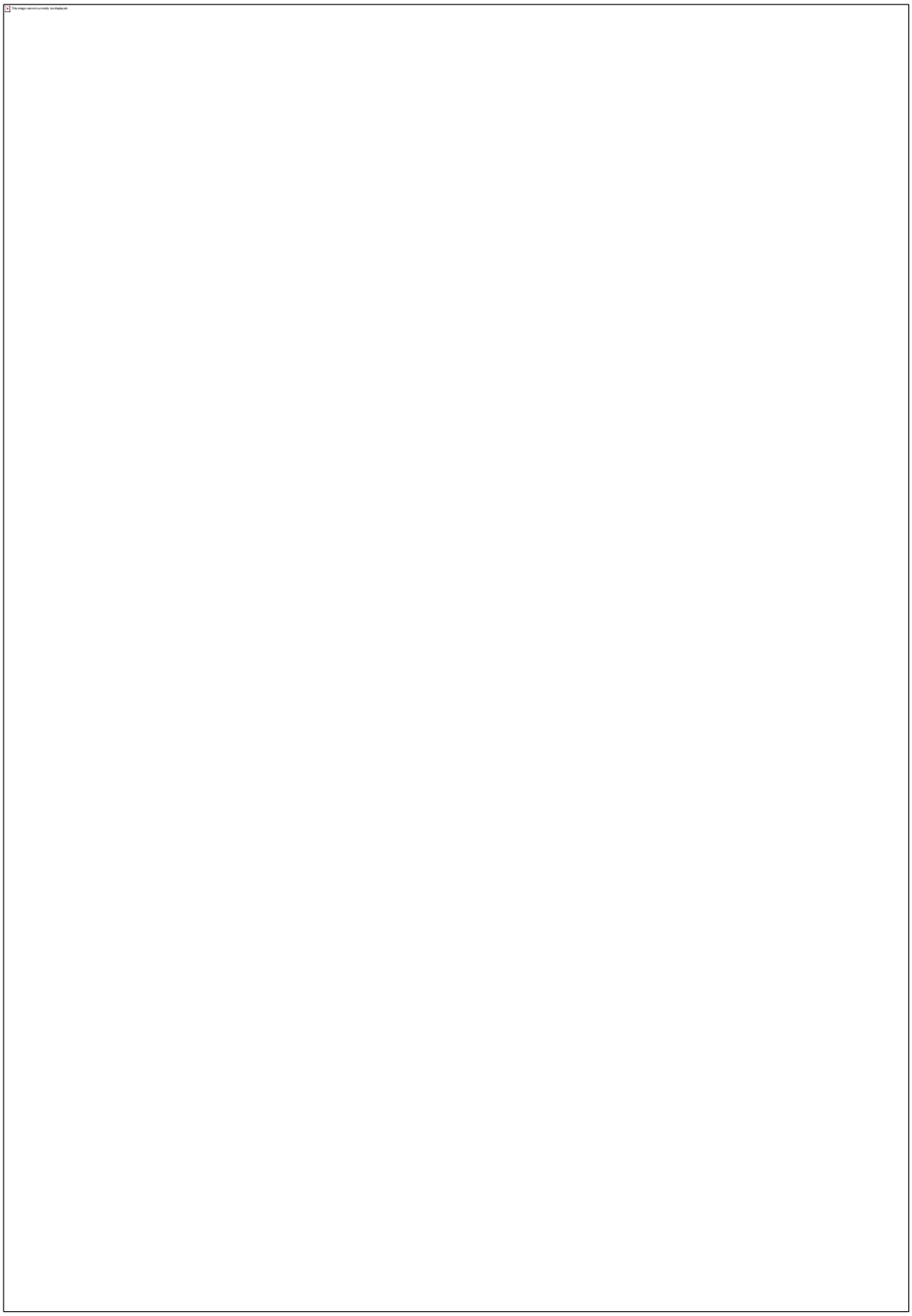

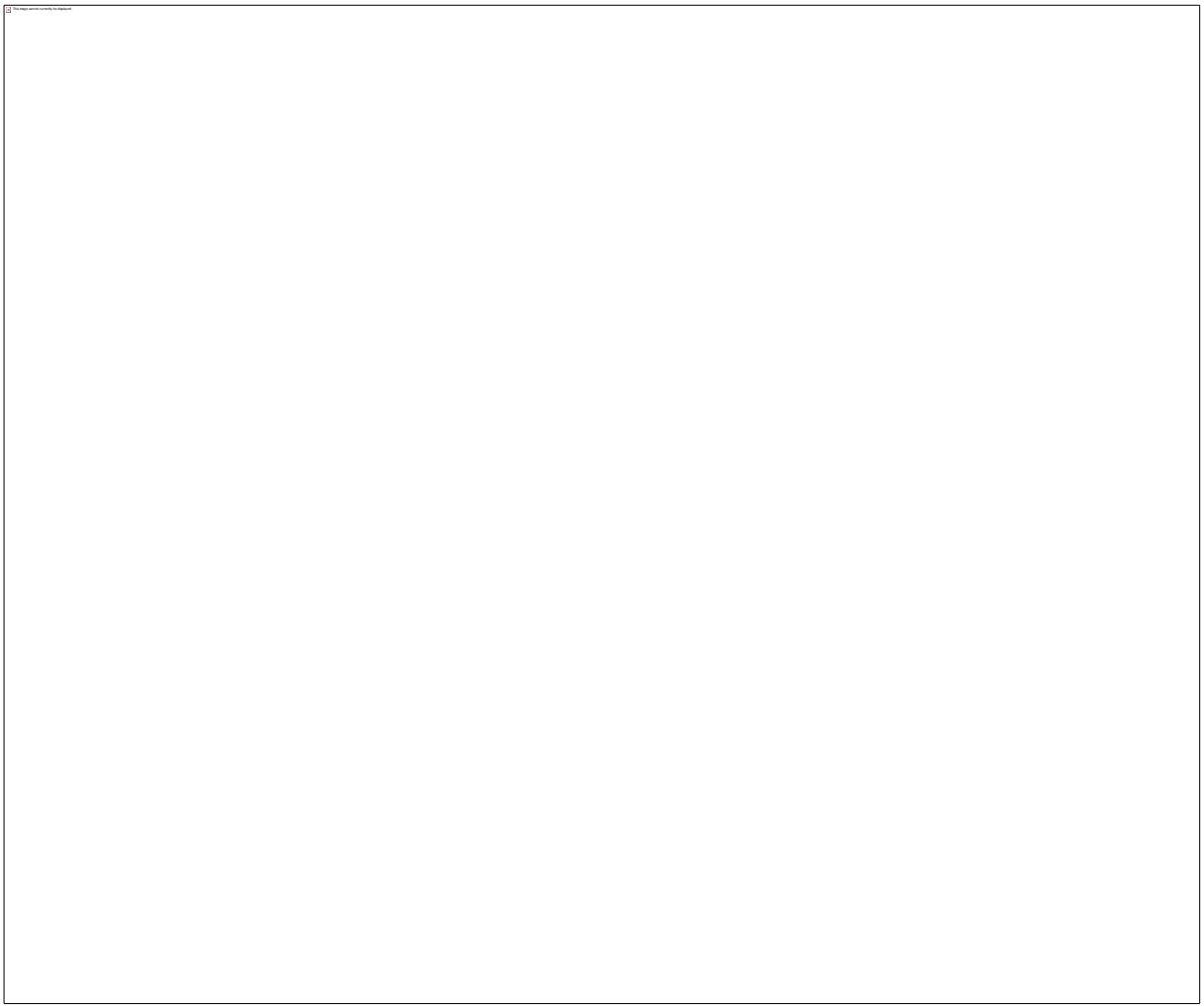

^{1}H NMR and ^{13}C NMR SPECTRA 6.3

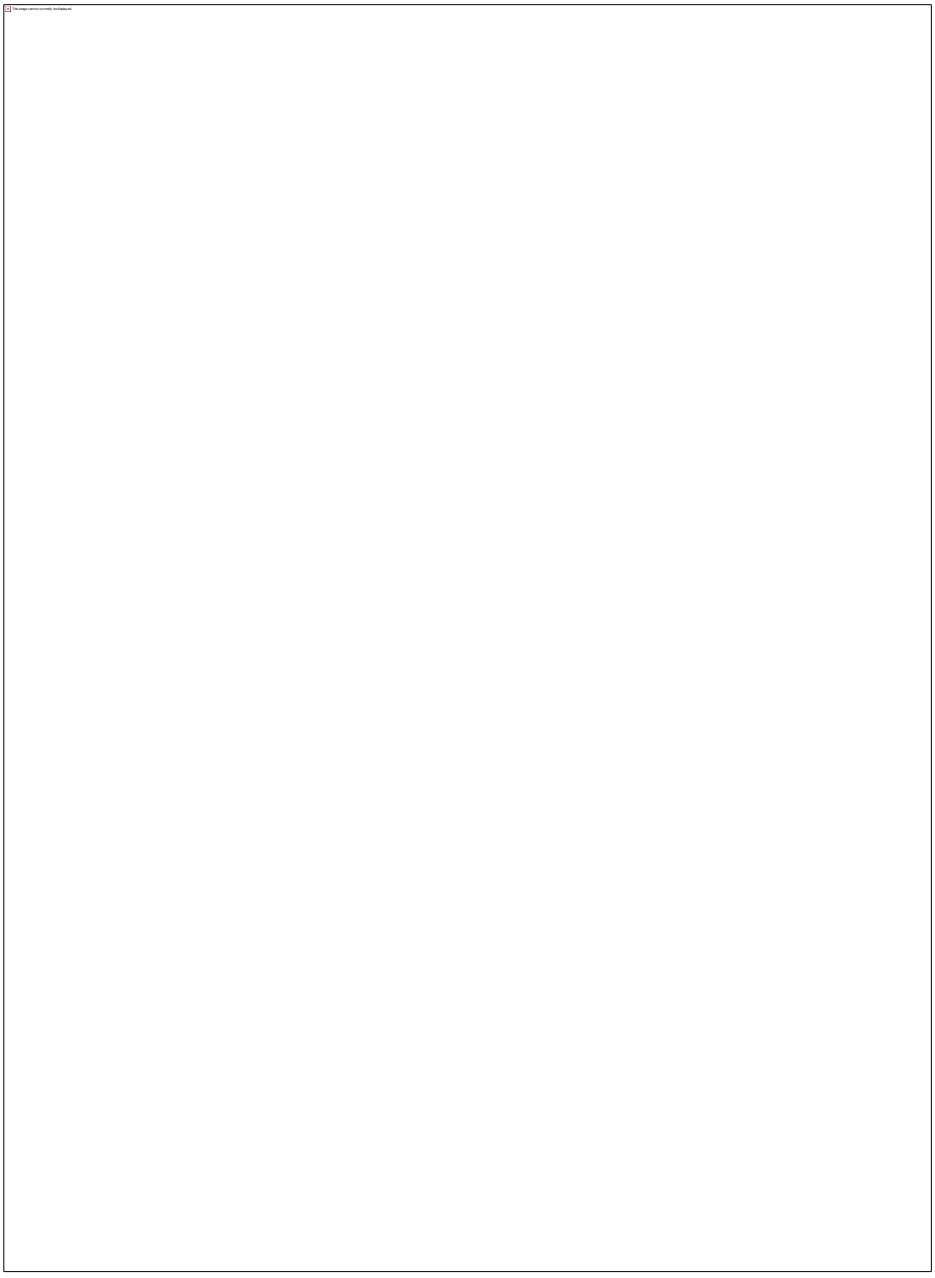

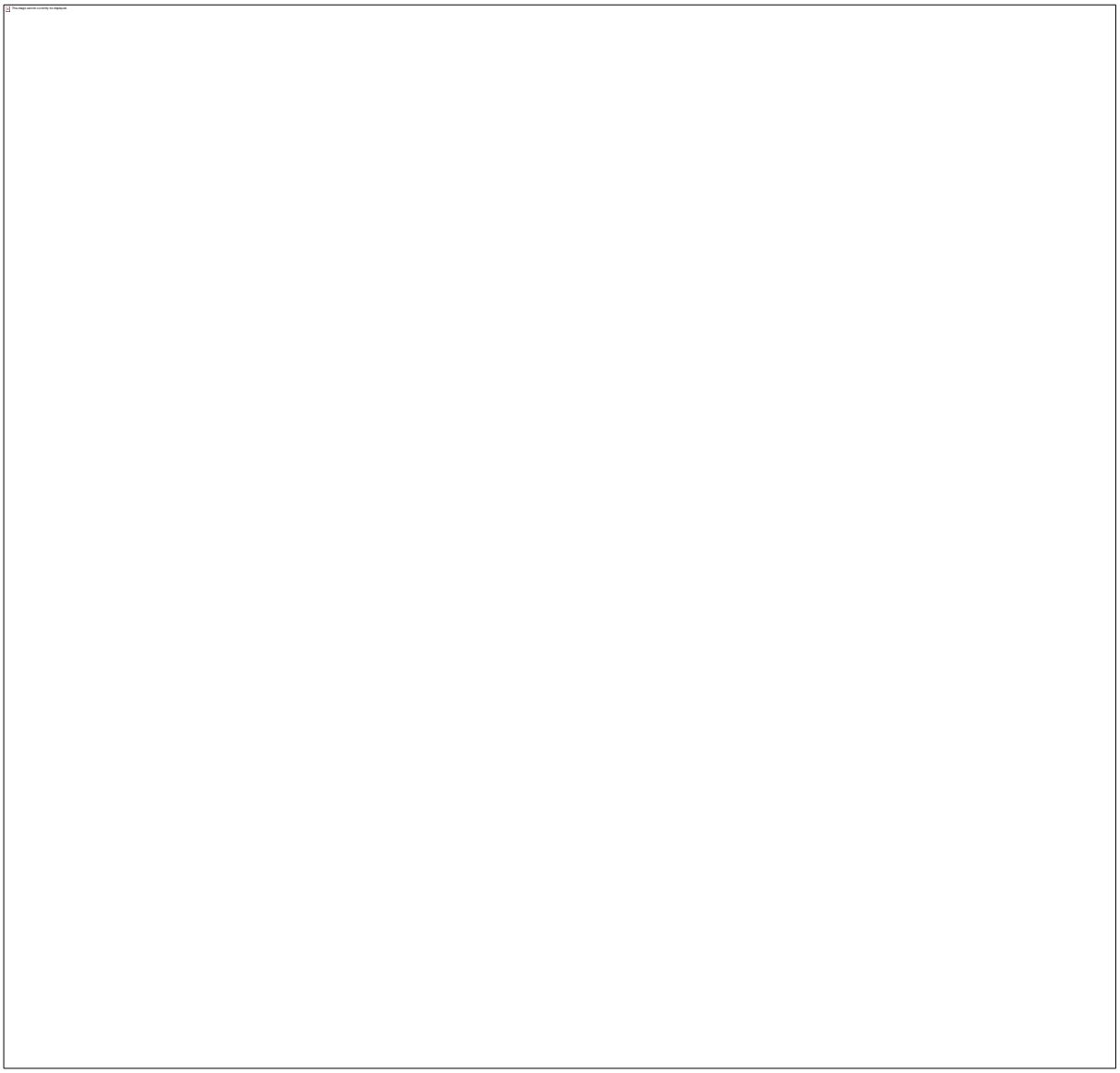

^{1}H NMR AND ^{13}C NMR SPECTRA 6.4

^{1}H NMR and ^{13}C NMR SPECTRA 6.5

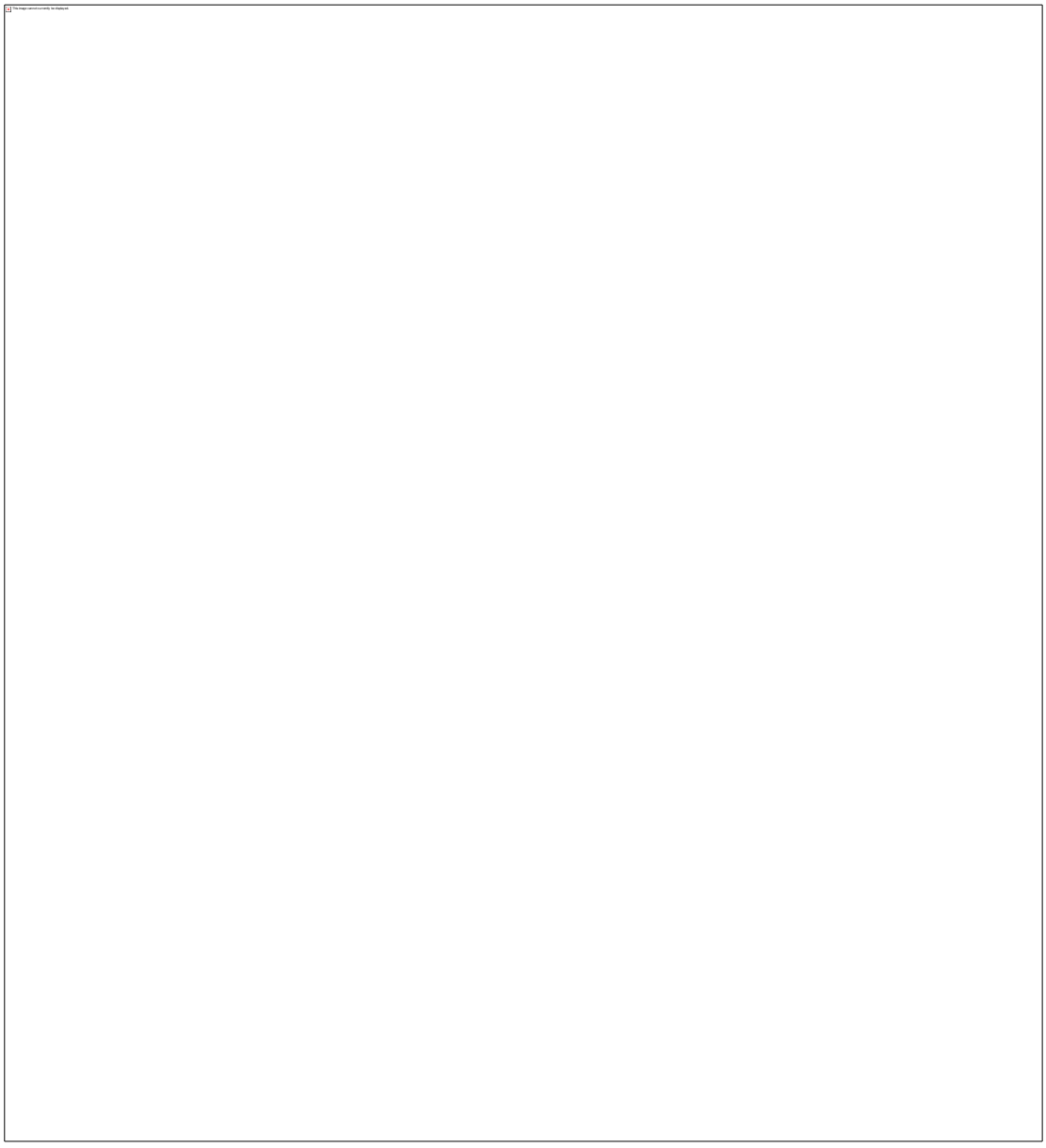

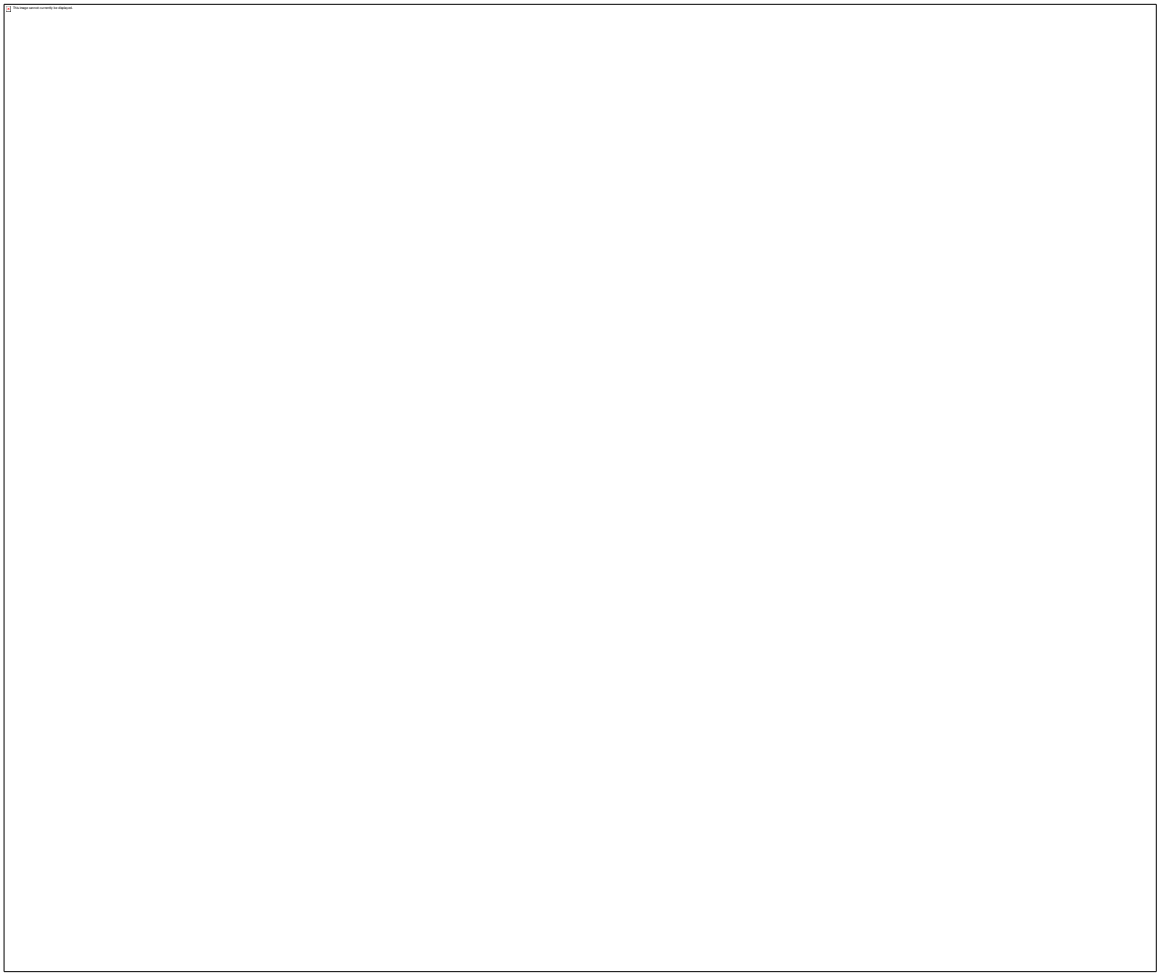

^{1}H NMR and ^{13}C NMR SPECTRA 6.7

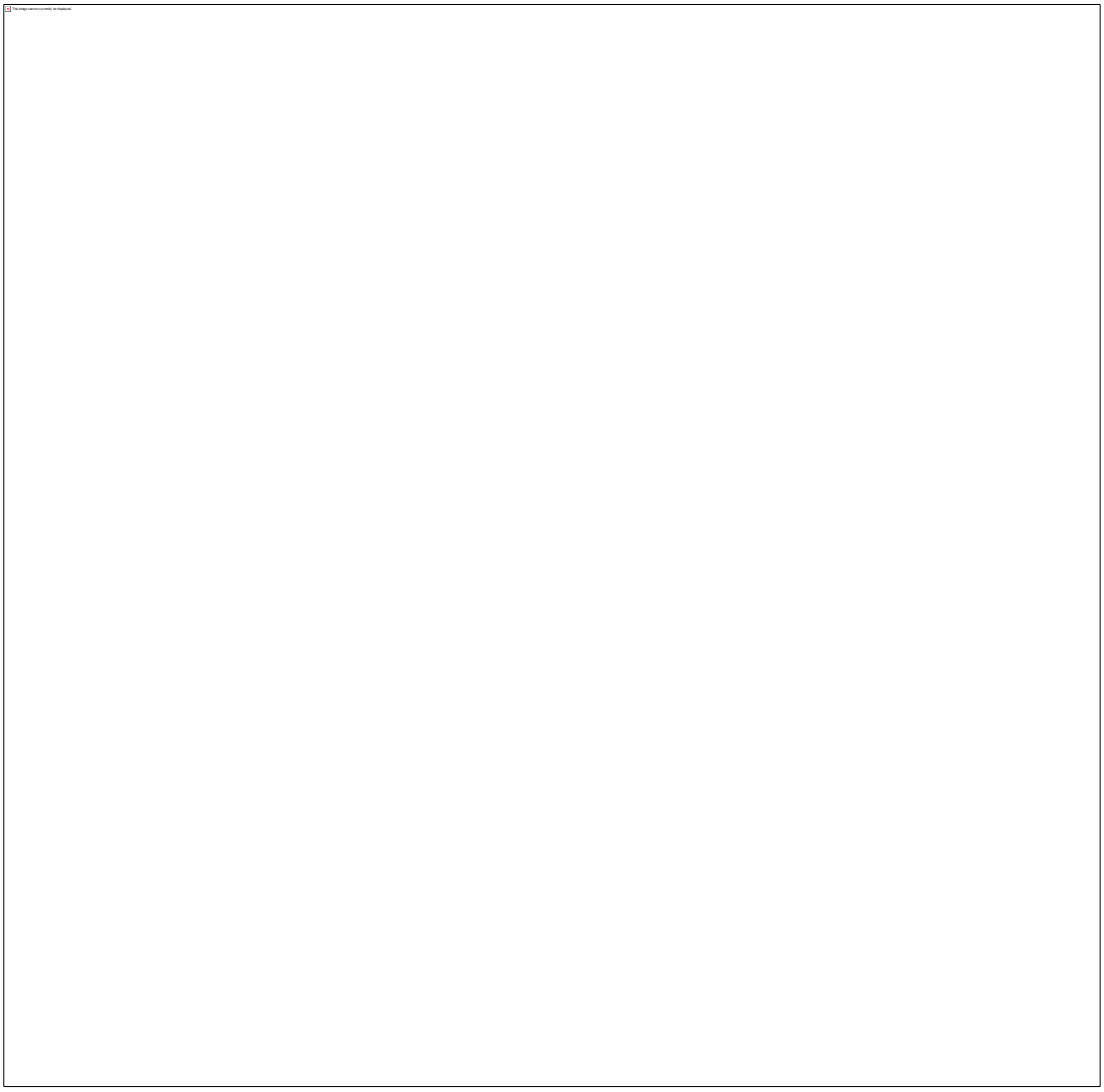

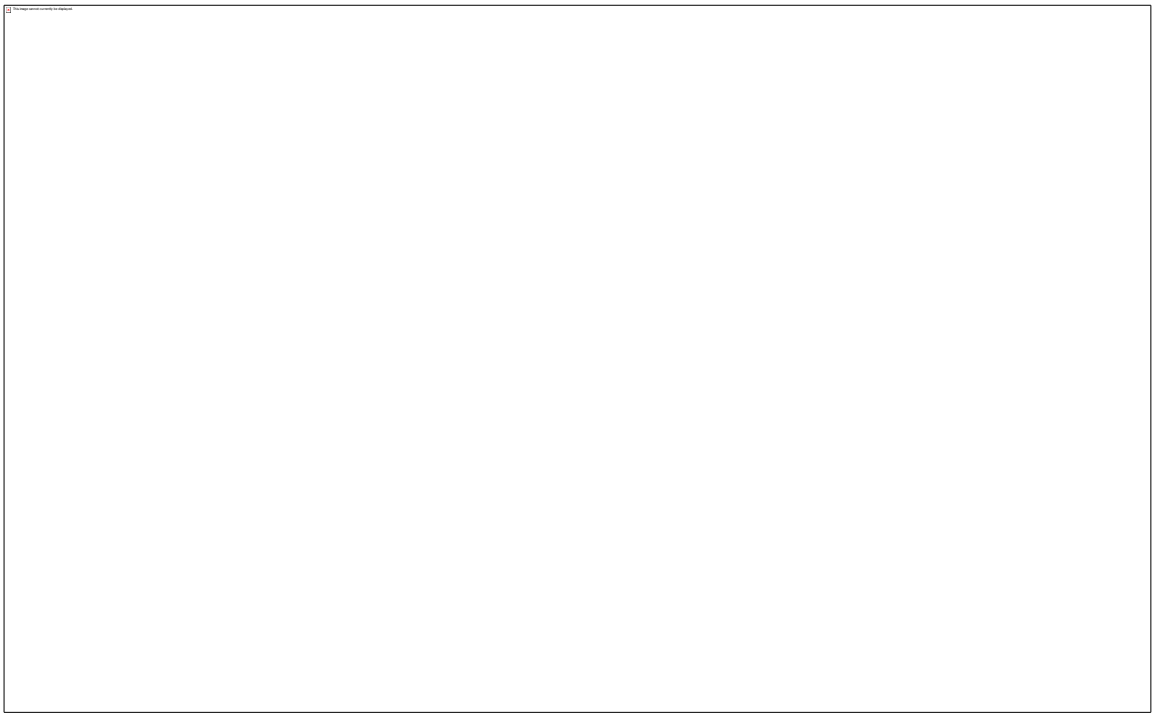

2. HPLC traces of final products

Chapter 4

4.9

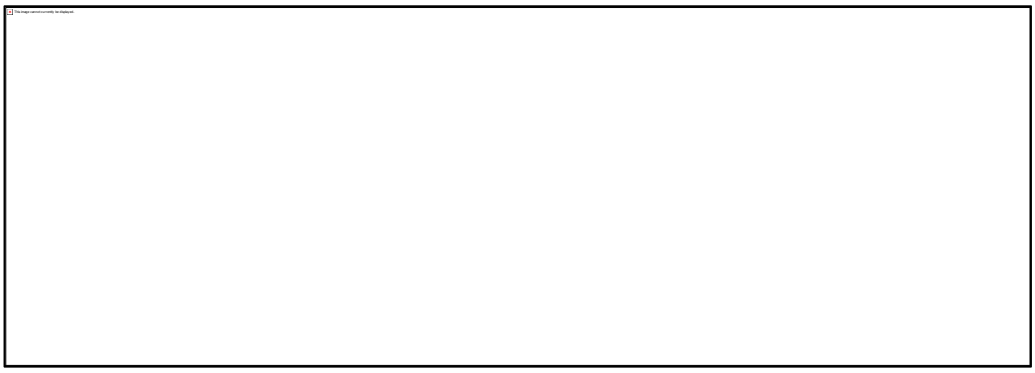

	Time	Area %
1	1.671	0.802
2	10.213	1.316
3	10.523	96.473
4	15.009	0.511
5	16.314	0.299
6	16.652	0.599

4.10

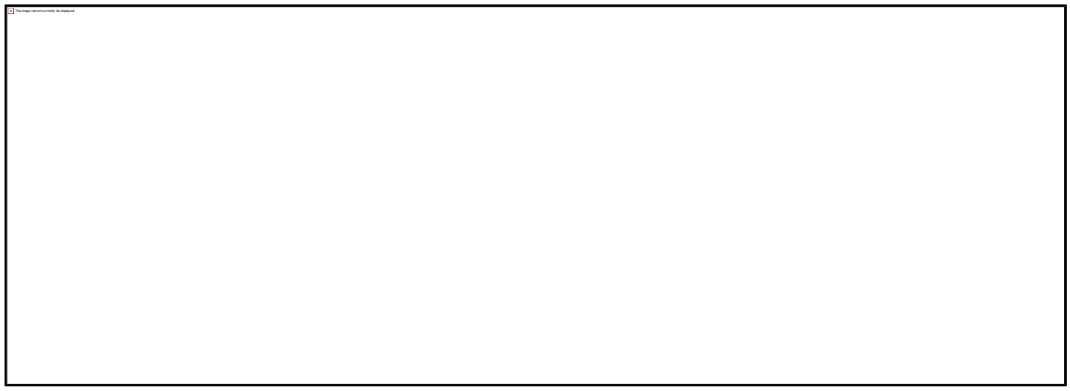

	Time	Area %
1	1.658	0.027
2	12.418	0.048
3	12.729	0.107
4	13.138	99.269
5	14.320	0.021
6	14.765	0.528

4.11

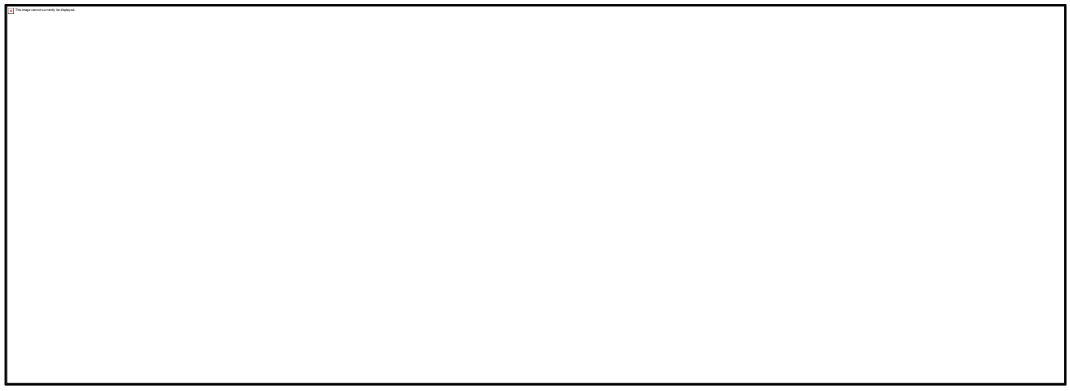

	Time	Area %
1	5.918	0.097
2	10.864	95.562
3	11.317	1.291
4	11.79	0.019
5	12.829	0.048
6	12.963	1.117
7	13.612	1.308
8	16.595	0.558

4.12

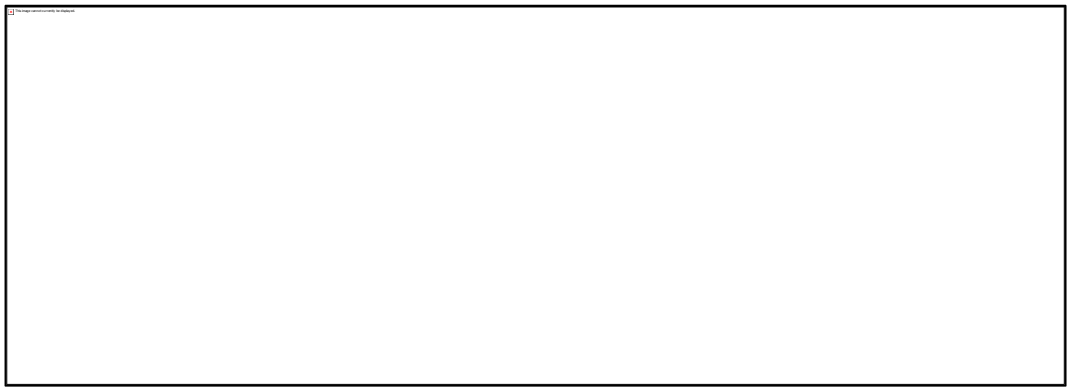

	Time	Area %
1	1.693	0.465
2	1.834	0.112
3	14.181	99.423

4.13

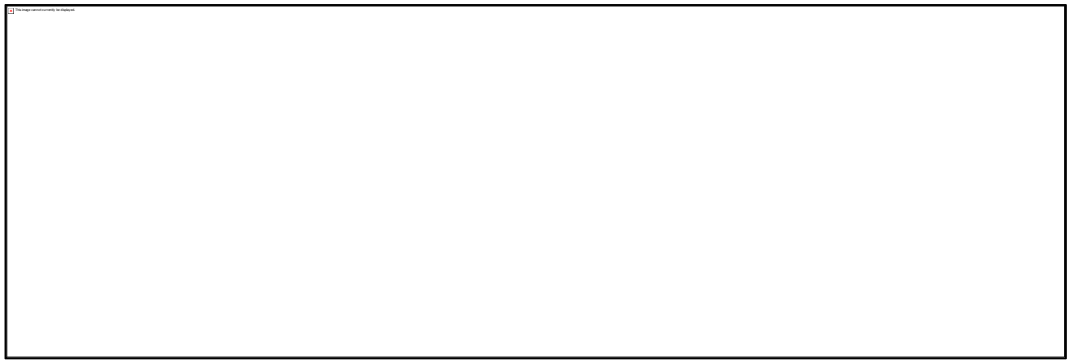

	Time	Area %
1	1.624	0.301
2	1.711	0.202
3	14.714	95.295
4	16.965	2.724
5	19.289	1.487

4.14

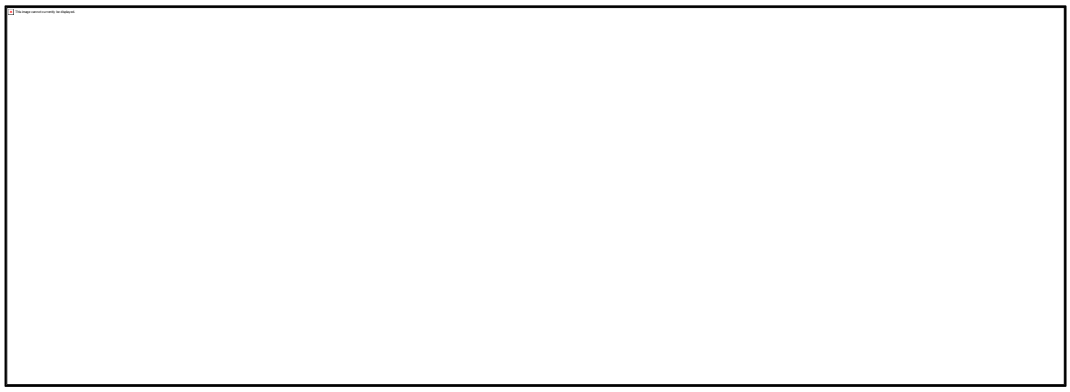

	Time	Area %
1	1.672	0.018
2	10.513	96.723
3	11.741	1.098
4	12.503	0.677
5	19.144	0.384

4.15

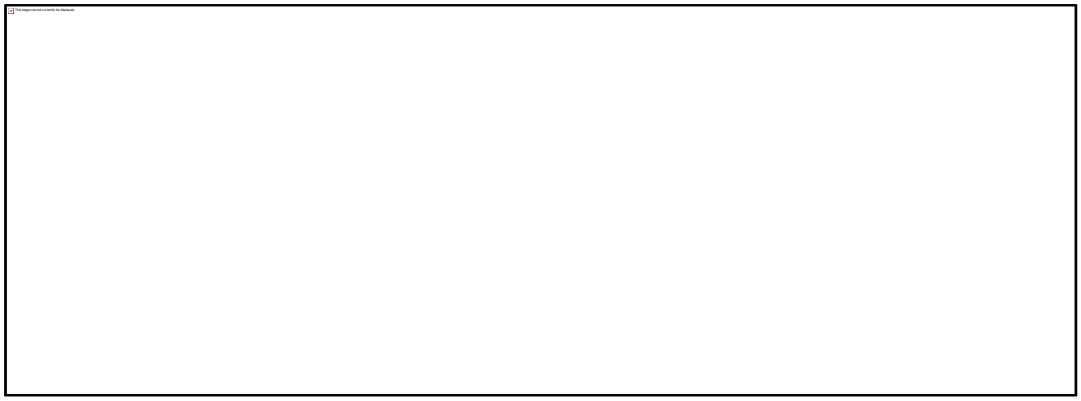

	Time	Area %
1	9.186	1.687
2	13.625	96.963
3	14.142	1.233
4	23.731	0.117

4.16

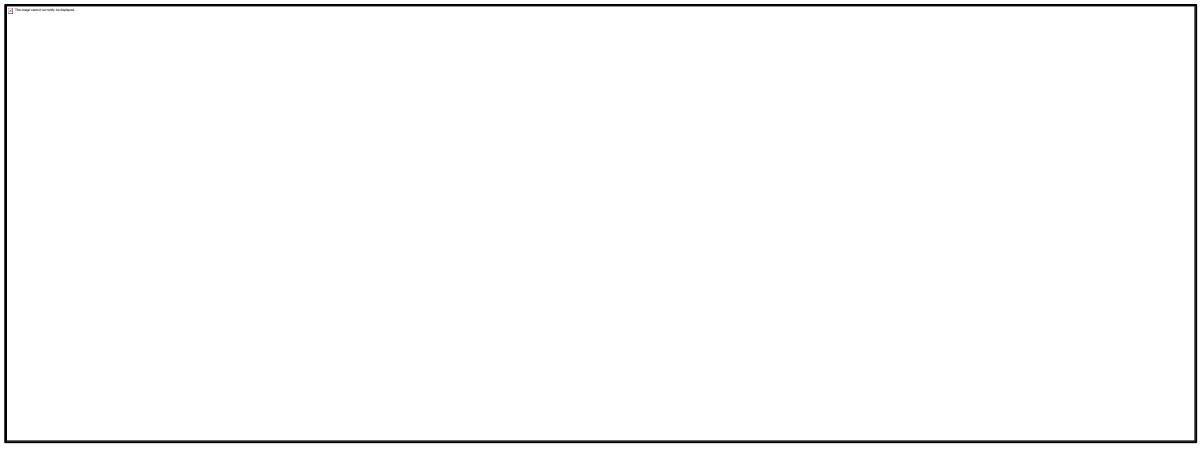

	Time	Area %
1	12.228	97.504
2	13.844	0.575
3	15.481	0.281
4	15.639	0.123
5	16.293	0.127
6	20.117	1.390

4.17

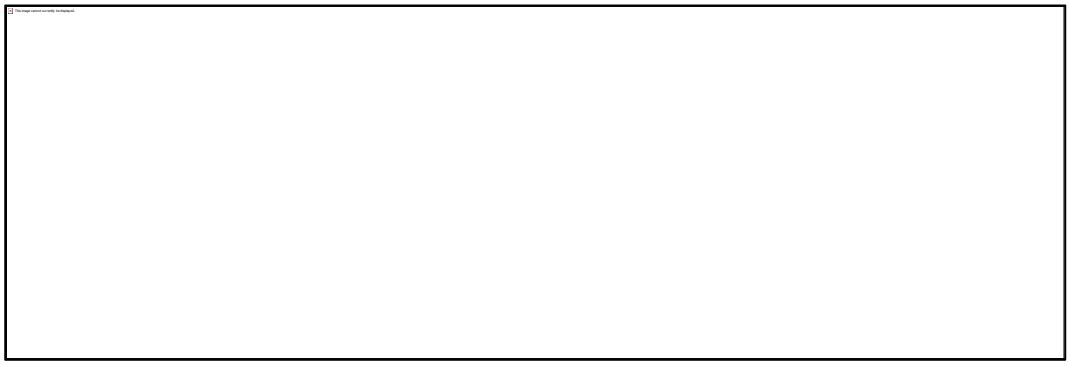

	Time	Area %
1	3.617e-2	0.032
2	6.620	0.700
3	9.322	1.192
4	12.305	0.041
5	13.726	95.728
6	14.307	1.078
7	15.756	1.041
8	16.184	0.189

4.18

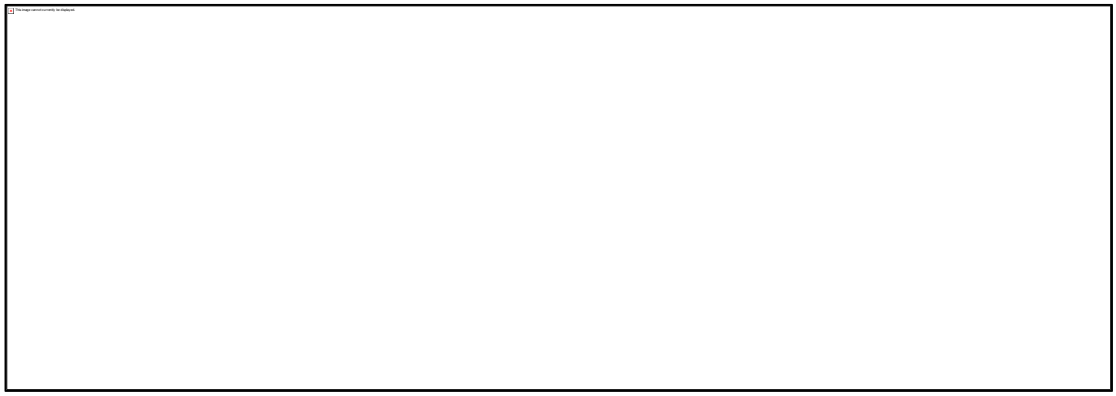

	Time	Area %
1	3.628e-2	0.010
2	8.904	1.343
3	11.988	97.936
4	12.311	0.0865

4.19

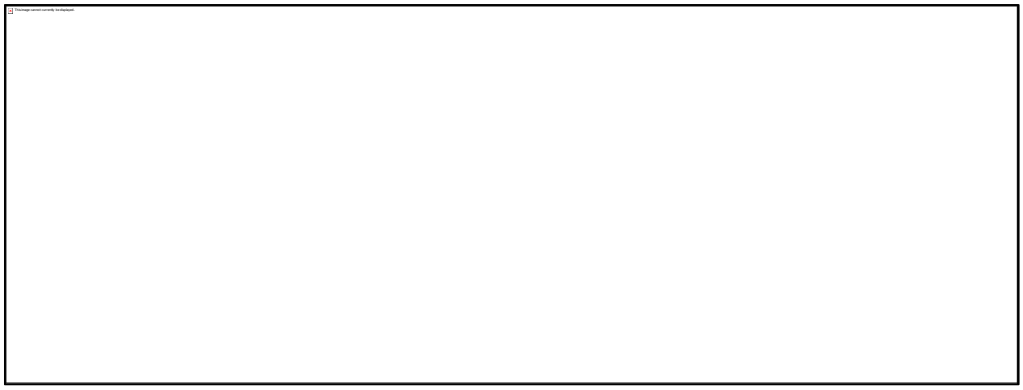

	Time	Area %
1	1.722	0.077
2	1.786	0.040
3	10.826	0.369
4	10.976	0.579
5	12.246	94.008
6	14.002	1.026
7	14.676	2.031
8	15.201	0.914
9	17.795	0.355

4.20

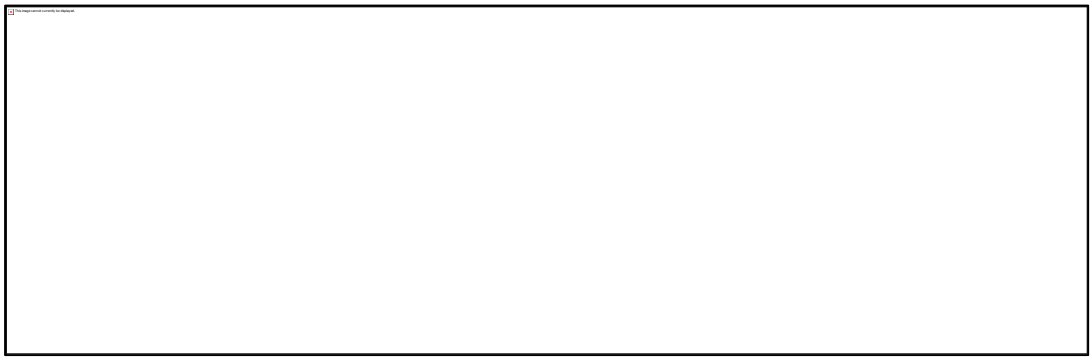

	Time	Area %
1	10.624	98.223
2	13.832	1.343
3	19.1	0.460

4.21

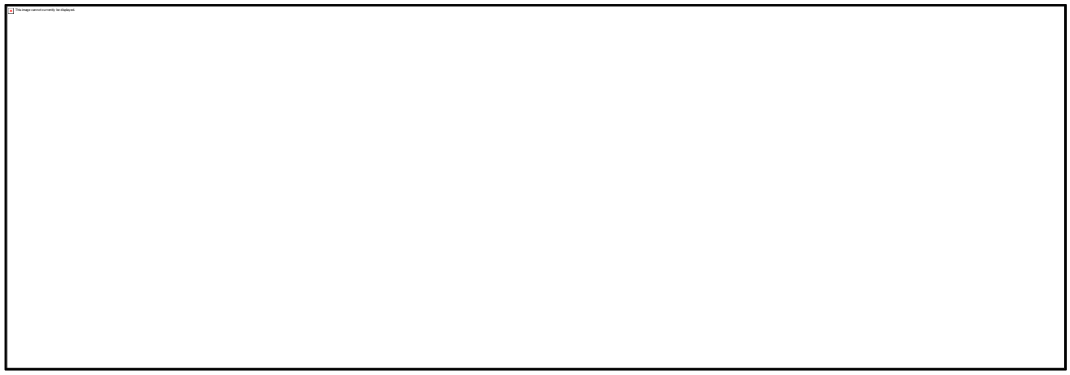

	Time	Area %
1	1.568	0.196
2	11.259	94.045
3	11.484	2.064
4	12.082	0.535
5	13.72	2.499
6	13.921	0.399
7	16.354	0.262

4.22

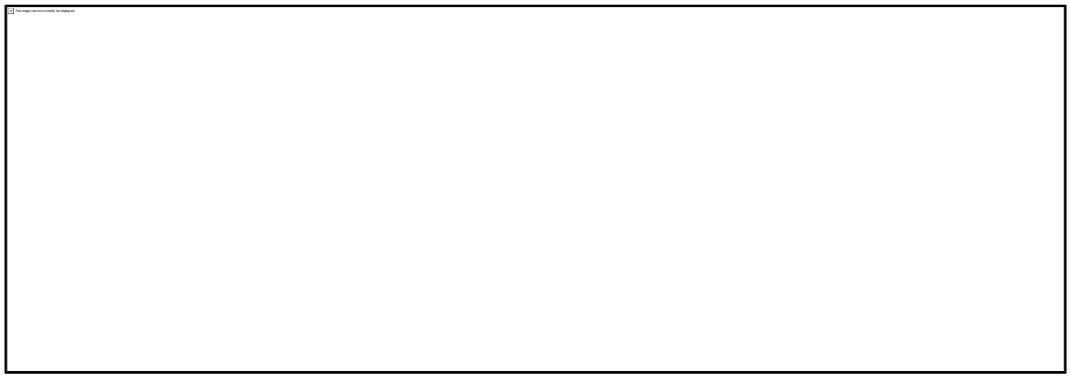

	Time	Area %
1	10.277	3.273
2	10.912	95.135
3	11.232	1.592

4.23

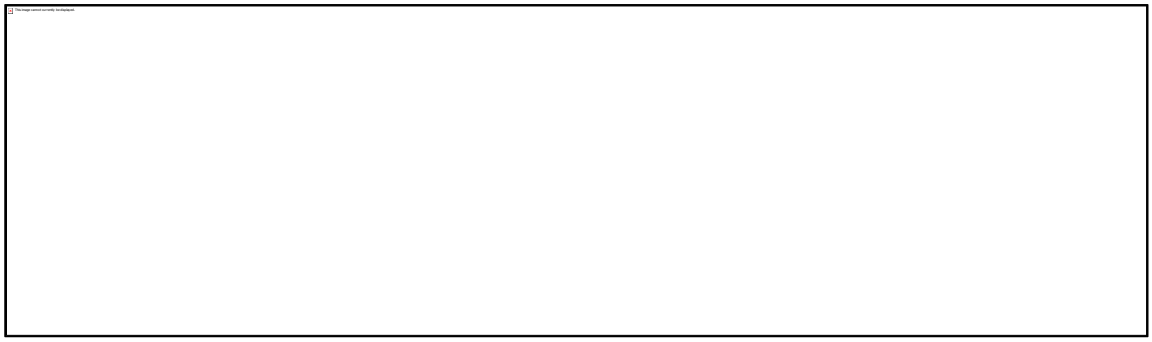

	Time	Area %
1	6.821	0.960
2	10.913	94.617
3	11.143	1.741
4	11.723	1.080
5	13.288	1.052
6	13.505	0.349
7	17.572	0.201

4.24

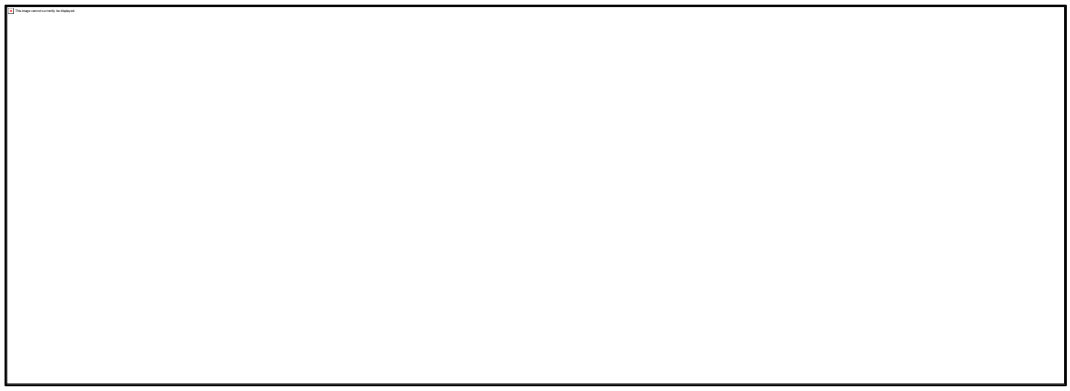

	Time	Area %
1	1.619	2.831
2	13.618	97.169

4.25

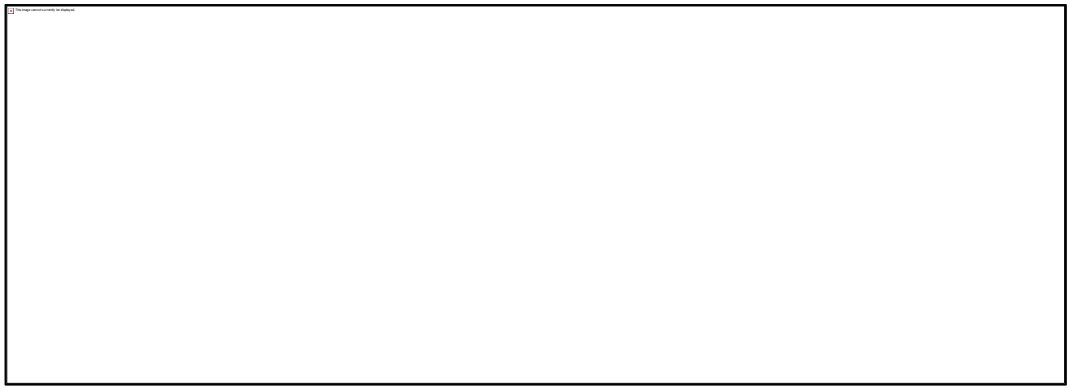

	Time	Area %
1	10.29	0.077
2	11.469	98.531
3	19.045	0.238

4.26

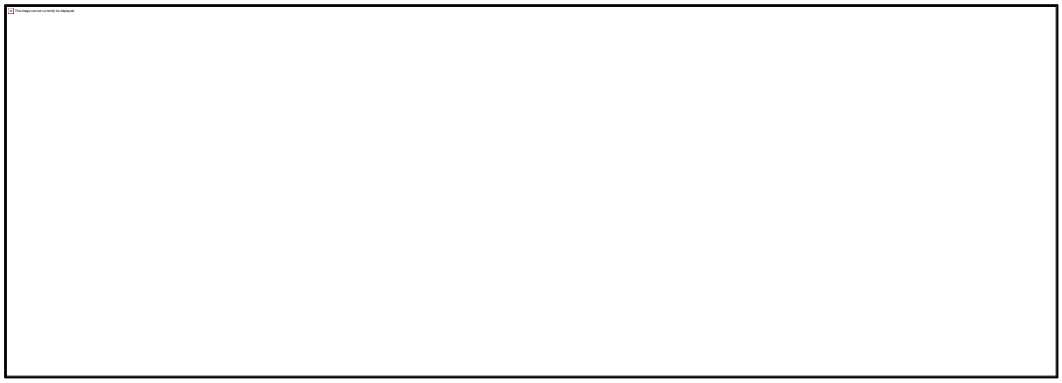

	Time	Area %
1	1.625	0.754
2	1.686	0.286
3	1.847	0.053
	16.20	95.879
	17.23	3.027

4.27

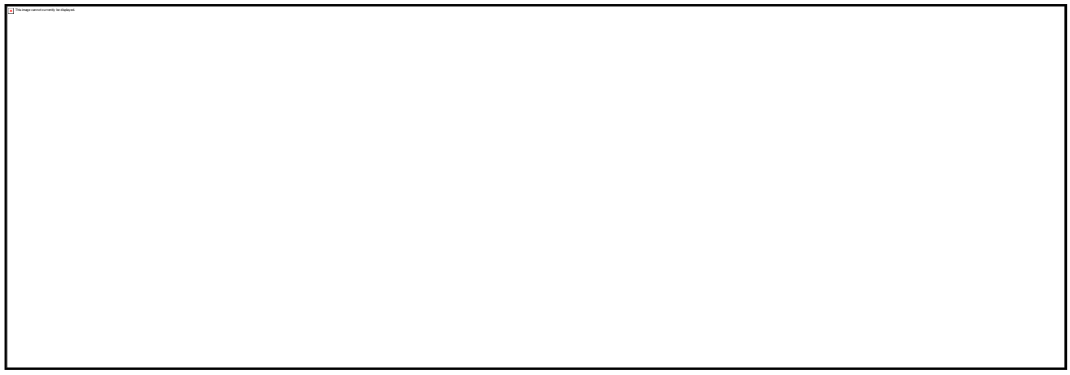

	Time	Area %
1	5.878	0.467
2	6.138	2.030
3	10.104	95.501
4	10.472	1.000
5	12.308	1.002

Chapter 5

5.1

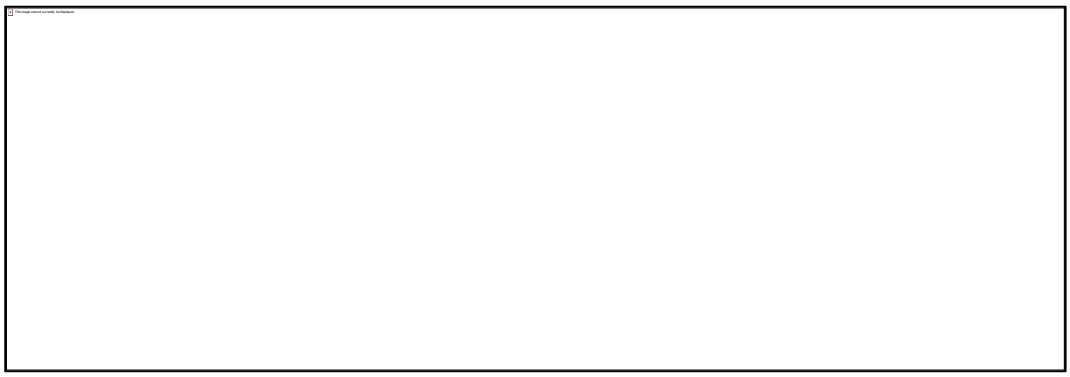

	Time	Area %
1	9.816	1.710
2	13.625	98.290

5.2

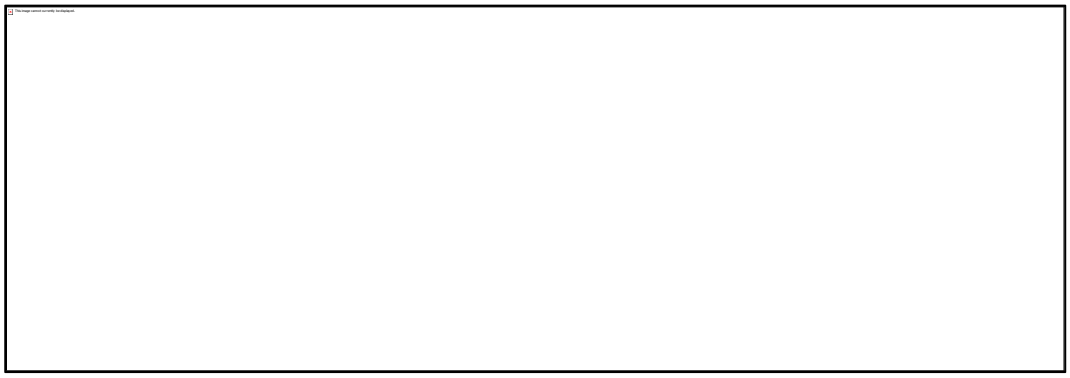

	Time	Area %
1	12.003	0.040
2	12.25	98.585
3	12.685	0.258
4	13.394	0.965
5	13.576	0.151

5.6

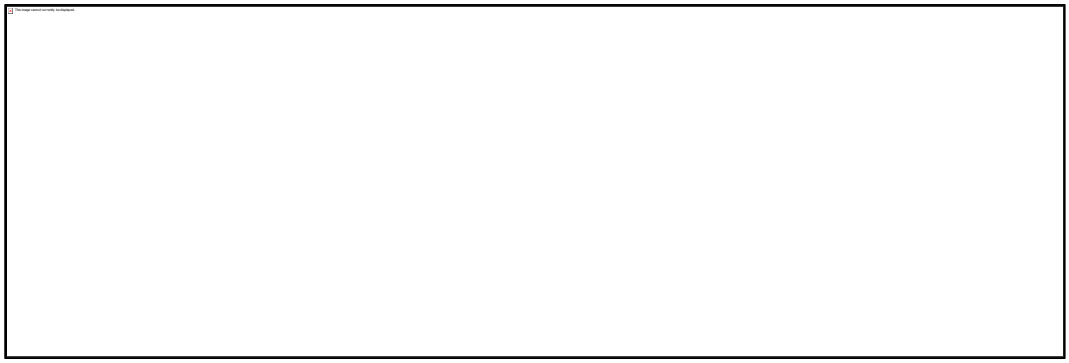

	Time	Area %
1	5.669e-2	0.115
2	14.723	1.1341
3	15.379	97.758
4	15.934	0.599
5	18.326	0.188

5.7

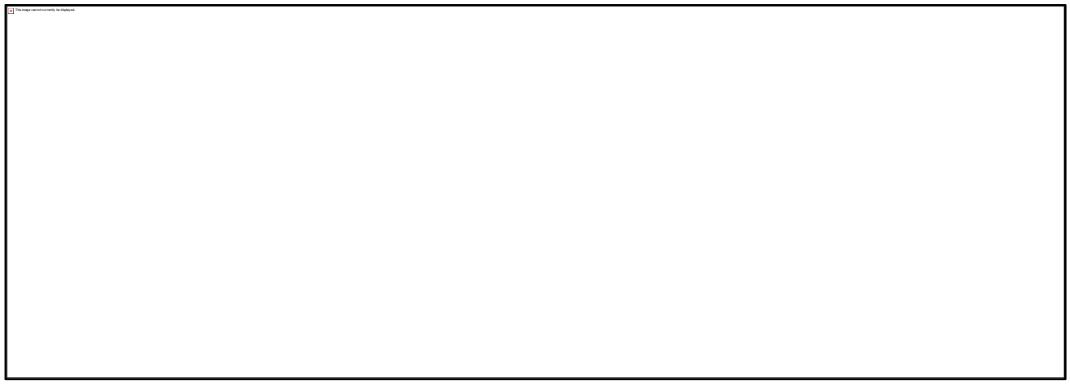

	Time	Area %
1	2.077	0.496
2	14.699	1.696
3	15.099	97.808

5.8

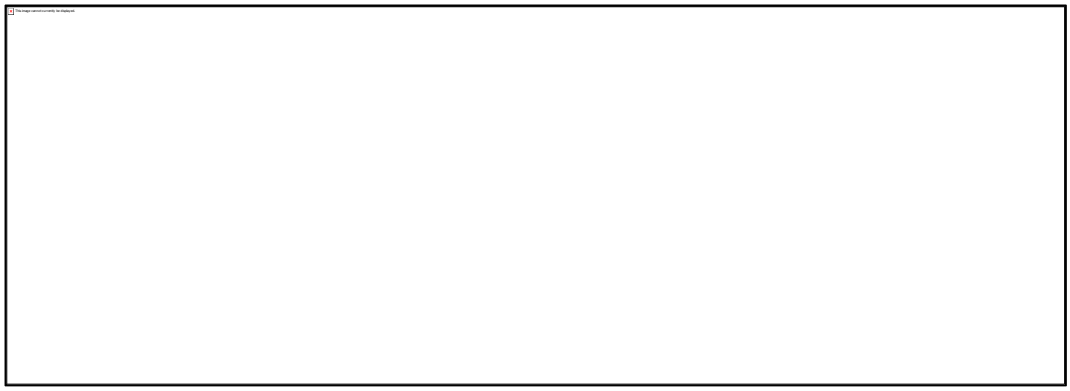

	Time	Area %
1	14.626	1.536
2	15.068	98.464

Chapter 6

6.7

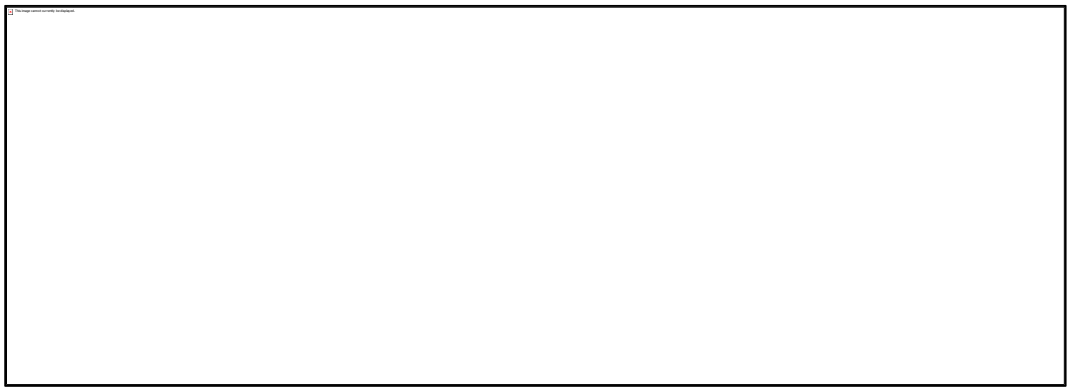

	Time	Area %
1	12.008	95.356%
2	12.808	1.426
3	12.944	2.047
4	14.91	1.171

Bibliography

(1) Szyf, M. Lamarck Revisited: Epigenetic Inheritance of Ancestral Odor Fear Conditioning. *Nat. Neurosci.* **2014**, *17*, 2–4.

(2) Goldberg, A. D.; Allis, C. D.; Bernstein, E. Epigenetics: A Landscape Takes Shape. *Cell* **2007**, *128*, 635–638.

(3) Herceg, Z.; Vaissière, T. Epigenetic Mechanisms and Cancer: An Interface between the Environment and the Genome. *Epigenetics* **2011**, *6*, 804–819.

(4) Genuis, S. J. Our Genes Are Not Our Destiny: Incorporating Molecular Medicine into Clinical Practice. *J. Eval. Clin. Pract.* **2008**, *14*, 94–102.

(5) Skinner, M. K. Environmental Epigenetics and a Unified Theory of the Molecular Aspects of Evolution: A Neo-Lamarckian Concept That Facilitates Neo-Darwinian Evolution. *Genome Biol. Evol.* **2015**, *7*, 1296–1302.

(6) Feinberg, A. P. Phenotypic Plasticity and the Epigenetics of Human Disease. *Nature* **2007**, *447*, 433–440.

(7) Fusco, G.; Minelli, A. Phenotypic Plasticity in Development and Evolution: Facts and Concepts. Introduction. *Philos. Trans. R. Soc. Lond. B. Biol. Sci.* **2010**, *365*, 547–556.

(8) Herb, B. R.; Wolschin, F.; Hansen, K. D.; Aryee, M. J.; Langmead, B.; Irizarry, R.; Amdam, G. V; Feinberg, A. P. Reversible Switching between Epigenetic States in Honeybee Behavioral Subcastes. *Nat. Neurosci.* **2012**, *15*, 1371–1373.

(9) Herceg, Z.; Hainaut, P. Genetic and Epigenetic Alterations as Biomarkers for Cancer Detection, Diagnosis and Prognosis. *Mol. Oncol.* **2007**, *1*, 26–41.

(10) Feinberg, A. P.; Tycko, B. The History of Cancer Epigenetics. *Nat. Rev. Cancer* **2004**, *4*, 143–153.

(11) Berdasco, M.; Esteller, M. Aberrant Epigenetic Landscape in Cancer: How Cellular Identity Goes Awry. *Dev. Cell* **2010**, *19*, 698–711.

(12) Greer, E. L.; Shi, Y. Histone Methylation: A Dynamic Mark in Health, Disease and Inheritance. *Nat. Rev. Genet.* **2012**, *13*, 343–357.

(13) Waldmann, T.; Schneider, R. Targeting Histone Modifications--Epigenetics in Cancer. *Curr. Opin. Cell Biol.* **2013**, *25*, 184–189.

(14) Portela, A.; Esteller, M. Epigenetic Modifications and Human Disease. *Nat. Biotechnol.* **2010**, *28*, 1057–1068.

(15) Pasqualucci, L.; Dominguez-Sola, D.; Chiarenza, A.; Fabbri, G.; Grunn, A.; Trifonov, V.; Kasper, L. H.; Lerach, S.; Tang, H.; Ma, J.; Rossi, D.; Chadburn, A.; Murty, V. V; Mullighan, C. G.; Gaidano, G.; Rabadan, R.; Brindle, P. K.; Dalla-Favera, R. Inactivating Mutations of Acetyltransferase Genes in B-Cell Lymphoma. *Nature* **2011**, *471*, 189–195.

(16) Yan, X.-J.; Xu, J.; Gu, Z.-H.; Pan, C.-M.; Lu, G.; Shen, Y.; Shi, J.-Y.; Zhu, Y.-

M.; Tang, L.; Zhang, X.-W.; Liang, W.-X.; Mi, J.-Q.; Song, H.-D.; Li, K.-Q.; Chen, Z.; Chen, S.-J. Exome Sequencing Identifies Somatic Mutations of DNA Methyltransferase Gene DNMT3A in Acute Monocytic Leukemia. *Nat. Genet.* **2011**, *43*, 309–315.

(17) Esteller, M. Epigenetic Lesions Causing Genetic Lesions in Human Cancer: Promoter Hypermethylation of DNA Repair Genes. *Eur. J. Cancer* **2000**, *36*, 2294–2300.

(18) Kristensen, L. S.; Nielsen, H. M.; Hansen, L. L. Epigenetics and Cancer Treatment. *Eur. J. Pharmacol.* **2009**, *625*, 131–142.

(19) Clark, S. J. Action at a Distance: Epigenetic Silencing of Large Chromosomal Regions in Carcinogenesis. *Hum. Mol. Genet.* **2007**, *16 Spec No*, R88–R95.

(20) Guenther, M. G.; Lawton, L. N.; Rozovskaia, T.; Frampton, G. M.; Levine, S. S.; Volkert, T. L.; Croce, C. M.; Nakamura, T.; Canaani, E.; Young, R. A. Aberrant Chromatin at Genes Encoding Stem Cell Regulators in Human Mixed-Lineage Leukemia. *Genes Dev.* **2008**, *22*, 3403–3408.

(21) Bernt, K. M.; Zhu, N.; Sinha, A. U.; Vempati, S.; Faber, J.; Krivtsov, A. V; Feng, Z.; Punt, N.; Daigle, A.; Bullinger, L.; Pollock, R. M.; Richon, V. M.; Kung, A. L.; Armstrong, S. A. MLL-Rearranged Leukemia Is Dependent on Aberrant H3K79 Methylation by DOT1L. *Cancer Cell* **2011**, *20*, 66–78.

(22) Fenaux, P.; Mufti, G. J.; Hellstrom-Lindberg, E.; Santini, V.; Finelli, C.; Giagounidis, A.; Schoch, R.; Gattermann, N.; Sanz, G.; List, A.; Gore, S. D.; Seymour, J. F.; Bennett, J. M.; Byrd, J.; Backstrom, J.; Zimmerman, L.; McKenzie, D.; Beach, C.; Silverman, L. R. Efficacy of Azacitidine Compared with that of Conventional Care Regimens in the Treatment of Higher-Risk Myelodysplastic Syndromes: A Randomised, Open-Label, Phase III Study. *Lancet Oncol.* **2009**, *10*, 223–232.

(23) Luger, K.; Mäder, A. W.; Richmond, R. K.; Sargent, D. F.; Richmond, T. J. Crystal Structure of the Nucleosome Core Particle at 2.8 A Resolution. *Nature* **1997**, *389*, 251–260.

(24) Biel, M.; Wascholowski, V.; Giannis, A. Epigenetics--an Epicenter of Gene Regulation: Histones and Histone-Modifying Enzymes. *Angew. Chem. Int. Ed. Engl.* **2005**, *44*, 3186–3216.

(25) Koch, C. M.; Andrews, R. M.; Flicek, P.; Dillon, S. C.; Karaoz, U.; Clelland, G. K.; Wilcox, S.; Beare, D. M.; Fowler, J. C.; Couttet, P.; James, K. D.; Lefebvre, G. C.; Bruce, A. W.; Dovey, O. M.; Ellis, P. D.; Dhami, P.; Langford, C. F.; Weng, Z.; Birney, E.; Carter, N. P.; Vetrie, D.; Dunham, I. The Landscape of Histone Modifications across 1% of the Human Genome in Five Human Cell Lines. *Genome Res.* **2007**, *17*, 691–707.

(26) Egger, G.; Liang, G.; Aparicio, A.; Jones, P. A. Epigenetics in Human Disease and Prospects for Epigenetic Therapy. *Nature* **2004**, *429*, 457–463.

(27) Beisel, C.; Paro, R. Silencing Chromatin: Comparing Modes and Mechanisms. *Nat. Rev. Genet.* **2011**, *12*, 123–135.

(28) Li, E.; Beard, C.; Jaenisch, R. Role for DNA Methylation in Genomic Imprinting. *Nature* **1993**, *366*, 362–365.

(29) Kulis, M.; Esteller, M. DNA Methylation and Cancer. *Adv. Genet.* **2010**, *70*, 27–56.

(30) Okano, M.; Bell, D. W.; Haber, D. A.; Li, E. DNA Methyltransferases Dnmt3a and Dnmt3b Are Essential for de Novo Methylation and Mammalian Development. *Cell* **1999**, *99*, 247–257.

(31) Jin, B.; Li, Y.; Robertson, K. D. DNA Methylation: Superior or Subordinate in the Epigenetic Hierarchy? *Genes Cancer* **2011**, *2*, 607–617.

(32) Hirasawa, R.; Chiba, H.; Kaneda, M.; Tajima, S.; Li, E.; Jaenisch, R.; Sasaki, H. Maternal and Zygotic Dnmt1 Are Necessary and Sufficient for the Maintenance of DNA Methylation Imprints during Preimplantation Development. *Genes Dev.* **2008**, *22*, 1607–1616.

(33) Neelamegam, R.; Ricq, E. L.; Malvaez, M.; Patnaik, D.; Norton, S.; Carlin, S. M.; Hill, I. T.; Wood, M. A.; Haggarty, S. J.; Hooker, J. M. Brain-Penetrant LSD1 Inhibitors Can Block Memory Consolidation. *ACS Chem. Neurosci.* **2012**, *3*, 120–128.

(34) Schaefer, M.; Pollex, T.; Hanna, K.; Tuorto, F.; Meusburger, M.; Helm, M.; Lyko, F. RNA Methylation by Dnmt2 Protects Transfer RNAs against Stress-Induced Cleavage. *Genes Dev.* **2010**, *24*, 1590–1595.

(35) Bernstein, B. E.; Meissner, A.; Lander, E. S. The Mammalian Epigenome. *Cell* **2007**, *128*, 669–681.

(36) Santos, F.; Hendrich, B.; Reik, W.; Dean, W. Dynamic Reprogramming of DNA Methylation in the Early Mouse Embryo. *Dev. Biol.* **2002**, *241*, 172–182.

(37) Sharma, S.; Kelly, T. K.; Jones, P. A. Epigenetics in Cancer. *Carcinogenesis* **2010**, *31*, 27–36.

(38) Chi, P.; Allis, C. D.; Wang, G. G. Covalent Histone Modifications--Miswritten, Misinterpreted and Mis-Erased in Human Cancers. *Nat. Rev. Cancer* **2010**, *10*, 457–469.

(39) Arrowsmith, C. H.; Bountra, C.; Fish, P. V; Lee, K.; Schapira, M. Epigenetic Protein Families: A New Frontier for Drug Discovery. *Nat. Rev. Drug Discov.* **2012**, *11*, 384–400.

(40) Gius, D.; Cui, H.; Bradbury, C. M.; Cook, J.; Smart, D. K.; Zhao, S.; Young, L.; Brandenburg, S. A.; Hu, Y.; Bisht, K. S.; Ho, A. S.; Mattson, D.; Sun, L.; Munson, P. J.; Chuang, E. Y.; Mitchell, J. B.; Feinberg, A. P. Distinct Effects on Gene Expression of Chemical and Genetic Manipulation of the Cancer Epigenome Revealed by a Multimodality Approach. *Cancer Cell* **2004**, *6*, 361–371.

(41) Lakshmikuttyamma, A.; Scott, S. A.; DeCoteau, J. F.; Geyer, C. R. Reexpression of Epigenetically Silenced AML Tumor Suppressor Genes by SUV39H1 Inhibition. *Oncogene* **2010**, *29*, 576–588.

(42) Brenner, C.; Fuks, F. A Methylation Rendezvous: Reader Meets Writers. *Dev. Cell* **2007**, *12*, 843–844.

(43) Falkenberg, K. J.; Johnstone, R. W. Histone Deacetylases and Their Inhibitors in Cancer, Neurological Diseases and Immune Disorders. *Nat. Rev. Drug Discov.* **2014**, *13*, 673–691.

(44) Dekker, F. J.; Haisma, H. J. Histone Acetyl Transferases as Emerging Drug Targets. *Drug Discov. Today* **2009**, *14*, 942–948.

(45) Chopra, M.; Bohlander, S. K. Disturbing the Histone Code in Leukemia: Translocations and Mutations Affecting Histone Methyl Transferases. *Cancer Genet.* **2015**, *208*, 192–205.

(46) Mai, A.; Altucci, L. Epi-Drugs to Fight Cancer: From Chemistry to Cancer Treatment, the Road Ahead. *Int. J. Biochem. Cell Biol.* **2009**, *41*, 199–213.

(47) Klose, R. J.; Zhang, Y. Regulation of Histone Methylation by Demethylimination and Demethylation. *Nat. Rev. Mol. Cell Biol.* **2007**, *8*, 307–318.

(48) Copeland, R. A.; Olhava, E. J.; Scott, M. P. Targeting Epigenetic Enzymes for Drug Discovery. *Curr. Opin. Chem. Biol.* **2010**, *14*, 505–510.

(49) Ropero, S.; Esteller, M. The Role of Histone Deacetylases (HDACs) in Human Cancer. *Mol. Oncol.* **2007**, *1*, 19–25.

(50) Leoni, F.; Fossati, G.; Lewis, E. C.; Lee, J.-K.; Porro, G.; Pagani, P.; Modena, D.; Moras, M. L.; Pozzi, P.; Reznikov, L. L.; Siegmund, B.; Fantuzzi, G.; Dinarello, C. A.; Mascagni, P. The Histone Deacetylase Inhibitor ITF2357 Reduces Production of pro-Inflammatory Cytokines in Vitro and Systemic Inflammation in Vivo. *Mol. Med. 11*, 1–15.

(51) Bolden, J. E.; Peart, M. J.; Johnstone, R. W. Anticancer Activities of Histone Deacetylase Inhibitors. *Nat. Rev. Drug Discov.* **2006**, *5*, 769–784.

(52) Shi, Y.; Lan, F.; Matson, C.; Mulligan, P.; Whetstine, J. R.; Cole, P. A.; Casero, R. A.; Shi, Y. Histone Demethylation Mediated by the Nuclear Amine Oxidase Homolog LSD1. *Cell* **2004**, *119*, 941–953.

(53) Thinnes, C. C.; England, K. S.; Kawamura, A.; Chowdhury, R.; Schofield, C. J.; Hopkinson, R. J. Targeting Histone Lysine Demethylases - Progress, Challenges, and the Future. *Biochim. Biophys. Acta* **2014**, *1839*, 1416–1432.

(54) Højfeldt, J. W.; Agger, K.; Helin, K. Histone Lysine Demethylases as Targets for Anticancer Therapy. *Nat. Rev. Drug Discov.* **2013**, *12*, 917–930.

(55) Tian, X.; Fang, J. Current Perspectives on Histone Demethylases. *Acta Biochim. Biophys. Sin. (Shanghai).* **2007**, *39*, 81–88.

(56) Maes, T.; Carceller, E.; Salas, J.; Ortega, A.; Buesa, C. Advances in the Development of Histone Lysine Demethylase Inhibitors. *Curr. Opin. Pharmacol.* **2015**, *23*, 52–60.

(57) King, O. N. F.; Li, X. S.; Sakurai, M.; Kawamura, A.; Rose, N. R.; Ng, S. S.; Quinn, A. M.; Rai, G.; Mott, B. T.; Beswick, P.; Klose, R. J.; Oppermann, U.;

Jadhav, A.; Heightman, T. D.; Maloney, D. J.; Schofield, C. J.; Simeonov, A. Quantitative High-Throughput Screening Identifies 8-Hydroxyquinolines as Cell-Active Histone Demethylase Inhibitors. *PLoS One* **2010**, *5*, e15535.

(58) Liang, Y.; Vogel, J.; Arbuckle, J. Targeting the JMJD2 Histone Demethylases to Epigenetically Control Herpesvirus Infection and Reactivation from Latency. *Sci. Transl. Med.* **2013**.

(59) Kruidenier, L.; Chung, C.; Cheng, Z.; Liddle, J.; Che, K.; Joberty, G.; Bantscheff, M.; Bountra, C.; Bridges, A.; Diallo, H.; Eberhard, D.; Hutchinson, S.; Jones, E.; Katso, R.; Leveridge, M.; Mander, P. K.; Mosley, J.; Ramirez-Molina, C.; Rowland, P.; Schofield, C. J.; Sheppard, R. J.; Smith, J. E.; Swales, C.; Tanner, R.; Thomas, P.; Tumber, A.; Drewes, G.; Oppermann, U.; Patel, D. J.; Lee, K.; Wilson, D. M. A Selective Jumonji H3K27 Demethylase Inhibitor Modulates the Proinflammatory Macrophage Response. *Nature* **2012**, *488*, 404–408.

(60) Musselman, C. A.; Lalonde, M.-E.; Côté, J.; Kutateladze, T. G. Perceiving the Epigenetic Landscape through Histone Readers. *Nat. Struct. Mol. Biol.* **2012**, *19*, 1218–1227.

(61) Filippakopoulos, P.; Knapp, S. Targeting Bromodomains: Epigenetic Readers of Lysine Acetylation. *Nat. Rev. Drug Discov.* **2014**, *13*, 337–356.

(62) Tanaka, M.; Roberts, J. M.; Qi, J.; Bradner, J. E. Inhibitors of Emerging Epigenetic Targets for Cancer Therapy: A Patent Review (2010-2014). *Pharm. Pat. Anal.* **2015**, *4*, 261–284.

(63) Spannhoff, A.; Hauser, A.-T.; Heinke, R.; Sippl, W.; Jung, M. The Emerging Therapeutic Potential of Histone Methyltransferase and Demethylase Inhibitors. *ChemMedChem* **2009**, *4*, 1568–1582.

(64) Nottke, A.; Colaiácovo, M. P.; Shi, Y. Developmental Roles of the Histone Lysine Demethylases. *Development* **2009**, *136*, 879–889.

(65) Roizman, B.; Zhou, G.; Du, T. Checkpoints in Productive and Latent Infections with Herpes Simplex Virus 1: Conceptualization of the Issues. *J. Neurovirol.* **2011**, *17*, 512–517.

(66) Rotili, D.; Mai, A. Targeting Histone Demethylases: A New Avenue for the Fight against Cancer. *Genes Cancer* **2011**, *2*, 663–679.

(67) Harris, W. J.; Huang, X.; Lynch, J. T.; Spencer, G. J.; Hitchin, J. R.; Li, Y.; Ciceri, F.; Blaser, J. G.; Greystoke, B. F.; Jordan, A. M.; Miller, C. J.; Ogilvie, D. J.; Somervaille, T. C. P. The Histone Demethylase KDM1A Sustains the Oncogenic Potential of MLL-AF9 Leukemia Stem Cells. *Cancer Cell* **2012**, *21*, 473–487.

(68) Amente, S.; Lania, L.; Majello, B. The Histone LSD1 Demethylase in Stemness and Cancer Transcription Programs. *Biochim. Biophys. Acta* **2013**, *1829*, 981–986.

(69) Dent, S. Y. R.; Chandra, J. The Lasting Influence of LSD1 in the Blood. *Elife* **2013**, *2*, e00963.

(70) Fang, R.; Barbera, A. J.; Xu, Y.; Rutenberg, M.; Leonor, T.; Bi, Q.; Lan, F.; Mei,

P.; Yuan, G.-C.; Lian, C.; Peng, J.; Cheng, D.; Sui, G.; Kaiser, U. B.; Shi, Y.; Shi, Y. G. Human LSD2/KDM1b/AOF1 Regulates Gene Transcription by Modulating Intragenic H3K4me2 Methylation. *Mol. Cell* **2010**, *39*, 222–233.

(71) Maes T., Tirapu I., Mascaro C., Ortega A., Estiarte A., Valls N., Castro-Palomino J., Buesa Arjol C., K. G. Preclinical Characterization of a Potent and Selective Inhibitor of the Histone Demethylase KDM1A for MLL Leukemia. *ASCO Meet. Abstr.* **2013**, *31*.

(72) Wang, J.; Scully, K.; Zhu, X.; Cai, L.; Zhang, J.; Prefontaine, G. G.; Krones, A.; Ohgi, K. A.; Zhu, P.; Garcia-Bassets, I.; Liu, F.; Taylor, H.; Lozach, J.; Jayes, F. L.; Korach, K. S.; Glass, C. K.; Fu, X.-D.; Rosenfeld, M. G. Opposing LSD1 Complexes Function in Developmental Gene Activation and Repression Programmes. *Nature* **2007**, *446*, 882–887.

(73) Whyte, W. A.; Bilodeau, S.; Orlando, D. A.; Hoke, H. A.; Frampton, G. M.; Foster, C. T.; Cowley, S. M.; Young, R. A. Enhancer Decommissioning by LSD1 during Embryonic Stem Cell Differentiation. *Nature* **2012**, *482*, 221–225.

(74) Adamo, A.; Sesé, B.; Boue, S.; Castaño, J.; Paramonov, I.; Barrero, M. J.; Izpisua Belmonte, J. C. LSD1 Regulates the Balance between Self-Renewal and Differentiation in Human Embryonic Stem Cells. *Nat. Cell Biol.* **2011**, *13*, 652–659.

(75) Zhu, X.; Wang, J.; Ju, B.-G.; Rosenfeld, M. G. Signaling and Epigenetic Regulation of Pituitary Development. *Curr. Opin. Cell Biol.* **2007**, *19*, 605–611.

(76) Ge, W.; Liu, Y.; Chen, T.; Zhang, X.; Lv, L.; Jin, C.; Jiang, Y.; Shi, L.; Zhou, Y. The Epigenetic Promotion of Osteogenic Differentiation of Human Adipose-Derived Stem Cells by the Genetic and Chemical Blockade of Histone Demethylase LSD1. *Biomaterials* **2014**, *35*, 6015–6025.

(77) Shi, Y.-J.; Matson, C.; Lan, F.; Iwase, S.; Baba, T.; Shi, Y. Regulation of LSD1 Histone Demethylase Activity by Its Associated Factors. *Mol. Cell* **2005**, *19*, 857–864.

(78) Kim, H.-J.; Rosenfeld, M. G. Epigenetic Control of Stem Cell Fate to Neurons and Glia. *Arch. Pharm. Res.* **2010**, *33*, 1467–1473.

(79) Fuentes, P.; Cánovas, J.; Berndt, F. A.; Noctor, S. C.; Kukuljan, M. CoREST/LSD1 Control the Development of Pyramidal Cortical Neurons. *Cereb. Cortex* **2012**, *22*, 1431–1441.

(80) Schulte, J. H.; Lim, S.; Schramm, A.; Friedrichs, N.; Koster, J.; Versteeg, R.; Ora, I.; Pajtler, K.; Klein-Hitpass, L.; Kuhfittig-Kulle, S.; Metzger, E.; Schüle, R.; Eggert, A.; Buettner, R.; Kirfel, J. Lysine-Specific Demethylase 1 Is Strongly Expressed in Poorly Differentiated Neuroblastoma: Implications for Therapy. *Cancer Res.* **2009**, *69*, 2065–2071.

(81) Cai, C.; He, H. H.; Chen, S.; Coleman, I.; Wang, H.; Fang, Z.; Chen, S.; Nelson, P. S.; Liu, X. S.; Brown, M.; Balk, S. P. Androgen Receptor Gene Expression in Prostate Cancer Is Directly Suppressed by the Androgen Receptor through Recruitment of Lysine-Specific Demethylase 1. *Cancer Cell* **2011**, *20*, 457–471.

(82) Bracarda, S.; de Cobelli, O.; Greco, C.; Prayer-Galetti, T.; Valdagni, R.; Gatta, G.; de Braud, F.; Bartsch, G. Cancer of the Prostate. *Crit. Rev. Oncol. Hematol.* **2005**, *56*, 379–396.

(83) Lim, S.; Janzer, A.; Becker, A.; Zimmer, A.; Schüle, R.; Buettner, R.; Kirfel, J. Lysine-Specific Demethylase 1 (LSD1) Is Highly Expressed in ER-Negative Breast Cancers and a Biomarker Predicting Aggressive Biology. *Carcinogenesis* **2010**, *31*, 512–520.

(84) Lynch, J. T.; Harris, W. J.; Somervaille, T. C. P. LSD1 Inhibition: A Therapeutic Strategy in Cancer? *Expert Opin. Ther. Targets* **2012**, *16*, 1239–1249.

(85) Huang, Y.; Vasilatos, S. N.; Boric, L.; Shaw, P. G.; Davidson, N. E. Inhibitors of Histone Demethylation and Histone Deacetylation Cooperate in Regulating Gene Expression and Inhibiting Growth in Human Breast Cancer Cells. *Breast Cancer Res. Treat.* **2012**, *131*, 777–789.

(86) Schenk, T.; Chen, W. C. W.; Göllner, S.; Howell, L.; Jin, L.; Hebestreit, K.; Klein, H.-U.; Popescu, A. C.; Burnett, A.; Mills, K.; Casero, R. A.; Marton, L.; Woster, P.; Minden, M. D.; Dugas, M.; Wang, J. C. Y.; Dick, J. E.; Müller-Tidow, C.; Petrie, K.; Zelent, A. Inhibition of the LSD1 (KDM1A) Demethylase Reactivates the All-Trans-Retinoic Acid Differentiation Pathway in Acute Myeloid Leukemia. *Nat. Med.* **2012**, *18*, 605–611.

(87) Huang, Z.; Li, S.; Song, W.; Li, X.; Li, Q.; Zhang, Z.; Han, Y.; Zhang, X.; Miao, S.; Du, R.; Wang, L. Lysine-Specific Demethylase 1 (LSD1/KDM1A) Contributes to Colorectal Tumorigenesis via Activation of the Wnt/β-Catenin Pathway by down-Regulating Dickkopf-1 (DKK1) [Corrected]. *PLoS One* **2013**, *8*, e70077.

(88) Hsu, H.-C.; Liu, Y.-S.; Tseng, K.-C.; Yang, T.-S.; Yeh, C.-Y.; You, J.-F.; Hung, H.-Y.; Chen, S.-J.; Chen, H.-C. CBB1003, a Lysine-Specific Demethylase 1 Inhibitor, Suppresses Colorectal Cancer Cells Growth through down-Regulation of Leucine-Rich Repeat-Containing G-Protein-Coupled Receptor 5 Expression. *J. Cancer Res. Clin. Oncol.* **2015**, *141*, 11–21.

(89) Jin, L.; Hanigan, C. L.; Wu, Y.; Wang, W.; Park, B. H.; Woster, P. M.; Casero, R. A. Loss of LSD1 (Lysine-Specific Demethylase 1) Suppresses Growth and Alters Gene Expression of Human Colon Cancer Cells in a p53- and DNMT1(DNA Methyltransferase 1)-Independent Manner. *Biochem. J.* **2013**, *449*, 459–468.

(90) Hayami, S.; Kelly, J. D.; Cho, H.-S.; Yoshimatsu, M.; Unoki, M.; Tsunoda, T.; Field, H. I.; Neal, D. E.; Yamaue, H.; Ponder, B. A. J.; Nakamura, Y.; Hamamoto, R. Overexpression of LSD1 Contributes to Human Carcinogenesis through Chromatin Regulation in Various Cancers. *Int. J. Cancer* **2011**, *128*, 574–586.

(91) Kahl, P.; Gullotti, L.; Heukamp, L. C.; Wolf, S.; Friedrichs, N.; Vorreuther, R.; Solleder, G.; Bastian, P. J.; Ellinger, J.; Metzger, E.; Schüle, R.; Buettner, R. Androgen Receptor Coactivators Lysine-Specific Histone Demethylase 1 and Four and a Half LIM Domain Protein 2 Predict Risk of Prostate Cancer Recurrence. *Cancer Res.* **2006**, *66*, 11341–11347.

(92) Lim, S.; Janzer, A.; Becker, A.; Zimmer, A.; Schüle, R.; Buettner, R.; Kirfel, J. Lysine-Specific Demethylase 1 (LSD1) Is Highly Expressed in ER-Negative Breast Cancers and a Biomarker Predicting Aggressive Biology. *Carcinogenesis* **2010**, *31*, 512–520.

(93) Willmann, D.; Lim, S.; Wetzel, S.; Metzger, E.; Jandausch, A.; Wilk, W.; Jung, M.; Forne, I.; Imhof, A.; Janzer, A.; Kirfel, J.; Waldmann, H.; Schüle, R.; Buettner, R. Impairment of Prostate Cancer Cell Growth by a Selective and Reversible Lysine-Specific Demethylase 1 Inhibitor. *Int. J. Cancer* **2012**, *131*, 2704–2709.

(94) Schulz, W. A.; Hatina, J. Epigenetics of Prostate Cancer: Beyond DNA Methylation. *J. Cell. Mol. Med.* **2006**, *10*, 100–125.

(95) Etani, T.; Suzuki, T.; Naiki, T.; Naiki-Ito, A.; Ando, R.; Iida, K.; Kawai, N.; Tozawa, K.; Miyata, N.; Kohri, K.; Takahashi, S. NCL1, a Highly Selective Lysine-Specific Demethylase 1 Inhibitor, Suppresses Prostate Cancer without Adverse Effect. *Oncotarget* **2015**, *5*, 2865–2878.

(96) Huang, Y.; Hager, E. R.; Phillips, D. L.; Dunn, V. R.; Hacker, A.; Frydman, B.; Kink, J. A.; Valasinas, A. L.; Reddy, V. K.; Marton, L. J.; Casero, R. A. . J.; Davidson, N. E. A Novel Polyamine Analog Inhibits Growth and Induces Apoptosis in Human Breast Cancer Cells. *Clin. Cancer Res.* **2003**, *9*, 2769–2777.

(97) Wang, Y.; Zhang, H.; Chen, Y.; Sun, Y.; Yang, F.; Yu, W.; Liang, J.; Sun, L.; Yang, X.; Shi, L.; Li, R.; Li, Y.; Zhang, Y.; Li, Q.; Yi, X.; Shang, Y. LSD1 Is a Subunit of the NuRD Complex and Targets the Metastasis Programs in Breast Cancer. *Cell* **2009**, *138*, 660–672.

(98) Burg, J. M.; Link, J. E.; Morgan, B. S.; Heller, F. J.; Hargrove, A. E.; McCafferty, D. G. KDM1 Class Flavin-Dependent Protein Lysine Demethylases. *Biopolymers* **2015**, *104*, 213–246.

(99) Cortez, V.; Mann, M.; Tekmal, S.; Suzuki, T.; Miyata, N.; Rodriguez-Aguayo, C.; Lopez-Berestein, G.; Sood, A. K.; Vadlamudi, R. K. Targeting the PELP1-KDM1 Axis as a Potential Therapeutic Strategy for Breast Cancer. *Breast Cancer Res.* **2012**, *14*, R108.

(100) Zhou, G.; Du, T.; Roizman, B. The Role of the CoREST/REST Repressor Complex in Herpes Simplex Virus 1 Productive Infection and in Latency. *Viruses* **2013**, *5*, 1208–1218.

(101) Shi, Y.; Lan, F.; Matson, C.; Mulligan, P.; Whetstine, J. R.; Cole, P. A.; Casero, R. A.; Shi, Y. Histone Demethylation Mediated by the Nuclear Amine Oxidase Homolog LSD1. *Cell* **2004**, *119*, 941–953.

(102) Anand, R.; Marmorstein, R. Structure and Mechanism of Lysine-Specific Demethylase Enzymes. *J. Biol. Chem.* **2007**, *282*, 35425–35429.

(103) Chen, Y.; Yang, Y.; Wang, F.; Wan, K.; Yamane, K.; Zhang, Y.; Lei, M. Crystal Structure of Human Histone Lysine-Specific Demethylase 1 (LSD1). *Proc. Natl. Acad. Sci. U. S. A.* **2006**, *103*, 13956–13961.

(104) Forneris, F.; Binda, C.; Vanoni, M. A.; Battaglioli, E.; Mattevi, A. Human

Histone Demethylase LSD1 Reads the Histone Code. *J. Biol. Chem.* **2005**, *280*, 41360–41365.

(105) Baron, R.; Binda, C.; Tortorici, M. Molecular Mimicry and Ligand Recognition in Binding and Catalysis by the Histone Demethylase LSD1-CoREST Complex. *Structure* **2011**.

(106) Lee, M. G.; Wynder, C.; Cooch, N.; Shiekhattar, R. An Essential Role for CoREST in Nucleosomal Histone 3 Lysine 4 Demethylation. *Nature* **2005**, *437*, 432–435.

(107) Yang, M.; Gocke, C. B.; Luo, X.; Borek, D.; Tomchick, D. R.; Machius, M.; Otwinowski, Z.; Yu, H. Structural Basis for CoREST-Dependent Demethylation of Nucleosomes by the Human LSD1 Histone Demethylase. *Mol. Cell* **2006**, *23*, 377–387.

(108) Forneris, F.; Binda, C.; Vanoni, M. A.; Mattevi, A.; Battaglioli, E. Histone Demethylation Catalysed by LSD1 Is a Flavin-Dependent Oxidative Process. *FEBS Lett.* **2005**, *579*, 2203–2207.

(109) Forneris, F.; Binda, C.; Battaglioli, E.; Mattevi, A. LSD1: Oxidative Chemistry for Multifaceted Functions in Chromatin Regulation. *Trends Biochem. Sci.* **2008**, *33*, 181–189.

(110) Forneris, F.; Binda, C.; Adamo, A.; Battaglioli, E.; Mattevi, A. Structural Basis of LSD1-CoREST Selectivity in Histone H3 Recognition. *J. Biol. Chem.* **2007**, *282*, 20070–20074.

(111) Baron, R.; Binda, C.; Tortorici, M.; McCammon, J. A.; Mattevi, A. Molecular Mimicry and Ligand Recognition in Binding and Catalysis by the Histone Demethylase LSD1-CoREST Complex. *Structure* **2011**, *19*, 212–220.

(112) Perillo, B.; Ombra, M. N.; Bertoni, A.; Cuozzo, C.; Sacchetti, S.; Sasso, A.; Chiariotti, L.; Malorni, A.; Abbondanza, C.; Avvedimento, E. V. DNA Oxidation as Triggered by H3K9me2 Demethylation Drives Estrogen-Induced Gene Expression. *Science* **2008**, *319*, 202–206.

(113) Karytinos, A.; Forneris, F.; Profumo, A.; Ciossani, G.; Battaglioli, E.; Binda, C.; Mattevi, A. A Novel Mammalian Flavin-Dependent Histone Demethylase. *J. Biol. Chem.* **2009**, *284*, 17775–17782.

(114) Dallman, J. E.; Allopenna, J.; Bassett, A.; Travers, A.; Mandel, G. A Conserved Role but Different Partners for the Transcriptional Corepressor CoREST in Fly and Mammalian Nervous System Formation. *J. Neurosci.* **2004**, *24*, 7186–7193.

(115) Foster, C. T.; Dovey, O. M.; Lezina, L.; Luo, J. L.; Gant, T. W.; Barlev, N.; Bradley, A.; Cowley, S. M. Lysine-Specific Demethylase 1 Regulates the Embryonic Transcriptome and CoREST Stability. *Mol. Cell. Biol.* **2010**, *30*, 4851–4863.

(116) Su, S.-T.; Ying, H.-Y.; Chiu, Y.-K.; Lin, F.-R.; Chen, M.-Y.; Lin, K.-I. Involvement of Histone Demethylase LSD1 in Blimp-1-Mediated Gene Repression during Plasma Cell Differentiation. *Mol. Cell. Biol.* **2009**, *29*, 1421–1431.

(117) Lin, Y.; Wu, Y.; Li, J.; Dong, C.; Ye, X.; Chi, Y.-I.; Evers, B. M.; Zhou, B. P. The SNAG Domain of Snail1 Functions as a Molecular Hook for Recruiting Lysine-Specific Demethylase 1. *EMBO J.* **2010**, *29*, 1803–1816.

(118) Yokoyama, A.; Takezawa, S.; Schüle, R.; Kitagawa, H.; Kato, S. Transrepressive Function of TLX Requires the Histone Demethylase LSD1. *Mol. Cell. Biol.* **2008**, *28*, 3995–4003.

(119) Hu, X.; Li, X.; Valverde, K.; Fu, X.; Noguchi, C.; Qiu, Y.; Huang, S. LSD1-Mediated Epigenetic Modification Is Required for TAL1 Function and Hematopoiesis. *Proc. Natl. Acad. Sci. U. S. A.* **2009**, *106*, 10141–10146.

(120) Xue, Y.; Wong, J.; Moreno, G. T.; Young, M. K.; Côté, J.; Wang, W. NURD, a Novel Complex with Both ATP-Dependent Chromatin-Remodeling and Histone Deacetylase Activities. *Mol. Cell* **1998**, *2*, 851–861.

(121) Shi, Y. Y.; Sawada, J.; Sui, G.; Affar, E. B.; Whetstine, J. R.; Lan, F.; Ogawa, H.; Luke, M. P.-S.; Nakatani, Y.; Shi, Y. Y. Coordinated Histone Modifications Mediated by a CtBP Co-Repressor Complex. *Nature* **2003**, *422*, 735–738.

(122) Hu, X.; Ybarra, R.; Qiu, Y.; Bungert, J.; Huang, S. Transcriptional Regulation by TAL1: A Link between Epigenetic Modifications and Erythropoiesis. *Epigenetics* **2009**, *4*, 357–361.

(123) Li, Y.; Deng, C.; Hu, X.; Patel, B.; Fu, X.; Qiu, Y.; Brand, M.; Zhao, K.; Huang, S. Dynamic Interaction between TAL1 Oncoprotein and LSD1 Regulates TAL1 Function in Hematopoiesis and Leukemogenesis. *Oncogene* **2012**, *31*, 5007–5018.

(124) Sun, G.; Alzayady, K.; Stewart, R.; Ye, P.; Yang, S.; Li, W.; Shi, Y. Histone Demethylase LSD1 Regulates Neural Stem Cell Proliferation. *Mol. Cell. Biol.* **2010**, *30*, 1997–2005.

(125) Sun, G.; Ye, P.; Murai, K.; Lang, M.-F.; Li, S.; Zhang, H.; Li, W.; Fu, C.; Yin, J.; Wang, A.; Ma, X.; Shi, Y. miR-137 Forms a Regulatory Loop with Nuclear Receptor TLX and LSD1 in Neural Stem Cells. *Nat. Commun.* **2011**, *2*, 529.

(126) Soto, F.; Kerschensteiner, D. Synaptic Remodeling of Neuronal Circuits in Early Retinal Degeneration. *Front. Cell. Neurosci.* **2015**, *9*, 395.

(127) Sun, G.; Alzayady, K.; Stewart, R.; Ye, P.; Yang, S.; Li, W.; Shi, Y. Histone Demethylase LSD1 Regulates Neural Stem Cell Proliferation. *Mol. Cell. Biol.* **2010**, *30*, 1997–2005.

(128) Smith, A.; Teknos, T. N.; Pan, Q. Epithelial to Mesenchymal Transition in Head and Neck Squamous Cell Carcinoma. *Oral Oncol.* **2013**, *49*, 287–292.

(129) Smits, A. H.; Jansen, P. W. T. C.; Poser, I.; Hyman, A. A.; Vermeulen, M. Stoichiometry of Chromatin-Associated Protein Complexes Revealed by Label-Free Quantitative Mass Spectrometry-Based Proteomics. *Nucleic Acids Res.* **2013**, *41*, e28.

(130) Li, Q.; Shi, L.; Gui, B.; Yu, W.; Wang, J.; Zhang, D.; Han, X.; Yao, Z.; Shang, Y. Binding of the JmjC Demethylase JARID1B to LSD1/NuRD Suppresses Angiogenesis and Metastasis in Breast Cancer Cells by Repressing Chemokine

CCL14. *Cancer Res.* **2011**, *71*, 6899–6908.

(131) Zhao, L.-Z.; Chinnadurai, G. Incapacitating CtBP to Kill Cancer. *Cell Cycle* **2010**, *9*, 3645–3646.

(132) Chinnadurai, G. The Transcriptional Corepressor CtBP: A Foe of Multiple Tumor Suppressors. *Cancer Res.* **2009**, *69*, 731–734.

(133) Chinnadurai, G. Transcriptional Regulation by C-Terminal Binding Proteins. *Int. J. Biochem. Cell Biol.* **2007**, *39*, 1593–1607.

(134) Cowger, J. J. M.; Zhao, Q.; Isovic, M.; Torchia, J. Biochemical Characterization of the Zinc-Finger Protein 217 Transcriptional Repressor Complex: Identification of a ZNF217 Consensus Recognition Sequence. *Oncogene* **2007**, *26*, 3378–3386.

(135) Gocke, C. B.; Yu, H. ZNF198 Stabilizes the LSD1-CoREST-HDAC1 Complex on Chromatin through Its MYM-Type Zinc Fingers. *PLoS One* **2008**, *3*, e3255.

(136) Christofori, G. Snail1 Links Transcriptional Control with Epigenetic Regulation. *EMBO J.* **2010**, *29*, 1787–1789.

(137) Chiang, C.; Ayyanathan, K. Snail/Gfi-1 (SNAG) Family Zinc Finger Proteins in Transcription Regulation, Chromatin Dynamics, Cell Signaling, Development, and Disease. *Cytokine Growth Factor Rev.* **2013**, *24*, 123–131.

(138) Mani, S. A.; Guo, W.; Liao, M.-J.; Eaton, E. N.; Ayyanan, A.; Zhou, A. Y.; Brooks, M.; Reinhard, F.; Zhang, C. C.; Shipitsin, M.; Campbell, L. L.; Polyak, K.; Brisken, C.; Yang, J.; Weinberg, R. A. The Epithelial-Mesenchymal Transition Generates Cells with Properties of Stem Cells. *Cell* **2008**, *133*, 704–715.

(139) von Burstin, J.; Eser, S.; Paul, M. C.; Seidler, B.; Brandl, M.; Messer, M.; von Werder, A.; Schmidt, A.; Mages, J.; Pagel, P.; Schnieke, A.; Schmid, R. M.; Schneider, G.; Saur, D. E-Cadherin Regulates Metastasis of Pancreatic Cancer in Vivo and Is Suppressed by a SNAIL/HDAC1/HDAC2 Repressor Complex. *Gastroenterology* **2009**, *137*, 361–371, 371.e1–e5.

(140) Barrallo-Gimeno, A.; Nieto, M. A. Evolutionary History of the Snail/Scratch Superfamily. *Trends Genet.* **2009**, *25*, 248–252.

(141) Barrallo-Gimeno, A.; Nieto, M. A. The Snail Genes as Inducers of Cell Movement and Survival: Implications in Development and Cancer. *Development* **2005**, *132*, 3151–3161.

(142) Ferrari-Amorotti, G.; Fragliasso, V.; Esteki, R.; Prudente, Z.; Soliera, A. R.; Cattelani, S.; Manzotti, G.; Grisendi, G.; Dominici, M.; Pieraccioli, M.; Raschellà, G.; Chiodoni, C.; Colombo, M. P.; Calabretta, B. Inhibiting Interactions of Lysine Demethylase LSD1 with Snail/slug Blocks Cancer Cell Invasion. *Cancer Res.* **2013**, *73*, 235–245.

(143) Tsai, M.-C.; Manor, O.; Wan, Y.; Mosammaparast, N.; Wang, J. K.; Lan, F.; Shi, Y.; Segal, E.; Chang, H. Y. Long Noncoding RNA as Modular Scaffold of Histone Modification Complexes. *Science* **2010**, *329*, 689–693.

(144) Boyer, L. A. Polycomb Complexes Repress Developmental Regulators in Murine

Embryonic Stem Cells. *Nature* **2006**, *441*, 349–353.

(145) Garcia-Bassets, I.; Kwon, Y.-S.; Telese, F.; Prefontaine, G. G.; Hutt, K. R.; Cheng, C. S.; Ju, B.-G.; Ohgi, K. A.; Wang, J.; Escoubet-Lozach, L.; Rose, D. W.; Glass, C. K.; Fu, X.-D.; Rosenfeld, M. G. Histone Methylation-Dependent Mechanisms Impose Ligand Dependency for Gene Activation by Nuclear Receptors. *Cell* **2007**, *128*, 505–518.

(146) Metzger, E.; Wissmann, M.; Yin, N.; Müller, J. M.; Schneider, R.; Peters, A. H. F. M.; Günther, T.; Buettner, R.; Schüle, R. LSD1 Demethylates Repressive Histone Marks to Promote Androgen-Receptor-Dependent Transcription. *Nature* **2005**, *437*, 436–439.

(147) Mangelsdorf, D. J.; Thummel, C.; Beato, M.; Herrlich, P.; Schütz, G.; Umesono, K.; Blumberg, B.; Kastner, P.; Mark, M.; Chambon, P.; Evans, R. M. The Nuclear Receptor Superfamily: The Second Decade. *Cell* **1995**, *83*, 835–839.

(148) Heinlein, C. A.; Chang, C. Androgen Receptor in Prostate Cancer. *Endocr. Rev.* **2004**, *25*, 276–308.

(149) Metzger, E.; Wissmann, M.; Schüle, R. Histone Demethylation and Androgen-Dependent Transcription. *Curr. Opin. Genet. Dev.* **2006**, *16*, 513–517.

(150) Cai, C.; Wang, H.; Xu, Y.; Chen, S.; Balk, S. P. Reactivation of Androgen Receptor-Regulated TMPRSS2:ERG Gene Expression in Castration-Resistant Prostate Cancer. *Cancer Res.* **2009**, *69*, 6027–6032.

(151) Schmitt, M. L.; Hauser, A.-T.; Carlino, L.; Pippel, M.; Schulz-Fincke, J.; Metzger, E.; Willmann, D.; Yiu, T.; Barton, M.; Schüle, R.; Sippl, W.; Jung, M. Nonpeptidic Propargylamines as Inhibitors of Lysine Specific Demethylase 1 (LSD1) with Cellular Activity. *J. Med. Chem.* **2013**, *56*, 7334–7342.

(152) Metzger, E.; Imhof, A.; Patel, D.; Kahl, P.; Hoffmeyer, K.; Friedrichs, N.; Müller, J. M.; Greschik, H.; Kirfel, J.; Ji, S.; Kunowska, N.; Beisenherz-Huss, C.; Günther, T.; Buettner, R.; Schüle, R. Phosphorylation of Histone H3T6 by PKCbeta(I) Controls Demethylation at Histone H3K4. *Nature* **2010**, *464*, 792–796.

(153) Thomas, C.; Gustafsson, J.-Å. The Different Roles of ER Subtypes in Cancer Biology and Therapy. *Nat. Rev. Cancer* **2011**, *11*, 597–608.

(154) Kim, J.; Park, U.-H.; Moon, M.; Um, S.-J.; Kim, E.-J. Negative Regulation of ERα by a Novel Protein CAC1 through Association with Histone Demethylase LSD1. *FEBS Lett.* **2013**, *587*, 17–22.

(155) Yang, M.; Culhane, J. C.; Szewczuk, L. M.; Gocke, C. B.; Brautigam, C. A.; Tomchick, D. R.; Machius, M.; Cole, P. A.; Yu, H. Structural Basis of Histone Demethylation by LSD1 Revealed by Suicide Inactivation. *Nat. Struct. Mol. Biol.* **2007**, *14*, 535–539.

(156) Nair, S. S.; Nair, B. C.; Cortez, V.; Chakravarty, D.; Metzger, E.; Schüle, R.; Brann, D. W.; Tekmal, R. R.; Vadlamudi, R. K. PELP1 Is a Reader of Histone H3 Methylation That Facilitates Oestrogen Receptor-Alpha Target Gene Activation by Regulating Lysine Demethylase 1 Specificity. *EMBO Rep.* **2010**,

11, 438–444.

(157) Wissmann, M.; Yin, N.; Müller, J. M.; Greschik, H.; Fodor, B. D.; Jenuwein, T.; Vogler, C.; Schneider, R.; Günther, T.; Buettner, R.; Metzger, E.; Schüle, R. Cooperative Demethylation by JMJD2C and LSD1 Promotes Androgen Receptor-Dependent Gene Expression. *Nat. Cell Biol.* **2007**, *9*, 347–353.

(158) Szewczuk, L. M.; Culhane, J. C.; Yang, M.; Majumdar, A.; Yu, H.; Cole, P. A. Mechanistic Analysis of a Suicide Inactivator of Histone Demethylase LSD1. *Biochemistry* **2007**, *46*, 6892–6902.

(159) Yang, M.; Culhane, J. C.; Szewczuk, L. M.; Jalili, P.; Ball, H. L.; Machius, M.; Cole, P. A.; Yu, H. Structural Basis for the Inhibition of the LSD1 Histone Demethylase by the Antidepressant Trans-2-Phenylcyclopropylamine. *Biochemistry* **2007**, *46*, 8058–8065.

(160) Culhane, J. C.; Wang, D.; Yen, P. M.; Cole, P. A. Comparative Analysis of Small Molecules and Histone Substrate Analogues as LSD1 Lysine Demethylase Inhibitors. *J. Am. Chem. Soc.* **2010**, *132*, 3164–3176.

(161) Finberg, J. P. M.; Gillman, K. Selective Inhibitors of Monoamine Oxidase Type B and The "cheese Effect". *Int. Rev. Neurobiol.* **2011**, *100*, 169–190.

(162) Schmidt, D. M. Z.; McCafferty, D. G. Trans-2-Phenylcyclopropylamine Is a Mechanism-Based Inactivator of the Histone Demethylase LSD1. *Biochemistry* **2007**, *46*, 4408–4416.

(163) Mimasu, S.; Sengoku, T.; Fukuzawa, S.; Umehara, T.; Yokoyama, S. Crystal Structure of Histone Demethylase LSD1 and Tranylcypromine at 2.25 A. *Biochem. Biophys. Res. Commun.* **2008**, *366*, 15–22.

(164) Prusevich, P.; Kalin, J. H.; Ming, S. A.; Basso, M.; Givens, J.; Li, X.; Hu, J.; Taylor, M. S.; Cieniewicz, A. M.; Hsiao, P.-Y.; Huang, R.; Roberson, H.; Adejola, N.; Avery, L. B.; Casero, R. A.; Taverna, S. D.; Qian, J.; Tackett, A. J.; Ratan, R. R.; McDonald, O. G.; Feinberg, A. P.; Cole, P. A. A Selective Phenelzine Analogue Inhibitor of Histone Demethylase LSD1. *ACS Chem. Biol.* **2014**, *9*, 1284–1293.

(165) Kozikowski, A. P.; Chen, Y.; Subhasish, T.; Lewin, N. E.; Blumberg, P. M.; Zhong, Z.; D'Annibale, M. A.; Wang, W.-L.; Shen, Y.; Langley, B. Searching for Disease Modifiers-PKC Activation and HDAC Inhibition - a Dual Drug Approach to Alzheimer's Disease That Decreases Abeta Production While Blocking Oxidative Stress. *ChemMedChem* **2009**, *4*, 1095–1105.

(166) Burger, A.; Yost, W. L. Arylcycloalkylamines. I. 2-Phenylcyclopropylamine. *J. Am. Chem. Soc.* **1948**, *70*, 2198–2201.

(167) Weber-Grandke, H.; Hahn, G.; Mutschler, E.; Möhrke, W.; Langguth, P.; Spahn-Langguth, H. The Pharmacokinetics of Tranylcypromine Enantiomers in Healthy Subjects after Oral Administration of Racemic Drug and the Single Enantiomers. *Br. J. Clin. Pharmacol.* **1993**, *36*, 363–365.

(168) Moises, H. W.; Beckmann, H. Antidepressant Efficacy of Tranylcypromine Isomers: A Controlled Study. *J. Neural Transm.* **1981**, *50*, 185–192.

(169) Lee, M. G.; Wynder, C.; Schmidt, D. M.; McCafferty, D. G.; Shiekhattar, R. Histone H3 Lysine 4 Demethylation Is a Target of Nonselective Antidepressive Medications. *Chem. Biol.* **2006**, *13*, 563–567.

(170) Benelkebir, H.; Hodgkinson, C.; Duriez, P. J.; Hayden, A. L.; Bulleid, R. A.; Crabb, S. J.; Packham, G.; Ganesan, A. Enantioselective Synthesis of Tranylcypromine Analogues as Lysine Demethylase (LSD1) Inhibitors. *Bioorg. Med. Chem.* **2011**, *19*, 3709–3716.

(171) Gooden, D. M.; Schmidt, D. M. Z.; Pollock, J. A.; Kabadi, A. M.; McCafferty, D. G. Facile Synthesis of Substituted Trans-2-Arylcyclopropylamine Inhibitors of the Human Histone Demethylase LSD1 and Monoamine Oxidases A and B. *Bioorg. Med. Chem. Lett.* **2008**, *18*, 3047–3051.

(172) Ueda, R.; Suzuki, T.; Mino, K.; Tsumoto, H.; Nakagawa, H.; Hasegawa, M.; Sasaki, R.; Mizukami, T.; Miyata, N. Identification of Cell-Active Lysine Specific Demethylase 1-Selective Inhibitors. *J. Am. Chem. Soc.* **2009**, *131*, 17536–17537.

(173) Ogasawara, D.; Suzuki, T.; Mino, K.; Ueda, R.; Khan, M. N. A.; Matsubara, T.; Koseki, K.; Hasegawa, M.; Sasaki, R.; Nakagawa, H.; Mizukami, T.; Miyata, N. Synthesis and Biological Activity of Optically Active NCL-1, a Lysine-Specific Demethylase 1 Selective Inhibitor. *Bioorg. Med. Chem.* **2011**, *19*, 3702–3708.

(174) Mimasu, S.; Umezawa, N.; Sato, S.; Higuchi, T.; Umehara, T.; Yokoyama, S. Structurally Designed Trans-2-Phenylcyclopropylamine Derivatives Potently Inhibit Histone Demethylase LSD1/KDM1 . *Biochemistry* **2010**, *49*, 6494–6503.

(175) Binda, C.; Valente, S.; Romanenghi, M.; Pilotto, S.; Cirilli, R.; Karytinos, A.; Ciossani, G.; Botrugno, O. A.; Forneris, F.; Tardugno, M.; Edmondson, D. E.; Minucci, S.; Mattevi, A.; Mai, A. Biochemical, Structural, and Biological Evaluation of Tranylcypromine Derivatives as Inhibitors of Histone Demethylases LSD1 and LSD2. *J. Am. Chem. Soc.* **2010**, *132*, 6827–6833.

(176) Rotili, D.; Tomassi, S.; Conte, M.; Benedetti, R.; Tortorici, M.; Ciossani, G.; Valente, S.; Marrocco, B.; Labella, D.; Novellino, E.; Mattevi, A.; Altucci, L.; Tumber, A.; Yapp, C.; King, O. N. F.; Hopkinson, R. J.; Kawamura, A.; Schofield, C. J.; Mai, A. Pan-Histone Demethylase Inhibitors Simultaneously Targeting Jumonji C and Lysine-Specific Demethylases Display High Anticancer Activities. *J. Med. Chem.* **2014**, *57*, 42–55.

(177) Guibourt, N.; Ortega Munoz, A.; Castro-Palomino, L. Phenylcyclopropylamine Derivatives and Their Medical Use. *Pat. WO 2010/084160 A1, Oryzon Genomics S.A.*, **2010**.

(178) Tomita, N.; Kajiii, S.; Cary, D. R.; Tomita, D.; Imamura, S.; Tsuchida, K.; Matsuda, S.; Hara, R. Cyclopropanamine Compound and Use Thereof. *Pat. WO2014058071A1; Tak. Pharm. Co. Limited. Osaka, Japan* **2014**.

(179) Mohammad, H. P.; Smitheman, K. N.; Kamat, C. D.; Soong, D.; Federowicz, K. E.; Van Aller, G. S.; Schneck, J. L.; Carson, J. D.; Liu, Y.; Butticello, M.; Bonnette, W. G.; Gorman, S. A.; Degenhardt, Y.; Bai, Y.; McCabe, M. T.; Pappalardi, M. B.; Kasparec, J.; Tian, X.; McNulty, K. C.; Rouse, M.; McDevitt,

P.; Ho, T.; Crouthamel, M.; Hart, T. K.; Concha, N. O.; McHugh, C. F.; Miller, W. H.; Dhanak, D.; Tummino, P. J.; Carpenter, C. L.; Johnson, N. W.; Hann, C. L.; Kruger, R. G. A DNA Hypomethylation Signature Predicts Antitumor Activity of LSD1 Inhibitors in SCLC. *Cancer Cell* **2015**, *28*, 57–69.

(180) Vianello, P.; Botrugno, O. A.; Cappa, A.; Ciossani, G.; Dessanti, P.; Mai, A.; Mattevi, A.; Meroni, G.; Minucci, S.; Thaler, F.; Tortorici, M.; Trifiró, P.; Valente, S.; Villa, M.; Varasi, M.; Mercurio, C. Synthesis, Biological Activity and Mechanistic Insights of 1-Substituted Cyclopropylamine Derivatives: A Novel Class of Irreversible Inhibitors of Histone Demethylase KDM1A. *Eur. J. Med. Chem.* **2014**, *86*, 352–363.

(181) Burger, A.; Davis, C. S.; Green, H.; Tedeschi, D. H.; Zirkle, C. L. 1-Methyl-2-Phenylcyclopropylamine. *J. Med. Pharm. Chem.* **1961**, *4*, 571–574.

(182) Pieroni, M.; Annunziato, G.; Azzali, E.; Dessanti, P.; Mercurio, C.; Meroni, G.; Trifiró, P.; Vianello, P.; Villa, M.; Beato, C.; Varasi, M.; Costantino, G. Further Insights into the SAR of α-Substituted Cyclopropylamine Derivatives as Inhibitors of Histone Demethylase KDM1A. *Eur. J. Med. Chem.* **2015**, *92*, 377–386.

(183) Abdulla, A.; Zhao, X.; Yang, F. Natural Polyphenols Inhibit Lysine-Specific Demethylase-1 in Vitro. *J. Biochem. Pharmacol. Res.* **2013**, *1*, 56–63.

(184) Sakane, C.; Okitsu, T.; Wada, A.; Sagami, H.; Shidoji, Y. Inhibition of Lysine-Specific Demethylase 1 by the Acyclic Diterpenoid Geranylgeranoic Acid and Its Derivatives. *Biochem. Biophys. Res. Commun.* **2014**, *444*, 24–29.

(185) Saab, N. H.; West, E. E.; Bieszk, N. C.; Preuss, C. V.; Mank, A. R.; Casero, R. A.; Woster, P. M. Synthesis and Evaluation of Unsymmetrically Substituted Polyamine Analogs as Modulators of Human Spermidine/spermine-N1-Acetyltransferase (SSAT) and as Potential Antitumor Agents. *J. Med. Chem.* **1993**, *36*, 2998–3004.

(186) Wang, Y.; Murray-Stewart, T.; Devereux, W.; Hacker, A.; Frydman, B.; Woster, P. M.; Casero, R. A. Properties of Purified Recombinant Human Polyamine Oxidase, PAOh1/SMO. *Biochem. Biophys. Res. Commun.* **2003**, *304*, 605–611.

(187) Thomas, T.; Thomas, T. J. Polyamines in Cell Growth and Cell Death: Molecular Mechanisms and Therapeutic Applications. *Cell. Mol. Life Sci.* **2001**, *58*, 244–258.

(188) Sharma, S. K.; Hazeldine, S.; Crowley, M. L.; Hanson, A.; Beattie, R.; Varghese, S.; Senanayake, T. M. D.; Hirata, A.; Hirata, F.; Huang, Y.; Wu, Y.; Steinbergs, N.; Murray-Stewart, T.; Bytheway, I.; Casero, R. A.; Woster, P. M. Polyamine-Based Small Molecule Epigenetic Modulators. *Medchemcomm* **2012**, *3*, 14–21.

(189) Bi, X.; Lopez, C.; Bacchi, C. J.; Rattendi, D.; Woster, P. M. Novel Alkylpolyaminoguanidines and Alkylpolyaminobiguanides with Potent Antitrypanosomal Activity. *Bioorg. Med. Chem. Lett.* **2006**, *16*, 3229–3232.

(190) Huang, Y.; Greene, E.; Murray Stewart, T.; Goodwin, A. C.; Baylin, S. B.; Woster, P. M.; Casero, R. A. Inhibition of Lysine-Specific Demethylase 1 by Polyamine Analogues Results in Reexpression of Aberrantly Silenced Genes.

Proc. Natl. Acad. Sci. U. S. A. **2007**, *104*, 8023–8028.

(191) Huang, Y.; Stewart, T. M.; Wu, Y.; Baylin, S. B.; Marton, L. J.; Perkins, B.; Jones, R. J.; Woster, P. M.; Casero, R. A. Novel Oligoamine Analogues Inhibit Lysine-Specific Demethylase 1 and Induce Reexpression of Epigenetically Silenced Genes. *Clin. Cancer Res.* **2009**, *15*, 7217–7228.

(192) Sharma, S. K.; Wu, Y.; Steinbergs, N.; Crowley, M. L.; Hanson, A. S.; Casero, R. A.; Woster, P. M. (Bis)urea and (Bis)thiourea Inhibitors of Lysine-Specific Demethylase 1 as Epigenetic Modulators. *J. Med. Chem.* **2010**, *53*, 5197–5212.

(193) Huang, Y.; Marton, L. J.; Woster, P. M.; Casero, R. A. Polyamine Analogues Targeting Epigenetic Gene Regulation. *Essays Biochem.* **2009**, *46*, 95–110.

(194) Wang, J.; Lu, F.; Ren, Q.; Sun, H.; Xu, Z.; Lan, R.; Liu, Y.; Ward, D.; Quan, J.; Ye, T.; Zhang, H. Novel Histone Demethylase LSD1 Inhibitors Selectively Target Cancer Cells with Pluripotent Stem Cell Properties. *Cancer Res.* **2011**, *71*, 7238–7249.

(195) Sorna, V.; Theisen, E. R.; Stephens, B.; Warner, S. L.; Bearss, D. J.; Vankayalapati, H.; Sharma, S. High-Throughput Virtual Screening Identifies Novel N'-(1-Phenylethylidene)-Benzohydrazides as Potent, Specific, and Reversible LSD1 Inhibitors. *J. Med. Chem.* **2013**, *56*, 9496–9508.

(196) Lynch, J. T.; Cockerill, M. J.; Hitchin, J. R.; WiSTDan, D. H.; Somervaille, T. C. P. CD86 Expression as a Surrogate Cellular Biomarker for Pharmacological Inhibition of the Histone Demethylase Lysine-Specific Demethylase 1. *Anal. Biochem.* **2013**, *442*, 104–106.

(197) Mould, D. P.; McGonagle, A. E.; WiSTDan, D. H.; Williams, E. L.; Jordan, A. M. Reversible Inhibitors of LSD1 as Therapeutic Agents in Acute Myeloid Leukemia: Clinical Significance and Progress to Date. *Med. Res. Rev.* **2014**.

(198) Baell, J. B.; Holloway, G. A. New Substructure Filters for Removal of Pan Assay Interference Compounds (PAINS) from Screening Libraries and for Their Exclusion in Bioassays. *J. Med. Chem.* **2010**, *53*, 2719–2740.

(199) Ifa, D. .; Rodrigues, C. .; de Alencastro, R. .; Fraga, C. A. .; Barreiro, E. . A Possible Molecular Mechanism for the Inhibition of Cysteine Proteases by Salicylaldehyde N-Acylhydrazones and Related Compounds. *J. Mol. Struct. THEOCHEM* **2000**, *505*, 11–17.

(200) Auld, D. S.; Southall, N. T.; Jadhav, A.; Johnson, R. L.; Diller, D. J.; Simeonov, A.; Austin, C. P.; Inglese, J. Characterization of Chemical Libraries for Luciferase Inhibitory Activity. *J. Med. Chem.* **2008**, *51*, 2372–2386.

(201) Ledesma, G. N.; Gonzalez Sierra, M.; Escandar, G. M. Spectroscopic and Theoretical Study of Aromatic α-Hydroxy Hydrazones and Their copper(II) Complexes in Dioxane-Water Mixtures. *Polyhedron* **1998**, *17*, 1517–1523.

(202) Fiskus, W.; Sharma, S.; Shah, B.; Portier, B. P.; Devaraj, S. G. T.; Liu, K.; Iyer, S. P.; Bearss, D.; Bhalla, K. N. Highly Effective Combination of LSD1 (KDM1A) Antagonist and Pan-Histone Deacetylase Inhibitor against Human AML Cells. *Leukemia* **2014**, *28*, 2155–2164.

(203) Sankar, S.; Theisen, E. R.; Bearss, J.; Mulvihill, T.; Hoffman, L. M.; Sorna, V.; Beckerle, M. C.; Sharma, S.; Lessnick, S. L. Reversible LSD1 Inhibition Interferes with Global EWS/ETS Transcriptional Activity and Impedes Ewing Sarcoma Tumor Growth. *Clin. Cancer Res.* **2014**, *20*, 4584–4597.

(204) Hitchin, J. R.; Blagg, J.; Burke, R.; Burns, S.; Cockerill, M. J.; Fairweather, E. E.; Hutton, C.; Jordan, A. M.; McAndrew, C.; Mirza, A.; Mould, D.; Thomson, G. J.; Waddell, I.; Ogilvie, D. J. Development and Evaluation of Selective, Reversible LSD1 Inhibitors Derived from Fragments. *Medchemcomm* **2013**, *4*, 1513.

(205) Hazeldine, S.; Pachaiyappan, B.; Steinbergs, N.; Nowotarski, S.; Hanson, A. S.; Casero, R. A.; Woster, P. M. Low Molecular Weight Amidoximes That Act as Potent Inhibitors of Lysine-Specific Demethylase 1. *J. Med. Chem.* **2012**, *55*, 7378–7391.

(206) Wetzel, S.; Wilk, W.; Chammaa, S.; Sperl, B.; Roth, A. G.; Yektaoglu, A.; Renner, S.; Berg, T.; Arenz, C.; Giannis, A.; Oprea, T. I.; Rauh, D.; Kaiser, M.; Waldmann, H. A Scaffold-Tree-Merging Strategy for Prospective Bioactivity Annotation of Gamma-Pyrones. *Angew. Chem. Int. Ed. Engl.* **2010**, *49*, 3666–3670.

(207) Zhou, C.; Kang, D.; Xu, Y.; Zhang, L.; Zha, X. Identification of Novel Selective Lysine-Specific Demethylase 1 (LSD1) Inhibitors Using a Pharmacophore-Based Virtual Screening Combined with Docking. *Chem. Biol. Drug Des.* **2014**.

(208) Dulla, B.; Kirla, K. T.; Rathore, V.; Deora, G. S.; Kavela, S.; Maddika, S.; Chatti, K.; Reiser, O.; Iqbal, J.; Pal, M. Synthesis and Evaluation of 3-Amino/guanidine Substituted Phenyl Oxazoles as a Novel Class of LSD1 Inhibitors with Anti-Proliferative Properties. *Org. Biomol. Chem.* **2013**, *11*, 3103–3107.

(209) Dhanak, D.; Jackson, P. Development and Classes of Epigenetic Drugs for Cancer. *Biochem. Biophys. Res. Commun.* **2014**, *455*, 58–69.

(210) Jie, Z.; Li, T.; Jia-Yun, H.; Qiu, J.; Ping-Yao, Z.; Houyan, S. Trans-2-Phenylcyclopropylamine Induces Nerve Cells Apoptosis in Zebrafish Mediated by Depression of LSD1 Activity. *Brain Res. Bull.* **2009**, *80*, 79–84.

(211) Rostovtsev, V. V; Green, L. G.; Fokin, V. V; Sharpless, K. B. A Stepwise Huisgen Cycloaddition Process: copper(I)-Catalyzed Regioselective "ligation" of Azides and Terminal Alkynes. *Angew. Chem. Int. Ed. Engl.* **2002**, *41*, 2596–2599.

(212) Zheng, Y.-C.; Duan, Y.-C.; Ma, J.-L.; Xu, R.-M.; Zi, X.; Lv, W.-L.; Wang, M.-M.; Ye, X.-W.; Zhu, S.; Mobley, D.; Zhu, Y.-Y.; Wang, J.-W.; Li, J.-F.; Wang, Z.-R.; Zhao, W.; Liu, H.-M. Triazole-Dithiocarbamate Based Selective Lysine Specific Demethylase 1 (LSD1) Inactivators Inhibit Gastric Cancer Cell Growth, Invasion, and Migration. *J. Med. Chem.* **2013**, *56*, 8543–8560.

(213) Culhane, J. C.; Szewczuk, L. M.; Liu, X.; Da, G.; Marmorstein, R.; Cole, P. A. A Mechanism-Based Inactivator for Histone Demethylase LSD1. *J. Am. Chem. Soc.* **2006**, *128*, 4536–4537.

(214) Tortorici, M.; Borrello, M. T.; Tardugno, M.; Chiarelli, L. R.; Pilotto, S.;

Ciossani, G.; Vellore, N. a.; Bailey, S. G.; Cowan, J.; O'Connell, M.; Crabb, S. J.; Packham, G. K.; Mai, A.; Baron, R.; Ganesan, a.; Mattevi, A. Protein Recognition by Short Peptide Reversible Inhibitors of the Chromatin-Modifying LSD1/CoREST Lysine Demethylase. *ACS Chem. Biol.* **2013**, *8*, 1677–1682.

(215) Ye, X.-W.; Zheng, Y.-C.; Duan, Y.-C.; Wang, M.-M.; Yu, B.; Ren, J.-L.; Ma, J.-L.; Zhang, E.; Liu, H.-M. Synthesis and Biological Evaluation of coumarin–1,2,3-Triazole–dithiocarbamate Hybrids as Potent LSD1 Inhibitors. *Medchemcomm* **2014**, *5*, 650.

(216) Lin, T.; Ponn, A.; Hu, X.; Law, B. K.; Lu, J. Requirement of the Histone Demethylase LSD1 in Snai1-Mediated Transcriptional Repression during Epithelial-Mesenchymal Transition. *Oncogene* **2010**, *29*, 4896–4904.

(217) Wu, Y.; Zhou, B. P. New Insights of Epithelial-Mesenchymal Transition in Cancer Metastasis. *Acta Biochim. Biophys. Sin. (Shanghai).* **2008**, *40*, 643–650.

(218) Thiery, J. P.; Acloque, H.; Huang, R. Y. J.; Nieto, M. A. Epithelial-Mesenchymal Transitions in Development and Disease. *Cell* **2009**, *139*, 871–890.

(219) Saleque, S.; Kim, J.; Rooke, H. M.; Orkin, S. H. Epigenetic Regulation of Hematopoietic Differentiation by Gfi-1 and Gfi-1b Is Mediated by the Cofactors CoREST and LSD1. *Mol. Cell* **2007**, *27*, 562–572.

(220) Lin, T.; Ponn, A.; Hu, X.; Law, B. K.; Lu, J. Requirement of the Histone Demethylase LSD1 in Snai1-Mediated Transcriptional Repression during Epithelial-Mesenchymal Transition. *Oncogene* **2010**, *29*, 4896–4904.

(221) Li, H.; Wang, H.; Wang, F.; Gu, Q.; Xu, X. Snail Involves in the Transforming Growth Factor β1-Mediated Epithelial-Mesenchymal Transition of Retinal Pigment Epithelial Cells. *PLoS One* **2011**, *6*, e23322.

(222) Merrifield, B. Solid Phase Synthesis. *Science (80-.).* **1986**, *232*, 341–347.

(223) Palomo, J. M. Solid-Phase Peptide Synthesis: An Overview Focused on the Preparation of Biologically Relevant Peptides. *RSC Adv.* **2014**, *4*, 32658.

(224) Krchnák, V.; Flegelová, Z.; Vágner, J. Aggregation of Resin-Bound Peptides during Solid-Phase Peptide Synthesis. Prediction of Difficult Sequences. *Int. J. Pept. Protein Res.* **1993**, *42*, 450–454.

(225) Pearson, D. A.; Blanchette, M.; Baker, M. Lou; Guindon, C. A. Trialkylsilanes as Scavengers for the Trifluoroacetic Acid Deblocking of Protecting Groups in Peptide Synthesis. *Tetrahedron Lett.* **1989**, *30*, 2739–2742.

(226) Kaiser, E.; Colescott, R. L.; Bossinger, C. D.; Cook, P. I. Color Test for Detection of Free Terminal Amino Groups in the Solid-Phase Synthesis of Peptides. *Anal. Biochem.* **1970**, *34*, 595–598.

(227) Alnabari, M.; Bittner, S. New Quinone-Amino Acid Conjugates Linked via a Vinylic Spacer. *Amino Acids* **2001**, *20*, 381–387.

(228) Alnabari, M.; Bittner, S. Quinonic Enaminones; Synthesis of New Dialkylaminovinyl and Bis(dialkylaminovinyl) Derivatives of Quinones. *Synthesis (Stuttg).* **2000**, *2000*, 1087–1090.

(229) Tam, J. P.; Lu, Y.-A. Coupling Difficulty Associated with Interchain Clustering and Phase Transition in Solid Phase Peptide Synthesis. *J. Am. Chem. Soc.* **1995**, *117*, 12058–12063.

(230) Lefevre, F. Alanine-Stretch Scanning Mutagenesis: A Simple and Efficient Method to Probe Protein Structure and Function. *Nucleic Acids Res.* **1997**, *25*, 447–448.

(231) Robertson, J. C.; Hurley, N. C.; Tortorici, M.; Ciossani, G.; Borrello, M. T.; Vellore, N. A.; Ganesan, A.; Mattevi, A.; Baron, R. Expanding the Druggable Space of the LSD1/CoREST Epigenetic Target: New Potential Binding Regions for Drug-Like Molecules, Peptides, Protein Partners, and Chromatin. *PLoS Comput. Biol.* **2013**, *9*, e1003158.

(232) Lv, T.; Yuan, D.; Miao, X.; Lv, Y.; Zhan, P.; Shen, X.; Song, Y. Over-Expression of LSD1 Promotes Proliferation, Migration and Invasion in Non-Small Cell Lung Cancer. *PLoS One* **2012**, *7*, e35065.

(233) Devlin, J.; Panganiban, L.; Devlin, P. Random Peptide Libraries: A Source of Specific Protein Binding Molecules. *Science (80-.).* **1990**, *249*, 404–406.

(234) Cwirla, S. E.; Peters, E. A.; Barrett, R. W.; Dower, W. J. Peptides on Phage: A Vast Library of Peptides for Identifying Ligands. *Proc. Natl. Acad. Sci. U. S. A.* **1990**, *87*, 6378–6382.

(235) Cwirla, S. E.; Balasubramanian, P.; Duffin, D. J.; Wagstrom, C. R.; Gates, C. M.; Singer, S. C.; Davis, A. M.; Tansik, R. L.; Mattheakis, L. C.; Boytos, C. M.; Schatz, P. J.; Baccanari, D. P.; Wrighton, N. C.; Barrett, R. W.; Dower, W. J. Peptide Agonist of the Thrombopoietin Receptor as Potent as the Natural Cytokine. *Science* **1997**, *276*, 1696–1699.

(236) Krumpe, L.; Mori, T. Potential of Phage-Displayed Peptide Library Technology to Identify Functional Targeting Peptides. **2007**.

(237) Rothe, A.; Hosse, R. J.; Power, B. E. In Vitro Display Technologies Reveal Novel Biopharmaceutics. *FASEB J.* **2006**, *20*, 1599–1610.

(238) Sidhu, S. Phage Display in Pharmaceutical Biotechnology. *Curr. Opin. Biotechnol.* **2000**.

(239) Smith, G. P.; Petrenko, V. A. Phage Display. *Chem. Rev.* **1997**, *97*, 391–410.

(240) Sergeeva, A.; Kolonin, M. G.; Molldrem, J. J.; Pasqualini, R.; Arap, W. Display Technologies: Application for the Discovery of Drug and Gene Delivery Agents. *Adv. Drug Deliv. Rev.* **2006**, *58*, 1622–1654.

(241) Remy, I. Erythropoietin Receptor Activation by a Ligand-Induced Conformation Change. *Science (80-.).* **1999**, *283*, 990–993.

(242) Mintz, P. J.; Kim, J.; Do, K.-A.; Wang, X.; Zinner, R. G.; Cristofanilli, M.; Arap, M. A.; Hong, W. K.; Troncoso, P.; Logothetis, C. J.; Pasqualini, R.; Arap, W. Fingerprinting the Circulating Repertoire of Antibodies from Cancer Patients. *Nat. Biotechnol.* **2003**, *21*, 57–63.

(243) Leurs, U.; Lohse, B.; Rand, K. D.; Ming, S.; Riise, E. S.; Cole, P. A.; Kristensen,

J. L.; Clausen, R. P. Substrate- and Cofactor-Independent Inhibition of Histone Demethylase KDM4C. *ACS Chem. Biol.* **2014**, *9*, 2131–2138.

(244) Leurs, U.; Lohse, B.; Ming, S.; Cole, P. A.; Clausen, R. P.; Kristensen, J. L.; Rand, K. D. Dissecting the Binding Mode of Low Affinity Phage Display Peptide Ligands to Protein Targets by Hydrogen/deuterium Exchange Coupled to Mass Spectrometry. *Anal. Chem.* **2014**, *86*, 11734–11741.

(245) Smith, G. Filamentous Fusion Phage: Novel Expression Vectors That Display Cloned Antigens on the Virion Surface. *Science (80-.).* **1985**, *228*, 1315–1317.

(246) Kehoe, J.; Kay, B. Filamentous Phage Display in the New Millennium. *Chem. Rev.* **2005**.

(247) Lee, C. M. Y.; Iorno, N.; Sierro, F.; Christ, D. Selection of Human Antibody Fragments by Phage Display. *Nat. Protoc.* **2007**, *2*, 3001–3008.

(248) Løset, G. Å.; Roos, N.; Bogen, B.; Sandlie, I. Expanding the Versatility of Phage Display II: Improved Affinity Selection of Folded Domains on Protein VII and IX of the Filamentous Phage. *PLoS One* **2011**, *6*, e17433.

(249) Krebber, C.; Spada, S.; Desplancq, D.; Krebber, A.; Ge, L.; Pluckthun, A. Selectively-Infective Phage (SIP): A Mechanistic Dissection of a Novel in Vivo Selection for Protein-Ligand Interactions. *J. Mol. Biol.* **1997**, *268*, 607–618.

(250) Spada, S.; Plückthun, A. Selectively Infective Phage (SIP) Technology: A Novel Method for in Vivo Selection of Interacting Protein–ligand Pairs. *Nat. Med.* **1997**, *3*, 694–696.

(251) Riechmann, L.; Holliger, P. The C-Terminal Domain of TolA Is the Coreceptor for Filamentous Phage Infection of E. Coli. *Cell* **1997**, *90*, 351–360.

(252) Kay, B. K.; Kurakin, A. V.; Hyde-DeRuyscher, R. From Peptides to Drugs via Phage Display. *Drug Discov. Today* **1998**, *3*, 370–378.

(253) Carmen, S.; Jermutus, L. Concepts in Antibody Phage Display. *Brief. Funct. Genomic. Proteomic.* **2002**, *1*, 189–203.

(254) Ullman, C. G.; Frigotto, L.; Cooley, R. N. In Vitro Methods for Peptide Display and Their Applications. *Brief. Funct. Genomics* **2011**, *10*, 125–134.

(255) Butler, J. E.; Ni, L.; Nessler, R.; Joshi, K. S.; Suter, M.; Rosenberg, B.; Chang, J.; Brown, W. R.; Cantarero, L. A. The Physical and Functional Behavior of Capture Antibodies Adsorbed on Polystyrene. *J. Immunol. Methods* **1992**, *150*, 77–90.

(256) Phage Display: Solution-phase Panning with Affinity Bead Capture | NEB https://www.neb.com/protocols/1/01/01/phage-display-solution-phase-panning-with-affinity-bead-capture (accessed Aug 25, 2015).

(257) Koide, A.; Wojcik, J.; Gilbreth, R. N.; Reichel, A.; Piehler, J.; Koide, S. Accelerating Phage-Display Library Selection by Reversible and Site-Specific Biotinylation. *Protein Eng. Des. Sel.* **2009**, *22*, 685–690.

(258) Galasso, G. J.; Sharp, D. G. Virus Particle Aggregation and the Plaque-Forming

Unit. *J. Immunol.* **1962**, *88*, 339–347.

(259) Meulemans, E. V; Slobbe, R.; Wasterval, P.; Ramaekers, F. C.; van Eys, G. J. Selection of Phage-Displayed Antibodies Specific for a Cytoskeletal Antigen by Competitive Elution with a Monoclonal Antibody. *J. Mol. Biol.* **1994**, *244*, 353–360.

(260) Young, C. L.; Britton, Z. T.; Robinson, A. S. Recombinant Protein Expression and Purification: A Comprehensive Review of Affinity Tags and Microbial Applications. *Biotechnol. J.* **2012**, *7*, 620–634.

(261) Marbach, A.; Bettenbrock, K. Lac Operon Induction in Escherichia Coli: Systematic Comparison of IPTG and TMG Induction and Influence of the Transacetylase LacA. *J. Biotechnol.* **2012**, *157*, 82–88.

(262) Lee, Y. C. High-Performance Anion-Exchange Chromatography for Carbohydrate Analysis. *Anal. Biochem.* **1990**, *189*, 151–162.

(263) Rocklin, R. D.; Pohl, C. A. Determination of Carbohydrates by Anion Exchange Chromatography with Pulsed Amperometric Detection. *J. Liq. Chromatogr.* **2006**, *6*, 1577–1590.

(264) Noble, J. E.; Bailey, M. J. A. Quantitation of Protein. *Methods Enzymol.* **2009**, *463*, 73–95.

(265) Kay, B.; Kasanov, J.; Knight, S.; Kurakin, A. Convergent Evolution with Combinatorial Peptides. *FEBS Lett.* **2000**.

(266) Barbas, C. F.; Rosenblum, J. S.; Lerner, R. A. Direct Selection of Antibodies That Coordinate Metals from STDisynthetic Combinatorial Libraries. *Proc. Natl. Acad. Sci. U. S. A.* **1993**, *90*, 6385–6389.

(267) Vodnik, M.; Zager, U.; Strukelj, B.; Lunder, M. Phage Display: Selecting Straws instead of a Needle from a Haystack. *Molecules* **2011**, *16*, 790–817.

(268) Thomas, W. D.; Golomb, M.; Smith, G. P. Corruption of Phage Display Libraries by Target-Unrelated Clones: Diagnosis and Countermeasures. *Anal. Biochem.* **2010**, *407*, 237–240.

(269) Cao, J.; Zhao, P.; Miao, X. H.; Zhao, L. J.; Xue, L. J.; Qi Zt, Z. tian. Phage Display Selection on Whole Cells Yields a Small Peptide Specific for HCV Receptor Human CD81. *Cell Res.* **2003**, *13*, 473–479.

(270) Sundell, G. N.; Ivarsson, Y. Interaction Analysis through Proteomic Phage Display. *Biomed Res. Int.* **2014**, *2014*, 176172.

(271) Gray, B. P.; Li, S.; Brown, K. C. From Phage Display to Nanoparticle Delivery: Functionalizing Liposomes with Multivalent Peptides Improves Targeting to a Cancer Biomarker. *Bioconjug. Chem.* **2013**, *24*, 85–96.

(272) Kay, B. K.; Hamilton, P. T. Identification of Enzyme Inhibitors from Phage-Displayed Combinatorial Peptide Libraries. *Comb. Chem. High Throughput Screen.* **2001**, *4*, 535–543.

(273) Leurs, U.; Lohse, B.; Ming, S.; Cole, P. A.; Clausen, R. P.; Kristensen, J. L.;

Rand, K. D. Dissecting the Binding Mode of Low Affinity Phage Display Peptide Ligands to Protein Targets by Hydrogen/deuterium Exchange Coupled to Mass Spectrometry. *Anal. Chem.* **2014**, *86*, 11734–11741.

(274) Lin, X.-M.; Zhong, W.-T.; Wang, C.-L.; Wang, S.-Q. [Expression of Histone Demethylase Lysine Specific Demethylase 1 in Acute Leukemia and Its Clinical Significance]. *Zhongguo Shi Yan Xue Ye Xue Za Zhi* **2011**, *19*, 1348–1352.

(275) Suzuki, T.; Miyata, N. Lysine Demethylases Inhibitors. *J. Med. Chem.* **2011**, *54*, 8236–8250.

(276) Mohammad, H.; Smitheman, K.; Cusan, M.; Liu, Y.; Pappalardi, M.; Federowicz, K.; Aller, G. Van; Kasparec, J.; Tian, X.; Suarez, D.; Rouse, M.; Schneck, J.; Carson, J.; McDevitt, P.; Ho, T.; McHugh, C.; Miller, W.; Johnson, N.; Armstrong, S. A.; Tummino, P. Inhibition Of LSD1 As a Therapeutic Strategy For The Treatment Of Acute Myeloid Leukemia. *Blood* **2013**, *122*, 3964.

(277) Shen, H.; Laird, P. W. Interplay between the Cancer Genome and Epigenome. *Cell* **2013**, *153*, 38–55.

(278) Welch, J. S.; Ley, T. J.; Link, D. C.; Miller, C. A.; Larson, D. E.; Koboldt, D. C.; Wartman, L. D.; Lamprecht, T. L.; Liu, F.; Xia, J.; Kandoth, C.; Fulton, R. S.; McLellan, M. D.; Dooling, D. J.; Wallis, J. W.; Chen, K.; Harris, C. C.; Schmidt, H. K.; Kalicki-Veizer, J. M.; Lu, C.; Zhang, Q.; Lin, L.; O'Laughlin, M. D.; McMichael, J. F.; Delehaunty, K. D.; Fulton, L. A.; Magrini, V. J.; McGrath, S. D.; Demeter, R. T.; Vickery, T. L.; Hundal, J.; Cook, L. L.; Swift, G. W.; Reed, J. P.; Alldredge, P. A.; Wylie, T. N.; Walker, J. R.; Watson, M. A.; Heath, S. E.; Shannon, W. D.; Varghese, N.; Nagarajan, R.; Payton, J. E.; Baty, J. D.; Kulkarni, S.; Klco, J. M.; Tomasson, M. H.; Westervelt, P.; Walter, M. J.; Graubert, T. A.; DiPersio, J. F.; Ding, L.; Mardis, E. R.; Wilson, R. K. The Origin and Evolution of Mutations in Acute Myeloid Leukemia. *Cell* **2012**, *150*, 264–278.

(279) Lerch, E.; Espeli, V.; Zucca, E.; Leoncini, L.; Scali, G.; Mora, O.; Bordoni, A.; Cavalli, F.; Ghielmini, M.; Juliusson, G.; Antunovic, P.; Derolf, A.; Lehmann, S.; Möllgård, L.; Stockelberg, D.; Tidefelt, U.; Wahlin, A.; Höglund, M. Prognosis of Acute Myeloid Leukemia in the General Population: Data from Southern Switzerland. *Blood* **2009**, *113*, 303–310.

(280) Alibhai, S. M. H.; Leach, M.; Minden, M. D.; Brandwein, J. Outcomes and Quality of Care in Acute Myeloid Leukemia over 40 Years. *Cancer* **2009**, *115*, 2903–2911.

(281) Kon Kim, T.; Gore, S. D.; Zeidan, A. M. Epigenetic Therapy in Acute Myeloid Leukemia: Current and Future Directions. *STDin. Hematol.* **2015**, *52*, 172–183.

(282) Sprüssel, A.; Schulte, J. H.; Weber, S.; Necke, M.; Händschke, K.; Thor, T.; Pajtler, K. W.; Schramm, A.; König, K.; Diehl, L.; Mestdagh, P.; Vandesompele, J.; Speleman, F.; Jastrow, H.; Heukamp, L. C.; Schüle, R.; Dührsen, U.; Buettner, R.; Eggert, A.; Göthert, J. R. Lysine-Specific Demethylase 1 Restricts Hematopoietic Progenitor Proliferation and Is Essential for Terminal Differentiation. *Leukemia* **2012**, *26*, 2039–2051.

(283) Kerenyi, M. A.; Shao, Z.; Hsu, Y.-J.; Guo, G.; Luc, S.; O'Brien, K.; Fujiwara, Y.; Peng, C.; Nguyen, M.; Orkin, S. H. Histone Demethylase Lsd1 Represses Hematopoietic Stem and Progenitor Cell Signatures during Blood Cell Maturation. *Elife* **2013**, *2*, e00633.

(284) Niebel, D.; Kirfel, J.; Janzen, V.; Höller, T.; Majores, M.; Gütgemann, I. Lysine-Specific Demethylase 1 (LSD1) in Hematopoietic and Lymphoid Neoplasms. *Blood* **2014**, *124*, 151–152.

(285) Lokken, A. A.; Zeleznik-Le, N. J. Breaking the LSD1/KDM1A Addiction: Therapeutic Targeting of the Epigenetic Modifier in AML. *Cancer Cell* **2012**, *21*, 451–453.

(286) Rathke, M. W.; Nowak, M. The Horner-Wadsworth-Emmons Modification of the Wittig Reaction Using Triethylamine and Lithium or Magnesium Salts. *J. Org. Chem.* **1985**, *50*, 2624–2626.

(287) Riches, S. L.; Saha, C.; Filgueira, N. F.; Grange, E.; McGarrigle, E. M.; Aggarwal, V. K. On the Mechanism of Ylide-Mediated Cyclopropanations: Evidence for a Proton-Transfer Step and Its Effect on Stereoselectivity. *J. Am. Chem. Soc.* **2010**, *132*, 7626–7630.

(288) Montalbetti, C. A. G. N.; Falque, V. Amide Bond Formation and Peptide Coupling. *Tetrahedron* **2005**, *61*, 10827–10852.

(289) Quentmeier, H.; Martelli, M. P.; Dirks, W. G.; Bolli, N.; Liso, A.; Macleod, R. A. F.; Nicoletti, I.; Mannucci, R.; Pucciarini, A.; Bigerna, B.; Martelli, M. F.; Mecucci, C.; Drexler, H. G.; Falini, B. Cell Line OCI/AML3 Bears Exon-12 NPM Gene Mutation-A and Cytoplasmic Expression of Nucleophosmin. *Leukemia* **2005**, *19*, 1760–1767.

(290) Amit Jathoul, E. L. O. G. M. P. L. T. and J. M. *Bioluminescence - Recent Advances in Oceanic Measurements and Laboratory Applications*; Lapota, D., Ed.; InTech, 2012.

(291) Mah, R.; Thomas, J. R.; Shafer, C. M. Drug Discovery Considerations in the Development of Covalent Inhibitors. *Bioorg. Med. Chem. Lett.* **2014**, *24*, 33–39.

(292) Slavik, J. M.; Hutchcroft, J. E.; Bierer, B. E. CD28/CTLA-4 and CD80/CD86 Families: Signaling and Function. *Immunol. Res.* **1999**, *19*, 1–24.

(293) Sansom, D. M. CD28, CTLA-4 and Their Ligands: Who Does What and to Whom? *Immunology* **2000**, *101*, 169–177.

(294) Ziegler-Heitbrock, H. W.; Ulevitch, R. J. CD14: Cell Surface Receptor and Differentiation Marker. *Immunol. Today* **1993**, *14*, 121–125.

(295) Tagliafico, E.; Tenedini, E.; Bergamaschi, A.; Manfredini, R.; Percudani, R.; Siena, M.; Zanocco-Marani, T.; Grande, A.; Montanari, M.; Gemelli, C.; Torelli, U.; Ferrari, S. Gene Expression Profile of Vitamin D3 Treated HL60 Cells Shows an Incomplete Molecular Phenotypic Conversion to Monocytes. *Cell Death Differ.* **2002**, *9*, 1185–1195.

(296) Rigby, W. F.; Shen, L.; Ball, E. D.; Fanger, M. W. 1,25-Dihydroxyvitamin D3 Induces a Myelomonocytic Phenotype with Enhanced Effector Cell Function in

the HL-60 Promyelocytic Leukemia Cell Line. *Mol. Immunol.* **1985**, *22*, 567–572.

(297) Rigby, W. F.; Shen, L.; Ball, E. D.; Guyre, P. M.; Fanger, M. W. Differentiation of a Human Monocytic Cell Line by 1,25-Dihydroxyvitamin D3 (Calcitriol): A Morphologic, Phenotypic, and Functional Analysis. *Blood* **1984**, *64*, 1110–1115.

(298) Loken, M. R.; Shah, V. O.; Dattilio, K. L.; Civin, C. I. Flow Cytometric Analysis of Human Bone Marrow. II. Normal B Lymphocyte Development. *Blood* **1987**, *70*, 1316–1324.

(299) Tagliafico, E.; Tenedini, E.; Bergamaschi, A.; Manfredini, R.; Percudani, R.; Siena, M.; Zanocco-Marani, T.; Grande, A.; Montanari, M.; Gemelli, C.; Torelli, U.; Ferrari, S. Gene Expression Profile of Vitamin D3 Treated HL60 Cells Shows an Incomplete Molecular Phenotypic Conversion to Monocytes. *Cell Death Differ.* **2002**, *9*, 1185–1195.

(300) Rushworth, S. A.; Murray, M. Y.; Zaitseva, L.; Bowles, K. M.; MacEwan, D. J. Identification of Bruton's Tyrosine Kinase as a Therapeutic Target in Acute Myeloid Leukemia. *Blood* **2014**, *123*, 1229–1238.

(301) Siddiqui, N.; Andalip; Bawa, S.; Ali, R.; Afzal, O.; Akhtar, M. J.; Azad, B.; Kumar, R. Antidepressant Potential of Nitrogen-Containing Heterocyclic Moieties: An Updated Review. *J. Pharm. Bioallied Sci.* **2011**, *3*, 194–212.

(302) Casini, A.; Scozzafava, A.; Mastrolorenzo, A.; Supuran, L. T. Sulfonamides and Sulfonylated Derivatives as Anticancer Agents. *Curr. Cancer Drug Targets* **2002**, *2*, 55–75.

(303) Scozzafava, A.; Owa, T.; Mastrolorenzo, A.; Supuran, C. T. Anticancer and Antiviral Sulfonamides. *Curr. Med. Chem.* **2003**, *10*, 925–953.

(304) Seiter, K.; Feldman, E. J.; Dorota Halicka, H.; Deptala, A.; Traganos, F.; Burke, H. B.; Hoang, A.; Goff, H.; Pozzuoli, M.; Kancherla, R.; Darzynkiewicz, Z.; Ahmed, T. Clinical and Laboratory Evaluation of All-Trans Retinoic Acid Modulation of Chemotherapy in Patients with Acute Myelogenous Leukaemia. *Br. J. Haematol.* **2000**, *108*, 40–47.

(305) Honigberg, L. A.; Smith, A. M.; Sirisawad, M.; Verner, E.; Loury, D.; Chang, B.; Li, S.; Pan, Z.; Thamm, D. H.; Miller, R. A.; Buggy, J. J. The Bruton Tyrosine Kinase Inhibitor PCI-32765 Blocks B-Cell Activation and Is Efficacious in Models of Autoimmune Disease and B-Cell Malignancy. *Proc. Natl. Acad. Sci.* **2010**, *107*, 13075–13080.

(306) Dalton, W. T.; Ahearn, M. J.; McCredie, K. B.; Freireich, E. J.; Stass, S. A.; Trujillo, J. M. HL-60 Cell Line Was Derived from a Patient with FAB-M2 and Not FAB-M3. *Blood* **1988**, *71*, 242–247.

(307) Palis, J.; King, B.; Keng, P. Separation of Spontaneously Differentiating and Cell Cycle-Specific Populations of HL-60 Cells. *Leuk. Res.* **1988**, *12*, 339–344.

(308) Quentmeier, H.; Reinhardt, J.; Zaborski, M.; Drexler, H. G. FLT3 Mutations in Acute Myeloid Leukemia Cell Lines. *Leukemia* **2003**, *17*, 120–124.

(309) Shih, A. H.; Jiang, Y.; Meydan, C.; Shank, K.; Pandey, S.; Barreyro, L.; Antony-

Debre, I.; Viale, A.; Socci, N.; Sun, Y.; Robertson, A.; Cavatore, M.; de Stanchina, E.; Hricik, T.; Rapaport, F.; Woods, B.; Wei, C.; Hatlen, M.; Baljevic, M.; Nimer, S. D.; Tallman, M.; Paietta, E.; Cimmino, L.; Aifantis, I.; Steidl, U.; Mason, C.; Melnick, A.; Levine, R. L. Mutational Cooperativity Linked to Combinatorial Epigenetic Gain of Function in Acute Myeloid Leukemia. *Cancer Cell* **2015**, *27*, 502–515.

(310) Laubach, J. P.; Moreau, P.; San-Miguel, J. F.; Richardson, P. G. Panobinostat for the Treatment of Multiple Myeloma. *Clin. Cancer Res.* **2015**.

(311) Li, H.; Xue, F.; Kraus, J. M.; Ji, H.; Labby, K. J.; Mataka, J.; Delker, S. L.; Martásek, P.; Roman, L. J.; Poulos, T. L.; Silverman, R. B. Cyclopropyl- and Methyl-Containing Inhibitors of Neuronal Nitric Oxide Synthase. *Bioorg. Med. Chem.* **2013**, *21*, 1333–1343.

(312) Warner, J. K.; Wang, J. C. Y.; Takenaka, K.; Doulatov, S.; McKenzie, J. L.; Harrington, L.; Dick, J. E. Direct Evidence for Cooperating Genetic Events in the Leukemic Transformation of Normal Human Hematopoietic Cells. *Leukemia* **2005**, *19*, 1794–1805.

(313) Lynch, J. T.; Spencer, G. J.; Harris, W. J.; Maiques-Díaz, A.; Ciceri, F.; Huang, X.; Somervaille, T. C. P. Pharmacological Inhibitors of LSD1 Promote Differentiation of Myeloid Leukemia Cells through a Mechanism Independent of Histone Demethylation. *Blood* **2014**, *124*, 267.

(314) Hock, H.; Hamblen, M. J.; Rooke, H. M.; Traver, D.; Bronson, R. T.; Cameron, S.; Orkin, S. H. Intrinsic Requirement for Zinc Finger Transcription Factor Gfi-1 in Neutrophil Differentiation. *Immunity* **2003**, *18*, 109–120.

(315) Khanna-Gupta, A.; Sun, H.; Zibello, T.; Lee, H. M.; Dahl, R.; Boxer, L. A.; Berliner, N. Growth Factor Independence-1 (Gfi-1) Plays a Role in Mediating Specific Granule Deficiency (SGD) in a Patient Lacking a Gene-Inactivating Mutation in the C/EBPepsilon Gene. *Blood* **2007**, *109*, 4181–4190.

(316) Upadhyay, G.; Chowdhury, A. H.; Vaidyanathan, B.; Kim, D.; Saleque, S. Antagonistic Actions of Rcor Proteins Regulate LSD1 Activity and Cellular Differentiation. *Proc. Natl. Acad. Sci. U. S. A.* **2014**, *111*, 8071–8076.

(317) Fonovic, M.; Bogyo, M. Activity Based Probes for Proteases: Applications to Biomarker Discovery,Molecular Imaging and Drug Screening. *Curr. Pharm. Des.* **2007**, *13*, 253–261.

(318) Sadaghiani, A. M.; Verhelst, S. H.; Bogyo, M. Tagging and Detection Strategies for Activity-Based Proteomics. *Curr. Opin. Chem. Biol.* **2007**, *11*, 20–28.

(319) Prescher, J. A.; Bertozzi, C. R. Chemistry in Living Systems. *Nat. Chem. Biol.* **2005**, *1*, 13–21.

(320) Heal, W. P.; Dang, T. H. T.; Tate, E. W. Activity-Based Probes: Discovering New Biology and New Drug Targets. *Chem. Soc. Rev.* **2011**, *40*, 246–257.

(321) Speers, A. E.; Cravatt, B. F. Profiling Enzyme Activities in Vivo Using Click Chemistry Methods. *Chem. Biol.* **2004**, *11*, 535–546.

(322) Yang, Y.; Yang, X.; Verhelst, S. Comparative Analysis of Click Chemistry

Mediated Activity-Based Protein Profiling in Cell Lysates. *Molecules* **2013**.

(323) Heal, W. P.; Dang, T. H. T.; Tate, E. W. Activity-Based Probes: Discovering New Biology and New Drug Targets. *Chem. Soc. Rev.* **2011**, *40*, 246–257.

(324) Li, X.; Kapoor, T. M. Approach to Profile Proteins That Recognize Post-Translationally Modified Histone "tails". *J. Am. Chem. Soc.* **2010**, *132*, 2504–2505.

(325) Krysiak, J. M.; Kreuzer, J.; Macheroux, P.; Hermetter, A.; Sieber, S. A.; Breinbauer, R. Activity-Based Probes for Studying the Activity of Flavin-Dependent Oxidases and for the Protein Target Profiling of Monoamine Oxidase Inhibitors. *Angew. Chem. Int. Ed. Engl.* **2012**, *51*, 7035–7040.

(326) Willems, L. I.; van der Linden, W. A.; Li, N.; Li, K.-Y.; Liu, N.; Hoogendoorn, S.; van der Marel, G. A.; Florea, B. I.; Overkleeft, H. S. Bioorthogonal Chemistry: Applications in Activity-Based Protein Profiling. *Acc. Chem. Res.* **2011**, *44*, 718–729.

(327) Cunningham, C. W.; Mukhopadhyay, A.; Lushington, G. H.; Blagg, B. S. J.; Prisinzano, T. E.; Krise, J. P. Uptake, Distribution and Diffusivity of Reactive Fluorophores in Cells: Implications toward Target Identification. *Mol. Pharm.* **2010**, *7*, 1301–1310.

(328) Agard, N. J.; Prescher, J. A.; Bertozzi, C. R. A Strain-Promoted [3 + 2] Azide-Alkyne Cycloaddition for Covalent Modification of Biomolecules in Living Systems. *J. Am. Chem. Soc.* **2004**, *126*, 15046–15047.

(329) Saxon, E. Cell Surface Engineering by a Modified Staudinger Reaction. *Science (80-.).* **2000**, *287*, 2007–2010.

(330) Zhang, X.; Zhang, Y. Applications of Azide-Based Bioorthogonal Click Chemistry in Glycobiology. *Molecules* **2013**.

(331) Himo, F.; Lovell, T.; Hilgraf, R.; Rostovtsev, V. V; Noodleman, L.; Sharpless, K. B.; Fokin, V. V. Copper(I)-Catalyzed Synthesis of Azoles. DFT Study Predicts Unprecedented Reactivity and Intermediates. *J. Am. Chem. Soc.* **2005**, *127*, 210–216.

(332) Berg, R.; Straub, B. F. Advancements in the Mechanistic Understanding of the Copper-Catalyzed Azide-Alkyne Cycloaddition. *Beilstein J. Org. Chem.* **2013**, *9*, 2715–2750.

(333) Chan, T. R.; Hilgraf, R.; Sharpless, K. B.; Fokin, V. V. Polytriazoles as copper(I)-Stabilizing Ligands in Catalysis. *Org. Lett.* **2004**, *6*, 2853–2855.

(334) Long, S.; Chen, L.; Xiang, Y.; Song, M.; Zheng, Y.; Zhu, Q. An Activity-Based Fluorogenic Probe for Sensitive and Selective Monoamine Oxidase-B Detection. *Chem. Commun. (Camb).* **2012**, *48*, 7164–7166.

(335) Duvvuri, M.; Konkar, S.; Funk, R. S.; Krise, J. M.; Krise, J. P. A Chemical Strategy To Manipulate the Intracellular Localization of Drugs in Resistant Cancer Cells †. *Biochemistry* **2005**, *44*, 15743–15749.

(336) Duvvuri, M.; Krise, J. P. Intracellular Drug Sequestration Events Associated with

the Emergence of Multidrug Resistance: A Mechanistic Review. *Front. Biosci.* **2005**, *10*, 1499–1509.

(337) Duvvuri, M.; Gong, Y.; Chatterji, D.; Krise, J. P. Weak Base Permeability Characteristics Influence the Intracellular Sequestration Site in the Multidrug-Resistant Human Leukemic Cell Line HL-60. *J. Biol. Chem.* **2004**, *279*, 32367–32372.

(338) Gong, Y.; Duvvuri, M.; Krise, J. P. Separate Roles for the Golgi Apparatus and Lysosomes in the Sequestration of Drugs in the Multidrug-Resistant Human Leukemic Cell Line HL-60. *J. Biol. Chem.* **2003**, *278*, 50234–50239.

(339) Rosania, G. R. Supertargeted Chemistry: Identifying Relationships between Molecular Structures and Their Sub-Cellular Distribution. *Curr. Top. Med. Chem.* **2003**, *3*, 659–685.

(340) Wang, Q.; Chan, T. R.; Hilgraf, R.; Fokin, V. V; Sharpless, K. B.; Finn, M. G. Bioconjugation by copper(I)-Catalyzed Azide-Alkyne [3 + 2] Cycloaddition. *J. Am. Chem. Soc.* **2003**, *125*, 3192–3193.

(341) Presolski, S. I.; Hong, V. P.; Finn, M. G. Copper-Catalyzed Azide-Alkyne Click Chemistry for Bioconjugation. *Curr. Protoc. Chem. Biol.* **2011**, *3*, 153–162.

(342) Suikki, H. E.; Kujala, P. M.; Tammela, T. L. J.; van Weerden, W. M.; Vessella, R. L.; Visakorpi, T. Genetic Alterations and Changes in Expression of Histone Demethylases in Prostate Cancer. *Prostate* **2010**, *70*, 889–898.

(343) Malcomson, T.; Yelekci, K.; Borrello, M. T.; Ganesan, A.; STDina, E.; De Kimpe, N.; Mangelinckx, S.; Ramsay, R. R. Cis-Cyclopropylamines as Mechanism-Based Inhibitors of Monoamine Oxidases. *FEBS J.* **2015**, *282*, 3190–3198.

(344) Huang, Z.-P.; Du, J.-T.; Zhao, Y.-F.; Li, Y.-M. Synthesis of Site-Specifically Dimethylated and Trimethylated Peptides Derived from Histone H3 N-Terminal Tail. *Int. J. Pept. Res. Ther.* **2006**, *12*, 187–193.

(345) Pardin Cristophe, Keillor W. Jeffrey, L. D. W. Cinnamoyl Inhibitors of Transglutaminase, 2013.

(346) Peh, G.-R.; Kantchev, E. A. B.; Zhang, C.; Ying, J. Y. N-Heterocycle Carbene (NHC)-Ligated Cyclopalladated N,N-Dimethylbenzylamine: A Highly Active, Practical and Versatile Catalyst for the Heck–Mizoroki Reaction. *Org. Biomol. Chem.* **2009**, *7*, 2110.

(347) Ahn, Y.-H.; Hwang, Y.; Liu, H.; Wang, X. J.; Zhang, Y.; Stephenson, K. K.; Boronina, T. N.; Cole, R. N.; Dinkova-Kostova, A. T.; Talalay, P.; Cole, P. A. Electrophilic Tuning of the Chemoprotective Natural Product Sulforaphane. *Proc. Natl. Acad. Sci. U. S. A.* **2010**, *107*, 9590–9595.